EMERGING INFECTIOUS DISEASES®

CDC
Centers for Disease Control and Prevention

Respiratory Infections

November 2021

Berthe Morisot (1841–1895), *Hanging the Laundry Out to Dry*, 1875. Oil on canvas, 13 in x 16 in/33 cm x 40.6 cm. Public domain image, National Gallery of Art, Washington, DC, USA.

EMERGING INFECTIOUS DISEASES®

Emerging Infectious Diseases is published monthly by the Centers for Disease Control and Prevention, 1600 Clifton Rd NE, Mailstop H16-2, Atlanta, GA 30329-4027, USA. Telephone 404-639-1960; email, eideditor@cdc.gov

EMERGING INFECTIOUS DISEASES®

Respiratory Infections **November 2021**

On the Cover

Berthe Morisot (1841–1895), *Hanging the Laundry Out to Dry*, 1875. Oil on canvas, 13 in x 16 in/33 cm x 40.6 cm. Public domain image, National Gallery of Art, Washington, DC, USA.

About the Cover p. 2977

Synopses

Research

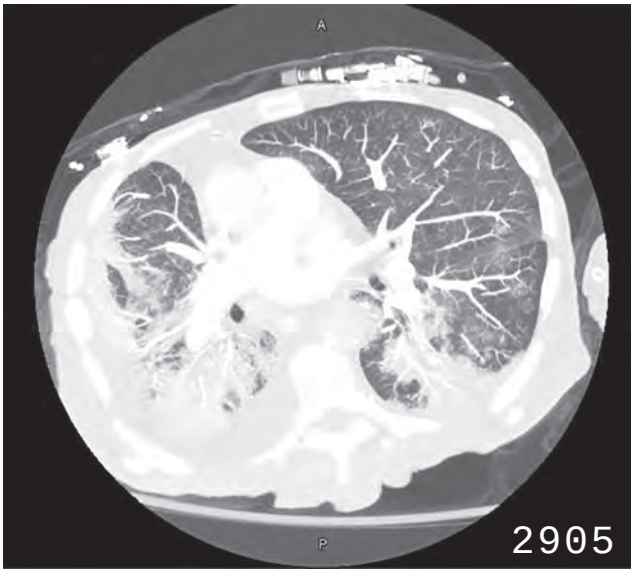

Dispatches

EMERGING INFECTIOUS DISEASES®
November 2021

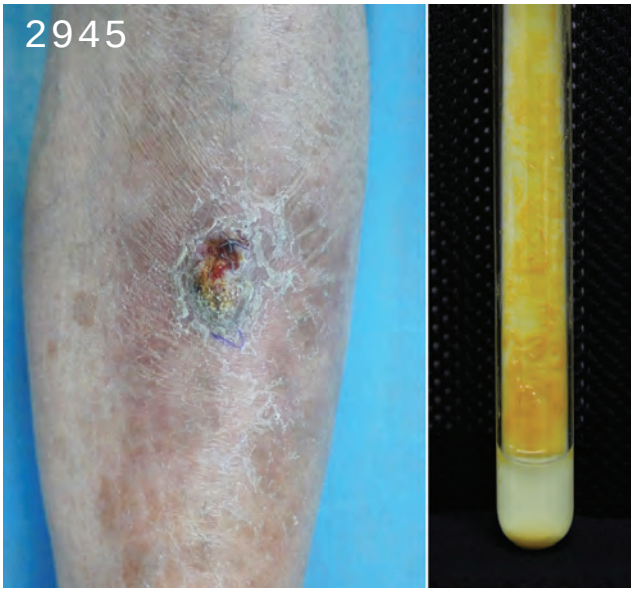

EMERGING INFECTIOUS DISEASES®
November 2021

Research Letters

Books and Media

About the Cover

Etymologia

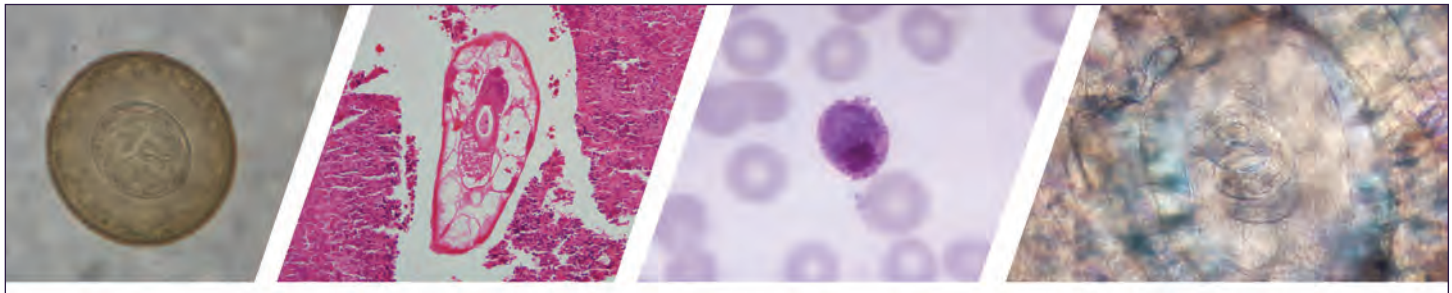

DPDx

Diagnostic Assistance and Training in Laboratory Identification of Parasites

A free service of CDC available to laboratorians, pathologists, and other health professionals in the United States and abroad

- Diagnosis from photographs of worms, histological sections, fecal, blood, and other specimen types
- Expert diagnostic review
- Formal diagnostic laboratory report
- Submission of samples via secure file share

Visit the DPDx website for information on laboratory diagnosis, geographic distribution, clinical features, parasite life cycles, and training via Monthly Case Studies of parasitic diseases.

www.cdc.gov/dpdx
dpdx@cdc.gov

U.S. Department of Health and Human Services
Centers for Disease Control and Prevention

CS272346-DE

Policy Review and Modeling Analysis of Mitigation Measures for Coronavirus Disease Epidemic Control, Health System, and Disease Burden, South Korea

Hae-Young Kim, In-Hwan Oh, Jacob Lee, Jeong-Yeon Seon, Woo-Hwi Jeon, Jae Seok Park, Sung-Il Nam, Niket Thakkar, Prashanth Selvaraj, Jessica McGillen, Daniel Klein, Scott Braithwaite, Anna Bershteyn, Seung Heon Lee

We reviewed the timeline of key policies for control of the coronavirus disease epidemic and determined their impact on the epidemic and hospital burden in South Korea. Using a discrete stochastic transmission model, we estimated that multilevel policies, including extensive testing, contact tracing, and quarantine, reduced contact rates by 90% and rapidly decreased the epidemic in Daegu and nationwide during February–March 2020. Absence of these prompt responses could have resulted in a >10-fold increase in infections, hospitalizations, and deaths by May 15, 2020, relative to the status quo. The model suggests that reallocation of persons who have mild or asymptomatic cases to community treatment centers helped avoid overwhelming hospital capacity and enabled healthcare workers to provide care for more severely and critically ill patients in hospital beds and negative-pressure intensive care units. As small outbreaks continue to occur, contact tracing and maintenance of hospital capacity are needed.

Since the first reported outbreak in Wuhan, China, on December 31, 2019, severe acute respiratory syndrome coronavirus 2 has infected >210 million persons and resulted in nearly 4.4 million deaths worldwide as of August 2021 (*1*). Many countries have responded to the coronavirus disease (COVID-19) pandemic with unprecedented large-scale anticontagion policies, including closure of nonessential businesses and stay-at-home restrictions (*2*). Such policies have had measurable effects on slowing down the epidemic during the early months of the COVID-19 pandemic (*1*–*4*).

In South Korea, the first case of COVID-19 was reported on January 20, 2020, and an additional 27 cases were confirmed by February 10. All confirmed case-patients either had international travel histories linked to the cities with confirmed cases or were the contacts of index case-patients. Many of these early cases were likely linked to travel between Wuhan and South Korea during the Lunar New Year holiday on January 24–28, 2020. However, on February 18, a woman in Daegu, the epicenter of the initial COVID-19 outbreak in South Korea, was the first case-patient who had no international travel history or contact with another index case-patient. Epidemiologic surveillance showed that she attended a large Shincheonji Church meeting before her diagnosis. Subsequently, >2,500 cases (62% of all confirmed cases in Daegu) were confirmed positive and epidemiologically linked to this church. The rapid surge in cases quickly overwhelmed all available hospital beds and intensive care unit (ICU) capacity in Daegu (*5*,*6*).

In response to the rapid surge, the government of South Korea implemented intensive policies for testing, contact tracing, and quarantining of all close and potential contacts of index cases, and social distancing (*7*). We review the timeline of key policies and practices implemented for COVID-19 epidemic control during the early 2020 epidemic in South Korea. We then used a stochastic transmission model to retrospectively evaluate the probable impact of these

Author affiliations: New York University Grossman School of Medicine, New York, NY, USA (H.-Y. Kim, J. McGillen, S. Braithwaite, A. Bershteyn); Kyung Hee University School of Medicine, Seoul, South Korea (I.-H. Oh, J.-Y. Seon, W.-H. Jeon); Hallym University Kangnam Hospital, Seoul (J. Lee); Keimyung University School of Medicine, Daegu, South Korea (J.S. Park, S.-I. Nam); Institute of Disease Modeling, Seattle, Washington, USA (N. Thakkar, P. Selvaraj, D. Klein); Korea University Ansan Hospital, Ansan, South Korea (S.H. Lee)

DOI: https://doi.org/10.301/eid2711.203779

policies and practices on the epidemic control. Our findings offer lessons for future health system planning and epidemic control during an initial outbreak of a respiratory disease.

Methods

Review of Country-Level Responses to COVID-19 Outbreak

We reviewed and summarized the key policies for COVID-19 epidemic control in South Korea during January 1–May 15, 2020. Our review used the World Health Organization (WHO) operational guidelines for COVID-19 strategic preparedness and response plan to categorize components of the response (*8*). The guidelines focus on 9 major pillars: 1) country-level coordination, planning, and monitoring; 2) risk communication and community engagement; 3) surveillance, rapid-response teams, and case investigation; 4) points of entry, international travel, and transport; 5) national laboratories; 6) infection prevention and control; 7) case management; 8) operational support and logistics; and 9) maintaining essential health services and systems. The details of the epidemic, policies, and health system use were collected from the official site of the Korea Center for Disease Control and Prevention (KCDC) and Daegu Disaster Management Headquarters (*5*,*9*), which were made public daily. We provide major policies at each governmental level, facility level, congregate setting, and household/personal level in chronological order (Table 1, https://wwwnc.cdc.gov/EID/article/27/11/20-3779-T1.htm; Appendix Figure, https://wwwnc.cdc.gov/EID/article/27/11/20-3779-App1.pdf).

Mathematical Model

We adapted an existing stochastic, discrete-time compartment model of community transmission of severe acute respiratory syndrome coronavirus 2 (*10*) to simulate the COVID-19 epidemic in South Korea (Appendix) . The model represents persons who are susceptible (S), exposed (E), infectious (I), or removed/recovered (R). We assumed that initial infections were imported through international travelers.

After the daily cases peaked at 813/day on March 1, the daily cases decreased below 100/day, and >99% of all Shincheonji Church members in Daegu were successfully traced and tested by mid-March. By March 18, there were 8,413 confirmed cases, 270,888 confirmed negative tests results, and 16,346 tests in progress, yielding a positive test rate of 3.0% and a case-fatality rate of 1.00%. Given that testing was widely conducted with intensive efforts for contact tracing during the initial outbreak, we assumed that the case-fatality rate is not far above the infection-fatality rate (IFR). To be conservative, we assumed that the true IFR would be slightly lower by a factor of 5%, resulting in the overall IFR estimate of 0.95.

Model Assumptions and Calibration

As of May 15, there were 10,991 confirmed cases, 695,854 confirmed negative test results, 19,875 in progress for test results, and 260 cumulative deaths. According to the data published by KCDC and Daegu Disaster Management Headquarters, 69.1% of all case-patients were asymptomatic or mildly symptomatic, 22.4% had mild symptoms, 10.0% had severe symptoms leading to hospitalization, and 3.6% had critical illness requiring ICU admission (*5*).

The government of South Korea encouraged all case-patients, including mild symptomatic and asymptomatic case-patients, to be hospitalized to prevent community transmission, yielding a high case-hospitalization rate. Although 49.4% of all case-patients were hospitalized before March 2, a total of 82.6% of all infected case-patients were either hospitalized or admitted to community treatment centers (CTCs) after these centers were established to provide care for asymptomatic or mildly ill patients after March 2, 2020. We assumed that the average time from infection to symptom onset was 5.1 days (*11*) and from symptom onset to hospitalization was 4 (range 0–11) days (*12*–*14*) (Table 2). Our previous study used the claims made in the National Health Insurance System (NHIS) (*15*), a mandatory health insurance system covering 96.6% of the entire population of South Korea. On the basis of those data and data from the literature, we assumed that the average length of stay at hospitals among non–ICU-admitted patients would be 21 (7.2–32.6) days and that for case-patients quarantined at CTCs would be 16 (7–20) days (*15*–*18*).

Critically ill patients were assumed to be first admitted to non-ICU hospital beds for 3 days, then transferred to the ICUs for 30 (range 11.6–47.2) days before returning to non-ICU hospital beds for another 5 days (*5*,*15*,*16*). On the basis of KCDC data, we assumed that 60% of the critically ill patients would die and have an average length of time in the ICU of 10 (range 0–13) days before death (*5*,*15*,*16*).

We calibrated the susceptible-exposed-infectious-removed (SEIR) model to the data for confirmed COVID-19 case-patients, hospital census, CTC census, ICU census, and deaths as reported by KCDC and Daegu Disaster Management Headquarters during February 1–May 15, 2020 (*5*,*9*). We estimated the basic reproduction number (R_0) at the beginning of

Table 2. Input parameters for COVID-19 transmission compartmental model, South Korea*

Characteristic	Baseline value	Range†	Reference
Hospitalizations for all confirmed cases by disease severity before March 2, %	49.4		(*5*)
Asymptomatic or mild symptomatic cases	17.0		(*5*)
Mild symptomatic cases	22.4		(*5*)
Severely ill cases	6.4		(*5*)
Critically ill cases	3.6		(*5*)
Hospitalizations for all confirmed cases by disease severity after March 2, %	82.6		(*5*,*9*)
Asymptomatic or mild symptomatic cases (admitted to CTCs)	38.2		(*5*,*9*)
Asymptomatic or mild symptomatic cases (admitted to hospitals)	12.0		(*5*,*9*)
Mild symptomatic cases	22.4		(*5*,*9*)
Severe symptomatic cases	6.4		(*5*,*9*)
Critically ill cases	3.6		(*5*,*9*)
Proportion admitted to the ICU among hospitalized patients	8.1		(*5*,*9*)
Time to outcome, d			
Time to symptom onsets	5.1	4.5–5.8	(*11*)
Time from symptom onset to hospitalization	4.0	0–11	(*12*–*14*)
Time from symptom onset to ICU hospitalization	7.0	6–8	(*12*–*14*)
Time from symptom onset to death	17.0	0–27	(*14*)
Length of stay at CTC	16.0	7–20	(*9*,*18*)
Length of stays at hospital without ICU admission	20.9	7.2–34.6	(*15*–*17*)
ICU length of stay among survivors	30.0	11.6–47.2	(*5*,*15*,*16*)
ICU length of stay among nonsurvivors	10.0	0 –13	(*5*,*15*,*16*)
Case-fatality rate for critically ill patients, %	60.0		(*5*,*9*)

*COVID-19, coronavirus disease; CTC, community treatment center; ICU, intensive care unit.
†Range was used for sensitivity analysis where available. For parameters that were calculated as proportions, baseline values were used as fixed values.

the epidemic in South Korea and the effective reproduction number (R_e) after the first epidemic peak in early March 2020. We adjusted the estimated R_e to minimize the sum of squared residuals between the data and the corresponding model outputs after the epidemic started decreasing in late February. To enable stochasticity in transmission, we applied a log-normal stochastic process with an SD of 0.722, a value determined on the basis of fitting this model to the 2018–19 influenza season for Seattle, Washington, USA (*10*). We implemented the model in Python version 3.7 (https://www.python.org) and analyzed and graphed outputs by using R version 3.6.1 https://www.r-project.org). Ethics approval was not required because the study was based on a simulated cohort of patients and used publicly available epidemiologic data.

Model Scenarios for Impact of Mitigation Measures

Rapid testing and effective contact tracing of index cases enable health authorities to test and quickly quarantine infectious persons and isolate the contacts of index case-patients from the susceptible population, reducing the number of infectious persons in the population and thus preventing onward transmissions. Several studies, including 2 meta-analyses of respiratory diseases caused by coronaviruses, showed that social distancing and mask-wearing reduce viral transmission among contacts (*19*,*20*). In our SEIR model, we assumed that social distancing and mask-wearing would reduce transmissibility or contact rates for infectious persons. Given that all mitigation measures and interventions, including contact tracing and testing, social distancing, and mask-wearing, had simultaneously occurred, we did not separately model and measure the effects of individual interventions but estimated the overall impact of combined interventions.

We measured outcomes of the epidemic (infections, cases, and deaths) and health system burden (hospital census, CTC census, and ICU census) by May 15, 2020, in South Korea associated with the actual response and compared them with hypothetical, less intensive mitigation efforts. Specifically, we considered 2 scenarios where R_e was estimated to be reduced by 50% of the initial R_0 by February 28, then would remain at 50% (scenario 1) or 70% (scenario 2) of the initial R_0 after February 28. We also conducted sensitivity analysis by varying the key parameter values affecting health system burden (Appendix Figure 2).

Results

We present a summary of key policies and practices for COVID-19 response and control in South Korea. This summary was conducted according to WHO guidelines (Table 1; Appendix Figure 1).

Key Policies and Practices

Country-Level Coordination, Planning, and Monitoring

A special COVID-19 task force was organized on January 3, 2020. As soon as the first COVID-19 case was confirmed, the government of South Korea promptly declared its political commitment on January 22 to

prepare a response to COVID-19 in advance of the Lunar New Year holidays (*21*).

Risk Communication and Community Engagement

The government raised the alarm level in the 4-level national crisis management system (blue, yellow, orange, red) from yellow (stage 2) to orange (stage 3) on January 27 and to red (stage 4) on February 23, after the WHO Public Health Emergency of International Concern announcement on January 30. The KCDC held daily briefings to provide status updates and policy guidance to the public.

Surveillance, Rapid-Response Teams, and Case Investigations

We implemented intensive contact investigation and quarantine for all potential contacts of index case-patients (*5*,*21*,*22*). Epidemiologic Intelligence Service officers rapidly traced the contacts of every confirmed index case-patient by using cell phones and novel mobile applications (*23*). During January 20–March 27, 2020, the number of index case-patients traced was 5,706, and the number of contacts traced was 59,073, yielding a ratio of contacts traced/index case patient of 10.4 (*24*). The contacts who were successfully traced were monitored for an average of 9.9 days (*24*).

Points of Entry, International Travel, and Transport

After March 19, all in-bound passengers received health screenings at airport immigration checkpoints (*9*,*25*,*26*). These screenings were performed to identify new case-patients coming into South Korea.

National Laboratories

The Academy of Korean Laboratory Medicine developed reverse transcription PCR (RT-PCR)–based COVID-19 diagnostic kits, which were rapidly approved by the Korean Food and Drug Administration and distributed to 18 public laboratory centers on January 31. Rapid approval by the Korean Food and Drug Administration was possible because the government had established a system that enables emergency-use authorization in vitro diagnostics after the outbreak of Middle East respiratory syndrome (MERS) during 2015 (*27*).

Infection Prevention and Control at Hospitals

All hospitals and public health centers set up COVID-19 screening clinics after the first case was confirmed in South Korea. The transmission risk among healthcare workers was low; only 241 (2.4%) of all confirmed cases were healthcare workers as of April 5 (*9*).

Congregate Settings

On March 25, the government completed a full screening of high-risk congregate facilities, as well as nursing homes (*28*,*29*). This screening showed a positivity rate of 0.7% (224/32,990) in Daegu.

Social Distancing

The government announced a nationwide social distancing campaign for 2 weeks starting March 22, 2020. This campaign included staying home except for essential travel, limiting social gatherings, working from home whenever possible, and keeping 6 feet of distancing from others outside the home (*30*). In addition, after the mass outbreak occurred in Daegu in February, persons voluntarily reduced mobility and increased social distancing (e.g., the total number of riders taking the Seoul subway decreased to half of its previous total) (*31*). The government later established guidelines for implementing 3 levels of social distancing based on the number of confirmed cases in the local area (*25*).

Use of Face Masks

Since 2014, a yellow dust storm that originated in the deserts of Mongolia and northern China during the spring has been a public health issue in South Korea, and persons were advised to wear a face mask outdoors to avoid inhaling particulate matter. In addition, because of an outbreak of MERS during 2015 that resulted in 186 cases and 38 deaths, public acceptance of wearing a mask was high in the event of respiratory disease outbreak. Wearing a face mask in public areas was regarded as a sign of thoughtfulness and modesty to prevent transmission to others (*32*). The 2 surveys conducted in late February and mid-March 2020 showed that 63% (*33*) and 94% (*34*) of persons in South Korea reported always wearing face masks when they were outside.

Case Management

Several CTCs were established on March 2 to quarantine and monitor asymptomatic and mild symptomatic case-patients and to enable reallocation of hospital beds in Daegu, when the total number of isolated patients, including self-quarantined cases at home waiting for admission (4,159), exceeded the number of available hospital isolation beds. Shortly afterward, CTCs were implemented nationwide (*18*). In addition, Daegu Dongsan Hospital and Daegu Medical Center were designated as COVID-19 central hospitals for effective COVID-19 case management (*35*).

Operational Support and Logistics in Hospitals

South Korea had the second-highest number of hospital beds per capita (12.3 beds/1,000 population) worldwide during 2019 (*36*). The number of negative-pressure beds increased to 1,077 by February 22 during the early part of the outbreak (*9*). In addition, to accommodate the rapid surge of COVID-19 patients, most tertiary hospitals constructed and renovated their isolation rooms with airborne infection isolation using common outlet duct systems or mobile negative-air machines (*37*).

Human Resources

Public health and army doctors dispatched as a substitute for their obligatory military service. These doctors were the main workforces, in addition to thousands of medical volunteers.

Maintaining Essential Health Services and Systems

Some private and public hospitals were designated as COVID-19 central hospitals. This designation was conducted to care only for patients with confirmed COVID-19.

Estimated Impacts of Policy and Interventions

The epidemic rapidly increased in the early phase, and the number of new daily cases peaked at 656 on February 29 (Appendix Figure 1). However, new daily cases declined in March and reached fewer than 100 daily confirmed cases after April 2. The reported hospital census peaked on March 14 at ≈3,600 cases and the CTC census on March 15 at 3,025 cases (Figure). The ICU census reached its peak in mid-March at ≈160. Given the limited capacity of ≈3,600 available hospital beds for isolation and 300 ICU beds with negative pressure in South Korea (*6*,*16*), a delay in governmental response for epidemic control is likely to have caused the epidemic to exceed the existing hospital capacity nationwide.

The SEIR model estimated that R_0 was 3.24 at the beginning of the outbreak but decreased by 35% as of February 26, 50% as of February 28, and 90% as of March 2 (Figure 1). Such a reduction can be attributed to the combination of different mitigation efforts and individual practices as described earlier in this report, including contact tracing of ≈99% contacts in the Shincheonji Church outbreak in Daegu and isolation of contacts at hospitals or CTC, social distancing and voluntary reductions in population mobility, near-universal mask wearing in public, and widespread testing.

The SEIR model estimated that the number of new daily cases would have exceeded 750 by April

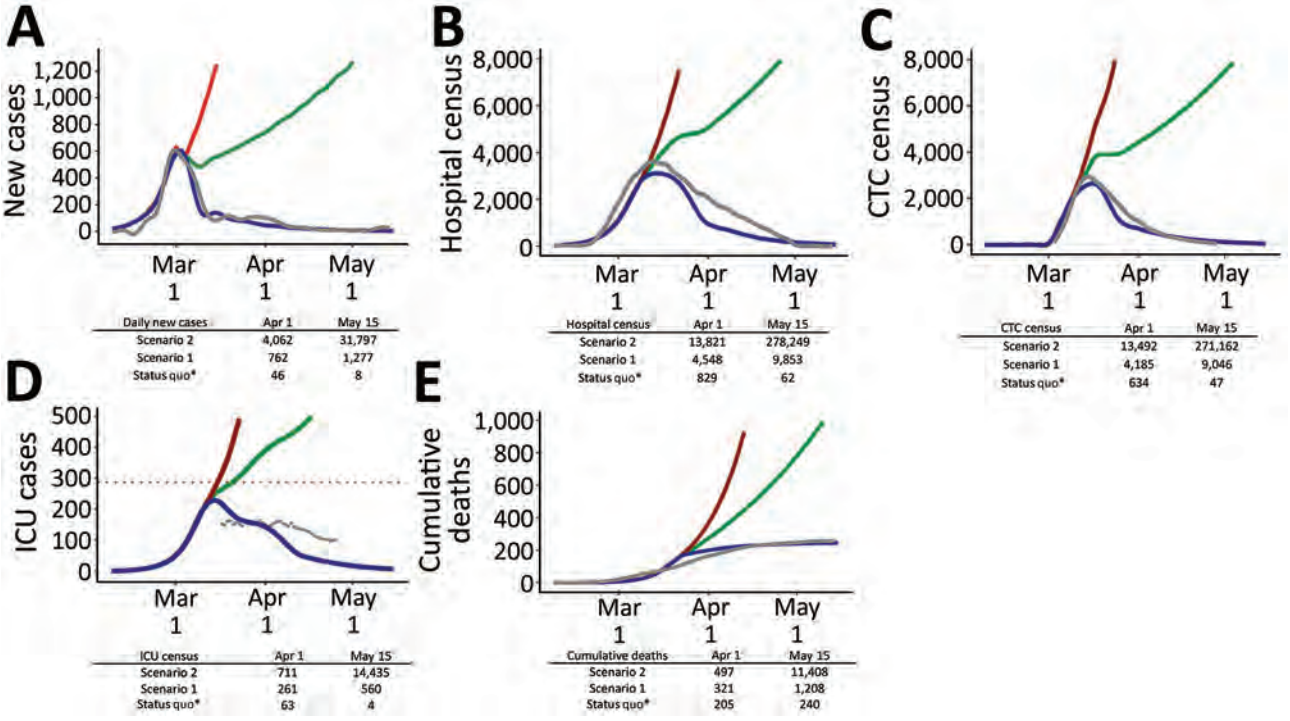

Figure. Estimated and confirmed numbers for coronavirus disease, South Korea, 2020. A) New daily cases; B) hospital census; C) CTC census; D) ICU census; E) cumulative deaths. Gray lines indicate observed data (*5*,*6*,*9*,*16*). Blue lines indicate estimated numbers with 35%, 50%, and 90% reductions in the basic reproduction number by February 26, February 28, and March 2, respectively, as the status quo. Additional scenarios are shown where R_0 was assumed to be reduced by 70% (scenario 1, green line) or stayed the same at 50% (scenario 2, red line) after February 28. CTC, community treatment center; ICU, intensive care unit; R_0, basic reproduction number.

1 and resulted in ≈27,000 cumulative infections if R_0 had been reduced only by 70%, which showed ≈25% lower composite effects of mitigation measures on reducing contact rates and transmissibility compared with the status quo (scenario 1) (Figure). R_0 would have remained at ≈1, sustaining the continued epidemic growth and outbreak clusters. By May 15, the cumulative infections would have reached 82,000 and the hospital census would have reached 9,900, which is ≈3 times higher than the total hospital beds available for isolation in South Korea. Cumulative deaths would have exceeded 1,200, which is >5-fold increase over the number of cumulative deaths observed as of May 15. This result would have prompted nationwide stage 2.5 social distancing measures and restrictions in which persons are advised to stay at home, and private or public gatherings of >50 persons indoors are prohibited (*31*).

If R_0 had been reduced by only 50% after February 28, the epidemic would have reached 4,000 new daily cases and 83,900 cumulative infections by April 1 and 31,800 new daily cases and >1.7 million cumulative infections by May 15 (scenario 2) (Figure). R_0 would have reached ≈1.6, exponentially increasing and doubling the cases by 7.9 days nationwide. This result would have prompted nationwide stage 3 social distancing measures and restrictions, the highest level of restriction, in which persons are advised to strictly stay at home, all nonessential businesses and in-person schooling are closed, and private or public gatherings of >10 persons indoors are prohibited (*31*).

Discussion

Our SEIR model showed that swift and comprehensive coordination and preparation of the government in response to the spring 2020 COVID-19 outbreak achieved rapid epidemic control in Daegu and nationwide by reducing R_0 by 90% through various interventions, including widespread testing, contact tracing, and quarantine without strict lockdown of the city or stay-at-home orders. Without these prompt multilevel responses, the epidemic could have led to a >10-fold increase in cumulative infections and deaths by May 15. The model also estimated that a delay in the government's response or an absence of rapid triage of mild symptomatic case-patients from hospitals to CTCs would have exceeded the hospital system capacity for hospital beds and negative- pressure rooms and potentially resulted in more deaths by overburdening the health system.

Several key factors contributed to slowing down the epidemic without a citywide or nationwide lockdown. The government intensively used an active tracing system that consisted of location tracking, card transactions, closed-circuit television recording, and a digital tracing mobile application to trace not only close contacts but also all potential contacts and offer testing to them. This system was possible because of the rapid set-up of RT-PCR capacity to perform 15,000–20,000 tests/day by early February and publicly disclosing the trajectories of confirmed COVID-19 case-patients so that anyone who might have contacted confirmed case-patients could self-identify and receive testing. Many of these lessons were learned from the MERS outbreak in South Korea during 2015.

A delayed response would have resulted in a surge of case-patients that would have overwhelmed the available hospital capacity nationwide. In Daegu, where 75% of the confirmed cases were located, the ICU census already exceeded the available ICU bed capacity (≈60) in public hospitals by late February, and an additional 50–60 critically ill patients were transferred to hospitals outside Daegu (*5*). In addition, establishing CTCs to isolate and manage asymptomatic case-patients was critical to effectively control further community transmission and to reduce burden on the hospital system (*38*).

Since mid-May 2020, South Korea has experienced several clustered outbreaks, including 1 at the Itaewon night club and others at multiple logistics centers (*39*). These outbreaks suggest that community transmission can quickly escalate and could lead to a large surge in cases after relaxing social distancing polices. In preparation for potential community outbreaks and surges in cases, the government arranged an additional 1,077 hospital beds, negative-pressure areas, and 300 ICU beds nationwide. It also eased the hospital discharge criteria for a shorter turnover time of hospital beds so that symptomatic patients could be discharged if their clinical symptoms improved without fever for 10 days after symptom onset, or if RT-PCR results were negative for >24 hours after the confirmed diagnosis (*9*). Monitoring and contact tracing continued to be central to the COVID-19 response in South Korea, especially for high-risk groups (*40*), and hospital bed capacity was maintained at designated COVID-19 management facilities in the event of further outbreaks.

The first limitation of our study is that we have not explicitly modeled quarantine or contact tracing and did not estimate the effects of individual interventions. Instead, we assumed that the combination of all interventions and policies reduced overall transmission rates in the population. Second, our SEIR compartment model did not capture any spatial networks

among different cities in South Korea. Third, data that informed input parameters for modeling are subject to uncertainties and should be validated with further clinical data.

In summary, our model estimates that South Korea reduced contact rates by 90% through various interventions without strict lockdown of the city or stay-at-home restrictions. At the same time, allocation and management of mild and moderate symptomatic case-patients helped to avoid overburdening the hospital system. However, continuous monitoring, contact tracing, securing hospital and isolating beds, and social distancing will remain critical as long as COVID-19 outbreaks remain a public health threat.

Acknowledgments

We thank Hyungseok Park, Yoonji Choi, Jisoon Lee, and Soriul Kim for editing the figures.

About the Author

Dr. Kim is a research fellow at the Department of Population Health, New York University Grossman School of Medicine, New York, NY. Her primary research interests include patient-centered interventions for HIV, tuberculosis prevention and treatment, and infectious disease modeling.

References

1. World Health Organization. WHO coronavirus disease (COVID-19) dashboard, 2021 [cited 2021 Aug 12]. https://covid19.who.int
2. Flaxman S, Mishra S, Gandy A, Unwin HJ, Mellan TA, Coupland H, et al.; Imperial College COVID-19 Response Team. Estimating the effects of non-pharmaceutical interventions on COVID-19 in Europe. Nature. 2020;584:257–61. https://doi.org/10.1038/s41586-020-2405-7
3. Hsiang S, Allen D, Annan-Phan S, Bell K, Bolliger I, Chong T, et al. The effect of large-scale anti-contagion policies on the COVID-19 pandemic. Nature. 2020;584:262–7. https://doi.org/10.1038/s41586-020-2404-8
4. Wise J. COVID-19: risk of second wave is very real, say researchers. BMJ. 2020;369:m2294. https://doi.org/10.1136/bmj.m2294
5. Daegu Disaster Management Headquarters. COVID-19 daily briefing in Daegu metropolitan City, 2020 [cited 2020 Jun 30]. http://www.daegu.go.kr/dgcontent/index.do?menu_id=00936590
6. Korea Central Emergency Medical Central. Comprehensive situation dashboard in National Emergency Department Information System 2020, 2020 [cited 2020 Aug 12]. http://portal.nemc.or.kr/medi_info/dashboards/dash_total_emer_org_popup_for_egen.do
7. Song JY, Yun JG, Noh JY, Cheong HJ, Kim WJ. COVID-19 in South Korea: challenges of subclinical manifestations. N Engl J Med. 2020;382:1858–9. https://doi.org/10.1056/NEJMc2001801
8. World Health Organization. COVID19 strategic preparedness and response plan: operational planning guidelines to support country preparedness and response, 2020 [cited 2021 Jul 26]. https://www.who.int / publications/m/item/covid-19-strategic-preparedness -and-response-plan-operational-planning-guideline
9. Central Department of Mental Health. Cases in Korea by city/province, 2020 [cited 2020 Aug 12]. http://ncov.mohw.go.kr/en/bdBoardList.do?brdId=16&brdGubun=162&dataGubun=&ncvContSeq=&contSeq=&board_id=&gubun=
10. Thakkar N, Klein D, Selvaraj P, Famulare M. COVID in New York City: a model-based perspective, 2020 [cited 2021 Jun 26]. https://iazpvnewgrp01.blob.core.windows.net/source/archived/COVID_Modeling_NYC.pdf
11. Lauer SA, Grantz KH, Bi Q, Jones FK, Zheng Q, Meredith HR, et al. The incubation period of coronavirus disease 2019 (COVID-19) from publicly reported confirmed cases: estimation and application. Ann Intern Med. 2020;172:577–82. https://doi.org/10.7326/M20-0504
12. Kim ES, Chin BS, Kang CK, Kim NJ, Kang YM, Choi JP, et al.; Korea National Committee for Clinical Management of COVID-19. Clinical course and outcomes of patients with severe acute respiratory syndrome coronavirus 2 infection: a preliminary report of the first 28 patients from the Korean cohort study on COVID-19. J Korean Med Sci. 2020;35:e142. https://doi.org/10.3346/jkms.2020.35.e142
13. Kim M, Kweon S, Lee JH, Baek S, Jeon B-H, Joo H, et al. Weekly report on the COVID-19 situation in the Republic of Korea (as of March 28, 2020). Public Health Wkly Rep. 2020;13:800–6.
14. COVID-19 National Emergency Response Center, Epidemiology and Case Management Team, Korea Centers for Disease Control and Prevention. Coronavirus disease-19: the first 7,755 cases in the Republic of Korea. Osong Public Health Res Perspect. 2020;11:85–90. https://doi.org/10.24171/j.phrp.2020.11.2.05
15. Jang SY, Seon JY, Yoon S-J, Park S-Y, Lee S-H, Oh I-H. Comorbidities and factors determining medical expenses and length of stay for admitted COVID-19 patients in Korea. Risk Manag Healthc Policy. 2021;14:2021–33. https://doi.org/10.2147/RMHP.S292538
16. Health Insurance Review and Assessment Service. Facility and equipment status. Healthcare Bigdata Hub, 2020 [cited 2020 Jun 3]. http://opendata.hira.or.kr/op/opc/olapInfraEquipmentStatInfo.do#none
17. Choi MH, Ahn H, Ryu HS, Kim BJ, Jang J, Jung M, et al. Clinical characteristics and disease progression in early-stage COVID-19 patients in South Korea. J Clin Med. 2020;9:E1959. https://doi.org/10.3390/jcm9061959
18. Kang E, Lee SY, Jung H, Kim MS, Cho B, Kim YS. Operating protocols of a community treatment center for isolation of patients with coronavirus disease, South Korea. Emerg Infect Dis. 2020;26:2329–37. https://doi.org/10.3201/eid2610.201460
19. Liang M, Gao L, Cheng C, Zhou Q, Uy JP, Heiner K, et al. Efficacy of face mask in preventing respiratory virus transmission: a systematic review and meta-analysis. Travel Med Infect Dis. 2020;36:101751. https://doi.org/10.1016/j.tmaid.2020.101751
20. Chu DK, Akl EA, Duda S, Solo K, Yaacoub S, Schünemann HJ, et al.; COVID-19 Systematic Urgent Review Group Effort (SURGE) study authors. Physical distancing, face masks, and eye protection to prevent person-to-person transmission of SARS-CoV-2 and COVID-19: a systematic review and meta-analysis. Lancet. 2020;395:1973–87. https://doi.org/10.1016/S0140-6736(20)31142-9
21. Korean Society of Infectious Diseases; Korean Society of Pediatric Infectious Diseases; Korean Society of Epidemiology; Korean Society for Antimicrobial Therapy; Korean Society

for Healthcare-Associated Infection Control and Prevention; Korea Centers for Disease Control and Prevention. Report on the epidemiological features of coronavirus disease 2019 (COVID-19) outbreak in the Republic of Korea from January 19 to March 2, 2020. J Korean Med Sci. 2020;35:e112. https://doi.org/10.3346/jkms.2020.35.e112
22. Park SY, Kim YM, Yi S, Lee S, Na BJ, Kim CB, et al. Coronavirus disease outbreak in call center, South Korea. Emerg Infect Dis. 2020;26:1666–70. https://doi.org/10.3201/eid2608.201274
23. COVID-19 National Emergency Response Center, Epidemiology & Case Management Team, Korea Centers for Disease Control & Prevention. Contact transmission of COVID-19 in South Korea: novel investigation techniques for tracing contacts. Osong Public Health Res Perspect. 2020;11:60–3. https://doi.org/10.24171/j.phrp.2020.11.1.09
24. Park YJ, Choe YJ, Park O, Park SY, Kim YM, Kim J, et al.; COVID-19 National Emergency Response Center, Epidemiology and Case Management Team. Contact tracing during coronavirus disease outbreak, South Korea, 2020. Emerg Infect Dis. 2020;26:2465–8. https://doi.org/10.3201/eid2610.201315
25. Ministry of Health and Welfare. Republic of Korea. COVID-19 response: Korean government's response system (as of February 25, 2020), 2020 [cited 2021 Apr 15]. http://ncov.mohw.go.kr/en/baroView.do?brdId=11&brdGubun=111&dataGubun=&ncvContSeq=&contSeq=&board_id=&gubun=
26. Government of the Republic of Korea. Ministry of Foreign Affairs. All about Korea's response to COVID-19, 2020 [cited 2021 Jul 26]. https://www.mofa.go.kr/eng/brd/m_22591/view.do?seq=35&srchFr=&srchTo=&srchWord=&srchTp=&multi_itm_seq=0&itm_seq_1=0&itm_seq_2=0&company_cd=&company_nm=&page=1&titleNm=
27. Kim YJ, Sung H, Ki CS, Hur M. COVID-19 testing in South Korea: current status and the need for faster diagnostics. Ann Lab Med. 2020;40:349–50. https://doi.org/10.3343/alm.2020.40.5.349
28. Fulop T, Pawelec G, Castle S, Loeb M. Immunosenescence and vaccination in nursing home residents. Clin Infect Dis. 2009;48:443–8. https://doi.org/10.1086/596475
29. Strausbaugh LJ, Sukumar SR, Joseph CL. Infectious disease outbreaks in nursing homes: an unappreciated hazard for frail elderly persons. Clin Infect Dis. 2003;36:870–6. https://doi.org/10.1086/368197
30. Korea Center for Disease Control. Coronavirus disease-19, Republic of Korea: enhanced social distancing campaign, 2020 [cited 2021 Apr 15]. https://ncov.mohw.go.kr/en/infoBoardView.do?brdId=14&brdGubun=141&dataGubun=&ncvContSeq=1551&contSeq=1551&board_id=&gubun=
31. Park IN, Yum HK. Stepwise strategy of social distancing in Korea. J Korean Med Sci. 2020;35:e264. https://doi.org/10.3346/jkms.2020.35.e264
32. Lim S, Yoon HI, Song KH, Kim ES, Kim HB. Face masks and containment of COVID-19: experience from South Korea. J Hosp Infect. 2020;106:206–7. https://doi.org/10.1016/j.jhin.2020.06.017
33. Lee M, You M. Psychological and behavioral responses in South Korea during the early tages of coronavirus disease 2019 (COVID-19). Int J Environ Res Public Health. 2020;17:E2977. https://doi.org/10.3390/ijerph17092977
34. Gallup International Association. Coronavirus 19 prevention behavior and related perceptions, 2020 [cited 2021 Jul 26]. https://news.gallup.com/opinion/gallup/308126/roundup-gallup-covid-coverage.aspx
35. Kim SW, Lee KS, Kim K, Lee JJ, Kim JY; Daegu Medical Association. A brief telephone severity scoring system and therapeutic living centers solved acute hospital-bed shortage during the COVID-19 outbreak in Daegu, Korea. J Korean Med Sci. 2020;35:e152. https://doi.org/10.3346/jkms.2020.35.e152
36. Organization for Economic Co-operation and Development (OECD). OECD Health Statistics 2019, 2020 [cited 2020 Aug 12]. https://www.oecd.org/health/health-data.htm
37. Lee SY, Choi SH, Park JE, Hwang S, Kwon KT. Crucial role of temporary airborne infection isolation rooms in an intensive care unit: containing the COVID-19 outbreak in South Korea. Crit Care. 2020;24:238. https://doi.org/10.1186/s13054-020-02944-0
38. Lee Y, Lim J. Korean Goverment says, "Transferring critially ill patients with COVID-19 to dedicated non-ICU beds as their conditions improve... especially to a single-occupancy room" [in Korean]. Newsis. 2020 Dec 15 [cited 2021 Jun 28]. https://www.newsis.com/view/?id=NISX20201215_0001270622
39. Kang CR, Lee JY, Park Y, Huh IS, Ham HJ, Han JK, et al.; Seoul Metropolitan Government COVID-19 Rapid Response Team (SCoRR Team). Coronavirus disease exposure and spread from nightclubs, South Korea. Emerg Infect Dis. 2020;26:2499–501. https://doi.org/10.3201/eid2610.202573
40. US Department of Health and Human Services, Centers for Disease Control and Prevention. Interim guidance on developing a COVID-19 case investigation & contact tracing plan: overview, 2020 [cited 2020 Jun 5]. https://www.cdc.gov/coronavirus/2019-ncov/php/contact-tracing/contact-tracing-plan/overview.html

Address for correspondence: Seung Heon Lee, Division of Pulmonary, Sleep, and Critical Care Medicine, Department of Internal Medicine, Korea University Ansan Hospital, 123, Jeokgeum-ro, Danwon-gu, Ansan-si, Gyeonggi-do 15355, South Korea; email: lee-sh@korea.ac.kr

Effectiveness of Abbott BinaxNOW Rapid Antigen Test for Detection of SARS-CoV-2 Infections in Outbreak among Horse Racetrack Workers, California, USA

Krishna Surasi, Kristin J. Cummings, Carl Hanson, Mary Kate Morris, Maria Salas, David Seftel, Liza Ortiz, Ruwan Thilakaratne, Cameron Stainken, Debra A. Wadford

The Abbott BinaxNOW rapid antigen test is cheaper and faster than real-time reverse transcription PCR (rRT-PCR) for detecting severe acute respiratory syndrome coronavirus 2. We compared BinaxNOW with rRT-PCR in 769 paired specimens from 342 persons during a coronavirus disease outbreak among horse racetrack workers in California, USA. We found positive percent agreement was 43.3% (95% CI 34.6%–52.4%), negative percent agreement 100% (95% CI 99.4%–100%), positive predictive value 100% (95% CI 93.5%–100%), and negative predictive value 89.9% (95% CI 87.5%–92.0%). Among 127 rRT-PCR–positive specimens, the 55 with paired BinaxNOW-positive results had a lower mean cycle threshold than the 72 with paired BinaxNOW-negative results (17.8 vs. 28.5; p<0.001). Of 100 specimens with cycle threshold <30, a total of 51 resulted in positive virus isolation; 45 (88.2%) of those were BinaxNOW-positive. Our comparison supports immediate isolation for BinaxNOW-positive persons and confirmatory testing for negative persons.

Rapid antigen tests, such as Abbott BinaxNOW (https://www.abbott.com) test kits, offer a less expensive and faster alternative to nucleic acid amplification tests, such as real-time reverse transcription PCR (rRT-PCR), in the diagnosis of coronavirus disease (COVID-19) (*1*,*2*). Previous studies of BinaxNOW compared with rRT-PCR have demonstrated a high negative percent agreement (NPA) (99.4%–100%) but variable positive percent agreement (PPA) (52.5%–89.0%). Performance was better among symptomatic persons, specimens with cycle threshold (C_t) <30 (suggestive of higher viral loads), and specimens with positive viral cultures (*3*–*8*). These reports have focused on community testing sites and outbreaks in healthcare facilities.

Throughout the pandemic, certain nonhealthcare occupational groups (e.g., meat and poultry processing workers) have experienced higher risk of contracting COVID-19; this higher risk is attributable to workplace hazards, such as lack of appropriate personal protective equipment, densely populated work areas, poorly ventilated workspaces, and prolonged close contact (*9*,*10*). These workplaces might benefit from effective rapid antigen tests that enable employers to quickly identify persons infected with severe acute respiratory syndrome coronavirus 2 (SARS-CoV-2) for isolation and to guide contact tracing, thereby reducing workplace transmission. Despite the need for research on this topic, information on the performance of BinaxNOW in the setting of nonhealthcare workplace outbreaks is lacking.

During October 20, 2020–January 15, 2021, a horse racetrack (the facility) in California, USA, experienced a COVID-19 outbreak among its 563 employees and independent contractor workers (hereafter collectively called facility staff). Nearly half (n = 278; 49.4%) of the staff lived onsite in facility-provided housing, and many performed essential

Author affiliations: Centers for Disease Control and Prevention, Atlanta, Georgia, USA (K. Surasi); California Department of Public Health, Richmond, California, USA (K. Surasi, K.J. Cummings, C. Hanson, M.K. Morris, M. Salas, R. Thilakaratne, C. Stainken, D.A. Wadford); Golden Gate Fields, Berkeley, California, USA (D. Seftel); City of Berkeley Public Health Officer Unit, Berkeley (L. Ortiz); Kaiser Permanente San Francisco Internal Medicine Residency Program, San Francisco, California, USA (C. Stainken); University of California San Francisco School of Medicine, San Francisco (C. Stainken).

DOI: https://doi.org/10.3201/eid2711.211449

duties (e.g., grooming, feeding) related to the basic care of the >1,100 horses stabled there.

The outbreak was discovered by the contact tracing efforts of the local health department (LHD), the City of Berkeley Public Health Officer Unit. In response, the LHD ordered that all nonessential work activities (e.g., horse racing) be stopped until mass testing of all staff demonstrated no further transmission. The initial round of rRT-PCR testing (round 0) occurred on November 14–15, 2020, and identified 169 SARS-CoV-2–positive staff who were subsequently isolated. At this time, all staff were assumed to have been exposed. Those living onsite were moved to hotel rooms to quarantine, and those living offsite quarantined in their homes. No staff were permitted to return to onsite residence until the outbreak had ended. However, some quarantined employees were permitted to return to work if they were needed to perform duties related to essential care of the horses. Additional rounds of testing were needed to monitor ongoing transmission and determine when the outbreak had ended. The LHD decided to use BinaxNOW as a supplement to rRT-PCR to more quickly identify SARS-CoV-2–positive employees for isolation. This use provided an opportunity to assess the effectiveness of the BinaxNOW rapid antigen test in detecting SARS-CoV-2 infection in a nonhealthcare workplace outbreak. The purpose of this analysis is to compare BinaxNOW with rRT-PCR in paired specimens from persons during a COVID-19 outbreak among horse racetrack workers. These findings could inform testing protocols used to contain future outbreaks of COVID-19 in nonhealthcare workplaces.

Methods

The facility, in collaboration with the LHD and the California Department of Public Health (CDPH) laboratory, conducted 6 rounds of serial testing of its staff with paired BinaxNOW rapid antigen and rRT-PCR tests during November 25–December 22 (rounds 1–6). Testing frequency was determined by the LHD and changed as the outbreak progressed. Each round was intended to test all staff who had not yet tested positive by BinaxNOW or rRT-PCR to continue identifying potentially infectious persons. Staff who tested positive by either BinaxNOW or rRT-PCR were isolated and excluded from further testing.

All specimen collection and antigen testing occurred outdoors in the parking lot of the facility. On the day of testing, a facility administrative employee conducted registration and collected demographic data, including self-reported race and ethnicity. Symptom information was elicited by asking staff if they were experiencing any COVID symptoms, such as fever, headache, or loss of taste. Bilateral anterior nasal swab specimens were collected by either the racetrack physician or one of the racetrack veterinarians trained in collection procedures. A first swab specimen was used for onsite BinaxNOW testing; a second swab specimen was placed in viral transport medium and chilled on ice packs before transport to the CDPH laboratory for rRT-PCR testing 24–72 hours after collection. All specimens in viral transport medium were frozen at –70°C within 12 hours of delivery to the laboratory. BinaxNOW test results were interpreted immediately at the 15-minute read time by the racetrack physician in accordance with the test kit instructions, along with the updated scoring criteria described by Pilarowski et al. (*5*), which indicates that bands are scored as positive only if they extend across the full width of the strip, irrespective of the intensity of the band. Because BinaxNOW testing was not performed for round 0, those 169 rRT-PCR–positive specimens were not included in this analysis.

For rRT-PCR, we isolated and purified viral nucleic acid (NA) from the swab specimens by using the KingFisher Flex Purification System and the MagMAX Viral/Pathogen Nucleic Acid Isolation Kit (ThermoFisher Scientific, https://www.thermofisher.com). We performed rRT-PCR by using the ThermoFisher TaqPath COVID-19 Combo Kit, which targets 3 SARS-CoV-2 viral regions (nucleocapsid protein gene, spike protein gene, and open reading frame 1ab), and the Applied Biosystems 7500 Fast Dx Real-Time PCR Instrument (ThermoFisher Scientific), according to the manufacturer's instructions. Real-time RT-PCR–positive specimens with C_t <30 were also cultured for SARS-CoV-2 at CDPH in a Biosafety Level 3 laboratory. For cultures, 200 μL of patient specimen was diluted 1:1 with diluent containing 0.75% bovine serum albumin, and 50 μL was added to 8 replicate wells in a 96-well plate containing confluent Vero-81 cells at 37°C with 5% CO_2. After 1 h, the inoculum was removed and 200 μL of minimum essential medium containing 5% fetal bovine serum and antibiotics was added to each well. Cells were monitored for cytopathic effect. Cells with positive cytopathic effect were tested by rRT-PCR to confirm presence of SARS-CoV-2. Cells with no cytopathic effect or negative rRT-PCR results were passaged after 7 d onto fresh confluent Vero-81 and monitored for an additional 7 d before performing rRT-PCR again. Viral replication in these specimens was defined as a decrease in C_t over the culture period.

We used the paired BinaxNOW and rRT-PCR results to calculate the BinaxNOW PPA, NPA, negative predictive value (NPV), and positive predictive value (PPV), using $C_t \leq 37$ to define rRT-PCR–positive specimens. As described in Pilarowski et al. (*5*), we also calculated performance by using $C_t < 30$ to define rRT-PCR–positive specimens. The exact binomial method was used to calculate 95% CIs. Comparison of mean C_t was performed using the Welch t-test. We performed statistical analyses using R version 4.0.1 (R Foundation for Statistical Computing, https://www.r-project.org).

This activity was reviewed by the Centers for Disease Control and Prevention (CDC) and was conducted consistent with applicable federal law and CDC policy (45 C.F.R. part 46, 21 C.F.R. part 56; 42 U.S.C. §241(d); 5 U.S.C. §552a; 44 U.S.C. §3501 et seq.). In addition, this activity was conducted as part of a COVID-19 project determined to be nonresearch by the California Health and Human Services Agency's Committee for the Protection of Human Subjects.

Results

Including testing performed in round 0 and results reported by outside laboratories from staff seeking testing on their own, the cumulative incidence over the course of the outbreak in the entire staff was 62.3% (351/563). A total of 342 different staff participated in testing rounds 1 through 6. These persons ranged in age from 18 to 92 years (median 52 years). Self-reported race and ethnicity produced cell sizes that are too small to report, so only Hispanic ethnicity is presented in this study. Most staff identified as Hispanic (62.0%) (Table 1). Symptoms were reported by 11 different persons at the time of testing, which accounted for 11/769 (1.4%) of collected paired specimens. A total of 6 persons were hospitalized, and 1 of those patients died. The number of staff tested in each round, which varied because of attrition and exclusion of SARS-CoV-2–positive staff from further testing, ranged from 333 persons (round 1) to 57 persons (round 4). The number of rRT-PCR–positive results in each round ranged from 98 (round 1) to 0 (round 4) (Table 2).

In total, 769 valid, paired rRT-PCR and BinaxNOW antigen test results were reported and analyzed. Among all paired testing rounds with rRT-PCR, BinaxNOW produced these results when rRT-PCR tests with $C_t \leq 37$ were considered positive: PPA, 43.3% (95% CI 34.6%–52.4%); NPA, 100% (95% CI 99.4%–100.0%); PPV, 100.0% (95% CI 93.5%–100.0%); and NPV, 89.9% (95% CI 87.5%–92.0%). When only rRT-PCR tests with $C_t < 30$ were considered positive, BinaxNOW produced these results: PPA, 55.6% (95% CI 45.2%–65.6%); NPA, 100% (95% CI 99.5%–100%), PPV, 100.0% (95% CI 93.5%–100%); and NPV, 93.8% (95% CI 91.8%–95.5%) (Table 3).

Of 127 rRT-PCR–positive specimens, BinaxNOW detected 55, did not detect 72 (44 specimens with $C_t < 30$, 5 specimens with $C_t \leq 20$, and 6 specimens with positive viral cultures), and produced no false-positive results (Table 3). Among rRT-PCR–positive specimens, those with paired BinaxNOW-positive results had a lower mean C_t (17.8) than those with paired BinaxNOW-negative results (28.5) ($p < 0.001$). No rRT-PCR–positive results with a $C_t > 29.4$ were detected by BinaxNOW (Figure 1).

In dual-positive pairs, the median time between rRT-PCR specimen collection date and results reported date was 4 days (range 1–6 days). For BinaxNOW false-negative pairs, the median time between rRT-PCR specimen collection date and results reported date was 5 days (range 1–7 days). In contrast, the 15-minute read time of the BinaxNOW antigen test kit provided results to the facility and LHD the same day as testing.

Table 1. Characteristics of horse racetrack staff providing paired anterior nasal swab specimens for the BinaxNOW rapid antigen test and real-time reverse transcription PCR for coronavirus disease, California, USA, November–December 2020*

Characteristic	rRT-PCR result		Overall
	Detected	Not detected	
Total	127 (100)	215 (100)	342 (100)
Sex			
F	26 (20.5)	62 (28.8)	88 (25.7)
M	101 (79.5)	153 (71.2)	254 (74.3)
Median age (range), y	46 (18–82)	54 (18–92)	52 (18–92)
Age groups, y			
18–44	57 (44.9)	75 (34.9)	132 (38.6)
45–64	56 (44.1)	103 (47.9)	159 (46.5)
≥65	14 (11.0)	37 (17.2)	51 (14.9)
Ethnicity			
Hispanic	99 (78.0)	113 (52.6)	212 (62.0)
Non-Hispanic	28 (22.0)	102 (47.4)	130 (38.0)

*Values are no. (%) except as indicated. rRT-PCR, real-time reverse transcription PCR.

Table 2. BinaxNOW rapid antigen test compared with real-time reverse transcription PCR for coronavirus disease among all horse racetrack staff undergoing paired testing, California, USA, November–December 2020*

BinaxNOW result	rRT-PCR result		Total
	Detected	Not detected	
Round 1, n = 333, November 25, 27, 28†			
Detected	40	0	40
Not detected	58	235	293
Total	98	235	333
Round 2, n = 197, December 4			
Detected	12	0	12
Not detected	10	175	185
Total	22	175	197
Round 3, n = 65, December 13			
Detected	2	0	2
Not detected	3	60	63
Total	5	60	65
Round 4, n = 57, December 16			
Detected	0	0	0
Not detected	0	57	57
Total	0	57	57
Round 5, n = 58, December 20			
Detected	0	0	0
Not detected	1	57	58
Total	1	57	58
Round 6, n = 59, December 22			
Detected	1	0	1
Not detected	0	58	58
Total	1	58	59
Overall, N = 769, November 25–December 22			
Detected	55	0	55
Not detected	72	642	714
Total	127	642	769

*Inconclusive (n = 4) and invalid (n = 3) rRT-PCR test results excluded from table. rRT-PCR, real-time reverse transcription PCR.
†All employees who had not yet tested positive were meant to return for subsequent testing rounds. However, participant attrition occurred, likely because of employees leaving their jobs or logistical obstacles to being on-site for testing during mass testing days.

Of the 127 rRT-PCR–positive specimens, we attempted virus isolation and culture for all 100 specimens with C_t <30. Of those specimens, 51 resulted in positive virus isolation. Of those culture-positive specimens, 45 (88.2%) were BinaxNOW-positive (Table 4; Figure 2). The mean C_t of culture-positive specimens (17.4) was significantly lower than culture-negative specimens (25.5) (p<0.001).

Table 3. BinaxNOW rapid antigen test performance compared with real-time reverse transcription PCR for coronavirus disease in using 2 different cycle threshold values to define positive results, California, USA, November–December 2020*

BinaxNOW performance	% (95% CI)	
	$C_t \leq 37$†	C_t <30‡
PPA	43.3 (34.6–52.4)	55.6 (45.2–65.6)
NPA	100.0 (99.4–100.0)	100.0 (99.5–100)
PPV	100.0 (93.5–100.0)	100.0 (93.5–100)
NPV	89.9 (87.5–92.0)	93.8 (91.8–95.5)

*Results for 769 paired specimens from 342 horse racetrack staff. C_t, cycle threshold; NPA, negative percent agreement; NPV, negative predictive value; PPA, positive percent agreement; PPV, positive predictive value; rRT-PCR, real-time reverse transcription PCR.
†127 rRT-PCR–positive specimens.
‡100 rRT-PCR–positive specimens.

Discussion

In the setting of a nonhealthcare workplace outbreak of COVID-19 with high attack rate (62.3%), we found that BinaxNOW was a useful adjunct to rRT-PCR testing. BinaxNOW showed NPA and PPV of 100%. A total of 55 participants were concordantly identified as positive by BinaxNOW and rRT-PCR, and no false-positive BinaxNOW results were noted. This low false-positive rate is consistent with results from Pilarowski et al. (*5*) that established the updated BinaxNOW card-reading technique used by the racetrack physician in this outbreak. Results of BinaxNOW testing were available the same day, which enabled more rapid identification of infected workers for isolation than reliance on rRT-PCR alone.

Negative BinaxNOW results were less concordant with rRT-PCR results. The PPA of BinaxNOW was 43.0% and the NPV was 89.9%. Real-time RT-PCR confirmation of BinaxNOW negative results identified 72 additional positive specimens. The median time between rRT-PCR specimen collection date and results reported date for these BinaxNOW false-negative specimens was 5 days (range 1–7 days).

Although C_t cannot be used to define viral load or infectivity of a given person, C_t is inversely related to the amount of target genetic material present in the specimen (*11*). Therefore, the significantly lower mean C_t for true-positive BinaxNOW specimens (17.8) compared with false-negative BinaxNOW specimens (28.5) indicates that more viral genetic material was present in those specimens. BinaxNOW demonstrated better concordance with positive viral culture results (88.2%) than with positive rRT-PCR results (43.3%). Positive viral culture is further evidence of the presence of infectious virus, so these findings might indicate that some BinaxNOW false-negative participants were not infectious at the time of specimen collection (i.e., they had low viral RNA load at the beginning or end of their infection trajectory) (*12*). Numerous factors can affect the outcome of a viral culture; therefore, negative culture results do not necessarily mean that no viable virus was present in those specimens, nor that the participants from whom those specimens were collected were not infectious at the time of specimen collection.

With serial BinaxNOW testing, some of the persons with discordant paired results could have tested positive with subsequent BinaxNOW testing. Further studies are needed to determine whether serial rapid antigen testing alone can identify infectious persons as efficiently as rRT-PCR alone or a combination of rRT-PCR and rapid antigen testing (*13*).

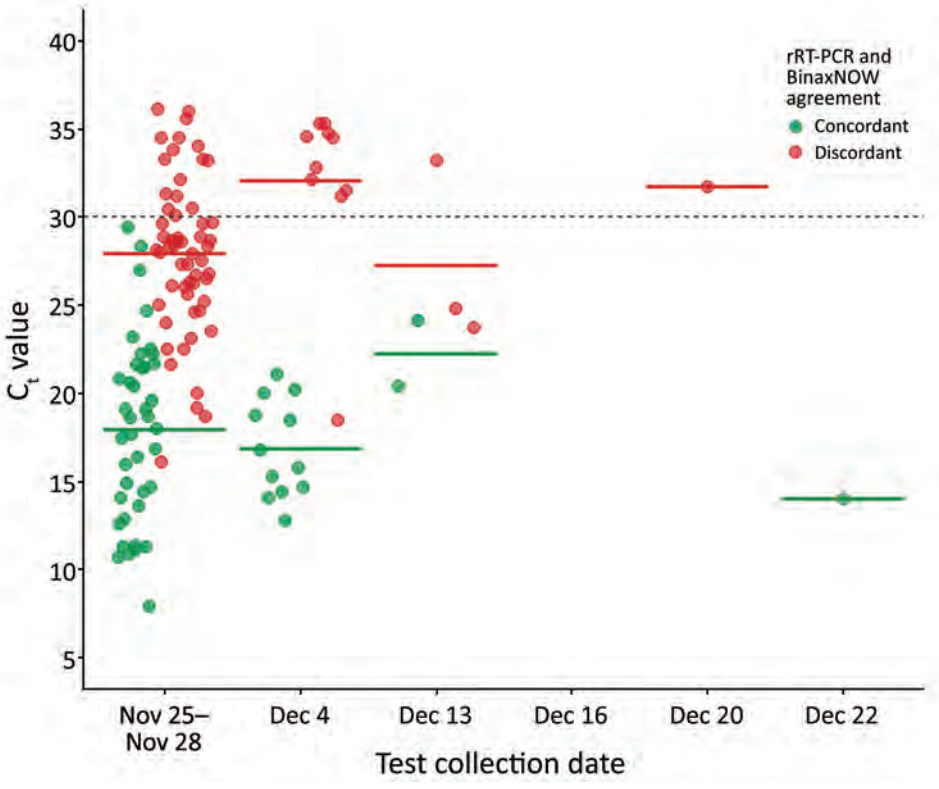

Figure 1. Concordance of BinaxNOW rapid antigen test results with positive rRT-PCR results over 6 testing rounds among staff at a horse racetrack, California, USA, November–December 2020. All rRT-PCR–negative results (n = 642) were concordant with BinaxNOW results, so only rRT-PCR–positive results (n = 127) are shown. Crossbars represent mean C_t for the concordant and discordant pair groups in each testing period. The dashed line represents C_t = 30. C_t, cycle threshold; rRT-PCR, real-time reverse transcription PCR.

The first limitation of our study is that, although other studies have demonstrated differential BinaxNOW test performance in symptomatic and asymptomatic persons (*3*,*6*–*8*), we were unable to examine test performance by symptom status, because symptom reporting might not have been reliable. At the time of specimen collection, only 11 persons reported symptoms to the facility administrative employee registering them for testing. This number conflicts with data previously collected from the racetrack physician as part of a prospective cohort drug trial on this same population which, out of an enrolled cohort of 113 BinaxNOW-positive staff, identified 60 (53%) persons who were symptomatic at the time of testing (*14*). This discrepancy might have resulted from staff feeling less comfortable discussing symptoms with the administrative employee versus the racetrack physician or it could be associated with the incomplete list of COVID-19 symptoms in the administrative employee's question. It might also reflect a language barrier, because the question about symptoms was asked only in English by the administrative employee. According to onsite interactions with staff and reports from racetrack leadership, many staff were native Spanish speakers, although this language difference was not quantified.

Second, the BinaxNOW tests may have been performed in ambient temperatures below the manufacturer's recommended range. The BinaxNOW test kit instructions recommend that all test components be at room temperature (15°C–30°C) before use; the mean daily minimum and maximum air temperature recordings from a nearby National Oceanic and Atmospheric Administration weather station in Richmond, CA, on testing days were 7.9°C and 15.1°C (*15*). Performing BinaxNOW tests in the recommended temperature range might have improved performance.

Third, some missing data limit this analysis from encompassing the entire outbreak. The first mass testing dates (round 0) only used rRT-PCR testing, so no comparison with BinaxNOW was possible. Furthermore, each round of testing was intended to capture all staff who had not yet tested positive; however, participant attrition occurred between testing rounds.

Table 4. BinaxNOW rapid antigen test performance compared with viral culture among 100 real-time reverse transcription PCR–positive specimens with cycle threshold <30 from horse racetrack staff, California, USA, November–December 2020

BinaxNOW results	Viral culture results		Total
	Positive	Negative	
Detected	45	10	55
Not detected	6	39	45
Total	51	49	100

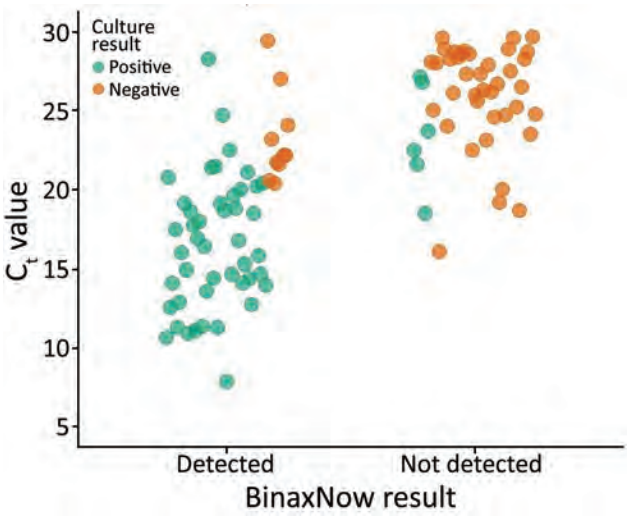

Figure 2. BinaxNOW rapid antigen test results and viral culture results among 100 real-time reverse transcription PCR–positive specimens with cycle threshold <30 among staff at a horse racetrack, California, USA, November–December 2020. Of 51 viral culture–positive specimens, 45 were detected by BinaxNOW (88.2% concordance).

We attribute this attrition to the logistical obstacles of staff getting to the testing site or to staff leaving their jobs during the outbreak. More complete paired-testing data could have provided better insight as to the usefulness of rapid antigen testing when used for the entire duration of an outbreak.

Our results support considering BinaxNOW-positive employees as infectious without waiting for rRT-PCR confirmation. The rapid turnaround time and high PPV of BinaxNOW enabled some SARS-CoV-2–positive employees to be identified and isolated faster than if rRT-PCR had been used alone. In outbreak situations in which access to laboratory rRT-PCR services is limited, it might be reasonable to act on BinaxNOW-positive results and forgo rRT-PCR confirmation. In contrast, our findings suggest that BinaxNOW negative results in an outbreak investigation should be confirmed with rRT-PCR, because false negatives do occur.

Our results indicate that BinaxNOW performs better at identifying rRT-PCR–positive specimens with lower C_t (suggestive of higher viral loads) and positive viral cultures, although these factors are not precise proxies for infectiousness. Real-time RT-PCR remains a more sensitive test for identifying persons that might be infectious, and our results support the current recommendation that rRT-PCR (or another nucleic acid amplification test) should be used in outbreak situations to confirm BinaxNOW-negative results (*2*). Clinical discretion informed by COVID-19 incidence in the relevant population, as well as individual exposure history and symptoms, should be used to determine whether to quarantine persons who test negative for SARS-CoV-2 by BinaxNOW but are awaiting results of rRT-PCR testing (*16*).

Acknowledgments

We thank Lisa B. Hernandez, James Allard, Beimnet Taye, the California Department of Public Health Viral and Rickettsial Disease Laboratory staff, and the racetrack staff described in this report.

About the Author

Dr. Surasi is an Epidemic Intelligence Service Officer with the Center for Surveillance, Epidemiology, and Laboratory Services, Centers for Disease Control and Prevention. He is positioned at the California Department of Public Health within the Occupational Health Branch and the Environmental Health Investigations Branch. His research interests are workplace health and safety.

References

1. Food and Drug Administration. BinaxNOW COVID-19 Ag card (PN 195–000)—instructions for use. 2020 Dec [cited 2021 Mar 15]. https://www.fda.gov/media/141570/download
2. Centers for Disease Control and Prevention. Interim guidance for antigen testing for SARS-CoV-2. 2020 Dec 5 [cited 2021 Mar 15]. https://www.cdc.gov/coronavirus/2019-ncov/lab/resources/antigen-tests-guidelines.html
3. James AE, Gulley T, Kothari A, Holder K, Garner K, Patil N. Performance of the BinaxNOW COVID-19 antigen card test relative to the SARS-CoV-2 real-time reverse transcriptase polymerase chain reaction assay among symptomatic and asymptomatic healthcare employees. Infect Control Hosp Epidemiol. 2021 Jan 25 [Epub ahead of print]. https://doi.org/10.1017/ice.2021.20
4. Okoye NC, Barker AP, Curtis K, Orlandi RR, Snavely EA, Wright C, et al. Performance characteristics of BinaxNOW COVID-19 antigen card for screening asymptomatic individuals in a university setting. J Clin Microbiol. 2021;59:e03282–20. https://doi.org/10.1128/JCM.03282-20
5. Pilarowski G, Lebel P, Sunshine S, Liu J, Crawford E, Marquez C, et al. Performance characteristics of a rapid severe acute respiratory syndrome coronavirus 2 antigen detection assay at a public plaza testing site in San Francisco. J Infect Dis. 2021;223:1139–44.
6. Pilarowski G, Marquez C, Rubio L, Peng J, Martinez J, Black D, et al. Field performance and public health response using the BinaxNOW TM Rapid SARS-CoV-2 antigen detection assay during community-based testing. Clin Infect Dis. 2020 Dec 26 [Epub ahead of print]. https://doi.org/10.1093/cid/ciaa1890
7. Pollock NR, Jacobs JR, Tran K, Cranston AE, Smith S, O'Kane CY, et al. Performance and implementation evaluation of the Abbott BinaxNOW rapid antigen test in a high-throughput drive-through community testing site in Massachusetts. J Clin Microbiol. 2021;59:e00083–21. https://doi.org/10.1128/JCM.00083-21

8. Prince-Guerra JL, Almendares O, Nolen LD, Gunn JKL, Dale AP, Buono SA, et al. Evaluation of Abbott BinaxNOW rapid antigen test for SARS-CoV-2 infection at two community-based testing sites—Pima County, Arizona, November 3–17, 2020. MMWR Morb Mortal Wkly Rep. 2021;70:100–5. https://doi.org/10.15585/mmwr.mm7003e3
9. Carlsten C, Gulati M, Hines S, Rose C, Scott K, Tarlo SM, et al. COVID-19 as an occupational disease. Am J Ind Med. 2021;64:227–37. https://doi.org/10.1002/ajim.23222
10. Waltenburg MA, Victoroff T, Rose CE, Butterfield M, Jervis RH, Fedak KM, et al.; COVID-19 Response Team. Update: COVID-19 among workers in meat and poultry processing facilities—United States, April–May 2020. MMWR Morb Mortal Wkly Rep. 2020;69:887–92. https://doi.org/10.15585/mmwr.mm6927e2
11. Dahdouh E, Lázaro-Perona F, Romero-Gómez MP, Mingorance J, García-Rodriguez J. C_t values from SARS-CoV-2 diagnostic PCR assays should not be used as direct estimates of viral load. J Infect. 2021;82:414–51. https://doi.org/10.1016/j.jinf.2020.10.017
12. Sethuraman N, Jeremiah SS, Ryo A. Interpreting diagnostic tests for SARS-CoV-2. JAMA. 2020;323:2249–51. https://doi.org/10.1001/jama.2020.8259
13. Mina MJ, Parker R, Larremore DB. Rethinking Covid-19 test sensitivity—a strategy for containment. N Engl J Med. 2020;383:e120. https://doi.org/10.1056/NEJMp2025631
14. Seftel D, Boulware DR. Prospective cohort of fluvoxamine for early treatment of coronavirus disease 19. Open Forum Infect Dis. 2021 Feb 1 [Epub ahead of print]. https://doi.org/10.1093/ofid/ofab050
15. National Oceanic and Atmospheric Administration. Temperature data from the weather station in Richmond, CA, on the following dates: Nov. 25, 27, 28; Dec. 4, 13, 16, 20, 22 [cited 2021 Mar 15]. https://www.noaa.gov
16. Centers for Disease Control and Prevention. Interim guidance for SARS-CoV-2 testing in non-healthcare workplaces. 2021 Mar 17 [cited 2021 June 11]. https://www.cdc.gov/coronavirus/2019-ncov/community/organizations/testing-non-healthcare-workplaces.html

Address for correspondence: Krishna Surasi, State of California Department of Public Health, 850 Marina Bay Pkwy, Bldg P, 3rd Fl, Richmond, CA 94804, USA; email: okt3@cdc.gov

Originally published in June 2019

etymologia revisited

Neospora caninum [ne-os′ pə-rə ca-nin′ um]

From the *neo-* (Latin, "new") + *spora* (Greek, "seed") and *canis* (Latin, "dog"), *Neospora caninum* is a sporozoan parasite that was first described in 1984. It is a major pathogen of cattle and dogs but can also infect horses, goats, sheep, and deer. Antibodies to *N. caninum* have been found in humans, predominantly in those with HIV infection, although the role of this parasite in causing or exacerbating illness is unclear.

Sources:

1. Bjerkås I, Mohn SF, Presthus J. Unidentified cyst-forming sporozoon causing encephalomyelitis and myositis in dogs. Z Parasitenkd. 1984;70:271–4. http://dx.doi.org/10.1007/BF00942230
2. Dubey JP. Review of *Neospora caninum* and neosporosis in animals. Korean J Parasitol. 2003; 41:1–16. http://dx.doi.org/10.3347/kjp.2003.41.1.1
3. Lobato J, Silva DA, Mineo TW, Amaral JD, Segundo GR, Costa-Cruz JM, et al. Detection of immunoglobulin G antibodies to *Neospora caninum* in humans: high seropositivity rates in patients who are infected by human immunodeficiency virus or have neurological disorders. Clin Vaccine Immunol. 2006;13:84–9. http://dx.doi.org/10.1128/CVI.13.1.84-89.2006

https://wwwnc.cdc.gov/eid/article/25/6/et-2506_article

Ehrlichiosis and Anaplasmosis among Transfusion and Transplant Recipients in the United States

Sanjida J. Mowla, Naomi A. Drexler, Cara C. Cherry, Pallavi D. Annambholta, Ian T. Kracalik, Sridhar V. Basavaraju

Medscape EDUCATION ACTIVITY

In support of improving patient care, this activity has been planned and implemented by Medscape, LLC and Emerging Infectious Diseases. Medscape, LLC is jointly accredited by the Accreditation Council for Continuing Medical Education (ACCME), the Accreditation Council for Pharmacy Education (ACPE), and the American Nurses Credentialing Center (ANCC), to provide continuing education for the healthcare team.

Medscape, LLC designates this Journal-based CME activity for a maximum of 1.00 ***AMA PRA Category 1 Credit(s)™***. Physicians should claim only the credit commensurate with the extent of their participation in the activity.

Successful completion of this CME activity, which includes participation in the evaluation component, enables the participant to earn up to 1.0 MOC points in the American Board of Internal Medicine's (ABIM) Maintenance of Certification (MOC) program. Participants will earn MOC points equivalent to the amount of CME credits claimed for the activity. It is the CME activity provider's responsibility to submit participant completion information to ACCME for the purpose of granting ABIM MOC credit.

All other clinicians completing this activity will be issued a certificate of participation. To participate in this journal CME activity: (1) review the learning objectives and author disclosures; (2) study the education content; (3) take the post-test with a 75% minimum passing score and complete the evaluation at http://www.medscape.org/journal/eid; and (4) view/print certificate. For CME questions, see page 2950.

Release date: October 13, 2021; Expiration date: October 13, 2022

Learning Objectives

Upon completion of this activity, participants will be able to:

- Assess donor-derived ehrlichiosis and anaplasmosis cases in the United States among solid organ transplant recipients, based on a case series, review of Centers for Disease Control and Prevention (CDC) investigations, and literature review
- Evaluate donor-derived ehrlichiosis and anaplasmosis cases in the United States among transfusion recipients, based on a case series, review of CDC investigations, and literature review
- Determine the clinical implications of donor-derived ehrlichiosis and anaplasmosis cases in the United States among solid organ transplant and transfusion recipients, based on a case series, review of CDC investigations, and literature review

CME Editor

Tony Pearson-Clarke, MS, Technical Writer/Editor, Emerging Infectious Diseases. *Disclosure: Tony Pearson-Clarke, MS, has disclosed no relevant financial relationships.*

CME Author

Laurie Barclay, MD, freelance writer and reviewer, Medscape, LLC. *Disclosure: Laurie Barclay, MD, has disclosed no relevant financial relationships.*

Authors

Disclosures: ***Sanjida J. Mowla, MPH; Naomi A. Drexler, MPH, DrPH; Cara C. Cherry, DVM; Pallavi Annambholta, DrPH; Ian T. Kracalik, PhD;*** *and* ***Sridhar V. Basavaraju, MD,*** *have disclosed no relevant financial relationships.*

Author affiliations: Oak Ridge Institute for Science and Education, Oak Ridge, Tennessee, USA (S.J. Mowla); Centers for Disease Control and Prevention, Atlanta, Georgia, USA (S.J. Mowla, N.A. Drexler, C.C. Cherry, P.D. Annambholta, I.T. Kracalik, S.V. Basavaraju)

DOI: https://doi.org/10.3201/eid2711.211127

Ehrlichiosis and anaplasmosis are emerging tickborne diseases that can also be transmitted through blood transfusions or organ transplants. Since 2000, ehrlichiosis and anaplasmosis cases in the United States have increased substantially, resulting in potential risk to transplant and transfusion recipients. We reviewed ehrlichiosis and anaplasmosis cases among blood transfusion and solid organ transplant recipients in the United States from peer-reviewed literature and Centers for Disease Control and Prevention investigations. We identified 132 cases during 1997–2020, 12 transfusion-associated cases and 120 cases in transplant recipients; 8 cases were donor-derived, and in 13 cases illness occurred <1 year after transplant. Disease in the remaining 99 cases occurred ≥1 year after transplant, suggesting donor-derived disease was unlikely. Severe illness or death were reported among 15 transfusion and transplant recipients. Clinicians should be alert for these possible infections among transfusion and transplant recipients to prevent severe complications or death by quickly treating them.

Ehrlichiosis and anaplasmosis are emerging tickborne diseases caused by *Ehrlichia* and *Anaplasma* spp. obligate intracellular bacteria (*1*,*2*). Tick bites are the primary route of infection, but transmission can also occur through blood transfusion or solid organ transplantation, because these pathogens infect leukocytes and circulate throughout the blood stream (*2*). In the United States, human ehrlichiosis is caused primarily by *Ehrlichia chaffeensis* but can also result from *E. ewingii* or *E. muris eauclairensis* infections (*1*,*3*). Anaplasmosis is caused by *Anaplasma phagocytophilum* (*1*). Although distinct diseases, ehrlichiosis and anaplasmosis share clinical and laboratory features. Early symptoms often include fever, chills, headache, malaise, myalgia, or nausea, and many infections go unrecognized and undiagnosed (*3*–*5*). Laboratory features often include leukopenia, thrombocytopenia, anemia, and elevated hepatic transaminases (*3*–*5*).

Both diseases have incubation periods of 5–14 days from the time of tick transmission, and during early illness infected asymptomatic persons or those with mild illness might be unknowingly accepted as blood donors (*3*,*5*). In general, higher rates of ehrlichiosis and anaplasmosis are reported among adults >40 years of age, and most patients are men (*5*–*7*). Illness onset is most commonly reported during June and July, corresponding to peak tick activity (*3*,*5*). Approximately half of ehrlichiosis and anaplasmosis patients require hospitalization, and 7% require critical care (*3*,*8*). Case-fatality rates are ≈1% for *E. chaffeensis* ehrlichiosis and 0.3% for anaplasmosis patients based on national surveillance reports (*3*,*5*). In part because of immunosuppressive therapies to prevent organ rejection, transplant and transfusion recipients may be more susceptible to ehrlichiosis and anaplasmosis. Relative risk (RR) for severe outcomes among immunosuppressed compared with immunocompetent case-patients was higher for hospitalization (RR 1.4), life-threatening complications (RR 2.4), and death (RR 2.3), highlighting the potential severity of disease in immunocompromised populations (*3*,*9*–*15*).

In the United States, ehrlichiosis was first reported in 1987 and anaplasmosis in 1994, and both became nationally notifiable diseases in 1999 (*3*,*5*,*16*,*17*). Since 2000, reported cases of ehrlichiosis and anaplasmosis in the United States have increased substantially. Reported *E. chaffeensis* ehrlichiosis cases have increased >10-fold, from 200 in 2000 to 2,093 in 2019 (*18*,*19*). Reported anaplasmosis cases increased >16-fold, from 348 cases in 2000 to 5,655 in 2019 (*19*,*20*).

Increasing rates of reported ehrlichiosis and anaplasmosis might be related to several factors, including improved diagnostics, changes in reporting practices, and expanded human contact with animal reservoirs and tick vectors (*2*,*3*,*21*,*22*). *E. chaffeensis* and *E. ewingii* are primarily transmitted by the lone star tick (*Amblyomma americanum*); *A. phagocytophilum* is transmitted by either the blacklegged tick (*Ixodes scapularis*) or the western blacklegged tick (*I. pacificus*) (*3*,*5*). *E. muris eauclaurensis* is transmitted by *I. scapularis* ticks. *E. chaffeensis* ehrlichiosis is most frequently reported in the southeastern and south-central regions of the United States, and anaplasmosis is most often reported in the upper midwestern and northeastern regions.

PCR and serologic testing using an indirect immunofluorescence antibody assay are the primary laboratory methods for diagnosing ehrlichiosis and anaplasmosis (*3*,*5*). Because infection transmitted through blood or organs is rare, it might not be diagnosed in solid organ transplant and transfusion recipients. In addition, nonspecific signs and symptoms and a higher index of suspicion for other opportunistic infections might complicate diagnosis (*14*), which is unfortunate because early detection and treatment can prevent severe illness and death (*23*). Here, we summarize and discuss the risks of ehrlichiosis and anaplasmosis cases in the United States among solid organ transplant and transfusion recipients, with a focus on donor-derived infections.

Methods

We conducted a literature search to identify articles published during January–August 2020 describing ehrlichiosis and anaplasmosis in solid organ

transplant or blood transfusion recipients in the United States. We used PubMed search terms "ehrlichiosis AND transfusion," "ehrlichiosis AND transplant," "anaplasmosis AND transfusion," and "anaplasmosis AND transplant." We included articles describing case reports, case series, or other clinical descriptions related to *Ehrlichia* and *Anaplasma* spp. infections in the setting of solid organ transplantation or transfusion of blood products in the United States. We excluded infections in hematopoietic stem cell recipients because these are not reported to a national notifiable disease system. For articles meeting inclusion criteria, we further reviewed references to identify any case reports or case descriptions not found in the initial PubMed search. Duplicate cases were only counted once for this review. We summarized transplant- and transfusion-associated cases as presented in the literature; we made no additional exclusions based on diagnostic criteria, and we only determined cases to be donor-derived if the authors presented them as such in the literature or investigations.

In the United States, all suspected or confirmed cases of donor-derived diseases are reported to the Organ Procurement and Transplantation Network and are investigated by the Disease Transmission Advisory Committee (DTAC). Nationally notifiable diseases such as ehrlichiosis and anaplasmosis are referred to the Centers for Disease Control and Prevention (CDC) for investigation and determination of whether the infection was transmitted from a donor to a recipient. We also included cases of transplant-associated ehrlichiosis and anaplasmosis identified as part of these DTAC investigations by CDC if not already accounted for in the peer-reviewed literature (Figure 1). From each reviewed article or CDC-led case investigation, we collected available information on geographic region, recipient characteristics, *Ehrlichia* or *Anaplasma* species, transmission route, age of blood component transfused or type of organ transplanted, time between transplantation and infection, symptoms and clinical details, diagnostic methods, donor and recipient histories of tick exposure, donor characteristics, likely source of infection, and whether the recipient survived or died.

Results

Ehrlichiosis and Anaplasmosis Cases Reported among Transfusion Recipients

During the 1997–2020 investigation period, 12 cases of transfusion-transmitted ehrlichiosis or anaplasmosis were reported in the United States (Appendix Table 1,

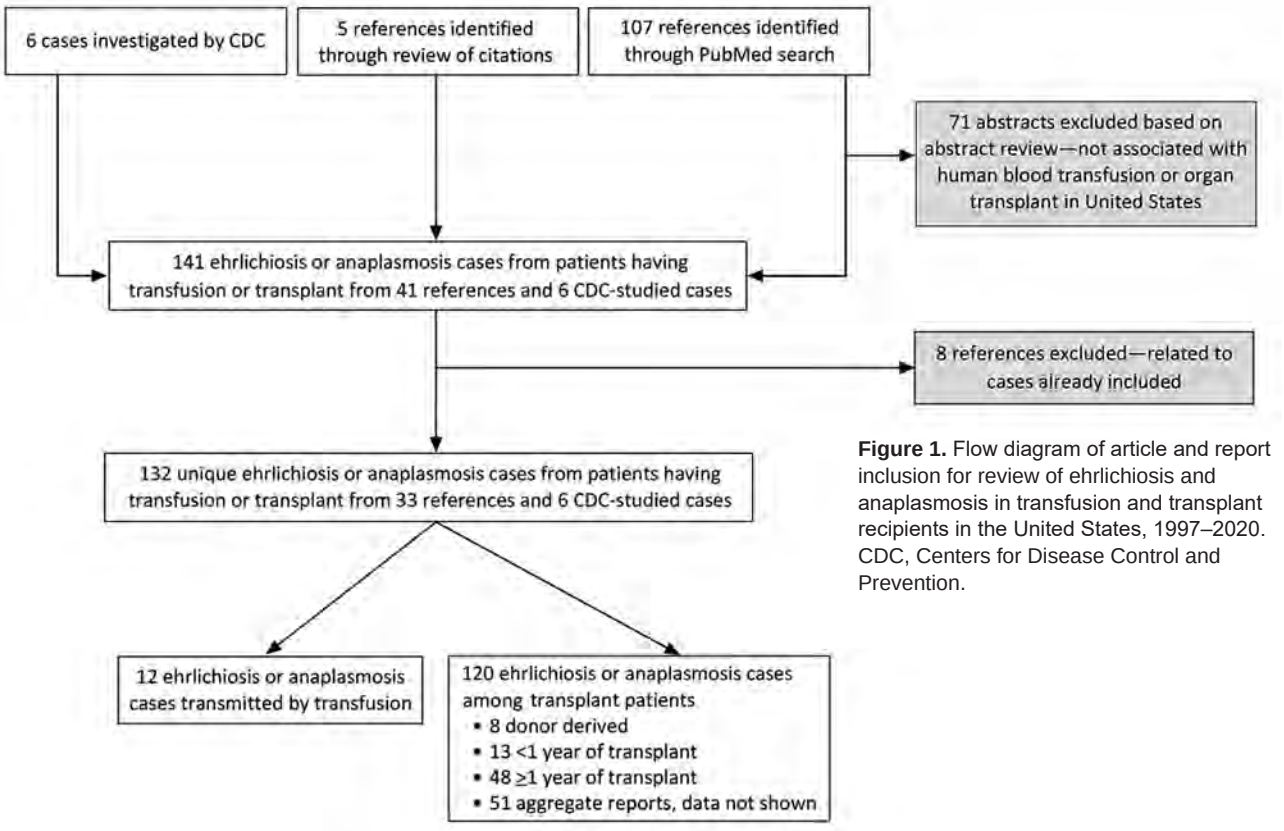

Figure 1. Flow diagram of article and report inclusion for review of ehrlichiosis and anaplasmosis in transfusion and transplant recipients in the United States, 1997–2020. CDC, Centers for Disease Control and Prevention.

https://wwwnc.cdc.gov/EID/article/27/11/21-1127-App1.pdf). Of the 12 transfusion-transmitted cases, 8 resulted from transfused red blood cell components and 3 from transfused platelet components (2 apheresis and 1 whole blood–derived); the component for 1 case was not identified. Ten (83.3%) of 12 transfusion-associated cases were *A. phagocytophilum* infections; 1 case was associated with *E. ewingii* and 1 with *E. chaffeensis* (Figure 2, panels C, D). Median age of transfusion recipients was 66 years (range 9–85 years); sex was equally distributed. Of the transfusion-associated cases of ehrlichiosis and anaplasmosis, 3 occurred in Minnesota; 2 in Wisconsin; and 1 each in Georgia, Rhode Island, Connecticut, Massachusetts, New York, and Oklahoma (Figure 2, panels A, B). Disease in all cases was diagnosed using PCR, and additional serologic testing was used for 2 cases. Most (83.3%) transfusion case-patients survived infection; one third of cases were associated with mild symptoms. Intensive care unit (ICU) treatment was noted for 2 anaplasmosis patients, prompted by respiratory failure, hypotension, and hypoxia. In addition, 3 anaplasmosis patients had multisystem organ failure, but ICU treatment was not mentioned for these cases. Two patients died, one from anaplasmosis and the other from other medical complications.

Ehrlichiosis and Anaplasmosis Cases Reported among Solid Organ Transplant Recipients

During the investigation period, 107 cases of ehrlichiosis and 7 cases of anaplasmosis were described in the literature among solid organ transplant recipients. Of these, 63 included patient-specific information. We described the remaining 51 cases in aggregate and reported on them separately. An additional 6 cases of ehrlichiosis among solid organ transplant recipients were investigated by CDC, resulting in a total of 120 cases of ehrlichiosis or anaplasmosis described among transplant recipients during the investigation period.

E. chaffeensis ehrlichiosis was the most common organ donor-derived infection, reported among 8 solid organ transplant recipients: 2 cases we identified from the literature and the 6 investigated by CDC (Appendix Table 2). Of these, 7 (87.5%) case-patients were kidney transplant recipients and 1 was a liver transplant recipient. Fever was reported among all solid organ transplant recipients. Diagnostic methods were PCR (87.5%) and serologic testing (12.5%). Most (87.5%) patients were male, median age was 57 years (range 5–69 years), and median time between transplantation and infection was 13.5 days (range 10–25 days). Of the donor-derived ehrlichiosis cases, 2 occurred in Maryland; 3 in Missouri; and 1 each in New York, New Jersey, and Illinois (Figure 2, panel E). Among the 8 donor-derived ehrlichiosis cases, 2 deaths were reported among the kidney transplant recipients, both occurring <1 month after transplantation (Appendix Table 3). None of the confirmed transplant-derived case reports described ICU admission among the patients.

Thirteen cases of ehrlichiosis and anaplasmosis occurred <1 year after transplantation but could not be confirmed as donor-derived. The median time between transplantation and symptom onset in these 13 cases was 5 months (range 2 weeks–9 months) (Table 4). Of those cases, 4 were identified in Tennessee (Figure 2, panel F). *E. chaffeensis* infection was associated with 11 (84.6%) cases, and *A. phagocytophilum* infection was associated with 2 (15.4%) cases. Of the 13 cases, 5 (38.5%) occurred in kidney recipients, 4 (30.8%) in heart recipients, 2 (15.4%) in kidney and pancreas recipients, and 1 (7.7%) in a liver and lung recipient. Most (76.9%) patients were male, median age was 50 years (range 35–63 years), and PCR was the most common (76.9%) diagnostic method. Most (92.3%) patients infected <1 year after transplantation survived; however, 1 kidney and pancreas recipient with *A. phagocytophilum* infection died.

Forty-eight records of individual cases of ehrlichiosis or anaplasmosis that occurred ≥1 year after transplant were most likely attributable to posttransplant infections acquired through tick bites (Table 5). Median time from transplant to symptom onset was 6 years (range 1–21 years), most patients (75.0%) were male, and median age was 51 years (range 11–73 years). Among these patients, records described *Ehrlichia* infection for 43 (89.6%) and *Anaplasma* infection for 5 (10.4%). *E. chaffeensis* was implicated in 30 (69.8%) of 43 cases of ehrlichiosis, *E. ewingii* in 12 (27.9%), and an unspecified *Ehrlichia* sp. in 1 (2.3%). Twenty-three patients (53.5%) received kidneys, 8 (18.6%) livers, 7 (16.3%) lungs, 4 (9.3%) hearts, and 1 (2.3%) a pancreas. Of the 5 reported cases of anaplasmosis occurring ≥1 year after transplant, 4 (80.0%) occurred in kidney recipients and 1 (20.0%) in a liver recipient. Among the 43 cases of ehrlichiosis in solid organ transplant recipients who had illness onset ≥1 year after transplant, 26 (60.6%) occurred in Missouri and 12 (27.9%) in Tennessee; exact location was not specified in 1 report, but the case occurred in Alabama, Tennessee, or Mississippi. Among the 5 cases of anaplasmosis, 2 occurred in Minnesota, 1 in Maine, 1 in Wisconsin, and 1 in Connecticut. One patient had possible reactivation of a previous *Anaplasma* infection secondary to potent immunosuppression 9 months after the

original infection. There were 2 reports of *Ehrlichia* reinfection that described distinct strains of *E. chaffeensis* and *E. ewingii* found in a secondary infection. Secondary hemophagocytic lymphohistiocytosis, which is characterized by severe and potentially fatal inflammation, developed in 1 kidney transplant recipient. Of the solid organ transplant recipients with ehrlichiosis or anaplasmosis occurring ≥1 year after transplant, 47 (97.9%) of 48 survived. One pancreas recipient with an *E. chaffeensis* infection died. Seven cases occurring ≥1 year of solid organ transplantation did report ICU admission, possibly relating to long-term immunosuppression among transplant recipients.

Of the 51 cases of ehrlichiosis from Missouri for which we report data in aggregate, 18 (35.3%) occurred in kidney recipients, 12 (23.5%) in heart recipients, 12

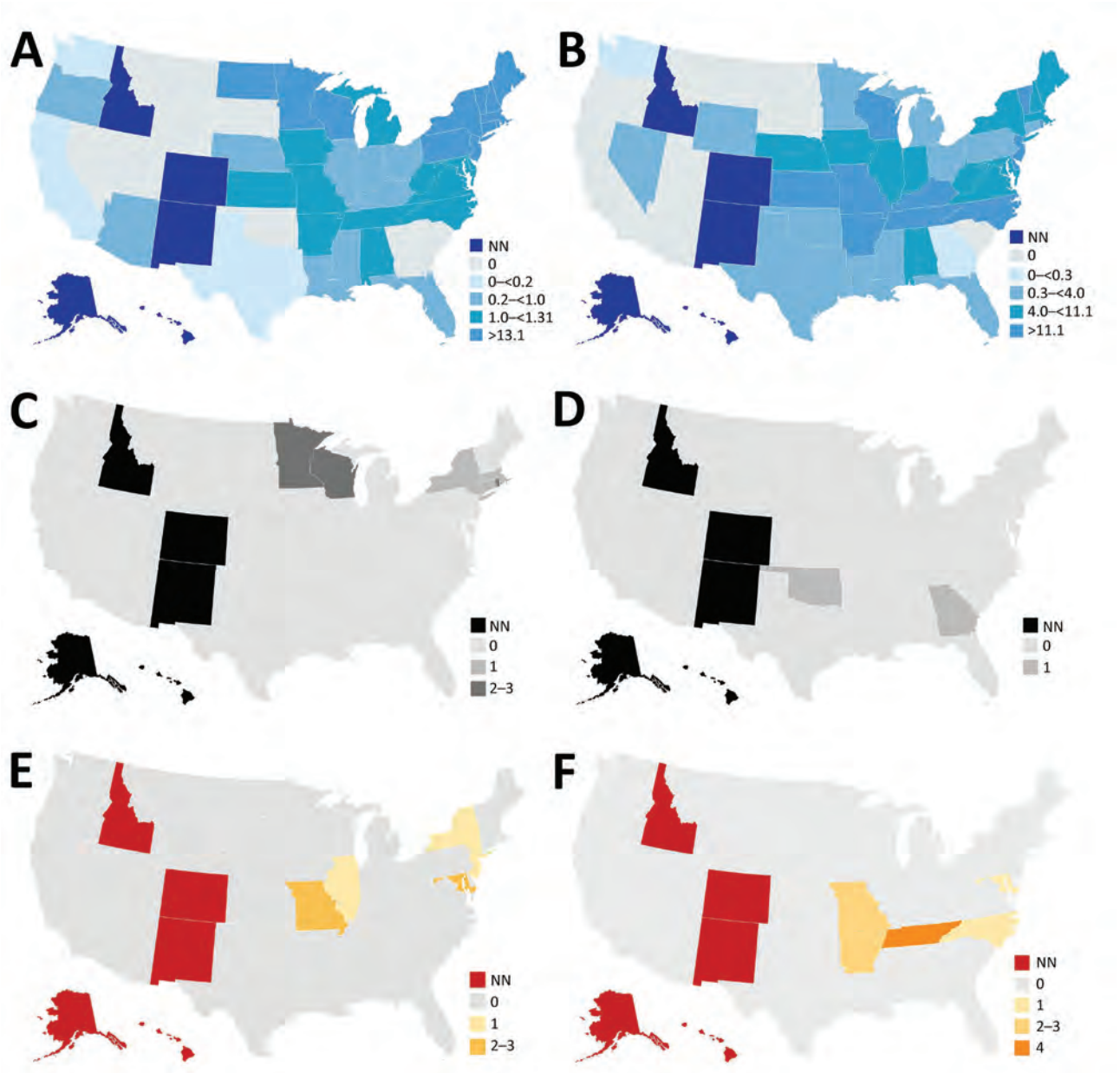

Figure 2. Incidence of ehrlichiosis and anaplasmosis in the United States, 2019, and of cases among transfusion and transplant recipients, 1997–2020. A) Incidence of anaplasmosis per 1 million US residents in 2019. B) Incidence of ehrlichiosis per 1 million US residents in 2019. C) Transfusion-transmitted anaplasmosis cases by recipient state of residence. D) Transfusion-transmitted ehrlichiosis cases by recipient state of residence. E) Organ donor–derived ehrlichiosis cases by recipient state of residence. We identified no organ donor–derived anaplasmosis cases. F) Organ donor–derived ehrlichiosis cases with onset <1 year after transplant by recipient state of residence. We identified 2 additional donor-derived ehrlichiosis cases with onset <1 year after transplant; however, recipient state of residence was unknown. NN, not notifiable.

(23.5%) in lung recipients, 7 (13.7%) in liver recipients, and 2 (4.0%) in kidney-pancreas recipients. Additional information on disease, pathogen species, and demographics was not available for these 51 cases.

Discussion

This study reviewed ehrlichiosis and anaplasmosis cases among transfusion and solid organ transplant recipients described in published literature and reports from 6 CDC investigations. During the study period, 12 cases of transfusion-transmitted ehrlichiosis or anaplasmosis were reported, 2 of which resulted in death. In addition, 8 cases of organ donor–derived ehrlichiosis were reported (7 kidney transplant recipients and 1 liver recipient), 2 of which resulted in death. *A. phagocytophilum* was the most common causative agent among transfusion-derived infections. In contrast, among transplant recipients, *E. chaffeensis* was the most common causative agent. Donor-derived infections were observed among patients of a broad range of ages (5–85 years). Although children are not considered a high-risk group for anaplasmosis in particular, pediatric infection should not be discounted among transfusion and transplant recipients. Time from transplant or transfusion to the development of signs and symptoms varied widely and in most cases was longer than the typical incubation period for a tick-transmitted infection. Delays in symptom onset might be affected by the colony size and the site of the inoculated bacteria. Transfusion- or transplant-transmitted ehrlichiosis and anaplasmosis are rare but can result in severe outcomes including the death of the recipient.

Although known cases of transfusion- and transplant-transmitted ehrlichiosis or anaplasmosis are uncommon, studies of asymptomatic infection among blood donors and the survivability of infection in blood suggest the risk of transmission is greater than previously recognized. In endemic areas, seroprevalence studies found 11.3% of blood donors in New York, 0.5% in Wisconsin, and 3.5% in Connecticut had detectable antibodies against *A. phagocytophilum* (*24*,*25*). In Iowa, ≈1% of blood donors studied were seropositive for and displayed symptoms of ehrlichiosis after blood donation, although recipient lookback reported by physicians indicated that these transfusions did not result in transfusion-transmitted illnesses (*26*). However, serosurveys do not report active or incident infections, only the proportion of participants previously exposed to an *Ehrlichia* or *Anaplasma* agent. Some studies also examined the survivability of *Ehrlichia* and *Anaplasma* species in donor blood. Blood from anaplasmosis patients in 2 studies found viable *A. phagocytophilum* survived under refrigerated storage conditions for up to 18 days in whole blood (*27*,*28*). One in vitro study reported *E. chaffeensis* remained viable for up to 11 days within refrigerated packed red blood cells (*29*).

Donor-derived ehrlichiosis and anaplasmosis highlight the importance of donor risk mitigation strategies in the setting of blood transfusion and solid organ transplantation and the potential role of laboratory-based screening. Recognizing and diagnosing tickborne diseases is complicated by long incubation periods and potential asymptomatic or mildly symptomatic infections. Although several laboratory tests are used to diagnose ehrlichiosis and anaplasmosis, no tests have been approved by the US Food and Drug Administration (FDA) to screen blood or organ donors for these diseases. Furthermore, serologic screening of donors might not identify active *Ehrlichia* or *Anaplasma* infections or could exclude healthy donors (*28*). PCR testing would more accurately screen contaminated blood and organ products, but no FDA-licensed test is available. Donor deferral on the basis of travel or residence would be impractically broad because of the widespread endemicity of ehrlichiosis and anaplasmosis across regions of the United States. To minimize blood supply disruptions based on travel deferrals for Zika virus and babesia, FDA previously recommended universal antibody testing and regional nucleic acid testing in states with the highest rates of risk for infection (*30*,*31*). Similar screening may eventually be necessary for ehrlichiosis and anaplasmosis as the prevalence and incidence of these infections increases in the United States. CDC will continue to monitor the occurrence of transfusion- or transplant-transmitted ehrlichiosis and anaplasmosis.

Among this study's limitations, for sources identified through the literature we were limited to the information provided in the case reports, which might not always have represented a full account of the patient experience. Data on donor demographics were extremely limited. Donor state of residence might have provided a more accurate insight on likelihood of donor infection by state which might have broader implications for blood and organ screening criteria. Next, for the purposes of this evaluation, we relied on the characterizations by the original authors or investigators to categorize cases as donor- or transplant-derived ehrlichiosis or anaplasmosis. Finally, we included only cases published in peer-reviewed literature or reported to CDC, possibly underreporting transfusion- and transplant-associated infections. In 2019, the Rickettsial Zoonoses Branch,

Division of Vector-Borne Diseases, National Center for Emerging and Zoonotic Infectious Diseases, CDC, added questions relating to recent transfusion and organ transplant to their tickborne rickettsial disease surveillance system (https://www.cdc.gov/ticks/forms/Tick_TBRD_FILL_508.pdf) to better track donor-derived infections.

Because *Ehrlichia* and *Anaplasma* species primarily infect leukocytes, leukoreduction has been presumed to reduce risk for ehrlichiosis and anaplasmosis through passive removal (*23*,*32*,*33*). However, 83% (10/12) of components implicated in transfusion-transmitted cases in this study were leukoreduced. In cell culture models, because of their presence in plasma also, *E. chaffeensis* survived in red blood cells stored in additive solution, suggesting leukoreduction alone will not prevent transmission of *Ehrlichia* and *Anaplasma* species (*29*). Adopting pathogen reduction technology, such as psoralen and ultraviolet light to inactivate infectious agents, for platelet and plasma products would provide additional safety measures to reduce risk for transfusion-transmitted *Ehrlichia* and *Anaplasma* infections. Pathogen-reduced plasma has demonstrated a ≥3.6-log reduction in viable *A. phagocytophilum* (*34*). However, this method has not been approved for red blood cell products, which were implicated in 8 of 12 cases of transfusion-transmitted ehrlichiosis and anaplasmosis in this study.

Identifying risk factors for *Ehrlichia* and *Anaplasma* infections among deceased organ donors is challenging because clinical, demographic, and social information about deceased donors is often obtained from family members, who might not have access to or recall all historical details (*35*). Also, routine laboratory screening of organ donors, required for multiple infectious diseases, including HIV/AIDS, does not yet include testing for infection with *Ehrlichia* and *Anaplasma* species. In addition, the number of posttransplant infections reported in this review highlights the risk among blood product or organ recipients. Therefore, clinicians must closely monitor recipients of blood transfusions or solid organs during long-term management and consider these pathogens when recipients develop signs or symptoms of infection. Because the prevalence of tickborne disease infections is rising, additional risk mitigation interventions will likely be necessary to enhance blood and organ safety.

Acknowledgments

We thank Paige Armstrong for her contributions to preparing this manuscript.

Organ Procurement and Transplantation Network data provided for this report was supported in part by the US Health Resources and Services Administration (https://www.hrsa.gov).

About the Author

Ms. Mowla is an ORISE fellow in the Office of Blood, Organ, and Other Tissue Safety, Division of Healthcare Quality Promotion, National Center for Emerging and Zoonotic Infectious Diseases, CDC, in Atlanta. Her primary research interests are transfusion- and transplant-transmitted infections.

References

1. Vannorsdall MD, Thomas S, Smith RP, Zimmerman R, Christman R, Vella JP, et al. Human granulocytic ehrlichiosis in a renal allograft recipient: review of the clinical spectrum of disease in solid organ transplant patients. Transpl Infect Dis. 2002;4:97–101. https://doi.org/10.1034/j.1399-3062.2002.01015.x
2. Ismail N, Bloch KC, McBride JW. Human ehrlichiosis and anaplasmosis. Clin Lab Med. 2010;30:261–92. https://doi.org/10.1016/j.cll.2009.10.004
3. Nichols Heitman K, Dahlgren FS, Drexler NA, Massung RF, Behravesh CB. Increasing incidence of ehrlichiosis in the United States: a summary of national surveillance of *Ehrlichia chaffeensis* and *Ehrlichia ewingii* infections in the United States, 2008–2012. Am J Trop Med Hyg. 2016;94:52–60. https://doi.org/10.4269/ajtmh.15-0540
4. Bakken JS, Dumler JS. Human granulocytic anaplasmosis. Infect Dis Clin North Am. 2015;29:341–55. https://doi.org/10.1016/j.idc.2015.02.007
5. Dahlgren FS, Heitman KN, Drexler NA, Massung RF, Behravesh CB. Human granulocytic anaplasmosis in the United States from 2008 to 2012: a summary of national surveillance data. Am J Trop Med Hyg. 2015;93:66–72. https://doi.org/10.4269/ajtmh.15-0122
6. Fishbein DB, Dawson JE, Robinson LE. Human ehrlichiosis in the United States, 1985 to 1990. Ann Intern Med. 1994;120:736–43. https://doi.org/10.7326/0003-4819-120-9-199405010-00003
7. Paddock CD, Childs JE. *Ehrlichia chaffeensis*: a prototypical emerging pathogen. Clin Microbiol Rev. 2003;16:37–64. https://doi.org/10.1128/CMR.16.1.37-64.2003
8. Dumler JS. *Anaplasma* and *Ehrlichia* infection. Ann N Y Acad Sci. 2005;1063:361–73. https://doi.org/10.1196/annals.1355.069
9. Alhumaidan H, Westley B, Esteva C, Berardi V, Young C, Sweeney J. Transfusion-transmitted anaplasmosis from leukoreduced red blood cells. Transfusion. 2013;53:181–6. https://doi.org/10.1111/j.1537-2995.2012.03685.x
10. Cotant C, Okulicz JF, Brezina B, Riley DJ, Conger NG. Human monocytic ehrlichiosis in a renal transplant patient. Scand J Infect Dis. 2006;38:699–702. https://doi.org/10.1080/00365540500444694
11. Fine AB, Sweeney JD, Nixon CP, Knoll BM. Transfusion-transmitted anaplasmosis from a leukoreduced platelet pool. Transfusion. 2016;56:699–704. https://doi.org/10.1111/trf.13392
12. Goel R, Westblade LF, Kessler DA, Sfeir M, Slavinski S, Backenson B, et al. Death from transfusion-transmitted anaplasmosis, New York, USA, 2017. [Erratum in Emerg

Infect Dis. 2018;24:1773.]. Emerg Infect Dis. 2018;24:1548–50. https://doi.org/10.3201/eid2408.172048
13. Sachdev SH, Joshi V, Cox ER, Amoroso A, Palekar S. Severe life-threatening *Ehrlichia chaffeensis* infections transmitted through solid organ transplantation. Transpl Infect Dis. 2014;16:119–24. https://doi.org/10.1111/tid.12172
14. Safdar N, Love RB, Maki DG. Severe *Ehrlichia chaffeensis* infection in a lung transplant recipient: a review of ehrlichiosis in the immunocompromised patient. Emerg Infect Dis. 2002;8:320–3. https://doi.org/10.3201/eid0803.010249
15. Trofe J, Reddy KS, Stratta RJ, Flax SD, Somerville KT, Alloway RR, et al. Human granulocytic ehrlichiosis in pancreas transplant recipients. Transpl Infect Dis. 2001; 3:34–9. https://doi.org/10.1034/j.1399-3062.2001.003001034.x
16. Chen SM, Dumler JS, Bakken JS, Walker DH. Identification of a granulocytotropic *Ehrlichia* species as the etiologic agent of human disease. J Clin Microbiol. 1994;32:589–95. https://doi.org/10.1128/jcm.32.3.589-595.1994
17. Maeda K, Markowitz N, Hawley RC, Ristic M, Cox D, McDade JE. Human infection with *Ehrlichia canis*, a leukocytic rickettsia. N Engl J Med. 1987;316:853–6. https://doi.org/10.1056/NEJM198704023161406
18. CDC. Ehrlichiosis: epidemiology and statistics [cited 2021 June 23]. https://www.cdc.gov/ehrlichiosis/stats/index.html
19. CDC. Nationally notifiable infectious diseases and conditions, United States: annual tables [cited 2021 June 23]. https://wonder.cdc.gov/nndss/static/2019/annual/2019-table2f.html
20. CDC. Anaplasmosis: epidemiology and statistics [cited 2021 June 23]. https://www.cdc.gov/anaplasmosis/stats/index.html
21. Dahlgren FS, Mandel EJ, Krebs JW, Massung RF, McQuiston JH. Increasing incidence of *Ehrlichia chaffeensis* and *Anaplasma phagocytophilum* in the United States, 2000–2007. Am J Trop Med Hyg. 2011;85:124–31. https://doi.org/10.4269/ajtmh.2011.10-0613
22. Springer YP, Eisen L, Beati L, James AM, Eisen RJ. Spatial distribution of counties in the continental United States with records of occurrence of *Amblyomma americanum* (Ixodida: Ixodidae). J Med Entomol. 2014;51:342–51. https://doi.org/10.1603/ME13115
23. Biggs HM, Behravesh CB, Bradley KK, Dahlgren FS, Drexler NA, Dumler JS, et al. Diagnosis and management of tickborne rickettsial diseases: Rocky Mountain spotted fever and other spotted fever group rickettsioses, ehrlichioses, and anaplasmosis—United States. A practical guide for health care and public health professionals. MMWR Recomm Rep. 2016;65:1–44. https://doi.org/10.15585/mmwr.rr6502a1
24. Aguero-Rosenfeld ME, Donnarumma L, Zentmaier L, Jacob J, Frey M, Noto R, et al. Seroprevalence of antibodies that react with *Anaplasma phagocytophila*, the agent of human granulocytic ehrlichiosis, in different populations in Westchester County, New York. J Clin Microbiol. 2002; 40:2612–5. https://doi.org/10.1128/JCM.40.7.2612-2615.2002
25. Leiby DA, Chung AP, Cable RG, Trouern-Trend J, McCullough J, Homer MJ, et al. Relationship between tick bites and the seroprevalence of *Babesia microti* and *Anaplasma phagocytophila* (previously *Ehrlichia* sp.) in blood donors. Transfusion. 2002;42:1585–91. https://doi.org/10.1046/j.1537-2995.2002.00251.x
26. Arguin PM, Singleton J, Rotz LD, Marston E, Treadwell TA, Slater K, et al. An investigation into the possibility of transmission of tick-borne pathogens via blood transfusion. Transfusion-Associated Tick-Borne Illness Task Force. Transfusion. 1999;39:828–33. https://doi.org/10.1046/j.1537-2995.1999.39080828.x
27. Kalantarpour F, Chowdhury I, Wormser GP, Aguero-Rosenfeld ME. Survival of the human granulocytic ehrlichiosis agent under refrigeration conditions. J Clin Microbiol. 2000;38:2398–9. https://doi.org/10.1128/JCM.38.6.2398-2399.2000
28. McQuiston JH, Childs JE, Chamberland ME, Tabor E. Transmission of tick-borne agents of disease by blood transfusion: a review of known and potential risks in the United States. [Erratum in Transfusion. 2000;40:891.] Transfusion. 2000;40:274–84. https://doi.org/10.1046/j.1537-2995.2000.40030274.x
29. McKechnie DB, Slater KS, Childs JE, Massung RF, Paddock CD. Survival of *Ehrlichia chaffeensis* in refrigerated, ADSOL-treated RBCs. Transfusion. 2000;40:1041–7. https://doi.org/10.1046/j.1537-2995.2000.40091041.x
30. Food and Drug Administration. Recommendations for reducing the risk of transfusion-transmitted babesiosis [cited on 2021 June 23]. https://www.fda.gov/media/114847/download
31. Food and Drug Administration. Information for blood establishments regarding FDA's determination that Zika virus is no longer a relevant transfusion-transmitted infection [cited 2021 September 7]. https://www.fda.gov/vaccines-blood-biologics/blood-blood-products/information-blood-establishments-regarding-fdas-determination-zika-virus-no-longer-relevant
32. Annen K, Friedman K, Eshoa C, Horowitz M, Gottschall J, Straus T. Two cases of transfusion-transmitted *Anaplasma phagocytophilum.* Am J Clin Pathol. 2012;137:562–5. https://doi.org/10.1309/AJCP4E4VQQQOZIAQ
33. Proctor MC, Leiby DA. Do leukoreduction filters passively reduce the transmission risk of human granulocytic anaplasmosis? Transfusion. 2015;55:1242–8. https://doi.org/10.1111/trf.12976
34. Food and Drug Administration. INTERCEPT blood system for cryoprecipitation package insert for the manufacturing of pathogen reduced plasma, cryoprecipitate reduced [cited on 2021 June 23]. https://www.fda.gov/media/90594/download
35. Vora NM, Basavaraju SV, Feldman KA, Paddock CD, Orciari L, Gitterman S, et al.; Transplant-Associated Rabies Virus Transmission Investigation Team. Raccoon rabies virus variant transmission through solid organ transplantation. JAMA. 2013;310:398–407. https://doi.org/10.1001/jama.2013.7986

Address for correspondence: Sridhar V. Basavaraju, Centers for Disease Control and Prevention, 1600 Clifton Rd NE, Mailstop V18-4, Atlanta, GA 30329-4027, USA; email: smowla1@uga.edu

Interventions to Disrupt Coronavirus Disease Transmission at a University, Wisconsin, USA, August–October 2020

Dustin W. Currie,[1] Gage K. Moreno,[1] Miranda J. Delahoy, Ian W. Pray, Amanda Jovaag, Katarina M. Braun, Devlin Cole, Todd Shechter, Geroncio C. Fajardo, Carol Griggs, Brian S. Yandell, Steve Goldstein, Dena Bushman, Hannah E. Segaloff, G. Patrick Kelly, Collin Pitts, Christine Lee, Katarina M. Grande, Amanda Kita-Yarbro, Brittany Grogan, Sara Mader, Jake Baggott, Allen C. Bateman, Ryan P. Westergaard, Jacqueline E. Tate, Thomas C. Friedrich, Hannah L. Kirking, David H. O'Connor, Marie E. Killerby

University settings have demonstrated potential for coronavirus disease (COVID-19) outbreaks; they combine congregate living, substantial social activity, and a young population predisposed to mild illness. Using genomic and epidemiologic data, we describe a COVID-19 outbreak at the University of Wisconsin–Madison, Madison, Wisconsin, USA. During August–October 2020, a total of 3,485 students, including 856/6,162 students living in dormitories, tested positive. Case counts began rising during move-in week, August 25–31, 2020, then rose rapidly during September 1–11, 2020. The university initiated multiple prevention efforts, including quarantining 2 dormitories; a subsequent decline in cases was observed. Genomic surveillance of cases from Dane County, in which the university is located, did not find evidence of transmission from a large cluster of cases in the 2 quarantined dorms during the outbreak. Coordinated implementation of prevention measures can reduce COVID-19 spread in university settings and may limit spillover to the surrounding community.

Author affiliations: Centers for Disease Control and Prevention, Atlanta, Georgia, USA (D.W. Currie, M.J. Delahoy, I.W. Pray, G.C. Fajardo, D. Bushman, H.E. Segaloff, C. Lee, J.E. Tate, H.L. Kirking, M.E. Killerby); University of Wisconsin–Madison, Madison, Wisconsin, USA (G.K. Moreno, A. Jovaag, K.M. Braun, D. Cole, T. Shechter, C. Griggs, B.S. Yandell, S.Goldstein, P. Kelly, C. Pitts, J. Baggott, R.P. Westergaard, T.C. Friedrich, D.H. O'Connor); Wisconsin Department of Health Services, Madison (I.W. Pray, D. Cole, H.E. Segaloff, R.P. Westergaard); Public Health Madison and Dane County, Madison (K.M. Grande·A. Kita-Yarbro, B. Grogan, S. Mader); Wisconsin State Laboratory of Hygiene, Madison (A.C. Bateman)

DOI: https://doi.org/10.3201/eid2711.211306

Severe acute respiratory syndrome coronavirus 2 (SARS-CoV-2), which causes coronavirus disease (COVID-19), can spread rapidly within congregate settings, including institutions of higher education (IHEs) (*1*,*2*). During August–December 2020, as IHEs around the United States resumed in-person instruction, IHE-associated SARS-CoV-2 cases began to rise (*3*). By February 2021, >530,000 COVID-19 cases linked to US IHEs had been identified (*4*). In many IHE settings populated substantially by young adults 18–24 years of age (*5*), susceptibility to severe COVID-19 is lower than for older populations (≥65 years of age) (*6*). Adhering to physical distancing is also challenging for young adults, for whom interaction with peers and social networks is important (*7*).

As students returned to in-person learning, high-density clustering within on-campus housing may have increased transmission and resulted in community outbreaks (*8*–*10*; M.S. Andersen, et al., unpub. data, https://doi.org/10.1101/2020.09.22.2019604; C.S. Richmond, et al., unpub. data, https://doi.org/10.1101/2020.10.12.20210294). One study using whole-genome sequencing (WGS) data, which can be used to track specific SARS-CoV-2 lineages through space and time (*11*–*16*; M. Zeller et al., unpub. data, https://doi.org/10.1101/2021.02.05.21251235), suggested that SARS-CoV-2 transmission chains beginning or proliferating on IHE campuses may lead to spread within the surrounding community, including to populations at higher risk for severe disease (C.S. Richmond, et al., unpub. data). Therefore, strategies to prevent SARS-CoV-2 spread on IHE campuses and between IHEs and the community are needed.

[1]These authors contributed equally to this article.

We used epidemiologic and genomic data to describe an outbreak of SARS-CoV-2 infection at the University of Wisconsin–Madison (UW-Madison; Madison, WI, USA) shortly after its reopening for the fall 2020 semester. We report the trajectory of the outbreak and describe measures taken to reduce transmission. In addition, using genomic data, we investigated whether SARS-CoV-2 lineages associated with outbreaks at dormitories may have spread into the community surrounding UW-Madison.

The Western Institutional Review Board obtained a waiver of Health Insurance Portability and Accountability Act authorization (WIRB #1-1290953-1) to obtain the clinical specimens for whole-genome sequencing. Our analysis was reviewed by Centers for Disease Control and Prevention (CDC) and was conducted consistent with applicable federal law and CDC policy (45 C.F.R. part 46.102(l)(2), 21 C.F.R. part 56; 42 U.S.C. Sect. 241(d); 5 U.S.C. Sect. 552a; 44 U.S.C. Sect. 3501 et seq.). The Institutional Review Board at UW-Madison determined these activities were nonresearch public health surveillance.

Methods

Setting

UW-Madison is a large public university in the midwestern United States; during the fall 2020 semester, the university had ≈45,540 enrolled students and 23,917 staff (*17*). UW-Madison offered a combination of in-person and virtual classes for this semester. Undergraduate students living in on-campus dormitories and moved in on preassigned days during August 25–31, 2020. They were tested for SARS-CoV-2 on move-in day and subsequently required to undergo testing every 2 weeks regardless of symptoms. Appointment-based testing for all students and staff was also available free of charge. Testing was conducted on anterior nasal swab specimens using real-time reverse transcription PCR (rRT-PCR) tests authorized by the Food and Drug Administration. UW-Madison instituted a mandatory COVID-19 student pledge at the start of the semester, which required mask usage at all times (except within students' own rooms), physical distancing when possible, self-monitoring for symptoms, and limited gatherings in accordance with local public health guidelines (*18*). Students were provided a symptom screening tool for symptom self-monitoring; those screening positive were instructed to schedule a test and self-isolate (except for medical care) until receiving a negative result.

Isolation facilities were established in designated dormitories to temporarily house students living on-campus who tested positive for SARS-CoV-2. Students living on campus who were identified as close contacts of persons testing positive for SARS-CoV-2 (defined as being within 6 feet of an infected person for ≥15 minutes within a 24-hour period from 2 days before illness onset or positive specimen collection through the end of isolation) were quarantined in individual single rooms in local hotels for 14 days; meals were delivered to the rooms, and students were tested for SARS-CoV-2 during the first and second week of quarantine. If a quarantined student tested positive, they isolated in the same quarantine location. Nonquarantined students who tested positive were transferred to designated isolation dormitories. Isolation lasted for 10 days after symptom onset, or 10 days after positive specimen collection for those who were asymptomatic, consistent with CDC recommendations (*19*).

As the semester progressed, some modifications to the quarantine procedure were required. Given the high frequency of positivity within 2 dormitories (dorms A and B) during universal testing events, all students living in these 2 dormitories were asked to quarantine within their hall for 2 weeks to mitigate transmission. During the dormitory quarantine period, students were asked to wear a face covering when leaving their room, refrain from congregating, self-monitor for symptoms, test onsite, and stay in their dormitory. Residents testing positive were moved to an isolation facility, and roommates of residents testing positive initially quarantined within their dormitory room. Approximately 1 week into the dormitory quarantine, roommates of those with positive cases were moved to alternative quarantine facilities. Students could also choose to quarantine at their permanent home; those students could return to the dormitory after the quarantine ended and they provided a negative test result.

County-level ordinances passed earlier in the summer also applied to the UW-Madison community. As of July 13, 2020, emergency order no. 8 from Dane County, which includes Madison, mandated the use of face coverings when in public, limited the size of public gatherings, limited restaurant capacity, and closed bars except for takeout and socially distanced outdoor seating (*20*).

Epidemiologic Data Analysis

We used Wisconsin Electronic Disease Surveillance System (WEDSS) data to describe demographic characteristics, location of on-campus clusters, and symptoms of COVID-19 cases. We defined a UW-Madison–affiliated SARS-CoV-2 infection as a positive

rRT-PCR test result in a specimen collected from a UW-Madison student or staff member during August 1–October 31, 2020. We calculated daily percent positivity (defined as the number positive SARS-CoV-2 specimens collected on a given day divided by the total number of specimens collected) and attack rates within 19 dormitories (occupancy range 26–1,195 residents) using campus testing program data. We merged campus testing data with data from the University Housing department to determine housing location of students living on-campus as of September 22, 2020. We defined index cases for roommate attack rate calculations as the resident with the first positive SARS-CoV-2 test result within a room in a dormitory. We defined roommate attack rate as the proportion of susceptible students (roommates of an index case that had not previously tested positive for SARS-CoV-2) who had a positive SARS-CoV-2 specimen collected 2–14 days after the index case specimen collection. We performed epidemiologic data analyses using SAS software version 9.4 (SAS Institute, https://www.sas.com), and RStudio version 1.2.1335 (RStudio Team, https://www.rstudio.com).

Whole-Genome Sequencing

Sequences for this investigation were derived from 262 anterior nasal swab samples collected during September 8–22, 2020, from UW-Madison students living in dormitories A and B. We selected these samples for sequencing because they were the largest outbreaks among students living in on-campus housing; we sought to determine whether the outbreaks between the 2 dormitories were distinct. We extracted viral RNA from 100 μL of viral transport medium by using the Viral Total Nucleic Acid Purification kit (Promega, https://www.promega.com) on a Maxwell RSC 48 (Promega) instrument and eluted it in 50 μL of nuclease-free H_2O. We synthesized cDNA using a modified ARTIC Network approach (*21*–*23*). In brief, we reverse transcribed 11 μL of virual RNA with SuperScript IV Reverse transcription (Invitrogen, https://www.thermofisher.com) according to the manufacturer's guidelines. We used ARTIC version 3 primers (IDT, https://www.idtdna.com/pages/landing/coronavirus-research-reagents/ngs-assays) for SARS-CoV-2–specific multiplex PCR for nanopore sequencing (Appendix Table 2). We amplified cDNA (2.5 μL) in 2 multiplexed PCR reactions using Q5 Hot-Start DNA High-fidelity Polymerase (New England Biolabs, https://www.neb.com). We performed all consensus-level sequencing of SARS-CoV-2 using nanopore sequencing as described previously (*11*).

Phylogenetic Analysis

We processed sequencing data using the ARTIC bioinformatics pipeline (https://github.com/artic-network/artic-ncov2019) scaled up for on-campus computing cores. The entire nanopore analysis pipeline is available at https://github.com/gagekmoreno/SARS-CoV-2-in-Southern-Wisconsin. We used all available full-length sequences from Dane County through January 31, 2021, for phylogenetic analysis using the tools implemented in Nextstrain custom builds (https://github.com/nextstrain/ncov) (*24*,*25*). We included 262 samples from students in dormitories A and B and 875 samples from persons tested at University of Wisconsin Hospital and Clinics (UWHC) from September 1, 2020–January 31, 2021; these samples represented ≈3% of all cases within Dane County, where UW-Madison is located, during this period. Persons using UWHC testing services included community members receiving preoperative testing, employees, inpatient and emergency department patients, patients from associated hospitals, and persons with known exposures. Of the 875 UWHC samples sequenced, 714 were collected on or after September 23, 2020, when the quarantine of dormitories A and B ended. We used this convenience sample to assess strains circulating within the Dane County community following the UW-Madison outbreak. We built time-resolved and divergence phylogenetic trees using standard Nextstrain tools and scripts. We filtered and cleaned metadata using custom Python (version 3.8; https://www.anaconda.com) scripts.

Analyses Comparing Roommate Sequences

To test the hypothesis that roommate pairs are more likely to have similar viral sequences than nonroommate pairs, we linked data from 33 roommate pairs in which both roommates had sequencing data and performed a permutation test comparing the percent overlap in single-nucleotide polymorphism (SNP) identities between roommate pairs and random pairs of sequences derived from dormitories A and B. We performed a Mann-Whitney U test to compare the amount of diversity shared in roommate pairs and random pairs.

Results

Demographics, Symptom Manifestation, and Measures to Reduce Transmission

During August 1–October 31, 2020, a total of 3,485 students and 245 staff affiliated with UW-Madison tested positive for SARS-CoV-2 by rRT-PCR, out of ≈45,540 enrolled students and 23,917 staff (Table 1). Cases in fraternity and sorority life (FSL) housing and

Table 1. Characteristics of University of Wisconsin-Madison student and staff coronavirus disease cases, Dane County, Wisconsin, USA, August 1–October 31, 2020*

Characteristic	Students, n = 3,485	Staff, n = 245
Mean age, y (range)	19.8 (17–72)	40.0 (20–88)
Sex		
M	1,677 (48.1)	114 (46.5)
F	1,807 (51.9)	131 (53.5)
Cluster affiliation†		
Dormitories	902 (25.9)	NA
Fraternity and sorority life	460 (13.2)	NA
Off-campus apartment	1,019 (29.2)	NA
No known affiliation with cluster	1,134 (32.5)	NA
Hospitalized		
Yes	4 (0.1)	1 (0.4)
No/unknown‡	3,481 (99.9)	244 (99.6)
Presence of symptoms§		
Symptomatic	2,838 (81.4)	197 (80.4)
Asymptomatic	647 (18.6)	48 (19.6)
Symptoms		
Headache	1,562 (44.8)	132 (53.9)
Sore throat	1,454 (41.7)	81 (33.1)
Fatigue	1,417 (40.7)	106 (43.3)
Cough	1,311 (37.6)	116 (47.4)
Runny nose	1,122 (32.2)	80 (32.7)
Muscle ache	1,021 (29.3)	100 (40.8)
Fever	918 (26.3)	75 (30.6)
Loss of smell	879 (25.2)	63 (25.7)
Loss of taste	777 (22.3)	53 (21.6)
Chills	822 (23.6)	56 (22.9)
Shortness of breath	336 (9.6)	19 (7.8)
Nausea	286 (8.2)	23 (9.4)
Diarrhea	247 (7.1)	19 (7.8)
Abdominal pain	126 (3.6)	12 (4.9)
Vomiting	43 (1.2)	7 (2.9)
Meets CSTE clinical criteria¶		
Yes	2,371 (68.0)	178 (72.7)
No	1,114 (32.0)	67 (27.3)
Timing of specimen collection relative to symptom onset		
Specimen collected on or after symptom onset date	2,275 (65.3)	162 (66.1)
Specimen collected before symptom onset date	162 (4.6)	7 (2.9)
No symptoms reported	647 (18.6)	48 (19.6)
Symptomatic, missing symptom onset date	401 (11.5)	28 (11.4)
Timing of positive report relative to symptom onset		
Positive reported on or after symptom onset date	2,411 (69.2)	167 (68.2)
Positive reported before symptom onset date	26 (0.7)	2 (0.8)
No symptoms reported	647 (18.6)	48 (19.6)
Symptomatic, missing symptom onset date	401 (11.5)	28 (11.4)

*Values are no. (%) except as indicated. Student affiliation was prioritized over staff, such that those identified as both students and staff are categorized as students. NA, not applicable.
†Cluster affiliation categories are not mutually exclusive.
‡Cannot distinguish between no and unknown; there is only 1 checkbox in which hospitalization can be selected.
§Anyone with ≥1 symptom is considered symptomatic; asymptomatic does not distinguish between those who were truly asymptomatic and those who were missing symptom information.
¶CSTE clinical criteria are met if the case-patient has either cough or shortness of breath, or ≥2 of the following symptoms: fever, chills, myalgia, headache, sore throat, loss of smell, or loss of taste.

other off-campus housing began rising before dormitory move-in week. UW-Madison–associated cases peaked during the week of September 6–12, 2020; soon after, cases began declining, showing a sustained decline through September and consistently low case counts in October (Figure 1). Most student (81.4%) and staff (80.4%) case-patients reported ≥1 symptom of COVID-19; 68.0% of students and 72.7% of staff met the Council of State and Territorial Epidemiologists clinical criteria for a COVID-19 case (Table 1) (*26*). Hospitalization was rare for both students and staff (<1.0%). Specimen collection occurred before symptom onset for 4.6% of student cases, whereas a positive result was reported before symptom onset for 0.7% of student cases. Among student case-patients, 902 (25.9%) were associated with an on-campus dormitory, 1,019 (29.2%) were associated with off-campus housing clusters, and 460 (13.2%) were associated with FSL (Table 1); the remainder were not linked to housing-specific clusters.

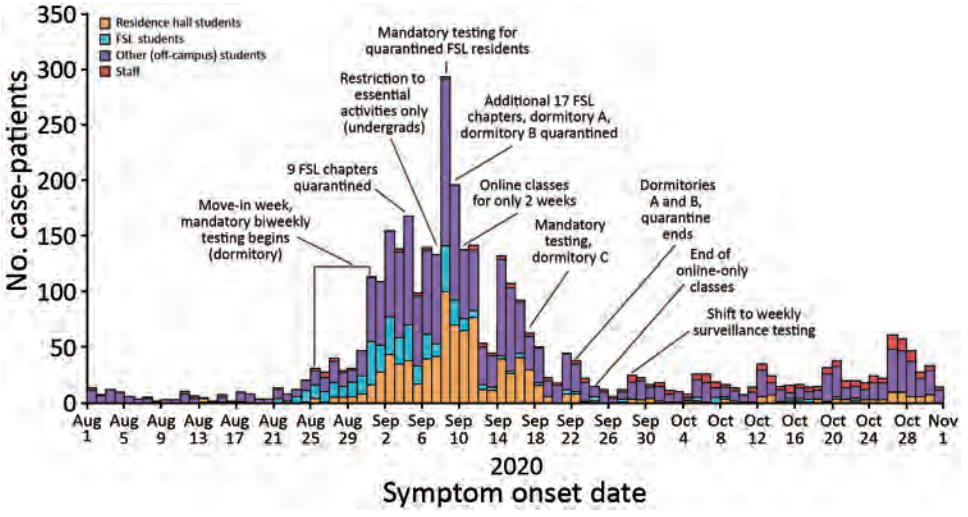

Figure 1. Overall epidemic curves of coronavirus disease cases among University of Wisconsin–Madison students and staff, Dane County, Wisconsin, USA, August 1–October 31, 2020. We categorized 10 student case-patients affiliated with both a dormitory and FSL as dormitory students. Student was considered the primary affiliation, such that any student who was also a staff member was categorized as a student. FSL, fraternity and sorority life.

Multiple mitigation measures were put into place to reduce transmission during September 6–12, 2020. Those measures included suspending in-person classes and events, prohibiting nonsanctioned social activities, holding additional mass testing events, and quarantining all students in dormitories A and B during September 9–23, 2020 (Figure 1). The local health department also required testing and quarantine for 26 FSL house chapters.

Infections among Students in Dormitories

Across all dormitories, 5,820/6,162 students (94.4%) were tested during move-in week (August 25–31, 2020); mean turnaround time from test to result was 2 days (interquartile range 1–2 days). Thirty-four students (0.6%) tested positive at move-in without documentation of a previous positive test in the previous 90 days; these students were moved into isolation dorms. Overall, 856/6,162 (13.9%) students living in the 19 on-campus dormitories had a positive SARS-CoV-2 specimen collected through campus testing during August 25–October 31, 2020; attack rates in dormitories were 1.9%–31.9% (Table 2) during this time. Fifteen dormitories had attack rates of <10.0%, 2 had attack rates of 10.0%–20.0%, and 2 had attack rates >20.0%. Dormitories A and B accounted for 68.5% of all dormitory cases (586/856), but only 34.4% of all students living in dormitories (2,119/6,162) (Figure 2).

In addition, we used a divergence phylogeny, colored by dormitory, to compare the number of mutations present in each sequence relative to the initial SARS-CoV-2 reference virus (GenBank accession no. MN908947.3). If dormitories A and B had distinct but contemporaneous outbreaks, we might expect viral sequences from the 2 halls to segregate into distinct taxa on a divergence tree. However, the tree illustrates that substantial mixing of viral genetic lineages between the dormitories occurred, indicating that outbreaks of COVID-19 within these dormitories were not distinct and resulted from intermingling between residents (Figure 3, panel C).

Table 2. Attack rates of coronavirus disease within dormitories and within roommates for dormitories with ≥10 cases, University of Wisconsin—Madison, Dane County, Wisconsin, USA, August 25–October 31, 2020*

Dormitory	No. residents	Residents with confirmed SARS-CoV-2 infection	Attack rates in roommates 2–14 d after index case†
Dormitory A	1,195	291/1,195 (24.4)	41/165 (24.8)
Dormitory B	924	295/924 (31.9)	32/172 (18.6)
Dormitory C	478	58/478 (12.1)	7/35 (20.0)
Dormitory D	181	19/181 (10.5)	2/9 (22.2)
Dormitory E	532	51/532 (9.6)	4/37 (10.8)
Dormitory F	384	31/384 (8.1)	5/23 (21.7)
Dormitory G	372	27/372 (7.3)	2/15 (13.3)
Dormitory H	319	20/319 (6.3)	1/14 (7.1)
Dormitory I	435	13/435 (3.0)	2/11 (18.2)
All other dormitories‡	1,342	51/1,342 (3.8)	5/33 (15.2)
Total†	6,162	856/6,162 (13.9)	101/514 (19.6)

*Values are no. positive/no. in category (%).
†One room included in the roommate attack rate analysis housed 3 residents, whereas all others housed 2 residents; in the room with 2 susceptible residents, neither tested positive within 2–14 d of the index case.
‡Includes aggregated data from 10 dormitories not listed here that had <10 total cases each; attack rates in these halls were 1.9%–5.6%.

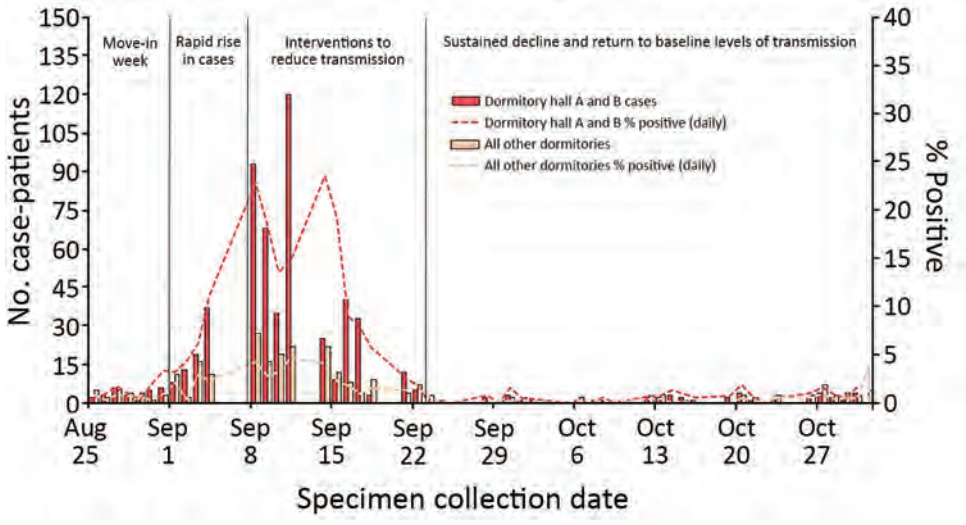

Figure 2. Coronavirus disease epidemic curves and percent positivity for University of Wisconsin–Madison students living in dormitories A and B versus all other dormitories, Dane County, Wisconsin, USA, August 25–October 31, 2020.

Whole-Genome Sequencing among Student Samples from Dormitories A and B

We sequenced complete viral genomes from 262 (44.7%) of 586 specimens from students living in dormitories A and B (Figure 3). Using a Dane County–centric phylogeny, we visualized the relationship of SARS-CoV-2 viruses circulating in dormitories A and B (Figure 3). Almost two thirds of sequences from the dormitories (172/262; 65.6%) formed a cluster in the 20A clade (PANGO lineage B.1.369) (Figure 3, panel B). This cluster contains a unique spike mutation encoding a glutamic acid-to-glutamine substitution at spike residue 780 (S E780Q), which was not seen in Dane County before this outbreak. This mutation was not subsequently found in 467 sequenced specimens from Dane County (of 15,740 positive tests, a sequencing coverage of 2.96%) during November 11, 2020–January 31, 2021.

The remaining 90 dormitory sequences clustered with the 20A (32/262), 20G (30/262), 20C (24/262), and 20B (4/262) clades. Sequences clustering in those remaining clades were more closely related to viral lineages concurrently circulating in Dane County, suggesting these persons became infected in the community. During September 23, 2020–January 31, 2021, a total of 75.3% (538/714) of new sequences in Dane County were classified as 20G clade, 15.1% (108/714) as 20A clade, 7.0% (50/714) as 20C clade, and 2.5% (18/714) as 20B clade. The large cluster in dormitories A and B was almost exclusively among case-patients 17–23 years of age (Figure 4).

Risk for Transmission between Roommates

Across all dormitories, 81.6% of residents had a roommate. Percentage positivity was higher overall among students with roommates (15.4%) than those without roommates (7.3%) ($p<0.0001$). Of the 514 students who had a roommate test positive but had not yet tested positive themselves, 101 (19.6%) tested positive within 2–14 days. (Table 2). Genetic distance comparisons between roommate pairs and nonroommate pairs within dormitories A and B revealed significantly higher levels of overlap in SNV identities between roommate pairs compared to random pairs. Specifically, 32/33 (97.0%) roommate pairs had viruses that contained 100.0% identical consensus sequences, whereas identical consensus sequences were found in 1,062/33,930 (3.1%) of randomly assigned pairs ($p<0.0001$).

Discussion

An outbreak of COVID-19 occurred at UW-Madison at the beginning of the fall semester. Over the course of our investigation, ≈14.0% of students living in dormitories tested positive; those living with roommates were more likely to test positive. Shortly after the UW-Madison outbreak began, mitigation measures were rapidly implemented, and a rapid decline in cases was observed. Ninety residence-hall sequences clustered with viruses circulating in Dane County, suggesting mixing between the university and Dane County. However, we did not detect evidence of transmission of the predominant viral lineages associated with dormitories A or B beyond these dormitories within Dane County in a convenience sample of sequenced specimens collected in the months following the outbreak.

Testing at the time students moved into dormitories identified some introductions of SARS-CoV-2 onto campus, and UW-Madison isolated infected students. However, the average 2-day turnaround

time for test results meant transmission might have occurred while students were awaiting their results. Therefore, when implementing move-in testing, quarantining students until results have been received may help prevent transmission among asymptomatic students awaiting results (*27*). Move-in testing also may fail to identify students who have recently been infected and do not yet have detectable levels of SARS-CoV-2 virus (*28*) and cannot prevent new infections if the virus is already circulating in the community. Our results suggest the importance of supplementing move-in testing with ongoing serial testing

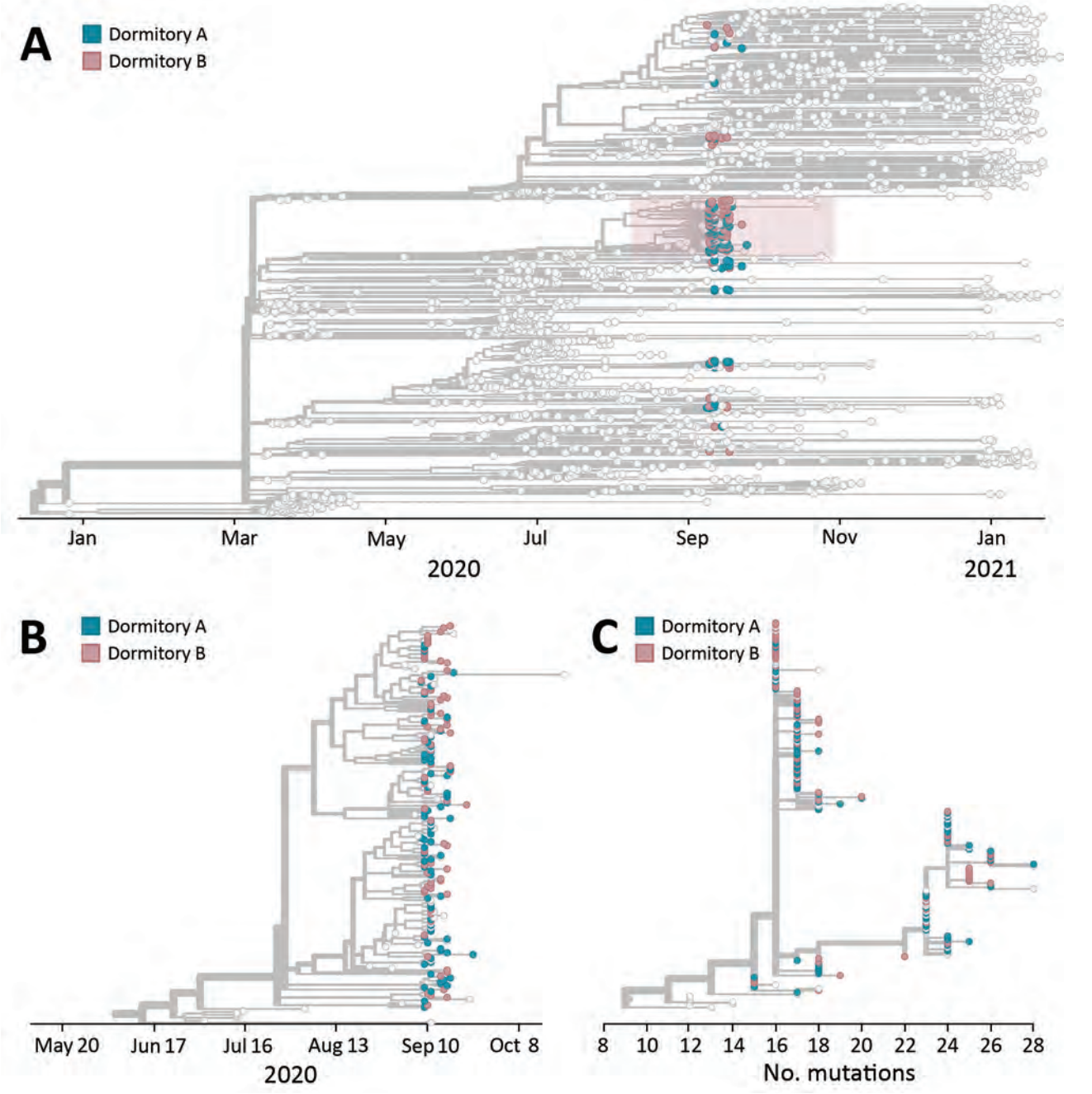

Figure 3. Phylogenetic tree of the coronavirus disease outbreak in dormitories A and B, University of Wisconsin–Madison, Dane County, Wisconsin, USA, January 2020–January 2021. A) Phylogenetic tree of all cases sequenced in Dane County, Wisconsin (light gray tips) during January 2020–January 2021 and cases sequenced in each dormitory. Pink shading indicates cluster associated with dormitories A and B. B) Expanded view of phylogenetic tree of the large cluster of cases associated with dormitories A and B during the September 2020 outbreak. C) Mutations relative to the initially identified severe acute respiratory syndrome coronavirus 2 genome in Wuhan, China (GenBank accession no. MN908947.3), during the outbreak in dormitories A and B.

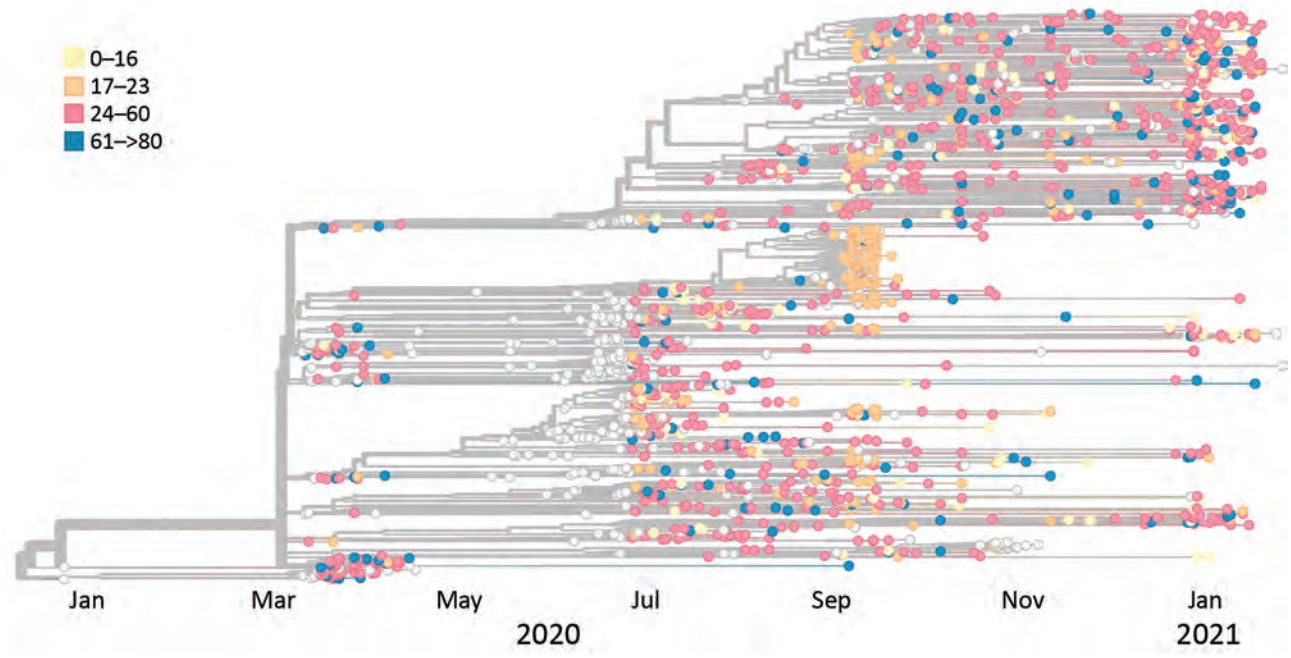

Figure 4. Phylogenetic tree of severe acute respiratory syndrome coronavirus 2 specimens sequenced in Dane County, Wisconsin, USA, January 2020–January 2021, coded by age of case-patient providing specimen.

and additional mitigation steps to effectively prevent ongoing transmission and community spread.

UW-Madison conducted biweekly serial screening testing for students in dormitories with relatively short turnaround time (mean 2 days), enabling the university to identify and isolate students with SARS-CoV-2 infections, quarantine roommates, and conduct contact tracing. Still, more frequent testing may have enabled more rapid case detection and initiation of isolation and quarantine procedures, preventing further transmission. A modeling study of COVID-19 spread within IHEs suggested that testing every 2 days would be needed to control the spread of SARS-CoV-2 (*29*). Recognizing this potential for rapid spread, UW-Madison increased the frequency of testing to twice per week for students living on-campus and off-campus in nearby ZIP codes and reduced turnaround time for results to <24 hours for the spring 2021 semester (*30*,*31*). Further evaluation of serial testing strategies is needed to determine optimal testing frequency in IHE settings and to prioritize populations for testing when capacity is limited. The high proportion of infected students who were symptomatic (>80.0%) suggests that, even in young adults, SARS-CoV-2 infection is frequently associated with at least mild symptoms, reinforcing the importance of educating students on COVID-19 symptoms, symptom monitoring, testing, and self-isolation when even mild symptoms develop (*32*).

Roommates live in close contact with each other, providing substantial opportunities for transmission (*32*). At UW-Madison, roommates were not required to wear masks within their rooms because this measure was considered impractical and unenforceable. Roommates of confirmed case-patients within dormitories had an estimated attack rate of 19.6%, and a larger proportion of students with roommates tested positive over the investigation period than those without. Furthermore, SARS-CoV-2 genomes collected from 33 roommate pairs found a high proportion of identical sequences, suggesting transmission occurred either within the roommate pair or from a shared exposure. Given the elevated risk for infection associated with having a roommate, efforts to reduce the density of dormitories, including single-occupancy rooms when available, may reduce transmission (*1*).

Two dormitories accounted for more than two thirds of all confirmed cases among students living in dormitories during the investigation period, although these 2 halls accounted for only one third of students living in on-campus housing. Transmission may have occurred within the dormitories but may have also occurred in other undetected settings (e.g., bars, private residences, fraternities, or sororities) that residents of dormitories A and B might have visited more frequently than did students living in other dormitories (*33*,*34*). The sequencing data strongly suggest that the clusters in dormitories A and B, which are located close to each other and share dining and recreation spaces, were not independent and were the result of intermingling. Viral genome sequencing is an important tool

in understanding the transmission dynamics between UW-Madison students and the broader community (*11–16*; C.S. Richmond et al., unpub. data; M. Zeller et al., unpub. data). Our sequencing data covering 44.7% of student case-patients living in dormitories A and B, 7.5% of all student case-patients, and 3.0% of community samples from Dane County did not find evidence that viruses from this cluster subsequently circulated at high frequencies in the community.

The first limitation of our analysis is that full lists of off-campus students and staff and their COVID-19 testing histories were not available; therefore, attack rates could be calculated only for students living in on-campus dormitories. We did not examine data related to race, ethnicity, and other social determinants of health. Occupancy levels remained fluid throughout the semester, but available data used for dormitory census calculations represented a single point in time at the end of the outbreak, when occupancy was lower than at the start of the semester. UW-Madison's rapid implementation of multiple interventions limits our ability to determine the effectiveness of individual interventions. Specimens from students living in dormitories A and B were targeted for sequencing to understand transmission patterns within and across these housing units. Therefore, our sequencing results should not be generalized to the campus at large; transmission events may have occurred after campus-related clusters outside of dormitories A and B. Other studies assessing trends in cases over time have suggested that university outbreaks preceding broader community outbreaks may be caused by transmission from universities to community members, a possibility that we cannot rule out (*10*). In addition, sequencing of Dane County specimens in Nextstrain represented a small proportion of the total number infections within the county (≈3.0%) and were sampled nonrandomly among clients of a large testing provider. Therefore, it is possible that descendant infections from dormitory A and B clusters occurred in Dane County but were not captured in the convenience sample from the community.

This investigation described an outbreak in which COVID-19 spread rapidly among university students at UW-Madison. Given the swift rise in cases, being able to quickly identify outbreaks and rapidly implement mitigation strategies by a coordinated universitywide response in collaboration with public health authorities is critical in halting transmission. Large-scale quarantines in congregate living situations (e.g., dormitories) and suspension of on-campus activities may be effective during large-scale outbreaks, if put in place rapidly and effectively. This investigation demonstrates using genomic surveillance to provide a more comprehensive understanding of transmission dynamics both in specific outbreak settings and in the general population. These tools can be used by universities and health departments to monitor spillover into the community and inform campus and community mitigation efforts.

This article was preprinted at https://www.medrxiv.org/content/10.1101/2021.05.07.21256834v1.

This research was performed using the computing resources and assistance of the UW-Madison Center for High Throughput Computing (CHTC) in the Department of Computer Sciences. The CHTC is supported by UW-Madison, the Advanced Computing Initiative, the Wisconsin Alumni Research Foundation, the Wisconsin Institutes for Discovery, and the National Science Foundation and is an active member of the Open Science Grid, which is supported by the National Science Foundation and the US Department of Energy Office of Science. G.K.M. is supported by a National Libraries of Medicine training grant to the Computation and Informatics in Biology and Medicine Training Program (NLM 5T15LM007359). This work was funded in part by the Centers for Disease Control and Prevention (contract no. 75D30120C09870: Defining the Role of College Students in SARS-CoV-2 Spread in the Upper Midwest).

About the Author

Dr. Currie is an Epidemic Intelligence Service officer in the Epidemiology and Surveillance Branch, Division of Global HIV and Tuberculosis, Center for Global Health, Centers for Disease Control and Prevention, Atlanta, Georgia, USA. His research interests include general population HIV surveillance, COVID-19 outbreak investigation, testing strategies for SARS-CoV-2 infection, and the relationship between behavioral science and communicable diseases.

References

1. Wilson E, Donovan CV, Campbell M, Chai T, Pittman K, Seña AC, et al. Multiple COVID-19 clusters on a university campus—North Carolina, August 2020. MMWR Morb Mortal Wkly Rep. 2020;69:1416–8. https://doi.org/10.15585/mmwr.mm6939e3
2. Fox MD, Bailey DC, Seamon MD, Miranda ML. Response to a COVID-19 outbreak on a university campus—Indiana, August 2020. MMWR Morb Mortal Wkly Rep. 2021;70:118–22. https://doi.org/10.15585/mmwr.mm7004a3
3. Salvatore PP, Sula E, Coyle JP, Caruso E, Smith AR, Levine RS, et al. Recent increase in COVID-19 cases reported among adults aged 18–22 years—United States, May 31–September 5, 2020. MMWR Morb Mortal Wkly Rep. 2020;69:1419–24. https://doi.org/10.15585/mmwr.mm6939e4
4. Cai W, Ivory D, Semple K, Smith M, Lemonides A, Higgins L et al. Tracking coronavirus cases at U.S. colleges and universities. The New York Times. 2021 [cited 2021

Mar 1]. https://www.nytimes.com/interactive/2021/us/college-covid-tracker.html
5. Centers for Disease Control and Prevention. COVID-19 parental resources kit—young adulthood. Updated December 28, 2020 [cited 2021 Apr 15]. https://www.cdc.gov/coronavirus/2019-ncov/daily-life-coping/parental-resource-kit/young-adulthood.html
6. Centers for Disease Control and Prevention; COVID-19 Response Team. Severe outcomes among patients with coronavirus disease 2019 (COVID-19)—United States, February 12–March 16, 2020. MMWR Morb Mortal Wkly Rep. 2020;69:343–46. https://doi.org/10.15585/mmwr.mm6912e2
7. Andrews JL, Foulkes L, Blakemore SJ. Peer influence in adolescence: public-health implications for COVID-19. Trends Cogn Sci. 2020;24:585–7. https://doi.org/10.1016/j.tics.2020.05.001
8. Walke HT, Honein MA, Redfield RR. Preventing and responding to COVID-19 on college campuses. JAMA. 2020;324:1727–8. https://doi.org/10.1001/jama.2020.20027
9. Leidner AJ, Barry V, Bowen VB, Silver R, Musial T, Kang GJ, et al. Opening of large institutions of higher education and county-level COVID-19 incidence—United States, July 6–September 17, 2020. MMWR Morb Mortal Wkly Rep. 2021;70:14–9. https://doi.org/10.15585/mmwr.mm7001a4
10. Pray IW, Kocharian A, Mason J, Westergaard R, Meiman J. Trends in outbreak-associated cases of COVID-19—Wisconsin, March–November 2020. MMWR Morb Mortal Wkly Rep. 2021;70:114–7. https://doi.org/10.15585/mmwr.mm7004a2
11. Moreno GK, Braun KM, Riemersma KK, Martin MA, Halfmann PJ, Crooks CM, et al. Revealing fine-scale spatiotemporal differences in SARS-CoV-2 introduction and spread. Nat Commun. 2020;11:5558. https://doi.org/10.1038/s41467-020-19346-z
12. Fauver JR, Petrone ME, Hodcroft EB, Shioda K, Ehrlich HY, Watts AG, et al. Coast-to-coast spread of SARS-CoV-2 during the early epidemic in the United States. Cell. 2020;181:990–996.e5. https://doi.org/10.1016/j.cell.2020.04.021
13. Lemieux JE, Siddle KJ, Shaw BM, Loreth C, Schaffner SF, Gladden-Young A, et al. Phylogenetic analysis of SARS-CoV-2 in Boston highlights the impact of superspreading events. Science 2021;371:eabe3261. https://doi.org/10.1126/science.abe3261
14. Miller D, Martin MA, Harel N, Tirosh O, Kustin T, Meir M, et al. Full genome viral sequences inform patterns of SARS-CoV-2 spread into and within Israel. Nat Commun. 2020;11:5518. https://doi.org/10.1038/s41467-020-19248-0
15. Maurano MT, Ramaswami S, Zappile P, Dimartino D, Boytard L, Ribeiro-Dos-Santos AM, et al. Sequencing identifies multiple early introductions of SARS-CoV-2 to the New York City region. Genome Res. 2020;30:1781–8. https://doi.org/10.1101/gr.266676.120
16. Bedford T, Greninger AL, Roychoudhury P, Starita LM, Famulare M, Huang ML, et al.; Seattle Flu Study Investigators. Cryptic transmission of SARS-CoV-2 in Washington state. Science. 2020;370:571–5. https://doi.org/10.1126/science.abc0523
17. University of Wisconsin—Madison. At a glance factsheet. 2021 [cited 2021 Mar 22]. https://www.wisc.edu/pdfs/uwmadison-factsheet-jan-2021.pdf
18. University of Wisconsin—Madison. COVID-19 response: Badger pledge for students. Madison (WI): The University; 2020.
19. Centers for Disease Control and Prevention. Interim guidance on duration of isolation and precautions for adults with COVID-19. February 13, 2021 [cited 2021 Mar 31]. https://www.cdc.gov/coronavirus/2019-ncov/hcp/duration-isolation.html
20. Public Health Madison & Dane County. Emergency order #8. July 7, 2020 [cited 2021 Mar 1]. https://publichealthmdc.com/documents/2020-07-07_Order_8.pdf
21. Quick J, Grubaugh ND, Pullan ST, Claro IM, Smith AD, Gangavarapu K, et al. Multiplex PCR method for MinION and Illumina sequencing of Zika and other virus genomes directly from clinical samples. Nat Protoc. 2017;12:1261–76. https://doi.org/10.1038/nprot.2017.066
22. Quick J. nCoV-2019 sequencing protocol v3 (LoCost) version 3. August 25, 2020 [cited 2021 Mar 9]. https://www.protocols.io/view/ncov-2019-sequencing-protocol-v3-locost-bh42j8ye
23. Quick J. nCoV-2019 sequencing protocol v2 (GunIt) version 2. April 9, 2020 [cited 2021 Mar 9]. https://www.protocols.io/view/ncov-2019-sequencing-protocol-v2-bdp7i5rn?version_warning=no
24. Hadfield J, Megill C, Bell SM, Huddleston J, Potter B, Callender C, et al. Nextstrain: real-time tracking of pathogen evolution. Bioinformatics. 2018;34:4121–3. https://doi.org/10.1093/bioinformatics/bty407
25. Sagulenko P, Puller V, Neher RA. TreeTime: maximum-likelihood phylodynamic analysis. Virus Evol. 2018;4:vex042. https://doi.org/10.1093/ve/vex042
26. Centers for Disease Control and Prevention. Coronavirus disease 2019 (COVID-19) 2020 interim case definition, approved August 5, 2020. CSTE position statement: interim-20-ID-02 [cited 2021 Jan 7]. https://ndc.services.cdc.gov/case-definitions/coronavirus-disease-2019-2020-08-05
27. Yamey G, Walensky RP. Covid-19: re-opening universities is high risk. BMJ. 2020;370:m3365. https://doi.org/10.1136/bmj.m3365
28. Centers for Disease Control and Prevention. COVID-19 testing overview. 2021 [cited 2021 Feb 23]. https://www.cdc.gov/coronavirus/2019-ncov/symptoms-testing/testing.html
29. Paltiel AD, Zheng A, Walensky RP. Assessment of SARS-CoV-2 screening strategies to permit the safe reopening of college campuses in the United States. JAMA Netw Open. 2020;3:e2016818. https://doi.org/10.1001/jamanetworkopen.2020.16818
30. University of Wisconsin. What is the testing process for undergraduates living in residence halls for spring semester? Madison (WI): The University; 2021.
31. University of Wisconsin. What is the testing process for undergraduates living off campus for spring semester? Madison (WI): The University; 2021
32. Centers for Disease Control and Prevention. COVID-19 guidance for shared or congregate housing. Last updated December 31, 2020 [cited 2021 Feb 23]. https://www.cdc.gov/coronavirus/2019-ncov/community/shared-congregate-house/guidance-shared-congregate-housing.html
33. Harris JE. Geospatial analysis of the September 2020 coronavirus outbreak at the University of Wisconsin—Madison: did a cluster of local bars play a critical role? National Bureau of Economic Research Working Paper 28132. 2020. [cited 2021 Aug 31]. https://www.nber.org/papers/w28132. https://doi.org/10.3386/w28132
34. Vang KE, Krow-Lucal ER, James AE, Cima MJ, Kothari A, Zohoori N, et al. Participation in fraternity and sorority activities and the spread of COVID-19 among residential university communities—Arkansas, August 21–September 5, 2020. MMWR Morb Mortal Wkly Rep. 2021;70:20–3. https://doi.org/10.15585/mmwr.mm7001a5

Address for correspondence: Dustin Currie, Centers for Disease Control and Prevention, 1600 Clifton Rd NE, Mailstop US1-2, Atlanta, GA 30329-4027, USA; email: pif7@cdc.gov

Probability-Based Estimates of Severe Acute Respiratory Syndrome Coronavirus 2 Seroprevalence and Detection Fraction, Utah, USA

Matthew H. Samore, Adam Looney, Brian Orleans, Tom Greene, Nathan Seegert, Julio C. Delgado, Angela Presson, Chong Zhang, Jian Ying, Yue Zhang, Jincheng Shen, Patricia Slev, Maclean Gaulin, Mu-Jeung Yang, Andrew T. Pavia, Stephen C. Alder

We aimed to generate an unbiased estimate of the incidence of severe acute respiratory syndrome coronavirus 2 (SARS-CoV-2) infection in 4 urban counties in Utah, USA. We used a multistage sampling design to randomly select community-representative participants ≥12 years of age. During May 4–June 30, 2020, we collected serum samples and survey responses from 8,108 persons belonging to 5,125 households. We used a qualitative chemiluminescent microparticle immunoassay to detect SARS-CoV-2 IgG in serum samples. We estimated the overall seroprevalence to be 0.8%. The estimated seroprevalence-to-case count ratio was 2.5, corresponding to a detection fraction of 40%. Only 0.2% of participants from whom we collected nasopharyngeal swab samples had SARS-CoV-2–positive reverse transcription PCR results. SARS-CoV-2 antibody prevalence during the study was low, and prevalence of PCR-positive cases was even lower. The comparatively high SARS-CoV-2 detection rate (40%) demonstrates the effectiveness of Utah's testing strategy and public health response.

By May 2021, >150 million severe acute respiratory syndrome coronavirus 2 (SARS-CoV-2) infections and >3 million deaths from coronavirus disease (COVID-19) had been reported worldwide (*1*). The real infection count likely is much higher but continues to be a point of uncertainty. Case reporting underestimates the total number of SARS-CoV-2 infections because of underdetection of asymptomatic or mildly symptomatic cases and variation in the use and availability of diagnostic testing. Serologic testing provides an independent method to estimate the true cumulative incidence of SARS-CoV-2 infection because it relies on evidence of immune response as an indication of previous infection. Seroprevalence has been touted as a more standardized way to estimate the incidence of SARS-CoV-2 infection across different populations, but inconsistencies in test performance and sampling methods continue to cause challenges for use of seroprevalence.

In May 2020, the University of Utah (Salt Lake City, Utah, USA) launched the Utah Health and Economic Recovery Outreach project, in partnership with state government agencies, to collect community-based data on SARS-CoV-2 infection rates. Our goal was to estimate the cumulative incidence of SARS-CoV-2 infection to benchmark case detection in community populations based on public health surveillance. In addition to measuring SARS-CoV-2 seroprevalence, we collected nasopharyngeal swab samples to concurrently estimate the prevalence of reverse transcription PCR (RT-PCR) positivity. We applied methods of recruitment and analysis to minimize bias and maximize relevance for policymaking. We describe the results of the first phase of the project, which was conducted in the Wasatch Front, the major population center of Utah, comprising a chain of contiguous cities and towns stretched along the Wasatch Mountain Range.

Author affiliation: Veterans Affairs Salt Lake City Health Care System, Salt Lake City, Utah, USA (M.H. Samore); University of Utah, Salt Lake City (M.H. Samore, A. Looney, B. Orleans, T. Greene, N. Seegert, J.C. Delgago, A. Presson, C. Zhang, J. Ying, Y. Zhang, J. Shen, P. Slev, M. Gaulin, M.-J. Yang, A.T. Pavia, S.C. Alder)

DOI: https://doi.org/10.3201/eid2711.204435

Methods

Sampling Design and Participant Recruitment

We conducted serologic survey in 4 counties: Utah, Salt Lake, Davis, and Summit. The total estimated population of the study area is ≈2.2 million, which represents ≈68% of the population of Utah. Overall, 29% of the population is <18 years of age, compared with 22% of the US population (*2*). The fraction of residents of the 4 counties that are non-Hispanic White is 76%, which is higher than the US population of 60%. During March 14–June 30, 2020, the 4 counties reported 17,316 cases of SARS-CoV-2 infection (*3*).

We recruited and enrolled participants during May 4–June 30, 2020. The sampling frame consisted of a list of all residential addresses in the 4 counties curated by the state of Utah. The 657,870 total addresses were grouped hierarchically into 16,677 census blocks, 1,089 census block groups, 389 census tracts, and 229 groups of adjacent tracts, termed tract groups. We categorized tract groups into 15 strata based on combinations of county, ethnicity, median age, and reported positive case count from the Utah Department of Health.

We used 2 address-based probability sampling designs that differed in intensity of recruitment and geographic clustering. Both methods followed a random sampling design. Our primary sampling design included 11,563 addresses that were selected by randomly choosing 26 of the tract groups from the 15 strata, weighted by tract group population. We then selected ≈420 addresses from each tract group by first randomly choosing 30 census block groups per census tract group and then selecting 14 addresses per census block group. The geographic address clustering facilitated recruitment and data collection and followed methods recommended by the Centers for Disease Control and Prevention (https://www.cdc.gov/nceh/casper/sampling-methodology.htm).

Our secondary sampling frame comprised 14,012 addresses. We selected these addresses by proportionately oversampling the same strata as our primary sampling frame and excluding the tract groups selected in our primary sampling frame. The secondary sampling frame enabled us to expand the pool of participants and to broaden the geographic reach within the 4 counties.

To recruit our sample, we sent each address a postcard and a letter encouraging household members to participate. Participants were asked to complete a household survey, and household members ≥12 years of age were invited to take an individual participant survey and to undergo testing for IgG and viral RT-PCR at a specified mobile testing site. In our primary sampling frame, home addresses also were visited by a recruitment field team that attempted ≤3 in-person contacts. All household members who completed the survey and were tested received a $10 gift card as compensation for their time

Each mobile testing site location included 4 sequential drive-through stations. The first station collected basic information about the persons in the vehicle; the second conducted the viral RT-PCR sample via nasopharyngeal swab; the third conducted the IgG test via blood draw; and the last quality-checked participation, provided information about receiving test results, and responded to participant questions. The analyses described here are limited to persons who completed the participant survey and underwent serologic testing.

Laboratory Methods

We analyzed serum specimens by using the SARS-CoV-2 IgG assay (Abbott Laboratories, https://www.abbott.com) on an Architect i2000 instrument (Abbott Laboratories), according to the manufacturer's instructions. The SARS-CoV-2 IgG assay is a qualitative chemiluminescent microparticle immunoassay that detects IgG binding to an undisclosed epitope of the SARS-CoV-2 nucleocapsid protein. The assay relies on an assay-specific calibrator to report a ratio of specimen absorbance to calibrator absorbance. The assay can be interpreted as positive (ratio >1.4) or negative (ratio <1.4). The manufacturer reports a sensitivity of 86.4% (95% CI 65.1%–97.1%) 8–13 days after symptom onset and 100% (95% CI 95.9%–100%) ≥14 days after symptom onset, and a specificity of 99.6% (95% CI 99.1%–99.9%) (*4*,*5*). The manufacturer's estimate of sensitivity ≥14 days after symptom onset was derived from 88 symptomatic patients. However, other studies using this assay have reported lower sensitivities, ranging from 85% to 97%, when used in the general population (*6*–*8*). We observed that 20/24 (83.3%) participants who reported a prior positive SARS-COV-2 test >14 days before we collected serum samples were seropositive. By using a cutoff of 10 days after a prior positive SARS-COV-2, 25/30 (83.3%) participants who reported prior positive tests also were IgG positive. Therefore, we assumed a sensitivity of 83% in our primary analysis.

We used the cobas SARS-CoV-2 assay (Roche Diagnostics, https://www.roche.com) to detect viral RNA in nasopharyngeal swabs, according to the manufacturer's instructions. The cobas SARS-CoV-2 assay detects the nonstructural open reading frame (ORF) 1a/b region unique to SARS-CoV-2 at a limit

of detection of 1,800 copies/mL. All testing was performed at ARUP Laboratories (https://www.aruplab.com), a nonprofit national reference laboratory associated with the University of Utah.

For data analysis, we used a series of steps to account for the sampling design, nonresponse, demographic balance, and the sensitivity and specificity of the serology assay. The University of Utah Institutional Review Board designated this surveillance project nonresearch because it was launched to support public health and governmental response to the COVID-19 pandemic.

Statistical Methods

Sampling Design

We computed sampling design weights to account for varying probabilities of sampling of households (Appendix, https://wwwnc.cdc.gov/EID/article/27/11/20-4435-App1.pdf) (*9*). These weights depended primarily on the ratios of the numbers of sampled households to the total numbers of households within each stratum of the primary and secondary sampling designs (Appendix Tables 1–6). We computed 3 further sets of weights to account for nonresponse at the household, participant, and serology testing levels. We determined household response weights from estimated propensities of household response based on characteristics of the census block group where the household was located and participant response weights from estimated propensities of response by persons within households based on characteristics of the census block group and the primary household respondent. We determined serology response weights from estimated propensities for the provision of a serology sample based on participant survey responses.

We estimated propensities separately in the primary and secondary sampling designs by using nonparametric boosted regression for household and serology response and logistic regression for participant response (Appendix Table 1) (*10*). We used estimated propensities for membership in the primary versus the secondary design to align the secondary sampling design's characteristics to those of the primary sampling design. Multiplication of each of the described weights provided 2 sets of comprehensive weights that accounted for the design and nonresponse for the primary and secondary sampling designs. We then scaled the weights for 2 sampling designs based on the proportions of respondents in the 2 designs to provide a single final set of weights for estimating seroprevalence across the 4-county area. To prevent extreme variation in weights, we truncated weights that were either <10% or >10-fold greater than the median weight. Finally, we used iterative proportional fitting to optimize agreement of the marginal distributions of age, sex, Hispanic ethnicity, and education level between the weighted study sample and the US census data for the 4-county area (*11*).

Data Analysis

We defined the primary sampling units (PSUs) for data analysis by 54 census tracts included in the primary sampling design and mainly by block groups in the secondary sampling design. For Summit County, sampling was performed without clustering at the household level in the secondary sampling frame, so the household served as the PSU. We modeled the relationship of seroprevalence to predictor variables, such as county, demographic and clinical factors, behaviors, and attitudes, by using survey weighted generalized linear models for binary outcomes and assessed variability based on replicate jackknife weights (*12*,*13*). We tested for the presence of a detectable temporal trend in seroprevalence by including calendar time as a continuous variable in models relating seroprevalence to the Utah Department of Health case count. These analyses showed no trend for an effect of calendar time. Hence, we performed analyses for seroprevalence without adjustment for calendar time.

We corrected estimates of seroprevalence for assay error by applying the following formula:

$$\frac{\text{P1} - (1 - \text{specificity})}{\text{sensitivity} + \text{specificity} - 1}$$

where P1 is the estimated prevalence within a given category of a predictor variable provided by the generalized linear models. We then used the parametric bootstrap to account for the sampling error and 95% CI of the manufacturer's estimate of specificity. We estimated the seroprevalence-to-case-count ratio by computing the ratio between the adjusted prevalence estimates we described in the previous section to the weighted average case count rates corresponding to the respondent's ZIP code 10–17 days before the respondent's serology test reported by the Utah Department of Health. The inverse of the ratio of adjusted prevalence and average case counts is the detection fraction, the estimated proportion of the total number of infections that were reported. We performed hypothesis tests comparing prevalence between categories directly on the estimates of seroprevalence without assay error adjustment because assay error adjustment does not affect equality of seroprevalences between subgroups when sensitivity plus specificity is >1.

Results

Participant Characteristics

During May 4–June 30, 2020, we randomly selected 11,563 households for a combined mailed recruitment and home visit and randomly selected another 14,012 households for mailed recruitment only. Altogether, 8,108 persons from 5,125 households completed surveys and testing for SARS-CoV-2 antibodies. Among participants, 5,791 were in the combined home visit and mailed recruitment frame and 2,317 were in the mailed recruitment only frame. The median age of participants was 44 (interquartile range [IQR] 30–62) years; only 9.3% of participants were 12–18 years of age (Tables 1, 2). Overall, 6.6% of participants self-reported ethnicity as Hispanic, compared with 15.3% of the 4-county population based on census data. The source population also differed from participants with respect to age distribution and education level. Accounting for response bias through iterative proportional fitting resolved these differences in county-level marginal distributions.

Estimated Seroprevalence

Among participants, 89 persons from 75 households were seropositive, corresponding to an unadjusted seroprevalence of 1.1% (Table 3). The 4-county seroprevalence adjusted for sampling fraction, nonresponse, and test performance was 0.8% (95% CI 0.1%–1.6%). We estimated adjusted SARS-CoV-2 seroprevalence to be 5.7% (95% CI 1.2%–19.4%) among persons residing in households where the primary language was Spanish and 2.7% (95% CI 0.6%–8.0%) among persons who self-reported as Hispanic; both estimates were significantly greater than the comparator groups ($p = 0.01$ for Spanish as primary language; $p = 0.03$ for self-report as Hispanic) (Table 3). Seroprevalence was 4.6% in Summit County, which includes the ski resort town, Park City, an early infection hot spot in Utah, and was significantly higher than the other counties ($p = 0.03$); the variation in seroprevalence across Utah, Salt Lake, and Davis counties was not statistically different.

Seroprevalence correlated with cumulative incidence estimated on the basis of reported case counts (Table 3). The adjusted seroprevalence was 2.2% in ZIP codes where cumulative incidence calculated from reported cases was >500/100,000 population compared with 0.2% in ZIP codes in where the reported cumulative incidence was ≤200/100,000 population. The overall seroprevalence-to-case count ratio was estimated to be 2.5 (95% CI 0.3–5.0), corresponding to a detected fraction of 0.40. This ratio was not statistically different across the 4 counties.

Other Descriptive Analyses

Among participants, 360 (4.4%) reported contact with a person with diagnosed COVID-19 and 26 (7.2%) of these participants were seropositive (Table 4). Among participants who reported contact with a family member with known SARS-CoV-2 infection, 14.4% were seropositive. In contrast, among 38 persons who reported exposure to SARS-CoV-2 infection in their role as healthcare workers, none were seropositive. Among 62 households with ≥2 members who tested positive, our analysis revealed 53 households with

Table 1. Characteristics of participants and households in a study of SARS-CoV-2 seroprevalence, Utah, United States

Household-level factors	No. (%) participating households	No. (%) participants, n = 8,108
County	n = 5,125	
Davis	1,023 (20)	1,703 (21.0)
Salt Lake	2,695 (52.6)	4,021 (49.6)
Summit, including Park City	283 (5.5)	345 (4.3)
Utah	1,124 (21.9)	2,039 (25.1)
No. participating household members	n = 5,088	
1	1,738 (34.2)	1,027 (12.7)
2	2,277 (44.8)	3,683 (45.4)
3	541 (10.6)	1,307 (16.1)
≥4	532 (10.5)	2,091 (25.8)
No. household members <12 years of age	n = 5,033	
0	3,537 (70.3)	5,407 (67.6)
1	589 (11.7)	1,053 (13.2)
2	499 (9.9)	850 (10.6)
3	239 (4.7)	424 (5.3)
≥4	169 (3.4)	269 (3.4)
Primary language spoken in household	n = 5,053	
English	4,866 (96.3)	7,785 (97.1)
Spanish	132 (2.6)	169 (2.1)
Other	55 (1.1)	61 (0.8)

*Participants completed a survey and had serum collected to test for SARS-CoV-2 IgG. n values indicate number of responses available in that category.
SARS-CoV-2, severe acute respiratory syndrome coronavirus 2.

Table 2. Characteristics of participants in a study of SARS-CoV-2 seroprevalence, Utah, USA*

Characteristics	No. (%) participants, n = 8,108
Sex	
F	4,335 (53.5)
M	3,773 (46.5)
Age, y	
12–<18	755 (9.3)
18–<45	3,366 (41.5)
45–64	2,345 (28.9)
65–74	1,087 (13.4)
≥75	555 (6.8)
Ethnicity, n = 8044	
Hispanic	528 (6.6)
Non-Hispanic	7,516 (93.4)
Race, n = 7,839	
White	7,452 (95.1)
Black or African American	34 (0.4)
American Indian or Alaska Native	32 (0.4)
Asian	159 (2.0)
Native Hawaiian or other Pacific Islander	40 (0.5)
Multiracial	122 (1.6)
Underlying conditions	
Diabetes	508 (6.3)
Hypertension	1,078 (13.3)
Cardiovascular disease	354 (4.4)
Asthma	841 (10.4)
Emphysema	72 (0.9)
Cancer	130 (1.6)
Immunosuppressive therapy	79 (1.0)
Exposure, n = 8,084	
Contact with COVID-19 case	360 (4.5)
Prior testing	
Tested for COVID-19 at any time	716 (8.8)

*Participants completed survey and had serum collected to test for SARS-CoV-2 IgG. n values indicate number of responses available in that category COVID-19, coronavirus disease; SARS-CoV-2, severe acute respiratory syndrome coronavirus 2.

exactly 1 seropositive member and 9 households with ≥1 seropositive member. Among the 123 members of 62 households with SARS-CoV-2–positive residents, 23 (18.7%) participants were seropositive. We assumed that infection for 1 of the infected members of each household was imported and that other household cases were transmissions from the index member of the household; thus, our crude estimate the secondary household attack rate was 12%.

Overall, 798 (9.9%) persons reported having a prior COVID-19 test. Among 30 participants who reported having a positive COVID-19 test ≥14 days before serum collection, 25 (83.3%) were SARS-CoV-2 seropositive; we used that figure to estimate the sensitivity of the serologic assay. Among seropositive participants, 7 (28.0%) reported a prior RT-PCR–positive SARS-CoV-2 test. If we assume a true seroprevalence of 0.8%, assay sensitivity of 83%, and specificity of 99.6%, the corrected point estimate for the detection fraction based on history of a prior positive RT-PCR test is 0.28/0.614 = 0.46, which is close to our estimated detection fraction based on the seroprevalence-to-case count ratio.

Among 6,251 participants from whom a nasopharyngeal swab specimen was collected, 14 (0.2%) had SARS-CoV-2 virus detected by RT-PCR; 9 (64.3%) of those persons were seropositive. The small number of positive RT-PCR tests precluded statistical analysis of factors associated with positivity or adjustment for response bias.

Discussion

By using a statistical sampling frame and adjusting for test performance and non-response, we estimated the prevalence of IgG to SARS-CoV-2 in 4 urban counties in Utah during May–June 2020 to be only 0.8%. Thus, consistent with other community surveys, most of the population lacked immunity to SARS-CoV-2. Comparing seroprevalence to the cumulative incidence of SARS-CoV-2 infection based on case reporting, we found that the estimated ratio of total-to-detected cases was 2.5, corresponding to a detection fraction of 40%. We found participants in Summit County had higher seroprevalence of 4.6%, which is compatible with the extensive outbreak in the resort community of Park City that began in March 2020. Seroprevalence was higher (2.7%) among persons who identified as Hispanic than among those who identified as non-Hispanic (0.5%); seroprevalence was 5.7% among persons who lived in a household where Spanish was the primary language, much higher than the 0.5% seroprevalence among persons who lived in households where English was the primary language. This finding adds to the substantial body of evidence regarding ethnic and racial disparities in the spread of SARS-CoV-2 across populations.

Our estimates of seroprevalence and of the seroprevalence-to-case count ratio are generally lower than has been reported in Utah and elsewhere in the United States during a similar time. Several seroprevalence studies conducted in the United States and other countries have been published (*14*–*24*) and use a variety of assays and sampling methods (*25*). Some studies have relied on convenience samples or did not adequately control for response bias. The specificity of serologic methods for SARS-CoV-2 testing varies widely, which can lead to substantial overestimation in a low-prevalence population (*26*). Not all studies have adjusted for test performance, and the differences in methods make comparisons between studies challenging.

Our project involved random sampling of >25,000 households and used intensive recruiting methods. Our analytical approach accounted for

multiple sources of error, including response bias and imperfect test performance. We also were able to generate an internal estimate of the detection fraction by using self-reported histories of prior RT-PCR test results. After accounting for test error, the estimate of the detection fraction based on participant histories was 0.46, a value that corroborates our population estimate of the detected fraction of 0.40.

We used a serologic test that is reported by the manufacturer to have a specificity at 99.6% (*4*,*5*); however, even at this level of accuracy, statistically accounting for false positive results is necessary given the low population prevalence of IgG to SARS-CoV-2. To better account for the possibility of reduced sensitivity when asymptomatic infections are included (*27*), we assumed a sensitivity of 83% because of an analysis of project participants who reported having had a positive RT-PCR test in the past. We note that our estimate of sensitivity is substantially lower than the manufacturer's estimate of sensitivity of 97.2% (*5*). Because antibody to nucleocapsid protein appears to decrease more rapidly than antibody to the spike protein, our analysis requires us to account for waning immunity (*27*,*28*). Our internal estimate of sensitivity is conditional on the distribution of time between infection and antibody testing for persons reported to be infected in our sample, which enhances its utility for adjusting the estimate of seroprevalence. Of note, among persons who reported having a prior test, 83% of serum samples were collected within 2 months following the previous RT-PCR SARS-CoV-2 test.

With these considerations in mind, our estimate of the detection fraction is substantially higher than what has been reported in other serologic surveys. A study that used residual clinical samples collected during March–May 2020 to measure SARS-CoV-2 antibody at 10 US sites estimated a detection fraction of 0.10 for residents of the country (*17*). That study estimated the seroprevalence in Utah at 2.2% (95% CI 1.2%–3.4%), and those CIs overlap with our estimate. Similarly, our estimate of seroprevalence is lower than what has been reported in most other geographic regions during a comparable period of the pandemic. In a meta-analysis that included 17 studies, the seroprevalence was estimated to be <1% in 5 of the studies examined (*29*). In another study, the projected prevalence of SARS-CoV-2 antibodies was 9.2% in the US adult population, based on an analysis of 28,000

Table 3. Overall and subgroup-specific seroprevalence of participants in a study of SARS-CoV-2 seroprevalence, Utah, USA*

Characteristics	Total	No. (%) seropositive	Adjusted seroprevalence, % (95% CI)†	p value
Overall	8,108	89 (1.1)	0.8 (0.1–1.6)	
County				
Davis	1,703	16 (0.9)	0.1 (0–1.3)	0.06
Salt Lake	4,021	38 (0.9)	0.7 (0–1.8)	
Summit, including Park City	345	10 (2.9)	4.6 (1.0–15.1)	
Utah	2,039	25 (1.2)	1.2 (0.1–3.4)	
Sex				
M	3,773	41 (1.1)	0.7 (0–1.6)	0.65
F	4,293	48 (1.1)	0.9 (0.2–1.9)	
Age, y				
<45	4,119	39 (0.9)	0.9 (0.1–2.1)	0.62
45–64	2,345	31 (1.3)	0.8 (0.1–1.7)	
≥65	1,642	19 (1.2)	0.4 (0–1.4)	
Ethnicity				
Non-Hispanic	7,516	75 (1)	0.5 (0–1.1)	0.03
Hispanic	528	14 (2.7)	2.7 (0.6–8.0)	
Primary language spoken in household				
English	7,785	78 (1)	0.5 (0–1.2)	0.01
Spanish	169	11 (6.5)	5.7 (1.2–19.4)	
No. participants in household				
1	1,027	15 (1.5)	0.7 (0–1.8)	0.60
2	3,683	35 (1)	0.5 (0–1.7)	
≥3	3,398	39 (1.1)	1.0 (0.2–2.3)	
No. participants <12 years of age				
0	5,407	64 (1.2)	0.6 (0–1.3)	0.33
≥1	2,596	20 (0.8)	1.1 (0.1–3)	
Cumulative incidence per 100,000 residents in participant's ZIP code				
<200	3,718	26 (0.7)	0.2 (0–0.9)	0.02
200–500	3,012	34 (1.1)	0.8 (0.1–2.0)	
>500	1,378	29 (2.1)	2.2 (0.6–5.5)	

*Participants completed survey and had serum collected to test for SARS-CoV-2 IgG. COVID-19, coronavirus disease; SARS-CoV-2, severe acute respiratory syndrome coronavirus 2.
†Adjusted for sampling design and test sensitivity (0.83) and specificity (0.996)

Table 4. Relationship between COVID-19 exposures and serologic results of participants in a study of SARS-CoV-2 seroprevalence, Utah, USA*

Exposures	Total	No. (%) seronegative, n = 8,019	No. (%) seropositive, n = 89	% Adjusted seroprevalence (95% CI)†
Contact with diagnosed COVID-19 case	360	334 (92.8)	26 (7.2)	8.5 (3.3–19.5)
Participant's relationship with contact				
Family member	97	83 (85.6)	14 (14.4)	14.8 (4.0–40.8)
Friend	42	38 (90.5)	4 (9.5)	14.0
Healthcare worker‡	38	38 (100)	0 (0)	0.0
Coworker	105	102 (97.1)	3 (2.9)	3.4
Other	78	73 (93.6)	5 (6.4)	3.1 (0.3–12.9)
Reside in household with ≥1 seropositive person	123	100 (81.3)	23 (18.7)	24.9 (10.5–48.7)

*COVID-19, coronavirus disease; SARS-CoV-2, severe acute respiratory syndrome coronavirus 2.
†Adjusted for sampling design and test sensitivity (0.83) and specificity (0.996). Confidence intervals are omitted for subgroups with fewer than 5 seropositive persons.
‡Participant reported that their exposure was related to their work as a healthcare worker.

dialysis patients; in Utah it was 3.1%. Discrepancies between results of other studies and our findings are likely due to our use of probabilistic sampling to reduce bias (*30*).

Our results suggest that Utah's public health response to SARS-COV-2 was effective in case detection. Factors that likely contributed to the success of Utah's approach to case detection include early expansion of access to testing, mobile testing that targeted heavily impacted communities, and a strong commitment to contact tracing and contact testing by the state and local health departments. This conclusion also is supported by our finding that 29% of seropositive persons reported exposure to a known case.

We observed that seropositivity was much more frequent than RT-PCR positivity, a finding that contrasts with selected other studies that combined viral detection and measurement of seroprevalence. For example, among randomly sampled residents of the US state of Indiana, the unadjusted prevalence of a positive RT-PCR was 1.74%, compared with an unadjusted SARS-CoV-2 seroprevalence of 1.01% (*31*). The ratio of prevalence of antibody detection to prevalence of viral detection, as observed in our community survey, suggests that infections were accumulating linearly rather than exponentially during the study period.

One limitation of our study is that it covers the early period of the COVID-19 pandemic, which reflects the cumulative incidence of SARS-CoV-2 infection through mid-June 2020. An updated analysis is needed to examine the secular trend in seroprevalence and determine whether the detection fraction continues to be high. Additional data also will enhance the feasibility of examining possible geographically localized hot spots. Our application of weighting and iterative proportional fitting should minimize nonresponse bias because of ethnicity and other measured factors at each stage of the sampling. However, our analytic approach cannot fully account for all sources of bias, particularly due to unmeasured factors that influenced the decision to participate at the household level. Thus, despite weighting techniques, the generalizability of our results might be limited by residual bias due to nonresponse. Nonetheless, our sampling frame likely reflects population seroprevalence more accurately than convenience-based samples. Recruitment efforts should focus on increasing the ease and appeal of participation of a wide range of demographic and geographic groups, especially for populations that traditionally have lower response rates and have been disproportionately affected by the COVID-19 pandemic.

In conclusion, we used a project design in which we randomly selected all participants, detected SARS-CoV-2 antibodies with a highly specific assay, applied rigorous analytical methods to account for bias and test error, and analyzed survey responses to support population-level inferences. The most distinctive finding in our analysis was that the detection fraction was estimated to be 40%. Further analysis is needed to determine whether this pattern has continued in subsequent months of the COVID-19 pandemic and to assess the factors that influence SARS-CoV-2 transmission and detection. High rates of testing and enhanced case detection are key initial steps for effective public health response.

This article was preprinted at https://www.medrxiv.org/content/10.1101/2020.10.26.20219907v1.

Acknowledgments

We thank Kristina Stratford for project management and for supporting data collection. We thank Elizabeth Rabon, Alicen Bringard, Jeanette Nelson, and Jill Stephenson for managing field operations and for administering the different parts of this project. We thank Carrie Milligan for review and editing of this manuscript.

This project was funded by a State of Utah Cooperative Contract (contract no. AR3473), with support in part from the University of Utah Study Design and Biostatistics Center, which receives funding from the National Center for Research Resources and the National Center for Advancing Translational Sciences, NIH (grant no. UL1TR002538).

About the Author

Dr. Samore chairs the Division of Epidemiology in the Department of Internal Medicine, University of Utah School of Medicine. He also directs the Department of Veterans Affairs IDEAS Center of Innovation in Salt Lake City, Utah. His research interests focus on infectious diseases and biomedical informatics.

References

1. Center for Systems Science and Engineering at Johns Hopkins University. COVID-19 dashboard. 2020 [cited 2021 May 3]. https://coronavirus.jhu.edu/map.html
2. United States Census Bureau. Quick facts 2020 [cited 2020 October 23]. https://www.census.gov/quickfacts/fact/table/US,daviscountyutah,summitcountyutah,utahcountyutah,UT/PST045219
3. Kem C. Gardner Policy Institute of the University of Utah. US Census Bureau estimates for race and Hispanic origin, vintage 2019 [cited 2020 Oct 5]. https://gardner.utah.edu/demographics/current-census-bureau-estimates
4. Abbott Laboratories Diagnostics Division. SARS-CoV-2 IgG reagent kit for use with Architect, June 2020 [package insert] [cited 2021 May 3]. https://www.fda.gov/media/137383/download
5. Abbott Laboratories Diagnostics Division. SARS-CoV-2 IgG calibrator kit for use with Architect, April 2020 [package insert] [cited 2021 May 3]. https://www.henryschein.com/assets/Medical/Abbott%20IFU%20-%20Calibration.pdf
6. Perkmann T, Perkmann-Nagele N, Breyer MK, Breyer-Kohansal R, Burghuber OC, Hartl S, et al. Side by side comparison of three fully automated SARS-CoV-2 antibody assays with a focus on specificity. Clin Chem. 2020;66:1405–13. https://doi.org/10.1093/clinchem/hvaa198
7. Theel ES, Harring J, Hilgart H, Granger D. Performance characteristics of four high-throughput immunoassays for detection of IgG antibodies against SARS-CoV-2. J Clin Microbiol. 2020;58:e01243-20. https://doi.org/10.1128/JCM.01243-20
8. Bryan A, Pepper G, Wener MH, Fink SL, Morishima C, Chaudhary A, et al. Performance characteristics of the Abbott Architect SARS-CoV-2 IgG assay and seroprevalence in Boise, Idaho. J Clin Microbiol. 2020;58:e00941-20. https://doi.org/10.1128/JCM.00941-20
9. Valliant R, Dever JA, Kreuter F. Practical tools for designing and weighting survey samples. New York: Springer; 2013.
10. Ridgeway G, McCaffrey D, Morral A, Burgette L, Griffin BA. Toolkit for weighting and analysis of nonequivalent groups: a tutorial for the twang package. Santa Monica (CA, USA): RAND Corporation; 2017 [cited 2021 May 3]. https://www.rand.org/pubs/tools/TL136z1.html
11. Lumley T. Post-stratification, raking and calibration. In: Complex surveys: a guide to analysis using R, volume 565. Hoboken (NJ, USA): John Wiley & Sons; 2011. p. 135–56.
12. Shao J, Tu D. The jackknife and bootstrap. New York: Springer-Verlag Inc; 1995.
13. Lumley T. Complex surveys: a guide to analysis using R, vol. 565. Hoboken (NJ, USA): John Wiley & Sons; 2011.
14. Bendavid E, Mulaney B, Sood N, Shah S, Ling E, Bromley-Dulfano R, et al. COVID-19 antibody seroprevalence in Santa Clara County, California. Int J Epidemiol. 2021;50:410–9. https://doi.org/10.1093/ije/dyab010
15. Biggs HM, Harris JB, Breakwell L, Dahlgren FS, Abedi GR, Szablewski CM, et al.; CDC Field Surveyor Team. Estimated community seroprevalence of SARS-CoV-2 antibodies—two Georgia Counties, April 28–May 3, 2020. MMWR Morb Mortal Wkly Rep. 2020;69:965–70. https://doi.org/10.15585/mmwr.mm6929e2
16. Flannery DD, Gouma S, Dhudasia MB, Mukhopadhyay S, Pfeifer MR, Woodford EC, et al. SARS-CoV-2 seroprevalence among parturient women in Philadelphia. Sci Immunol. 2020;5:eabd5709. https://doi.org/10.1126/sciimmunol.abd5709
17. Havers FP, Reed C, Lim T, Montgomery JM, Klena JD, Hall AJ, et al. Seroprevalence of Antibodies to SARS-CoV-2 in 10 Sites in the United States, March 23–May 12, 2020. JAMA Intern Med. 2020 Jul 21 [Epub ahead of print]. https://doi.org/10.1001/jamainternmed.2020.4130
18. Self WH, Tenforde MW, Stubblefield WB, Feldstein LR, Steingrub JS, Shapiro NI, et al.; CDC COVID-19 Response Team; IVY Network. Seroprevalence of SARS-CoV-2 among frontline health care personnel in a multistate hospital network—13 academic medical centers, April–June 2020. MMWR Morb Mortal Wkly Rep. 2020;69:1221–6. https://doi.org/10.15585/mmwr.mm6935e2
19. Sood N, Simon P, Ebner P, Eichner D, Reynolds J, Bendavid E, et al. Seroprevalence of SARS-CoV-2–specific antibodies among adults in Los Angeles County, California, on April 10–11, 2020. JAMA. 2020;323:2425–7. https://doi.org/10.1001/jama.2020.8279
20. Sutton M, Cieslak P, Linder M. Notes from the field: seroprevalence estimates of SARS-CoV-2 infection in convenience sample—Oregon, May 11–June 15, 2020. MMWR Morb Mortal Wkly Rep. 2020;69:1100–1. https://doi.org/10.15585/mmwr.mm6932a4
21. Percivalle E, Cambiè G, Cassaniti I, Nepita EV, Maserati R, Ferrari A, et al. Prevalence of SARS-CoV-2 specific neutralising antibodies in blood donors from the Lodi Red Zone in Lombardy, Italy, as at 06 April 2020. Euro Surveill. 2020;25:2001031. https://doi.org/10.2807/1560-7917.ES.2020.25.24.2001031
22. Pollán M, Pérez-Gómez B, Pastor-Barriuso R, Oteo J, Hernán MA, Pérez-Olmeda M, et al.; ENE-COVID Study Group. Prevalence of SARS-CoV-2 in Spain (ENE-COVID): a nationwide, population-based seroepidemiological study. Lancet. 2020;396:535–44. https://doi.org/10.1016/S0140-6736(20)31483-5
23. Stringhini S, Wisniak A, Piumatti G, Azman AS, Lauer SA, Baysson H, et al. Seroprevalence of anti-SARS-CoV-2 IgG antibodies in Geneva, Switzerland (SEROCoV-POP): a population-based study. Lancet. 2020;396:313–9. https://doi.org/10.1016/S0140-6736(20)31304-0
24. Xu X, Sun J, Nie S, Li H, Kong Y, Liang M, et al. Seroprevalence of immunoglobulin M and G antibodies against SARS-CoV-2 in China. Nat Med. 2020;26:1193–5. https://doi.org/10.1038/s41591-020-0949-6
25. Shook-Sa BE, Boyce RM, Aiello AE. Estimation without representation: early severe acute respiratory syndrome coronavirus 2 seroprevalence studies and the path forward. J Infect Dis. 2020;222:1086–9. https://doi.org/10.1093/infdis/jiaa429

26. Sempos CT, Tian L. Adjusting coronavirus prevalence estimates for laboratory test kit error. Am J Epidemiol. 2020;190:109–15. https://doi.org/10.1093/aje/kwaa174
27. Long QX, Tang XJ, Shi QL, Li Q, Deng HJ, Yuan J, et al. Clinical and immunological assessment of asymptomatic SARS-CoV-2 infections. Nat Med. 2020;26:1200–4. https://doi.org/10.1038/s41591-020-0965-6
28. Peluso MJ, Takahashi S, Hakim J, Kelly JD, Torres L, Iyer NS, et al. SARS-CoV-2 antibody magnitude and detectability are driven by disease severity, timing, and assay. Sci Adv. 2021;7:eabh3409. https://doi.org/10.1126/sciadv.abh3409
29. Byambasuren O, Dobler CC, Bell K, Rojas DP, Clark J, McLaws ML, et al. Comparison of seroprevalence of SARS-CoV-2 infections with cumulative and imputed COVID-19 cases: systematic review. PLoS One. 2021;16:e0248946. https://doi.org/10.1371/journal.pone.0248946
30. Anand S, Montez-Rath M, Han J, Bozeman J, Kerschmann R, Beyer P, et al. Prevalence of SARS-CoV-2 antibodies in a large nationwide sample of patients on dialysis in the USA: a cross-sectional study. Lancet. 2020;396:1335–44. https://doi.org/10.1016/S0140-6736(20)32009-2
31. Menachemi N, Yiannoutsos CT, Dixon BE, Duszynski TJ, Fadel WF, Wools-Kaloustian KK, et al. Population point prevalence of SARS-CoV-2 infection based on a statewide random sample—Indiana, April 25–29, 2020. MMWR Morb Mortal Wkly Rep. 2020;69:960–4. https://doi.org/10.15585/mmwr.mm6929e1

Address for correspondence: Matthew H. Samore, University of Utah 50 N Medical Dr, Salt Lake City, UT 84132, USA; email: matthew.samore@hsc.utah.edu

Seroprevalence of SARS-CoV-2–Specific Antibodies among Quarantined Close Contacts of COVID-19 Patients, Faroe Islands, 2020

Maria Skaalum Petersen, Marnar Fríðheim Kristiansen, Halla Weihe Reinert, Jógvan Páll Fjallsbak, Debes Hammershaimb Christiansen, Shahin Gaini, Bjarni á Steig, Lars Fodgaard Møller, Marin Strøm, Pál Weihe

Close contacts of coronavirus disease (COVID-19) patients are at high risk for severe acute respiratory syndrome 2 (SARS-CoV-2) infection. We assessed the seroprevalence of SARS-CoV-2–specific antibodies among quarantined close contacts of COVID-19 patients in the Faroe Islands. We invited quarantined close contacts of COVID-19 index patients identified during March 3–April 22, 2020, to participate in this study; 584 (81%) contacts consented and underwent serologic testing. Among the 584 participants, 32 (5.5%) were seropositive for total antibody against SARS-CoV-2. Household and young or elderly contacts had higher risk for seropositivity than other contacts.We found a secondary attack rate of 19.2%. Seroprevalence among close contacts was almost 10-fold higher than among the general population of the Faroe Islands. Regularly testing household close contacts of COVID-19 patients might help track the transmission of SARS-CoV-2.

Reverse transcription PCR (RT-PCR) is a standard tool for diagnosing severe acute respiratory syndrome coronavirus 2 (SARS-CoV-2) infection. However, different testing strategies might cause wide variation in the number of identified subclinical and asymptomatic cases, which could remain undetected (*1*). In May 2020, the Faroe Islands, an autonomous country that is part of the kingdom of Denmark with a population of 52,554 persons, had a 0.6% seroprevalence of antibodies against SARS-CoV-2 (*2*), among the lowest reported seroprevalences worldwide (*3*,*4*). This low seroprevalence is probably influenced by large-scale testing in the Faroes (*5*,*6*). However, the study also identified a few previously undetected cases, implying that persons had been infected without knowing and without spreading the contagion (*2*).

Since the identification of the first imported case of coronavirus disease (COVID-19) in the Faroe Islands on March 3, 2020, the territory has complied with World Health Organization recommendations to use an active suppression strategy focusing on testing and isolating patients and their close contacts. Accordingly, all close contacts of COVID-19 patients in the Faroe Islands were advised to quarantine for 2 weeks (*5*). In the Faroe Islands, the first wave of the COVID-19 pandemic ended on April 22, 2020; no local cases were detected until August 3, 2020, when a second surge began (*6*). During the first wave, the Faroe Islands' per capita testing rates were among the highest in the world. The seroprevalence study showed that, perhaps because of low levels of community transmission, few cases remained undetected (*2*). As a result, this context provides a unique opportunity to investigate the transmission dynamics of SARS-CoV-2 using serologic tests.

SARS-CoV-2 is highly contagious. Family members and other close contacts of COVID-19 patients are at higher risk for SARS-CoV-2 infection, potentially furthering the transmission of disease (*7*). Most studies estimating the secondary attack rate of

Author affiliations: University of the Faroe Islands, Tórshavn, Faroe Islands (M.S. Petersen, M.F. Kristiansen, S. Gaini, M. Strøm, P. Weihe); The Faroese Hospital System, Tórshavn (M.S. Petersen, H.W. Reinert, P. Weihe); National Hospital of the Faroe Islands, Tórshavn (M.F. Kristiansen, S. Gaini, B. á Steig); COVID-19 Task Force, Ministry of Health, Tórshavn (M.F. Kristiansen, B. á Steig); Faroese Food and Veterinary Authority, Tórshavn (J.P. Fjallsbak, D.H. Christiansen); Odense University Hospital, Odense, Denmark (S. Gaini); University of Southern Denmark, Odense (S. Gaini); Chief Medical Officer Office, Tórshavn (L.F. Møller); Statens Serum Institut, Copenhagen, Denmark (M. Strøm)

DOI: https://doi.org/10.3201/eid2711.204948

SARS-CoV-2 use RT-PCR, not serologic testing (*8*–*13*). One review of 22 studies from 10 countries estimated an overall household secondary attack rate of 17.1% (95% CI 13.7%–21.2%) (*8*), whereas another review found a pooled rate of 27% (95% CI 21%−32%) (*9*). Studies assessing the seroprevalence among close contacts, whether as a focus group or as part of national sample, have documented higher seroprevalences among close contacts than among persons who had not been in contact with patients who had suspected or confirmed COVID-19. A study in Singapore reported that 5.5% of household, 2.9% of work, and 2.1% of social contacts of COVID-19 patients were seropositive (*13*), whereas a study in Norway found that 31% of close contacts were seropositive (*14*). A large national serosurvey in England reported seroprevalences of 18.8% among those who had been in close contact with a confirmed COVID-19 patient and 16.9% among those who had been in contact with a suspected COVID-19 patient, compared with 4.3% among other participants (*15*). In addition, a nationwide population-based study in Spain reported seroprevalences of 31.4% among household members, 13.2% among noncohabitating family members or friends, and 10.6% among coworkers of COVID-19 patients (*16*). We assessed seroprevalence among close contacts of persons with COVID-19 in the Faroe Islands during the first wave of the pandemic in March and April 2020.

Methods

Data Collection

In this retrospective cohort study, we invited all close contacts of the 187 patients with confirmed COVID-19 in the Faroe Islands (crude prevalence 0.4%; https://corona.fo) during March 3–April 22, 2020. No local transmission occurred for the next 104 days, April 23–August 3, 2020 (*5*,*6*).

During this initial outbreak period, contact tracing was conducted by the Chief Medical Officer Office in the Faroes (Tórshavn, Faroe Islands), which communicated with all close contacts and requested that contacts quarantine for 14 days from the time of exposure. Close contacts of COVID-19 patients during the 48 hours before symptom onset, or of asymptomatic persons during the ≥48 hours before diagnosis, were traced. Household members and contacts who were within 2 meters of an infected person for ≥15 minutes, who had direct physical contact or provided caregiving without using personal protective equipment, or who had similar exposures, were defined as close contacts.

All infected persons were asked to avoid contact with other persons in their household and to use separate bathrooms. Close contacts also were asked to self-quarantine and to avoid contact with other members of the household. Most patients and close contacts could successfully self-quarantine, except for those in households with small children. When patients or contacts were unable to adequately separate from household members, hotel rooms were offered free of charge by the government.

During their quarantine periods, close contacts were interviewed by telephone to monitor potential onset of symptoms (*5*). RT-PCR, which required a physician's referral, was not used as a criterion for the end of quarantine. Only symptomatic contacts were tested for SARS-CoV-2 infection, although some asymptomatic contacts were also tested. Thus, no routine RT-PCR of all close contacts occurred during their quarantines.

The Chief Medical Officer's Office emailed a participation request to all 854 close contacts of COVID-19 patients identified during March 3–April 22, 2020. Among the 854 close contacts, 132 had tested positive for SARS-CoV-2 infection by PCR; as a result, 722 contacts were eligible to participate in this study (Figure).

Participants gave informed consent to provide a blood sample and answer a short questionnaire. The questionnaire asked about demographic information, smoking habits, and medical history, as well as their experience in quarantine. For example, the questionnaire inquired whether participants had been tested by RT-PCR, whether they had experienced symptoms during quarantine, if other members of the household had also been quarantined, and whether they knew the identity of the infected person with whom they had contact. We used these data to classify all participants as household, workplace, or other (e.g., single event, social, or noncohabitating family) contacts. In total, 82 (14%) participants could not be classified on the basis of available data. We collected blood samples and administered questionnaires mainly during May 27–July 14, 2020; we also collected data from 3 participants earlier in May 2020 and 4 participants later in August and September 2020. No local cases were diagnosed in the Faroes during April 23–August 3, 2020. We telephoned seropositive participants about their results and asked them to recall symptoms experienced during the quarantine, which we registered alongside data from the telephone interviews conducted during quarantine. Parents responded on behalf of children <18 years of age. We used serum samples to determine patient serologic status by the

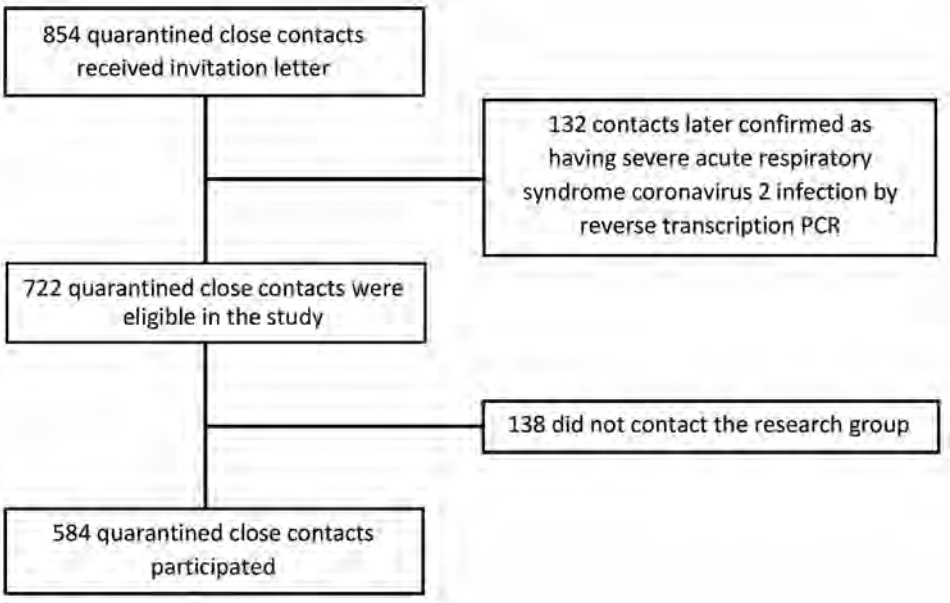

Figure. Recruitment of quarantined close contacts of coronavirus disease patients for study of seroprevalence of severe acute respiratory syndrome coronavirus 2–specific antibodies, Faroe Islands, 2020.

commercially available Wantai SARS-CoV-2 Ab ELISA kit (Beijing Wantai Biologic Pharmacy Enterprise, http://www.ystwt.cn), according to the manufacturer's instructions.

Informed consent was obtained from all participants. The study was approved by the Faroese Ethical Committee and the Data Protection Agency.

Statistical Analysis

We estimated the crude seroprevalence by dividing the total number of seropositive cases by the total number of close contacts. We calculated categorical variables as percentages and continuous variables as means and SDs. We estimated 95% CIs for crude prevalence using exact binomial models. We adjusted for test performance as reported by independent evaluation (*17*) (sensitivity [96.7%, 95% CI 92.4%–98.6%] and specificity [99.5%, 95% CI 98.7%–99.8%]) by using bootstrap methods (*18*). To investigate possibly associated factors, we conducted regression analysis by using a binary outcome of seropositivity with the covariates of sex, age group (0–9, 10–17, 18–34, 35–49, 50–66, >67 years), history of smoking (ever/never), daily medication use (yes/no), chronic diseases (yes/no), and type of contact (household, workplace, other). We found that only contact type and age group were statistically significant; we included these covariates in the final model. We used SPSS Statistics 25.0 (IBM, https://www.ibm.com) for the analysis.

Results

During March 3–April 22, 2020 in the Faroe Islands, 854 close contacts of COVID-19 patients were identified and quarantined, including 132 who were later confirmed to have SARS-CoV-2 infection. As a result, 722 close contacts that had not tested positive by RT-PCR were eligible for participation in this study (Figure); 584 participated, a participation rate of 80.9%. The mean participant age was 36 years (range 0–84 years), and 58% were women. Most participants were in the younger age groups; only 5.5% were >67 years of age (Table 1).

A total of 32 (5.5% [exact binomial 95% CI 3.8%–7.7%]) persons, comprised of 17 women and 15 men who had not previously tested positive by RT-PCR, were seropositive for total antibody against SARS-CoV-2. After adjustment for test sensitivity and specificity, we calculated the prevalence of SARS-CoV-2–specific antibodies as 5.3% (95% CI 3.5%–7.5%). A total of 43.8% of the seropositive close contacts retrospectively reported symptoms, mainly fever, running nose, and loss of taste or smell. Most seropositive participants were in the youngest age group (0–9 years, mean 4.5 years, range 1.4–9.6 years) (Table 2). Among seropositive participants, 21 had received negative RT-PCR results during their quarantine; 11 participants recalled symptoms, whereas 10 did not. The other 11 seropositive participants did not have RT-PCR during quarantine, of whom 3 retrospectively recalled symptoms. Median time between quarantine and RT-PCR was 0 days (range –1 to 15 days); 11 participants had RT-PCR upon or before going into quarantine. RT-PCR was most prevalent among the youngest age group, of which all 8 participants had RT-PCR (Table 2). The presence of symptoms was not significantly different among the age groups ($p = 0.9$).

Table 1. Demographic and clinical characteristics of 584 quarantined close contacts of coronavirus disease patients in study of seroprevalence of SARS-CoV-2–specific antibodies, Faroe Islands, 2020*

Characteristic	Close contacts			p value†
	Total	Seronegative	Seropositive	
Total	584 (100.0)	552 (100.0)	32 (100.0)	
Sex				0.8
F	339 (58.0)	321 (58.2)	17 (53.1)	
M	245 (42.0)	231 (41.8)	15 (46.9)	
Mean age, y (SD) [range]	36.5 (20.2) [0.2–83.8]	37.0 (19.9) [0.2–81.7]	28.1 (24.0) [1.4–83.8]	0.02
Age group, y				<0.01
0–9	69 (11.8)	61 (11.1)	8 (25.0)	
10–17	68 (11.6)	62 (11.2)	6 (18.8)	
18–34	134 (22.9)	125 (22.6)	9 (28.1)	
35–49	131 (22.4)	128 (23.2)	3 (9.4)	
50–66	150 (25.7)	148 (26.8)	2 (6.3)	
>67	32 (5.5)	28 (5.1)	4 (12.5)	
Smoking status‡				0.1
Active	93 (16.7)	92 (17.4)	1 (3.6)	
Occasional	41 (7.3)	40 (7.5)	1 (3.6)	
Former	127 (22.8)	121 (22.8)	6 (21.4)	
Never	297 (53.2)	277 (52.3)	20 (71.4)	
Daily medication use§				0.6
Yes	145 (27.8)	137 (27.6)	8 (32.0)	
No	376 (72.2)	359 (72.4)	17 (68.0)	
Self-reported chronic diseases‡				0.06
Yes	278 (49.8)	268 (50.6)	10 (35.7)	
No	280 (50.2)	262 (49.4)	18 (64.3)	
Had PCR during quarantine¶				0.2
Yes	263 (48.3)	249 (47.8)	21 (65.6)	
No	281 (51.7)	272 (52.2)	11 (34.4)	
Had symptoms during quarantine#				0.7
Yes	116 (21.4)	112 (21.6)	14 (43.8)	
No	345 (63.5)	327 (63.1)	18 (56.3)	
Not sure	82 (15.1)	79 (15.3)	0	
Had other family members in quarantine**				0.2
No	120 (21.8)	118 (22.5)	2 (7.4)	
Yes, together	373 (67.7)	352 (67.2)	21 (77.8)	
Yes, separated	58 (10.5)	54 (10.3)	4 (14.8)	
Type of contact††				<0.01
Household	145 (28.9)	125 (26.5)	20 (64.5)	
Workplace	184 (36.7)	179 (38.0)	5 (16.1)	
Other	173 (34.5)	167 (35.5)	6 (19.4)	

*Values are no. (%) except as indicated. SARS-CoV-2, severe acute respiratory syndrome coronavirus 2.
†p values determined by χ^2 test for categorical variables or analysis of variance for continuous variables.
‡Questionnaire data missing for 26 quarantined close contacts, including 4 seropositive contacts.
§Questionnaire data missing for 63 quarantined close contacts, including 7 seropositive contacts.
¶Questionnaire data missing for 40 quarantined close contacts, including 9 seropositive contacts. However, all seropositive patients were asked about PCR; as a result, values do not add up.
#Questionnaire data missing for 41 quarantined close contacts, including 7 seropositive contacts. However, all seropositive patients were asked about symptoms; as a result, values do not add up.
**Questionnaire data missing for 33 quarantined close contacts, including 5 seropositive contacts.
††Questionnaire data missing for 82 quarantined close contacts, including 1 seropositive contact.

According to the multivariable logistic regression analysis, type of contact (p<0.01) and age group (p = 0.02) were significantly associated with seropositivity. The risk for seropositivity was significantly higher for household contacts compared with other contacts (adjusted odds ratio [aOR] 5.4, 95% CI 1.9–15.2). We did not find a statistically significant difference for workplace contacts compared with other contacts (p = 0.8). Overall, age was significantly associated with seropositivity (p = 0.02). Most age groups had lower aORs than the youngest age group (0–9 years), although these associations were statistically significant only for the 35–49-year (aOR 0.18, 95% CI 0.04–0.9) and 50–66-year (aOR, 95% CI 0.03–0.8) age groups. Participants >67 years of age had an increased aOR compared with the youngest age group; however, this association was not statistically significant (aOR CI 0.6–9.9).

In this study, we identified 32 secondary SARS-CoV-2 infections by later serologic assay in addition to the 132 identified through initial RT-PCR, indicating a secondary attack rate of 19.2%. Most (67.5%) seropositive persons had been in quarantine with their families. In total, 65% of seropositive persons were

infected by household members; when including noncohabitating close family members, this total rose to 71%. The other persons were infected by extended family, workplace, or social contacts. We identified 3 sibling pairs, 2 sets of spouses, and 3 parent–child pairs among the seropositive persons.

Discussion

In this retrospective cohort study of close contacts of COVID-19 patients, we found a 5.5% seropositivity rate among contacts who were not previously identified as positive by RT-PCR. Seroprevalence was highest among household contacts. We found the highest seropositivity rate among children who were infected by their parents. The risk for seropositivity among household contacts was 5-fold that of the risk posed by other close contacts, probably because household members might have closer and more prolonged interactions than work or social contacts. In total, 56% of secondary infections were asymptomatic.

The rapid spread of COVID-19 is partly attributable to transmission by asymptomatic or presymptomatic persons; many of these cases remain undetected because patients might not seek healthcare or undergo testing (*19*). As a result of the large-scale testing and tracing protocols used in the Faroe Islands, the risk for transmission from persons with undetected cases is probably low. A study of 1,075 randomly selected persons from the Faroe Islands in April 2020 found a 0.6% seropositivity rate (exact binomial 95% CI 0.2%–1.2%), which corresponds to 313 COVID-19 patients (*2*), somewhat higher than the observed 0.4% crude prevalence of confirmed cases in the Faroe Islands [https://corona.fo]). Our results for close contacts of patients with confirmed COVID-19 are in accordance with the seroprevalence study (*2*) indicating the existence of some undetected (i.e., not documented in the official records) cases of SARS-CoV-2 infection in the Faroe Islands. Our results highlight the importance of tracing close contacts, who have a much higher seroprevalence than the general population, despite a high proportion of asymptomatic seropositive persons. These findings underscore that testing only symptomatic contacts will miss infections and underestimate the true number of cases. In addition, we emphasize that a negative RT-PCR result might not rule out SARS-CoV-2 infection in a household contact. The close contacts who underwent RT-PCR were tested at a median 0 days (range −1 to 15 days) from start of quarantine (Table 2), possibly indicating that most patients were tested before symptoms developed. Because most of the seropositive contacts in this study were infected by household members, our findings emphasize the importance of isolating infected persons.

Our overall prevalence estimate is lower than that of a study comprising 100,000 participants in England, which found an 18.8% (742/3,946) seroprevalence among those who had unspecified contact with a COVID-19 patient (*15*). Our estimate is more comparable with that of a study in Singapore that found a 5.5% (29/524) seroprevalence among household contacts who did not have a COVID-19 diagnosis (*13*). In a seroprevalence study of household members of COVID-19 outpatients in Norway, Cox et al. (*14*) found that 24/77 (31%) household members were seropositive 6 weeks after the index patient had first tested positive by RT-PCR. Similarly, a study of 61,075 participants in Spain found a 10.6% seroprevalence among coworkers, compared with 31.4% among household members of COVID-19 patients (*16*). These prevalence estimates are higher than our overall prevalence of 5.5% among close contacts who were not previously identified as positive by RT-PCR. However, comparing seroprevalence studies can be challenging because of differences in the nature and closeness of contacts, classification of contact types, methods of measuring antibodies, and characteristics of eligible study participants. In addition, the level of community transmission in each country would affect prevalence.

Table 2. Self-reported prevalence of symptoms and RT-PCR among 32 seropositive quarantined close contacts of coronavirus disease patients in study of seroprevalence of SARS-CoV-2–specific antibodies, by age, Faroe Islands, 2020*

Age, y	Total no. contacts	Had symptoms in quarantine	RT-PCR conducted	Mean days from start of quarantine to first RT-PCR (SD)	Median days from start of quarantine to first RT-PCR (range)
0–9	8	6 (75.0)	8 (100.0)†	5.5 (5.5)	6.0 (0–15)
10–17	6	0	4 (66.7)	7.0 (4.8)	8.5 (0–11)
18–34	9	5 (55.6)	3 (33.3)‡	0.3 (0.6)	0 (0–1)
35–49	3	1 (33.3)	3 (100.0)§	0.7 (2.1)	0 (–1 to 3)
50–66	2	1 (50.0)	1 (50.0)	0	0
>67	4	1 (25.0)	2 (50.0)	0	0

*Values are no. (%) except as indicated. RT-PCR, reverse transcription PCR; SARS-CoV-2, severe acute respiratory syndrome coronavirus 2.
†Three contacts had 2 RT-PCRs.
‡One contact had 2 RT-PCRs and 1 had 4 RT-PCRs.
§One contact had 2 RT-PCRs.

Among the 32 seropositive persons we identified, 21 had tested negative by RT-PCR, including 11 (52.4%) who had reported symptoms. The sensitivity of RT-PCR is dependent on multiple factors, primarily the presence of viral RNA on the test swab, which can vary by swabbing technique and whether viral RNA is present at the anatomic site of the test. Therefore, the timing of testing in relation to infection onset is critical. Among participants who underwent RT-PCR, most were tested during the early stage of quarantine, probably before symptom onset, and thus perhaps also before infection onset (e.g., among contacts who were in quarantine with the infected family member), which might explain their negative RT-PCR results (Table 2). In addition, many of the quarantined close contacts who were tested by RT-PCR were young children, in whom collecting adequate swab samples might be difficult.

The major strengths of this study are its nationwide nature, in which all close contacts of confirmed COVID-19 patients from the first wave in the Faroe Islands were directly contacted, and the high participation rate. As a result, the likelihood of selection bias is low. Because the Faroe Islands eliminated COVID-19 for 104 days after the last patient in this wave was identified, there was little risk for exposure from sources other than the index cases.

One limitation of our study is that contacts were asked retrospectively about symptoms during quarantine, introducing the possibility for recall bias. The risk for bias is especially relevant for children, whose questionnaires were answered by parents. However, because most index cases occurred in a family member, parents were probably vigilant for potential symptoms in children. Another limitation might be the classification of participants as household, workplace, or other contacts. Because this classification was based on whether participants knew the identity of the index patient, this measure might be imprecise. However, we were able to classify most participants into 3 groups on the basis of available information. We found that the primary exposure route is within families, and we believe this information is valuable, even if the data might be flawed. Finally, RT-PCR was not routinely conducted for quarantined persons. Because symptomatic persons were probably prioritized for RT-PCR, this selection might have introduced bias.

In conclusion, our study found that seroprevalence among close contacts of COVID-19 patients is higher than that among the general population. Close contacts, especially household members, of COVID-19 patients are at higher risk for infection. Thus, routinely testing household contacts of COVID-19 patients, regardless of symptoms, might improve detection of SARS-CoV-2 infection. Our results also indicate that close contacts should maintain quarantine even if they receive negative RT-PCR results early in quarantine.

Acknowledgments

We thank all the participants and the technicians who drew blood samples. We also thank the staff at the Department of Occupational Medicine and Public Health in The Faroese Hospital System, the Chief Medical Officer Office, and the Faroese Food and Veterinary Authority for assistance throughout the project. We thank Bodil H. Heimustovu for assistance with data curation.

The project is funded by the special COVID-19 funding from the Faroese Research Council.

About the Author

Dr. Petersen is an associate professor at the University of the Faroe Islands, senior researcher at The Faroese Hospital System, and head of Centre of Health Sciences, University of the Faroe Islands. Her primary research interests include epidemiology and coronavirus disease.

References

1. Meyerowitz EA, Richterman A, Gandhi RT, Sax PE. Transmission of SARS-CoV-2: a review of viral, host, and environmental factors. Ann Intern Med. 2021;174:69–79. https://doi.org/10.7326/M20-5008
2. Petersen MS, Strøm M, Christiansen DH, Fjallsbak JP, Eliasen EH, Johansen M, et al. Seroprevalence of SARS-CoV-2–specific antibodies, Faroe Islands. Emerg Infect Dis. 2020;26:2760–3. https://doi.org/10.3201/eid2611.202736
3. Arora RK, Joseph A, Van Wyk J, Rocco S, Atmaja A, May E, et al. SeroTracker: a global SARS-CoV-2 seroprevalence dashboard. Lancet Infect Dis. 2021;21:e75–6. https://doi.org/10.1016/S1473-3099(20)30631-9
4. Rostami A, Sepidarkish M, Leeflang MMG, Riahi SM, Nourollahpour Shiadeh M, Esfandyari S, et al. SARS-CoV-2 seroprevalence worldwide: a systematic review and meta-analysis. Clin Microbiol Infect. 2021;27:331–40. https://doi.org/10.1016/j.cmi.2020.10.020
5. Kristiansen MF, Heimustovu BH, Borg SÁ, Mohr TH, Gislason H, Møller LF, et al. Epidemiology and clinical course of first wave coronavirus disease cases, Faroe Islands. Emerg Infect Dis. 2021;27:749–58. https://doi.org/10.3201/eid2703.202589
6. Strøm M, Kristiansen MF, Christiansen DH, Weihe P, Petersen MS. Elimination of COVID-19 in the Faroe Islands: effectiveness of massive testing and intensive case and contact tracing. The Lancet Regional Health—Europe. 2021;1:10011.
7. Ye F, Xu S, Rong Z, Xu R, Liu X, Deng P, et al. Delivery of infection from asymptomatic carriers of COVID-19 in a familial cluster. Int J Infect Dis. 2020;94:133–8. https://doi.org/10.1016/j.ijid.2020.03.042
8. Fung HF, Martinez L, Alarid-Escudero F, Salomon JA, Studdert DM, Andrews JR, et al.; SC-COSMO Modeling

Group. The household secondary attack rate of severe acute respiratory syndrome coronavirus 2 (SARS-CoV-2): a rapid review. Clin Infect Dis. 2020 Oct 12 [Epub ahead of print]. https://doi.org/10.1093/cid/ciaa1558
9. Lei H, Xu X, Xiao S, Wu X, Shu Y. Household transmission of COVID-19-a systematic review and meta-analysis. J Infect. 2020;81:979–97. https://doi.org/10.1016/j.jinf.2020.08.033
10. Chen Y, Wang AH, Yi B, Ding KQ, Wang HB, Wang JM, et al. Epidemiological characteristics of infection in COVID-19 close contacts in Ningbo city [in Chinese]. Zhonghua Liu Xing Bing Xue Za Zhi. 2020;41:667–71.
11. Bi Q, Wu Y, Mei S, Ye C, Zou X, Zhang Z, et al. Epidemiology and transmission of COVID-19 in 391 cases and 1,286 of their close contacts in Shenzhen, China: a retrospective cohort study. Lancet Infect Dis. 2020;20:911–9. https://doi.org/10.1016/S1473-3099(20)30287-5
12. Li W, Zhang B, Lu J, Liu S, Chang Z, Peng C, et al. Characteristics of household transmission of COVID-19. Clin Infect Dis. 2020;71:1943–6. https://doi.org/10.1093/cid/ciaa450
13. Ng OT, Marimuthu K, Koh V, Pang J, Linn KZ, Sun J, et al. SARS-CoV-2 seroprevalence and transmission risk factors among high-risk close contacts: a retrospective cohort study. Lancet Infect Dis. 2021;21:333–43. https://doi.org/10.1016/S1473-3099(20)30833-1
14. Cox RJ, Brokstad KA, Krammer F, Langeland N, Blomberg B, Kuwelker K, et al.; Bergen COVID-19 Research Group. Seroconversion in household members of COVID-19 outpatients. Lancet Infect Dis. 2021;21:168. https://doi.org/10.1016/S1473-3099(20)30466-7
15. Ward H, Atchison C, Whitaker M, Ainslie KEC, Elliott J, Okell L, et al. SARS-CoV-2 antibody prevalence in England following the first peak of the pandemic. Nat Commun. 2021;12:905. https://doi.org/10.1038/s41467-021-21237-w
16. Pollán M, Pérez-Gómez B, Pastor-Barriuso R, Oteo J, Hernán MA, Pérez-Olmeda M, et al.; ENE-COVID Study Group. Prevalence of SARS-CoV-2 in Spain (ENE-COVID): a nationwide, population-based seroepidemiological study. Lancet. 2020;396:535–44. https://doi.org/10.1016/S0140-6736(20)31483-5
17. Harritshøj LH, Gybel-Brask M, Afzal S, Kamstrup PR, Jørgensen CS, Thomsen MK, et al. Comparison of 16 serological SARS-CoV-2 immunoassays in 16 clinical laboratories. J Clin Microbiol. 2021;59:e02596–20. https://doi.org/10.1128/JCM.02596-20
18. Speybroeck N, Devleesschauwer B, Joseph L, Berkvens D. Misclassification errors in prevalence estimation: Bayesian handling with care. Int J Public Health. 2013;58:791–5. https://doi.org/10.1007/s00038-012-0439-9
19 Nikolai LA, Meyer CG, Kremsner PG, Velavan TP. Asymptomatic SARS coronavirus 2 infection: invisible yet invincible. Int J Infect Dis. 2020;100:112–6. https://doi.org/10.1016/j.ijid.2020.08.076

Address for correspondence: Maria Skaalum Petersen, Department of Occupational Medicine and Public Health, the Faroese Hospital System, Sigmundargøta 5, FO-100 Tórshavn, Faroe Islands; email: maria@health.fo

Rapid Increase in SARS-CoV-2 P.1 Lineage Leading to Codominance with B.1.1.7 Lineage, British Columbia, Canada, January–April 2021

Catherine A. Hogan,[1] Agatha N. Jassem,[1] Hind Sbihi, Yayuk Joffres, John R. Tyson, Kyle Noftall, Marsha Taylor, Tracy Lee, Chris Fjell, Amanda Wilmer, John Galbraith, Marc G. Romney, Bonnie Henry, Mel Krajden, Eleni Galanis, Natalie Prystajecky, Linda M.N. Hoang

Several severe acute respiratory syndrome coronavirus 2 variants of concern (VOCs) emerged in late 2020; lineage B.1.1.7 initially dominated globally. However, lineages B.1.351 and P.1 represent potentially greater risk for transmission and immune escape. In British Columbia, Canada, B.1.1.7 and B.1.351 were first identified in December 2020 and P.1 in February 2021. We combined quantitative PCR and whole-genome sequencing to assess relative contribution of VOCs in nearly 67,000 infections during the first 16 weeks of 2021 in British Columbia. B.1.1.7 accounted for <10% of screened or sequenced specimens early on, increasing to >50% by week 8. P.1 accounted for <10% until week 10, increased rapidly to peak at week 12, and by week 13 codominated within 10% of rates of B.1.1.7. B.1.351 was a minority throughout. This rapid expansion of P.1 but suppression of B.1.351 expands our understanding of population-level VOC patterns and might provide clues to fitness determinants for emerging VOCs.

Characterizing mutations in the severe acute respiratory syndrome coronavirus 2 (SARS-CoV-2) genome has led to the identification of variants of concern (VOCs) on the basis of such criteria as increased transmissibility, clinical severity, effect on diagnostic testing, and reduced vaccine efficacy (*1*–*5*). Globally, the B.1.1.7 (Alpha), B.1.351 (Beta), and P.1 (Gamma) lineages represented the 3 main actively circulating VOCs in late 2020 and early 2021 (*6*). B.1.1.7 was first detected in England in September 2020 and progressed to become the dominant lineage in this setting within months (*4*,*7*). By early January 2021, >40 countries had documented B.1.1.7 cases, demonstrating rapid international spread (*8*). This lineage has been associated with an estimated 40%–90% increase in transmissibility (*4*,*7*), variable effects on clinical severity and mortality rates (*5*,*9*,*10*), and limited effect on vaccine effectiveness (*11*). In contrast, whereas B.1.351 and P.1 also emerged in fall 2020 and spread rapidly locally, initial evidence of international transmission beyond South Africa and Brazil was limited (*8*,*12*,*13*). The P.1 lineage poses concern given its associations with an estimated 70%–240% increase in transmissibility (*12*), decreased neutralization capacity by monoclonal and serum-derived polyclonal antibodies (*14*), and increased risk for reinfection (*12*). Limited evidence from Italy, where B.1.1.7 and P.1 lineages have cocirculated, has shown the potential for B.1.1.7 to surpass P.1 for dominant VOC status in a short timeframe (*15*; P. Stefanelli et al., unpub. data, https://www.medrxiv.org/content/10.1101/2021.04.06.21254923v1). However, recent evidence from the United States suggests that infection after vaccination might be attributed to variants characterized by such mutations as E484K, T95I, del142–144, and D614G (*16*). The SARS-CoV-2 spike E484K mutation, which is present in the P.1 and B.1.351 lineages,

Author affiliations: British Columbia Centre for Disease Control, Vancouver, British Columbia, Canada (C.A. Hogan, A.N. Jassem, H. Sbihi, Y. Joffres, J.R. Tyson, K. Noftall, M. Taylor, T. Lee, C. Fjell, M. Krajden, E. Galanis, N. Prystajecky, L.M.N. Hoang); University of British Columbia, Vancouver (C.A. Hogan, A.N. Jassem, H. Sbihi, B. Henry, M. Krajden, E. Galanis, N. Prystajecky, L.M.N. Hoang); Kelowna General Hospital, Kelowna, British Columbia, Canada (A. Wilmer); Victoria General Hospital, Victoria, British Columbia, Canada (J. Galbraith); St. Paul's Hospital, Vancouver (M.G. Romney); Ministry of Health, Victoria (B. Henry)

DOI: https://doi.org/10.3201/eid2711.211190

[1]These authors contributed equally to this article.

is most concerning for its potential vaccine response resistance and therefore might theoretically drive selective emergence of these lineages in vaccinated populations (*6*). The factors that lead to the establishment of one strain over another are under study; uncertainty remains regarding the dynamics of VOCs in the context of recent global SARS-CoV-2 vaccine rollout. Understanding the dynamics of VOC rates is critical given the importance of implementing stringent measures to mitigate the spread of more transmissible variants (*17*) and to guide vaccine program development, planning, and delivery.

The province of British Columbia (BC), Canada, population 5.1 million, experienced 3 coronavirus disease (COVID-19) waves during 2020 and early 2021, consistent with other regions in North America and Europe. BC reached a single-day peak of 1,318 cases on April 7, 2021, at the height of the third wave and a cumulative total of 106,985 cases by that point (*18*). For delivery of healthcare services, the province is partitioned into 5 regional health authorities (Appendix Figure 1, https://wwwnc.cdc.gov/EID/article/27/11/21-1190-App1.pdf). B.1.1.7 and B.1.351 lineages were first identified in BC in December 2020 (*19*). BC initiated SARS-CoV-2 vaccination campaigns in December 2020 in predefined phases according to priority populations (*19*). Vaccine administration, which had covered >25% of the population by the end of the study period (epidemiologic week [epiweek] 16), involved three 2-dose vaccines: BNT162b2 mRNA (Pfizer-BioNTech, https://www.pfizer.com), mRNA-1273 (Moderna, https://www.modernatx.com), and ChAdOx1 (AstraZeneca/SII COVISHIELD, https://www.astrazeneca.com) (*19*). The objective of this study was to summarize provincewide VOC surveillance observations over a 16-week period in 2021 spanning epiweek 1 (beginning January 3) to epiweek 16 (beginning April 24), including changes in relative population contribution over time.

Methods

VOC Detection by Single-Nucleotide Polymorphism Quantitative PCR and Whole-Genome Sequencing

The British Columbia Centre for Disease Control (BCCDC) Public Health Laboratory (PHL) (Vancouver, BC, Canada) serves as the reference laboratory for the province. In addition, hospital and private laboratories across BC offer frontline SARS-CoV-2 diagnostic testing. Testing using quantitative PCR (qPCR) is largely restricted to symptomatic persons, with the exception of outbreak investigations, which might include asymptomatic testing. We used a combined VOC testing strategy using targeted VOC single-nucleotide polymorphism (SNP) qPCR and whole-genome sequencing (WGS) to monitor VOC prevalence and assessed concordance between the 2 methods. Specimens tested by WGS were from priority populations, such as cases from an outbreak or cluster. Specimens not tested directly by WGS were screened by VOC qPCR. We performed an initial VOC proportion assessment during January 30–February 6, 2021, to evaluate the testing strategy and benchmark VOC prevalence.

VOC SNP qPCR Implementation

During January 30–March 31, 2021, N501Y qPCR testing was performed at the BCCDC PHL and adopted by the Victoria General Hospital Laboratory (Vancouver Island, BC, Canada). At the same time, St. Paul's Hospital Virology Laboratory (Vancouver) implemented a sequential qPCR testing algorithm targeting several mutations identified in VOCs, including N501Y and K417T (*20*). The N501Y mutation has been detected in the 3 main currently circulating VOCs: B.1.1.7, B.1.351, and P.1. Among those 3 VOCs, the K417T mutation is found only in P.1. During April 1–24, 2021, VOC qPCR testing was modified to incorporate both N501Y and E484K mutation screening at the BCCDC PHL; this method was adopted by Victoria General Hospital on April 16. Full VOC SNP qPCR used at the BCCDC PHL is described separately (Appendix). This change was performed to account for circulating VOCs and to optimize testing capacity. The E484K mutation has been detected in lineages B.1.351 and P.1 but is very rarely detected in B.1.1.7. In addition, in April 2021, the Kelowna General Hospital Microbiology Laboratory (Kelowna, BC, Canada) implemented a commercially available VOC qPCR targeting N501Y and E484K (Allplex SARS-CoV-2 Variant I Assay; Seegene, https://www.seegene.com). For this study, integrated provincewide surveillance was coordinated by the BCCDC to capture VOC prevalence during January 3–April 24, 2021.

Confirmation by WGS

Until March 31, 2021, all presumptive positive SNP qPCR results were confirmed by WGS at the BCCDC PHL. After March 31, specimens that tested positive for N501Y alone were identified as presumptive B.1.1.7 lineage; ≈10% were confirmed by WGS. In addition, only ≈25% of specimens that tested positive for N501Y and another mutation were confirmed by WGS. The full WGS methodology performed at the BCCDC PHL is described separately (Appendix).

Data Linkages and Analysis

We included all cases of SARS-CoV-2 infection diagnosed during January 3–April 24, 2021, for a total of 66,982 cases and 74,057 unique samples. Laboratory data collection was achieved by linking diagnostic SARS-CoV-2 qPCR, VOC SNP qPCR, and WGS databases housed in the BCCDC PHL COVID-19 database. Laboratory sites performing VOC testing provided daily or weekly data transfers of their results to enable the same linkages at the BCCDC PHL. We extracted epidemiologic (demographic and geographic [address of residence] information) and vaccination data (from the Provincial Immunization Registry) on May 15 from the BCCDC Public Health Reporting Data Warehouse and linked that information to laboratory data by using unique personal identifiers shared across the databases. To measure VOC lineage prevalence while better representing community-level dynamics, we did not include VOC lineages that were identified through WGS (as part of cluster investigations or targeted surveillance [e.g., testing after travel]) in this investigation. As part of the WGS testing sample selection, we processed a random selection of samples (background surveillance) by WGS without first conducting SNP qPCR testing. We estimated prevalence of each lineage on the basis of a weighted sum of VOC proportion through each of the 2 pathways of detection, SNP qPCR and WGS (Appendix). We defined a SARS-CoV-2 case as SARS-CoV-2 infection laboratory-confirmed by PCR. To measure VOC proportions among vaccinated case-patients, we defined breakthrough infection as a confirmed SARS-CoV-2 infection reported ≥21 days after the first (single) vaccine dose and ≥7 days after the second dose. This definition refers to the number of vaccine doses received across all 2-dose vaccines administered. We calculated descriptive analyses and 95% CI for VOC proportions among vaccinated and unvaccinated persons and for VOC prevalence by using R version 3.5.2 (R Foundation for Statistical Computing, https://www.r-project.org). We used the number of specimens screened by SNP qPCR (N501Y/E484K duplex or sequential qPCR algorithm) or background WGS as the denominator. We used Kruskal-Wallis analysis for comparison of continuous variables and the Fisher exact test for categorical variables. This work was conducted under the public health mandate, and institutional review board approval was waived.

Results

During the study period, 66,982 cases of SARS-CoV-2 infection were identified in BC, of which 19,768 (31.9%) were identified as infections with a VOC. Most VOC case-patients were young adults, median age was 33 (range <1 to 99) years, and sex distribution was approximately equal (52.2% male) (Appendix Table). Age and sex distribution varied significantly by VOC, however; P.1 case-patients were younger and more likely to be men than case-patients who tested positive for the other 2 VOCs.

During the initial BC VOC prevalence assessment, 3,024 specimens were tested during January 30–February 6, 2021, representing 97.5% of all laboratory-confirmed SARS-CoV-2–positive specimens in the province. Just 28 (0.93%) of these 3,024 SARS-CoV-2–positive specimens were identified as VOCs. Of those identified as VOCs, 22/28 (79%) were identified through screening qPCR and 6/28 (21%) through direct WGS. Of the 22 qPCR-screened specimens, 21 were successfully sequenced; the qPCR VOC confirmation rate by WGS was 95.5%, reinforcing the value of the VOC qPCR as a screening strategy. VOC cases were characterized as 23 (85.2%) B.1.1.7 lineage and 4 (14.8%) B.1.351 lineage. Continued surveillance by VOC screening of nearly all SARS-CoV-2–positive specimens identified through diagnostic testing showed a progressive increase in overall VOC-positivity in BC, reaching >10% by the end of February 2021, >50% by the end of March 2021, and >70% by mid-April 2021 (Table). By VOC case count, the B.1.1.7 lineage increased progressively from 0% to 7.9% during epiweeks 1–6, then increased more rapidly to 52.2% during epiweeks 6–8 (Figure 1, panel A); estimated doubling rate was <1 week. The P.1 lineage was initially recognized in BC at the end of February 2021, and rapidly increased to account for 39.4% of VOCs by epiweek 12; the minimal estimated doubling time was <1 week during epiweeks 10–12 (Figure 1, panel A). By epiweek 14, the proportion of B.1.1.7 and P.1 was similar, ranging from 32.3%–36.5%, and both stabilized. This rapid P.1 increase was clearly observed in 3 regional health authorities in BC (regions 1, 2, and 5); B.1.1.7 was initially predominant (Figure 1, panels B, C, F). In the 2 other BC health regions (regions 3 and 4) (Figure 1, panels D, E), P.1 increased modestly overall and did not compete with B.1.1.7 as the dominant lineage. However, when we restricted the analysis to a single smaller geographic unit of region 3 in which B.1.1.7 had been circulating for >8 weeks, we observed a rapid increase in P.1, after which the 2 lineages coexisted (Appendix Figure 2). Despite earlier detection of B.1.351 in BC in epiweek 9, B.1.351 remained stable or decreased over time and represented <10% of all VOC cases across the entire study (Figure 1, panel A).

During this study period, 1,280 breakthrough infections were identified. Among those, 497 (1.7%) cases in persons who had received 1 vaccine dose were

Table. Number of specimens positive for severe acute respiratory syndrome coronavirus 2, proportion screened VOC assay, and proportion positive for variants of concern, British Columbia, Canada, January 3–April 24, 2021*

Epiweek	Start date	No. positive specimens	No. (%) specimens	
			Screened by VOC assay	Presumptive VOC-positive†
1	2021 Jan 3	3,857	19 (0.49)	0
2	2021 Jan 10	3,498	235 (6.72)	2 (0.85)
3	2021 Jan 17	3,477	867 (24.94)	9 (1.04)
4	2021 Jan 24	3,325	793 (23.85)	8 (1.01)
5	2021 Jan 31	3,125	2,200 (70.40)	24 (1.09)
6	2021 Feb 7	3,126	2,263 (72.39)	57 (2.52)
7	2021 Feb 14	3,464	2,821 (81.44)	105 (3.72)
8	2021 Feb 21	3,638	3,291 (90.46)	231 (7.02)
9	2021 Feb 28	3,867	3,813 (98.86)	442 (11.59)
10	2021 Mar 7	3,862	3,862 (100)	626 (16.20)
11	2021 Mar 14	4,155	4,128 (99.35)	1,081 (26.19)
12	2021 Mar 21	5,723	5,636 (98.48)	2,162 (38.36)
13	2021 Mar 28	7,036	7,032 (99.94)	3,622 (51.51)
14	2021 Apr 4	8,195	8,185 (99.88)	5,404 (66.02)
15	2021 Apr 11	7,278	6,560 (90.13)	4,644 (70.79)
16	2021 Apr 18	6,441	6,127 (95.12)	4,681 (76.40)

*Epiweek, epidemiologic week; VOC, variant of concern.
†Presumptive VOC detection refers to VOC identification by quantitative PCR testing without confirmation by whole-genome sequencing; includes all specimens tested for VOCs.

attributed to B.1.1.7 and P.1 lineage strains, and 18 (0.2%) cases in persons who had received 2 doses were attributed to B.1.1.7 and P.1 lineage strains (Appendix Table). Infections after 2 doses of vaccine were excluded from downstream analyses given their small number. Almost all (96.4%) of the VOC infections occurred in unvaccinated persons, but approximately the same proportion of VOC cases occurred among partially vaccinated and unvaccinated persons. Specifically, during epiweeks 9–16, when B.1.1.7 was widespread and case counts were high, B.1.1.7 infections were identified in 37%–55% of cases in unvaccinated persons and in 30%–65% of cases in persons who had received 1 dose (Figure 2). During epiweeks 10–16, after P.1 emerged in the study population, the proportion of infections with P.1 was 14%–39% among cases in partially vaccinated persons and 11%–40% among cases in unvaccinated persons (Figure 2). Conversely, at the same time (epiweeks 9–16), 6%–50% of breakthrough infections were non-VOC lineages in persons who had received 1 dose of a 2-dose vaccine.

Discussion

Results from this analysis of VOC laboratory and epidemiologic surveillance data demonstrated initially low prevalence of VOC and predominance of the B.1.1.7 lineage in BC, Canada, in early 2021, consistent with trends documented across North America. An earlier study that tested 2,618 SARS-CoV-2–positive samples in BC over a 7-day period in a single regional health authority reported an outbreak of 13 P.1 cases; however, whether this occurrence represented a single confined outbreak or potential for more disseminated spread of this lineage is uncertain, and WGS data were limited (*20*). Building on those earlier findings, our study performed ongoing surveillance of >74,000 SARS-CoV-2–positive specimens across the entire province over 16 weeks. This surveillance led to the detection of a rapid and substantial increase in P.1 lineage, demonstrating its potential for codominance with B.1.1.7 at the provincial level. The pattern of population-level lineage change over time reflected the largest outbreak of the P.1 lineage outside of Brazil at that time (*21*,*22*). This study documented the parallel rapid increase of the P.1 lineage in 3 regional health authorities in which B.1.1.7 was previously established, contrasting with previous reports in Italy showing sustained dominance of B.1.1.7 after the introduction of P.1 (*15*; P. Stefanelli et al., unpub. data). In 2 regions, the proportion of P.1 exceeded that of B.1.1.7 for a sustained period. Of note, P.1 arose to codominance before broad vaccination of the most likely implicated young adult age group, and the proportion of VOCs was similar between vaccinated and unvaccinated groups, suggesting that vaccination was not driving the observed trends of P.1 increase. Although our findings contradict those of Hacisuleyman et al. (*16*), which cautioned that infections after vaccination might be characterized by variant mutations such as E484K, the difference might reflect the small sample size in that study. Comprehensive comparative demographic data to characterize the P.1 lineage are lacking; however, early data from Brazil demonstrate increased case-fatality rates among younger age groups that coincide temporally with the rise of this lineage there (M.H.S. de Oliveira, unpub. data, https://www.medrxiv.org/content/10.1101/2021.03.24.21254046v1). Further work investigating

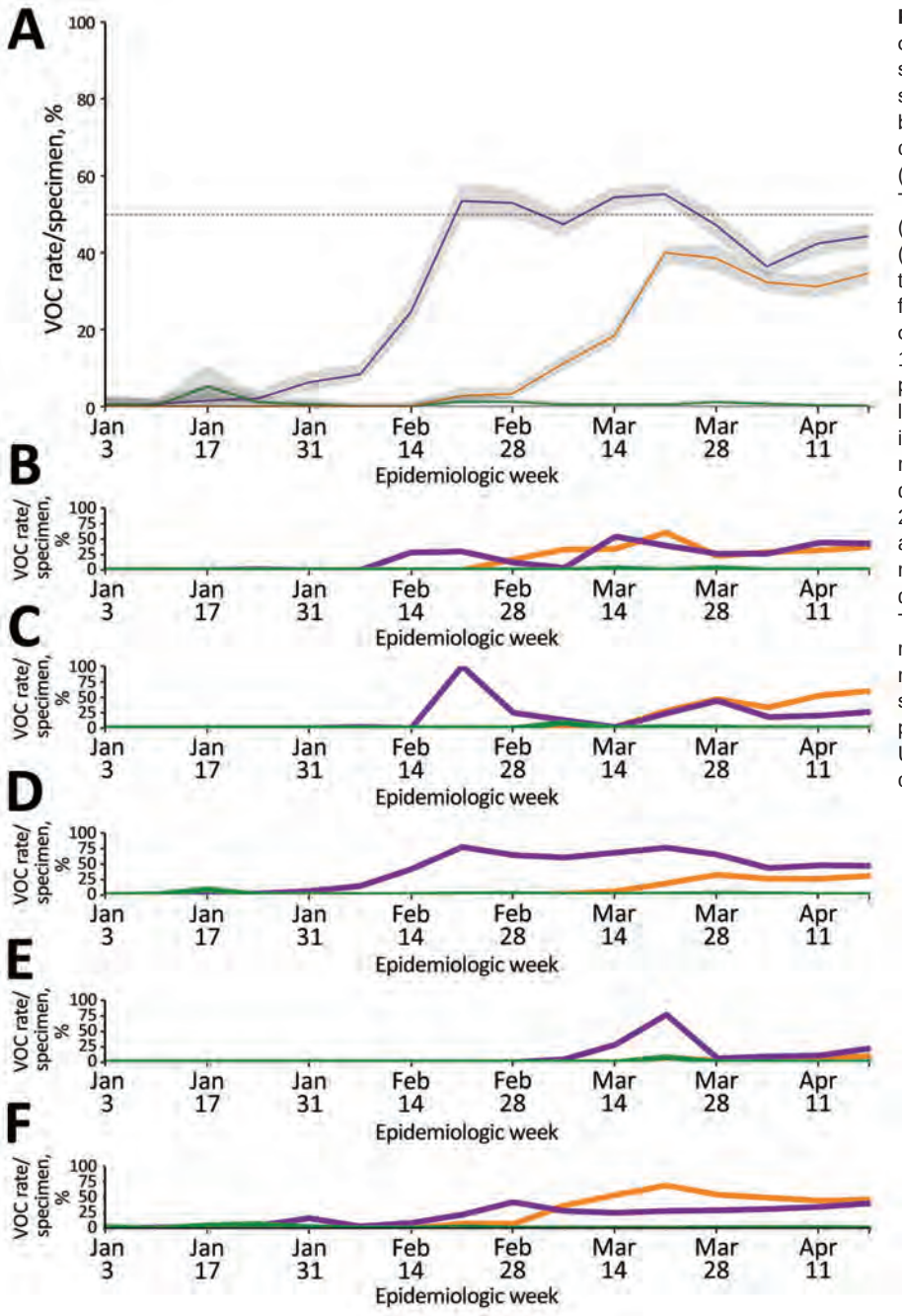

Figure 1. Weekly rate estimates of each severe acute respiratory syndrome coronavirus 2 VoC (per 100 specimens screened or sequenced), by epidemiologic week and specimen collection date, British Columbia (BC), Canada, January–April 2021. The 3 main VoC are shown in purple (B.1.1.7), green (B.1.351), and orange (P.1). The P.1 lineage was confirmed through whole-genome sequencing or from an N501Y- and E484K-positive or K417T-positive result from epiweek 12 onward. A) VOC data for the whole province. Shaded areas around the line represent 95% CI; dashed line indicates 50%. B) VOC data for BC regional health authority 1. C) VOC data for BC regional health authority 2. D) VOC data for BC regional health authority 3. E) VOC data for BC regional health authority 4. F) VOC data for BC regional health authority 5. The 95% CIs are not shown for health regions because of low numbers and rates and the resulting wide uncertainty seen across regions for extended periods. BR, Brazil; SA, South Africa; UK, United Kingdom; VOC, variant of concern.

the full epidemiologic characteristics and clinical implications, including disease severity, of the P.1 increase will complement the findings of this study.

The first limitation of our study is that the VOC qPCR and WGS confirmation testing strategies were modified over time, which might partially limit comparability of positivity estimates over time and could overestimate rates of P.1 because of the use of E484K-positivity as its surrogate in some instances. Nonetheless, background surveillance data during the same timeframe (data not shown) supported the identification of most E484K-positive specimens as P.1 lineage. Second, to avoid oversampling bias, we based the WGS selection strategy on the inclusion of specimens from persons tested for background surveillance purposes, not for outbreak investigation or targeted (e.g., travel-related) surveillance. Third, the populations that were vaccinated during this study period do not necessarily reflect the persons at highest risk for VOC infection, which might have modified

breakthrough VOC proportions. Of note, this study was not designed to assess vaccine effectiveness; we did not adjust for confounders in the relationship between vaccination and infection, such as age, underlying conditions, vaccination program roll-out, and temporal-spatial epidemic risk. More comprehensive studies considering characteristics of the vaccine roll-out strategy are needed for analyses beyond overall comparisons between lineages in unvaccinated and vaccinated groups.

In summary, this population-level study based on a combined qPCR and WGS VOC testing strategy demonstrated the rapid increase of the P.1 lineage and its later codominance, contrasting with studies in settings such as Italy, where the B.1.1.7 and P.1 lineages have cocirculated. Further work is required to elucidate the biologic and social factors that enabled the establishment of this lineage and to assess the clinical implications of these findings.

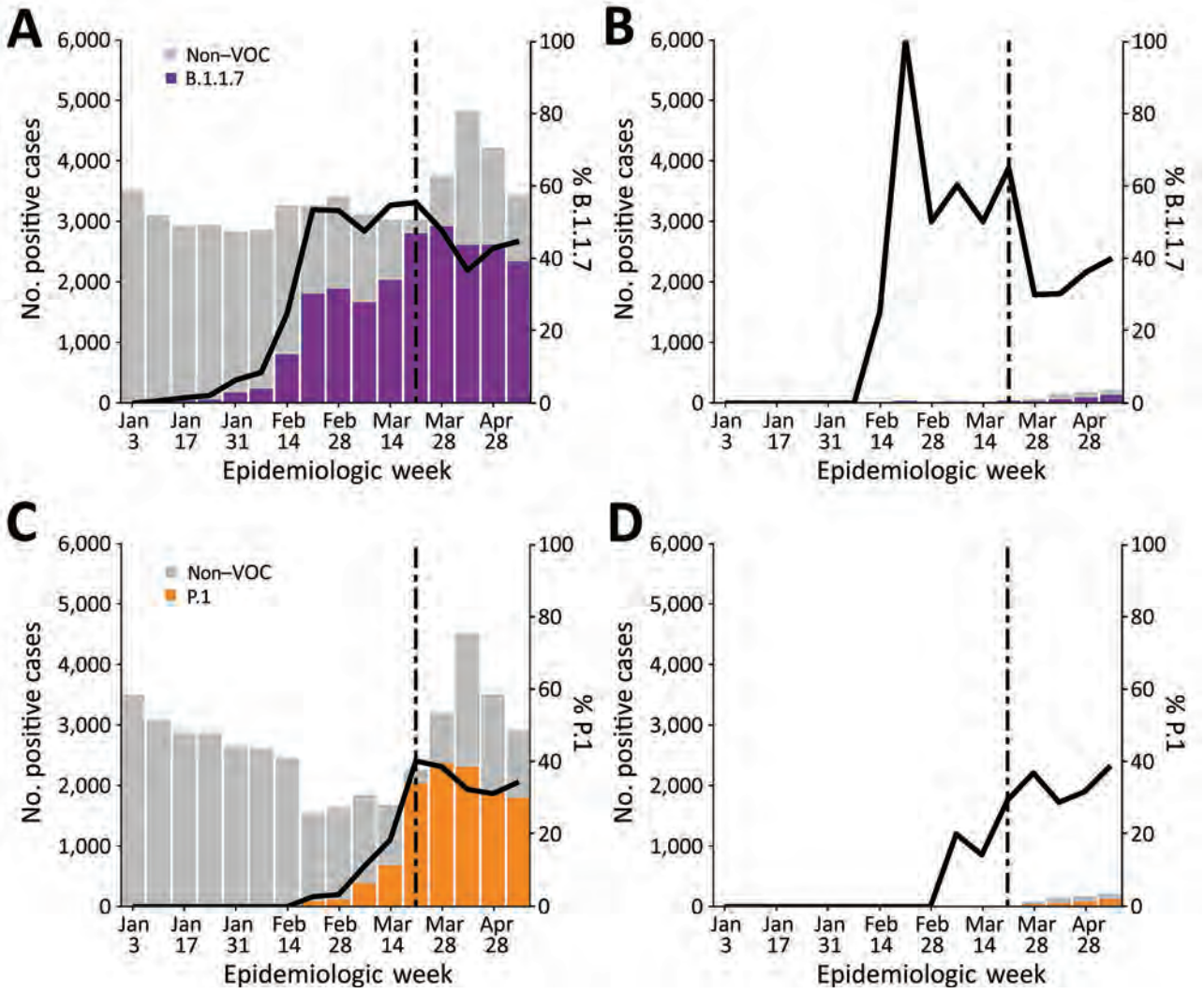

Figure 2. Distribution of all severe acute respiratory syndrome coronavirus 2 cases and VoC cases by vaccination status, British Columbia, Canada, January–April 2021. Vaccinated persons included those who had received 1 dose of a 2-dose vaccine with diagnosis confirmed by PCR ≥21 days after the first dose (on the basis of specimen collection date). Stacked bars (left-hand y-axis) represent the absolute number of VOC cases and non-VOC cases. Solid lines (right-hand y-axis) show the percentage of VOC among all cases identified in a given week. Dotted lines show the date when VOC quantitative PCR (qPCR) including E484K mutation detection was adopted at the British Columbia Centre for Disease Control Public Health Laboratory. A) B.1.1.7 and non-VOC cases in nonvaccinated persons. B) B.1.1.7 and non-VOC cases in vaccinated persons. VOC cases in panels A and B included B.1.1.7 confirmed for lineage by whole-genome sequencing and presumptive B.1.1.7 positives based on a VOC qPCR result of N501Y-positive and E484K-negative. C) P.1 and non-VOC cases in nonvaccinated persons. D) P.1 and non-VOC cases in vaccinated persons. VOC cases in panels C and D included P.1 and B.1.351 confirmed for lineage by whole-genome sequencing and presumptive P.1 positives based on a VOC qPCR result of N501Y-positive and E484K-positive or K417T-positive. VOC, variant of concern.

Acknowledgments

We thank the molecular, virology, and bacteriology staff and microbiologists of the British Columbia Centre for Disease Control Public Health Laboratory (BCCDC PHL) for their contribution toward testing, without which this work would not have been possible. We thank Rebecca Hickman, Ji-In Hum, Jason Nguyen, Frankie Tsang, Branco Cheung, Michael Chan, Corrinne Ng, Loretta Janz, Rob Azana, Ana Paccagnella, Kim Macdonald, Kimia Kamelian, Diane Eisler, Dan Fornika, and Yin Chang for their contributions toward test procedure development, interpretation, and implementation. We thank Karen Mooder and senior members of the BCCDC PHL operations team for their role in building the infrastructure that enabled this work. We thank Braeden Klaver and the BCCDC data analytics team for implementing the data collection and entry systems that enabled this work. We thank Nancy Matic and Christopher Lowe and the virology laboratory staff from St. Paul's Hospital, Vancouver Island Health Authority (VIHA), and Interior Health Authority (IHA) laboratories for sharing and verifying variant of concern data. We thank the British Columbia Association of Medical Microbiologists for sharing samples and data that enabled provincewide data collection and testing. We also thank medical health officers across all 5 health authorities, and regional and provincial public health staff, for providing case-level data.

This work was supported by funding from Genome BC, Genome Canada/CanCOGen, Canadian Institutes for Health Research and MetroVancouver to N.P. This work was also funded by a Public Health Agency of Canada COVID-19 Immunology Task Force COVID-19 Hot Spots Competition Grant (grant no. 2021-HQ-000120) to M.G.R.

About the Author

Dr. Hogan is a medical microbiologist and infectious diseases physician and the British Columbia Centre for Disease Control Public Health Laboratory program head for the Parasitology Laboratory. Her research interests include novel diagnostic methods, clinical impact of diagnostics, and global health. Dr. Jassem is a clinical microbiologist and the British Columbia Centre for Disease Control Public Health Laboratory program head for the Virology/Molecular Diagnostics Laboratory. Her research interests include evaluation of molecular- and serology-based strategies for virus detection or exposure.

References

1. Walensky RP, Walke HT, Fauci AS. SARS-CoV-2 variants of concern in the United States—challenges and opportunities. JAMA. 2021;325:1037–8. https://doi.org/10.1001/jama.2021.2294
2. Galloway SE, Paul P, MacCannell DR, Johansson MA, Brooks JT, MacNeil A, et al. Emergence of SARS-CoV-2 B.1.1.7 lineage—United States, December 29, 2020–January 12, 2021. MMWR Morb Mortal Wkly Rep. 2021;70:95–9. https://doi.org/10.15585/mmwr.mm7003e2
3. Muik A, Wallisch AK, Sänger B, Swanson KA, Mühl J, Chen W, et al. Neutralization of SARS-CoV-2 lineage B.1.1.7 pseudovirus by BNT162b2 vaccine-elicited human sera. Science. 2021;371:1152–3. https://doi.org/10.1126/science.abg6105
4. Davies NG, Abbott S, Barnard RC, Jarvis CI, Kucharski AJ, Munday JD, et al.; CMMID COVID-19 Working Group; COVID-19 Genomics UK (COG-UK) Consortium. Estimated transmissibility and impact of SARS-CoV-2 lineage B.1.1.7 in England. Science. 2021;372:eabg3055. https://doi.org/10.1126/science.abg3055
5. Challen R, Brooks-Pollock E, Read JM, Dyson L, Tsaneva-Atanasova K, Danon L. Risk of mortality in patients infected with SARS-CoV-2 variant of concern 202012/1: matched cohort study. BMJ. 2021;372:n579. https://doi.org/10.1136/bmj.n579
6. GISAID. Tracking of variants. 2021 [cited 2021 May 20]. https://www.gisaid.org/hcov19-variants
7. Volz E, Mishra S, Chand M, Barrett JC, Johnson R, Geidelberg L, et al.; COVID-19 Genomics UK (COG-UK) consortium. Assessing transmissibility of SARS-CoV-2 lineage B.1.1.7 in England. Nature. 2021;593:266–9. https://doi.org/10.1038/s41586-021-03470-x
8. O'Toole A, Hill V, Pybus OG, Watts A, Bogoch II, Khan K, et al. Tracking the international spread of SARS-CoV-2 lineages B.1.1.7 and B.1.351/501Y–V2. 2021 [cited 2021 May 8]. https://virological.org/t/tracking-the-international-spread-of-sars-cov-2-lineages-b-1-1-7-and-b-1-351-501y-v2/592
9. Frampton D, Rampling T, Cross A, Bailey H, Heaney J, Byott M, et al. Genomic characteristics and clinical effect of the emergent SARS-CoV-2 B.1.1.7 lineage in London, UK: a whole-genome sequencing and hospital-based cohort study. Lancet Infect Dis. 2021 Apr 12 [Epub ahead of print].
10. Peter Horby CH. Nick Davies, John Edmunds, Neil Ferguson, Graham Medley CS. NERVTAG. 2021 [cited 2021 May 1]. https://assets.publishing.service.gov.uk/government/uploads/system/uploads/attachment_data/file/961037/NERVTAG_note_on_B.1.1.7_severity_for_SAGE_77__1_.pdf
11. World Health Organization. COVID-19 weekly epidemiological update. 2021 [cited 2021 Apr 28]. https://www.who.int/docs/default-source/coronaviruse/situation-reports/20210413_weekly_epi_update_35.pdf
12. Faria NR, Mellan TA, Whittaker C, Claro IM, Candido DDS, Mishra S, et al. Genomics and epidemiology of the P.1 SARS-CoV-2 lineage in Manaus, Brazil. Science. 2021;372:815–21. https://doi.org/10.1126/science.abh2644
13. PANGO lineages. P.1 [cited 2021 Apr 28]. https://cov-lineages.org/global_report_P.1.html
14. Chen RE, Zhang X, Case JB, Winkler ES, Liu Y, VanBlargan LA, et al. Resistance of SARS-CoV-2 variants to neutralization by monoclonal and serum-derived polyclonal antibodies. Nat Med. 2021;27:717–26. https://doi.org/10.1038/s41591-021-01294-w
15. Di Giallonardo F, Puglia I, Curini V, Cammà C, Mangone I, Calistri P, et al. Emergence and spread of SARS-CoV-2 lineages B.1.1.7 and P.1 in Italy. Viruses. 2021;13:794. https://doi.org/10.3390/v13050794
16. Hacisuleyman E, Hale C, Saito Y, Blachere NE, Bergh M, Conlon EG, et al. Vaccine breakthrough infections with

SARS-CoV-2 variants. N Engl J Med. 2021;384:2212–8. https://doi.org/10.1056/NEJMoa2105000
17. Public Health Agency of Canada. Update on COVID-19 in Canada: epidemiology and modelling. 2021 Feb 19 [cited 2021 Feb 19]. https://www.canada.ca/content/dam/phac-aspc/documents/services/diseases-maladies/coronavirus-disease-covid-19/epidemiological-economic-research-data/update-covid-19-canada-epidemiology-modelling-20210219-en.pdf
18. British Columbia Centre for Disease Control. British Columbia COVID-19 dashboard. 2021 [cited 2021 May 20]. https://experience.arcgis.com/experience/a6f23959a8b14bfa989e3cda29297ded
19. British Columbia Government. COVID-19 immunization plan. 2021 [cited 2021 May 20]. https://www2.gov.bc.ca/gov/content/covid-19/vaccine/plan
20. Matic N, Lowe CF, Ritchie G, Stefanovic A, Lawson T, Jang W, et al. Rapid detection of SARS-CoV-2 variants of concern, Including B.1.1.28/P.1, British Columbia, Canada. Emerg Infect Dis. 2021;27:1673–6. https://doi.org/10.3201/eid2706.210532
21. Government of Canada. COVID-19 epidemiology update. 2021 [cited 2021 May 20]. https://health-infobase.canada.ca/covid-19/epidemiological-summary-covid-19-cases.html
22. Centers for Disease Control and Prevention. COVID-19 data tracker; variant proportions. 2021 [cited 2021 May 20]. https://covid.cdc.gov/covid-data-tracker/#variant-proportions

Address for correspondence: Catherine A. Hogan, British Columbia Centre for Disease Control, 655 W 12th Ave, Rm 2054, Vancouver, BC, V6R 2M7, Canada; email: catherine.hogan@bccdc.ca

Changing Patterns of Disease Severity in *Blastomyces dermatitidis* Infection, Quebec, Canada

Alex Carignan, Chiheb Boudhrioua, Sandrine Moreira, Andrée Ann Pelletier, Kevin Dufour, Jacques Pépin, Catherine Allard, Dominique Marcoux, Philippe J. Dufresne

This retrospective multicenter cohort study assessed temporal changes in the severity and mortality rate of blastomycosis in Quebec, Canada, and identified risk factors for death in patients with blastomycosis in 1988–2016. The primary outcome was 90-day all-cause deaths. Among 185 patients, 122 (66%) needed hospitalization and 30 (16%) died. We noted increases in the proportion of severe cases, in age at diagnosis and in the proportion of diabetic and immunocompromised patients over time. Independent risk factors for death were age (adjusted odds ratio [aOR] 1.04, 95% CI 1.00–1.07), immunosuppression (aOR 4.2, 95% CI 1.5–11.6), and involvement of ≥2 lung lobes (aOR 5.3, 95% CI 1.9–14.3). There was no association between the *Blastomyces* genotype group and all-cause mortality. The proportion of severe cases of blastomycosis has increased in Quebec over the past 30 years, partially explained by the higher number of immunosuppressed patients.

Blastomyces dermatitidis, a dimorphic fungus, causes a localized or disseminated pyogranulomatous fungal infection called blastomycosis. Various descriptive studies have shown predominantly pulmonary, skin, bone, and genitourinary involvement (*1*). The clinical spectrum of blastomycosis is wide, ranging from subclinical infection to critical cases of acute respiratory distress syndrome. Retrospective studies conducted in recent years have shown an increased incidence of blastomycosis in both Canada and the United States (*2*–*5*). Blastomycosis is endemic to the St. Lawrence River Valley; a study that focused on the incidence of blastomycosis in the province of Quebec, Canada (*6*), showed an increasing incidence from 1988 to 2011. Similar trends have been observed in several regions in the United States (*7*), although the underlying causes are poorly understood. The absence of robust reporting and lack of reportability in many jurisdictions may hamper the ability to know whether cases are increasing more broadly. Some authors suggested a possible relationship with certain climatic factors (*3*,*8*). In the wake of the increased incidence of blastomycosis in Quebec, clinicians have observed a possible worsening of the disease severity in patients, with occasional deaths.

This study aimed to assess temporal changes in the severity and mortality of blastomycosis in Quebec and to identify risk factors for blastomycosis-related deaths. In Quebec, all suspected *B. dermatitidis* isolates are sent for molecular species confirmation at the Quebec Public Health Laboratory (Laboratoire de Santé Publique du Québec; LSPQ; Sainte-Anne-de-Bellevue, QC, Canada), a Containment Level 3 laboratory. In addition, these strains are maintained in a strain biorepository. Therefore, we also aimed to establish a genetic diversity profile of the circulating *Blastomyces* strains in Quebec and assess whether major genotypes may be associated with increased disease severity or death. The institutional review board of Centre Intégré Universitaire de Santé et de Services Sociaux de l'Estrie—Centre Hospitalier Universitaire de Sherbrooke (CIUSSSE-CHUS) approved this study (project no. MP-31-2017-1597) and waived the need for individual informed consent because the study involved minimal to no risk to participants and this retrospective research could not practically be carried out without the waiver.

Methods

We conducted a retrospective cohort study in 39 acute-care facilities, including community hospitals and academic centers, in Quebec. The study population included all patients with culture-confirmed

Author affiliations: Université de Sherbrooke, Sherbrooke, Quebec, Canada (A. Carignan, A.A. Pelletier, K. Dufour, J. Pépin, C. Allard, D. Marcoux); Laboratoire de Santé Publique du Québec, Sainte-Anne-de-Bellevue, Québec, Canada (C. Boudhrioua, S. Moreira, P.J. Dufresne)

DOI: https://doi.org/10.3201/eid2711.210552

B. dermatitidis infection who were treated as inpatients or outpatients. Data on *B. dermatitidis* cultures were extracted from the database (1988–2017) of the LSPQ, where all *B. dermatitidis* isolates are confirmed by an in-house detection PCR coupled with confirmatory sequencing of the internal transcribed spacer region and stored in the repository.

Data Collection and Outcomes

Research assistants reviewed hospital records using a standardized questionnaire. The administrative region of residence was determined using postal codes (*9*). The medical history was delineated to calculate the Charlson Comorbidity Index (*10*), along with demographic, microbiological, clinical, and therapeutic data (antifungal drug, dose, route of administration, and start and end dates of treatment). Because there is no consensual definition of disseminated disease, we calculated the total number of organs involved, including the lungs. Immunosuppression included HIV infection, corticosteroid use, immunosuppressive therapy for inflammatory disease, chemotherapy, and transplantation. Severe cases were defined as patients with septic shock or acute respiratory distress syndrome or requiring mechanical ventilation, or any combination of those. The primary outcome was 90-day all-cause mortality.

Genotyping

A total of 157 *Blastomyces* isolates, out of 185 in the LSPQ collection for which a medical record was available, were successfully grown on inhibitory mold agar or potato dextrose agar. We obtained whole-genome sequences (WGS) of 108 of those isolates using the Illumina MiSeq system (Illumina, https://www.illumina.com) In brief, we obtained DNA extracts from mycelium culture with the DNeasy PowerSoil extraction kit (QIAGEN, https://www.qiagen.com) and used for whole-genome pair-end sequencing with Nextera XT DNA Library Prep kit and reagent V3 (2 × 300 bp) kit (Illumina). We used the WGS data to detect single-nucleotide polymorphism (SNP) and genotypes calling by an in-house pipeline. Only high-quality SNPs having genotype calls (read depth >10 and mapping score >30) across all samples, from which ≥5% carried the minor allele, were stored. These SNPs were used to conduct population structure analysis with fastSTRUCTURE (https://rajanil.github.io/fastStructure) to identify major genetic groups present in the population.

Statistical Analysis

We double-entered data into an electronic input tool, Research Electronic Data Capture (REDcap; Vanderbilt University, Nashville, TN, USA), and analyzed data using Stata version 15.1 for Mac (StataCorp, https://www.stata.com). Proportions were compared using the χ^2 or Fisher exact test, as appropriate. We compared continuous variables by Wilcoxon rank-sum test. We excluded cases with missing data from the analyses. To establish risk factors for death, we selected the variables to be included in the multivariable unconditional logistic regression model by applying a 10% significance level after univariate analysis. We added variables one at a time and retained them only if they were found to be significant in the multivariable model based on the likelihood ratio test ($p<0.05$); the final model retained variables that significantly enhanced the fit of the model. To avoid potential confounding by indication, we excluded antifungal therapies from the multivariable analysis. We also excluded the variable representing case severity because it is on the causal pathway between the infection and the primary study outcome of 90-day all-cause mortality.

Results

In total, 224 *B. dermatitidis*–positive culture results were extracted from the public health laboratory database. We included 185 cases of blastomycosis in 181 different patients with complete medical records in the analysis dataset of this study; of those, 157 isolates could be grown in culture, and 143 yielded high-quality WGS data. The remaining isolates were nonviable.

Case Characteristics and Clinical and Radiologic Manifestations

Most patients were male (143/185; 77%), and the median age was 55 (interquartile range [IQR] 44–67) years. The median duration between the onset of the first symptoms and diagnosis was 56 (IQR 25–123) days. Pulmonary infection (n = 149; 81%) was predominant in this cohort, followed by cutaneous (n = 75; 40.5%), osteoarticular (n = 27, 15%), central nervous system (n = 8, 4%), and urinary (n = 11, 6%) involvement. Two or more organs were involved in 35% (64/185) of the patients. The most frequent symptoms when patients initially sought care were cough (n = 120; 65%) and dyspnea (n = 97; 52%). Fever was documented in 65 (35%) patients and weight loss in 62 (34%) patients. In patients with pulmonary infections, chest radiograph or computed tomography (CT) scan showed the involvement of >2 lobes in 64 (43%) patients. Radiologic manifestations on chest radiograph, chest CT, or both included, among others, nodular infiltrates (53; 36%), focal masses (27; 18%), and miliary patterns (n = 9; 6%). Furthermore, 122 patients (66%) needed hospitalization for a median duration of 15

Table 1. Characteristics of patients in study of blastomycosis in Quebec, Canada*

Characteristic	1988–1997, n = 33	1998–2007, n = 57	2008–2017, n = 95	p value
Median age, y (IQR)	47.4 (42.9–61.2)	50.0 (40.4–62.8)	58.9 (48.6–70.6)	0.02†
Sex				
F	11 (33)	13 (23)	18 (19)	
M	22 (67)	44 (77)	77 (81)	0.2
No. involved organs				
1	17 (52)	34 (60)	70 (74)	
≥2	16 (48)	23 (40)	25 (26)	0.04
Underlying conditions				
Chronic obstructive pulmonary disease	6 (18)	7 (12)	21 (22)	0.3
Diabetes	1 (3)	9 (16)	22 (23)	0.03
Immunosuppression	2 (6)	11 (19)	31 (33)	0.005
Charlson Comorbidity Index				
0	20 (61)	28 (49)	33 (35)	
1–2	11 (33)	12 (21)	30 (32)	
≥3	2 (6)	17 (30)	32 (34)	0.01
First antifungal administered				
Amphotericin B, lipid formulations	0	5 (9)	20 (21)	
Amphotericin B, deoxycholate	5 (15)	6 (11)	6 (6)	
Azole	20 (61)	33 (58)	58 (61)	
No treatment	8 (24)	13 (23)	11 (12)	0.008‡
Blastomyces genotype group				
I	1 (6)	1 (2)	1 (2)	
II	3 (17)	11 (24)	11 (24)	
III	4 (22)	13 (29)	14 (30)	
IV	10 (56)	20 (44)	20 (44)	0.9
Severe illness	1 (3)	8 (15)	21 (22)	0.03
90-day all-cause mortality	2 (6)	10 (18)	18 (19)	0.2

*Values are no. (%) except as indicated. IQR, interquartile range.
†By Mood's equality of medians test.
‡By Fisher exact test.

(IQR 7–29) days. Of these, 37/122 (30%) patients were admitted to the intensive care unit (median duration 4 days, IQR 2–9 days). A severe form of blastomycosis was observed in 30/185 patients (16%), and the 90-day all-cause mortality was 16% (30/185).

Temporal Changes in Characteristics, Treatment, and Outcomes of Blastomycosis

To further investigate temporal changes in blastomycosis, we compared the characteristics of case-patients from 1988–1997 (n = 33) with those identified in 1998–2007 (n = 57) and 2008–2017 (n = 95) (Table 1). We observed a significant increase over time in the age of patients with blastomycosis over the study periods (p = 0.02). In addition, we saw increases in the proportion of diabetic patients, immunocompromised patients, and patients with a Charlson Comorbidity Index score ≥3. Among the case-patients diagnosed during the 2008–2017 period, we noted an increasing use of the lipid formulations of amphotericin B over that of amphotericin B deoxycholate. There was no significant change in the distribution of *B. dermatitidis* genotypes over time: we observed an increase in the proportion of severe cases over the study periods (1988–1997, 1/33 [3%]; 1998–2007, 8/57 [15%]; 2008–2016, 21/95 [22%]; p = 0.03) (Figure), as well as in the 90-day all-cause mortality (1988–1997, 2/33 [6%]; 1998–2007, 11/54 [18%]; 2008–2016, 18/89 [19%]), but the differences between the study periods were not significant (p = 0.15).

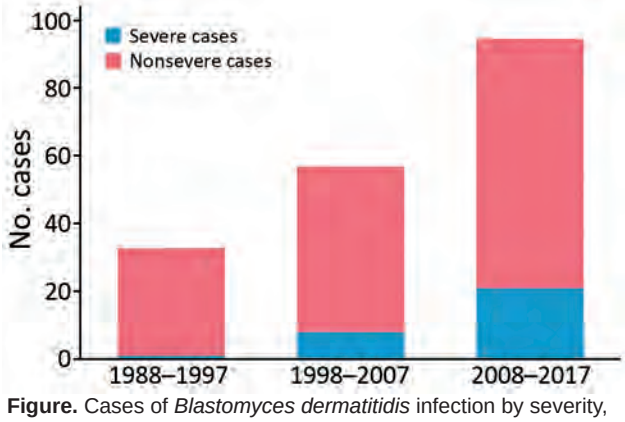

Figure. Cases of *Blastomyces dermatitidis* infection by severity, Quebec, Canada, 1988–2017.

Risk Factors for Mortality

Several variables were associated with mortality in univariate analysis but were no longer significant after adjusting for confounders. There was no significant association between genotype and mortality. The independent risk factors associated with mortality included age (p = 0.04), immunosuppression (p = 0.005), and the involvement of ≥2 lung lobes on chest radiograph (p = 0.001) (Table 2).

Table 2. Risk factors for 90-day all-cause mortality among patients with blastomycosis, Quebec, Canada*

Risk factor	Survived, n = 155	Died, n = 30	Crude odds ratio (95% CI)	p value	Adjusted odds ratio (95% CI)	p value
Study period						
1988–1997	31 (94)	2 (6)	1			
1998–2007	47 (82)	10 (18)	3.3 (0.7–16.1)	0.1	2.7 (0.5–15.3)	0.3
2008–2017	77 (81)	18 (19)	3.6 (0.8–16.6)	0.1	1.2 (0.2–6.5)	0.8
Median no. days of symptoms before diagnosis (IQR)	71 (26–141)	37 (18–45)	0.99 (0.99–1.00)	0.04	0.99 (0.99–1.00)	0.07
Median age, y (IQR)	54 (44–64)	62 (53–71)	1.04 (1.01–1.07)	0.004	1.04 (1.00–1.07)	0.04
Sex						
F	34 (81)	8 (19)				
M	121 (85)	22 (15)	0.8 (0.3–1.9)	0.6		
Charlson Comorbidity Index score						
0	76 (94)	5 (6)				
1–2	43 (81)	10 (19)	3.5 (1.1–16.1)	0.03		
≥3	36 (71)	15 (29)	6.3 (2.1–18.8)	0.001		
Underlying condition						
Diabetes	23 (72)	9 (28)	2.5 (1.00–6.04)	0.05		
COPD	27 (79)	7 (21)	1.4 (0.6–3.7)	0.5		
Immunosuppression	27 (61)	17(39)	6.2 (2.7–14.3)	<0.001	4.2 (1.5–11.6)	0.005
No. organs involved						
1–2	105 (87)	16 (13)				
>2	50 (78)	14 (22)	1.8 (0.8–4.1)	0.1		
Radiologic manifestations						
No. lobes						
0–2	112 (93)	8 (7)				
>2	43 (66)	22 (34)	7.2 (3.0–17.3)	<0.001	5.3 (1.9–14.3)	0.001
Miliary presentation	6 (67)	3 (33)	2.8 (0.7–11.7)	0.2		
First antifungal received						
Amphotericin, lipid formulations	20 (80)	5 (20)	1			
Amphotericin B, deoxycholate	13 (76)	4 (24)	1.2 (0.3–5.5)	0.08		
Azole	107 (96)	4 (4)	0.1 (0.04–0.61)	0.008		
No treatment	15 (47)	17 (53)	4.5 (1.4–15.1)	0.01		

*Values are no. (%) except as indicated. COPD, Chronic obstructive pulmonary disease; IQR, interquartile range.

Genotype

A total of 108 *Blastomyces* isolates were available for WGS genotyping. Using WGS data, we detected a total of 97,403 high-quality SNPs among all the isolates sequenced. For the purpose of this study, we used SNP genotype calls across all isolates for structure analysis to underline the major genetic groups present in the population and to assess if they could correlate with disease outcome and severity. We identified 4 main genotypes in the population. Genotype IV (n = 50; 46%) was most frequently isolated, followed by genotype III (n = 31; 28%) and II (n = 25; 23%). Genotype I was isolated infrequently in this study (n = 3; 2%); it formed an outlier group representing the cryptic species *B. gilchristii*. We saw a correlation between administrative regions and genotypes (Table 3); however, we detected no association between genotypes and the proportion of severe cases or all-cause mortality. Sequences from this study have been deposited in the National Center for Biotechnology Information (project no. PRJNA752385).

Discussion

This study demonstrated a gradual modification in the clinical characteristics and underlying conditions associated with *B. dermatitidis* infection in Quebec, Canada, over the last 3 decades, 1988–2017. We documented an increase in the proportion of severe cases and an increase in the age and proportion of diabetic and immunocompromised patients. The 90-day all-cause mortality rate remained stable at ≈20% for the last 2 decades despite this change in disease severity. Because blastomycosis is often misdiagnosed as bacterial pneumonia initially (*11*), and given this changing pattern of disease severity, clinicians in blastomycosis-endemic regions must recognize the possibility of *Blastomyces* infection earlier to avoid delays in both diagnosis and treatment initiation.

The increased proportion of severe cases observed within our cohort may be related to changes in the underlying characteristics of the affected patients. We observed an increase in the proportion of immunocompromised patients. The prevalence of immunosuppressed adults in Quebec is unknown; an estimated 2.7% of US adults self-reported that they were immunosuppressed in 2013 (*12*), and this number is thought to be increasing because of both greater life expectancy among immunosuppressed adults and new indications for immunosuppressive therapies (*13*,*14*). Furthermore, population aging

and increasing prevalence of chronic disease and multiple underlying conditions within the population of Quebec may explain the increased proportion of severe cases that were observed since 1998 (*15*). In addition, there was a similar increase in the prevalence of diabetes in Quebec, from 4.7% in 2000–2001 to 7.2% in 2014–2015 (*16*). Because our definition of severe cases included, among others, the use of mechanical ventilation, the increase in the proportion of severe cases may also be partially explained by changes leading to increasing use of mechanical ventilation over the years (*17*).

We observed an overall mortality rate of 16.2% in this study cohort, which is higher than the mortality rate observed in recently published large cohorts. A US nationwide study found an overall in-hospital mortality rate of 6.9% (*18*), and an overall case-fatality rate in a cohort of 671 cases in Minnesota during 1999–2018 was 10% (*19*). In a systematic review and meta-analysis, the mortality estimate for general clinical cases of blastomycosis was 6.6% overall (*20*); substantial heterogeneity between the included studies was mainly attributed to inconsistent definitions of mortality. We used 90-day all-cause mortality, a more robust outcome than other studies that used outcomes such as attributable mortality, which might explain the higher mortality rate in our findings compared with previously published results. Despite the increasing proportion of severe cases, we observed that the case-fatality ratio remained stable over the past 20 years. This observation may reflect improvements in severe sepsis management (*21*) or mechanical ventilation strategies (*22*), such as extracorporeal membrane oxygenation, for blastomycosis-related acute respiratory distress syndrome (*23*). Extracorporeal membrane oxygenation use increased substantially since 2002 (*24*); this treatment has been shown to decrease deaths in adults with severe acute respiratory failure (*25*). In addition, we documented the gradual replacement of amphotericin B deoxycholate by lipid formulations of amphotericin B. Despite its well-demonstrated effectiveness, amphotericin B deoxycholate is associated with renal toxicity (*26*). Patients with AIDS who had disseminated histoplasmosis and were treated with liposomal amphotericin B have demonstrated better clinical outcomes compared with patients who were treated with the deoxycholate forms (*27*). The increasing use of lipid formulations of amphotericin B may have contributed to the improved patient outcomes in this study, although a head-to-head comparison of amphotericin B formulations for *B. dermatitidis* infection has not been performed in clinical trials. Our study was not adequately powered to verify this hypothesis.

We used WGS to characterize the complete genome of our isolates. The high reproducibility and discriminatory power of WGS (*28*) enabled us to detect a strong association between genotype groups and the region where patients lived, where we assumed they acquired infection. These findings are similar to those of a study in Canada (*29*) that showed that the populations of both *Blastomyces* species were associated with major freshwater drainage. Other studies have used polymorphic microsatellite markers to genotype *B. dermatitidis* and have suggested potential associations

Table 3. Characteristics of patients according to *Blastomyces* genotype groups, Quebec, Canada*

Characteristic	Genotype I, n = 3	Genotype II, n = 25	Genotype III, n = 31	Genotype IV, n = 49	p value
Quebec administrative region					
Bas-St-Laurent	0	0	0	0 (10)	
Saguenay-Lac-St-Jean	0	0	0	1 (2)	
Capitale-Nationale	0	0	0	13 (27)	
Mauricie	0	0	1 (3)	5 (10)	
Estrie	1 (33)	0	25 (81)	4 (8)	
Montréal	1 (33)	3 (12)	3 (10)	3 (6)	
Outaouais	1 (33)	10 (40)	0	0	
Chaudière-Appalaches	0	0	1 (3)	5 (10)	
Laval	0	1 (4)	0	0	
Lanaudière	0	7 (28)	0	0	
Laurentides	0	1 (4)	0	0	
Montérégie	0	3 (12)	1 (3)	4 (8)	
Centre-du-Québec	0	0	0	9 (18)	<0.001†
Severe case					
No	3 (100)	20 (80)	27 (87)	43 (86)	
Yes	0	5 (20)	4 (13)	7 (14)	0.8†
90-day all-cause mortality					
No	3 (100)	19 (76)	26 (84)	41 (82)	
Yes	0	6 (24)	5 (16)	9 (18)	0.9†

*Values are no. (%) except as indicated.
†By Fisher exact test.

between the clinical phenotype and genetic groups of *B. dermatitidis*. Frost et al. found that SNP alleles were substantially different in cases of pulmonary and disseminated disease (*30*) and identified associations between the group 1 genotype (*B. gilchristii)* and pulmonary infection and between the group 2 genotype and disseminated disease (*31*). We had a very limited number of *B. gilchristii* infections in our study population and were therefore unable to assess the potential of these 2 groups to cause disseminated diseases within the cohort. We identified 4 main distinct genetic groups that correlate with the geographic origins, but we did not find any association between the genotype and the proportion of severe cases or mortality rate. These results indicate that virulence of *B. dermatitidis* is not correlated with its population genetic structure in Quebec. Nevertheless, we cannot exclude the possibility that virulence may be controlled by specific regions or alleles in the genome. In this case, other approaches could be more suitable such as genome-wide association mapping which reveals SNPs strongly associated with a given virulence trait.

The main limitation of our study is its retrospective nature, which could introduce information bias. We were able to minimize this bias by including on the study team specialized research assistants and infectious diseases fellows who ensured the completeness of data collection. Moreover, this study had limited power to assess the potential factors that could affect mortality rate (e.g., increasing use of lipid formulations of amphotericin B). Furthermore, the cases we analyzed in this study were restricted to patients for whom a positive *Blastomyces* culture was sent to the provincial health laboratory. Given that the diagnosis of *Blastomyces* infection is not limited to culture results, this leads to an underestimation of cases and may have created bias in our data.

The proportion of severe cases of blastomycosis in Quebec has increased over the past 30 years. These changes could be explained in part by the higher proportion of immunosuppressed patients, as well as the older age of infected persons. The study data do not support an increasing virulence of *B. dermatitidis* strains in Quebec. Future studies may help understand whether climate changes or more specific genetic determinants may have played a role in the emergence of more severe *B. dermatitidis* infections, the incidence of which has tripled over time.

This work was supported by the Centre de recherche du Centre hospitalier universitaire de Sherbrooke and The Infectious Disease and Climate Change Fund from Public Health Agency of Canada.

About the Author

Dr Carignan is a professor at the Faculté de Médecine et des Sciences de la Santé de l'Université de Sherbrooke and a clinical research scholar from the Fonds de Recherche en Santé du Québec. His research interests include the epidemiology of emerging infections associated with climate change.

References

1. Bennett JE, Dolin R, Blaser MJ. Mandell, Douglas, and Bennett's principles and practice of infectious diseases. 8th ed. Philadelphia: Elsevier Health Sciences; 2014.
2. Dworkin MS, Duckro AN, Proia L, Semel JD, Huhn G. The epidemiology of blastomycosis in Illinois and factors associated with death. Clin Infect Dis. 2005;41:e107–11. https://doi.org/10.1086/498152
3. Baumgardner DJ, Knavel EM, Steber D, Swain GR. Geographic distribution of human blastomycosis cases in Milwaukee, Wisconsin, USA: association with urban watersheds. Mycopathologia. 2006;161:275–82. https://doi.org/10.1007/s11046-006-0018-9
4. Morris SK, Brophy J, Richardson SE, Summerbell R, Parkin PC, Jamieson F, et al. Blastomycosis in Ontario, 1994–2003. Emerg Infect Dis. 2006;12:274–9. https://doi.org/10.3201/eid1202.050849
5. Crampton TL, Light RB, Berg GM, Meyers MP, Schroeder GC, Hershfield ES, et al. Epidemiology and clinical spectrum of blastomycosis diagnosed at Manitoba hospitals. Clin Infect Dis. 2002;34:1310–6. https://doi.org/10.1086/340049
6. Litvinov IV, St-Germain G, Pelletier R, Paradis M, Sheppard DC. Endemic human blastomycosis in Quebec, Canada, 1988–2011. Epidemiol Infect. 2013;141:1143–7. https://doi.org/10.1017/S0950268812001860
7. Seitz AE, Younes N, Steiner CA, Prevots DR. Incidence and trends of blastomycosis-associated hospitalizations in the United States. PLoS One. 2014;9:e105466. https://doi.org/10.1371/journal.pone.0105466
8. Baumgardner DJ, Paretsky DP, Baeseman ZJ, Schreiber A. Effects of season and weather on blastomycosis in dogs: Northern Wisconsin, USA. Med Mycol. 2011;49:49–55. https://doi.org/10.3109/13693786.2010.488658
9. Elections Quebec. Administrative entities linked to a postal code. 2020 October 20 [cited 2020 Nov 3]. https://www.electionsquebec.qc.ca/english/provincial/electoral-map/administrative-entities-linked-to-a-postal-code.php
10. Charlson ME, Pompei P, Ales KL, MacKenzie CR. A new method of classifying prognostic comorbidity in longitudinal studies: development and validation. J Chronic Dis. 1987;40:373–83. https://doi.org/10.1016/0021-9681(87)90171-8
11. Lohrenz S, Minion J, Pandey M, Karunakaran K. Blastomycosis in southern Saskatchewan 2000–2015: unique presentations and disease characteristics. Med Mycol. 2018;56:787–95. https://doi.org/10.1093/mmy/myx131
12. Harpaz R, Dahl RM, Dooling KL. Prevalence of immunosuppression among US adults, 2013. JAMA. 2016;316:2547–8.
13. Novosad SA, Winthrop KL. Beyond tumor necrosis factor inhibition: the expanding pipeline of biologic therapies for inflammatory diseases and their associated infectious sequelae. Clin Infect Dis. 2014;58:1587–98. https://doi.org/10.1093/cid/ciu104

14. Memoli MJ, Athota R, Reed S, Czajkowski L, Bristol T, Proudfoot K, et al. The natural history of influenza infection in the severely immunocompromised vs nonimmunocompromised hosts. Clin Infect Dis. 2014;58:214–24. https://doi.org/10.1093/cid/cit725
15. Institut National de Santé Publique du Québec. Aging in Québec [cited 2020 Nov 3]. https://www.inspq.qc.ca/le-vieillissement-au-quebec
16. Ins Institut National de Santé Publique du Québec. Diabetes. 2020 [cited 2020 Nov 3]. https://www.inspq.qc.ca/santescope/syntheses/diabete
17. Mehta AB, Syeda SN, Wiener RS, Walkey AJ. Epidemiological trends in invasive mechanical ventilation in the United States: a population-based study. J Crit Care. 2015;30:1217–21. https://doi.org/10.1016/j.jcrc.2015.07.007
18. Rush B, Lother S, Paunovic B, Mooney O, Kumar A. Outcomes with severe blastomycosis and respiratory failure in the United States. Clin Infect Dis. 2021;72:1603–7. https://doi.org/10.1093/cid/ciaa294
19. Ireland M, Klumb C, Smith K, Scheftel J. Blastomycosis in Minnesota, USA, 1999–2018. Emerg Infect Dis. 2020;26:866–75. https://doi.org/10.3201/eid2605.191074
20. Carignan A, Denis M, Abou Chakra CN. Mortality associated with *Blastomyces dermatitidis* infection: a systematic review of the literature and meta-analysis. Med Mycol. 2020;58:1–10. https://doi.org/10.1093/mmy/myz048
21. Stevenson EK, Rubenstein AR, Radin GT, Wiener RS, Walkey AJ. Two decades of mortality trends among patients with severe sepsis: a comparative meta-analysis. Crit Care Med. 2014;42:625–31. https://doi.org/10.1097/CCM.0000000000000026
22. Kawai K, Gebremeskel BG, Acosta CJ. Systematic review of incidence and complications of herpes zoster: towards a global perspective. BMJ Open. 2014;4:e004833. https://doi.org/10.1136/bmjopen-2014-004833
23. Bednarczyk JM, Kethireddy S, White CW, Freed DH, Singal RK, Bell D, et al. Extracorporeal membrane oxygenation for blastomycosis-related acute respiratory distress syndrome: a case series. Can J Anaesth. 2015;62:807–15. https://doi.org/10.1007/s12630-015-0378-z
24. McCarthy FH, McDermott KM, Kini V, Gutsche JT, Wald JW, Xie D, et al. Trends in U.S. extracorporeal membrane oxygenation use and outcomes: 2002–2012. Semin Thorac Cardiovasc Surg. 2015;27:81–8. https://doi.org/10.1053/j.semtcvs.2015.07.005
25. Peek GJ, Mugford M, Tiruvoipati R, Wilson A, Allen E, Thalanany MM, et al.; CESAR trial collaboration. Efficacy and economic assessment of conventional ventilatory support versus extracorporeal membrane oxygenation for severe adult respiratory failure (CESAR): a multicentre randomised controlled trial. Lancet. 2009;374:1351–63. https://doi.org/10.1016/S0140-6736(09)61069-2
26. Girois SB, Chapuis F, Decullier E, Revol BG. Adverse effects of antifungal therapies in invasive fungal infections: review and meta-analysis. Eur J Clin Microbiol Infect Dis. 2006;25:138–49. https://doi.org/10.1007/s10096-005-0080-0
27. Johnson PC, Wheat LJ, Cloud GA, Goldman M, Lancaster D, Bamberger DM, et al.; US National Institute of Allergy and Infectious Diseases Mycoses Study Group. Safety and efficacy of liposomal amphotericin B compared with conventional amphotericin B for induction therapy of histoplasmosis in patients with AIDS. Ann Intern Med. 2002;137:105–9. https://doi.org/10.7326/0003-4819-137-2-200207160-00008
28. Araujo R. Towards the genotyping of fungi: methods, benefits and challenges. Curr Fungal Infect Rep. 2014;8:203–10.
29. McTaggart LR, Brown EM, Richardson SE. Phylogeographic analysis of *Blastomyces dermatitidis* and *Blastomyces gilchristii* reveals an association with North American freshwater drainage basins. PLoS One. 2016;11:e0159396. https://doi.org/10.1371/journal.pone.0159396
30. Frost HM, Anderson JL, Ivacic L, Sloss BL, Embil J, Meece JK. Development and validation of a novel single nucleotide polymorphism (SNP) panel for genetic analysis of *Blastomyces* spp. and association analysis. BMC Infect Dis. 2016;16:509. https://doi.org/10.1186/s12879-016-1847-x
31. Meece JK, Anderson JL, Gruszka S, Sloss BL, Sullivan B, Reed KD. Variation in clinical phenotype of human infection among genetic groups of *Blastomyces dermatitidis*. J Infect Dis. 2013;207:814–22. https://doi.org/10.1093/infdis/jis756

Address for correspondence: Alex Carignan, Department of Microbiology and Infectious Diseases, Université de Sherbrooke, 3001, 12th Ave N, Sherbrooke, QC J1H 5N4, Canada; email: Alex.Carignan@USherbrooke.ca

Hepatitis A Virus Incidence Rates and Biomarker Dynamics for Plasma Donors, United States

Stephanie Schoch, Martin Wälti, Mathias Schemmerer, Rick Alexander, Björn Keiner, Carol Kralicek, Keith Bycholski, Kelley Hyatt, Jon Knowles, Denis Klochkov, Toby Simon, Jürgen J. Wenzel, Nathan J. Roth, Eleonora Widmer

The United States is currently affected by widespread hepatitis A virus (HAV) outbreaks. We investigated HAV incidence rates among source plasma donors in the United States since 2016. Serial donations from HAV-positive frequent donors were analyzed for common biologic markers to obtain a detailed picture of the course of infection. We found a considerable increase in incidence rates with shifting outbreak hotspots over time. Although individual biomarker profiles were highly variable, HAV RNA typically had a high peak and a biphasic decrease and often remained detectable for several months. One donor had a biomarker pattern indicative of previous exposure. Our findings show that current HAV outbreaks have been spilling over into the plasma donor population. The detailed results presented improve our comprehension of HAV infection and related public health aspects. In addition, the capture of full RNA curves enables estimation of HAV doubling time.

Hepatitis A virus (HAV) is a small, nonenveloped RNA virus belonging to the family *Picornaviridae*. Its biology and transmission cycle have been reviewed elsewhere (*1*,*2*) and are therefore only briefly introduced. Six genotypes and 1 serotype have been described; genotypes I–III circulating in humans and IV–VI circulating in nonhuman primates. Virions exist in either of 2 forms (*3*): lipid-associated (main form in blood, also referred to as quasi-enveloped) or truly nonenveloped (main form in stool). Although parenteral transmission has also been reported, the predominant transmission route is the fecal–oral through contact with infected persons or uptake of contaminated food and water. Infection might involve an early, as of yet poorly characterized, extrahepatic replication phase (e.g., in gut epithelial cells [*4*]); from the gut, virions are then transported through the blood to their primary replication site, the liver. The transmission cycle ends with a transport of viral progeny via the bile to the gut, leading to massive virus shedding in stool (*2*). Although the course of disease is generally self-limiting, several serious complications can occur, especially in older persons or in combination with risk factors.

Since 1995, when the first HAV vaccine was licensed in the United States, the annual US incidence rate of acute hepatitis A has decreased tremendously (*1*,*5*). During 2015, the National Notifiable Diseases Surveillance System of the Centers for Disease Control and Prevention (CDC) recorded an annual average of 0.4 cases/100,000 inhabitants (*5*). However, since 2016, the downward trend has reversed (*6*). In mid-2016–early 2017, Michigan, California, Kentucky, and Utah began to report local person-to-person HAV outbreaks, which have since become a national concern: 38,031 cases affecting 35 states (status as of February 2021) (*7*). In 2018, the annual US incidence rate was 3.8 cases/100,000 population, and the true rate was estimated to be twice as high because of under-ascertainment and under-reporting (*6*). The current outbreak is enhanced by the fact that most (≈74%) of US-born adults are susceptible to HAV (*8*). This pattern is typical for industrialized countries that have good standards of sanitation and hygiene and a history of restrictive (mostly infant-targeted or risk group–targeted) vaccination practices (*9*). HAV genotype IB has been the most common genotype during this outbreak, whereas before 2017, most cases in the United States involved genotype IA (*10*).

Author affiliations: CSL Behring AG, Bern, Switzerland (S. Schoch, M. Wälti, D. Klochkov, N.J. Roth, E. Widmer); University Medical Center Regensburg, Regensburg, Germany (M. Schemmerer, J.J. Wenzel); CSL Plasma, Knoxville, Tennessee, USA (R. Alexander); CSL Behring GmbH, Marburg, Germany (B. Keiner); CSL Plasma, Boca Raton, Florida, USA (K. Bycholski, K. Hyatt, J. Knowles, T. Simon); CSL Plasma, Dallas, Texas, USA (C. Kralicek)

DOI: https://doi.org/10.3201/eid2711.204642

Human plasma is used as a starting material to produce several life-saving therapies, such as immunoglobulins. The safety of these products with regard to transmission of bloodborne viruses is based on 3 pillars: selecting low-risk donors, testing for relevant viral markers, and including process steps capable of removing or inactivating a broad range of viruses.

To ensure a reliable supply of therapies, CSL operates a large collection center network for source plasma, which is plasma serially collected from healthy, voluntary donors through plasmapheresis. CSL Plasma, a division of CSL, operates one of the largest global plasma collection networks, consisting of >260 collection centers throughout the United States. Each donation collected is tested for HAV RNA. These data provide a unique glimpse into how the HAV epidemiology trends in the United States have changed. Unlike whole blood donors, plasma donors are allowed to donate frequently, which can be useful from a research perspective.

During 2017, we noticed a trend toward higher HAV incidence rates among US donors. Because knowledge on the course of infection and host response during asymptomatic/subclinical infection is scant, we conducted this study. The aim of this study was to assess the effects of the current HAV outbreak on plasma donors in the United Sates and to complement existing knowledge on HAV biomarker dynamics.

Materials and Methods

Plasma and Routine Viral Marker Testing

Source plasma donors in the United States can donate ≤2 donations/week. Plasma donations and matching samples for routine viral marker testing (HIV, hepatitis B virus [HBV], hepatitis C virus [HCV], HAV, and parvovirus B19) were collected from donors by plasmapheresis in 4% sodium citrate and frozen at ≤–30°C. The freezing process was compliant with the European Pharmacopeia (*11*). We performed routine, qualitative nucleic acid testing (NAT) for HAV by using the Roche Cobas DPX Test (https://diagnostics.roche.com) on minipools of ≤96 donations. In the format used, the 95% limit of detection (LOD) of the assay was ≈105.6 IU/mL of HAV RNA/individual donation. We subjected HAV-positive minipools to resolution testing down to the individual donation. For all donors with a first HAV-positive donation, all previous/subsequent donations from a defined time period were put on quarantine and excluded from use for fractionation.

Donor Selection

We retrospectively included in this study 10 qualified US-source plasma donors with ≥1 HAV-positive NAT result; these donors had met all medical criteria for donation (*12*). To ensure optimal coverage of the viremic phase, donors had to fulfill 3 additional criteria: first, >10 serial donations from 1 month before to 2 months after the first HAV-positive donation available; second, ≥1 nonreactive donation preceding the first positive donation; and third, some coverage of the late phase of infection. The aim was to analyze all donations collected during the period −30 to +120 days of the first HAV NAT-positive donation (day 0). Nevertheless, for 7 of 10 donors, 1–7 donations were unavailable (plasma discarded or used for other research purposes).

Nonroutine Biomarker Testing

Testing was performed by accredited contract-testing laboratories using validated assays after having received approval for the study protocol by the WIRB Copernicus Group Institutional Review Board (https://www.wcgirb.com). Samples used were deidentified aliquots of quarantined donations stored at ≤–20°C; they had been subjected to 2 freeze–thaw cycles at the time of testing. We tested the following biomarkers at the individual donation level for each sample: HAV RNA, liver injury marker alanine aminotransferase (ALT), and HAV IgM and IgG.

HAV RNA was quantified at Interregional Blood Transfusion, Swiss Red Cross (IRB SRC), Bern, Switzerland (https://www.redcross.ch), by using a NAT assay targeted against the HAV 5′-noncoding region, which had a validated 95% LOD of 14 IU/mL and a linear range of 81.6–1.1 × 10^8 IU/mL (*13*). The remaining analytics were performed at the National Reference Laboratory for HAV, University Medical Center Regensburg, Regensburg, Germany. ALT was measured by using the quantitative Roche Cobas ALT Assay (Roche reference no. 05850797–190), which had a validated LOD of 5 IU/L for serum and upper limits of reference ranges of 35 IU/L for women and 50 IU/L for men. A control experiment with ALT-spiked samples confirmed that the citrate plasma matrix had no major impact on readout of the assay: at 50 IU/L and 150 IU/L ALT, average readouts for spiked serum and citrate plasma samples were within <5% of each other. A total of 13 ALT results from 3 donors were invalid because samples exceeded the lipemia threshold. We analyzed HAV IgM and IgG by using the Abbott Architect HAVAb IgM and IgG Assays (https://www.abbott.com). Finally, we identified the

HAV genotype by sequencing HAV coat protein viral protein 1/core protein P2A regions as described (*14*).

HAV Doubling Time

We calculated doubling time (Td) by using the formula Td = ln(2)/B based on an exponential trendline ($y = Ae^{Bx}$) determined in Excel (Microsoft, https://www.microsoft.com) for each donor's HAV RNA growth curve. In these equations A and B represent calculated coefficients standing for HAV RNA initial amount (A) and growth rate (B), e is base of the natural logarithm, x is time in days, and y is HAV RNA titer in IU per milliliter. To focus exclusively on the logarithmic growth phase, we excluded samples with a positive HAV IgM or IgG result and from visibly flattened areas of the RNA curve. Donor E was excluded from the analysis because the early growth phase was not represented.

Results

HAV Incidence Rates for Plasma Donors

During January 2016–December 2020, a total of 348 different donors from the United States donated plasma that tested positive for HAV RNA; these donations were excluded from further manufacturing processes. Monthly HAV incidence rates derived from these data showed a considerable increase from typically 0.0 cases/100,000 donors at the beginning of 2016 to a peak rate of 5.8 cases/100,000 donors during October 2019 (Figure 1). The highest rates were found during November 2018–November 2019; most cases were found in the states of Indiana, Ohio, Tennessee, Pennsylvania, and Florida.

After an intermittent decrease in case rates, a second main peak was observed during May–December 2020. This peak was driven by case numbers in South Carolina, Kansas, Texas and Georgia. The number of states that had donors affected increased, in parallel with the incidence rates, to 30 by December 2020 (Figure 2). The plasma donor case number map for December 2020 matches the CDC case number map (Figure 3) (*7*). One exception to this pattern is the state of Texas, where case numbers among plasma donors have lately increased, but so far no outbreak-associated cases were reported. Overall, data suggest that HAV outbreaks in the United States have been spilling over into the plasma donor population.

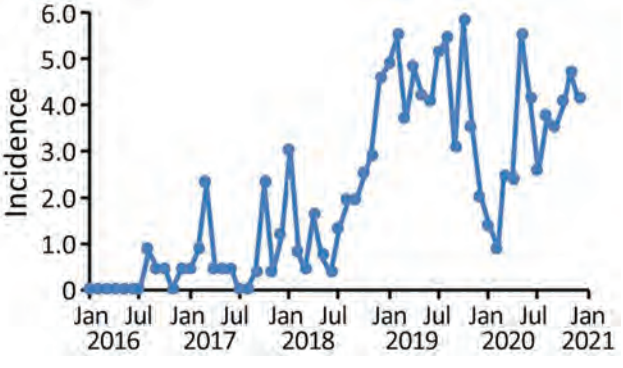

Figure 1. Incidence rates for hepatitis A virus (HAV) in source plasma donors, United States, 2016–2020. Shown are monthly HAV incidence rates based on routine viral marker testing. Incidence rates correspond to monthly number of previously HAV RNA-negative donors with a first positive HAV nucleic acid testing result per 100,000 donors.

HAV Biomarker Results for Donors who Showed Seroconversion

To assess the course of infection and immune response in the context of asymptomatic or subclinical HAV infection, we analyzed donations from 10 donors who had positive results (≥1 HAV RNA positive donation based on routine testing) by using a panel of nonroutine analytics. The panel included quantitative HAV RNA and ALT assays, semiquantitative HAV IgM and IgG assays, and HAV genotyping.

For 9 of 10 donors, HAV infection was clearly confirmed; these donors eventually showed seroconversion for HAV IgM and IgG, and 8 of them showed a transient increase in ALT (Figure 4). The finding that 2 (22%) of these donors were infected with HAV genotype IA and 7 (78%) with IB matches the genotype distribution reported for the current outbreak (15% IA, 84% IB, and <1% IIIA [*15*]). The overall sequence of events for HAV-infected plasma donors was similar to that reported for symptomatic patients: the HAV RNA peak typically preceded the ALT and IgM peak, which in turn preceded the IgG plateau, albeit with considerable individual variation in amplitude and timing (compare donors B, C, and J). Donor B had a particularly interesting profile: low RNAemia, weak IgM response, no increase in ALT, and an unusually early IgG response.

RNA curves obtained showed a maximum HAV RNA titer of 3.1×10^8 IU/mL whereby peak titers ≥10^7 IU/mL were common (6/10 donors). Earlier studies had reported an even higher RNAemia of 8.59×10^8 IU/mL (*16*), but suggested lower typical peak titers (*16*,*17*). Although the early phase of infection was characterized by rapid exponential growth and a median estimated HAV doubling time of 17.5 (range 14.1–24.7) hours (Table), the later phase often showed a more or less pronounced biphasic decrease, resulting in a skewed or shouldered RNA curve. Duration of RNAemia was highly variable among donors (Table) (mean 95 days, median 106 days). This duration was similar to

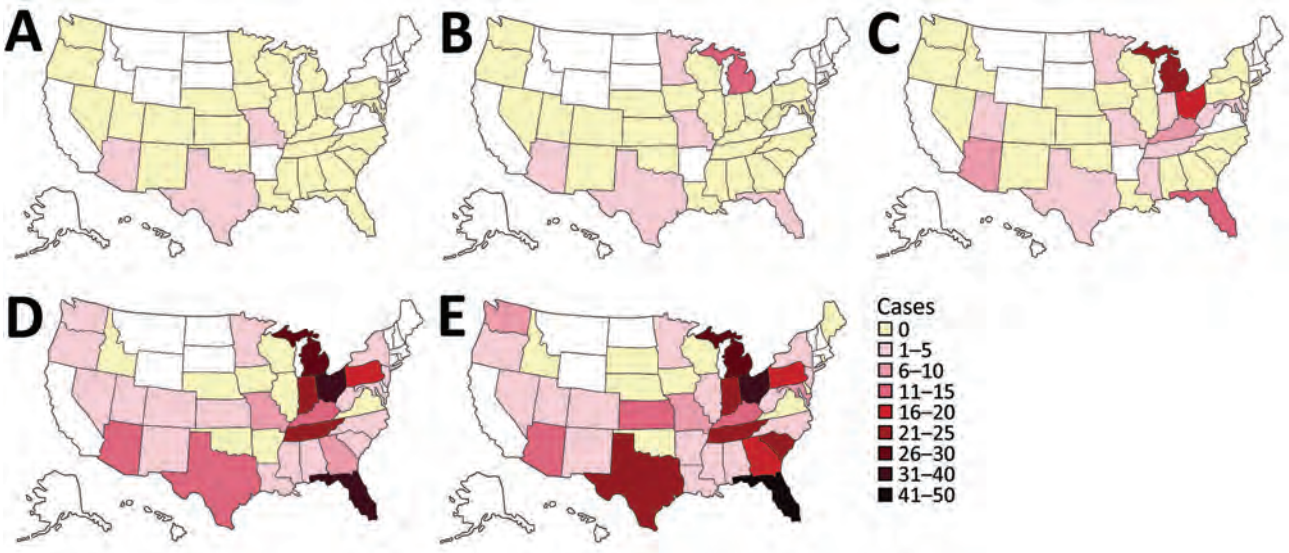

Figure 2. Geographic distribution of hepatitis A virus–positive plasma donors, United States, 2016–2020. Cumulative case counts are indicated: A) 2016; B) 2016–2017; C) 2016–2018; D) 2016–2019; E) 2016–2020. These counts reflect how hepatitis A outbreaks in the United States have spread and spilled over into the plasma donor population over time. No color indicates states for which no data are available (no plasma collection). Maps were created by using an Adobe Stock template (https://stock.adobe.com).

that reported for humans who had symptomatic HAV infection (mean 95 days, range 36–391 days) (*18*) but considerably longer than typically examples of RNAemia curves (*2*).

The first HAV IgM-reactive plasma donations occurred a mean (±SD) of 21 (±10) days from day 0; the first IgG-reactive donations were 25 (± 11) days from day 0. Day 0 is the first collection date that showed detectable HAV RNA. No clear association between key serologic and other parameters could be identified (e.g., higher HAV RNA titers were not associated with a faster IgM or IgG response). Analysis of IgM positivity patterns suggests that IgM remained reliably detectable for a median duration of 42 days (range 1–59 days) (Table) when measured by using the Abbot Architect HAVAb IgM assay. After this period, IgM might remain detectable (≤112 days after the first IgM-positive result), but not reliably, as suggested by IgM results fluctuating between positive, equivocal, and negative.

To assess whether liver function was affected during the course of asymptomatic/mild HAV infection, we measured ALT levels in all samples from donors who showed seroconversion. Only donor B lacked an ALT peak (Figure 4). For the other 8 donors, we found a median 27-fold increase in ALT over baseline (range 8- to 159-fold) and increased peak ALT titers (mean 452 IU/L, median 271 IU/L, range 40–1,262 IU/L) (Table). These data suggest that liver function is noticeably impacted during most infections, even if peak ALT levels in plasma donors were typically lower than those reported for cases of acute viral hepatitis in general (300–3,000 IU/L) (*19*) and acute hepatitis A in particular (mean 2,000 IU/L and levels >5,000 IU/L for 10% of cases) (*20*). In several instances, ALT levels remained high for prolonged periods (donors G and J) or showed a second peak (donor C).

HAV Biomarker Results for Donor F

One of 10 selected donors (donor F) had 1 HAV RNA-reactive donation on the basis of the Cobas DPX Assay but never showed seroconversion. All

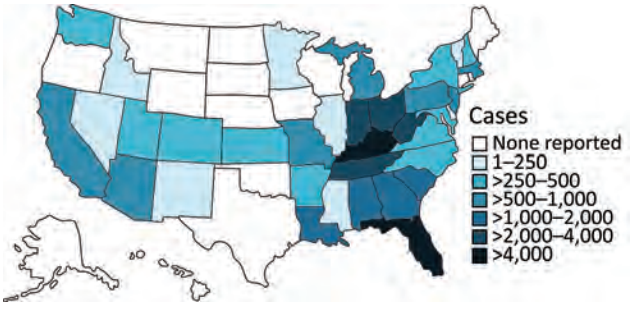

Figure 3. Geographic distribution of CDC-reported HAV outbreak cases, United States, as of February 2021, showing state-reported HAV outbreak cases as listed on the CDC website for the current outbreak since August 2016 (*7*). Outbreak-associated status is determined at state level in accordance with the respective outbreak case definition for each state. Therefore, HAV cases not classified as outbreak-associated are probably not captured in CDC data. CDC, Centers for Disease Control and Prevention; HAV, hepatitis A virus.

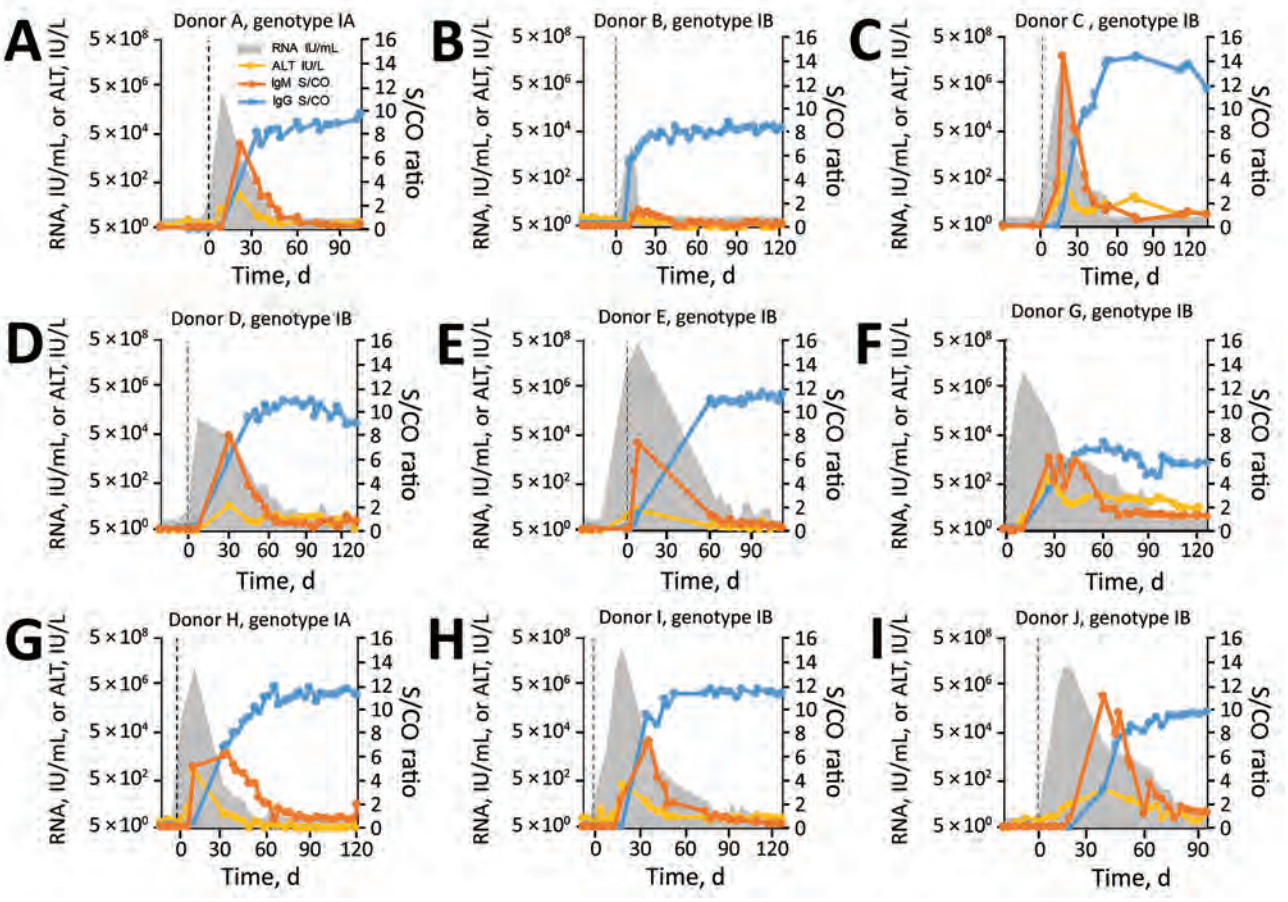

Figure 4. HAV biologic and clinical marker dynamics in plasma donors, United States. Quantitative HAV RNA and ALT results, as well as semiquantitative HAV IgM and IgG results, are shown for all 9 donors who seroconverted. Vertical dashed lines indicate day 0, the earliest collection date with detectable HAV RNA. Reactive nucleic acid testing results below the validated limit of detection of 14 IU/mL are not shown. The IgG result is defined as nonreactive/reactive for S/CO ratios <1 and ≥1, respectively. The IgM assay is defined as nonreactive/reactive for S/CO ratios <0.80 and >1.20, respectively, and as gray zone reactive for S/CO ratios of 0.80–1.20. The results of a tenth donor (donor F) who had 1 confirmed weak-positive HAV RNA result and all nonreactive IgM/IgG results are not shown but are described in the Results. The figure illustrates the extensive individual variation in viremia curves and timing of biomarker events. ALT, alanine aminotransferase; HAV, hepatitis A virus; S/CO, signal-to-cutoff ratio.

13 tested donations from day –10 to day +40 were IgM/IgG negative, and efforts to determine the HAV genotype were not successful. We performed several follow-up analyses to assess whether the initial reactive NAT result (cycle threshold value 35.7) might have been a false-positive result. However, we found no such evidence. First, a second independent HAV RNA test confirmed the low-level reactive result for the donation in question. Second, analysis of 12 immune status markers for common pathogens showed matching results between the index sample and 2 other samples from the same donor. Therefore, a sample or donation mixup is highly unlikely. Finally, analysis of routine donation screening results of 54 HAV RNA-positive donors showed that at least 7 donors (13%) had a positivity pattern similar to that for donor F, who had a single weak-positive donation among many negative donations. Further analyses are needed to clarify what is occurring in these examples.

Discussion

Our finding that HAV incidence rates among US-source plasma donors have increased in parallel with those in the general US population is not a concern for patients receiving plasma-derived medicinal products. A final product safety margin is considered adequate if the validated process virus reduction factor clearly exceeds the potential viral load of the starting material (*21*). When an epidemiologic situation worsens, safety is assured through appropriate measures associated with the

classical virus safety pillars (e.g., use of NAT to exclude viremic donations [22] or an adequate validated process virus reduction capacity).

According to industry standards (*22*), source plasma donations and manufacturing pools are tested for HAV RNA and are excluded from further manufacture if positive. Another common practice is to discard donations with negative test results before or after the donation that tested positive. This procedure is a regulatory requirement in the European Union and ensures that any residual virus titer of the starting material, the plasma pool, is minimal and well controlled. A worst-case residual virus titer (such as defined by the validated LOD of the pool testing assay) is generally taken into account when assessing final product safety.

Whether the incidence rates for source plasma donors can be extrapolated to other blood component donors is still unclear. In any case, such comparisons would be difficult because of probable differences in geographic sourcing, testing algorithms, donation frequencies, and potential differences in vaccination rates.

At least in the early phase of the HAV outbreaks, ≈57% of cases reported to CDC were associated with risk factors such as drug use or homelessness (*10*). Although our study did not include a retrospective risk factor investigation, which is a limitation, we consider it unlikely that these risk groups would be greatly represented in the donor population. Donors undergo a careful selection process, which includes extensive measures to prevent plasma collection from risk groups (e.g., medical examination, questionnaire addressing drug use, risk-based drug testing, proof of postal address). Although the donor selection process cannot fully exclude rare cases of noncompliance, it is only 1 of 3 complementary safety pillars (donor screening, donation testing, validated pathogen clearance) that have tremendously improved the safety of plasma products over the past few decades. A potential alternative explanation is that the outbreaks have spread from risk groups to the broader population, including plasma donors. A similar spillover was recently reported for an HAV outbreak that started among men who have sex with men (*23*). Perhaps a narrow confinement within risk groups, even if these are the drivers of an outbreak, cannot necessarily be expected for a highly resistant virus that often causes asymptomatic infections and undergoes fecal–oral transmission (*1*).

One aspect we observed is a shift in local HAV hotspots over time. Although collection centers in Indiana, Ohio, Tennessee, Pennsylvania, and Florida accounted for 57% of cases observed during 2018 (n = 65) and 59% of all cases observed during 2019 (n = 164), they represented only 13% of all cases during 2020 (n = 92). This abrupt decrease might indicate that measures taken by public health officials, such as information campaigns and vaccination programs, are beginning to bear fruit. Nevertheless, a confounding influence of coronavirus disease–related measures (e.g., heightened hygiene and social distancing) cannot be entirely excluded.

Our finding that most infected donors showed increased HAV RNA peak titers confirms that persons who have an asymptomatic/subclinical HAV infection might potentially be highly infectious. For instance, in a transfusion setting, as long as neither donor nor recipient have neutralizing antibodies, plasma RNA levels are typically expected to correlate with virus transmission risk. Therefore, adequate measures to prevent HAV transmission are needed.

Table. Descriptive statistics of HAV infection and immune response in plasma donors, United States*

Parameter	No. samples	Mean	SD	Median	Range
Time to peak RNA, d†	9	12.2	3.8	11.0	8–19
Peak RNA titer, IU/mL	9	7.77×10^7	1.12×10^8	2.61×10^7	1.2×10^4–3.1×10^8
Duration of viremia ≥100 IU/mL, d	9	54.8	23.4	55.0	14–88
Duration of detectable viremia, d	9	95.0	33.2	106.0	32–128
HAV doubling time, hours	8	18.0	3.5	17.5	14.1–24.7
Time to first positive IgM result, d†	9	21.1	10.3	19.0	7–37
Time to peak IgM S/CO ratio, d†	9	26.4	10.2	29.0	9–38
Peak IgM signal, S/CO	9	7.6	3.6	7.3	1.4–14.4
Duration of consecutive positive IgM, d	9	36.1	19.6	42.0	1–59
Days between first and last positive IgM result	9	61.3	37.6	58.0	7–112
Time to first positive IgG result, d†	9	25.2	10.7	29.0	9–37
Plateau IgG signal, S/CO	9	10.0	2.2	10.4	5.7–13.5
Time to peak ALT, d†	8	22.0	10.5	21.0	7–37
Maximum fold-change relative to baseline ALT	8	65.1	65.4	27.0	8–159
Peak ALT titer, IU/L	8	452.1	443.4	270.5	40–1,262
No. donations analyzed/donor	9	28.6	6.4	28.0	19–41

*Parameters listed were extracted based on donors who seroconverted (n = 9); donor F was excluded because of absence of seroconversion. For 4 cases, 1 additional donor was excluded from the analysis: donor B for ALT-related parameters (no visible ALT peak) and donor E for extrapolation of HAV doubling time (no early HAV RNA-positive sample available). ALT, alanine aminotransferase; HAV, hepatitis A virus; S/CO, signal-to-cutoff ratio.
†Relative to day 0 (defined as collection date with first detectable HAV RNA).

Whether the protracted low-level RNAemia observed during the late phase of infection is relevant from a pathophysiologic perspective is less clear and might depend on the HAV variant circulating. Although naked HAV virions are expected to be neutralized by HAV antibodies, this assumption might not apply to the more recently described quasi-enveloped HAV particles (*3*) and capsid-free HAV genomes, which are infectious because the RNA plus-strand orientation enables direct use as messenger RNA (*24*,*25*). The host cell entry of both of these variants is mediated by exosomes and relies on distinct host cell factors not used in the same way by naked virions (*25*).

On the basis of the unusual biomarker pattern (Figure 4), it is conceivable that donor B has had previous exposure to an HAV vaccine or natural HAV. Donor B had no ALT response, the lowest peak RNA (12,376 IU/mL), the lowest virus doubling time (24.7 hours), a weak IgM response, and a fast IgG response (positive IgG within 11 days after the first HAV RNA-positive result).

Clinical studies indicate that a small percentage of HAV vaccinees do not reach protective antibody titers or seroconversion after a single dose (*26*,*27*). Similarly, although natural HAV infection is generally believed to induce lifelong immunity (*1*,*9*), exposure to low infectious doses might not always result in a detectable humoral response. This finding highlights the case of donor F, who, after a single confirmed HAV RNA-positive donation, did not seroconvert and declared to never have been vaccinated against HAV. Finally, in rare instances, vaccinated or naturally infected persons might lose their IgG and become susceptible again. For example, a transient, asymptomatic HAV reinfection was reported for 1 patient (albeit one with detectable previous HAV immunity) who had received contaminated erythrocytes (*13*).

Virus doubling time is a useful infection parameter that has potential implications for virus transmission risk. Doubling time is probably influenced by both virus- and host-specific parameters, such as the initial number of infected cells, virus replication and egress strategy, or host cell metabolism. The following doubling times have been reported for bloodborne viruses in humans: HBV, 62.4 hours (range 31 hours−15 days) (*28*); HIV, 15.6 hours (range 8.9 hours–62.6 hours) (*29*); and HCV, 10.8 hours or 17.8 hours (range not specified) (*30*,*31*). HAV doubling time (median 17.5 hours, range 14.1–24.7 hours) partially overlaps with that reported for HCV. Whether this finding is the result of similarities (*32*) such as being a hepatotrophic plus-strand RNA virus remains unknown.

In summary, in parallel with HAV incidence rates in the general population in the United States, HAV infections among US source plasma donors have increased several-fold since January 2016. We leveraged the donors' frequent donation pattern to capture full RNA, ALT, and HAV IgM/IgG curves. This highly granular biomarker data consolidates our understanding of HAV infection and represents a highly useful resource for clinicians and other public health stakeholders.

Acknowledgments

We thank Martin Stolz for sharing his analytics expertise and Michael Schiffer for critically reviewing the manuscript.

S.S., M.W., D.K., N.J.R., E.W., R.A., B.K., K.B., K.H., T.S., and C.K. are employees of CSL, a manufacturer of plasma-derived biotherapies.

About the Author

Dr. S. Schoch is a senior scientist at CSL Behring AG, Bern, Switzerland. Her research interests are entry of enveloped viruses, in vitro virologic diagnostics, and pathogen safety aspects of bloodborne viruses.

References

1. Hollinger FB, Martin A. Hepatitis A virus. In: Knipe DM, Howley PM, editors. Fields virology, 6th ed. Philadelphia: Lippincott Williams & Wilkins; 2013. p.550–81.
2. Martin A, Lemon SM, Hepatitis A. Hepatitis A virus: from discovery to vaccines. Hepatology. 2006;43(Suppl 1):S164–72. https://doi.org/10.1002/hep.21052
3. Feng Z, Hensley L, McKnight KL, Hu F, Madden V, Ping L, et al. A pathogenic picornavirus acquires an envelope by hijacking cellular membranes. Nature. 2013;496:367–71. https://doi.org/10.1038/nature12029
4. Asher LV, Binn LN, Mensing TL, Marchwicki RH, Vassell RA, Young GD. Pathogenesis of hepatitis A in orally inoculated owl monkeys (*Aotus trivirgatus*). J Med Virol. 1995;47:260–8. https://doi.org/10.1002/jmv.1890470312
5. Centers for Disease Control and Prevention. Viral hepatitis surveillance—United States, 2015 [cited 2020 Sep 5]. https://www.cdc.gov/hepatitis/statistics/SurveillanceRpts.htm
6. Centers for Disease Control and Prevention. Viral hepatitis Surveillance—United States, 2018 [cited 2020 Sep 5]. https://www.cdc.gov/hepatitis/statistics/SurveillanceRpts.htm
7. Centers for Disease Control and Prevention. Widespread outbreaks of hepatitis A across the United States [cited 2021 Mar 4]. https://www.cdc.gov/hepatitis/outbreaks/2017March-HepatitisA.htm
8. Yin S, Barker L, Ly KN, Kilmer G, Foster MA, Drobeniuc J, et al. Susceptibility to hepatitis A virus infection in the United States, 2007–2016. Clin Infect Dis. 2020;71:e571–9. https://doi.org/10.1093/cid/ciaa298
9. World Health Organization. The immunological basis for immunization series: module 18: hepatitis A. 2019, 1–68 [cited 2021 Aug 2]. https://apps.who.int/iris/bitstream/handle/10665/326501/97892516327-eng.pdf

10. Foster M, Ramachandran S, Myatt K, Donovan D, Bohm S, Fiedler J, et al. Hepatitis A virus outbreaks associated with drug use and homelessness—California, Kentucky, Michigan, and Utah, 2017. MMWR Morb Mortal Wkly Rep. 2018;67:1208–10. https://doi.org/10.15585/mmwr.mm6743a3
11. European Pharmacopeia. Human plasma for fractionation (monograph 853) [cited 2021 Aug 2]. https://pharmacopoeia.ru/en/fs-3-3-2-0001-15-plazma-cheloveka-dlya-fraktsionirovaniya
12. Plasma Protein Therapeutics Association. International quality plasma program standards on donor health and donor management [cited 2021 Aug 2]. https://www.pptaglobal.org/safety-quality/standards/iqpp
13. Gowland P, Fontana S, Niederhauser C, Taleghani BM. Molecular and serologic tracing of a transfusion-transmitted hepatitis A virus. Transfusion. 2004;44:1555–61. https://doi.org/10.1111/j.1537-2995.2004.04071.x
14. Marosevic D, Belting A, Schönberger K, Carl A, Wenzel JJ, Brey R. Hepatitis A outbreak in the general population due to a MSM-associated HAV genotype linked to a food handler, November 2017 – February 2018, Germany. Food Environ Virol. 2019;11:149–56. https://doi.org/10.1007/s12560-019-09375-3
15. Foster MA, Hofmeister MG, Kupronis BA, Lin Y, Xia GL, Yin S, et al. Increase in hepatitis A virus infections—United States, 2013–2018. MMWR Morb Mortal Wkly Rep. 2019;68:413–5. https://doi.org/10.15585/mmwr.mm6818a2
16. Gallian P, Barlet V, Mouna L, Gross S, Lecam S, Ricard C, et al. Hepatitis A: an epidemiological survey in blood donors, France 2015 to 2017. Euro Surveill. 2018;23:1800237. https://doi.org/10.2807/1560-7917.ES.2018.23.21.1800237
17. Weimer T, Streichert S, Watson C, Gröner A. Hepatitis A virus prevalence in plasma donations. J Med Virol. 2002;67:469–71. https://doi.org/10.102/jmv.10124
18. Bower WA, Nainan OV, Han X, Margolis HS. Duration of viremia in hepatitis A virus infection. J Infect Dis. 2000;182:12–7. https://doi.org/10.1086/315701
19. Johnston DE. Special considerations in interpreting liver function tests. Am Fam Physician. 1999;59:2223–30.
20. Tong MJ, el-Farra NS, Grew MI. Clinical manifestations of hepatitis A: recent experience in a community teaching hospital. J Infect Dis. 1995;171(Suppl 1):S15–8. https://doi.org/10.1093/infdis/171.Supplement_1.S15
21. European Medicines Agency. Guideline on plasma-derived medicinal products (EMA/CHMP/BWP/706271/2010). Effective date: February 1, 2012 [cited 2021 Aug 2]. https://pdf4pro.com/view/guideline-on-plasma-derived-medicinal-products-2324eb.html
22. Plasma Protein Therapeutics Association. QSEAL NAT Testing Standard (version 2.0). Effective date: June 13, 2013 [cited 2021 Aug 2]. https://www.pptaglobal.org/safety-quality/standards/qseal
23. Friesema IH, Sonder GJ, Petrignani MW, Meiberg AE, van Rijckevorsel GG, Ruijs WL, et al. Spillover of a hepatitis A outbreak among men who have sex with men (MSM) to the general population, the Netherlands, 2017. Euro Surveill. 2018;23:1800265. https://doi.org/10.2807/1560-7917.ES.2018.23.23.1800265
24. Cohen JI, Ticehurst JR, Feinstone SM, Rosenblum B, Purcell RH. Hepatitis A virus cDNA and its RNA transcripts are infectious in cell culture. J Virol. 1987;61:3035–9. https://doi.org/10.1128/jvi.61.10.3035-3039.1987
25. Costafreda MI, Abbasi A, Lu H, Kaplan G. Exosome mimicry by a HAVCR1-NPC1 pathway of endosomal fusion mediates hepatitis A virus infection. Nat Microbiol. 2020;5:1096–106. https://doi.org/10.1038/s41564-020-0740-y
26. Ott JJ, Wiersma ST. Single-dose administration of inactivated hepatitis A vaccination in the context of hepatitis A vaccine recommendations. Int J Infect Dis. 2013;17:e939–44. https://doi.org/10.1016/j.ijid.2013.04.012
27. Garner-Spitzer E, Kundi M, Rendi-Wagner P, Winkler B, Wiedermann G, Holzmann H, et al. Correlation between humoral and cellular immune responses and the expression of the hepatitis A receptor HAVcr-1 on T cells after hepatitis A re-vaccination in high and low-responder vaccinees. Vaccine. 2009;27:197–204. https://doi.org/10.1016/j.vaccine.2008.10.045
28. Yoshikawa A, Gotanda Y, Itabashi M, Minegishi K, Kanemitsu K, Nishioka K. Hepatitis B NAT virus-positive blood donors in the early and late stages of HBV infection: analyses of the window period and kinetics of HBV DNA. Vox Sang. 2005;88:77–86. https://doi.org/10.1111/j.1423-0410.2005.00602.x
29. Ribeiro RM, Qin L, Chavez LL, Li D, Self SG, Perelson AS. Estimation of the initial viral growth rate and basic reproductive number during acute HIV-1 infection. J Virol. 2010;84:6096–102. https://doi.org/10.1128/JVI.00127-10
30. Busch MP, Giachetti C, Gallarda J, Mimms LT, Peddada L, Charles H, et al. Dynamics of HCV viremia during early HCV infection: Implications for minipool vs. individual donation nucleic acid amplification testing. Transfusion. 2000;40:S25.
31. Weusten JJ, van Drimmelen HA, Lelie PN. Mathematic modeling of the risk of HBV, HCV, and HIV transmission by window-phase donations not detected by NAT. Transfusion. 2002;42:537–48. https://doi.org/10.1046/j.1537-2995.2002.00099.x
32. Qu L, Lemon SM. Hepatitis A and hepatitis C viruses: divergent infection outcomes marked by similarities in induction and evasion of interferon responses. Semin Liver Dis. 2010;30:319–32. https://doi.org/10.1055/s-0030-1267534

Address for correspondence: Denis Klochkov, CSL Behring AG, Wankdorfstrasse 10, 3014 Bern, Switzerland; email: denis.klochkov@cslbehring.com

Multidrug-Resistant Methicillin-Resistant *Staphylococcus aureus* Associated with Bacteremia and Monocyte Evasion, Rio de Janeiro, Brazil

Alice Slotfeldt Viana,[1] Ana Maria Nunes Botelho,[1,2] Ahmed M. Moustafa,[1] Craig L.K. Boge, Adriana Lucia Pires Ferreira, Maria Cícera da Silva Carvalho, Márcia Aparecida Guimarães, Bruno de Souza Scramignon Costa,[3] Marcos Corrêa de Mattos, Sabrina Pires Maciel, Juliana Echevarria-Lima, Apurva Narechania, Kelsey O'Brien, Chanelle Ryan, Jeffrey S. Gerber, Bernadete Teixeira Ferreira Carvalho, Agnes Marie Sá Figueiredo,[4] Paul J. Planet[4]

We typed 600 methicillin-resistant *Staphylococcus aureus* (MRSA) isolates collected in 51 hospitals in the Rio de Janeiro, Brazil, metropolitan area during 2014–2017. We found that multiple new clonal complex (CC) 5 sequence types had replaced previously dominant MRSA lineages in hospitals. Whole-genome analysis of 208 isolates revealed an emerging sublineage of multidrug-resistant MRSA, sequence type 105, staphylococcal cassette chromosome *mec* II, *spa* t002, which we designated the Rio de Janeiro (RdJ) clone. Using molecular clock analysis, we hypothesized that this lineage began to expand in the Rio de Janeiro metropolitan area in 2009. Multivariate analysis supported an association between bloodstream infections and the CC5 lineage that includes the RdJ clone. Compared with other closely related isolates, representative isolates of the RdJ clone more effectively evaded immune function related to monocytic cells, as evidenced by decreased phagocytosis rate and increased numbers of viable unphagocytosed (free) bacteria after in vitro exposure to monocytes.

Author affiliations: Universidade Federal do Rio de Janeiro, Rio de Janeiro, Brazil (A.S. Viana, A.M.N. Botelho, A.L.P. Ferreira, M.C.S. Carvalho, M.A. Guimarães, B.S.S. Costa, M.C. Mattos, S.P. Maciel, J. Echevarria-Lima, B.T.F. Carvalho, A.M.S. Figueiredo); Children's Hospital of Philadelphia, Philadelphia, Pennsylvania, USA (A.M. Moustafa, C.L.K. Boge, K. O'Brien, C. Ryan, J.S. Gerber, P.J. Planet); Diagnósticos da América S.A., Duque de Caxias, Brazil (A.L.P. Ferreira); American Museum of Natural History, New York, New York, USA (A. Narechania, P.J. Planet); University of Pennsylvania, Philadelphia (J.S. Gerber, P.J. Planet)

DOI: https://doi.org/10.3201/eid2711.210097

Methicillin-resistant *Staphylococcus aureus* (MRSA) is characterized by the mainly clonal structure of bacterial populations and the worldwide spread of a few highly successful lineages, sequence types (STs), and clonal complexes (CCs) that cycle through waves of dominance (*1*,*2*). During the late 1990s, the Brazilian endemic clone (BEC), which belongs to the ST239(CC8)–staphylococcal cassette chromosome (SCC) *mec*III lineage, comprised ≈80% of MRSA isolates in hospitals in Brazil (*3*). In the 2000s, isolates of the ST1(CC1)-SCC*mec*IV lineage supplanted BEC in ≥2 hospitals in the Rio de Janeiro metropolitan area of Brazil (*4*). More recent analyses have suggested that CC5 isolates might be increasing in prevalence in Brazil (*5*).

Most studies on the molecular epidemiology of MRSA in Brazil have analyzed a small number of isolates from a limited number of hospitals (*5*–*9*). We used molecular and genomic approaches to characterize 600 MRSA isolates collected from 51 hospitals in the Rio de Janeiro metropolitan area and identified a novel MRSA clone of ST105-SCC*mec*II *spa* t002 (ST105-SCC*mec*II-t002), which we termed the Rio de Janeiro (RdJ) clone, as a predominant cause of MRSA bloodstream infections (BSIs).

[1]These first authors contributed equally to this article.

[2]Current affiliation: Fluminense Federal University, Niteroi, Brazil.

[3]Current affiliation: Fundação Oswaldo Cruz, Rio de Janeiro, Brazil.

[4]These authors were co–principal investigators.

Methods

Bacterial Isolates

We obtained the MRSA isolates from 600 patients at 51 hospitals in the Rio de Janeiro metropolitan area and confirmed MRSA using routine identification methods (Table 1; Appendix 1, https://wwwnc.cdc.gov/EID/article/27/11/21-0097-App1.xlsx). The sample comprised roughly equal numbers of isolates from blood samples from BSI patients, nonblood samples from patients with infections at another body site, and nasal swab samples; samples were collected during 2014–2017, most in 2015 and 2016. Patient age was available for 450 patients (Table 2). The research protocols were submitted to the Human Research Ethics Committee (CAAE submission no. 41614914.4.00005257) of the Hospital Universitário Clementino Fraga Filho, Universidade Federal do Rio de Janeiro (Rio de Janeiro, Brazil); the study was considered non–human subject research.

Molecular Typing and Susceptibility Testing

We used restriction-modification (RM) tests to determine CC (*10*) and multiplex PCR to type SCC*mec* (*11*). We used PCR to screen for the *lukSF-PV*, *agr*II, SCC*mec*III, and *seh* genes as previously described (*12*). We conducted antibiogram and susceptibility tests for glycopeptide drugs as recommended by Clinical and Laboratory Standards Institute guidelines (*13*).

Genome Sequencing and Analysis

We selected 208 isolates for whole-genome sequencing (WGS). Because of a strong predominance (179/208; 86.1%) of CC5 isolates, we focused our research on the CC5 lineage. We randomly selected isolates from blood (70/145; 48.3%), nonblood (52/114; 45.6%), and nasal swab (57/123; 46.3%) CC5 samples (Appendix 2, https://wwwnc.cdc.gov/EID/article/27/11/21-0097-App2.xlsx). The other 29 isolates used in WGS belonged to less abundant CCs. We prepared genomic DNA using the Wizard Genomic DNA Purification Kit (Promega Corporation, https://www.promega.com) and sequenced genome libraries by using Nextera XT DNA Library Prep Kit (Illumina, https://www.illumina.com) and the HiSeq 2500 system (Illumina) using paired-end reads of 125 bp. We trimmed reads using BBDuk Trimmer version 1.0 (Geneious, https://www.geneious.com) and assembled genomes using Velvet Assembly version 7.0.4 (*14*) and SPAdes version 3.13.0 (*15*). We used RAST (https://rast.nmpdr.org) and manual inspection to annotate the isolates. We determined the genotypes of the sequenced strains using the MLST 2.0, SCC*mec*Finder 1.2, and *spa* Typer 1.0 tools (https://cge.cbs.dtu.dk).

Table 1. Sample types of methicillin-resistant *Staphylococcus aureus* isolates from colonized and infected patients, Rio de Janeiro, Brazil, 2014–2017

Sample type	No. (%) samples
Blood	197 (32.8)
Nonblood	216 (36.0)
Anterior nasal swab	187 (31.2)
Total	600 (100.0)

Phylogenetic Analysis and Divergence Times

We constructed a maximum-likelihood tree for 661 CC5 genomes: 179 genomes from the current investigation and 482 assembled genomes available on GenBank, chosen from the list provided by Challagundla et al. (*8*) (Appendix 3, https://wwwnc.cdc.gov/EID/article/27/11/21-0097-App3.pdf). We used a single-nucleotide polymorphism (SNP) alignment produced by Snippy to infer an initial phylogenetic tree in RAxML version 8.2.4 (*16*).

To estimate when the ST105-SCC*mec*II-t002 lineage emerged in Rio de Janeiro, we used a Bayesian phylogenetic framework to analyze 73 genomes that passed our Mash Screen (*17*) quality cutoffs. We selected MRSA strain FCFHV36, the closest complete reference genome available in GenBank, using the WhatsGNU topgenome (-t) option (*18*). We used the SNP alignment to infer an initial phylogenetic tree in RAxML version 8.2.4 before using ClonalFrameML (*19*) to detect and mask areas of recombination. We used the SNP recombination-masked alignment to estimate divergence times in BEAST version 2.6.2 (*20*). We found a positive correlation between genetic divergence and isolation time using TempEst version 1.5.3 (*21*). We plotted the chronograms based on the maximum clade credibility tree using the TreeAnnotator program and visualized in FigTree version 1.4.3 (Appendix 3).

Genomic Island Characterization

We used Geneious Prime version 2020.1.2 to manually inspect the ΦSA3, vSa-α, vSa-β, vSa-β, and SaPI-1 genomic islands (*22*,*23*) and Swiss-Prot (Uniprot Consortium, https://www.uniprot.org) to

Table 2. Age distribution of patients who had methicillin-resistant *Staphylococcus aureus* infections or colonizations, Rio de Janeiro, Brazil, 2014–2017

Patient age range, y	No. (%)
<5	46 (10.2)
5–18	16 (3.6)
19–59	180 (40.0)
>60	208 (46.2)
Total	450 (100.0)

annotate paralogues. To map the genetic context of genomic islands, we randomly selected representative genome sequences from different phylogenetic locations of the tree showing the most common CC5 lineages in the Rio de Janeiro metropolitan area (Figure 1). We determined gene presence or absence using BLAST analysis (https://blast.ncbi.nlm.nih.gov).

Phagocytosis Assays

We subjected the selected isolates to phagocytosis (Appendix 3 Table 1). In this assay, we considered the entire process of phagocytosis (i.e., binding and uptake) by detecting all cell-associated bacteria, whether internalized or externally attached, after washing. We cultured bacteria at 37°C for 18 h at 250 rpm in brain–heart infusion broth (Becton Dickinson, https://www.bd.com) before treating with 25 nmol SYTO 9 stain (Thermo Fisher Scientific, https://www.thermofisher.com) for 15 min and washing in phosphate-buffered saline (1× phosphate-buffered saline, pH 7.2). We incubated bacterial cells at 37°C for 30 min in 5% carbon dioxide with THP-1 monocytes in Roswell Park Memorial Institute 1640 medium for a multiplicity of infection of 10 (*24*). We did not use antimicrobial drugs at any time during these assays. We washed the infected monocytes with PBS once and then centrifuged them at 200 × *g* for 5 min. We

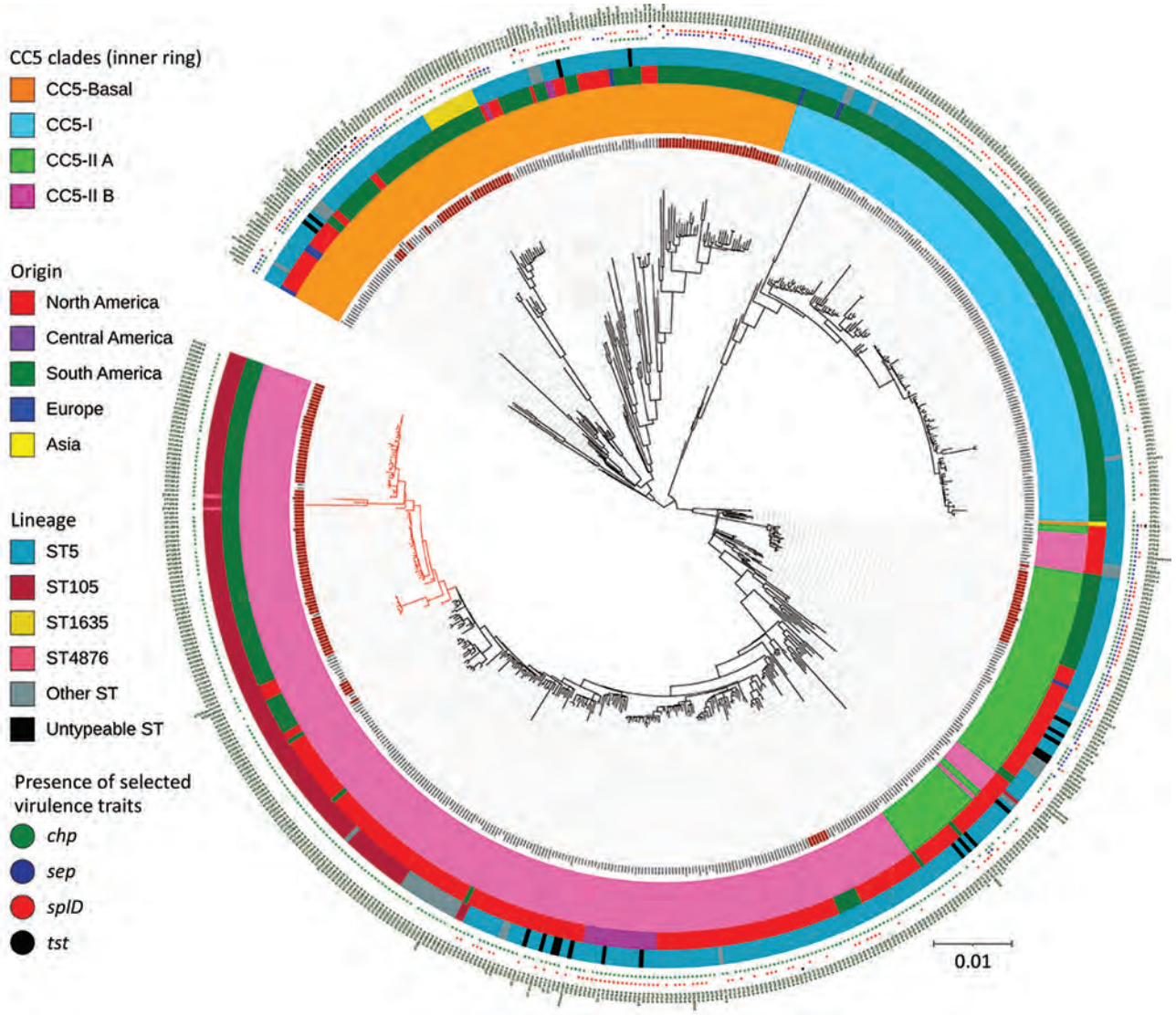

Figure 1. Maximum-likelihood phylogenetic tree of 179 methicillin-resistant *Staphylococcus aureus* CC5 isolates from Rio de Janeiro, Brazil, 2014–2017 (red text) and 482 reference genomes (*7*). Red branches indicate the Rio de Janeiro clone of the lineage ST105(CC5)-SCC*mec*II-t002. Scale indicates substitutions per site. CC, clonal complex; SCC, staphylococcal chromosome cassette; ST, sequence type.

resuspended THP-1 cells in PBS and analyzed them by flow cytometry (FACSCalibur; Becton Dickinson). We acquired 10,000 live THP-1 cells (as calculated by forward scatter and side scatter gating) and analyzed data using FlowJo10 software (https://www.flowjo.com). We calculated the number of bacteria-associated THP-1 cells as the frequency of fluorescent (i.e., SYTO 9–positive) THP-1 cells compared with total live THP-1 cells. In addition, we counted and compared the number of viable unphagocytosed bacterial cells in the culture supernatant of each assay at 0 and 30 min after incubation.

Statistical Analyses

We analyzed molecular typing, antimicrobial testing, and epidemiologic data using Pearson χ^2 tests. To assess the association of the CC5-SCC*mec*II group and the ST105-SCC*mec*II-t002 sublineage with BSI, we used Stata 16.0 (https://www.stata.com) to conduct a Mantel-Haenszel test stratified on a composite variable informed by participant age (≥60 years vs. <60 years), year of specimen collection (2014, 2015, or 2016–2017), and hospital type (public vs. private). For the analysis of year of specimen collection, we combined data from 2016 and 2017 because few isolates were collected during 2017. We analyzed phagocytosis assays using a 1-way analysis of variance and Tukey multiple comparison test in GraphPad Prism 6 (GraphPad Software, Inc., https://www.graphpad.com).

Results

Distribution of Genotypes (CC-SCC*mec*) and Antimicrobial Resistance

Among the 600 isolates that underwent CC and SCC*mec* typing, most were categorized as CC5-SCC*mec*II (245/600; 40.8%) or CC5-SCC*mec*IV (137/600; 22.8%). The second most common lineage was CC30, comprised of *lukSF-PV*–positive CC30-SCC*mec*IV (109/600; 18.2%) and *lukSF-PV*–negative CC30-SCC*mec*II (8/600; 1.3%) isolates. The previously dominant CC1-SCC*mec*IV lineage (79/600; 13.2%) and BEC clone (7/600; 1.2%) were much less frequent. In addition, we observed low frequencies of STs related to other international lineages such as CC45-SCC*mec*II/IV (related to USA600), CC8-SCC*mec*IV (related to USA300), and CC22-SCC*mec*IV (related to EMRSA-15) (Figure 2, panel A).

Compared with isolates of other frequent clonal lineages, CC5-SCC*mec*II isolates were more likely to be multidrug-resistant, defined as having resistance to ≥4 non-β-lactam antimicrobial drugs (48.6% vs. 5.8%) (Table 3). In contrast, CC5-SCC*mec*IV strains showed more susceptibility to non–β-lactams; only 4.4% were multidrug-resistant. All 109 strains belonging to the CC30-SCC*mec*IV lineage, which is related to the community-acquired MRSA USA1100/Oceania South West Pacific clone, were susceptible to all non–β-lactams tested (Table 3).

Distribution of Genotypes (CC-SCC*mec*) and Clinical Data

In the univariate analysis, we found that the distribution of genotypes was associated with MRSA infection site (Figure 2, panel B). CC5-SCC*mec*II isolates were more common among blood (115/245; 46.9%) than nonblood (62/245; 25.3%) and nasal swab (68/245; 27.8%) samples, whereas CC5-SCC*mec*IV isolates were more common among nasal swab (55/137; 40.1%) and nonblood (52/137; 38.0%) than blood (30/137; 21.9%) samples. The third most frequent lineage, CC30-SCC*mec*IV, was more common among nonblood (60/109; 55.0%) than nasal swab (30/109; 27.5%) and blood (19/109; 17.4%) samples.

The distribution of MRSA lineages varied among age groups. CC5-SCC*mec*II was more common among patients ≥60 years of age (100/208; 48.1%). CC30-SCC*mec*IV prevalence was higher among younger populations and diminished with increasing age range; prevalence was 50.0% (8/16) among children 5–18 years of age, 21.1% (38/180) among adults 19–59 years of age, and 10.6% (22/208) among adults ≥60 years of age. Among children <5 years of age, the most prevalent lineage was CC5-SCC*mec*IV, which is sometimes known as the pediatric clone (21/46; 45.7%) (Figure 2, panel C). Adults 19–59 and >60 years of age had a similar prevalence of CC5-SCC*mec*IV isolates (23.9% among adults 19–59 years of age vs. 22.1% among adults >60 years of age). The proportion of CC5-SCC*mec*II isolates was also similar between adults 19–59 years of age (57/180; 31.7%) and adults >60 years of age (62/208; 29.8%). CC5-SCC*mec*II was associated with BSIs even after stratifying for the composite variable of age, hospital type, and year of isolation ($p<0.01$).

Novel MRSA Clone

To better characterize the circulating clones, especially those belonging to CC5, we used whole-genome sequencing on 208 isolates: 76 (36.5%) from blood samples, 69 (33.2%) from nasal swab samples, and 63 (30.3%) from nonblood samples. Most (179; 86.1%) isolates belonged to CC5, whereas 29 did not (Appendix 3 Table 2). Multilocus and *spa*-typing using WGS revealed 4 CC5 clones that constituted >75% of isolates (Table 4). The dominant genotype,

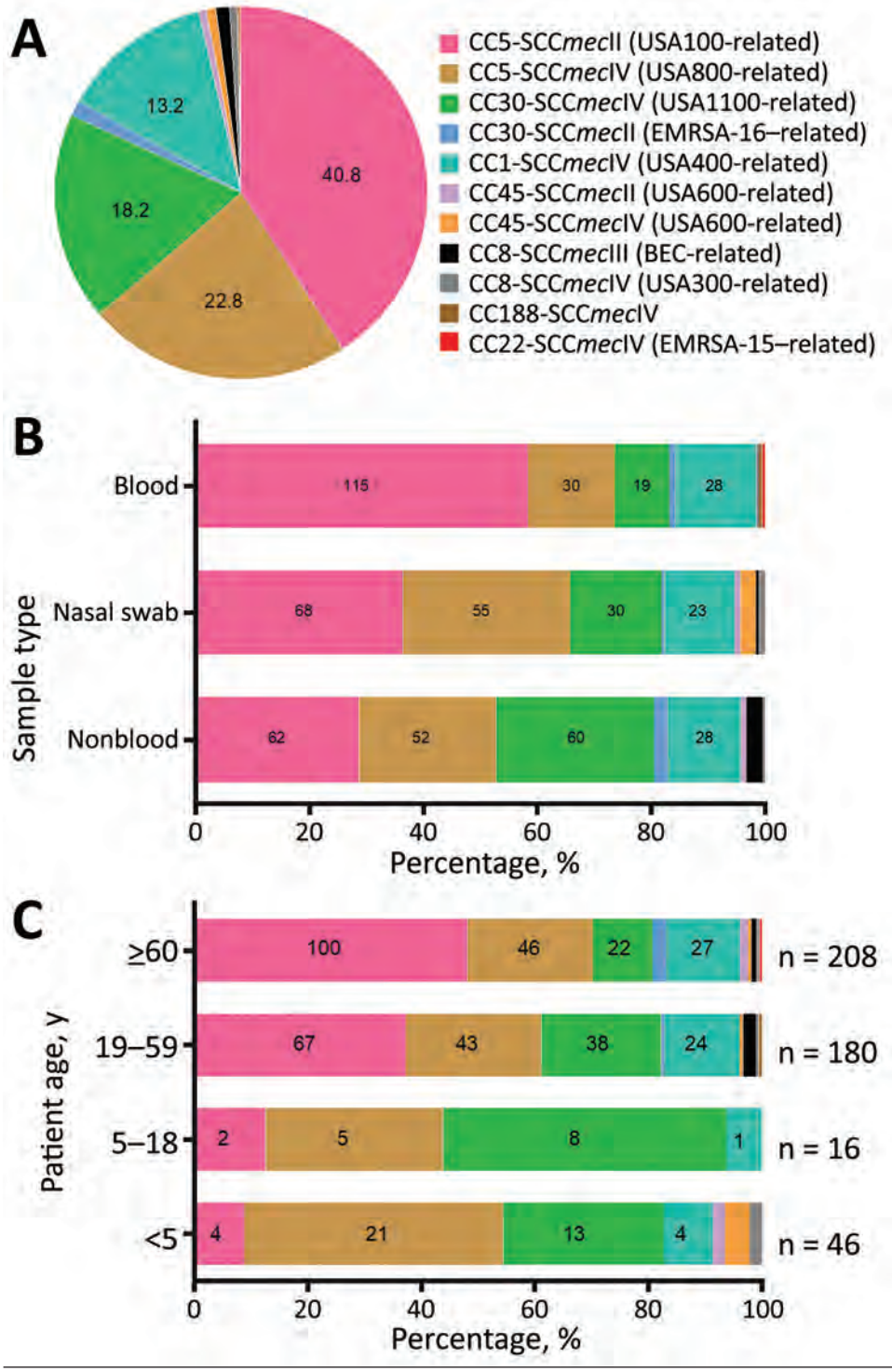

Figure 2. Distribution of 600 MRSA isolates by lineage (A), sample type (B), and patient age (C), Rio de Janeiro Brazil, 2014–2017. A) MRSA isolates by lineage (CC-SCC*mec* type) among 600 isolates. Labels indicate proportions. B) MRSA isolates by sample type. Labels indicate number of isolates. C) MRSA isolates by patient age (data available for 450 patients). Labels indicate number of isolates. BEC, Brazilian endemic clone; CC, clonal complex; EMRSA, epidemic methicillin-resistant *Staphylococcus aureus*; MRSA, methicillin-resistant *Staphylococcus aureus*; SCC, staphylococcal cassette chromosome.

ST105(CC5)-SCC*mec*II-t002, the RdJ clone, comprised 41.9% (75/179) of the CC5 isolates. RdJ showed the second highest proportion of multidrug resistance (41/75; 54.7%), superseded only by ST5-SCC*mec*II-t539 (14/17; 82.4%). In contrast, only 1 (2.3%) strain of ST5-SCC*mec*IV-t002 was multidrug-resistant. MRSA lineages coexisting in the same hospital often displayed different resistance profiles.

In addition to being the most frequent MRSA clone, RdJ might be responsible for the higher frequency of CC5-SCC*mec*II isolates from blood samples. ST105-SCC*mec*II-t002 isolates were more common among

blood (41/75; 54.7%) than nasal swab (20/75; 26.7%) and nonblood (14/75; 18.7%) samples; however, when adjusted for hospital type and year of isolation, this association became nonsignificant (p = 0.12).

Whole-Genome Phylogenetic Analysis of MRSA CC5 Isolates

The whole-genome phylogenetic analysis grouped CC5 isolates from this study into 3 of the 4 major phylogenetic groups corresponding mostly to the ST105(CC5)-SCC*mec*II-t002, ST5-SCC*mec*II-t539, and ST5-SCC*mec*IV-t002 genotypes and distributed widely throughout the CC5 tree (Figure 1). All SCC*mec*IV isolates clustered in the CC5-Basal clade. Isolates with the multidrug-resistant ST5(CC5)-SCC*mec*II-t539 genotype clustered with members of the paraphyletic group CC5-IIA described by Challagundla et al. (*8*). Most other CC5 isolates, including isolates of genotype ST105(CC5)-SCC*mec*II-t002, were grouped in clade CC5-IIB. Although most of these isolates form the RdJ clade, which is found mostly in Rio de Janeiro, nearby outgroups to this clade are composed of previously sequenced isolates from São Paulo and Porto Alegre (*25*) and North America, as well as a few isolates from this study (Appendix 3). This pattern might indicate multiple introductions into Brazil. Our Bayesian analysis of the RdJ clade suggests a recent date of introduction, probably 2009 (95% highest posterior density 2007–2010) (Figure 3).

Table 3. Antimicrobial resistance among 600 methicillin-resistant *Staphylococcus aureus* isolates, Rio de Janeiro, Brazil, 2014–2017*

Lineage	Total	No. multidrug-resistant isolates, %
CC5-SCC*mec*II	245	119 (48.6)†
CC5-SCC*mec*IV	137	6 (4.4)
CC30-SCC*mec*IV	109	0
CC1-SCC*mec*IV	79	13 (16.5)
CC30-SCC*mec*II	8	3 (37.5)
CC8-SCC*mec*III	7	7 (100.0)
CC45-SCC*mec*IV	5	0
CC45-SCC*mec*II	4	2 (50.0)
CC8-SCC*mec*IV	4	0
CC188-SCC*mec*IV	1	0
CC22-SCC*mec*IV	1	0

*Multidrug-resistant defined as an isolate carrying ≥4 additional antimicrobial resistance traits to non–β-lactam antimicrobial drugs.
†p<0.01 by Pearson χ^2 test.

In comparison with other CC5 genomes, the clade that includes the ST105 genomes lacked key virulence genes. In addition to the apparent loss of the enterotoxin P gene (*sep*) noted by Challagundla et al. (*8*), isolates from this clade uniformly lacked the *splD* gene encoding serine protease D (Figure 1).

Monocytic Evasion

To better ascertain differences in pathogenicity of RdJ isolates, we assessed the in vitro phagocytosis rate and

Table 4. Lineages of methicillin-resistant *Staphylococcus aureus* clonal complex 5 isolates, Rio de Janeiro, Brazil, 2014–2017*

Clones†	Blood	Anterior nasal swab	Nonblood	Total (%)
ST105-SCC*mec*II-t002	41	20	14	75 (41.9)‡
ST5-SCC*mec*IV-t002	11	13	19	43 (24.0)
ST5-SCC*mec*II-t539	5	4	8	17 (9.5)
ST1635-SCC*mec*IV-t002	2	4	4	10 (5.6)
ST5-SCC*mec*II-t067	2	3	1	6 (3.4)
ST5-SCC*mec*II-t2666	2	2	1	5 (2.8)
ST105-SCC*mec*II-NT	3	0	0	3 (1.7)
ST105-SCC*mec*II-t010	1	0	1	2 (1.1)
ST4876-SCC*mec*II-t002	1	0	1	2 (1.1)
ST5-SCC*mec*IV-t1154	1	1	0	2 (1.1)
ST5-SCC*mec*IV-NT	0	2	0	2 (1.1)
ST105-SCC*mec*II-t067	1	0	0	1 (0.6)
ST105-SCC*mec*II-t539	0	1	0	1 (0.6)
ST1635-SCC*mec*IV-t062	0	0	1	1 (0.6)
ST1635-SCC*mec*IV-t450	0	1	0	1 (0.6)
ST1635-SCC*mec*IV-t769	0	0	1	1 (0.6)
ST5-SCC*mec*II-t002	0	1	0	1 (0.6)
ST5-SCC*mec*II-NT	0	1	0	1 (0.6)
ST5-SCC*mec*IV-t061	0	1	0	1 (0.6)
ST5-SCC*mec*IV-t062	0	0	1	1 (0.6)
ST5-SCC*mec*IV-t105	0	1	0	1 (0.6)
ST5-SCC*mec*IV-t586	0	1	0	1 (0.6)
ST5-SCC*mec*IV-t777	0	1	0	1 (0.6)
Total sequenced/collected§	70/145	57/123	52/114	179/382

*SCC, staphylococcal chromosome cassette; NT, not typed by *spa* polymorphism; ST, sequence type.
†Clones defined by multilocus sequence type, SCC*mec* type, and *spa* polymorphism.
‡p<0.01 by single-variable analysis for blood samples compared with nasal swab and nonblood samples; p = 0.12 when adjusted for private vs. public hospital and year of isolation.
§Total isolates sequenced from total no. isolates collected.

viable counts of unphagocytosed (free) bacteria (Figures 4–6). Representative RdJ isolates showed very low rates of phagocytosis/host cell association (2.9%) compared with representatives of other CC5 lineages: 41.3% for ST5(CC5)-SCC*mec*II-t539 and 35.8% for ST5(CC5)-SCC*mec*IV-t002 strains (Figure 6, panel A). In addition, after a 30-minute interaction with THP-1 monocytes, the RdJ strains showed higher survival rates (5.58%) than other lineages: 0.88% for ST5(CC5)-SCC*mec*IV-t002 and 0.76% for ST5(CC5)-SCC*mec*II-t539 (Figure 6, panel B).

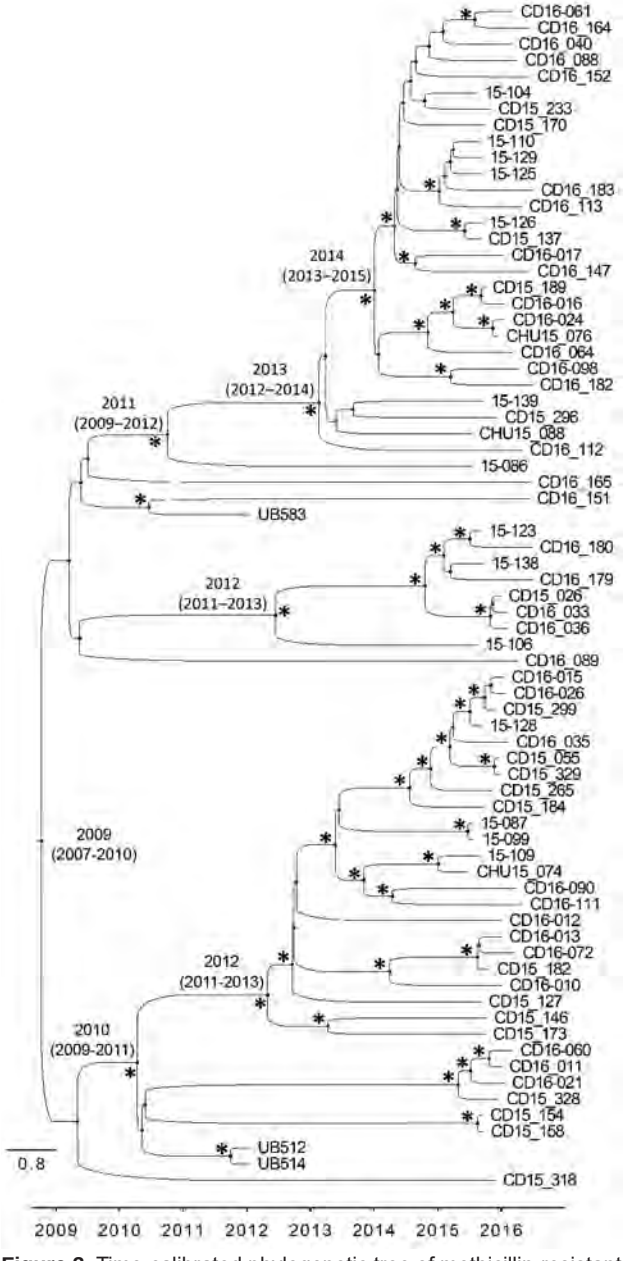

Figure 3. Time-calibrated phylogenetic tree of methicillin-resistant *Staphylococcus aureus* ST105(CC5)-SCC*mec*II-t002 lineage, Rio de Janeiro, Brazil, 2014–2017. Chronogram constructed using Bayesian phylogenetic analysis of single-nucleotide polymorphisms from 73 genomes. Maximum clade credibility tree estimated using a strict clock rate of 1.1927×10^{-6} substitutions/site/year (95% highest posterior density $1.5054–2.3351 \times 10^{-6}$). Node labels indicate 95% highest posterior density values of major clades. Asterisks (*) indicate posterior values >0.98. Scale indicates substitutions per site per year. CC, clonal complex; SCC, staphylococcal cassette chromosome; ST, sequence type.

Discussion

Using molecular typing and phylogenetic analysis, we identified a third epidemic lineage of MRSA in Rio de Janeiro. CC5, and to a lesser extent CC30, have become the most prevalent MRSA lineages in Rio de Janeiro hospitals, replacing the previously dominant ST1(CC1)-SCC*mec*IV lineage, which had replaced the BEC lineage ST239(CC8)-SCC*mec*III during 2004–2008 (*4*). At the time when the ST1(CC1)-SCC*mec*IV lineage replaced BEC, CC5 comprised only 10% of isolates (*4*); CC5 now constitutes >60% of isolates. Previously dominant clones, especially BEC, carried resistance to many non–β-lactam antimicrobial drugs, antiseptics, and heavy metals whereas the currently dominant strains are more susceptible (*1*).

Although CC5-SCC*mec*II was the predominant genotype in our sample, the proportions of the second and third most frequent genotypes, CC5-SCC*mec*IV and *lukSF-PV*–positive CC30-SCC*mec*IV, also had increased from prior studies (*4*). CC5-SCC*mec*IV (related to USA800), which was first isolated in children at a hospital in Portugal in 1992 (*26*), was overrepresented among patients <5 years of age in our sample. Some studies have suggested that this strain is more common among children (*27*), although the nature of this association remains unclear. The *lukSF-PV*–positive CC30-SCC*mec*IV genotype is related to the USA1100/Oceania South West Pacific clone (*1*), and is a distant relative of the historically epidemic and especially virulent phage type 80/81 lineage (*28*). We previously showed that, in contrast to the 80/81 lineage, ST30(CC30)-SCC*mec*IV MRSA from Brazil displays a natural attenuation of the Agr and SaeRS virulence regulators (*29*), which might explain why this lineage was responsible for only 9.6% of BSIs in this study.

The large number of MRSA isolates genotyped in this study enabled us to assess the distribution of MRSA genotypes by patient age and sites of infection or colonization. We identified associations between the CC5-SCC*mec*II genotype, BSIs, and older age, possibly because of the increased virulence or invasiveness of this genotype. The CC5-SCC*mec*II genotype also is found in the USA100 lineage ST5(CC5)-SCC*mec*II that was dominant among hospitals in the

United States during the late 1990s (*30*), before the emergence of the USA300 clone (*31*). USA100 is still found in hospitals in the United States (*32*) and around the world (*1*).

In our sample, most (75/114; 65.8%) CC5-SCC*mec*II isolates belonged to ST105 and shared *spa*-type t002, suggesting the emergence of a new clone. ST105(CC5)-SCC*mec*II strains have previously infected humans and domestic animals (*33*), and 4 isolates from this lineage were reported in a hospital in São Paulo (*7*). Reports from other countries have occasionally shown a substantial prevalence of this lineage, including a study that showed colonization among 22.4% of patients admitted to a hospital in Pennsylvania, USA (*34*). Another study showed that ST105(CC5)-SCC*mec*II was the predominant lineage among patients who had MRSA BSI in Switzerland (*35*). In Portugal, ST105(CC5)-SCC*mec*II has been reported as the most abundant MRSA colonizing patients >60 years of age (*33*); a multicenter study identified this lineage as the second most common clone among patients who had BSIs (*36*). The first vancomycin-resistant *S. aureus* isolate in Portugal belonged to this lineage (*33*), a troubling finding because most vancomycin-resistant *S. aureus* isolates have belonged to the CC5 lineage (*25*).

Few studies exist on the molecular epidemiology of MRSA in Brazil and in other countries from South America; existing studies are based on a limited number of samples (*5*–*7*,*9*). As a result, the full extent of the dissemination of the ST105-SCC*mec*II-t002 genotype in Latin America is unknown. Since the late 2000s, ST105-SCC*mec*II-t002 has been reported as the second or third most frequent MRSA lineage in hospitals in the United States and some countries in Europe (*33*–*35*). For example, researchers documented an outbreak of ST105-SCC*mec*II-t002 MRSA among 18 neonates at Mount Sinai Hospital (New York, NY, USA) during 2014–15 (*38*). In addition, ST105 isolates comprised 87.5% of delafloxacin-resistant MRSA strains collected in 7 hospitals in New York (*39*). Altogether, these data show that ST105 is a major MRSA lineage not only in Rio de Janeiro but also in other countries. ST105-SCC*mec*II-t002 also might have spread in other regions of Brazil; therefore, more studies are needed to better track and investigate this lineage.

We used Bayesian molecular clock analysis to estimate the expansion of the RdJ clade in Rio de Janeiro

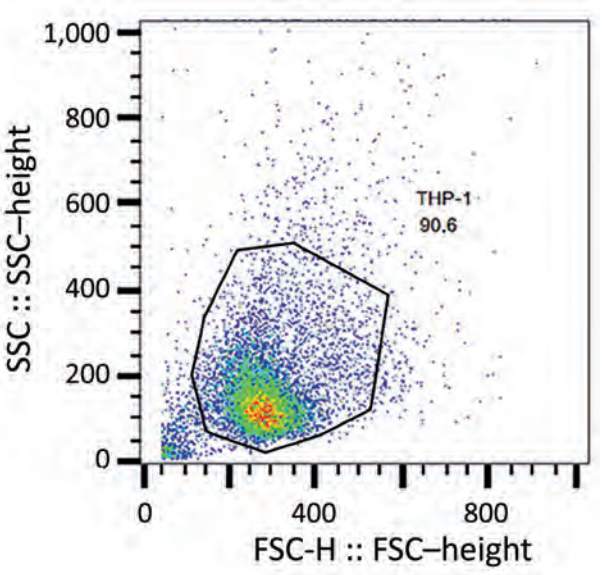

Figure 4. Scatter plot representing gating strategy for identifying monocytes in the FSC-H versus SSC-H analysis of methicillin-resistant *Staphylococcus aureus* isolates, Rio de Janeiro, Brazil, 2014–2017. Representative flow cytometry chart shows the acquisition of THP-1 cells not exposed to methicillin-resistant *Staphylococcus aureus*. FSC-H, forward scatter height; SSC-H, side scatter height.

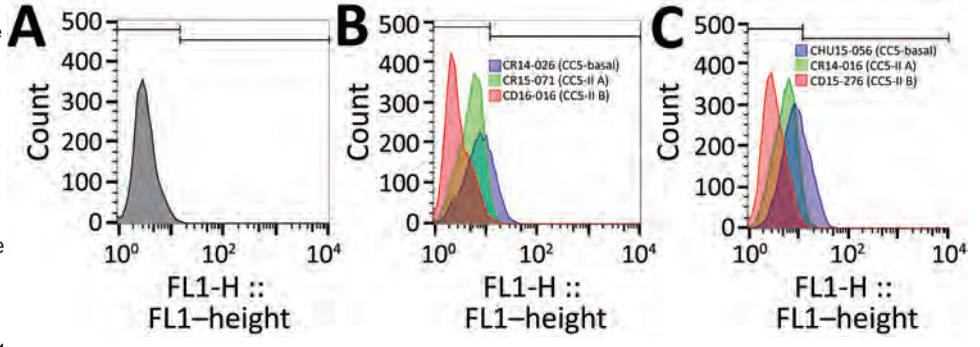

Figure 5. Histograms showing count versus green fluorescence intensity of THP-1 cells exposed or not to MRSA isolates, Rio de Janeiro, Brazil, 2014–2017. A) Acquisition of THP-1 cells not exposed to MRSA. B) Acquisition of THP-1 cells exposed to representative strains of 3 MRSA lineages. Blue indicates ST5-SCC*mec*IV-t002, strain CR14-026 (CC5-Basal lineage); green indicates ST5-SCC*mec*II-t539, strain CR15-071 (CC5-IIA lineage); and red indicates ST105-SCC*mec*II-t002, strain CD16–016 (CC5-IIB lineage). C) Acquisition of THP-1 cells exposed to representative strains of 3 MRSA lineages. Blue indicates ST5-SCC*mec*IV-t002, strain CHU15–056 (CC5-Basal lineage); green indicates ST5-SCC*mec*II-t539, strain CR14–016 (CC5-IIA lineage); and red indicates ST105-SCC*mec*II-t002 strain CD15–276 (CC5-IIB lineage). CC, clonal complex; FL1-H, forward light 1 height; MRSA, methicillin-resistant *Staphylococcus aureus*; SCC, staphylococcal cassette chromosome; ST, sequence type.

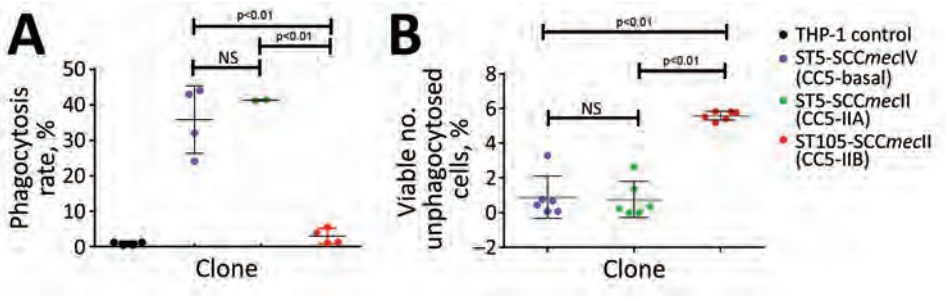

Figure 6. Scatter plots showing evasion of phagocytosis by MRSA isolates, Rio de Janeiro, Brazil, 2014–2017. A) Phagocytosis rates for representatives of the phylogenetic groups CC5-Basal, CC5-IIA, and CC5-IIB. Four independent experiments were conducted for each lineage using 1 fluorescence-activated single cell sorting determination for each experiment. Horizontal lines indicate means; whiskers indicate SDs. B) Viable count of unphagocytosed (free) bacteria after 30-min interaction with THP-1 monocytes. Six independent experiments were considered, with 2 replicates per lineage. Horizontal lines indicate means; whiskers indicate SDS. Statistical analyses conducted using 1-way analysis of variance and Tukey multiple comparison test. CC, clonal complex; NS, not significant; MRSA, methicillin-resistant *Staphylococcus aureus*; SCC, staphylococcal cassette chromosome; ST, sequence type.

in 2009 (95% highest posterior density 2007–2010), which is consistent with previous estimates that date the origin of the ST105 lineage to the mid-1990s (*8*). The ST105 clade is characterized by a lack of virulence genes that are common among other CC5 strains. All ST105(CC5)-SCC*mec*II isolates lacked the *sep* gene encoding enterotoxin P, as noted by Challagundla et al. (*8*). In addition to its emetic properties, enterotoxin P is a superantigen that induces T-cell proliferation and production of proinflammatory cytokines (*40*). ST105(CC5)-SCC*mec*II-t002 strains showed resistance to fluoroquinolones, macrolides, and lincosamides. ST105(CC5)-SCC*mec*II isolates also lacked the serine protease encoding gene *splD*, despite the presence of the *splABCF* genes of the *spl* operon. Although the specific role of SplD in *S. aureus* pathogenesis is not known, some researchers have proposed that Spl serine proteases might use proteolysis to modulate host proteins critical to bacterial pathogenesis (*41*). Future work should address implications of the absence of SplD in the ST105(CC5)-SCC*mec*II lineage.

Compared with representatives of the ST5-SCC*mec*II-t539 and ST5-SCC*mec*IV-t002 lineages, representative isolates of the RdJ clade showed increased evasion of phagocytosis mechanisms upon exposure to monocytic cells (i.e., THP-1). Multiple factors, including phagocytosis rate and the activity of toxic compounds released by monocytes, might affect the number of viable unphagocytosed bacterial cells (*42*). Moreover, we observed an increased number of viable RdJ free cells. The basis of this phenotype is unclear and deserves further study. Le Pabic et al. (*43*) implicated the small noncoding RNA, SprC, and its effect on regulation of the major autolysin Atl in *S. aureus* evasion of phagocytosis by human monocytes and macrophages. However, we did not find any differences in the *sprC* gene of the 6 representative strains tested, suggesting that the observed evasion might be multifactorial, probably linked to the production of several bacterial molecules (*42*).

One limitation of this study is the lack of more extensive clinical data such as the presence of indwelling catheters or lines and underlying conditions that might have affected our estimates. The association between ST105-SCC*mec*II-t002 and BSIs was attenuated when accounting for other variables such as hospital type and year of isolation, but still might be of clinical relevance. Access to more extensive clinical data would enable further exploration of this relationship. In addition, our reliance on samples from Rio de Janeiro might have affected our phylogenetic analysis; focused sampling in other geographic locations might show a more widespread epidemic.

In summary, we uncovered a new MRSA clone in hospitals in the Rio de Janeiro metropolitan area. Our findings emphasize the dynamic nature of the local rise and decline of various MRSA clones. In addition, these data indicate that MRSA clonal dynamics also might be associated with different manifestations of disease and host factors, such as age. This analysis revealed the emergence of a novel multidrug-resistant MRSA clone associated with BSIs. This association might be critical for assessing the clinical and epidemiologic risks associated with the spread of this clone and the biologic basis for its putative enhanced invasiveness.

Acknowledgments

We thank the microbiology department of Diagnósticos da América S.A. for providing the bacterial isolates included in this work.

This work was supported in part by Conselho Nacional de Desenvolvimento Científico e Tecnológico (CNPq grant no. 140774/2019-0 to A.S.V. and grant nos. 443804/2018-4 and 307672/2019-0 to A.M.S.F.), Fundação Carlos Chagas Filho de Amparo à Pesquisa do Estado do Rio de Janeiro

(grant no. E-26/210.193/2014 to A.M.S.F. and P.J.P.; grant nos. E-26/010.001280/2016, E-26.202.803/2017, and E-26/010.002435/2019 to A.M.S.F.); the Bill & Melinda Gates Foundation (grant no. OPP1193112 to A.M.S.F.) and the US National Institutes of Health (grant no. 1R01AI137526-01 to P.J.P. and A.M.M.).

About the Author

Ms. Viana is a doctoral candidate at Federal University of Rio de Janeiro, Rio de Janeiro, Brazil. Her main research interests are genomics and phylogenetic evolution of methicillin-resistant *Staphylococcus aureus*.

References

1. Figueiredo AMS, Ferreira FA. The multifaceted resources and microevolution of the successful human and animal pathogen methicillin-resistant *Staphylococcus aureus.* Mem Inst Oswaldo Cruz. 2014;109:265–78. https://doi.org/10.1590/0074-0276140016
2. Planet PJ, Narechania A, Chen L, Mathema B, Boundy S, Archer G, et al. Architecture of a species: phylogenomics of *Staphylococcus aureus.* Trends Microbiol. 2017;25:153–66. https://doi.org/10.1016/j.tim.2016.09.009
3. Teixeira LA, Resende CA, Ormonde LR, Rosenbaum R, Figueiredo AM, de Lencastre H, et al. Geographic spread of epidemic multiresistant *Staphylococcus aureus* clone in Brazil. J Clin Microbiol. 1995;33:2400–4. https://doi.org/10.1128/jcm.33.9.2400-2404.1995
4. Silva-Carvalho MC, Bonelli RR, Souza RR, Moreira S, dos Santos LCG, de Souza Conceição M, et al. Emergence of multiresistant variants of the community-acquired methicillin-resistant *Staphylococcus aureus* lineage ST1-SCC*mec*IV in 2 hospitals in Rio de Janeiro, Brazil. Diagn Microbiol Infect Dis. 2009;65:300–5. https://doi.org/10.1016/j.diagmicrobio.2009.07.023
5. Chamon RC, Ribeiro SD, da Costa TM, Nouér SA, Dos Santos KRN. Complete substitution of the Brazilian endemic clone by other methicillin-resistant *Staphylococcus aureus* lineages in two public hospitals in Rio de Janeiro, Brazil. Braz J Infect Dis. 2017;21:185–9. https://doi.org/10.1016/j.bjid.2016.09.015
6. Zuma AVP, Lima DF, Assef APDC, Marques EA, Leão RS. Molecular characterization of methicillin-resistant *Staphylococcus aureus* isolated from blood in Rio de Janeiro displaying susceptibility profiles to non-β-lactam antibiotics. Braz J Microbiol. 2017;48:237–41. https://doi.org/10.1016/j.bjm.2016.09.016
7. Caiaffa-Filho HH, Trindade PA, Gabriela da Cunha P, Alencar CS, Prado GVB, Rossi F, et al. Methicillin-resistant *Staphylococcus aureus* carrying SCC*mec* type II was more frequent than the Brazilian endemic clone as a cause of nosocomial bacteremia. Diagn Microbiol Infect Dis. 2013;76:518–20. https://doi.org/10.1016/j.diagmicrobio. 2013.04.024
8. Challagundla L, Reyes J, Rafiqullah I, Sordelli DO, Echaniz-Aviles G, Velazquez-Meza ME, et al. Phylogenomic classification and the evolution of clonal complex 5 methicillin-resistant *Staphylococcus aureus* in the Western Hemisphere. Front Microbiol. 2018;9:1901. https://doi.org/10.3389/fmicb.2018.01901
9. Arias CA, Reyes J, Carvajal LP, Rincon S, Diaz L, Panesso D, et al. A prospective cohort multicenter study of molecular epidemiology and phylogenomics of *Staphylococcus aureus* bacteremia in nine Latin American countries [Erratum in: Antimicrob Agents Chemother. 2017;61:e00095–18]. Antimicrob Agents Chemother. 2017;61:17. https://doi.org/10.1128/AAC.00816-17
10. Cockfield JD, Pathak S, Edgeworth JD, Lindsay JA. Rapid determination of hospital-acquired meticillin-resistant *Staphylococcus aureus* lineages. J Med Microbiol. 2007;56:614–9. https://doi.org/10.1099/jmm.0.47074-0
11. Milheiriço C, Oliveira DC, de Lencastre H. Update to the multiplex PCR strategy for assignment of *mec* element types in *Staphylococcus aureus* [Erratum in: Antimicrob Agents Chemother. 2007;51:4537]. Antimicrob Agents Chemother. 2007;51:3374–7. https://doi.org/10.1128/AAC.00275-07
12. Beltrame CO, Botelho AMN, Silva-Carvalho MC, Souza RR, Bonelli RR, Ramundo MS, et al. Restriction modification (RM) tests associated to additional molecular markers for screening prevalent MRSA clones in Brazil. Eur J Clin Microbiol Infect Dis. 2012;31:2011–6. https://doi.org/10.1007/s10096-011-1534-1
13. Clinical and Laboratory Standards Institute. Performance standards for antimicrobial susceptibility testing: 28th informational supplement (M100-S28). Wayne (PA): The Institute; 2018.
14. Zerbino DR, Birney E. Velvet: algorithms for de novo short read assembly using de Bruijn graphs. Genome Res. 2008;18:821–9. https://doi.org/10.1101/gr.074492.107
15. Bankevich A, Nurk S, Antipov D, Gurevich AA, Dvorkin M, Kulikov AS, et al. SPAdes: a new genome assembly algorithm and its applications to single-cell sequencing. J Comput Biol. 2012;19:455–77. https://doi.org/10.1089/cmb.2012.0021
16. Stamatakis A. RAxML version 8: a tool for phylogenetic analysis and post-analysis of large phylogenies. Bioinformatics. 2014;30:1312–3. https://doi.org/10.1093/bioinformatics/btu033
17. Ondov BD, Starrett GJ, Sappington A, Kostic A, Koren S, Buck CB, et al. Mash Screen: high-throughput sequence containment estimation for genome discovery. Genome Biol. 2019;20:232. https://doi.org/10.1186/s13059-019-1841-x
18. Moustafa AM, Planet PJ. WhatsGNU: a tool for identifying proteomic novelty. Genome Biol. 2020;21:58. https://doi.org/10.1186/s13059-020-01965-w
19. Didelot X, Wilson DJ. ClonalFrameML: efficient inference of recombination in whole bacterial genomes. PLOS Comput Biol. 2015;11:e1004041. https://doi.org/10.1371/journal.pcbi.1004041
20. Bouckaert R, Vaughan TG, Barido-Sottani J, Duchêne S, Fourment M, Gavryushkina A, et al. BEAST 2.5: An advanced software platform for Bayesian evolutionary analysis. PLOS Comput Biol. 2019;15:e1006650. https://doi.org/10.1371/journal.pcbi.1006650
21. Rambaut A, Lam TT, Max Carvalho L, Pybus OG. Exploring the temporal structure of heterochronous sequences using TempEst (formerly Path-O-Gen). Virus Evol. 2016;2:vew007. https://doi.org/10.1093/ve/vew007
22. Aswani V, Najar F, Pantrangi M, Mau B, Schwan WR, Shukla SK. Virulence factor landscape of a *Staphylococcus aureus* sequence type 45 strain, MCRF184. BMC Genomics. 2019;20:123. https://doi.org/10.1186/s12864-018-5394-2
23. Novick RP, Ram G. Staphylococcal pathogenicity islands-movers and shakers in the genomic firmament. Curr Opin Microbiol. 2017;38:197–204. https://doi.org/10.1016/j.mib.2017.08.001
24. Melehani JH, James DBA, DuMont AL, Torres VJ, Duncan JA. *Staphylococcus aureus* leukocidin A/B (LukAB) kills human

monocytes via host NLRP3 and ASC when extracellular, but not intracellular. PLoS Pathog. 2015; 11:e1004970. https://doi.org/10.1371/journal.ppat.1004970
25. Panesso D, Planet PJ, Diaz L, Hugonnet JE, Tran TT, Narechania A, et al. Methicillin-susceptible, vancomycin-resistant *Staphylococcus aureus*, Brazil. Emerg Infect Dis. 2015;21:1844–8. https://doi.org/10.3201/eid2110.141914
26. Sá-Leão R, Santos Sanches I, Dias D, Peres I, Barros RM, de Lencastre H. Detection of an archaic clone of *Staphylococcus aureus* with low-level resistance to methicillin in a pediatric hospital in Portugal and in international samples: relics of a formerly widely disseminated strain? J Clin Microbiol. 1999;37:1913–20. https://doi.org/10.1128/JCM.37.6.1913-1920.1999
27. Rokney A, Baum M, Ben-Shimol S, Sagi O, Anuka E, Agmon V, et al. Dissemination of the methicillin-resistant *Staphylococcus aureus* pediatric clone (ST5-T002-IV-PVL+) as a major cause of community-associated staphylococcal infections in Bedouin children, southern Israel. Pediatr Infect Dis J. 2019;38:230–5. https://doi.org/10.1097/INF.0000000000002126
28. DeLeo FR, Kennedy AD, Chen L, Bubeck Wardenburg J, Kobayashi SD, Mathema B, et al. Molecular differentiation of historic phage-type 80/81 and contemporary epidemic *Staphylococcus aureus*. Proc Natl Acad Sci U S A. 2011;108:18091–6. https://doi.org/10.1073/pnas.1111084108
29. Ramundo MS, Beltrame CO, Botelho AMN, Coelho LR, Silva-Carvalho MC, Ferreira-Carvalho BT, et al. A unique SaeS allele overrides cell-density dependent expression of *saeR* and *lukSF*-PV in the ST30-SCC*mec*IV lineage of CA-MRSA. Int J Med Microbiol. 2016;306:367–80. https://doi.org/10.1016/j.ijmm.2016.05.001
30. Roberts RB, Chung M, de Lencastre H, Hargrave J, Tomasz A, Nicolau DP, et al.; Tri-State MRSA Collaborative Study Group. Distribution of methicillin-resistant *Staphylococcus aureus* clones among health care facilities in Connecticut, New Jersey, and Pennsylvania. Microb Drug Resist. 2000;6:245–51. https://doi.org/10.1089/mdr.2000.6.245
31. Planet PJ. Life after USA300: the rise and fall of a superbug. J Infect Dis. 2017;215:S71–7. https://doi.org/10.1093/infdis/jiw444
32. Carrel M, Perencevich EN, David MZ. USA300 methicillin-resistant *Staphylococcus aureus*, United States, 2000–2013. Emerg Infect Dis. 2015;21:1973–80. https://doi.org/10.3201/eid2111.150452
33. Almeida ST, Nunes S, Paulo ACS, Faria NA, de Lencastre H, Sá-Leão R. Prevalence, risk factors, and epidemiology of methicillin-resistant *Staphylococcus aureus* carried by adults over 60 years of age. Eur J Clin Microbiol Infect Dis. 2015;34:593–600. https://doi.org/10.1007/s10096-014-2267-8
34. Verghese B, Schwalm ND III, Dudley EG, Knabel SJ. A combined multi-virulence-locus sequence typing and staphylococcal cassette chromosome *mec* typing scheme possesses enhanced discriminatory power for genotyping MRSA. Infect Genet Evol. 2012;12:1816–21. https://doi.org/10.1016/j.meegid.2012.07.026
35. Blanc DS, Petignat C, Wenger A, Kuhn G, Vallet Y, Fracheboud D, et al. Changing molecular epidemiology of methicillin-resistant *Staphylococcus aureus* in a small geographic area over an eight-year period. J Clin Microbiol. 2007;45:3729–36. https://doi.org/10.1128/JCM.00511-07
36. Faria NA, Miragaia M, de Lencastre H; Multi Laboratory Project Collaborators. Massive dissemination of methicillin resistant *Staphylococcus aureus* in bloodstream infections in a high MRSA prevalence country: establishment and diversification of EMRSA-15. Microb Drug Resist. 2013;19:483–90. https://doi.org/10.1089/mdr.2013.0149
37. Melo-Cristino J, Resina C, Manuel V, Lito L, Ramirez M. First case of infection with vancomycin-resistant *Staphylococcus aureus* in Europe. Lancet. 2013;382:205. https://doi.org/10.1016/S0140-6736(13)61219-2
38. Sullivan MJ, Altman DR, Chacko KI, Ciferri B, Webster E, Pak TR, et al. A complete genome screening program of clinical methicillin-resistant *Staphylococcus aureus* isolates identifies the origin and progression of a neonatal intensive care unit outbreak. J Clin Microbiol. 2019;57:e01261–19. https://doi.org/10.1128/JCM.01261-19
39. Iregui A, Khan Z, Malik S, Landman D, Quale J. Emergence of delafloxacin-resistant *Staphylococcus aureus* in Brooklyn, New York. Clin Infect Dis. 2020;70:1758–60. https://doi.org/10.1093/cid/ciz787
40. Omoe K, Imanishi K, Hu D-L, Kato H, Fugane Y, Abe Y, et al. Characterization of novel staphylococcal enterotoxin-like toxin type P. Infect Immun. 2005;73:5540–6. https://doi.org/10.1128/IAI.73.9.5540-5546.2005
41. Zdzalik M, Kalinska M, Wysocka M, Stec-Niemczyk J, Cichon P, Stach N, et al. Biochemical and structural characterization of SplD protease from *Staphylococcus aureus*. PLoS One. 2013;8:e76812. https://doi.org/10.1371/journal.pone.0076812
42. Flannagan RS, Heit B, Heinrichs DE. Antimicrobial mechanisms of macrophages and the immune evasion strategies of *Staphylococcus aureus*. Pathogens. 2015;4:826–68. https://doi.org/10.3390/pathogens4040826
43. Le Pabic H, Germain-Amiot N, Bordeau V, Felden B. A bacterial regulatory RNA attenuates virulence, spread and human host cell phagocytosis. Nucleic Acids Res. 2015;43:9232–48. https://doi.org/10.1093/nar/gkv783

Address for correspondence: Paul J. Planet, Division of Pediatric Infectious Diseases, Children's Hospital of Philadelphia, Philadelphia, PA 19104, USA; email: planetp@email.chop.edu; Agnes M.S. Figueiredo, Federal University of Rio de Janeiro, Rio de Janeiro 21941902, Brazil; email: agnes@micro.ufrj.br

Population Genomics and Inference of *Mycobacterium avium* Complex Clusters in Cystic Fibrosis Care Centers, United States

Nabeeh A. Hasan,[1] Rebecca M. Davidson,[1] L. Elaine Epperson, Sara M. Kammlade, Sean Beagle, Adrah R. Levin, Vinicius Calado de Moura, Joshua J. Hunkins, Natalia Weakly, Scott D. Sagel, Stacey L. Martiniano, Max Salfinger, Charles L. Daley, Jerry A. Nick, Michael Strong

Mycobacterium avium complex (MAC) species constitute most mycobacteria infections in persons with cystic fibrosis (CF) in the United States, but little is known about their genomic diversity or transmission. During 2016–2020, we performed whole-genome sequencing on 364 MAC isolates from 186 persons with CF from 42 cystic fibrosis care centers (CFCCs) across 23 states. We compared isolate genomes to identify instances of shared strains between persons with CF. Among persons with multiple isolates sequenced, 15/56 (27%) had >1 MAC strain type. Genomic comparisons revealed 18 clusters of highly similar isolates; 8 of these clusters had patients who shared CFCCs, which included 27/186 (15%) persons with CF. We provide genomic evidence of highly similar MAC strains shared among patients at the same CFCCs. Polyclonal infections and high genetic similarity between MAC isolates are consistent with multiple modes of acquisition for persons with CF to acquire MAC infections.

Nontuberculous mycobacteria (NTM) are ubiquitous microorganisms found in indoor and outdoor habitats, including water, soil, and dust. NTM can infect susceptible persons, including those with lung diseases such as cystic fibrosis (CF) (*1*). Previous surveys conducted in the United States have found that *Mycobacterium avium* complex (MAC) species are clinically relevant and the most frequently isolated NTM (*2*). MAC consists of 9 slow-growing mycobacterial species (*3*–*6*), of which the 2 most frequently observed are *M. avium* (MAV) and *M. intracellulare*, including its subspecies *intracellulare* (MINT) and subspecies *chimaera* (MCHIM) (*4*). In the United States, most persons with CF and positive NTM cultures (61%) had MAC species infections (*2*,*7*). MAC infections increased by 3% annually during 2010–2014.

MAC pulmonary infections are probably acquired by inhalation of aerosols (*8*), but the sources and modes of transmission of MAC remain unclear. Studies using various molecular genotyping methods have shown MAC isolates from human airway samples to have high genetic similarity to isolates from animals (*8*–*10*), water (*11*,*12*), bathroom faucets (*13*), showerheads (*14*,*15*), pools (*16*), and soil (*17*). Other potential MAC infection sources include fomites, zoonotic sources, and contaminated materials (*10*,*18*). Despite the clinical relevance of MAC and its prevalence among persons with CF, the genomic relationships of MAC isolates and the potential for person-to-person transmission are poorly understood. Whole-genome sequencing (WGS) to analyze the genetic diversity of MAC is aimed at identifying MAC infections that cluster by high bacterial genomic sequence similarity, particularly in susceptible populations such as persons with CF. Unclustered isolates are unrelated and are therefore not implicated in transmission, but clustering between MAC isolates suggests that they are derived from the same source (i.e., shared water, surfaces, or person-to-person transmission). To this end, we analyzed the WGS of NTM isolates

Author affiliations: National Jewish Health, Denver, Colorado, USA (N.A. Hasan, R.M. Davidson, L.E. Epperson, S.M. Kammlade, S. Beagle, A.R. Levin, V. Calado de Moura, J.J. Hunkins, N. Weakly, C.L. Daley, J.A. Nick, M. Strong); University of Colorado Anschutz Medical Campus and Children's Hospital Colorado, Aurora, Colorado, USA (S.D. Sagel, S.L. Martiniano); University of South Florida College of Public Health and Morsani College of Medicine, Tampa, Florida, USA (M. Salfinger)

DOI: https://doi.org/10.3201/eid2711.210124

[1]These first authors contributed equally to this article.

voluntarily sent from US CF care centers (CFCCs) during a 4-year period. The goals of this project were to support routine clinical care through high-resolution taxonomic identification, understand the genetic diversity of CF-associated MAC isolates, and identify genetically similar strains among persons with CF for epidemiologic follow-up.

Materials and Methods

Ethics approval for this work was obtained from the National Jewish Health Institutional Review Board (approval no. HS-3149). As part of Colorado Research and Development Program (https://www.nationaljewishhealth.org/cocfrdp), NTM isolates from US CFCCs were processed and biobanked with the goal of surveillance for genetically similar strains (Table 1). We cultured bacterial samples on Middlebrook 7H11 agar plates (ThermoFisher Scientific, https://www.thermofisher.com) supplemented with 10% oleic acid, albumin, dextrose, catalase growth supplement before subculturing single-colony isolates into Middlebrook 7H9 broth (ThermoFisher Scientific) supplemented with 10% albumin, dextrose, catalase growth supplement and 0.05% Tween 80 (Sigma-Aldrich, https://www.sigmaaldrich.com). We divided these cultures into 1-mL biobanked glycerol stock aliquot replicates that we stored at –20°C.

DNA Extraction and Whole-Genome Sequencing

We extracted NTM DNA as described previously (*19*). We used NexteraXT DNA or DNA FLEX sample preparation (Illumina, https://www.illumina.com) to prepare WGS libraries and sequenced the libraries by using the Illumina MiSeq or HiSeq 2500. WGS data are available at the National Center for Biotechnology Information (BioProject no. PRJNA319839).

Non-CF Sample Acquisition

To place RDP isolates in context with zoonotic, environmental, and clinical samples from around the world, we included additional MAC isolates with existing WGS in the study. We downloaded 874 MAC genomes from the National Center for Biotechnology Information, including MAV (559 total; 42 environmental, 467 non-CF clinical, and 50 zoonotic), MCHIM (114 total; 3 environmental and 111 non-CF clinical), and MINT (201 total; 4 environmental, 192 non-CF clinical, and 5 zoonotic) from 32 published studies (Appendix 1 Table 1, https://wwwnc.cdc.gov/EID/article/27/11/21-0124-App1.xlsx) for subsequent comparisons.

MAC Species Identification

We trimmed sequence reads of adapters and base calls with quality scores <Q20 by using Skewer (*20*). We then assembled trimmed reads into scaffolds by using Unicycler (*21*). We compared genome assemblies against a collection of reference genomes (Appendix 1 Table 1) to estimate average nucleotide identity (ANI) and assign a species call to each isolate (*22*,*23*). A cutoff ANI of ≥95% indicated the isolate and reference genome belonged to the same species.

Phylogenomic Analysis

On the basis of taxonomic assignment, with the highest ANI score >95% for each genome, we mapped trimmed sequence reads to respective reference genomes (e.g., *M. avium* strain H87 [*24*]; *M. intracellulare* subsp. *chimaera* CDC 2015-22-71 [*25*]) by using Bowtie2 (*26*). We identified single-nucleotide polymorphisms (SNPs) as previously described (*27*).

By using the genome coordinates that correspond to the partial *rpo*B region used in clinical diagnostics, we extracted sequences from each MAC isolate. We compared the partial *rpo*B sequences from MAV, MCHIM, and MINT phylogenetically by using neighbor-joining and 250 bootstraps of the observed SNPs in MEGA (*28*).

To evaluate relationships between MAV from US CFCCs and global strains, we assessed the phylogenetic relationships to publicly available genomes from 559 non-CF MAV isolates, including 465 clinical, 42 environmental, and 50 zoonotic isolates from Japan, Germany, Belgium, the United Kingdom, the United States, and 12 other countries (Appendix 1 Table 1). To evaluate relationships between MCHIM from US CFCCs with US and global strains, we assessed the phylogenetic relationships to publicly available genomes from 114 non-CF MCHIM isolates, including 109 clinical and 5 environmental isolates from the United Kingdom, the United States,

Table 1. Number of MAC isolates in a study of MAC clusters in cystic fibrosis centers, United States*

Category	MAV	MCHIM	MINT	Total
Patients with 1 isolate, no.	63	33	43	137
Patients with ≥2 isolates, no.	30	5	23	55
Total patients, no.	93	38	66	186
Total isolates, no.	186	44	134	364

*Some patients have isolates from multiple MAC species. MAC, *Mycobacterium avium* complex; MAV, *M. avium*; MCHIM, *M. intracellulare* subsp. *chimaera*; MINT, *M. intracellulare* subsp. *intracellulare*.

Switzerland, South Korea, Canada, and South Africa (Appendix 1 Table 1). To evaluate relationships between MINT from US CFCCs with US and global strains, we assessed the phylogenetic relationships to publicly available genomes from 201 non-CF MINT isolates, including 192 clinical, 4 environmental, and 5 zoonotic isolates from China, the United Kingdom, South Korea, and the United States (Appendix 1 Table 1).

Identifying Genetically Similar Isolate Clusters

To identify a SNP threshold for genetically similar isolates, we examined genomewide SNP distances between pairs of longitudinal isolates from the same person (within-patient isolates) and isolates from different persons (between-patient isolates) in the US CFCC MAC dataset, analogous to methods used previously for *M. abscessus* and MAV (*29*–*33*). The US CFCC MAC dataset included 56 persons with CF who had ≥2 isolates of the same species: 31 who had ≥2 MAV isolates, 5 who had ≥2 MCHIM isolates, and 23 who had ≥2 MINT isolates. We computed statistical comparisons between MAC groups by using Kruskal–Wallis tests. By using the distributions of within-patient and between-patient genomic SNPs (Figure 1, panel A), we defined a distance of ≤20 SNPs as the threshold difference for strain definition. We defined isolates found within a patient with a pairwise distance of >20 SNPs as different strains. We notified CFCCs of genetically similar isolates and offered participation in site-specific epidemiologic investigations as part of the ongoing HALT-NTM trial (https://clinicaltrials.gov/ct2/show/NCT04024423) (*34*).

Results

Distribution of MAC Species in US Cystic Fibrosis Care Centers

We sequenced the genomes of 364 MAC isolates, including 186 MAV (51%), 134 MINT (37%), and 44 MCHIM (12%) (Table 1). More than half (101/186 [54%]) of persons with CF were women or girls (average age 35 years [range 9–88 years]). Isolates were analyzed from a total of 42 CFCCs and 22 states (Figure 2). Two-thirds (129/186 [69%]) of persons with CF had only 1 isolate sequenced, 21 had 2 isolates (21/186 [12%]), and 36 had ≥3 isolates (36/186 [19%]); collection dates spanned a range of 0 to 1,376 days between the first and last isolate collected (Figure 3). Most (132/186 [71%]) persons with samples analyzed were from 41 CFCCs in 21 states, and the remainder received care at 1 CFCC.

To evaluate taxonomic relationships of closely related taxa, we analyzed isolates from persons with CF, reference genomes for MAV (Figure 4, panel A; Appendix 1 Table 2), and type strains of MINT and MCHIM (Figure 4, panel B; Appendix 1 Table 1). The MAV phylogeny shows that most isolates from persons with CF are *M. avium* subsp. *hominissuis*, except for 1 isolate that was *M. avium* subsp. *avium* (Figure 4, panel A). The *M. intracellulare* phylogeny supports the taxonomy of 2 *M. intracellulare* subspecies, including MCHIM that is distinct from MINT (Figure 4, panel B).

Polyclonal MAC infections in Persons with Cystic Fibrosis

Among 55 persons with CF who had ≥2 MAC isolates, we identified 15 (15/55 [27%]) who had multiple strains

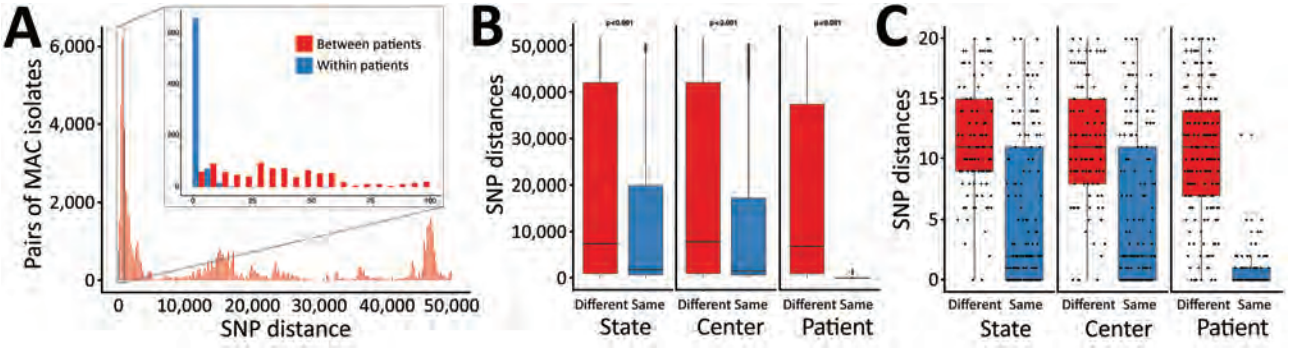

Figure 1. Cluster analysis of MAC in persons with cystic fibrosis to identify recent shared ancestry in a study of MAC clusters in cystic fibrosis centers, United States. A) Pairwise SNP distances of *Mycobacterium avium* and *M. intracellulare* subsp. *chimaera*, and *M. intracellulare* subsp. *intracellulare* isolates from within same patients (blue) and between different patients (red). B) Pairwise SNP distances of all CFCC MAC by state, CFCC, and patient comparisons. Kruskal–Wallis rank-sum test p values for comparing mean differences between categories are specified above each comparison. C) Pairwise SNP distances of CFCC MAC by state, CFCC, and patient comparisons under the clustering threshold. Box and scatterplots in panels B and C show SNPs between isolates at the same versus different states, same versus different CFCC, and same versus different patients. Horizontal lines within boxes indicate medians; top and bottom of boxes indicate 25th and 75th percentiles; error bars indicate the maximum and minimum values observed in the distribution. CFCC, cystic fibrosis care center; MAC, *Mycobacterium avium* complex; SNP, single-nucleotide polymorphism.

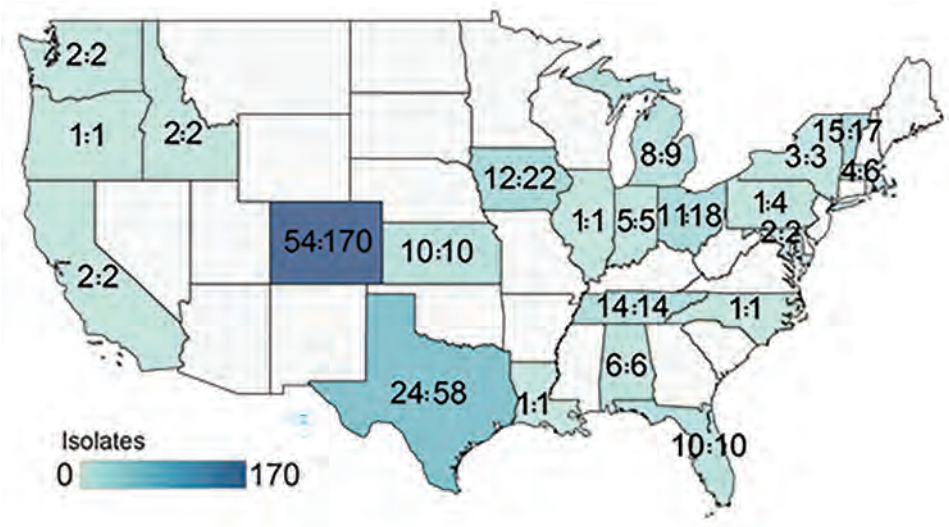

Figure 2. Geographic distribution of 364 *Mycobacterium avium* complex isolates from 186 patients, by cystic fibrosis care center state of origin in study of *M. avium* complex clusters in cystic fibrosis centers, United States. Numbers in each state are the number of patients with cystic fibrosis and total isolates contributed from centers within the state.

or species (Figure 5). Nine persons with CF (9/55 [16%]) had isolates from ≥2 MAC species; 1 (1/55 [2%]) had isolates of MAV, MCHIM, and MINT. Thirteen persons with CF who had MAV (13/30 [43%]) had ≥2 distinct MAV strains (>500 SNPs apart). Among these 13 persons with CF, we observed an average of 2.3 (range 2–5) different strains/patient; average within-patient diversity was 3,384 SNPs. Two (9%) of 23 persons with CF had 2 different strains of MINT; no persons with MCHIM had multiple strains. In total, 15/55 persons with CF had >1 strain or species, compared with 40/55 (73%) who had the same MAC strain isolated over time.

For the 15 persons with CF who had multiple strains of 1 MAC species, we generated time series plots of longitudinal isolates to visualize changes in strains over time (Figure 5; Appendix 2 Figure 1, https://wwwnc.cdc.gov/EID/article/27/11/21-0124-App2.pdf). The average time from first to last isolate collected was 259 days (range 5–1,262 days). In the case of the shortest interval, patient CF00193 was culture-positive with 2 different strains of MAV collected only 5 days apart. Patients CF00052, CF00060, and CF00193 each had 2 different strains of MAV collected within 30-day windows. Patient CF00002 was culture-positive for 3 different strains of MAV within a single week and had 5 different strains over nearly 3.5 years. In the 2 persons with CF harboring multiple strains of MINT, the second strain was detected 42 days (CF00004) and 138 days (CF00131) after the first isolate collected. Patients CF00029 and CF00776 showed alternating strains over time, suggesting persistent mixed populations of MAV in the airway.

Assessing Potential Transmission between Persons with Cystic Fibrosis

To evaluate routine molecular surveillance available in most diagnostic laboratories and compare it to the resolution afforded by WGS, we compared the *rpo*B partial sequences of each MAV, MCHIM, and MINT from US persons with CF. For MAV, 100% of patients belonged to 1 of 4 clusters (Appendix 2 Figure 2, panel A) based on analyses using *rpo*B, whereas 97.2% of MCHIM and 95.5% of MINT belonged to 5 clusters (Appendix 2 Figure 2, panel B). This result emphasizes that single-gene amplicon surveillance does not provide the resolution needed for genetic

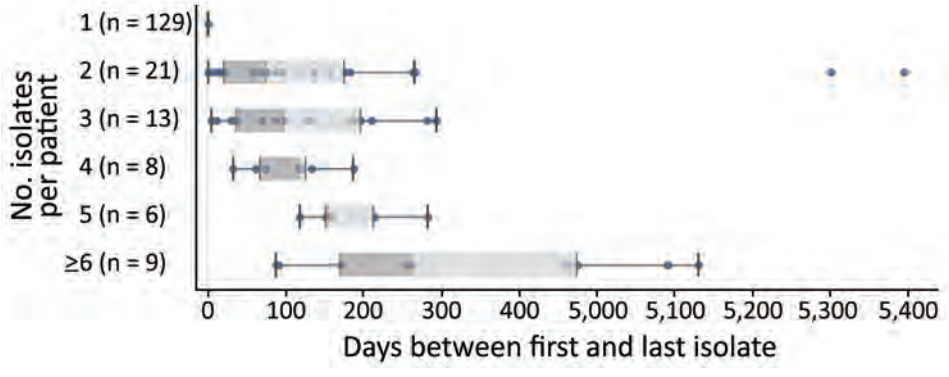

Figure 3. Numbers of isolates per patient and days between the patient's first and last isolate collected in the isolate cohort in a study of *Mycobacterium avium* complex clusters in cystic fibrosis centers, United States. Vertical lines within boxes indicate medians; top and bottom of boxes indicate 25th and 75th percentiles; error bars indicate the maximum and minimum values observed in the distribution.

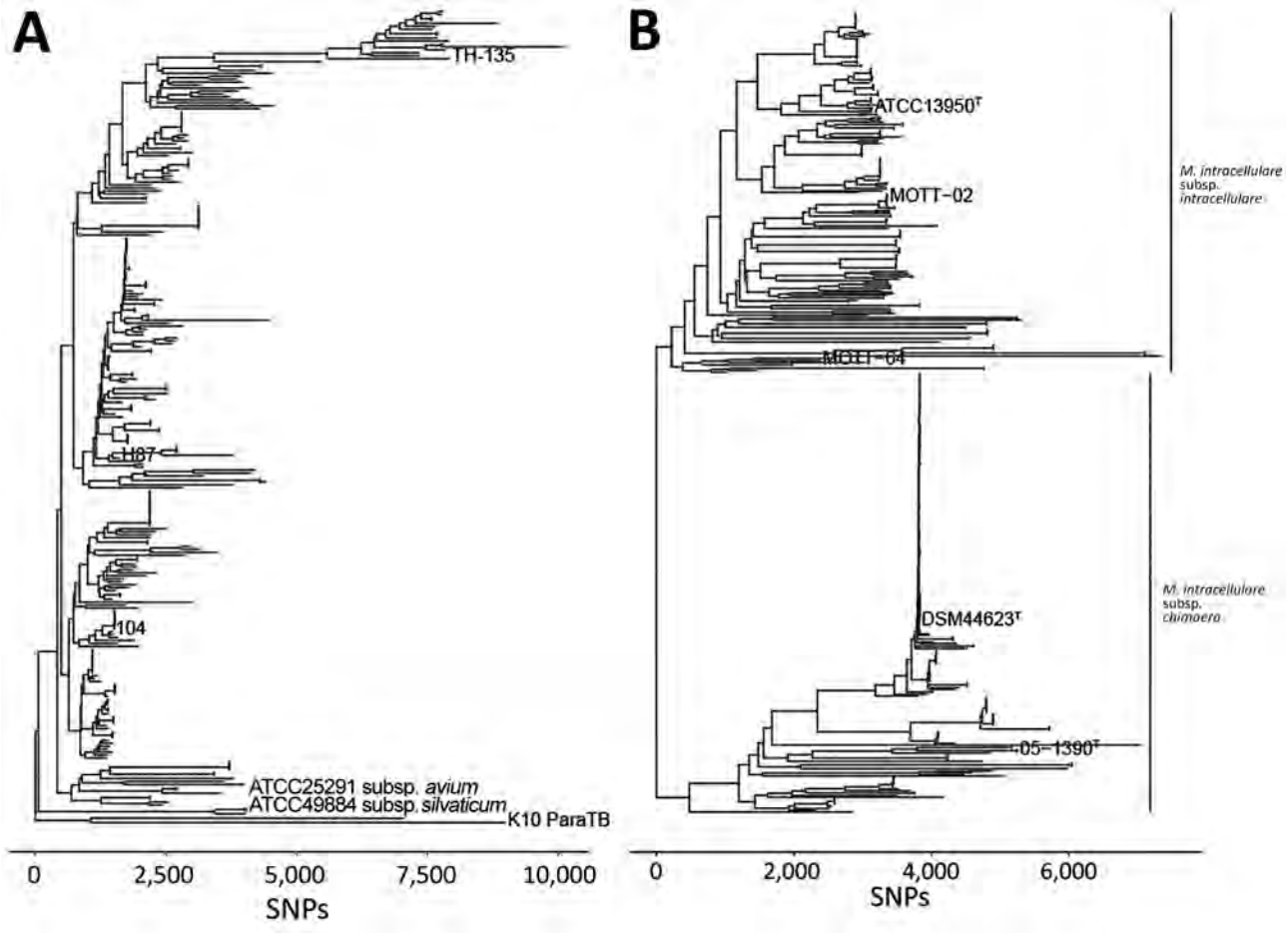

Figure 4. Phylogenetic relationships in a study of *Mycobacterium avium* complex isolates in cystic fibrosis care centers, United States. A) Phylogenetic tree of 207 *M. avium* isolates showing the relationships between *M. avium* cystic fibrosis care center and select non–cystic fibrosis, environmental, and zoonotic isolates. B). Phylogenetic tree of 235 isolates showing the relationships between cystic fibrosis care center and select non–cystic fibrosis *M. intracellulare* subsp. *chimaera* and *M. intracellulare* subsp. *intracellulare* isolates. Former species *M. yongonense* type strain 05–1380^T was also included as part of *M. intracellulare* subsp. *chimaera* to reflect current taxonomy. SNP, single-nucleotide polymorphism.

surveillance of NTM MAC species, whereas WGS does provide the necessary resolution.

To examine potential transmission of MAC isolates between persons with CF, we identified 20 SNPs as the threshold for recent shared ancestry on the basis of the distribution of SNPs among longitudinal isolates collected over time (Figure 1, panel A). By using this threshold, we identified a total of 18 genetically similar clusters, including 3 MAV, 5 MCHIM, and 10 MINT clusters (Figure 6). Of the 3 MAV clusters, 2 clusters consisting of 6 patients receiving treatment at 1 CFCC, and a third cluster consisting of 2 patients from a second CFCC. Most patients (15/27 [56%]) in 3/5 MCHIM clusters received treatment in the same CFCCs, whereas the remaining isolates in clusters originated from patients attending different CFCCs. Alternatively, a minority (4/21 [19%]) of patients in 2/10 MINT clusters received treatment in the same CFCC, suggesting that MINT may have different transmission routes compared with MAV or MCHIM. Among the entire US CFCC MAC dataset, 8/93 persons with MAV (9%), 15/36 with MCHIM (42%), and 4/66 with MINT (6%) belonged to clusters within the threshold of 20 SNPs and were treated at the same CFCCs, triggering epidemiologic follow-up in the HALT-NTM Trial (*34*). By using a 10-SNP threshold, we identified 2 *M. avium* clusters, 5 *M. chimaera*, and 6 *M. intracellulare* clusters (Appendix Figure 7). Overall, 4 patients included in 2 clusters defined by a 20-SNP threshold are removed when the threshold is reduced to 10 SNPs.

Overall, 27/186 persons with CF (15%) had MAC isolates that were genetically similar and received treatment at the same CFCC. Isolates collected within the same center were more similar than isolates

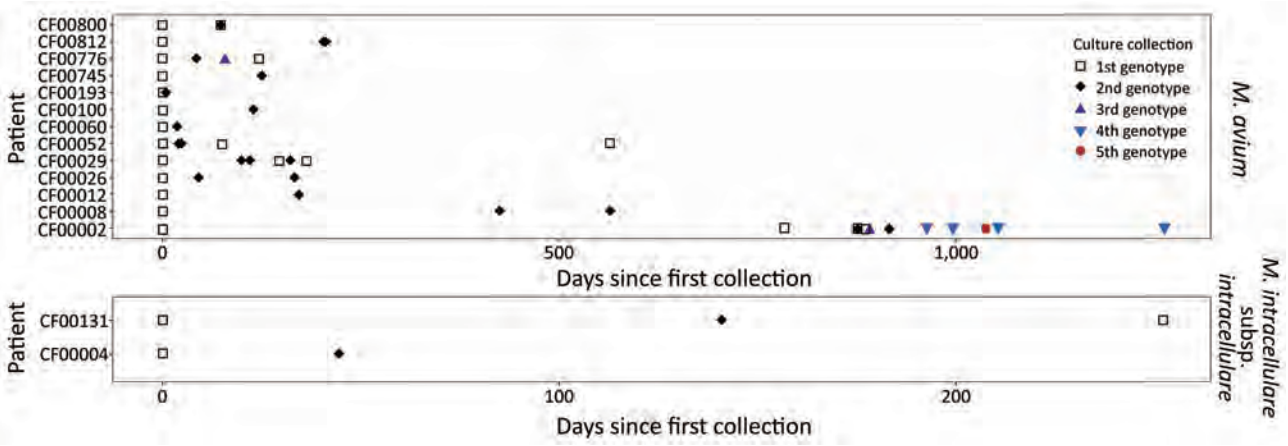

Figure 5. Polyclonal *Mycobacterium avium* complex (MAC) infections in 15 persons with CF in a study of MAC clusters in CF centers, United States. Persons with CF who had >1 MAC isolate were analyzed for the presence of multiple strains within a given MAC species. For *M. avium* (top) and *M. intracellulare* subsp. *intracellulare* (bottom), each row on the y-axis is a person with CF, and the x-axis represents the number of days after the first MAC isolate with whole-genome sequencing was collected. Each point represents a sequenced isolate and the shape represents a unique genotype. The plots do not represent all positive cultures in the patients' histories, but they illustrate how strains change, alternate, or both over time. In some cases, different strains were isolated on the same day or within a 1-week period. CF, cystic fibrosis.

collected from the same state (p = 0.014), whereas the mean SNPs observed between isolates coming from different centers were not significantly different from those coming from different states (Figure 1, panel B). The mean SNP differences observed between nearest-neighboring clustered MAC isolates from the same versus different CFCCs (5.47 vs. 11.21 SNPs; p<0.001) and the same versus different states (5.45 vs. 11.46 SNPs; p<0.001) were both significant (Figure 1, panel C). Only 2 clustered patient pairs (4/186 [2%]) were identified between different centers within a state, suggesting that clustering is more localized to CFCCs than to states.

For isolate clusters that included ≥3 isolates, we visualized the isolate relationships as phylogenetic clades (Figure 7). The patient with the isolate nearest to the base of each clade is ancestral to all descendants, and therefore is a potential source of transmission between the subsequent patients in the cluster. For example, patient CF00002 was the potential source of 2 separate clusters of MAV and MCHIM. In the MAV cluster (Figure 7, panel A), 4 isolates from patient CF00002 were ancestral to isolates from 3 other patients (CF00231, CF00776, and CF00812). In the MCHIM cluster, 2 isolates from patient CF00002 were ancestral to 1 isolate from patient CF00966 (Figure 7, panel E). Ancestral isolates and hypotheses about the order in which transmission events occurred can similarly be deduced for an additional MAV cluster (Figure 7, panel B), 3 MCHIM clusters (Figure 7, panels C–E), and 1 MINT cluster (Figure 7, panel F).

MAV

By using a genetic similarity threshold of 20 SNPs, we observed limited instances of genetic similarity between US CFCC MAV isolates from 11 persons with CF and 21 non-CF isolates (Appendix Figure 3). Four persons with CF had genetically similar MAV isolates to an environmental isolate collected from a household dust sample in Germany (Table 2; Appendix 2 Figure 4). Comparisons of US persons with CF MAV isolates to non-US clinical and zoonotic MAV isolates revealed similarities with 17 clinical isolates from patients in 6 countries (Belarus, Canada, Germany, Norway, United Kingdom, and United States), 3 zoonotic isolates from 2 birds (*35*), and 1 from an elephant. Overall, only 11/93 (12%) of persons with CF shared genetically similar isolates with non-CF MAV isolates.

MCHIM

A total of 30 MCHIM isolates from 28 persons with CF were similar to 37 non-CF isolates (Appendix 2 Figure 3). Matches to US CFCC isolates also include the MCHIM type strain DSM44623^T, 21 isolates from Oxford Hospital (Oxford, UK), and isolates from patients treated in Canada, Hawaii, and Virginia (Table 2; Appendix 2 Figure 5). US CFCC MCHIM isolates were all genetically different from isolates derived from contaminated heater–cooler units (*36*). No other environmental MCHIM isolates were available for comparisons. In total, 28/38 (74%) persons with CF and MCHIM had genetically similar isolates to non-CF isolates.

MINT

For MINT, we observed genetic similarities between isolates from 14 persons with CF and 24 non-CF isolates from North America, Europe, and Asia (Appendix 2 Figure 3). Eight MINT isolates were genetically similar to reference isolates, including MINT MOTT-02 (*37*), NCTC-13025 (*38*), and 22 nonpatient isolates from Michigan, Virginia, South Korea, and the United Kingdom (Table 2; Appendix 2 Figure 5). We did not observe similarities between environmental MINT and US CFCC isolates. Comparisons of US CFCC MINT isolates with zoonotic isolates identified similarity with isolates collected from a bird in a California zoo and the other from a penguin in a New York State zoo (*35*,*39*). Overall, 14/66 (21%) persons with CF and MINT had isolates with genetically similar matches to our non-CF isolate sample set.

Discussion

This study provides evidence of highly similar MAC isolates among persons with CF. However, the isolates from most MAC infections appear to be independently acquired and unclustered. We identified 18 genetically similar isolate clusters involving 54 persons with CF (including 8 patients with MAV, 27 patients with MCHIM, and 21 patients with MINT) within our threshold of recent shared ancestry (≤20 SNPs). We further determined that 8 of the identified clusters (8/18 [44%]) included 26 patients that received treatment at the same CFCCs. Person-to-person transmission may have occurred among those persons, and the genetic clusters are undergoing epidemiologic investigation (*34*). Epidemiologic follow-up will help us understand if genetic similarity is related to acquisition through common geography and environments. Most persons with CF (160/186 [86%]) in our study

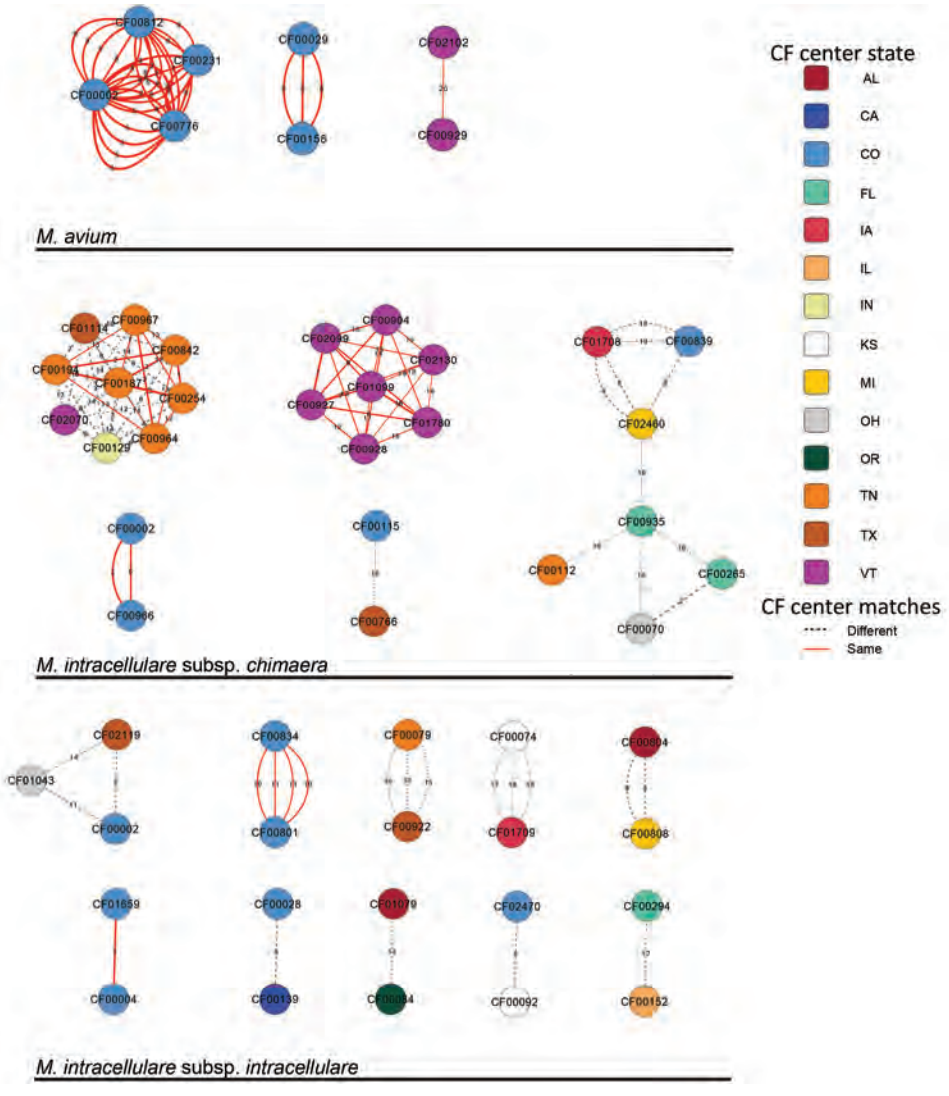

Figure 6. Genetic clusters of *Mycobacterium avium*, *M. intracellulare* subspecies *chimaera*, and *M. intracellulare* subsp. *intracellulare* in persons with CF in a study of *Mycobacterium avium* complex clusters in cystic fibrosis centers, United States. Three clusters *of M. avium*, 5 clusters of *M. intracellulare* subsp. *chimaera*, and 10 clusters of *M. intracellulare* subsp. *intracellulare* were identified. Each node represents a patient with ≥1 isolate having significant genetic similarity to an isolate in ≥1 patient. The color of each node represents the state of the submitting CF care center. Each edge represents genetic similarity between the isolates. Connecting edges are colored by matches within a center (red) or between different centers (dashed gray), and edge thickness is weighted from 0 SNPs (thickest) to 20 SNPs (thinnest) and the exact number of SNPs specified. Nodes with multiple connecting edges represent multiple isolates matching between patients. CF, cystic fibrosis; SNP, single-nucleotide polymorphism.

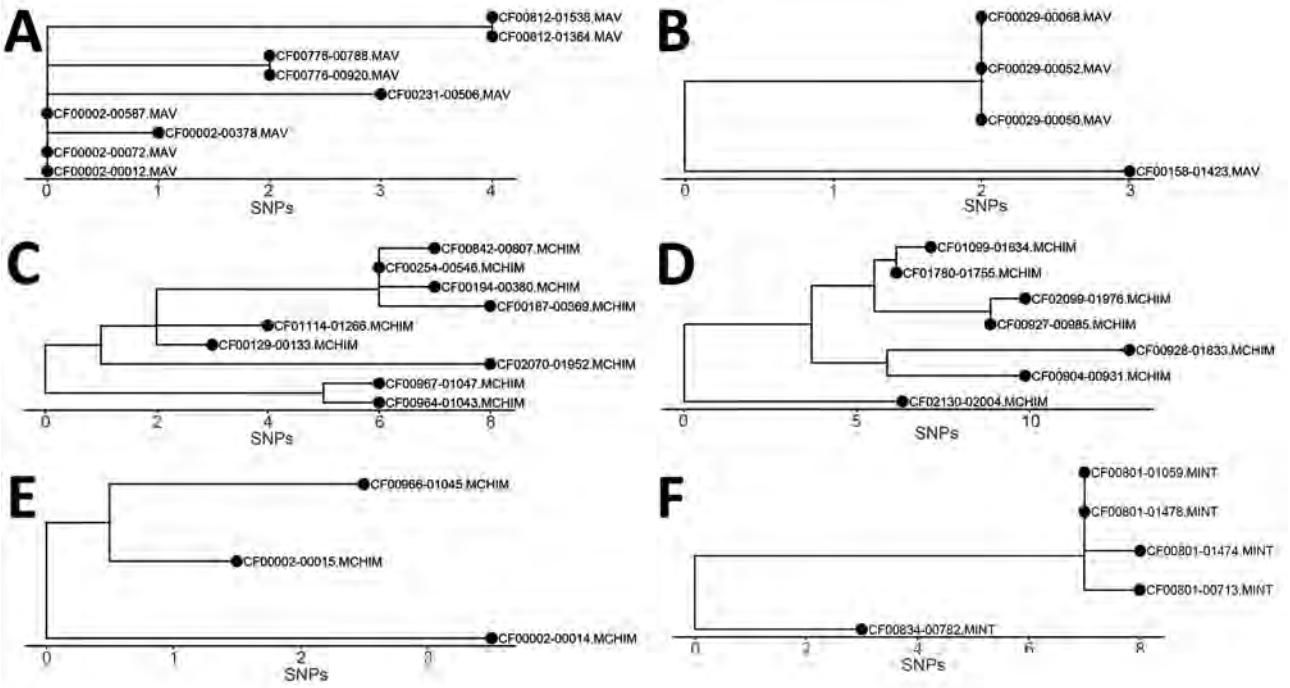

Figure 7. Phylogenetic visualization of *Mycobacterium avium* complex clusters in persons with CF in a study of *M. avium* complex clusters in CF centers, United States. Clusters with ≥3 isolates were visualized as clades to show the transition of patients' isolates over time. A) Cluster of 4 persons with MAV. B) Cluster of 2 persons with MAV. C) Cluster of 9 persons with MCHIM). D) Cluster of 7 persons with MCHIM. E) Cluster of 2 persons with MCHIM. F) Cluster of 2 persons with MINT. CF, cystic fibrosis; MAV, *M. avium*; MCHIM, *M. intracellulare* subsp. *chimaera*; MINT, *M. intracellulare* subsp. *intracellulare*; SNP, single-nucleotide polymorphism.

did not share similar strains; thus, we infer that most persons with CF do not transmit strains person-to-person or share acquisition sources of MAC.

In contrast with the clonality observed in *M. abscessus* (*27*,*29*), 27% of patients with MAC cultured multiple strains over time, as has also been observed for *Staphylococcus aureus* infections in persons with CF (*40*). This observation was considerably lower than the proportion of polyclonal MAC infections previously observed in patients with non-CF NTM lung disease (*29*). Although the analysis of single isolates instead of colony sweeps provides the clarity to genetically identify transmission clusters, it may underestimate the diversity of MAC populations present in patient airways. We surmise that MAV isolates found in most US persons with CF probably derive from the independent acquisition (or acquisitions) of strains in the environment. This interpretation is consistent with previously observed instances of genetically matched environmental and patient MAV isolates (*10*,*13*,*14*,*17*,*30*,*41*); however, it does not exclude the hypothesis of person-to-person transmission in persons with CF. Two hypotheses can explain the observations of multiple genotypes and species in persons with CF: patients were originally infected with multiple genotypes of MAC that were selected for during infection and treatment, or patients cleared the original infection and subsequently acquired a new, independent genotype. Our analyses provide evidence for both scenarios (Figure 5), though with limited sample sizes. Further studies of within-patient population diversity with

Table 2. Persons with CF with genetically similar MAC isolates compared with publicly available non-CF isolates collected from environmental, clinical, and zoonotic sources in a study of MAC clusters in CF centers, United States*

	No. (%)			
Taxon	Environmental	Non-CF clinical	Zoonotic	Total similar CF patients
MAV	4/93 (5)	9/93 (12)	3/93 (3)	11/93 (12)
MCHIM	0/38 (21)	28/38 (61)	0/38 (0)	28/38 (74)
MINT	0/66 (0)	14/66 (24)	3/66 (5)	14/66 (21)
Total				52/186 (28)

*Some patients have isolates that match to an isolate (or isolates) in >1 category. CF, cystic fibrosis; MAC, *Mycobacterium avium* complex; MAV, *M. avium*; MCHIM, *M. intracellulare* subsp. *chimaera*; MINT, *M. intracellulare* subsp. *intracellulare*.

corresponding environmental sampling are needed to address these questions.

Our WGS analysis of 364 MAC isolates, sent from 42 CFCCs in 23 states across the United States as part of a voluntary nationwide surveillance program, enabled us to examine genetic relationships among US isolates. WGS analyses greatly reduced the sizes of MAC clusters identified in US persons with CF compared with *rpo*B sequence information alone, highlighting the value of WGS resolution for epidemiologic follow-up. We also compared CF MAC isolates to isolates from previous studies, including those from environmental, zoonotic, and non-CF clinical sources. In our study, US MAV isolates from persons with CF were mostly distinct from non-CF clinical, environmental, and zoonotic samples from the United States (*30*), Europe (*42*–*44*), and Asia (*12*,*37*,*45*,*46*), although 12% of patients in our study had genetic matches to non-CF isolates. This finding is consistent with observations of human patients and animals harboring identical MAV in Europe (*8*,*9*,*12*,*13*,*42*,*47*,*48*). Similarly, only 21% of persons with CF and MINT had genetically similar isolates to non-CF samples, primarily clinical isolates. Few publicly available environmental isolates of MINT were available for comparison because of the lack of MINT found in water sources (*49*), suggesting that persons with CF likely acquire their MAV and MINT infections from nonhuman reservoirs that were not identified in this study.

In contrast, we observed many matches of MCHIM between CF and non-CF isolates. Indeed, a high proportion of MCHIM from US persons with CF (74% of patients) had matches to non-CF clinical isolates relative to MAV or MINT. One hypothesis to explain clustering of MCHIM is that the observed strains are well-adapted to colonize and persist in a human host. Alternatively, the high genetic similarity of MCHIM isolates may also suggest a lineage that has recently come to prominence in North America. Additional environmental and zoonotic sampling of MAV, MCHIM, and MINT isolates in the United States will be needed to better understand the species-specific risks of MAC infection from these sources.

Our study has some limitations. First, our empirically defined SNP threshold for recent common ancestry is specific for our patient cohort and is limited by the number of persons with CF with ≥2 isolates and the duration of sampling time frames. Thus, our threshold may miss transmission events that occurred before the sampling period. Second, despite observing genetic matches, epidemiologic links are required to support transmission. Our epidemiologic data were limited to isolate collection date and the CFCC where patients received care. Therefore, our analyses provide hypotheses for traditional epidemiologic follow-up at CFCCs that was beyond the scope of our current project but is being addressed in the HALT-NTM Trial (*34*). Third, the publicly available datasets did not allow a uniform comparison to non-CF clinical, environmental, or zoonotic isolates from each CFCC region for each species.

Our research study discovered potential instances of transmission between patients and assessed the dynamics of MAC infections in persons with CF. The findings of our US-based surveillance work in persons with CF were not possible without the resolution of WGS and underscore the need for continued epidemiologic follow-up in patients with MAC lung disease, with and without CF, to assist infectious disease control measures and limit the spread of MAC infections where possible.

This work was supported by the US Cystic Fibrosis Foundation's Colorado Research and Development Program (grant no. NICK15RO) and the Cystic Fibrosis National Resource Centers (grant nos. NICK20Y2SVC and NICK20Y2OUT). R.M.D was funded by National Institutes of Health–National Institute of Allergy and Infectious Diseases grant no. K01-AI125726. The funders had no role in study design, data collection and analysis, decision to publish, or preparation of the manuscript.

About the Author

Dr. Hasan is a bioinformatics analyst at the Center for Genes, Environment, and Health at National Jewish Health, Denver, Colorado. His main research interests are population genomics, acquisition, and environmental sources of nontuberculous mycobacteria.

References

1. Griffith DE, Aksamit T, Brown-Elliott BA, Catanzaro A, Daley C, Gordin F, et al.; ATS Mycobacterial Diseases Subcommittee; American Thoracic Society; Infectious Disease Society of America. An official ATS/IDSA statement: diagnosis, treatment, and prevention of nontuberculous mycobacterial diseases. Am J Respir Crit Care Med. 2007; 175:367–416. https://doi.org/10.1164/rccm.200604-571ST
2. Adjemian J, Olivier KN, Seitz AE, Holland SM, Prevots DR. Prevalence of nontuberculous mycobacterial lung disease in U.S. Medicare beneficiaries. Am J Respir Crit Care Med. 2012;185:881–6. https://doi.org/10.1164/rccm.201111-2016OC
3. Castejon M, Menéndez MC, Comas I, Vicente A, Garcia MJ. Whole-genome sequence analysis of the *Mycobacterium avium* complex and proposal of the transfer of *Mycobacterium yongonense* to *Mycobacterium intracellulare* subsp. *yongonense* subsp. nov. Int J Syst Evol Microbiol. 2018;68:1998–2005. https://doi.org/10.1099/ijsem.0.002767

4. Nouioui I, Carro L, García-López M, Meier-Kolthoff JP, Woyke T, Kyrpides NC, et al. Genome-based taxonomic classification of the phylum *Actinobacteria*. Front Microbiol. 2018;9:2007. https://doi.org/10.3389/fmicb.2018.02007
5. Tortoli E, Meehan CJ, Grottola A, Fregni Serpini G, Fabio A, Trovato A, et al. Genome-based taxonomic revision detects a number of synonymous taxa in the genus *Mycobacterium*. Infect Genet Evol. 2019;75:103983. https://doi.org/10.1016/j.meegid.2019.103983
6. van Ingen J, Turenne CY, Tortoli E, Wallace RJ Jr, Brown-Elliott BA. A definition of the *Mycobacterium avium* complex for taxonomical and clinical purposes, a review. Int J Syst Evol Microbiol. 2018;68:3666–77. https://doi.org/10.1099/ijsem.0.003026
7. Adjemian J, Olivier KN, Prevots DR. Epidemiology of pulmonary nontuberculous mycobacterial sputum positivity in patients with cystic fibrosis in the United States, 2010–2014. Ann Am Thorac Soc. 2018;15:817–26. https://doi.org/10.1513/AnnalsATS.201709-727OC
8. Arikawa K, Ichijo T, Nakajima S, Nishiuchi Y, Yano H, Tamaru A, et al. Genetic relatedness of *Mycobacterium avium* subsp. *hominissuis* isolates from bathrooms of healthy volunteers, rivers, and soils in Japan with human clinical isolates from different geographical areas. Infect Genet Evol. 2019;74:103923. https://doi.org/10.1016/j.meegid.2019.103923
9. Iwamoto T, Nakajima C, Nishiuchi Y, Kato T, Yoshida S, Nakanishi N, et al. Genetic diversity of *Mycobacterium avium* subsp. *hominissuis* strains isolated from humans, pigs, and human living environment. Infect Genet Evol. 2012;12:846–52. https://doi.org/10.1016/j.meegid.2011.06.018
10. Nishiuchi Y, Iwamoto T, Maruyama F. Infection sources of a common non-tuberculous mycobacterial pathogen, *Mycobacterium avium* complex. Front Med (Lausanne). 2017;4:27. https://doi.org/10.3389/fmed.2017.00027
11. Tzou CL, Dirac MA, Becker AL, Beck NK, Weigel KM, Meschke JS, et al. Association between *Mycobacterium avium* complex pulmonary disease and mycobacteria in home water and soil. Ann Am Thorac Soc. 2020;17:57–62. https://doi.org/10.1513/AnnalsATS.201812-915OC
12. Yano H, Iwamoto T, Nishiuchi Y, Nakajima C, Starkova DA, Mokrousov I, et al. Population structure and local adaptation of MAC lung disease agent *Mycobacterium avium* subsp. *hominissuis*. Genome Biol Evol. 2017;9:2403–17. https://doi.org/10.1093/gbe/evx183
13. Nishiuchi Y, Maekura R, Kitada S, Tamaru A, Taguri T, Kira Y, et al. The recovery of *Mycobacterium avium-intracellulare* complex (MAC) from the residential bathrooms of patients with pulmonary MAC. Clin Infect Dis. 2007;45:347–51. https://doi.org/10.1086/519383
14. Falkinham JOI III. Nontuberculous mycobacteria from household plumbing of patients with nontuberculous mycobacteria disease. Emerg Infect Dis. 2011;17:419–24. https://doi.org/10.3201/eid1703.101510
15. Feazel LM, Baumgartner LK, Peterson KL, Frank DN, Harris JK, Pace NR. Opportunistic pathogens enriched in showerhead biofilms. Proc Natl Acad Sci U S A. 2009;106:16393–9. https://doi.org/10.1073/pnas.0908446106
16. Thomson R, Tolson C, Carter R, Coulter C, Huygens F, Hargreaves M. Isolation of nontuberculous mycobacteria (NTM) from household water and shower aerosols in patients with pulmonary disease caused by NTM. J Clin Microbiol. 2013;51:3006–11. https://doi.org/10.1128/JCM.00899-13
17. De Groote MA, Pace NR, Fulton K, Falkinham JOI III. Relationships between *Mycobacterium* isolates from patients with pulmonary mycobacterial infection and potting soils. Appl Environ Microbiol. 2006;72:7602–6. https://doi.org/10.1128/AEM.00930-06
18. Honda JR, Hasan NA, Davidson RM, Williams MD, Epperson LE, Reynolds PR, et al. Environmental nontuberculous mycobacteria in the Hawaiian Islands. PLoS Negl Trop Dis. 2016;10:e0005068. https://doi.org/10.1371/journal.pntd.0005068
19. Epperson LE, Strong M. A scalable, efficient, and safe method to prepare high quality DNA from mycobacteria and other challenging cells. J Clin Tuberc Other Mycobact Dis. 2020;19:100150. https://doi.org/10.1016/j.jctube.2020.100150
20. Jiang H, Lei R, Ding S-W, Zhu S. Skewer: a fast and accurate adapter trimmer for next-generation sequencing paired-end reads. BMC Bioinformatics. 2014;15:182. https://doi.org/10.1186/1471-2105-15-182
21. Wick RR, Judd LM, Gorrie CL, Holt KE. Unicycler: Resolving bacterial genome assemblies from short and long sequencing reads. PLOS Comput Biol. 2017;13:e1005595. https://doi.org/10.1371/journal.pcbi.1005595
22. Goris J, Konstantinidis KT, Klappenbach JA, Coenye T, Vandamme P, Tiedje JM. DNA-DNA hybridization values and their relationship to whole-genome sequence similarities. Int J Syst Evol Microbiol. 2007;57:81–91. https://doi.org/10.1099/ijs.0.64483-0
23. Richter M, Rosselló-Móra R. Shifting the genomic gold standard for the prokaryotic species definition. Proc Natl Acad Sci U S A. 2009;106:19126–31. https://doi.org/10.1073/pnas.0906412106
24. Zhao X, Epperson LE, Hasan NA, Honda JR, Chan ED, Strong M, et al. Complete genome sequence of *Mycobacterium avium* subsp. *hominissuis* strain H87 isolated from an indoor water sample. Genome Announc. 2017;5:e00189–17. https://doi.org/10.1128/genomeA.00189-17
25. Hasan NA, Lawsin A, Perry KA, Alyanak E, Toney NC, Malecha A, et al. Complete genome sequence of *Mycobacterium chimaera* strain CDC 2015–22–71. Genome Announc. 2017;5:e00693–17. https://doi.org/10.1128/genomeA.00693-17
26. Langmead B, Salzberg SL. Fast gapped-read alignment with Bowtie 2. Nat Methods. 2012;9:357–9. https://doi.org/10.1038/nmeth.1923
27. Davidson RM, Hasan NA, Epperson LE, Benoit JB, Kammlade SM, Levin AR, et al. Population genomics of *Mycobacterium abscessus* from United States cystic fibrosis care centers. Ann Am Thorac Soc. 2021 Apr 15 [Epub ahead of print]. https://doi.org/10.1513/AnnalsATS.202009-1214OC
28. Stecher G, Tamura K, Kumar S. Molecular evolutionary genetics analysis (MEGA) for macOS. Mol Biol Evol. 2020;37:1237–9. https://doi.org/10.1093/molbev/msz312
29. Bryant JM, Brown KP, Burbaud S, Everall I, Belardinelli JM, Rodriguez-Rincon D, et al. Stepwise pathogenic evolution of *Mycobacterium abscessus*. Science. 2021;372:eabb8699. https://doi.org/10.1126/science.abb8699
30. Lande L, Alexander DC, Wallace RJ Jr, Kwait R, Iakhiaeva E, Williams M, et al. *Mycobacterium avium* in community and household water, suburban Philadelphia, Pennsylvania, USA, 2010–2012. Emerg Infect Dis. 2019;25:473–81. https://doi.org/10.3201/eid2503.180336
31. Bryant JM, Grogono DM, Greaves D, Foweraker J, Roddick I, Inns T, et al. Whole-genome sequencing to identify transmission of *Mycobacterium abscessus* between patients with cystic fibrosis: a retrospective cohort study. Lancet. 2013;381:1551–60. https://doi.org/10.1016/S0140-6736(13)60632-7

32. Tortoli E, Kohl TA, Trovato A, Baldan R, Campana S, Cariani L, et al. *Mycobacterium abscessus* in patients with cystic fibrosis: low impact of inter-human transmission in Italy. Eur Respir J. 2017;50:1602525. https://doi.org/10.1183/13993003.02525-2016
33. Yoon J-K, Kim TS, Kim J-I, Yim J-J. Whole genome sequencing of nontuberculous mycobacterium (NTM) isolates from sputum specimens of co-habiting patients with NTM pulmonary disease and NTM isolates from their environment. BMC Genomics. 2020;21:322. https://doi.org/10.1186/s12864-020-6738-2
34. Gross JE, Martiniano SL, Nick JA. Prevention of transmission of *Mycobacterium abscessus* among patients with cystic fibrosis. Curr Opin Pulm Med. 2019;25:646–53. https://doi.org/10.1097/MCP.0000000000000621
35. Pfeiffer W, Braun J, Burchell J, Witte CL, Rideout BA. Whole-genome analysis of mycobacteria from birds at the San Diego Zoo. PLoS One. 2017;12:e0173464. https://doi.org/10.1371/journal.pone.0173464
36. Hasan NA, Epperson LE, Lawsin A, Rodger RR, Perkins KM, Halpin AL, et al. Genomic analysis of cardiac surgery–associated *Mycobacterium chimaera* infections, United States. Emerg Infect Dis. 2019;25:559–63. https://doi.org/10.3201/eid2503.181282
37. Kim B-J, Choi B-S, Lim J-S, Choi I-Y, Lee J-H, Chun J, et al. Complete genome sequence of *Mycobacterium intracellulare* clinical strain MOTT-02. J Bacteriol. 2012;194:2771. https://doi.org/10.1128/JB.00365-12
38. Chand M, Lamagni T, Kranzer K, Hedge J, Moore G, Parks S, et al. Insidious risk of severe *Mycobacterium chimaera* infection in cardiac surgery patients. Clin Infect Dis. 2017;64:335–42. https://doi.org/10.1093/cid/ciw754
39. Rivas AE, Hollinger C, Oehler DA, Robbe-Austerman S, Paré JA. Diagnosis and management of mycobacteriosis in a colony of little penguins (*Eudyptula minor*). J Zoo Wildl Med. 2019;50:427–36. https://doi.org/10.1638/2018-0190
40. Long DR, Wolter DJ, Lee M, Precit M, McLean K, Holmes E, et al. Polyclonality, shared strains, and convergent evolution in chronic CF *S. aureus* airway infection. Am J Respir Crit Care Med. 2021;203:1127–37. https://doi.org/10.1164/rccm.202003-0735OC
41. Feazel LM, Baumgartner LK, Peterson KL, Frank DN, Harris JK, Pace NR. Opportunistic pathogens enriched in showerhead biofilms. Proc Natl Acad Sci U S A. 2009;106:16393–9. https://doi.org/10.1073/pnas.0908446106
42. Bruffaerts N, Vluggen C, Duytschaever L, Mathys V, Saegerman C, Chapeira O, et al. Genome sequences of four strains of *Mycobacterium avium* subsp. *hominissuis*, isolated from swine and humans, differing in virulence in a murine intranasal infection model. Genome Announc. 2016;4:e00533–16. https://doi.org/10.1128/genomeA.00533-16
43. Lahiri A, Kneisel J, Kloster I, Kamal E, Lewin A. Abundance of *Mycobacterium avium* ssp. *hominissuis* in soil and dust in Germany—implications for the infection route. Lett Appl Microbiol. 2014;59:65–70. https://doi.org/10.1111/lam.12243
44. Sanchini A, Semmler T, Mao L, Kumar N, Dematheis F, Tandon K, et al. A hypervariable genomic island identified in clinical and environmental *Mycobacterium avium* subsp. *hominissuis* isolates from Germany. Int J Med Microbiol. 2016;306:495–503. https://doi.org/10.1016/j.ijmm.2016.07.001
45. Uchiya K, Takahashi H, Yagi T, Moriyama M, Inagaki T, Ichikawa K, et al. Comparative genome analysis of *Mycobacterium avium* revealed genetic diversity in strains that cause pulmonary and disseminated disease. PLoS One. 2013;8:e71831. https://doi.org/10.1371/journal.pone.0071831
46. Uchiya KI, Tomida S, Nakagawa T, Asahi S, Nikai T, Ogawa K. Comparative genome analyses of *Mycobacterium avium* reveal genomic features of its subspecies and strains that cause progression of pulmonary disease. Sci Rep. 2017;7:39750. https://doi.org/10.1038/srep39750
47. Ichikawa K, van Ingen J, Koh WJ, Wagner D, Salfinger M, Inagaki T, et al. Genetic diversity of clinical *Mycobacterium avium* subsp. *hominissuis* and *Mycobacterium intracellulare* isolates causing pulmonary diseases recovered from different geographical regions. Infect Genet Evol. 2015;36:250–5. https://doi.org/10.1016/j.meegid.2015.09.029
48. Vluggen C, Soetaert K, Duytschaever L, Denoël J, Fauville-Dufaux M, Smeets F, et al. Genotyping and strain distribution of *Mycobacterium avium* subspecies *hominissuis* isolated from humans and pigs in Belgium, 2011-2013. Euro Surveill. 2016;21:30111. https://doi.org/10.2807/1560-7917.ES.2016.21.3.30111
49. Wallace RJ Jr, Iakhiaeva E, Williams MD, Brown-Elliott BA, Vasireddy S, Vasireddy R, et al. Absence of *Mycobacterium intracellulare* and presence of *Mycobacterium chimaera* in household water and biofilm samples of patients in the United States with *Mycobacterium avium* complex respiratory disease. J Clin Microbiol. 2013;51:1747–52. https://doi.org/10.1128/JCM.00186-13

Address for correspondence: Nabeeh A. Hasan, Center for Genes, Environment, and Health, National Jewish Health, 1400 Jackson St, Denver, CO 80206, USA; email: hasann@njhealth.org

Genomic Profiling of *Mycobacterium tuberculosis* Strains, Myanmar

Htin Lin Aung,[1] Wint Wint Nyunt,[1] Yang Fong, Patrick J. Biggs, Richard C. Winkworth, Peter J. Lockhart, Tsin Wen Yeo, Philip C. Hill, Gregory M. Cook, Si Thu Aung

Multidrug resistance is a major threat to global elimination of tuberculosis (TB). We performed phenotypic drug-susceptibility testing and whole-genome sequencing for 309 isolates from 342 consecutive patients who were given a diagnosis of TB in Yangon, Myanmar, during July 2016–June 2018. We identified isolates by using the GeneXpert platform to evaluate drug-resistance profiles. A total of 191 (62%) of 309 isolates had rifampin resistance; 168 (88%) of these rifampin-resistant isolates were not genomically related, indicating the repeated emergence of resistance in the population, rather than extensive local transmission. We did not detect resistance mutations to new oral drugs, including bedaquiline and pretomanid. The current GeneXpert MTB/RIF system needs to be modified by using the newly launched Xpert MTB/XDR cartridge or line-probe assay. Introducing new oral drugs to replace those currently used in treatment regimens for multidrug-resistant TB will also be useful for treating TB in Myanmar.

Tuberculosis (TB) is the infectious disease that causes the most deaths worldwide (≈5,000/day) (*1*). Of major concern is the increasing prevalence of drug resistance worldwide (*1*). There are different forms of TB drug resistance: pre–multidrug-resistant TB (pre–MDR TB, resistant to 1 of 2 first-line drugs: isoniazid or rifampin); multidrug-resistant TB (MDR TB, resistant to 2 first-line drugs: isoniazid and rifampin); pre–extensively drug-resistant (pre-XDR, resistant to either fluoroquinolones or injectable drugs in addition to MDR); and extensively drug-resistant TB (XDR TB, resistant to fluoroquinolones and injectable drugs in addition to MDR) (*1*). An estimated 0.5 million cases of MDR TB were reported in patients worldwide during 2018, but only one third had access to effective treatment, resulting in 56% of patients being successfully treated (*1*). In addition, an estimated 6% of diagnosed case of MDR TB cases are actually cases of XDR TB (*1*).

Myanmar is recognized by the World Health Organization (WHO) as having high burdens of TB (338 cases/100,000 population), MDR TB (21 cases/100,000 population), and co-infections of TB and HIV (29 cases/100,000 population) (*1*). A nationwide drug-resistant TB survey was conducted during 2012–2013 by the Myanmar National Tuberculosis Programme (NTP) to identify the drug susceptibility profile for first-line drugs (phenotypic drug susceptibility testing for second-line drugs was established during 2016) (*2*). This survey identified MDR TB among 5% of new cases and 27.1% of previously treated cases, and the Yangon region was identified as a hotspot for drug-resistant TB (*3*). Having an estimated population of 8 million persons, Yangon is the most populous city in Myanmar. All patients with suspected pulmonary TB are referred to a TB diagnostic center run by the NTP for testing by using the GeneXpert platform (https://www.cepheid.com). Routine, phenotypic drug-susceptibility testing (DST) of first-line or second-line drugs is rarely performed for new patients, and currently testing is based solely on the Xpert MTB/RIF (*M. tuberculosis*/rifampin) assay. Therefore, clinical decisions reflect the detection of rifampin resistance and national therapeutic guidelines on the basis of WHO recommendations.

Technological advances in next-generation, whole-genome sequencing (WGS) and downstream bioinformatic analyses now enable comprehensive detection of drug resistance and provide an alternative to existing

Author affiliations: University of Otago, Dunedin, New Zealand (H.L. Aung, P.C. Hill, G.M. Cook); Ministry of Health and Sports, Yangon, Myanmar (W.W. Nyunt); Massey University, Palmerston North, New Zealand (Y. Fong, P.J. Biggs, R.C. Winkworth, P.J. Lockhart); Nanyang Technological University, Singapore (T.W. Yeo); Ministry of Health and Sports, Naypyitaw, Myanmar (S.T. Aung)

DOI: https://doi.org/10.3201/eid2711.210726

[1]These authors contributed equally to this article.

approaches (*3*–*5*). Such sequence-based, drug-resistant profiles have high concordance with phenotypic DST (*3*,*4*). In addition, phylogenetic analyses of sequence data can be used to identify transmission patterns in the absence of epidemiologic data, which is often lacking in high-burden settings such as Myanmar (*3*,*6*). We combined clinical, genomic, and phenotypic drug-resistance data to provide insights into drug resistance and transmission patterns in Yangon. In this study, we used WGS analyses of 309 *M. tuberculosis* isolates to determine how the increasing burden of MDR TB has been driven in Yangon.

Methods

Study Design and Participants

This population-based, cross-sectional study included consenting participants ≥15 years of age who had GeneXpert-confirmed positive pulmonary TB at 3 major NTP TB diagnostic centers (Aung San, Latha, and North Oakkalapa) in Yangon during July 2016–June 2018. We aimed to recruit 250 patients consecutively given a diagnosis of infection with rifampin-resistant (RR) *M. tuberculosis* and 200 patients infected with rifampin-susceptible (RS) *M. tuberculosis*. Recruitment numbers at each facility reflected the relative numbers of patients given a diagnosis during the previous year. Patients were eligible to be included in the study if they had lived in Yangon at the time of registration, had a TB-positive confirmation by GeneXpert, and provided written informed consent. Patients were excluded if their residential address was outside Yangon at the time of registration or they did not provide informed consent. We obtained a brief clinical report for each patient (basic demographics, residential address, history of TB treatment, HIV status, and random blood glucose testing results for diabetes mellitus). The Institutional Review Boards of the Department of Medical Research, Ministry of Health and Sports of Myanmar, and the Human Health Ethics Review Committee of the University of Otago (Dunedin, New Zealand) approved this study.

Laboratory Procedures

We collected all clinical sputum samples at the time of diagnosis and before commencement of treatment. We sent samples to the National Tuberculosis Reference Laboratory in Yangon for DST. Testing for resistance to isoniazid, rifampin, ethambutol, streptomycin, para-aminosalicylic acid, ethionamide, D-cycloserine, fluoroquinolones (ofloxacin, levofloxacin, capreomycin), and aminoglycosides (amikacin, kanamycin) was performed by using the proportion method on Löwenstein–Jensen medium (https://apps.who.int/iris/bitstream/handle/10665/83807/WHO_CDS_TB_2001.288_eng.pdf). We determined resistance to new and repurposed drugs (i.e., pyrazinamide, bedaquiline, pretomanid, delamanid, linezolid, and clofazimine) on the basis of genomic markers known to be associated with resistance (*5*,*7*,*8*). Clinicians were provided with the WGS and accompanying phenotypic DST data as soon as it was available, and clinical decisions were made entirely at their discretion.

We extracted genomic DNA from cultures of single sputum specimens by using MoBio Microbial DNA Isolation Kits (https://www.qiagen.com) and sequenced DNA by using Illumina MiSeq (https://www.illumina.com) as described (*9*,*10*). All sequencing data from this study were deposited into the National Center for Biotechnology Information Sequence Read Archive (https://www.ncbi.nlm.nih.gov/sra; accession no. PRJNA638161).

Analysis

We performed genomic mapping by using Burrow-Wheeler Aligner-maximum exact matches (version 7.17-r1188; https://bio-bwa.sourceforge.net) and the *M. tuberculosis* reference genome H37Rv (GenBank accession no. NC_000962.3). Mapping used a custom *M. tuberculosis* masking browser extensible data file to exclude highly repetitive GC-rich conserved domains. We used SAMtools and BCFtools utilities version 1.9 to call single-nucleotide polymorphisms (SNPs) (*11*). *M. tuberculosis* TB-Profiler version 2.8.2 (https://github.com) was used to predict resistance to 17 drugs on the basis of genotyping of gene targets and classification to phylogenetic lineages by using SNP barcodes (*7*,*8*). Maximum-likelihood phylogenetic analyses were conducted by using RaxML, as implemented in the Gubbins pipeline version 2.3.4 (*12*). We used the online platform iTOL version 5.5 for annotation and management of phylogenetic trees (*13*). Isolates were considered closely related (genomically linked) if the pairwise distance between them was ≤12 SNPs (*5*). Statistical analyses were performed by using GraphPad Prism version 8.0 (https://www.graphpad.com) and the χ^2 test. A p value <0.05 was considered statistically significant.

Results

Over the recruitment period, 342 patients (194 with RR and 148 with RS *M. tuberculosis*) participated in the study; 33 case-patients were excluded because of laboratory contamination or failed sputum culture and DNA extraction. Of the final 309 GeneXpert-positive included participants, 200 (65%) were male (Table 1),

Table 1. Characteristics of patients who were infected with rifampin-susceptible and rifampin-resistant *Mycobacterium tuberculosis* strains that were identified by using Xpert MTB/RIF assay, Myanmar*

Characteristic	Resistant, n = 191	Susceptible, n = 118	p value
Sex			
M	120	80	0.39
F	71	38	
Treatment history			
Retreatment	108	31	<0.0001
New	83	87	
District			
North	64	74	<0.0001
South	7	3	
East	75	31	
West	45	10	
Age, y			
10–19	7	4	0.90
20–39	102	59	
40–59	67	44	
>60	15	11	
HIV			
Positive	6	1	0.28
Negative	200	102	
Random blood glucose, mg/dL			
≥200	13	8	0.64
<200	193	95	
Laboratory testing			
Lineage 2	164	37	<0.0001
Other	27	81	

*Xpert MTB/RIF (*M. tuberculosis*/rifampin), Cepheid (https://www.cepheid.com).

118 were RS and 191 were RR, and all had phenotypic DST successfully completed. RR was strongly associated with a history of TB treatment (p<0.0001) (Table 1).

We compared the results of the GeneXpert, phenotypic DST, and genomic analyses to further evaluate drug resistance (Figure 1). Of 118 cases diagnosed as RS by using GeneXpert, 16 (14%) were identified as isoniazid resistant on the basis of genomic analyses (Figure 1); resistance was conferred either by a mutation in the *katG* gene (S315T; 12 [75%] of 16) or in the promoter region of the *inhA* gene (c-15t; 4 [25%] of 16) (Table 2; Figure 1). All 16 cases were phenotypically confirmed as isoniazid resistant (Table 2).

All 191 RR isolates identified by GeneXpert were phenotypically resistant; the S450L mutation in the *rpoB* gene was the dominant mutation (137 [72%] of 191 (Table 2; Figure 2). WGS further identified that 10 (5%) were only rifampin resistant (pre-MDR), 144 (75%) were MDR, 31 (16%) were pre-XDR, and 6 (3%) were XDR; results were confirmed by phenotypic DST (Figure 1). All pre-XDR isolates harbored mutations in the *gyrA* gene, and D94G was most prevalent (12 [39%] of 31), followed by A90V (8 [26%] of 31) (Table 2; Figure 2). Resistance to aminoglycoside injectable drugs (XDR) was predominantly associated with *rrs* A1401G (4 [6 [67%] of 6) and G1484T (2 [33%] of 6) mutations. Mutations in the *embB* gene (M306V; 42 [53%] of 80), the M306I mutant (34 [43%] of 80), and mutations in the *rpsl* gene (K43R; 126 [90%] of 140) were present in all ethambutol-resistant and streptomycin-resistant isolates, resulting in a sensitivity of 70.2% and a specificity of 79.5% for ethambutol and a sensitivity of 84.3% and a specificity of 55.9% for streptomycin (Table 2; Figure 2). Known mutations conferring resistance to new and repurposed drugs, such as bedaquiline, delamanid, pretomanid, linezolid and clofizamine, were not identified by WGS in the 207 drug-resistant isolates (26 pre-MDR, 144 MDR, 31 pre-XDR, 6 XDR).

Using specific SNP barcodes, we classified the *M. tuberculosis* isolates as either lineage 1 (73, 24%), lineage 2 (201, 65%), lineage 3 (16, 5%) or lineage 4 (19, 6%) (Figure 3; Appendix Table 1, https://wwwnc.cdc.gov/EID/article/27/11/21-0726-App1.pdf). Most isolates were identified as belonging to sublineage 2.2.1, Beijing strain (Appendix Table 1). Isolates linked to TB lineage 2 were more commonly drug resistant than those belonging to other lineages (175 [85%] of 207 vs. 32 [15%] of 207; p<0.0001). In contrast, the other lineages were more commonly associated with drug susceptibility (76 [75%] of 102 vs. 26 [25%] of 102; p<0.001) (Table 1; Appendix Table 2). Drug-resistant isolates were also more commonly found in the East and West districts of Yangon (124 [60%] of 207; p<0.0001) (Table 1; Appendix Table 2) and to be associated with patients who had previously received treatment (112 [54%] of 207; p<0.0001) (Appendix Table 2). A total of 181 [87%] of 207

isolates were genomically unlinked on the basis of a standard pairwise distance threshold. The remaining 26 (13%) of 207 drug-resistant isolates formed 9 potential transmission chains (Figure 4).

Cases within most of these groups were located within the same districts (Figure 4), and each group contained a combination of new and previously treated TB patients. In 6 groups, all isolates had the same resistance profile; the remaining 3 (i.e., groups 5, 6, and 8) groups, had different resistance profiles. In group 6, an XDR isolate appears to have developed from an isoniazid-resistant (pre-MDR) isolate (Figure 4).

Discussion

This WGS study from Myanmar provides new insights into the landscape of drug-resistant TB in the country's largest city. A large proportion of isolates with high-level drug resistance, including pre-XDR and XDR, were identified. However, there was no resistance to new and repurposed drugs, such as bedaquiline, pretomanid, delamanid, and linezolid. Most drug-resistant cases were associated with previous treatment, and few were clearly associated with community transmission. These findings suggest an additional diagnostic tool, such as the Xpert MTB/XDR cartridge or line-probe assay (LPA), in addition to Xpert MTB/RIF, and new oral regimens, including bedaquiline and pretomanind, are needed for effective surveillance and treatment/management of MDR TB in Mynamar. Further studies are also required to investigate apparent cases of independent emergence and community transmission of MDR TB in Yangon.

Consistent with previous reports on lineage 2 from neighboring countries, this study identified a strong association between lineage 2 *M. tuberculosis* and drug resistance (*14*–*17*). There was strong agreement between WGS (presence of resistance-conferring mutations) and phenotypic DST to isoniazid and rifampin in this study (*18*). These findings indicate quality assurance in the TB laboratory diagnostic service provided by the Myanmar National Tuberculosis Reference Laboratory.

The Xpert MTB/RIF assay has been effective in the simultaneous detection of TB and resistance to rifampin. Because it can provide a diagnosis for a patient within 2 hours, GeneXpert is critical in TB control in high-burden settings. One of the limitations of current cartridges for Xpert is that resistance to

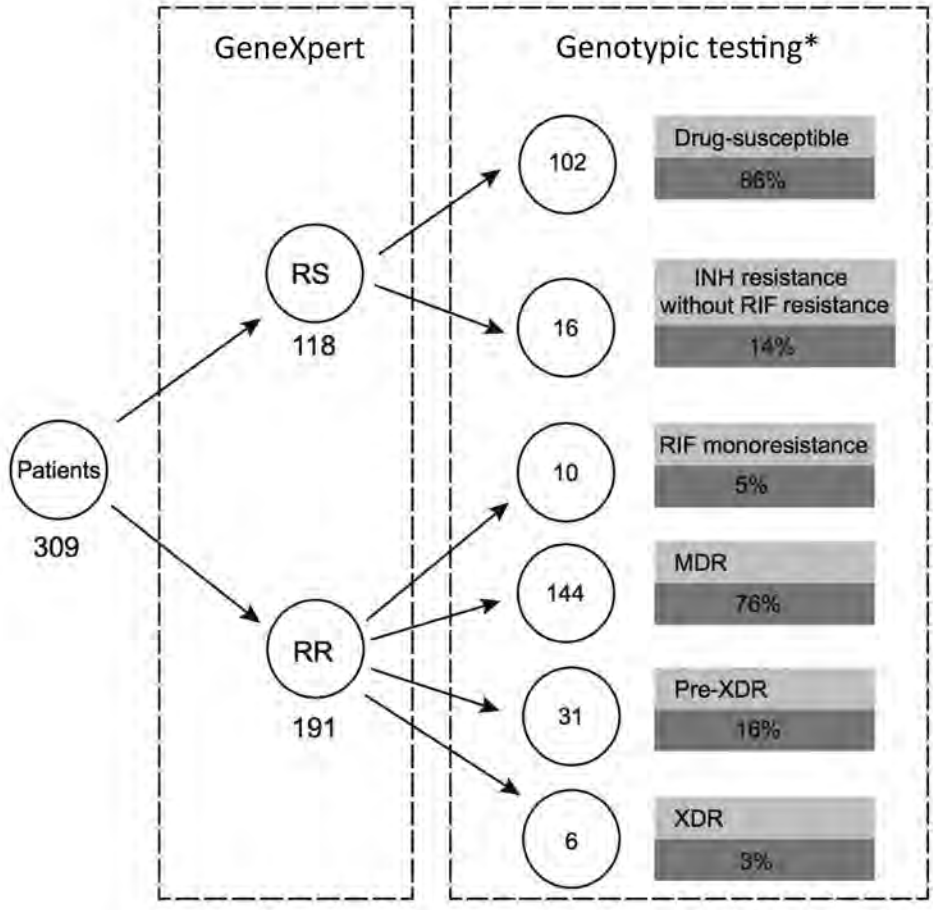

Figure 1. Genomic profiling of *Mycobacterium tuberculosis* strains, Myanmar, comparing discriminatory power offered by GeneXpert (Cepheid, https://www.cepheid.com) and additional genotypic testing, such as line-probe assay or whole-genome sequencing. RIF resistance and sensitivity were determined by using the Xpert MTB/RIF assay (Cepheid). INH, isoniazid; MDR, multidrug resistant; RIF, rifampin; RR, rifampin resistant; RS rifampin sensitive; XDR, extensively drug resistant. *Resistance profile confirmed by phenotypic testing.

Table 2. Comparison of phenotypic drug susceptibility testing and genomic resistance mutation results for *Mycobacterium tuberculosis* strains, Myanmar*

	Performance of genome-based† drug resistance profile prediction with respect to phenotypic drug-susceptibility testing					
	Mutation		No mutation			
Drug	Sensitive	Resistant	Sensitive	Resistant	Sensitivity, %	Specificity, %
Isonizaid	0	196	113	0	100.0	100.0
Rifampin	0	191	118	0	100.0	100.0
Ethambutol	34	80	155	40	70.2	79.5
Streptomycin	26	140	80	63	84.3	55.9
Ofloxacin/levofloxacin/capreomycin	13	31	263	2	70.4	99.2
Amikacin/kanamycin	0	6	303	0	100.0	100.0
Para-aminosalicylic acid	15	0	294	0	NA	100.0
Ethionamide	4	28	274	3	87.5	98.9
D-cycloserine	0	0	309	0	NA	100.0

*NA, not applicable.
†Whole-genome sequencing–based prediction.

isoniazid is assumed when rifampin resistance is detected. This approach captures a large portion of drug-resistant TB cases during diagnosis. However, for a few case-patients, which includes patients who have isoniazid resistance without concurrent rifampin resistance (14% in this study and 9.4% in the recently reported multicountry study [*19*]), treatment with a first-line regimen can contribute to the emergence of further drug resistance.

We previously reported that a patient with undiagnosed isoniazid resistance without concurrent rifampin resistance received a first-line treatment regimen that resulted in development of MDR TB (*20*). This finding highlights the limitations and real-world consequences of basing treatment decisions solely on results of the GeneXpert MTB/RIF system in a high-burden setting, where hundreds of cases are reported daily. This limitation is a serious impediment to con-

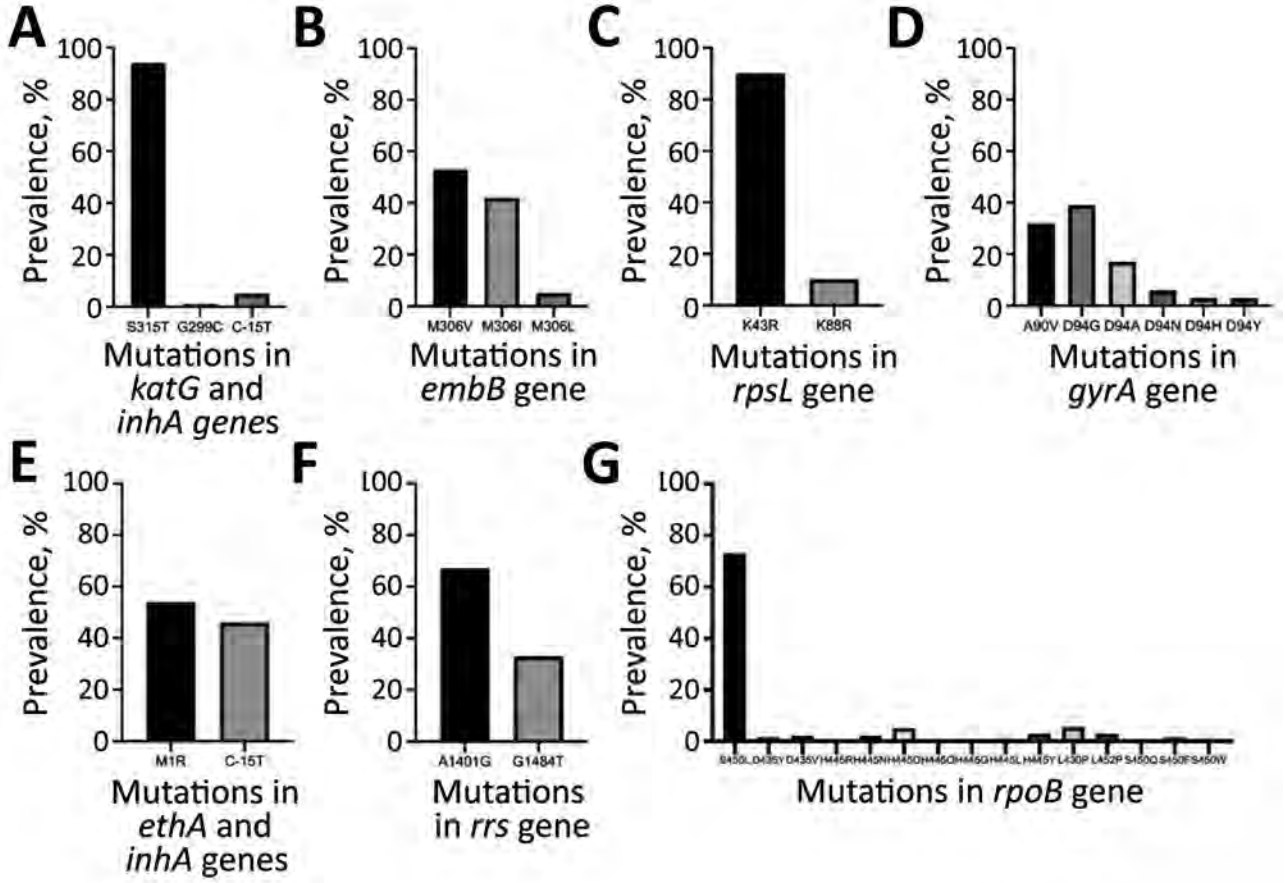

Figure 2. Prevalence of resistance-conferring mutations in genes of phenotypically resistant isolates of *Mycobacterium tuberculosis* strains, Myanmar. A) *katG* and *inhA*; B) *embB*; C) *rpsL*; D) *gyrA*; E) *ethA* and *inhA*; F) *rrs*; G) *rpoB*.

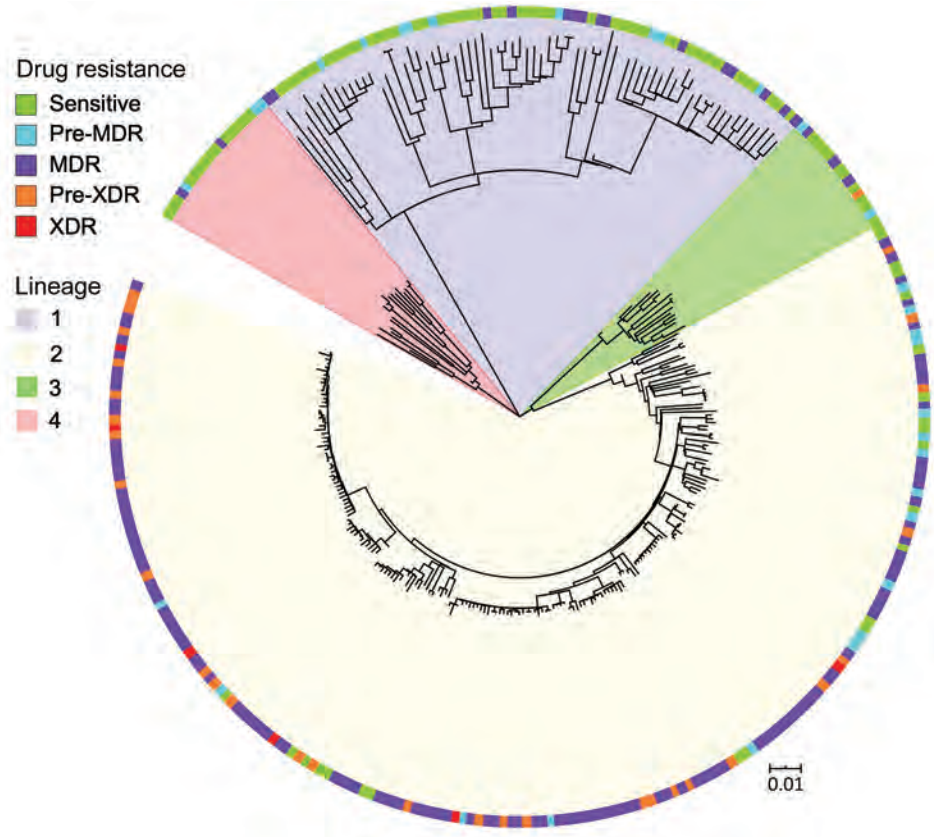

Figure 3. Maximum-likelihood tree based on whole-genome analysis of 309 *Mycobacterium tuberculosis* strains from Myanmar. Lineages and drug resistance status of isolates are shown. MDR indicates multidrug-resistant to 2 first-line drugs (isoniazid and rifampin); pre-MDR, resistant to 1 of 2 first-line drugs (isoniazid or rifampicin); pre-XDR, resistant to fluoroquinolones or injectable drugs in addition to MDR; XDR, resistant to fluoroquinolones and injectable drugs, in addition to MDR. Scale bar indicates nucleotide substitutions per site. MDR, multidrug resistant; XDR, extensively drug resistant.

trolling the spread of more extensive drug resistance (*21*). For example, although Xpert MTB/RIF can correctly diagnose RR MDR cases, it cannot detect pre-XDR and XDR cases. As identified in this study, 20% of rifampin-resistant cases identified by GeneXpert were pre-XDR (17%) and XDR (3%) cases, suggesting that ≈1 of 5 patients received limited treatment on the basis of treatment guidelines at the time of the study.

Most case-patients (including pre-XDR and XDR patients) in this study had drug-resistant isolates that were not closely related (genomically unlinked), which is suggestive of independent emergence of drug resistance because of limited diagnosis or treatment, as well as patient noncompliance. This finding is in contrast to previous studies from other high burden settings, such as China and South Africa, which showed a high proportion of drug-resistant cases that were genomically linked, suggesting community transmission (*15*,*21*–*23*).

Although it is possible that we simply did not have a high enough sampling fraction of all drug-resistant cases in the population under study, a high number of unclustered drug-resistant cases could be caused by differences in population density; the North, East, and West sections of Yangoon are in an urban industrial setting. These districts have a considerable factory-based workforce and thus draw in highly mobile migrant populations (internal migration), including members from neighboring states and regions, for employment (*24*). This finding enables a continuous flow of persons from outside Yangon, which could be independently introducing infections into the region. In addition, their status as migrants means they might have limited access to healthcare services, which is a barrier to rapid diagnosis and appropriate treatment for TB, underscoring the effect of migration on the TB burden in cities in Myanmar, particularly Yangon (*20*,*25*).

In addition to internal migration, cross-border migration has occurred in recent years, such as ≈6 million persons from fellow Greater Mekong Subregion (GMS) countries Cambodia, Laos, Thailand, and Vietnam. Therefore, the Myanmar NTP is collaborating with nongovernmental organizations and NTPs from other GMS countries to reduce the TB burden among Myanmar migrants. Further WGS studies outside Yangon and along these GMS borders are required to provide an insight into the transmission patterns of MDR TB in migrants. Coupling this collaboration with TB-related health education and

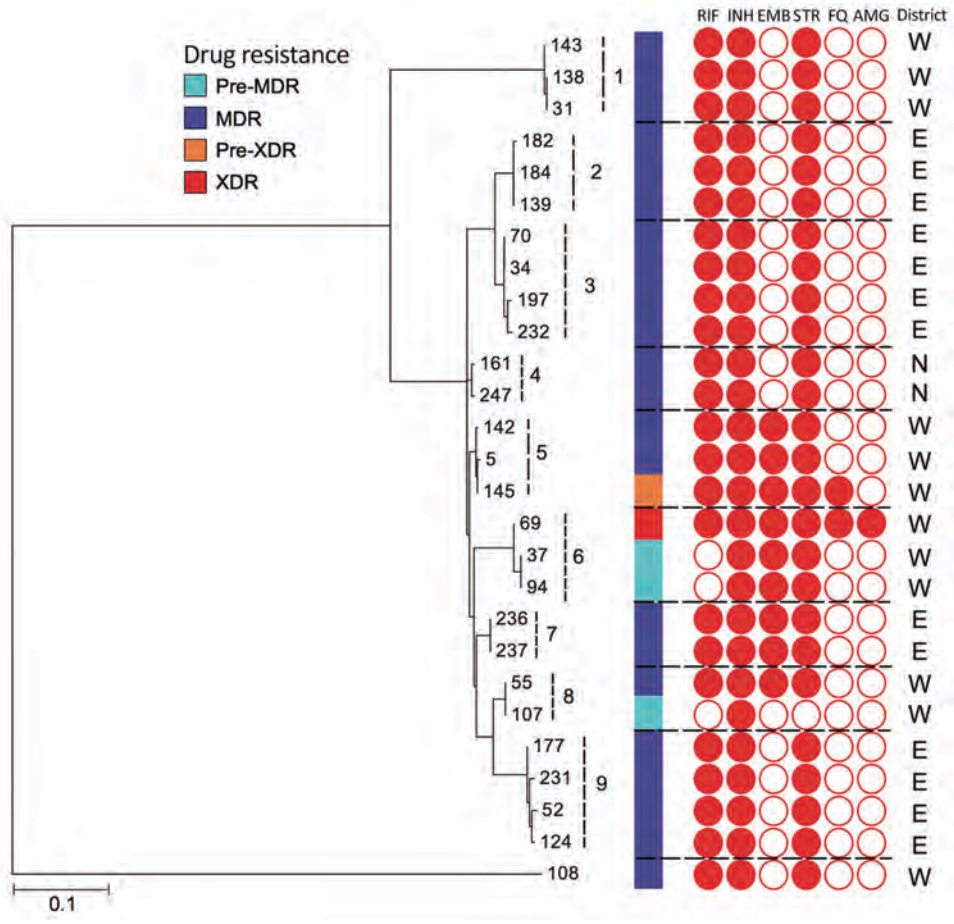

Figure 4. Maximum-likelihood tree of *Mycobacterium tuberculosis* strains, Myanmar, within 9 clusters and their drug resistance profiles. Dotted lines indicate boundaries of individual clusters. An outgroup (#108) differs by >100 single-nucleotide polymorphisms from the strains within 9 clusters. N, E, and W indicate the North, East, and West Districts of Yangon, respectively. MDR, resistant to 2 first-line drugs (isoniazid and rifampin); pre-MDR, resistant to 1 of 2 first-line drugs (isoniazid or rifampicin); pre-XDR, resistant to fluoroquinolones or injectable drugs in addition to MDR; XDR, resistant to fluoroquinolones and injectable drugs, in addition to MDR. AMG, aminoglycosides; ETH, ethambutol; FQ, fluoroquinolones; INH, isoniazid; RIF, rifampin; STR, streptomycin. Scale bar indicates nucleotide substitutions per site.

increase access to care could ultimately reduce the TB burden among migrants.

Further studies are also required to clarify the limitations and roles of both public and private healthcare providers in current treatment pathways for TB in Yangon, which might be contributing to the high rates of MDR TB. In our study, WGS showed a chain of infection, leading to the progression of pre-MDR cases toward XDR and subsequent transmission events, highlighting the need for effective diagnosis. This finding has implications for public health policies and also shows the need for local data to drive effective intervention.

Our study has major implications for clinical practice in Myanmar. First, effective treatment for MDR TB cases requires identification of the high proportion of pre-XDR and XDR TB, which cannot be achieved by current Xpert MTB/RIF testing (*27*,*28*). The drug resistance–conferring mutations reported in this study can be detected by first-line and second-line LPA, such as GenoType MTBDRplus and MTBDR*sl* (Hain Lifescience GmbH, https://www.hain-lifescience.de), or the recently launched Xpert MTB/XDR (*28*,*29*). These platforms can provide clinicians with an expanded drug-susceptibility report without the need for culturing and WGS. Recently, the Myanmar National Tuberculosis Programme diagnostic algorithm has been updated to extend first-line LPA for patients with a history of previous treatment. Second, several new or repurposed drugs (i.e., bedaquiline, delamanid linezolid, and pretomanid) are drugs already available in Myanmar. The apparent absence of preexisting mutations that confer resistance to these drugs justifies their introduction into treatment regimens for drug-resistant TB in Myanmar, as per WHO recommendations (*30*–*32*).

Our study has limitations that could lead to overestimation and underestimation of the true magnitude of the MDR epidemic and might not reflect the national situation. First, a large cohort of MDR TB, pre-XDR TB, and XDR TB cases was identified. The study region in Yangon is known to be a high-burden setting compared with other regions of Myanmar, accounting for ≈50% of all national cases (*26*). The 3 diagnostic centers in this study are also the major drug-resistant TB treatment centers in Yangon. Therefore,

it is likely that the landscape of infections is not representative of all Myanmar. Another limitation is that the study timeframe and size make it unlikely that we captured a full spectrum of MDR TB strains in the population and, as noted earlier, we might have missed identification of some transmission links, thus overestimating the proportion of resistant isolates that are independent.

Our study has major implications for clinical practice in Myanmar. First, effective treatment for MDR TB cases requires identification of the high proportion of pre-XDR and XDR TB, which cannot be achieved by current Xpert MTB/RIF testing (*27*,*28*). The drug resistance–conferring mutations reported in this study can be detected by first-line and second-line LPA, such as GenoType MTBDRplus and MTBDR*sl* (Hain Lifescience GmbH, https://www.hain-lifescience.de), or the recently launched Xpert MTB/XDR (*28*,*29*). These platforms can provide clinicians with an expanded drug-susceptibility report without the need for culturing and WGS. Recently, the Myanmar National Tuberculosis Programme diagnostic algorithm has been updated to extend first-line LPA for patients with a history of previous treatment. Second, several new or repurposed drugs (i.e., bedaquiline, delamanid linezolid, and pretomanid) are drugs already available in Myanmar. The apparent absence of preexisting mutations that confer resistance to these drugs justifies their introduction into treatment regimens for drug-resistant TB in Myanmar, as per WHO recommendations (*30*–*32*).

Our study is useful for public health officials in designing interventions for an evidence-based approach for early detection of cases (active case finding) with optimized diagnosis and treatment. Introducing additional diagnostic methods, such as routine LPA or Xpert MTB/XDR in tandem with Xpert MTB/RIF, and treatment regimens with new oral drugs would further assist in controlling and containing MDR TB in Myanmar. In addition, this study underscores the need for local data, rather than being based on general information from similar studies that have different healthcare delivery systems to drive public health policies for effective intervention.

Acknowledgments

We thank Aung San, Latha, North Oakkalapa, and the National Tuberculosis Reference Laboratory in Yangon for providing assistance.

This study was supported by the New Zealand Health Research Council through the e-ASIA funding scheme. H.L.A. is a Health Research Council Sir Charles Hercus Health Research Fellow.

About the Author

Dr. Htin Lin Aung is a molecular biologist in the Department of Microbiology and Immunology, University of Otago, Dunedin, New Zealand. His major research interests are antimicrobial resistance and health inequalities.

References

1. World Health Organization. Global tuberculosis report 2020 [cited 2020 Oct 15]. https://www.who.int/tb/publications/global_report/en
2. World Health Organization. Third nationwide drug-resistance survey 2012–2013; 2014 [cited 2021 Jun16]. https://www.who.int/docs/default-source/searo/tuberculosis/rglc-report--myanmar--2018.pdf
3. Meehan CJ, Goig GA, Kohl TA, Verboven L, Dippenaar A, Ezewudo M, et al. Whole genome sequencing of *Mycobacterium tuberculosis*: current standards and open issues. Nat Rev Microbiol. 2019;17:533–45. https://doi.org/10.1038/s41579-019-0214-5
4. Pankhurst LJ, Del Ojo Elias C, Votintseva AA, Walker TM, Cole K, Davies J, et al.; COMPASS-TB Study Group. Rapid, comprehensive, and affordable mycobacterial diagnosis with whole-genome sequencing: a prospective study. Lancet Respir Med. 2016;4:49–58. https://doi.org/10.1016/S2213-2600(15)00466-X
5. Walker TM, Kohl TA, Omar SV, Hedge J, Del Ojo Elias C, Bradley P, et al.; Modernizing Medical Microbiology (MMM) Informatics Group. Whole-genome sequencing for prediction of *Mycobacterium tuberculosis* drug susceptibility and resistance: a retrospective cohort study. Lancet Infect Dis. 2015;15:1193–202. https://doi.org/10.1016/S1473-3099(15)00062-6
6. Walker TM, Ip CL, Harrell RH, Evans JT, Kapatai G, Dedicoat MJ, et al. Whole-genome sequencing to delineate *Mycobacterium tuberculosis* outbreaks: a retrospective observational study. Lancet Infect Dis. 2013;13:137–46. https://doi.org/10.1016/S1473-3099(12)70277-3
7. Coll F, McNerney R, Preston MD, Guerra-Assunção JA, Warry A, Hill-Cawthorne G, et al. Rapid determination of anti-tuberculosis drug resistance from whole-genome sequences. Genome Med. 2015;7:51. https://doi.org/10.1186/s13073-015-0164-0
8. Phelan JE, O'Sullivan DM, Machado D, Ramos J, Oppong YE, Campino S, et al. Integrating informatics tools and portable sequencing technology for rapid detection of resistance to anti-tuberculous drugs. Genome Med. 2019;11:41. https://doi.org/10.1186/s13073-019-0650-x
9. Aung HL, Tun T, Moradigaravand D, Köser CU, Nyunt WW, Aung ST, et al. Whole-genome sequencing of multidrug-resistant *Mycobacterium tuberculosis* isolates from Myanmar. J Glob Antimicrob Resist. 2016;6:113–7. https://doi.org/10.1016/j.jgar.2016.04.008
10. Aung HL, Devine TJ, Mulholland CV, Arcus VL, Cook GM. Tackling tuberculosis in the indigenous people of New Zealand. Lancet Public Health. 2019;4:e496. https://doi.org/10.1016/S2468-2667(19)30180-X
11. Li H, Handsaker B, Wysoker A, Fennell T, Ruan J, Homer N, et al.; 1000 Genome Project Data Processing Subgroup. The sequence alignment/map format and SAMtools. Bioinformatics. 2009;25:2078–9. https://doi.org/10.1093/bioinformatics/btp352
12. Stamatakis A, Ludwig T, Meier H. RAxML-III: a fast program for maximum likelihood-based inference of large

phylogenetic trees. Bioinformatics. 2005;21:456–63. https://doi.org/10.1093/bioinformatics/bti191
13. Letunic I, Bork P. Interactive Tree Of Life (iTOL) v4: recent updates and new developments. Nucleic Acids Res. 2019;47(W1):W256–9. https://doi.org/10.1093/nar/gkz239
14. Holt KE, McAdam P, Thai PV, Thuong NT, Ha DT, Lan NN, et al. Frequent transmission of the *Mycobacterium tuberculosis* Beijing lineage and positive selection for the EsxW Beijing variant in Vietnam. Nat Genet. 2018;50:849–56. https://doi.org/10.1038/s41588-018-0117-9
15. Yang C, Luo T, Shen X, Wu J, Gan M, Xu P, et al. Transmission of multidrug-resistant *Mycobacterium tuberculosis* in Shanghai, China: a retrospective observational study using whole-genome sequencing and epidemiological investigation. Lancet Infect Dis. 2017;17:275–84. https://doi.org/10.1016/S1473-3099(16)30418-2
16. Merker M, Blin C, Mona S, Duforet-Frebourg N, Lecher S, Willery E, et al. Evolutionary history and global spread of the *Mycobacterium tuberculosis* Beijing lineage. Nat Genet. 2015;47:242–9. https://doi.org/10.1038/ng.3195
17. Zhang H, Li D, Zhao L, Fleming J, Lin N, Wang T, et al. Genome sequencing of 161 *Mycobacterium tuberculosis* isolates from China identifies genes and intergenic regions associated with drug resistance. Nat Genet. 2013;45:1255–60. https://doi.org/10.1038/ng.2735
18. CRyPTIC Consortium and the 100,000 Genomes Project; Wang T, Allix-Bégeuc C, Arandjelovic I, Bi L, Beckert P, Bonnet M, et al. Prediction of susceptibility to first-line tuberculosis drugs by DNA sequencing. N Engl J Med. 2018;379:1403–15. https://pubmed.ncbi.nlm,nih.gov/30280646
19. Dean AS, Zignol M, Cabibbe AM, Falzon D, Glaziou P, Cirillo DM, et al. Prevalence and genetic profiles of isoniazid resistance in tuberculosis patients: a multicountry analysis of cross-sectional data. PLoS Med. 2020;17:e1003008. https://doi.org/10.1371/journal.pmed.10030ic I, 08
20. Aung HL, Nyunt WW, Fong Y, Russell B, Cook GM, Aung ST. Acquired resistance to antituberculosis drugs. Emerg Infect Dis. 2018;24:2134. https://doi.org/10.3201/eid2411.180465
21. Yang C, Lu L, Warren JL, Wu J, Jiang Q, Zuo T, et al. Internal migration and transmission dynamics of tuberculosis in Shanghai, China: an epidemiological, spatial, genomic analysis. Lancet Infect Dis. 2018;18:788–95. https://doi.org/10.1016/S1473-3099(18)30218-4
22. Auld SC, Shah NS, Mathema B, Brown TS, Ismail N, Omar SV, et al. XDR tuberculosis in South Africa: genomic evidence supporting transmission in communities. Eur Respir J. 2018;52:1800246. https://doi.org/10.1183/13993003.00246-2018
23. Nelson KN, Shah NS, Mathema B, Ismail N, Brust JC, Brown TS, et al. Spatial patterns of extensively drug-resistant tuberculosis transmission in KwaZulu-Natal, South Africa. J Infect Dis. 2018;218:1964–73. https://doi.org/10.1093/infdis/jiy394
24. Myanmar Information Management Unit. The 2014 Myanmar Population and Housing Census [cited 2020 Jan 14]. https://themimu.info/census-data
25. Tun T, Nyunt WW, Latt KZ, Samaranayaka A, Crump JA, Thinn KK, et al. Drug-resistant tuberculosis among previously treated patients in Yangon, Myanmar. Int J Mycobacteriol. 2016;5:366–7. https://doi.org/10.1016/j.ijmyco.2016.06.004
26. National Tuberculosis Programme Myanmar. Annual tuberculosis report 2016 [cited 2021 Jul 13]. https://ghdx.healthdata.org/ record/myanmar-national-tuberculosis-programme-annual-report-20
27. Makhado NA, Matabane E, Faccin M, Pinçon C, Jouet A, Boutachkourt F, et al. Outbreak of multidrug-resistant tuberculosis in South Africa undetected by WHO-endorsed commercial tests: an observational study. Lancet Infect Dis. 2018;18:1350–9. https://doi.org/10.1016/S1473-3099(18)30496-1
28. Xie YL, Chakravorty S, Armstrong DT, Hall SL, Via LE, Song T, et al. Evaluation of a rapid molecular drug-susceptibility test for tuberculosis. N Engl J Med. 2017;377:1043–54. https://doi.org/10.1056/NEJMoa1614915
29. Cepheid. New rapid molecular test for tuberculosis can simultaneously detect resistance to first- and second-line drugs [cited 2020 Jul 23]. https://www.finddx.org/wp-content/uploads/2020/07/PR_Cepheid-2020-CID-RespiratoryXpert-MTB-XDR.pdf
30. World Health Organization. WHO consolidated guidelines on drug-resistant tuberculosis treatment, 2019 [cited 2020 Feb 15]. https://www.who.int/tb/publications/2019/consolidated-guidelines-drug-resistant-TB
31. Conradie F, Diacon AH, Ngubane N, Howell P, Everitt D, Crook AM, et al.; Nix-TB Trial Team. Treatment of highly drug-resistant pulmonary tuberculosis. N Engl J Med. 2020;382:893–902. https://doi.org/10.1056/NEJMoa1901814
32. Aung HL, Nyunt WW, Fong Y, Cook GM, Aung ST. First 2 extensively drug-resistant tuberculosis cases from Myanmar treated with bedaquiline. Clin Infect Dis. 2017;65:531–2. https://doi.org/10.1093/cid/cix365

Address for correspondence: Htin Lin Aung, Department of Microbiology and Immunology, School of Biomedical Sciences, University of Otago, PO Box 56, Dunedin, New Zealand; email: htin.aung@otago.ac.nz

Encephalitis and Death in Wild Mammals at a Rehabilitation Center after Infection with Highly Pathogenic Avian Influenza A(H5N8) Virus, United Kingdom

Tobias Floyd, Ashley C. Banyard, Fabian Z.X. Lean, Alexander M.P. Byrne, Edward Fullick, Elliot Whittard, Benjamin C. Mollett, Steve Bexton, Vanessa Swinson, Michele Macrelli, Nicola S. Lewis, Scott M. Reid, Alejandro Núñez, J. Paul Duff, Rowena Hansen, Ian H. Brown

We report a disease and mortality event involving swans, seals, and a fox at a wildlife rehabilitation center in the United Kingdom during late 2020. Five swans had onset of highly pathogenic avian influenza virus infection while in captivity. Subsequently, 5 seals and a fox died (or were euthanized) after onset of clinical disease. Avian-origin influenza A virus subtype H5N8 was retrospectively determined as the cause of disease. Infection in the seals manifested as seizures, and immunohistochemical and molecular testing on postmortem samples detected a neurologic distribution of viral products. The fox died overnight after sudden onset of inappetence, and postmortem tissues revealed neurologic and respiratory distribution of viral products. Live virus was isolated from the swans, seals, and the fox, and a single genetic change was detected as a potential adaptive mutation in the mammalian-derived viral sequences. No human influenza-like illness was reported in the weeks after the event.

Author affiliations: Animal and Plant Health Agency, Weybridge, UK (T. Floyd, A.C. Banyard, F.Z.X Lean, A.M.P. Byrne, E. Whittard, B.C. Mollett, S.M. Reid, A. Núñez, R. Hansen, I.H. Brown); Animal and Plant Health Agency, Thirsk, UK (E. Fullick, V. Swinson); Royal Society for Prevention of Cruelty to Animals, East Winch, UK (S. Bexton); Animal and Plant Health Agency, Bury St Edmunds, UK (M. Macrelli); , Royal Veterinary College Department of Pathobiology and Population Sciences, North Mymms, UK (N.S. Lewis); Animal and Plant Health Agency Diseases of Wildlife Scheme, Penrith, UK (J.P. Duff)

DOI: https://doi.org/10.3201/eid2711.211225

An episode of unusual disease resulting in deaths in different species at a wildlife rehabilitation center in the United Kingdom during late 2020 led to the retrospective detection of influenza A virus subtype H5N8 of avian origin in 5 mute swans, a fox, and 3 seals. The wildlife rehabilitation center admits >6,000 animals each year. New arrivals are initially housed in a quarantine facility upon admission. Four juvenile common seals (*Phoca vitulina*), 1 juvenile gray seal (*Halichoerus grypus*), and 1 juvenile red fox (*Vulpes vulpes*) died or were euthanized over a 2-day period. The fox died suddenly after a short period of nonspecific malaise and inappetence. The seals exhibited sudden-onset neurologic signs, including seizures before death or euthanasia (Figure 1).

This mortality event occurred ≈1 week after the deaths or euthanasia of 5 mute swans (*Cygnus olor*) held in isolation at the center because of acute-onset malaise and terminal seizures. The 5 swans were submitted for examination and testing under the Avian Influenza Wild Bird Surveillance Scheme (undertaken by the United Kingdom's Animal and Plant Health Agency) (*1*), and they tested positive for highly pathogenic avian influenza A(H5N8) virus.

The unusual spatiotemporal cluster of unexplained death and neurologic disease in multiple avian and nonavian species warranted further investigation. Influenza of avian origin was not suspected in the fox and seals, and none of the other captive birds at the center showed any clinical signs of disease. The linkage between the mortality event in the swans and that observed in the fox and seals was not

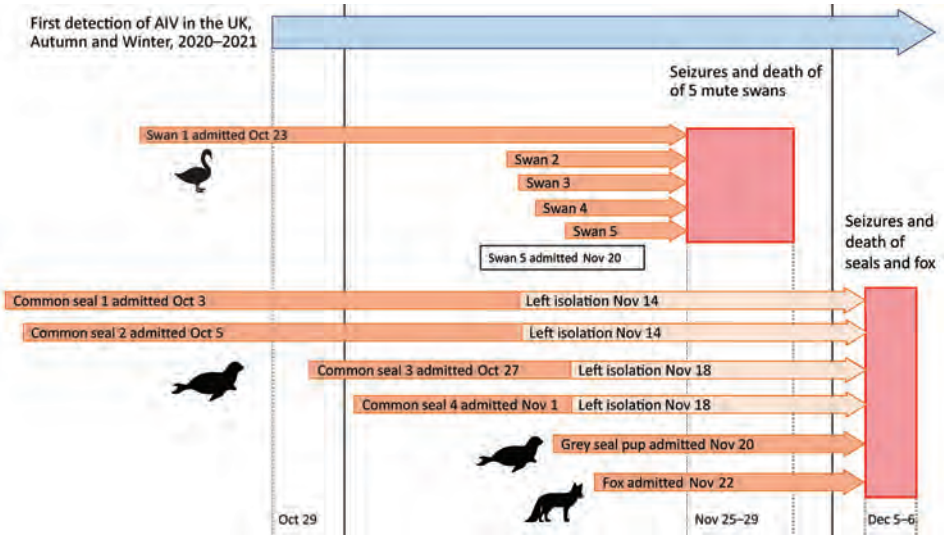

Figure 1. Timeline of the disease event, in which encephalitis and death in wild mammals at a rehabilitation center occurred after systemic infection with highly pathogenic avian influenza A subtype H5N8, United Kingdom. AIV, avian influenza virus; UK, United Kingdom.

made until many weeks after the event, when the fox and seal tissues were assessed to attempt to define an etiologic diagnosis.

Methods

Postmortem Examination, Tissue Sampling, and Histopathologic Investigation

We collected a thorough clinical history from the rehabilitation center. We subjected the carcasses of 3 of the 5 swans, the fox, and 3 of the 5 seals (1 gray seal and 2 common seals) full postmortem examination (PME). Two swans were submitted frozen and did not undergo PME, but we took oral and cloacal swab samples from these carcasses for virologic testing. We examined plain swab samples from the oropharynx and cloaca of each of the swans, and similarly from the nasal cavity and rectum of each of the 3 seals, for preliminary influenza virologic testing. After receipt of the avian influenza virus results, we sampled the 3 freshest seal carcasses because they were more likely to yield meaningful results and have suitable samples for histopathologic examination. We took tissue samples of brain, liver, kidney, spleen, lymph nodes, and lung from the seals and the fox and stored them at −80°C until required.

For histologic examination, we took samples of heart, lung, liver, spleen, and brain tissues from the swans, fox, and seals, as well as lymph nodes of the mammalian species, and fixed them in 10% neutral buffered formalin before processing for hematoxylin and eosin staining and immunohistochemical (IHC) examination. We performed IHC examination by using anti–influenza A nucleoprotein primary antibody (Statens Serum Institute, https://en.ssi.dk), as previously described (2), and anti–canine distemper virus nucleoprotein mouse monoclonal primary antibody (Bio-Rad, https://www.bio-rad.com) in selected fox tissues.

Virologic Investigation

We assessed swabs taken from the swans and seals and tissue samples taken from the seals and fox for influenza A nucleic acid by using a screening real-time reverse transcription PCR (rRT-PCR) assay (*3*), followed by an H5 subtype–specific rRT-PCR assay (*4*–*6*). Where the subtype-specific rRT-PCR assay detected positive samples, we determined the hemagglutinin cleavage-site sequence (*7*).

We performed virus isolation on PCR-positive samples from the swans, seals, and fox by using specified pathogen-free embryonated fowls' eggs (*8*,*9*). We used the 3 viral isolates recovered to generate whole-genome sequence (WGS) data by using a MiSeq platform (Illumina, https://www.illumina.com) (*10*). For comparative genetic analysis, we downloaded recent H5 2.3.4.4b virus hemagglutinin sequences from the GISAID EpiFlu database (https://platform.gisaid.org). We deposited sequences in the GISAID database (accession nos. EPI_ISL_1123360, EPI_ISL_2081527, and EPI_ISL_2081528).

Differential diagnosis for the fox samples included molecular testing for rabies virus and canine distemper virus (*11*,*12*). We assessed samples from all 3 seals for *Leptospira* infection (*13*). We subjected RNA obtained from the fox samples to sequence-independent single-primer amplification (*14*) to enable sequence generation. We then used the sequence data obtained from these samples to exclude other viral agents by removing reads that aligned with the *Vulpes*

vulpes genome (*15*,*16*) and then undertaking de novo assembly to produce contiguous sequences by using SPAdes (*17*). We then screened these sequences by using custom viral databases (*18*) against the *Bornaviridae*, *Circoviridae*, *Flaviviridae*, *Herpesviridae*, *Paramyxoviridae*, *Parvoviridae*, *Pheuiviridae*, and *Rhabdoviridae* viral families.

Results

Clinical Setting

The swans, gray seal, and fox were housed within the quarantine unit of the center, a suite of 17 individual cubicles accessed by a central corridor (Appendix Figure 1, https://wwwnc.cdc.gov/EID/article/27/11/21-1225-App1.pdf). This facility was designed to minimize transmission of microorganisms among residents; animals in separate cubicles had no direct contact. Basic biosecurity practices were in place, such as decontamination steps between cubicles and staff using respiratory protective equipment (e.g., N95 masks) and dedicated personal protective equipment for each cubicle.

The 5 juvenile mute swans were rescued from different locations and brought to the center for treatment during October 23–November 20, 2020 (Figure 1). These birds were admitted for various reasons, including trauma and being underweight and weak. Infection with avian influenza viruses was not suspected at admission. The juvenile mute swans were housed indoors within the center's isolation unit, mixed in groups of up to 4 with other rescued adult mute swans (Appendix Figure 1). Each of the juvenile swans had been recovering uneventfully until the sudden onset of lethargy and death or euthanasia during November 25–29 (Figure 1). Clinical signs were not observed in the remaining adult mute swans (n = 6) within the isolation unit. The isolation unit also contained 30 mallards (*Anas platyrhynchos*) housed across 3 rooms in groups of 10. No clinical disease or deaths were recorded in these birds.

The 4 common seals were estimated to be 5–6 months of age and arrived individually at the facility 1–2 months before the disease episode (Figure 1), admitted for various reasons, including poor body condition, superficial bite wounds, and lungworm. In each case, the animals had been responding well to treatment and supportive care up until the sudden onset of seizures and subsequent death or euthanasia. All 4 seals that died had been in the isolation unit (cubicles 6, 8, and 11) (Appendix Figure 1) at the time the swans (cubicles 15 and 17) were affected (Appendix Figure 1) but had subsequently been moved into another area of the facility. The affected seals had previously had close contact with other common seals in other areas of the facility; none of those animals became ill.

The gray seal was a 2-week-old pup admitted for care after maternal abandonment 2 weeks earlier (Figure 1). It was housed in the isolation unit in a cubicle opposite 1 of the swans (cubicle 1) (Appendix Figure 1). The seal was in good bodily condition and progressing well until the sudden onset of fever, facial twitching, and stupor that led to euthanasia on welfare grounds.

The fox had been in the isolation unit of the center for 2 weeks (Figure 1) in cubicle 10 (Appendix Figure 1). It had been brought to the facility with large areas of alopecia and skin crusts over the body and limbs, consistent with mange. It had been receiving treatment and was reported to be progressing well until the sudden onset of malaise and inappetence and was found dead the following morning.

Pathologic Investigation

The body condition of the 3 swans examined ranged from good to poor. Gross findings among the carcasses included petechiae in the liver and epicardium in 1 bird and opacity of the air sacs in another. Microscopic examination of tissues from 1 bird revealed multifocal, necrotizing, nonsuppurative myocarditis, hepatitis, splenitis, nephritis, and encephalitis, along with intralesional presence of influenza A virus antigen, observed during IHC examination.

The body condition of the 3 examined seals was judged to be fair. Gross examination of 2 common seals revealed generalized lymphadenomegaly and multiple pale foci in the lungs. One common seal also showed congested meninges. The gray seal pup showed generalized lymphadenomegaly but no other gross changes. Microscopic examination of the seal tissues revealed mild, eosinophilic, interstitial pneumonia in the 2 common seals, consistent with lungworm infection, and severe, necrotizing, nonsuppurative polioencephalitis in the 2 common seals and the gray seal. The lymph node sections showed nonspecific reactive hyperplasia, accounting for the gross enlargement of these organs. IHC examination for influenza A virus revealed multifocal immunolabelling in the neurons within the gray matter of the brain in all 3 seals, in close association with the inflammatory lesions (Figure 2, panel A), although virus antigen was absent in the lung, liver, kidney, and lymph node tissues of the seals.

The body condition of the fox was judged to be poor. The animal was visibly underweight, and

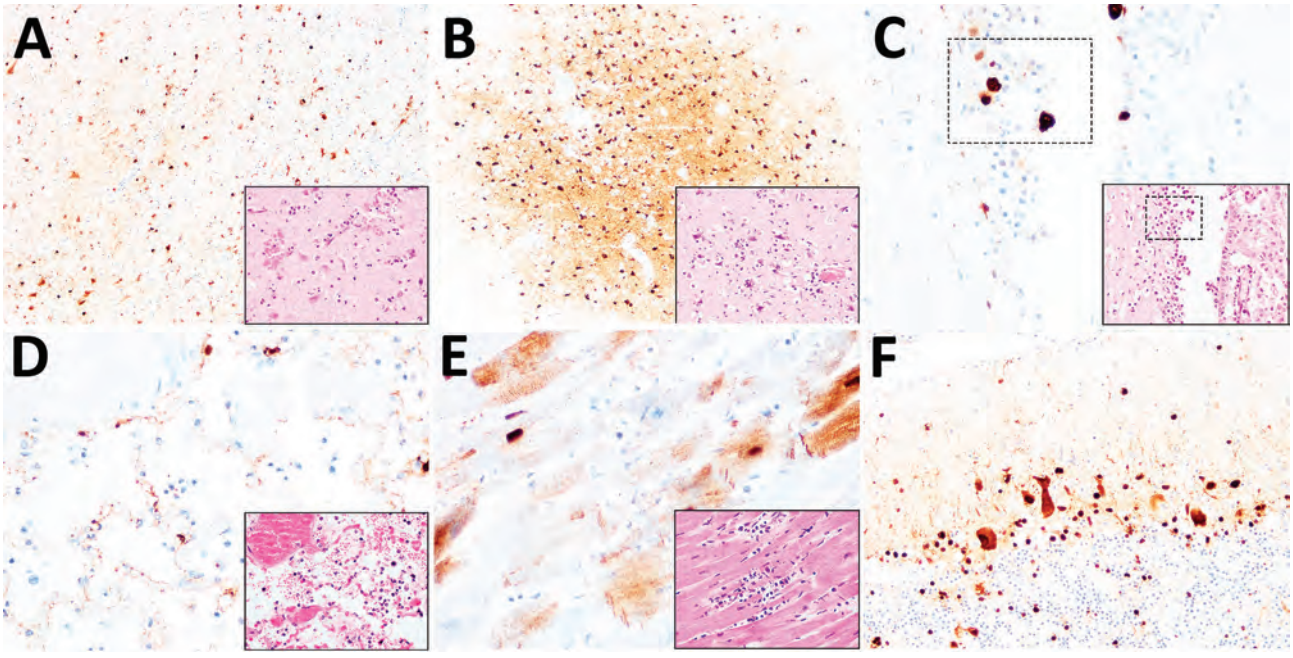

Figure 2. Histopathologic and immunohistochemical examination of the gray seal (*Halichoerus grypus*), common seal (*Phoca vitulina*), and red fox (*Vulpes vulpes*) infected with highly pathogenic avian influenza A subtype H5N8, United Kingdom. Serial tissue sections were stained with hematoxylin and eosin. Immunohistochemical examination was undertaken using anti–influenza A nucleoprotein primary antibody (Statens Serum Institute, https://en.ssi.dk). Insets show histopathologic study results. A) Nonsuppurative polioencephalitis and presence of virus antigens in neurons in the cerebrum, common seal (*Phoca vitulina*). Original magnification ×10, inset ×40. B) Nonsuppurative polioencephalitis with neuronophagia and association of virus antigens, red fox. Original magnification ×10, inset ×40. C) Ependymal necrosis and the association of virus antigens, fox. Original magnification and inset ×40; area of interest also shown. D) Diffuse alveolar damage and presence of virus in type I alveolar pneumocytes, red fox. Original magnification and inset ×40. E) Cardiomyonecrosis associated with virus antigens in cardiomyocytes, red fox. Original magnification and inset ×40. F) Virus antigens in granular and molecular layer of the cerebellum, red fox. Original magnification ×20, inset ×40. Serial tissue sections were stained with hematoxylin and eosin. Immunohistochemical examination was undertaken using anti–influenza A nucleoprotein primary antibody (Statens Serum Institute, https://en.ssi.dk). Insets show histopathologic study results.

gross examination revealed large areas of alopecia and crusts affecting the skin of the body and limbs, mild splenomegaly, and generalized reddening of the lungs. Microscopic examination of the brain, lung, and heart revealed severe, acute, nonsuppurative, polioencephalitis (Figure 2, panel B) and ventriculitis (Figure 2, panel C); severe, acute, necrotizing, nonsuppurative interstitial pneumonia (Figure 2, panel D); and mild, acute, nonsuppurative myocarditis (Figure 2, panel E). Within these lesions, IHC examination confirmed the presence of influenza virus antigens among neurons in the cerebrum (Figure 2, panel B) and cerebellum (Figure 2, panel F) and in ependymal cells (Figure 2, panel C), alveolar type I pneumocytes (Figure 2, panel D), and cardiomyocytes (Figure 2, panel E). IHC examination performed on sections of brain and lung showed no canine distemper virus.

Virologic Assessment

Oropharyngeal and cloacal swabs from all 5 swans tested positive for H5N8 (Appendix Table). WGS data were generated for 1 of the swans submitted (A/mute swan/England/234135/H5N8 2020/12/01).

Nasal and rectal swab samples taken during PME of the 3 seals tested negative by PCR for influenza A virus. However, we retrospectively detected influenza A(H5N8) virus nucleic acid in the brain and lung of the gray seal and the brain of 2 common seals (Appendix Table). We performed virus isolation on pooled samples and successfully isolated virus from the pooled brain tissue of seals (A/seal/England/AVP-031141/2020 [H5N8]).

We detected influenza A virus RNA in each of the fox samples (brain, liver, kidney, spleen, and lung), and PCR subtyping determined the influenza A virus subtype as H5N8 (Appendix Table). We isolated virus and generated WGS from the fox brain tissue (A/red fox/England/AVP-M1-21-01/2020 (H5N8)). The hemagglutinin cleavage site (CS) motif from selected fox and seal samples had the amino acid sequence PLREKRRKRGLF, consistent with 99% of CSs characterized across highly pathogenic

avian influenza (HPAI) H5N8 virus sequences from the United Kingdom during autumn and winter 2020–2021. Analysis of WGS data generated from the fox, seal, and swan samples demonstrated high sequence similarity (>99.9% nucleotide identity across all gene segments). Alignment of the viral hemagglutinin (Appendix Figure 2, panel A) and neuraminidase genes (Appendix Figure 2, panel B) demonstrated that virus from the fox and seals clustered closely with the viruses detected in the swans from the same wildlife center. Comparison of WGS data from the fox, seal, and swan identified a total of 33 aa substitutions that have been associated with altered virulence reported through natural or experimental infections. Almost all substitutions have been identified in the H5N8 virus sequences generated during the 2020–2021 epizootic in avian species (Appendix Figure 2, panel C). The genomes of the fox, seal, and swan-derived viruses were homologous at the amino-acid level, with the exception of a single amino-acid substitution at position 701 in the polymerase basic protein 2 gene (D701N) that was only present in the fox and seal sequences. Analysis of WGS data obtained from the fox samples demonstrated a lack of other viral agents, including canine distemper virus.

At the time of the outbreak, the rehabilitation center fell within a government-mandated protection zone because of previously confirmed detection of HPAI virus infections in the region; consequently, moving birds off the center was restricted around the time of the disease episode. Restrictions were also applied specifically to the rehabilitation center when suspicion of notifiable disease in the swans was reported. The cases investigated in this outbreak were limited to animals held within the quarantine ward, and over the subsequent months, no further cases of unusual or unexplained clinical disease or death occurred among the mammals and birds at the center. After the disease event, but before diagnosis of H5N8 in the seals and fox, the center was visited as part of surveillance activities within the protection zone. Resident bird species were examined for evidence of clinical disease, and 38 birds (6 swans, 30 mallards, 1 pigeon, and 1 widgeon) were sampled for virologic testing by PCR. All birds tested negative. Blood was not taken for analysis.

Discussion

We determined that avian-origin influenza A(H5N8) virus was the cause of death in a red fox and the cause of seizures in a gray seal and several common seals housed at a wildlife rehabilitation center. These events occurred roughly 1 week after 5 swans housed in the same quarantine unit died from infections with HPAI H5N8 virus. Genetic and epidemiologic investigations suggest that the swans were most likely the source of infection for the fox and seals; virus transmission likely occurred by fomite transfer or aerosol spread.

The severity of disease and pathologic findings in the seals and fox was unexpected. High-mortality outbreaks of disease associated with influenza A virus have been described in common seals and were associated with virus subtypes H10N7 (*19*–*21*), H7N7 (*22*), and H3N8 (*23*). In most of these cases, infection was limited to the respiratory tract. HPAI H5N8 clade 2.3.4.4b has also been detected recently in gray seals in Europe (*24*). However, the infection of a fox represents an unusual detection of this virus in association with inflammation of the central nervous system in terrestrial mammal species.

In 2016 and 2017, H5N8 virus was detected in lung tissue of 2 gray seals that were found dead, although pathologic findings typical of influenza virus infection was not reported in either carcass (*24*). The H5N8 virus of avian origin we have described was associated with acute inflammation of the central nervous system, in the absence of substantial respiratory involvement or detection in the nasal swab specimens collected before postmortem investigation; however, viral nucleic acid was indicated in the lung of the single gray seal tested. The negative result on nasal swab specimens of the seals in this outbreak is noteworthy and may have implications for surveillance for influenza in this species.

Natural infection of terrestrial carnivores with influenza A virus subtypes, although rare, has been previously reported in species such as domestic and wild felids, mustelids, and canids (*25*–*27*). Experimental infection of red foxes was previously conducted using the HPAI H5N1 subtype by intratracheal inoculation and through feeding virus-infected bird carcasses (a proxy for the putative natural route of infection) (*27*). This experimental H5N1 infection of foxes resulted in severe inflammation in the brain, lung, and heart of foxes that were challenged intratracheally, despite the animals showing no clinical signs. From the foxes fed virus-infected carcasses, only mild inflammation was observed, and it was restricted to the lungs. The study authors (Reperant et al. [*27*]) also refer in their discussion to detection of influenza A virus in foxes found dead in the field, although no further details are provided. The histopathologic findings in the intratracheally inoculated foxes are consistent with those observed

in the natural infection of the fox at the rehabilitation center and would support a respiratory or airborne infection route.

In our study, evaluation of WGS data demonstrated that the virus in the swans, the fox, and the seals clustered together phylogenetically, and minimal genetic differences were observed. The WGS analysis did not enable us to determine the direction of infection; however, the epidemiologic findings combined with the genetic data generated strongly suggest that the swans were the source of the infection for the fox and seals. The D701N amino acid substitution in the polymerase basic 2 gene identified in both sequences derived from the mammalian species was absent from all avian sequences generated during this 2020–2021 outbreak in the United Kingdom. This substitution has previously been associated with mammalian adaptation and increased replicative fitness in mammalian cells (*28*–*32*). However, the substitution, in isolation, is not considered to be a factor that may result in increased avian-to-mammalian transmission risk, given that a combination of adaptive and compensatory changes observed in human sequences that would likely be required for efficient adaptation. Analysis of available H5 and H7 influenza sequences from human infections found that the D701N mutation had low prevalence and was therefore not a strong correlate for zoonotic infection. Excluding the D701N mutation, the remaining amino-acid changes identified in the fox, seal, and swan we have described were common to the H5N8 sequences obtained from the UK and Europe during the 2020–2021 epizootic. Therefore, the assessment of the sequences derived from mammalian species, when compared against both avian influenza A virus sequences from the 2020–2021 UK outbreak and sequences derived from proposed human infection, demonstrated no human risk for infection over and above that already considered for the avian isolate.

A question that remains is why infection with a highly pathogenic H5N8 isolate of avian influenza produced such severe clinical disease in mammal species in this event, although contributing factors are likely to be multifactorial and involve both virus and host. For example, a combination of underlying conditions, nutrition, and physiologic stress might have contributed to disease onset in these animals, in addition to factors associated with temporary housing of wild animals. Several of the seals were admitted to the center with lungworm infection, which is not uncommon in wild pinnipeds, and although the infections were severe enough to require treatment, several of the seals had been at the center for at least 1 month and were reported to be responding well to treatment. The affected gray seal had been admitted as a neonate 2 weeks previously and was likely to have been abandoned immediately after birth, probably without opportunity to suckle; therefore, an immature immune system and reduced passive immunity could have been contributory factors for disease. The fox was malnourished and had mange, a common infection that causes severe illness and potentially increases susceptibility to other infections, although immunosuppressive viral infections were excluded after negative results on PCR, WGS, and IHC examination. No other pathologies or disease agents were identified in the seals and fox during postmortem examination. Malnutrition is also common in young seals admitted to rehabilitation centers and was evident in the history provided for 2 of the common seals (*33*). However, a standard commercial multivitamin–multimineral supplement is given to all seals after admission and is discontinued once they are self-feeding. Furthermore, the fish used at the center is blast-frozen at sea and therefore the risk for thiaminase activity is considered low; as such, nutrition is unlikely to have played a role in predisposing the seals to infection.

The retrospective detection of influenza A virus of avian origin in these mammalian species meant that evidence of human exposure was not evaluated. However, the disease event occurred during a nationwide coronavirus disease lockdown in the United Kingdom, during which the population was required to self-monitor for signs of coronavirus disease and be tested whenever clinical disease consistent with an influenza-like illness occurred. No staff reported any illness of this type during the 6-week period after the disease event, and so we can safely conclude that staff were not infected with severe acute respiratory syndrome coronavirus 2. Use of respiratory protective equipment at the quarantine facility also would have reduced the risk for infection.

In conclusion, we determined that avian-origin influenza A(H5N8) virus caused severe disease and death in juvenile seals and a fox held in a wildlife rehabilitation center, in addition to swans that had also succumbed to the virus. All evidence suggests that the swans were the most likely source of infection for the fox and seals. The location of affected animals within the quarantine facility (Appendix Figure 1) suggests either aerosol or fomite spread as the likely cause of dissemination of infectious virus between cubicles. Although the quarantine facility is designed to limit spread of infectious microorganisms through the use of good basic hygiene practices, it is not a

biosecure facility designed to handle Biosafety Level 3 pathogens; as such, highly transmissible agents such as avian influenza may well spread even with some infection prevention measures in place. Because influenza infection was not suspected at the time of the event, biosecurity practices at the center may have been less effective at preventing spread compared with those implemented at a heightened level of biosecurity, which would likely have been in place had there been an awareness of the presence of influenza infection. Determining the cause of disease in the seals and fox retrospectively was entirely reliant on collaboration between field veterinary services, pathologists, and virologists, and this case highlights the importance of wildlife disease surveillance. Although genetic analyses indicated no increased risk for human infection with the H5N8 viruses in this outbreak, the investigation shows how these viruses may have unexpected and severe health risks for mammalian species. Such spillover disease events in atypical host species constitute additional factors for veterinary authorities to consider during disease outbreaks and highlight the importance of wildlife disease surveillance that uses interdisciplinary and collaborative approaches.

Acknowledgments

We thank the scientific and support staff of the Pathology and Virology Departments of the Animal and Plant Health Agency (APHA) Weybridge and the Surveillance and Laboratory Services Department of the APHA Veterinary Investigation Centres. All authors acknowledge the originating and submitting laboratories for contributing sequences to the GISAID EpiFlu database (https://platform.gisaid.org), on which this research is based.

A.C.B., A.M.P.B., E.W., B.C.M., S.M.R., R.H., and I.B. were funded in part by the UK Department for the Environment, Food, and Rural Affairs and the devolved governments of Scotland and Wales (grant nos. SE2213, SV3400, and SV3006, respectively). A.C.B . and I.B were also part funded by the European Union's Horizon 2020 research and innovation programme "DELTA-FLU: Dynamics of avian influenza in a changing world" under grant agreement No 727922. The APHA Diseases of Wildlife Scheme is funded by the UK Department for the Environment, Food, and Rural Affairs and the devolved governments of Scotland and Wales (grant no. ED1600).

About the Author

Mr. Floyd is a veterinary pathologist working for the Animal and Plant Health Agency, UK. His main area of interest is pathology and surveillance for diseases of livestock.

References

1. European Commission. Decision of 25 June 2010 on the implementation by Member States of surveillance programmes for avian influenza in poultry and wild birds (2010/367/EU). Official Journal of the European Union; 2010. p. L 166/22 [cited 2021 Feb 14]. https://eur-lex.europa.eu/legal-content/EN/TXT/?uri=CELEX%3A32010D0367
2. Núñez A, Brookes SM, Reid SM, Garcia-Rueda C, Hicks DJ, Seekings JM, et al. Highly pathogenic avian influenza H5N8 clade 2.3.4.4 virus: equivocal pathogenicity and implications for surveillance following natural infection in breeder ducks in the United Kingdom. Transbound Emerg Dis. 2016;63:5–9. https://doi.org/10.1111/tbed.12442
3. Nagy A, Vostinakova V, Pirchanova Z, Cernikova L, Dirbakova Z, Mojzis M, et al. Development and evaluation of a one-step real-time RT-PCR assay for universal detection of influenza A viruses from avian and mammal species. Arch Virol. 2010;155:665–73. https://doi.org/10.1007/s00705-010-0636-x
4. Slomka MJ, Pavlidis T, Coward VJ, Voermans J, Koch G, Hanna A, et al. Validated RealTime reverse transcriptase PCR methods for the diagnosis and pathotyping of Eurasian H7 avian influenza viruses. Influenza Other Respir Viruses. 2009;3:151–64. https://doi.org/10.1111/j.1750-2659.2009.00083.x
5. Slomka MJ, Pavlidis T, Banks J, Shell W, McNally A, Essen S, et al. Validated H5 Eurasian real-time reverse transcriptase-polymerase chain reaction and its application in H5N1 outbreaks in 2005–2006. Avian Dis. 2007;51(Suppl):373–7. https://doi.org/10.1637/7664-060906R1.1
6. James J, Slomka MJ, Reid SM, Thomas SS, Mahmood S, Alexander MP, Byrne, et al. Proceedings paper: Avian Diseases 10th AI Symposium issue development and application of real-time PCR assays for specific detection of contemporary avian influenza virus subtypes N5, N6, N7, N8, and N9. Avian Dis. 2019;63(sp1):209–18.
7. Slomka MJ, To TL, Tong HH, Coward VJ, Hanna A, Shell W, et al. Challenges for accurate and prompt molecular diagnosis of clades of highly pathogenic avian influenza H5N1 viruses emerging in Vietnam. Avian Pathol. 2012;41:177–93. https://doi.org/10.1080/03079457.2012.656578
8. European Commission. European Commission decision 2006/437/EC of 4 August 2006 approving diagnostic manual for avian influenza as provided for in council directive 2005/94/EC. Official Journal of the European Union; 2006;237:1–27 [cited 2021 Feb 21]. https://eur-lex.europa.eu/legal-content/EN/TXT/?uri=celex%3A32006D0437
9. World Organisation for Animal Health (OIE). Avian influenza (including infection with high pathogenicity avian influenza viruses). 2019 [cited 2021 Feb 14]. https://www.oie.int/fileadmin/Home/eng/Health_standards/tahm/3.03.04_AI.pdf
10. Seekings AH, Warren CJ, Thomas SS, Mahmood S, James J, Byrne AMP, et al. Highly pathogenic avian influenza virus H5N6 (clade 2.3.4.4b) has a preferable host tropism for waterfowl reflected in its inefficient transmission to terrestrial poultry. Virology. 2021;559:74–85. https://doi.org/10.1016/j.virol.2021.03.010
11. Marston DA, Jennings DL, MacLaren NC, Dorey-Robinson D, Fooks AR, Banyard AC, et al. Pan-lyssavirus real time RT-PCR for rabies diagnosis. J Vis Exp. 2019;149. https://doi.org/10.3791/59709
12. Gordon CH, Banyard AC, Hussein A, Laurenson MK, Malcolm JR, Marino J, et al. Canine distemper in endangered Ethiopian wolves. Emerg Infect Dis. 2015;21:824–32. https://doi.org/10.3201/eid2105.141920

13. Fearnley C, Wakeley PR, Gallego-Beltran J, Dalley C, Williamson S, Gaudie C, et al. The development of a real-time PCR to detect pathogenic *Leptospira* species in kidney tissue. Res Vet Sci. 2008;85:8–16. https://doi.org/10.1016/j.rvsc.2007.09.005
14. Lewandowski K, Xu Y, Pullan ST, Lumley SF, Foster D, Sanderson N, et al. Metagenomic nanopore sequencing of influenza virus direct from clinical respiratory samples. J Clin Microbiol. 2019;58:58. https://doi.org/10.1128/JCM.00963-19
15. Li H, Durbin R. Fast and accurate short read alignment with Burrows-Wheeler transform. Bioinformatics. 2009;25:1754–60. https://doi.org/10.1093/bioinformatics/btp324
16. Danecek P, Bonfield JK, Liddle J, Marshall J, Ohan V, Pollard MO, et al. Twelve years of SAMtools and BCFtools. Gigascience. 2021;10:giab008.
17. Nurk S, Bankevich A, Antipov D, Gurevich AA, Korobeynikov A, Lapidus A, et al. Assembling single-cell genomes and mini-metagenomes from chimeric MDA products. J Comput Biol. 2013;20:714–37. https://doi.org/10.1089/cmb.2013.0084
18. Pickett BE, Greer DS, Zhang Y, Stewart L, Zhou L, Sun G, et al. Virus pathogen database and analysis resource (ViPR): a comprehensive bioinformatics database and analysis resource for the coronavirus research community. Viruses. 2012;4:3209–26. https://doi.org/10.3390/v4113209
19. Bodewes R, Bestebroer TM, van der Vries E, Verhagen JH, Herfst S, Koopmans MP, et al. Avian influenza A(H10N7) virus-associated mass deaths among harbor seals. Emerg Infect Dis. 2015;21:720–2. https://doi.org/10.3201/eid2104.141675
20. Krog JS, Hansen MS, Holm E, Hjulsager CK, Chriél M, Pedersen K, et al. Influenza A(H10N7) virus in dead harbor seals, Denmark. Emerg Infect Dis. 2015;21:684–7. https://doi.org/10.3201/eid2104.141484
21. Zohari S, Neimanis A, Härkönen T, Moraeus C, Valarcher JF. Avian influenza A(H10N7) virus involvement in mass mortality of harbour seals (*Phoca vitulina*) in Sweden, March through October 2014. Euro Surveill. 2014;19:20967. https://doi.org/10.2807/1560-7917.ES2014.19.46.20967
22. Geraci JR, St Aubin DJ, Barker IK, Webster RG, Hinshaw VS, Bean WJ, et al. Mass mortality of harbor seals: pneumonia associated with influenza A virus. Science. 1982;215:1129–31. https://doi.org/10.1126/science.7063847
23. Anthony SJ, St Leger JA, Pugliares K, Ip HS, Chan JM, Carpenter ZW, et al. Emergence of fatal avian influenza in New England harbor seals. MBio. 2012;3:e00166–12. https://doi.org/10.1128/mBio.00166-12
24. Shin DL, Siebert U, Lakemeyer J, Grilo M, Pawliczka I, Wu NH, et al. Highly pathogenic avian influenza A(H5N8) virus in gray seals, Baltic Sea. Emerg Infect Dis. 2019;25:2295–8. https://doi.org/10.3201/eid2512.181472
25. Fiorentini L, Taddei R, Moreno A, Gelmetti D, Barbieri I, De Marco MA, et al. Influenza A pandemic (H1N1) 2009 virus outbreak in a cat colony in Italy. Zoonoses Public Health. 2011;58:573–81. https://doi.org/10.1111/j.1863-2378.2011.01406.x
26. Patterson AR, Cooper VL, Yoon KJ, Janke BH, Gauger PC. Naturally occurring influenza infection in a ferret (*Mustela putorius furo*) colony. J Vet Diagn Invest. 2009;21:527–30. https://doi.org/10.1177/104063870902100417
27. Reperant LA, van Amerongen G, van de Bildt MW, Rimmelzwaan GF, Dobson AP, Osterhaus AD, et al. Highly pathogenic avian influenza virus (H5N1) infection in red foxes fed infected bird carcasses. Emerg Infect Dis. 2008;14:1835–41. https://doi.org/10.3201/eid1412.080470
28. Gao Y, Zhang Y, Shinya K, Deng G, Jiang Y, Li Z, et al. Identification of amino acids in HA and PB2 critical for the transmission of H5N1 avian influenza viruses in a mammalian host. PLoS Pathog. 2009;5:e1000709. https://doi.org/10.1371/journal.ppat.1000709
29. Le QM, Sakai-Tagawa Y, Ozawa M, Ito M, Kawaoka Y. Selection of H5N1 influenza virus PB2 during replication in humans. J Virol. 2009;83:5278–81. https://doi.org/10.1128/JVI.00063-09
30. Li Z, Chen H, Jiao P, Deng G, Tian G, Li Y, et al. Molecular basis of replication of duck H5N1 influenza viruses in a mammalian mouse model. J Virol. 2005;79:12058–64. https://doi.org/10.1128/JVI.79.18.12058-12064.2005
31. Steel J, Lowen AC, Mubareka S, Palese P. Transmission of influenza virus in a mammalian host is increased by PB2 amino acids 627K or 627E/701N. PLoS Pathog. 2009;5:e1000252. https://doi.org/10.1371/journal.ppat.1000252
32. Taft AS, Ozawa M, Fitch A, Depasse JV, Halfmann PJ, Hill-Batorski L, et al. Identification of mammalian-adapting mutations in the polymerase complex of an avian H5N1 influenza virus. Nat Commun. 2015;6:7491. https://doi.org/10.1038/ncomms8491
33. Colegrove KM, Burek-Huntington KA, Roe W, Siebert U. *Pinnipediae*. In: Terio KA, McAloose D, St. Leger J, editors. Pathology of wildlife and zoo animals. London: Academic Press; 2018. p. 569–92.

Address for correspondence: Ashley C. Banyard, Department of Virology, Animal and Plant Health Agency, Weybridge KT15 3NB, UK; email: ashley.banyard@apha.gov.uk

Co-infection with *Legionella* and SARS-CoV-2, France, March 2020

Camille Allam, Alexandre Gaymard, Ghislaine Descours, Christophe Ginevra, Laurence Josset, Maud Bouscambert, Laetitia Beraud, Marine Ibranosyan, Camille Golfier, Arnaud Friggeri, Bruno Lina, Christine Campèse, Florence Ader, Sophie Jarraud; COVID-19 diagnosis HCL consortium[1]

We describe a March 2020 co-occurrence of Legionnaires' disease (LD) and coronavirus disease in France. Severe acute respiratory syndrome coronavirus 2 co-infections were identified in 7 of 49 patients from LD case notifications. Most were elderly men with underlying conditions who had contracted severe pneumonia, illustrating the relevance of co-infection screening.

The coronavirus disease (COVID-19) pandemic spread to France in mid-February 2020 (*1*). Co-infections have been described in patients with COVID-19 (*2*,*3*), but only 3 co-infections with *Legionella* have been reported (*4*–*6*). We report 7 cases of severe acute respiratory syndrome coronavirus 2 (SARS-CoV-2) and Legionnaires' disease (LD) co-infections in France during March 2020.

The Study

In France, LD surveillance is based on mandatory notifications to Santé Publique France, the national public health agency. To evaluate LD and COVID-19 co-occurrence, we retrospectively studied all LD case notifications with symptom onset during March 2020 and included cases in which patients had clinical or radiologic signs of pneumonia combined with *Legionella* culture, positive *Legionella* PCR from broncho-pulmonary secretions, or positive *Legionella pneumophila* serogroup 1 urinary antigen test (UAT) results. There were 65 LD case notifications in March 2020 compared with 79 in March 2019. To evaluate the number of UATs, which are performed in 96% of LD cases (*7*), we contacted the 59 reporting laboratories (in 47 cities), 33 of which sent the relevant data. The number of UATs increased 2.5-fold (interquartile range: 1.6–2.8) from 3,203 in March 2019 to 8,004 in March 2020. Data obtained from 6 major UAT suppliers indicated a similar 2.1-fold (interquartile range 1.52–14.8-fold) increase in tests sold to laboratories in France, from 33,378 in March 2019 to 65,072 in March 2020. Despite these increases, the number of LD case notifications was 18% lower in March 2020 than in March 2019.

Among the 65 patients from the case notifications, 49 were tested for both LD and COVID-19 and 12 for LD only; no information was available for 4. The frequency of proven LD/COVID-19 co-infection was 14.3% (7/49). This finding may be an overestimate because COVID-19 incidence was <5 cases/100,000 persons in the region of residence of the 16 patients not tested at the time of symptom onset; actual co-infection frequency could be from 10.8% (7/65) to 14.3% (7/49).

Most patients (4/7) with co-infection lived in the Grand Est region, the area in France with the most COVID-19 cases during the study period and a region that usually reports a high number of LD cases. Median patient age was 72 years (range 37–83 years); male-to-female ratio was 6:1 (Table), higher than for the overall COVID-19–infected population (*8*). Of interest, the male-to-female ratio for LD has elsewhere been reported as ≈3:1 (*7*), similar to the ratio observed in the LD-positive/COVID-19–negative cases.

At hospital admission, co-infected patients had more underlying conditions; 6 (86%) of 7 patients had ≥1, compared with 25 (60%) of 42 LD-positive/COVID-19–negative patients (Table). For cardiovascular diseases, the proportions were 6 of 7 among co-infected and 1 of 42 among LD-positive/COVID-19–negative patients. Sources of LD exposure

Author affiliations: Hospices Civils de Lyon, Lyon, France (C. Allam, A. Gaymard, G. Descours, C. Ginevra, L. Josset, L. Beraud, M. Ibranosyan, C. Golfier, A. Friggeri, B. Lina, F. Ader, S. Jarraud); Université de Lyon, Lyon (C. Allam, A. Gaymard, G. Descours, C. Ginevra, L. Josset, M. Ibranosyan, B. Lina, F. Ader, S. Jarraud); Centre International de Recherche en Infectiologie, Lyon (C. Allam, A. Gaymard, G. Descours, C. Ginevra, L. Josset, B. Lina, F. Ader, S. Jarraud); Santé Publique France, Saint-Maurice, France (C. Campèse)

DOI: https://doi.org/10.3201/eid2711.202150

[1]Members are listed at the end of this article.

Table. Patient demographics, underlying conditions, and risk exposures for patients with LD, with and without co-occurring COVID-19, France, 2020*

Patient no.	LD-positive, COVID-19–negative	LD- and COVID-19–positive	LD- and COVID-19–positive patient details						
			1	2	3	4	5	6	7
Demographics†									
Sex	M:F ratio 23:18	M:F ratio 6:1	M	M	M	F	M	M	M
Age, y	Median (range), 67 (36–96)	Median (range), 72 (37–83)	72	71	71	83	73	73	37
ICU admission	10/31 (32)	7/7 (100)	Y	Y	Y	Y	Y	Y	Y
Outcome†									
Recovered	7/42 (17)	1/7 (14)	N	N	N	Y	N	N	N
Death	3/42 (7)	2/7 (29)	N	N	Y	N	N	Y	N
Ongoing disease	32/42 (76)	4/7 (71)	Y	Y	N	N	Y	N	Y
Underlying conditions									
Corticotherapy‡	1/42 (2)	2/7 (29)	Y	Y	N	N	N	N	N
Other immunosuppression‡	5/42 (12)	0/7 (0)	N	N	N	N	N	N	N
Smoking‡	15/42 (36)	2/7 (29)	N	Y	Y	N	N	N	N
Cardiovascular diseases	1/42 (2)	6/7 (90)	Y	Y	Y	Y	Y	Y	N
Chronic respiratory disease	4/42 (10)	1/7 (14)	N	Y	N	N	N	N	N
Chronic renal insufficiency	1/42 (2)	1/7 (14)	N	N	N	N	N	Y	N
Diabetes‡	10/42 (24)	2/7 (29)	N	Y	N	N	Y	N	N
Hemopathy or cancer‡	3/42 (7)	2/7 (29)	Y	N	Y	N	N	N	N
≥1 underlying condition	25/42 (60)	6/7 (86)	Y	Y	Y	Y	Y	Y	N
Exposures§									
Hospital‡	1/42 (2)	2/7 (0)	Y	Y	N	N	N	N	N
Nursing home‡	2/42 (5)	0/7 (0)	N	N	N	N	N	N	N
Travel associated/tourism‡¶	11/42 (26)	1/7 (29)	N	Y	N	N	N	N	N
Professional exposure‡#	2/42 (5)	0/7 (0)	N	N	N	N	N	N	N
Other exposure‡**	0/42 (0)	1/7 (29)	N	N	N	N	Y	N	N
≥1 exposure	14/42 (33)	3/7 (43)	Y	Y	N	N	Y	N	N

*Values are no. patients/total no. in category (%) except as indicated. COVID-19, coronavirus disease; ICU, intensive care unit; LD, Legionnaires' disease.
†Demographics and outcome at the LD notification date.
‡Elements indicated in mandatory LD notifications. LD risk exposures had to be reported if they occurred ≤14 d before LD symptom onset.
§Exposures were indicated in LD mandatory notifications.
¶Travel-associated/tourism exposures include hotels, holiday resorts, rental houses, and cruises.
#Professional exposures include using public showers during work hours.
**Other exposure: in-house plumbing.

were reported in case notifications for 3 (43%) of 7 co-infected versus 14 (33%) of 42 non–co-infected patients; the proportions of exposure sources reported was similar between the 2 groups. Despite the implementation on March 15 of the COVID-19 national lockdown in France, halting travel, 12 (24%) of 49 exposures from the LD notifications were travel associated, a ratio similar to that in a 2017 report (*9*). Therefore, the decrease in LD cases observed in March 2020 cannot be explained by decreased travel.

Community-acquired LD and COVID-19 were diagnosed at hospital admission in 5 of 7 patients with both infections. For patient 2 (Table), whose symptoms started 48 hours before admission, UAT was not performed until 7 days after admission. Hospital-acquired COVID-19 was suspected in patient 3 because he initially tested negative but was positive after a 4-week hospitalization (Figure 1). All 7 co-infected patients required admission to an intensive care unit (ICU; median stay 13 days,; range 2–34 days). In contrast, only 10 (32%) of 31 of LD-positive/COVID-19–negative patients required ICU, similar to LD-only patients in previous reports (*7*).

At admission, all 7 co-infected patients had hyperthermia, 6 had cough or dyspnea, and 2 had neurologic symptoms. Five patients needed orotracheal intubation for a median of 13 days (range 3–30 days); acute respiratory distress syndrome developed in 4 patients, and 1 required extracorporeal membrane oxygenation (Figure 1). The median follow-up was 24 days (range 2–34 days); 2 (29%) of 7 patients died, similar to death rates for known ICU LD patients (*7*,*10*) and severe COVID-19 patients (*8*). Three (7%) of 42 LD-positive/COVID-19–negative patients died, consistent with overall LD death rates (*7*). Patient 6 died within 3 days after co-infection diagnosis. Patient 3 had progressive pulmonary deterioration and died 6 days after COVID-19 diagnosis. First-line LD treatment was appropriate for all patients; 2 patients received COVID-19 treatment (Figure 1).

The longitudinal follow-up of patient 1, a 71-year-old man receiving chemotherapy for multiple myeloma, may help decipher the kinetics of each pathogen load. Hospitalized for fever (39°C) and productive cough, he required ICU admission on day 9 because of acute respiratory distress syndrome. A thoracic computed tomography scan found left lobar

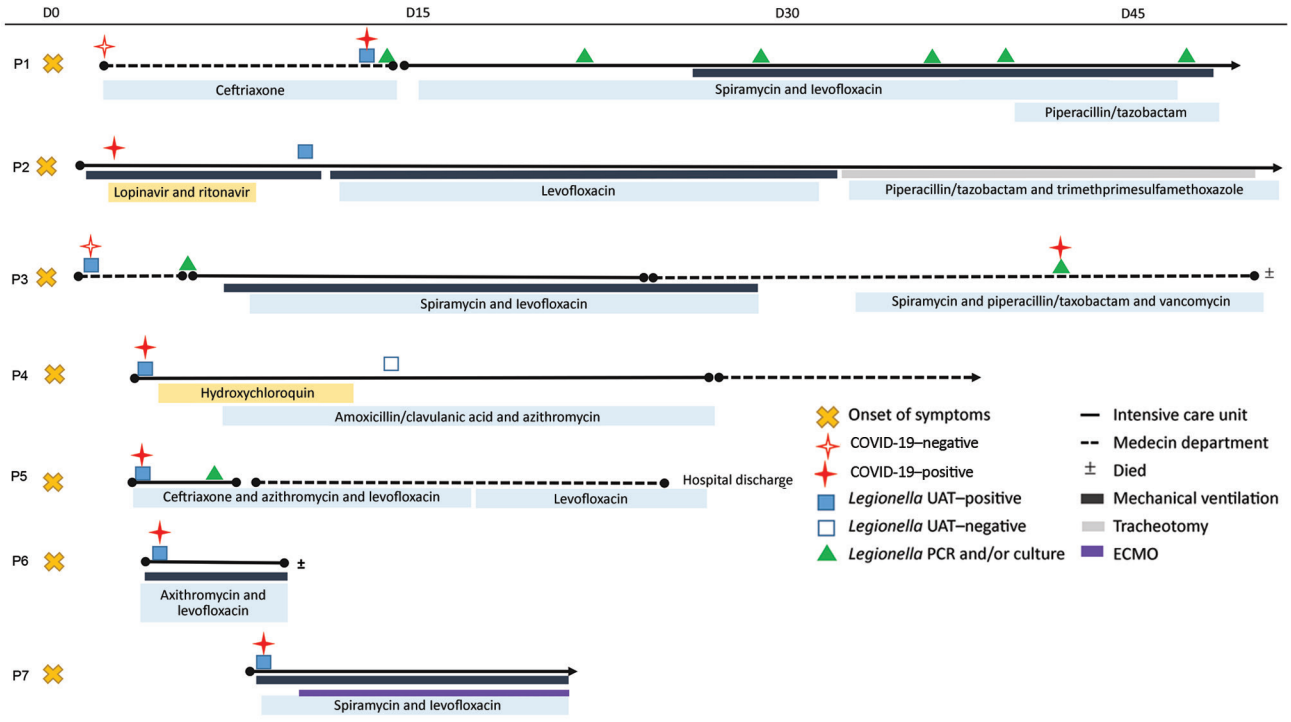

Figure 1. Timeline of first Legionnaires' disease symptoms among 7 Legionnaires' disease/COVID-19 co-infected patients, France, March 2020. COVID-19, coronavirus disease; D, day; ECMO, extracorporeal membrane oxygenation; UAT, urinary antigen test.

atelectasis, multiple ground-glass opacities compatible with COVID-19, and pleural effusion suggesting possible bacterial infection. Results of UAT and nasopharyngeal SARS-CoV-2 reverse transcription PCR were both positive. On day 10, a serum sample was PCR positive for both SARS-CoV-2 and *Legionella* (Figure 2, panel A); each pathogen has individually been associated with COVID-19 (*11*) and LD (*12*) severity. Beginning on day 10, longitudinal samples of the lower respiratory tract collected every 3–6 days showed a high SARS-CoV-2 viral load (7.5 $\log_{10}$ RNA copies/100 cells), followed by a decrease to 1.3 $\log_{10}$ RNA copies/100 cells within 21 days (Figure 2, panel B). In contrast, lung *Legionella* DNA load increased and remained high (cycle threshold 21.9) until day 31. To identify potential bacterial co-infections, we performed a lung microbiota analysis on a D19 bronchoalveolar lavage using 16S MinION long-read sequencing technology (Oxford Nanopore Technologies, https://nanoporetech.com). Similar to another study of LD microbiomes (*13*), we found a predominance of *Legionella* (61%) and the presence of commensal lung bacteria (Appendix Figure, https://wwwnc.cdc.gov/EID/article/27/11/20-

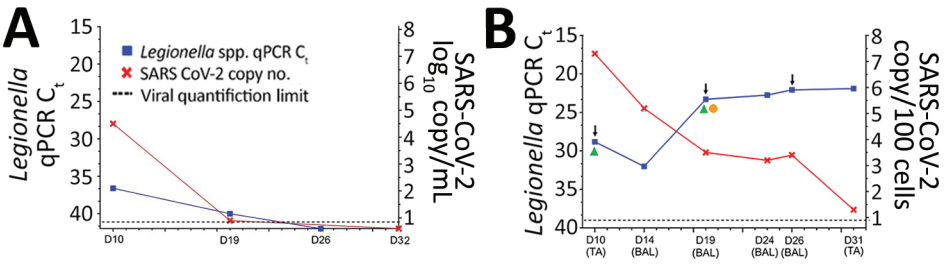

Figure 2. Timeline of detection of SARS-CoV-2 and *Legionella* in patient 1, a 71-year-old man receiving chemotherapy for multiple myeloma, France, March 2020. A) Serum *Legionella* DNA load estimated by qPCR C_t and SARS-CoV-2 RNA load expressed as the number of $\log_{10}$ RNA copies/mL serum. B) Pulmonary *Legionella* DNA load estimated by qPCR C_t, targeting the 16sRNA gene (R-DiaLeg, Diagenode, https://www.diagenode.com) and SARS-CoV-2 RNA load (Institut Pasteur, Paris protocol). Arrows indicate dates of computed tomography scans, green triangles indicates dates of positive *Legionella* cultures, and orange circle indicates date of lung microbiome testing. Values are normalized according to cellular quantification using the CELL Control r-gene kit (bioMérieux, https://www.biomerieux.com) and expressed as the number of $\log_{10}$ RNA copies/100 cells from pulmonary TA and BAL. BAL, broncho-alveolar lavage; C_t, cycle threshold; D, days after onset of symptoms; qPCR, quantitative PCR; SARS-CoV-2, severe acute respiratory syndrome coronavirus 2; TA, tracheal aspirations.

2150-App1.pdf) but no additional bacterial co-infection. On day 26, while high lung *Legionella* DNA load persisted, a third chest scan found pseudocavitation. Persistence of culture or PCR positivity in respiratory samples, or both, has been described in patients with *Legionella* lung abscesses, especially if immunocompromised (*14*).

Conclusions

Our study found a substantial proportion of patients in LD notifications in France during March 2020, mostly elderly men with underlying conditions, also had COVID-19. They required ICU admission more frequently and had a higher case-fatality rate than patients without SARS-CoV-2 co-infection, but these rates were similar to that for all ICU-admitted LD patients (*7*,*10*). Overall, health effects from co-infections were more severe than from single infections, perhaps because of cumulative effects or because patients with co-infections may be more likely to have risk factors associated with poor outcomes. Another possibility is that SARS-CoV-2 infection may be more severe in this population.

Longitudinal monitoring of a single co-infected patient found a first phase of predominant SARS-CoV-2 replication followed by a resurgence of *Legionella* and worsening of respiratory symptoms while SARS-CoV-2 decreased. Initial viral infection could establish pulmonary damage suitable for the bacteria to develop, similar to how bacterial superinfections develop in influenza-infected patients (*15*). Such co-infections may lead to poor prognoses as demonstrated here and elsewhere (*3*), underlining the importance of extensive screening for respiratory pathogens in patients with suspected or confirmed COVID-19. Because *Legionella* and other pulmonary microorganisms share clinical and radiological features with SARS-CoV-2 infection, they should be included in COVID-19 differential diagnoses (*3*).

Members of the COVID-19 diagnosis HCL consortium: Antonin Bal, Geneviève Billaud, Grégory Destras, Vanessa Escuret, Sibyle Etievant, Emilie Frobert, Florence Morfin, and Clément Munier

Acknowledgments

We thank all clinicians, microbiologists, and epidemiologists for providing clinical, laboratory, and epidemiologic data: Florent Wallet, Christelle Fabbro, Claire Plassart, Dominique Jusserand, Patricia Stroessel, Julie Kieffer, Agnes Scanvic, Carole Guillemet, Sarah Bassous, Arthur Luton, Christian Meyer, and Catherine Maine. We thank the authors, the originating and submitting laboratories for their sequence data and metadata shared through the Global Initiative on Sharing All Influenza Data (GISAID; https://www.gisaid.org) on which this research is based. We also thank Philip Robinson and Hélène Boyer for help in manuscript preparation.

According to legislation in France all patients have been fully informed of the project and of their right to decline participation in the study and written informed consent from patient 1 was obtained. The local ethics committee approved the study (number 20-57; Comité d'Ethique du CHU de Lyon).

About the Author

Dr. Allam is a medical biologist at the French National Reference Centre for *Legionella* at the Infective Agents Institute, North Hospital Network, in Lyon, France, and teaches bacteriology at the Claude Bernard Lyon 1 Medical University. She is seeking a PhD with a concentration in *Legionella* virulence and severity factors.

References

1. Spiteri G, Fielding J, Diercke M, Campese C, Enouf V, Gaymard A, et al. First cases of coronavirus disease 2019 (COVID-19) in the WHO European Region, 24 January to 21 February 2020. Euro Surveill. 2020;25:2000178. https://doi.org/10.2807/1560-7917.ES.2020.25.9.2000178
2. Hughes S, Troise O, Donaldson H, Mughal N, Moore LSP. Bacterial and fungal coinfection among hospitalized patients with COVID-19: a retrospective cohort study in a UK secondary-care setting. Clin Microbiol Infect. 2020;26:1395–9. https://doi.org/10.1016/j.cmi.2020.06.025
3. Lai C-C, Wang C-Y, Hsueh P-R. Co-infections among patients with COVID-19: The need for combination therapy with non-anti-SARS-CoV-2 agents? J Microbiol Immunol Infect. 2020;53:505–12. https://doi.org/10.1016/j.jmii.2020.05.013
4. Arashiro T, Nakamura S, Asami T, Mikuni H, Fujiwara E, Sakamoto S, et al. SARS-CoV-2 and *Legionella* co-infection in a person returning from a Nile cruise. J Travel Med. 2020;27:taaa053.
5. Bordi L, Nicastri E, Scorzolini L, Di Caro A, Capobianchi MR, Castilletti C, et al.; On Behalf Of Inmi Covid-Study Group And Collaborating Centers. Differential diagnosis of illness in patients under investigation for the novel coronavirus (SARS-CoV-2), Italy, February 2020. Euro Surveill. 2020;25:2000170. https://doi.org/10.2807/1560-7917.ES.2020.25.8.2000170
6. Verhasselt HL, Buer J, Dedy J, Ziegler R, Steinmann J, Herbstreit F, et al. COVID-19 Co-infection with *Legionella pneumophila* in 2 tertiary-care hospitals, Germany. Emerg Infect Dis. 2021;27:1535–7. https://doi.org/10.3201/eid2705.203388
7. Chidiac C, Che D, Pires-Cronenberger S, Jarraud S, Campèse C, Bissery A, et al.; French Legionnaires' Disease Study Group. Factors associated with hospital mortality in community-acquired legionellosis in France. Eur Respir J. 2012;39:963–70. https://doi.org/10.1183/09031936.00076911
8. Boëlle P-Y, Delory T, Maynadier X, Janssen C, Piarroux R, Pichenot M, et al. Trajectories of hospitalization in COVID-19

patients: an observational study in France. J Clin Med. 2020; 9:3148. https://doi.org/10.3390/jcm9103148
9. Beauté J; The European Legionnaires' Disease Surveillance Network. Legionnaires' disease in Europe, 2011 to 2015. Euro Surveill. 2017;22:30566 [Erratum in: Euro Surveill. 2017; 22:171116-1]. https://doi.org/10.2807/1560-7917.ES.2017.22.27.30566
10. Cecchini J, Tuffet S, Sonneville R, Fartoukh M, Mayaux J, Roux D, et al. Antimicrobial strategy for severe community-acquired Legionnaires' disease: a multicentre retrospective observational study. J Antimicrob Chemother. 2017;72: 1502–9. https://doi.org/10.1093/jac/dkx007
11. Rao SN, Manissero D, Steele VR, Pareja J. A systematic review of the clinical utility of cycle threshold values in the context of COVID-19. Infect Dis Ther. 2020;9:573–86 [Erratum in: Infect Dis Ther. 2020;9:587]. https://doi.org/10.1007/s40121-020-00324-3
12. van de Veerdonk FL, de Jager CPC, Schellekens JJA, Huijsmans CJJ, Beaumont F, Hermans MHA, et al. *Legionella pneumophila* DNA in serum samples during Legionnaires' disease in relation to C-reactive protein levels. Eur J Clin Microbiol Infect Dis. 2009;28:371–6. https://doi.org/10.1007/s10096-008-0638-8
13. Pérez-Cobas AE, Ginevra C, Rusniok C, Jarraud S, Buchrieser C. Persistent Legionnaires' disease and associated antibiotic treatment engender a highly disturbed pulmonary microbiome enriched in opportunistic microorganisms. MBio. 2020;11:e00889–20. https://doi.org/10.1128/mBio.00889-20
14. Pouderoux C, Ginevra C, Descours G, Ranc A-G, Beraud L, Boisset S, et al. Slowly or nonresolving Legionnaires' disease: case series and literature review. Clin Infect Dis. 2020;70:1933–40. https://doi.org/10.1093/cid/ciz538
15. Small C-L, Shaler CR, McCormick S, Jeyanathan M, Damjanovic D, Brown EG, et al. Influenza infection leads to increased susceptibility to subsequent bacterial superinfection by impairing NK cell responses in the lung. J Immunol. 2010;184:2048–56. https://doi.org/10.4049/jimmunol.0902772

Address for correspondence: Sophie Jarraud, Centre National de Reference des Legionella, Institut des Agents Infectieux, Hospices Civils de Lyon, 103 Grande rue de la Croix Rousse, 69317 Lyon CEDEX 04, France; email: sophie.jarraud@chu-lyon.fr

Epidemiologic Analysis of Efforts to Achieve and Sustain Malaria Elimination along the China–Myanmar Border

Fang Huang, Li Zhang, Hong Tu, Yan-Wen Cui, Shui-Sen Zhou, Zhi-Gui Xia, Hong-Ning Zhou

Malaria cases have dramatically declined in China along the Myanmar border, attributed mainly to adoption of the 1-3-7 surveillance and response approach. No indigenous cases have been reported in China since 2017. Counties in the middle and southern part of the border area have a higher risk for malaria importation and reestablishment after elimination.

In 2010, China issued the National Malaria Elimination Action Plan (2010–2020), with the goal of eliminating malaria nationwide by 2020 (*1*). Malaria cases in China subsequently decreased dramatically, and no indigenous cases have been reported since 2017 (*2*). In 2020, on the basis of successful subnational verification, China submitted an official request to the World Health Organization for certification of national malaria elimination, which requires a country to provide evidence that local malaria transmission has been fully interrupted, that zero indigenous human malaria cases have been reported for ≥3 consecutive years, and that an adequate program for preventing reestablishment of indigenous transmission is fully functional throughout the country (*3*). However, the China–Myanmar border of Yunnan Province has attracted considerable attention because of a substantial risk of reintroduction of malaria from bordering areas of Myanmar (*4*). This border region is extremely remote, has high rates of poverty, and is inhabited by local minority nationalities (*5*,*6*). A total of 18 counties in Yunnan Province share the 1,997-km border with the townships of Myanmar in which malaria is endemic; the border provides no natural barriers and poses a high risk for malaria reintroduction into China.

Author affiliations: National Institute of Parasitic Diseases, Chinese Center for Disease Control and Prevention (Chinese Center for Tropical Diseases Research), Shanghai, China (F. Huang, L. Zhang, H. Tu, Y.-W. Cui, S.-S. Zhou, Z.-G. Xia); NHC Key Laboratory of Parasite and Vector Biology, Shanghai (F. Huang, L. Zhang, H. Tu, Y.-W. Cui, S.-S. Zhou, Z.-G. Xia); World Health Organization Collaborating Centre for Tropical Diseases, Shanghai (F. Huang, L. Zhang, H. Tu, Y.-W. Cui, S.-S. Zhou, Z.-G. Xia); National Center for International Research on Tropical Diseases, Shanghai, China (F. Huang, L. Zhang, H. Tu, Y.-W. Cui, S.-S. Zhou, Z.-G. Xia); Yunnan Institute of Parasitic Diseases, Puer, China (H.-N. Zhou)

DOI: https://doi.org/10.3201/eid2711.204428

The Study

We extracted data on reported malaria cases and foci during 2013–2019 from the web-based China Information System for Disease Control and Prevention and comprised data from passive case detection, reactive case detection among foci residents and case co-travelers, and proactive case detection among at-risk populations. Indigenous cases were defined as cases in patients who contracted malaria by bites from *Anopheles* mosquitoes within China without direct link to transmission from an imported case, whereas imported cases were defined as cases in patients who had exposure history in any malaria-endemic areas abroad before the onset of illness (*7*,*8*). *Plasmodium* spp. were determined by microscopy or rapid diagnosis test and PCR (*8*). This study was an epidemiologic analysis of malaria along the China–Myanmar border to identify the risk for malaria reestablishment in the stage after elimination.

During 2013–2019, a total of 2,222 malaria cases were reported from the 18 border counties; 1 death occurred. Total cases fell from 465 in 2013 to 148 in 2019; indigenous cases dropped to zero by 2017, and the number of imported cases also declined (Table 1). This decrease was mainly attributed to the extensive adoption of the 1-3-7 approach to surveillance and response: case reporting within 1 day, investigation

within 3 days, and focus investigation and response within 7 days. Case-patients ranged in age from 19 to 59 years, and men and outdoor workers were at considerably higher risk of contracting malaria (p<0.0001) (Table 1).

In 2013, malaria cases reported from the 18 border counties accounted for 80.6% of total cases in Yunnan Province; 89.9% (418/465) were imported cases. Indigenous cases (10.1%, 47/465) were distributed in 10 border counties (Figure 1). Yingjiang County reported 38.3% (18/47) of total indigenous cases, along with the highest annual parasite index of 0.058. Five counties displayed an annual parasite index range of 0.01–0.05 (Figure 1). The number of counties reporting indigenous cases decreased from 10 in 2013 to 1 in 2016 (Figure 1). The last indigenous *P. falciparum* case in China was in Cangyuan County in 2015 and the last indigenous *P. vivax* case in Yingjiang County in 2016. Most imported malaria cases were distributed in the middle part of the borderline, especially Yingjiang and Tengchong Counties (Figure 1); 96.5% (2,056/2,130) of total imported cases in the 18 border counties were from Myanmar (Table 1). During 2017–2019, a total of 97.7% (562/575) of imported cases and 98.5% (542/550) of *P. vivax* cases were from Myanmar (Table 1). The counties bordering areas of Myanmar, where rates of malaria were highest, displayed higher numbers of imported cases (*9*).

P. vivax was the predominant species. *P. vivax* cases accounted for 95.7% of total reported cases during 2017–2019, whereas the proportion of *P. falciparum* declined to 1.4% (Figure 2, panel A). Four cases of *P. malariae* and 10 cases of mixed infections were reported; no *P. ovale* cases were reported. A total of 43

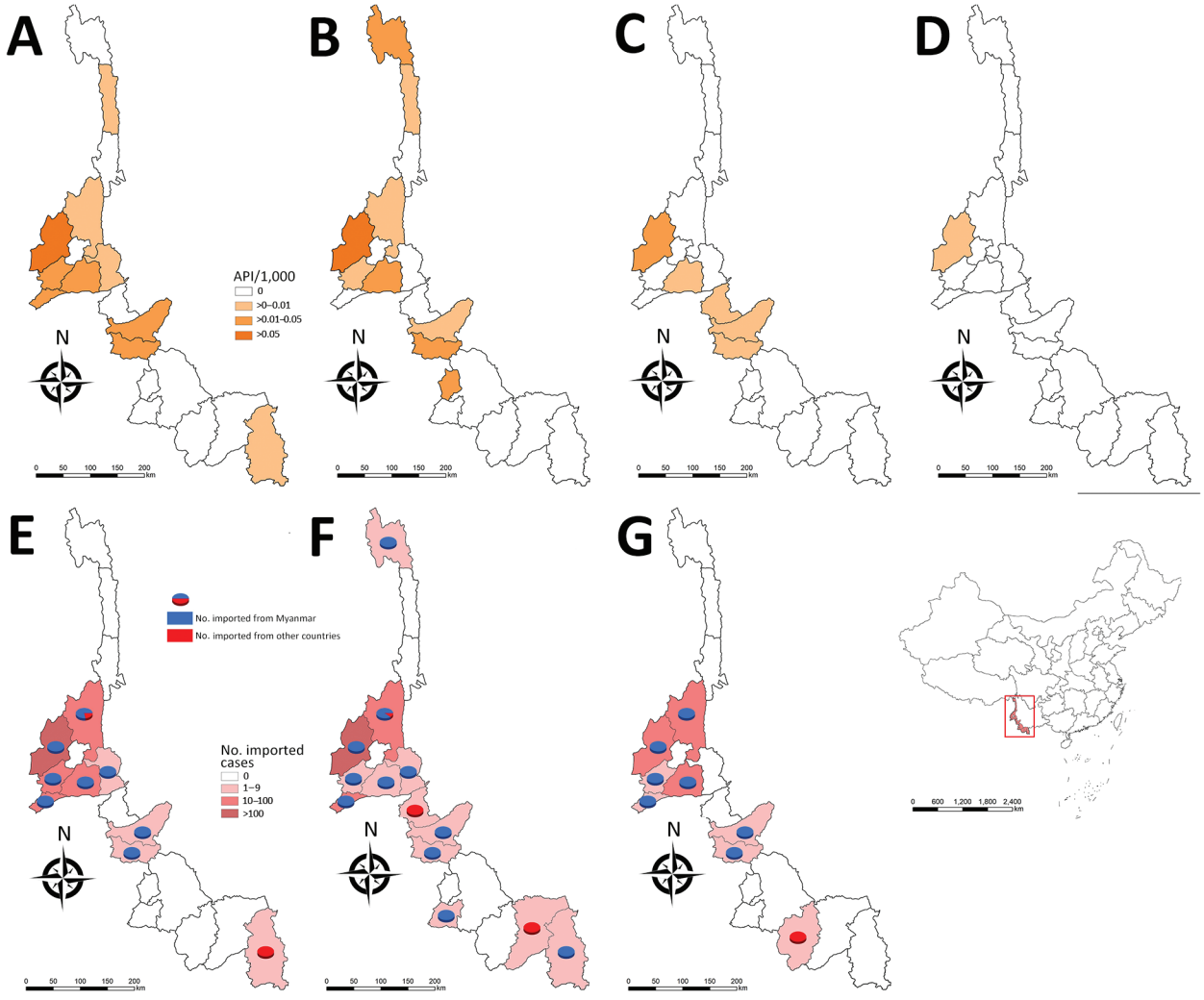

Figure 1. API per 1,000 persons and numbers of imported cases by year in the 18 China counties along the border with Myanmar, 2013–2019. A) 2013 API, B) 2014 API, C) 2015 API, D) 2016 API; E) 2017 imported cases, F) 2018 imported cases, G) 2019 imported cases. Inset map shows location of China–Myanmar border area (rectangle). API, annual parasite index.

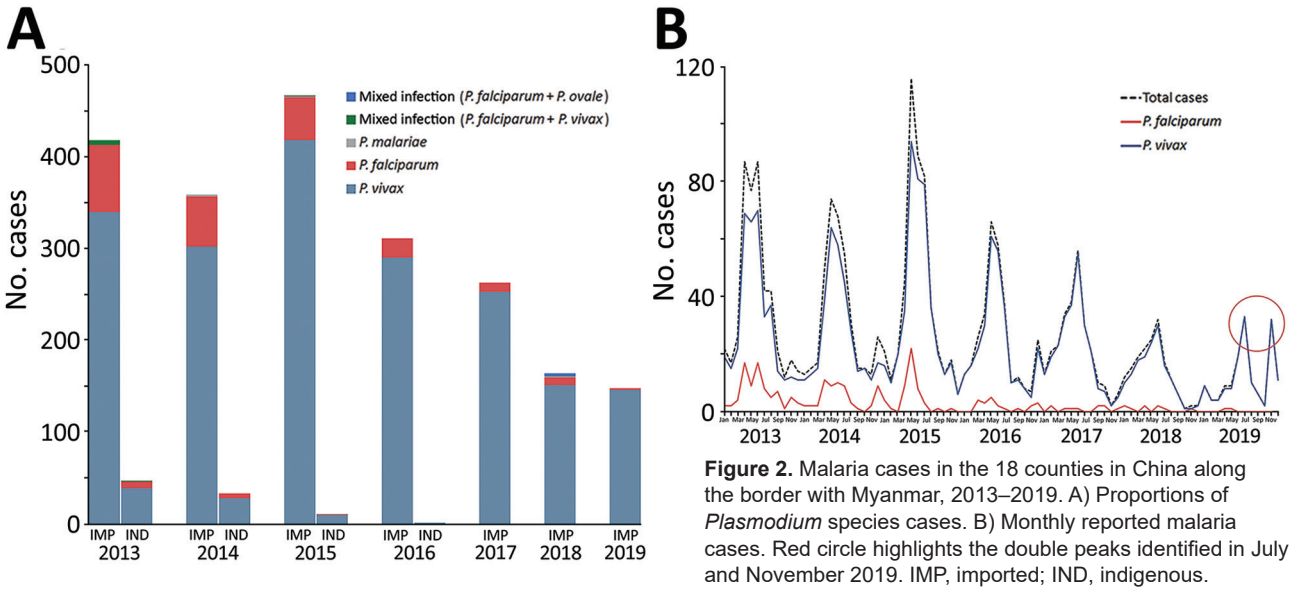

Figure 2. Malaria cases in the 18 counties in China along the border with Myanmar, 2013–2019. A) Proportions of *Plasmodium* species cases. B) Monthly reported malaria cases. Red circle highlights the double peaks identified in July and November 2019. IMP, imported; IND, indigenous.

relapsing cases (*P. vivax* cases that recurred 1 month later with neither evidence of an epidemiologic link to additional cases nor as a result of incomplete clearance of original asexual parasites) were reported during 2013–2019, which indicates the need for adherence to the full primaquine regimen and possible resistance to the drug for eliminating the hypnozoites.

The malaria transmission peak was from April to August; another slight peak occurred from December to the following January (Figure 2, panel B). This transmission coincided with the local natural environment and was strongly correlated with the abundance of *Anopheles* spp. mosquitoes. Of note, double peaks were identified in July and November 2019. The first peak was postponed, whereas the second peak shifted 1 month earlier. This change was primarily caused by migration in the local population. The temporal distribution pattern of *P. vivax* and *P. falciparum* was different (Figure 2, panel B) because *P. falciparum* cases were few and most were imported, mainly because of population movement and migration.

The median interval between onset of illness and diagnosis of malaria varied widely (range 2–10 days; Table 2), because the capability for diagnosis in some healthcare facilities was relatively low; training is needed to strengthen case detection and diagnosis capabilities. In addition, this range reflects the knowledge, attitudes, and practice gaps regarding malaria treatment-seeking of residents. The median interval between diagnosis and treatment was 0 days, except for in Ximeng County, which had a median interval of 0.5 days (Table 2). These rates indicate the capacity of hospital response was strong. The 1-3-7 approach was adopted nationally in China in early 2012 (*10*). During 2013–2019, all malaria cases were reported within 1 day, 95.6% of cases were investigated within 3 days, and in 8 of 18 counties 100% of cases were investigated within 3 days in all years studied. Longchuan, Gengma, and Yingjiang Centers for Disease Control and Prevention took >3 days to complete investigation of cases from remote areas. Malaria focus in China is defined as the circumscribed village or community with a reported case (*11*). During 2013–2019, a total of 97.9% (381/389) of foci were investigated and responded to within 7 days in 10 counties (Table 2). Depending on the nature of the focus and its state of transmission, the corresponding response actions were selected; these actions consisted of indoor residual spraying, reactive case detection, case treatment, and health education (*7*). No secondary cases have been reported because of the prompt and targeted interventions in all the foci.

Conclusions

China has set a goal to eliminate malaria by 2020, and Myanmar has set a goal to eliminate malaria by 2030 (*1*,*12*). This study demonstrated that local malaria transmission has been interrupted in Yunnan Province at the China–Myanmar border, although the risk for malaria reintroduction still exists. The complex geographic conditions and large migrant population along the border, in addition to reservoirs of symptomatic and asymptomatic infection in neighboring Myanmar (*13*), are obstacles to consolidating achievements in malaria elimination (*5*,*14*). Another noteworthy factor is the coronavirus

disease pandemic. Maintaining full engagement with malaria control is challenging given the simultaneous demands of the pandemic (*15*).

In summary, malaria elimination has been achieved in the counties in China along the border with Myanmar. However, continued strong surveillance,

Table 1. Demographic characteristics of reported malaria cases in the 18 counties in China along the border with Myanmar, 2013–2019*

Characteristics	No. cases by year							No. cases by type		Total cases	p value†
	2013	2014	2015	2016	2017	2018	2019	Imported	Indigenous		
Total cases	465	392	478	312	263	164	148	2,130	92		
Sex											
M	392	349	404	231	179	124	109	1,726	62	1,788	0.0012
F	73	43	74	81	84	40	39	404	30	434	
Age group, y											
<5	3	9	9	9	10	5	1	41	5	46	
5–18	42	20	36	35	37	19	7	176	20	196	<0.0001
19–59	415	357	423	253	202	127	132	1,850	59	1,909	
≥60	5	6	10	15	14	13	8	63	8	71	
Occupation‡											
Outdoor worker	371	323	323	235	160	95	85	1,536	56	1,592	
Indoor worker	37	28	81	10	13	15	21	204	1	205	<0.0001
Unclear	50	35	51	56	84	53	42	348	23	371	
Missing	7	6	23	11	6	1	0	42	12	54	
Plasmodium spp.											
P. vivax	379	330	428	291	253	151	146	1,900	78	1,978	
P. falciparum	80	60	48	21	10	9	2	217	13	230	
P. malariae	0	2	1	0	0	1	0	4	0	4	0.4653
P. falciparum + *P. vivax*	6	0	1	0	0	0	0	6	1	7	
P. falciparum + *P. ovale*	0	0	0	0	0	3	0	3	0	3	
Destination of oversea travel and species											
Myanmar										2,056	
P. falciparum	71	55	46	16	9	6	1	204	NA		
P. vivax	321	294	399	283	246	150	146	1,839	NA		
Other species	5	2	2	0	0	4	0	13	NA		
Other countries										74	
P. falciparum	2	0	1	5	1	3	1	13	NA		
P. vivax	19	8	19	7	7	1	0	61	NA		

*NA, not available.
†The number of cases over years were compared by using a χ^2 or Fisher exact test according to sample size (>5 or ≤5) by SAS software.
‡Outdoor workers are persons whose activity is mostly conducted outside, including architectural engineers, construction workers, farmers, fishermen, overseas migrant workers (expatriate Chinese nationals), open mine workers, sailors or truck drivers, field engineers, herdsmen, military or soldiers, etc. Indoor workers include businessmen, caterers, interpreters, medical staff, office workers, teachers, actors, flight attendants, babysitters, middlemen, cooks, diplomats, financial staff, journalists, underground mine workers, prisoners (although not a worker per se, prisoners were officially classified as an indoor worker since their time is spent indoors), researchers, waiters, etc. Unclear indicates those for whom risk exposure cannot clearly be estimated, including children, retirees, self-employed persons, students, unemployed persons, athletes, tourists, etc. Missing data were not included in the statistical analysis.

Table 2. Characteristics of implementation of the 1-3-7 approach to malaria surveillance and response in 18 counties in China along the border with Myanmar, 2013–2019*

County	No. reported cases	Days from illness onset to diagnosis, median (IQR)	Days from diagnosis to treatment, median (IQR)	Case reported within 1 d, %	Case investigated within 3 d, %	Foci response within 7 d, %
Zhenkang	6	4.5 (4–7.3)	0.0 (0–0.75)	100.0	100.0	–
Menghai	3	10.0 (6–12)	0.0 (0–0.5)	100.0	100.0	–
Lancang	9	7.0 (3–11)	0.0 (0)	100.0	100.0	–
Jinghong	14	5.0 (3–6)	0.0 (0)	100.0	92.9	–
Gengma	29	3.0 (1–6)	0.0 (0–1)	100.0	82.8	100.0 (4/4)
Mengla	30	2.0 (1–5)	0.0 (0–1)	100.0	93.3	100.0 (1/1)
Menglian	20	3.5 (0–7.5)	0.0 (0–2.25)	100.0	100.0	100.0 (1/1)
Lushui	18	6.5 (3–10)	0.0 (0)	100.0	100.0	–
Ximeng	4	4.5 (3.8–6)	0.5 (0–1)	100.0	100.0	–
Fugong	11	4.0 (3–6.5)	0.0 (0)	100.0	100.0	–
Cangyuan	35	4.0 (2–7.5)	0.0 (0)	100.0	97.1	–
Longchuan	69	2.0 (1–4)	0.0 (0–1)	100.0	82.6	100.0 (20/20)
Longling	75	3.0 (2–5)	0.0 (0)	100.0	98.7	85.7 (6/7)
Gongshan	5	4.0 (1–5)	0.0 (0–5)	100.0	100.0	100.0 (1/1)
Mangshi	112	3.0 (1–4)	0.0 (0–2)	100.0	92.0	96.2 (25/26)
Tengchong	525	2.0 (1–4)	0.0 (0–2)	100.0	95.6	98.0 (48/49)
Yingjiang	895	2.0 (1–4)	0.0 (0)	100.0	88.4	98.5 (256/261)
Ruili	362	2.5 (1–5)	0.0 (0)	100.0	97.2	100.0 (19/19)

*IQR, interquartile range, –, no focus reported.

multisectoral collaboration, and cross-border cooperation are of high priority to reduce the risk for malaria reintroduction and sustain its elimination.

This work was supported by the National Malaria Elimination Program of China and the Fifth Round of Three-Year Public Health Action Plan of Shanghai (No. GWV-10.1-XK13).

The datasets used and analyzed during this study are available from the corresponding author on request.

About the Author

Dr. Huang is a molecular epidemiologist in the National Institute of Parasitic Diseases, Chinese Center for Disease Control and Prevention. Her primary research interests are malaria epidemiology and antimalarial drug resistance.

References

1. The Central People's Government of the People's Republic of China. China malaria elimination action plan (2010–2020), 19 May 2010 [in Chinese]. 2010 [cited 2021 Apr 15]. http://www.gov.cn/zwgk/2010-05/26/content_1614176.htm
2. Feng J, Zhang L, Huang F, Yin JH, Tu H, Xia ZG, et al. Ready for malaria elimination: zero indigenous case reported in the People's Republic of China. Malar J. 2018;17:315. https://doi.org/10.1186/s12936-018-2444-9
3. World Health Organization. Preparing for certification of malaria elimination, 4 January 2021 [cited 2021 Apr 15]. https://www.who.int/publications/i/item/9789240005624
4. Yang WZ, Zhou XN. New challenges of malaria elimination in China [in Chinese]. Zhonghua Yu Fang Yi Xue Za Zhi. 2016;50:289–91. https://doi.org/10.3760/cma.j.issn.0253-9624.2016.04.001
5. Zhang J, Dong JQ, Li JY, Zhang Y, Tian YH, Sun XY, et al. Effectiveness and impact of the cross-border healthcare model as implemented by non-governmental organizations: case study of the malaria control programs by health poverty action on the China-Myanmar border. Infect Dis Poverty. 2016;5:80. https://doi.org/10.1186/s40249-016-0175-0
6. Feng J, Liu J, Feng X, Zhang L, Xiao H, Xia Z. Towards malaria elimination: monitoring and evaluation of the "1-3-7" approach at the China-Myanmar border. Am J Trop Med Hyg. 2016;95:806–10. https://doi.org/10.4269/ajtmh.15-0888
7. Chinese Center for Disease Control and Prevention. Technical scheme of malaria elimination in China, 2 September 2011 [in Chinese] [cited 2021 Apr 15]. http://www.chinacdc.cn/did/crbzt/jscb/nj/njzyzl/lgjbfk/lgfkfa/201507/P020150715347374233381.pdf
8. National Health and Family Planning Commission of the People's Republic of China. Diagnostic criteria for malaria (WS 259–2015) [in Chinese]. 2015 Nov 16 [cited 2021 Apr 15]. http://www.nhc.gov.cn/fzs/s7852d/201511/5a35d124469a4b69884c942c43ae3269.shtml
9. Huang F, Zhang L, Xue JB, Zhou HN, Thi A, Zhang J, et al. From control to elimination: a spatial-temporal analysis of malaria along the China-Myanmar border. Infect Dis Poverty. 2020;9:158. https://doi.org/10.1186/s40249-020-00777-1
10. Zhou SS, Zhang SS, Zhang L, Rietveld AE, Ramsay AR, Zachariah R, et al. China's 1-3-7 surveillance and response strategy for malaria elimination: is case reporting, investigation and foci response happening according to plan? Infect Dis Poverty. 2015;4:55. https://doi.org/10.1186/s40249-015-0089-2
11. Feng J, Tu H, Zhang L, Zhang S, Jiang S, Xia Z, et al. Mapping transmission foci to eliminate malaria in the People's Republic of China, 2010-2015: a retrospective analysis. BMC Infect Dis. 2018;18:115. 10.1186/s12879-018-3018-8 https://doi.org/10.1186/s12879-018-3018-8
12. National Malaria Control Program Myanmar. National plan for malaria elimination in Myanmar 2016–2030. 2017 [cited 2020 Apr 5]. https://apmen.org/sites/default/files/all_resources/National%20Strategic%20Plan_Myanmar_2016-2020.pdf.
13. Chen I, Clarke SE, Gosling R, Hamainza B, Killeen G, Magill A, et al. "Asymptomatic" malaria: a chronic and debilitating infection that should be treated. PLoS Med. 2016;13:e1001942. https://doi.org/10.1371/journal.pmed.1001942
14. Xu X, Zhou G, Wang Y, Hu Y, Ruan Y, Fan Q, et al. Microgeographic heterogeneity of border malaria during elimination phase, Yunnan Province, China, 2011–2013. Emerg Infect Dis. 2016;22:1363–70. https://doi.org/10.3201/eid2208.150390
15. Chiodini J. COVID-19 and the impact on malaria. Travel Med Infect Dis. 2020;35:101758. https://doi.org/10.1016/j.tmaid.2020.101758

Address for correspondence: Zhi-Gui Xia, National Institute of Parasitic Diseases, Chinese Center for Disease Control and Prevention (Chinese Center for Tropical Diseases Research), 207 Ruijin Er Rd, Shanghai 200025, China; email: xiazg@nipd.chinacdc.cn; Hong-Ning Zhou, Yunnan Institute of Parasitic Diseases, 6 Xiyuan Rd, Puer 665000, China; email: zhouhn66@163.com

Socioeconomic Patterns of COVID-19 Clusters in Low-Incidence City, Hong Kong

Gary K.K. Chung, Siu-Ming Chan, Yat-Hang Chan, Jean Woo, Hung Wong, Samuel Y. Wong, Eng Kiong Yeoh, Michael Marmot, Roger Y. Chung

Although coronavirus disease (COVID-19) outbreaks have been relatively well controlled in Hong Kong, containment remains challenging among socioeconomically disadvantaged persons. They are at higher risk for widespread COVID-19 transmission through sizable clustering, probably because of exposure to social settings in which existing mitigation policies had differential socioeconomic effects.

As coronavirus disease (COVID-19) continued to spread globally, studies of transmission mainly focused on clusters of ≥2 epidemiologically linked cases. Some governments, including those of New Zealand and Hong Kong, China, put specific focus on sizable infection clusters (i.e., clusters of ≥10 epidemiologically linked case-patients who are not all part of the same household) to detect widespread human-to-human COVID-19 infections with potentially greater numbers of successive transmission generations (*1*,*2*). These sizable infection clusters are closely linked to COVID-19 superspreading; as many as 7 superspreading events were related to the first few sizable infection clusters in Hong Kong (*3*). Given the widely observed higher COVID-19 incidence associated with socioeconomic disadvantages (*4*–*7*), determining whether the risk for sizable infection clustering is socioeconomically patterned is of public health significance. Such a pattern would imply not only higher risk for exposure to the virus but also increased risk of spreading the disease among socioeconomically disadvantaged communities.

Unlike many other parts of the world, Hong Kong has had a relatively low COVID-19 incidence, which made comprehensive contact tracing to identify sizable infection clusters possible and meaningful. In this study, we examined the association of socioeconomic position with sizable infection clustering in Hong Kong and explored the potential heterogeneity by case classification and different activity categories of clusters. For this study, we used data collected by the Centre for Health Protection (CHP), the Planning Department, and the Census and Statistics Department of the Hong Kong Government in compliance with the Declaration of Professional Ethics of the International Statistical Institute.

The Study

We collected data on individual laboratory-confirmed cases from CHP (*1*) and a COVID-19 information website (*8*), which shows compiled information released by the CHP. During January 23–October 31, 2020, a total of 5,324 cases and 30 sizable infection clusters were identified (Appendix Table 1, https://wwwnc.cdc.gov/EID/article/27/11/20-4840-App1.pdf). We included 3,587 local cases with recognizable residential addresses in this study; 778 of those cases were linked to sizable infection clusters (Table 1).

We assigned as the dependent variable whether a case belonged to a sizable infection cluster. These sizable infection cluster cases included the earliest identified unlinked source cases and their subsequent epidemiologically linked cases. We categorized these clusters as living, working, dining, or entertainment (>100 cases each) on the basis of the type of activities most closely associated with the venues at which the source cases of each corresponding cluster were identified.

We adopted self-reported residential addresses of the confirmed case-patients (*8*) to generate 2 proxy socioeconomic measures (Appendix). First, we calculated the area-level income poverty rates as the proportion of households living at <50% of the median

Author affiliations: The Chinese University of Hong Kong, Hong Kong, China (G.K.K. Chung, S.-M. Chan, Y.-H. Chan, J. Woo, H. Wong, S.Y. Wong, E.K. Yeoh, M. Marmot, R.Y. Chung); City University of Hong Kong, Hong Kong (S.-M. Chan); University College London, London, UK (M. Marmot)

DOI: https://doi.org/10.3201/eid2711.204840

Table 1. Characteristics of local coronavirus disease case-patients with a valid residential address, Hong Kong, 2020*

Characteristic	Total sample, N = 3,587	Area-level income poverty rate†			
		1st quartile	2nd quartile	3rd quartile	4th quartile
Mean age, y (SD)	47.92 (19.96)	44.20 (19.17)	47.66 (18.65)	49.93 (20.86)	46.63 (19.60)
Sex					
M	1,750 (48.8)	158 (51.6)	348 (47.4)	712 (50.6)	532 (46.6)
F	1,837 (51.2)	148 (48.4)	386 (52.6)	694 (49.4)	609 (53.4)
Sizable infection clustering					
Noncluster cases	2,809 (78.3)	275 (89.9)	617 (84.1)	1,033 (73.5)	884 (77.5)
Cluster cases‡	778 (21.7)	31 (10.1)	117 (15.9)	373 (26.5)	257 (22.5)
Living clusters	159 (4.4)	0 (0.0)	3 (0.4)	99 (7.0)	57 (5.0)
Working clusters	225 (6.3)	8 (2.6)	42 (5.7)	77 (5.5)	98 (8.6)
Dining clusters	248 (6.9)	15 (4.9)	35 (4.8)	137 (9.7)	61 (5.3)
Entertainment clusters	114 (3.2)	8 (2.6)	27 (3.7)	48 (3.4)	31 (2.7)
Others§	33 (0.9)	1 (0.3)	10 (1.4)	12 (0.9)	10 (0.9)
Case classification					
Infection source cases	1,455 (40.6)	133 (43.5)	317 (43.2)	528 (37.6)	477 (41.8)
Probable local cases	95 (2.6)	29 (9.5)	31 (4.2)	24 (1.7)	11 (1.0)
Local cases	1,360 (37.9)	104 (34.0)	286 (39.0)	504 (35.8)	466 (40.8)
Cases epidemiologically linked to infection source cases	2,132 (59.4)	173 (56.5)	417 (56.8)	878 (62.4)	664 (58.2)
Linked to probable local cases	62 (1.7)	12 (3.9)	20 (2.7)	22 (1.6)	8 (0.7)
Linked to local cases	2,070 (57.7)	161 (52.6)	397 (54.1)	856 (60.9)	656 (57.5)
Presence of symptoms					
Asymptomatic	590 (16.4)	44 (14.4)	89 (12.1)	262 (18.6)	195 (17.1)
Symptomatic	2,997 (83.6)	262 (85.6)	645 (87.9)	1144 (81.4)	946 (82.9)
Type of housing					
Public rental housing	1,479 (41.2)	6 (2.0)	243 (33.1)	591 (42.0)	639 (56.0)
Subsidized home ownership	409 (11.4)	6 (2.0)	137 (18.7)	171 (12.2)	95 (8.3)
Private housing	1,377 (38.4)	261 (85.3)	307 (41.8)	469 (33.4)	340 (29.8)
Residential care homes	116 (3.2)	3 (1.0)	6 (0.8)	86 (6.1)	21 (1.8)
Other	206 (5.7)	30 (9.8)	41 (5.6)	89 (6.3)	46 (4.0)
Area-level population density#					
1st quartile	409 (11.4)	82 (26.8)	165 (22.5)	102 (7.3)	60 (5.3)
2nd quartile	752 (21.0)	91 (29.7)	177 (24.1)	275 (19.6)	209 (18.3)
3rd quartile	888 (24.8)	55 (18.0)	200 (27.2)	310 (22.0)	323 (28.3)
4th quartile	1,538 (42.9)	78 (25.5)	192 (26.2)	719 (51.1)	549 (48.1)

*Values are no. (%) except as indicated. We used data current to October 31, 2020.
†The 1st quartile is the wealthiest group and 4th quartile the poorest group.
‡The number of cluster cases differed from the sum of cluster cases across cluster types because one case was involved in both dining and working clusters.
§Traveling, religious, grocery shopping activities.
#The 1st quartile is lowest population density and 4th quartile the highest density.

monthly household income for the corresponding household size in each of the 154 small-area Tertiary Planning Units (*9*); we then grouped these rates into quartiles. Second, we categorized the individual-level housing type into public rental housing, subsidized home ownership, private housing, residential care homes, and others (e.g., villages, industrial and commercial buildings, and staff quarters).

Results of multilevel binary logistic regression with random intercepts at area level showed that case-patients living in the wealthiest areas (i.e., 1st quartile) were 65% less likely to be cases in sizable infection clusters (adjusted OR [aOR] 0.35, 95% CI 0.19–0.65) than those living in the poorest areas (i.e., 4th quartile), after adjusting for confounding factors (Table 2). Area-level socioeconomic patterns of sizable clustering were more apparent among case-patients epidemiologically linked to previously confirmed cases (aOR 0.34, 95% CI 0.18–0.66) than among unlinked source cases (aOR 0.61, 95% CI 0.19–1.97). Such patterns were more pronounced for those in living and working clusters than in dining and entertainment clusters. At the individual level, persons living in residential care homes tended to be part of living-related sizable infection clusters. We observed stark variations in the effect of private housing across cluster categories; case-patients living in private housing had lower odds of being in working clusters (aOR 0.66, 95% CI .45–0.96) but increased odds of being in entertainment clusters (aOR 3.20, 95% CI 1.79–5.72) compared with case-patients living in public rental housing.

Conclusions

This study showed that socioeconomic disadvantage was associated with a wider COVID-19 transmission in the form of sizable infection clustering regardless of epidemic waves (Appendix Table 2); we observed a

stronger socioeconomic pattern in clusters of more essential activities (i.e., living and working) than in clusters of less essential activities (i.e., dining and entertainment). The more apparent socioeconomic pattern of sizable COVID-19 clustering among epidemiologically linked cases suggested that the socioeconomically disadvantaged were not necessarily more prone to contracting the disease from random infection sources but that, once they contracted the disease, their communities were at higher risk for wide transmission of disease.

The stringent social distancing policies imposed by the Hong Kong government seriously disrupted social activities and confined residents to their own homes or local communities. The socioeconomically disadvantaged are particularly likely to be infected if they live in small, overcrowded apartments with poorer ventilation (*10*,*11*). Residential-care homes constituted 6 of 7 living-related infection clusters; these care homes tend to be located in socioeconomically disadvantaged areas, and sizable infection clusters involving care homes started to form when community outbreaks of local transmission became severe in early July 2020 (*1*,*12*). This observation implies that residential care home clusters are usually not only sporadic but also possibly concomitant with an outbreak in the disadvantaged community (*13*).

Work arrangement is another major COVID-19 containment measure with differential socioeconomic impacts. Despite advocacy for the work-from-home arrangement, the socioeconomically disadvantaged often could hardly benefit from this option (*5*). These persons also tend to work in occupations demanding longer hours and more intense social interactions and rely heavily on public transport, which inevitably increased their risk of having contact with infected persons and subsequently spreading the disease within their community. Moreover, the lack of financial subsidies to confirmed case-patients before late November 2020 may have kept these workers or the self-employed, who had no paid sick leave, from opting for necessary COVID-19 testing, thereby hampering early transmission containment. Altogether, we were not surprised to see several sizable infection clusters in the construction, transport, and direct-selling industries in Hong Kong.

Our results shed light on the pervasive social inequalities deeply entrenched in society. The socioeconomically disadvantaged have limited resources and opportunities to overcome structural constraints of the social environment (*14*) and are the ones hardest hit in emergencies or adverse events. The wealthier groups are at risk for infection through entertainment activities, given the propensity for widespread

Table 2. Associations of poverty rate and housing type with sizable coronavirus disease clustering, Hong Kong, 2020*

		aOR (95% CI)†					
	Total	Case classification		Specific activity categories‡			
Category	samples‡	Unlinked‡	Linked‡	Living§	Working§	Dining§	Entertainment§
Area-level income poverty rate¶							
4th quartile	Referent	Referent	Referent	Referent	Referent	Referent	Referent
3rd quartile	0.89 (0.58–1.37)	1.27 (0.73–2.19)	0.81 (0.50–1.29)	0.61 (0.14–2.71)	0.83 (0.46–1.49)	1.00 (0.55–1.81)	1.13 (0.54–2.34)
2nd quartile	0.67 (0.42–1.06)	0.85 (0.42–1.74)	0.64 (0.39–1.07)	0.18 (0.02–1.52)	0.70 (0.37–1.34)	0.82 (0.43–1.56)	0.92 (0.42–2.06)
1st quartile	0.35 (0.19–0.65)	0.61 (0.19–1.97)	0.34 (0.18–0.66)	NA#	0.33 (0.13–0.87)	0.85 (0.37–1.92)	0.47 (0.16–1.35)
Individual-level housing type							
Public rental housing	Referent	Referent	Referent	Referent	Referent	Referent	Referent
Subsidized home ownership	0.97 (0.72–1.31)	1.26 (0.63–2.52)	0.99 (0.69–1.40)	1.22 (0.33–4.49)	0.72 (0.44–1.17)	1.06 (0.70–1.59)	1.27 (0.53–3.06)
Private housing	0.99 (0.77–1.26)	0.86 (0.49–1.51)	1.05 (0.79–1.39)	1.12 (0.46–2.72)	0.66 (0.45–0.96)	0.90 (0.62–1.32)	3.20 (1.79–5.72)
Residential care homes	27.20 (14.16–52.26)	4.69 (0.88–24.97)	22.35 (10.00–49.96)	720.16 (224.14–2,313.84)	NA**	NA#	NA#
Other	0.82 (0.51–1.33)	0.70 (0.22–2.27)	0.84 (0.49–1.46)	3.34 (0.87–12.81)	1.03 (0.53–1.99)	0.27 (0.09–0.82)	1.90 (0.71–5.09)

*Clustering for these data refers to ≥10 epidemiologically linked case-patients who are not all part of the same household, grouped by case classification and activity categories of clusters. aOR, adjusted odds ratio; NA, not available; Ref, reference.
†Variables in the regression model were age (continuous), sex, presence of symptoms, type of housing, area-level income poverty rate (by quartiles), and area-level population density (by quartiles).
‡With reference to confirmed cases who were not classified into any sizable infection clusters.
§With reference to confirmed cases who were not classified into the corresponding activity category of sizable infection clusters.
¶The 1st quartile is the wealthiest group and 4th quartile the poorest group.
#No living cluster cases in the 1st quartile of area-level income poverty rate.
**No cases living in residential homes for respective types of clusters.

dispersion and difficulty in COVID-19 containment in these settings (*15*). Infection control may thus work better for the wealthier groups through restriction of entertainment activities.

A limitation of this study lies in the potential residual confounding as a result of the limited information the CHP released on the confirmed cases. In addition, case-patients who experienced symptoms after COVID-19 diagnosis may have been misclassified as asymptomatic. Moreover, we categorized the sizable infection clusters by social activities; therefore, infected case-patients epidemiologically linked to the source of one cluster were classified into the same activity category of the cluster regardless of their involvement with the specific activities.

In summary, despite relatively low COVID-19 incidence in Hong Kong, transmission containment among socioeconomically disadvantaged persons and communities remains challenging. Consideration of social inequalities is crucial to deploying equitable containment and exit strategies.

Acknowledgments

We thank the team from the COVID-19 in HK (https://covid19.vote4.hk) online platform for integrating and extracting information on residential addresses of all infected cases in Hong Kong for this study.

The Research Grants Council supported G.K.K.C. by postdoctoral fellowship (reference no. PDFS2122-4H02). The US National Academy of Medicine supported R.Y.C. by International Health Policy fellowship.

About the Author

Dr. Chung is a postdoctoral fellow at the Chinese University of Hong Kong Institute of Health Equity. His research focuses primarily on how socioeconomic disadvantages (e.g., low education, poverty, and deprivation) affect population health and health inequalities from a life-course perspective.

References

1. Centre for Health Protection. Latest situation of cases of COVID-19 2020 [cited 2021 Feb 22]. https://www.chp.gov.hk/files/pdf/local_situation_covid19_en.pdf
2. New Zealand Ministry of Health. COVID-19: source of cases [cited 2021 Feb 22]. https://www.health.govt.nz/our-work/diseases-and-conditions/covid-19-novel-coronavirus/covid-19-data-and-statistics/covid-19-source-cases
3. Adam DC, Wu P, Wong JY, Lau EHY, Tsang TK, Cauchemez S, et al. Clustering and superspreading potential of SARS-CoV-2 infections in Hong Kong. Nat Med. 2020;26:1714–9. https://doi.org/10.1038/s41591-020-1092-0
4. Cordes J, Castro MC. Spatial analysis of COVID-19 clusters and contextual factors in New York City. Spat Spatio-Temporal Epidemiol. 2020;34:100355. https://doi.org/10.1016/j.sste.2020.100355
5. Office for National Statistics. Coronavirus (COVID-19) related deaths by occupation, England and Wales: deaths registered up to and including 20 April 2020. 2020 May 11 [cited 2021 Aug 13]. https://www.ons.gov.uk/peoplepopulationandcommunity/healthandsocialcare/causesofdeath/bulletins/coronaviruscovid19relateddeathsbyoccupationenglandandwales/deathsregistereduptoandincluding20april2020
6. Nicodemo C, Barzin S, Cavalli N, Lasserson D, Moscone F, Redding S, et al. Measuring geographical disparities in England at the time of COVID-19: results using a composite indicator of population vulnerability. BMJ Open. 2020;10:e039749. https://doi.org/10.1136/bmjopen-2020-039749
7. Whittle RS, Diaz-Artiles A. An ecological study of socioeconomic predictors in detection of COVID-19 cases across neighborhoods in New York City. BMC Med. 2020;18:271. https://doi.org/10.1186/s12916-020-01731-6
8. COVID-19 in HK. COVID-19 in HK [cited 2021 Feb 22]. https://covid19.vote4.hk
9. Census and Statistics Department. 2016 Population by-census: statistics by large Tertiary Planning Unit group. 2017 [cited 2021 Feb 22]. https://www.bycensus2016.gov.hk/en/bc-dp-tpu.html
10. Chung RY, Chung GK, Gordon D, Mak JK, Zhang LF, Chan D, et al. Housing affordability effects on physical and mental health: household survey in a population with the world's greatest housing affordability stress. J Epidemiol Community Health. 2020;74:164–72. https://doi.org/10.1136/jech-2019-212286
11. Wang J, Huang B, Zhang T, Wong H, Huang Y. Impact of housing and community conditions on multidimensional health among middle- and low-income groups in Hong Kong. Int J Environ Res Public Health. 2018;15:1132. https://doi.org/10.3390/ijerph15061132
12. Woo J. COVID-19 and residential care homes in Hong Kong. Jour Nursing Home Res. 2020;6:20–1. https://doi.org/10.14283/jnhrs.2020.4
13. Burton JK, Bayne G, Evans C, Garbe F, Gorman D, Honhold N, et al. Evolution and effects of COVID-19 outbreaks in care homes: a population analysis in 189 care homes in one geographical region of the UK. Lancet Healthy Longev. 2020;1:e21–31. https://doi.org/10.1016/S2666-7568(20)30012-X
14. Chung GK, Dong D, Wong SY, Wong H, Chung RY. Perceived poverty and health, and their roles in the poverty-health vicious cycle: a qualitative study of major stakeholders in the healthcare setting in Hong Kong. Int J Equity Health. 2020;19:13. https://doi.org/10.1186/s12939-020-1127-7
15. Wong NS, Lee SS, Kwan TH, Yeoh E-K. Settings of virus exposure and their implications in the propagation of transmission networks in a COVID-19 outbreak. Lancet Reg Health West Pac. 2020;4:100052. https://doi.org/10.1016/j.lanwpc.2020.100052

Address for correspondence: Roger Y. Chung, 4/F, School of Public Health and Primary Care, Prince of Wales Hospital, Shatin, NT, Hong Kong, China; email: rychung@cuhk.edu.hk

Prevalence of SARS-CoV-2 Antibodies after First 6 Months of COVID-19 Pandemic, Portugal

Luísa Canto e Castro, Ana Helena Guia Pereira, Rita Ribeiro, Catarina Alves, Luís Veloso, Vera Vicente, Dalila Alves, Inês Domingues, Cláudia Silva, Andreia Gomes, Marta Serrano, Ângela Afonso, Marc Veldhoen, Maria José Rego de Sousa, José Germano Rego de Sousa, Germano de Sousa, Maria M. Mota, Bruno Silva-Santos,[1] Ruy M. Ribeiro[1]

In September 2020, we tested 13,398 persons in Portugal for antibodies against severe acute respiratory syndrome coronavirus 2 by using a quota sample stratified by age and population density. We found a seroprevalence of 2.2%, 3–4 times larger than the official number of cases at the end of the first wave of the pandemic.

Severe acute respiratory syndrome coronavirus 2 (SARS-CoV-2) has spread rapidly worldwide during 2020–2021, but incidence has been highly variable in different countries and is difficult to estimate. In Portugal, which has ≈10.3 million inhabitants, the burden of disease, cases, and deaths was similar to or less than that for neighboring countries during the first wave of the coronavirus disease (COVID-19) pandemic, through September 2020 (Appendix Figure, https://wwwnc.cdc.gov/EID/article/27/11/21-0636-App1.pdf). However, it is difficult to estimate the true extent of SARS-CoV-2 infections in Portugal, although a previous study of clinical patients indicated a seropositivity ≤2.9% (*1*). We report a national, cross-sectional, epidemiologic survey that used quota sampling to quantify more accurately the cumulative number of infected persons in Portugal.

Author affiliations: Fundação Francisco Manuel dos Santos, Lisbon, Portugal (L. Canto e Castro); Universidade de Lisboa, Lisbon (L. Canto e Castro, I. Domingues, C. Silva, A. Gomes, M. Serrano, Â. Afonso, M. Veldhoen, M.M. Mota, B. Silva-Santos, R.M. Ribeiro); Centro de Medicina Laboratorial Germano de Sousa, Lisbon (A.H.G. Pereira, R. Ribeiro, M.J. Rego de Sousa, J.G. Rego de Sousa, G. de Sousa); CTI Clinical Trial and Consulting Services, Portugal (C. Alves, L. Veloso, V. Vicente, D. Alves); Los Alamos National Laboratory, Los Alamos, New Mexico, USA (R.M. Ribeiro)

DOI: https://doi.org/10.3201/eid2711.210636

The Study

We used a convenience quota sampling, quasi-proportional to the population of Portugal in 9 strata: age group (<18, 18–54, and ≥55 years of age), each subdivided by population density of place of residence (<60, 60–500, and >500 persons/km^2) (Appendix). After a widespread media campaign, we recruited participants by using voluntary registration on a website specifically designed for this study. We obtained informed consent from all participants ≥16 years of age and from legal guardians for participants <18 years of age. The study was approved by the Ethics Committee of the Centro Académico de Medicina de Lisboa (#350/20, July 30, 2020).

Blood collections and serologic tests were performed by Centro de Medicina Laboratorial Germano de Sousa (Lisbon, Portugal) by using standard procedures. We determined total antibodies against SARS-CoV-2 by using a chemiluminescent immunoassay test (COV2T; Advia Centaur Siemens, https://www.siemens-healthineers.com), which targets the spike protein. This antibody test has a sensitivity of 98.1% and a specificity of 99.9% (*2*), which we used to correct the seroprevalence estimates by using the Rogan–Gladen estimator (*3*). We used sample weights and poststratified by sex to adjust the seroprevalence, extrapolating from the strata to the whole population (Appendix Tables 1–4). Participants completed a questionnaire with demographic, clinical, and epidemiologic questions regarding SARS-CoV-2 exposure (Appendix). We use standard statistical analyses to compare results at an $\alpha = 0.05$ significance.

We enrolled 13,398 participants (55.3% women, age range 1–92 years) (Appendix Figure 2). Our sample reflected approximately the characteristics of the

[1]These authors were co-senior authors.

Table 1. Prevalence of antibodies against severe acute respiratory syndrome coronavirus 2, by person age, adjusted for sensitivity and specificity, Portugal, September 8–October 14, 2020

	Seroprevalence, % (95% CI), by age, y			
Population density	<18, n = 2,108	18–54, n = 6,495	≥55, n = 4,795	Overall, n = 13,398
Low, n = 2,298	0.6 (0.2–2.8)	1.5 (0.9–2.6)	1.7 (1.0–2.9)	1.4 (1.1–2.2)
Medium, n = 5,006	1.4 (0.8–2.7)	1.7 (1.3–2.4)	1.7 (1.2–2.5)	1.6 (1.4–2.1)
High, n = 6,094	3.5 (2.5–5.0)	3.1 (2.6–3.9)	2.2 (1.7–3.1)	2.9 (2.5–3.4)
Overall	2.4 (1.9–3.3)	2.3 (2.0–2.8)	1.9 (1.6–2.4)	2.2 (2.0–2.5)

population in Portugal, except for overrepresentation of women, persons who had higher levels of education, persons living in households that had >1 person, and workers in the education and health sectors (Appendix Tables 5–7).

We obtained blood samples during September 8–October 14, 2020; a total of ≈90% were obtained by September 19. Overall seroprevalence was 2.2% (95% CI 2.0%–2.5%; n = 296 positive participants) (Table 1). The differences seen among age groups did not reach statistical significance. We found a higher seroprevalence in regions of high population density (2.9%, 95% CI 2.5%–3.4%) versus regions of medium population density (1.6%, 95% CI 1.4%–2.1%) and low population density (1.4%, 95% CI 1.1%–2.2%) (Appendix Figure 3).

Comparing the seroprevalence (2.2% corresponds to ≈226,000 persons in Portugal) with the number of official cumulative confirmed cases (55,720 on August 24 and 76,396 on October 1) (4), we found a 3–4-fold larger number of persons who had antibodies than those reported infected. This factor varied across age groups; we found an ≈9-fold difference for young participants versus a 2–5-fold difference (depending on sex and age) in middle-age and older participants (Figure 1). With our estimate of cumulative cases, we calculated that the infection-fatality rate varied from ≤0.2% in younger persons to up to 9.0% in men >80 years of age (Figure 2). The estimated proportion of asymptomatic persons among seropositive persons was 17.4% (95% CI 14.1%–22.9%); this proportion was much higher for persons <18 years of age (Appendix Table 8).

We found no difference between seropositivity levels in men and women (2.3% vs. 2.1%) (Table 2; Appendix Table 9). There were small differences in seroprevalence by occupation and professional sector; and teleworkers had a lower seroprevalence (1.4%) than nonteleworkers (2.4%) (Table 2). We also did not find differences in seroprevalence for persons who had chronic conditions versus persons who did not (Appendix Table 10). One of the largest differences was between nonsmokers and smokers (2.4% vs. 1.0%) (Table 2).

Of the seropositive participants, 50.0% had never been given a diagnosis as being a case or a suspected case of infection (Appendix Table 11). However, 5% (n = 669) of participants were considered as having a suspected case of COVID-19 before the study (Table 2). This number is consistent with the number of suspected cases, which the national health authorities reported until August 16, 2020, two weeks before the start of our study, when there were a cumulative 468,937 suspected cases (only 54,102 confirmed), corresponding to 4.6% of the population of Portugal.

Conclusions

We found a seroprevalence of 2.2% for antibodies against SARS-CoV-2 in the population of Portugal,

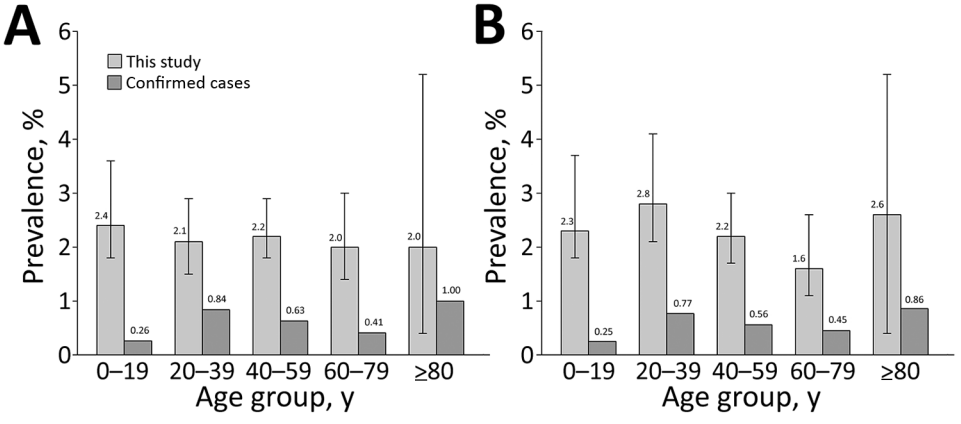

Figure 1. Seroprevalence of antibodies against severe acute respiratory syndrome coronavirus 2, Portugal, compared with official reported confirmed cases, by sex and age. A) Female; B) male. Adjusted seroprevalence measured in this study (numbers above light gray bars) is compared with confirmed cases (numbers above dark gray bars) as a fraction of the corresponding population group (on September 1, 2020). Error bars indicate 95% CIs for estimates. This figure includes different age ranges for consistency with the official data on number of cases by age.

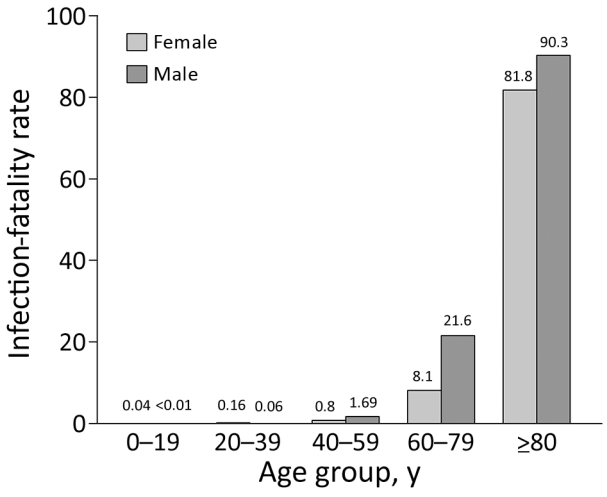

Figure 2. Inferred infection-fatality rate from seroprevalence estimates for antibodies against severe acute respiratory syndrome coronavirus 2, Portugal. We used the registered number of deaths (on September 21, 2020) by age and sex and our prevalence estimates based on seropositivity to infer the infection-fatality rate (Appendix, https://wwwnc.cdc.gov/EID/article/27/11/21-0636-App1.pdf) for more details. Numbers above bars indicate deaths per 1,000 persons.

which was lower than that in a previous smaller study (*1*). Our results suggest that 3–4-fold as many persons were infected by SARS-CoV-2 than was officially reported by health authorities. This factor is consistent with, albeit somewhat smaller than, results reported in other national seroprevalence studies (*5*–*7*) and varied across age groups.

The higher seroprevalence in younger participants is in contrast to the official number of confirmed cases in Portugal, where there is a higher prevalence in older persons (*4*), possibly because younger persons tend to have milder disease, often asymptomatic (*8*,*9*). We found that ≈40% of infections were asymptomatic in persons <18 years of age, whereas this proportion was much lower in older persons. Overall, if only ≈20% of cases are asymptomatic, a question is why so many cases go undetected even with higher testing rates, as in Portugal before our study (*10*). This discrepancy highlights the public health relevance of conducting seroprevalence studies.

Despite a similar prevalence, we found that the infection-fatality rate for men was higher than that for women, particularly in persons >40 years of age. The rate was more than twice as large for persons 60–79 years of age (2.16%) than for the overall group (0.81%). These values are consistent with those reported in Spain (*11*) and include only confirmed COVID-19 deaths, not all excess deaths during this period (*12*).

A limitation of our study is that we used quota sampling, relying on volunteers for the study. We chose our method of recruitment to achieve a fast enrollment process because, during a pandemic, the number of persons positive for antibodies is changing continuously. We reasoned that such changes could bias the study more than the method of recruitment. In addition, even studies with a fully random sample often have a large fraction of persons refusing to participate or unable to be contacted (*6*,*13*). Another limitation is that we used relatively large intervals for age groups. A more fine-grained stratification, along with other variables (e.g., sex), would be more representative of epidemiologic and clinical aspects of SARS-CoV-2, but would require a larger sample. We also did not correct for potential seroreversion (*14*), which reduces the fraction of seropositive results in relation to the actual number of infections and lowers the estimated infection-fatality rate. However, we expect seroreversion over the short 6-month period covered by our study to be minimal (*15*). These potential limitations are common to most seroprevalence studies but do not limit the need for conducting these studies during the evolving pandemic.

Overall, our results demonstrate a low incidence of SARS-CoV-2 during the first wave (spring and summer 2020) of the pandemic in Portugal. This incidence probably resulted from control measures that were relatively successful, in comparison with other countries with higher seroprevalence over similar (or shorter) periods (*6*).

Acknowledgments

We thank the 13,398 volunteers for participating in this study; colleagues at Universidade de Lisboa, Centro de Medicina Laboratorial Germano de Sousa, and CTI Clinical Trial and Consulting Services, in particular Filipa Robalo, Liliana Cunha, and Luis Graça for providing help and assistance; and the 5 anonymous reviewers, whose comments substantially improved the manuscript.

This study was supported by Sociedade Francisco Manuel dos Santos and Grupo Jerónimo Martins. Portions of this study were supported by the LANL LDRD Program (grant 20210730ER), Fundacao para a Ciencia e Tecnologia (Portugal) (grants PTDC/MAT-APL/31602/2017 and UID/MAT/00006/2019), and the European Union Horizon 2020 Research and Innovation Program (grant no. No 952377: iSTARS ERA Chair). M.V. was supported by the European Union H2020 ERA project (grant 667824: EXCELLtoINNOV).

About the Author

Dr. Canto e Castro is professor of statistics at the Faculdade de Ciências da Universidade de Lisboa, Lisbon, Portugal. Her primary research interests are biostatistics; extreme value theory; and collection, analysis, and dissemination of statistical information.

References

1. Kislaya I, Gonçalves P, Barreto M, Sousa R, Garcia AC, Matos R, et al.; ISNCOVID-19 Group. Seroprevalence of SARS-CoV-2 infection in Portugal in May–July 2020: results of the first National Serological Survey (ISNCOVID-19). Acta Med Port. 2021;34:87–94. https://doi.org/10.20344/amp.15122
2. Ainsworth M, Andersson M, Auckland K, Baillie JK, Barnes E, Beer S, et al.; National SARS-CoV-2 Serology Assay Evaluation Group. Performance characteristics of five immunoassays for SARS-CoV-2: a head-to-head benchmark comparison. Lancet Infect Dis. 2020;20:1390–400. https://doi.org/10.1016/S1473-3099(20)30634-4
3. Rogan WJ, Gladen B. Estimating prevalence from the results of a screening test. Am J Epidemiol. 1978;107:71–6. https://doi.org/10.1093/oxfordjournals.aje.a112510
4. Portuguese Ministry of Health. Status Report COVID-19 [in Portuguese] [cited 2021 May 14]. https://covid19.min-saude.pt/relatorio-de-situacao
5. Gudbjartsson DF, Norddahl GL, Melsted P, Gunnarsdottir K, Holm H, Eythorsson E, et al. Humoral immune response to SARS-CoV-2 in Iceland. N Engl J Med. 2020;383:1724–34. https://doi.org/10.1056/NEJMoa2026116
6. Pollán M, Pérez-Gómez B, Pastor-Barriuso R, Oteo J, Hernán MA, Pérez-Olmeda M, et al.; ENE-COVID Study Group. Prevalence of SARS-CoV-2 in Spain (ENE-COVID): a nationwide, population-based seroepidemiological study. Lancet. 2020;396:535–44. https://doi.org/10.1016/S0140-6736(20)31483-5
7. Poustchi H, Darvishian M, Mohammadi Z, Shayanrad A, Delavari A, Bahadorimonfared A, et al. SARS-CoV-2 antibody seroprevalence in the general population and high-risk occupational groups across 18 cities in Iran: a population-based cross-sectional study. Lancet Infect Dis. 2020.
8. Beale S, Hayward A, Shallcross L, Aldridge RW, Fragaszy E. A rapid review and meta-analysis of the asymptomatic proportion of PCR-confirmed SARS-CoV-2 infections in community settings. Wellcome Open Res. 2020;5:266 [cited 2021 Aug 16]. https://doi.org/10.12688/wellcomeopenres.16387.1
9. Syangtan G, Bista S, Dawadi P, Rayamajhee B, Shrestha LB, Tuladhar R, et al. Asymptomatic SARS-CoV-2 carriers: a systematic review and meta-analysis. Front Public Health. 2021;8:587374. https://doi.org/10.3389/fpubh.2020.587374
10. Triunfol M. High COVID-19 testing rate in Portugal. Lancet Infect Dis. 2020;20:783. https://doi.org/10.1016/S1473-3099(20)30499-0
11. Pastor-Barriuso R, Pérez-Gómez B, Hernán MA, Pérez-Olmeda M, Yotti R, Oteo-Iglesias J, et al.; ENE-COVID Study Group. Infection fatality risk for SARS-CoV-2 in community dwelling population of Spain: nationwide seroepidemiological study. BMJ. 2020;371:m4509. https://doi.org/10.1136/bmj.m4509
12. Nogueira PJ, Nobre MA, Nicola PJ, Furtado C, Vaz Carneiro A. Excess mortality estimation during the COVID-19 pandemic: preliminary data from Portugal. Acta Med Port. 2020;33:376–83. https://doi.org/10.20344/amp.13928
13. Hallal PC, Hartwig FP, Horta BL, Silveira MF, Struchiner CJ, Vidaletti LP, et al. SARS-CoV-2 antibody prevalence in Brazil: results from two successive nationwide serological household surveys. Lancet Glob Health. 2020;8:e1390–8. https://doi.org/10.1016/S2214-109X(20)30387-9
14. Shioda K, Lau MS, Kraay AN, Nelson KN, Siegler AJ, Sullivan PS, et al. Estimating the cumulative incidence of SARS-CoV-2 infection and the infection fatality ratio in light of waning antibodies. Epidemiology. 2021;32:518–24. https://doi.org/10.1097/EDE.0000000000001361
15. Figueiredo-Campos P, Blankenhaus B, Mota C, Gomes A, Serrano M, Ariotti S, et al. Seroprevalence of anti-SARS-CoV-2 antibodies in COVID-19 patients and healthy volunteers up to 6 months post disease onset. Eur J Immunol. 2020;50:2025–40. https://doi.org/10.1002/eji.202048970

Address for correspondence: Ruy M. Ribeiro, Department of Theoretical Biology and Biophysics, Los Alamos National Laboratory, Mailstop K710, Los Alamos, NM 87545, USA; email: ruy@lanl.gov

Association of Shared Living Spaces and COVID-19 in University Students, Wisconsin, USA, 2020

John Paul Bigouette, Laura Ford, Hannah E. Segaloff, Kimberly Langolf, Juliana Kahrs, Tara Zochert, Jacqueline E. Tate, Douglas Gieryn, Hannah L. Kirking, Ryan P. Westergaard, Marie E. Killerby

We describe characteristics associated with having coronavirus disease (COVID-19) among students residing on a university campus. Of 2,187 students, 528 (24.1%) received a COVID-19 diagnosis during fall semester 2020. Students sharing a bedroom or suite had approximately twice the odds of contracting COVID-19 as those living alone.

In 2020, multiple outbreaks of coronavirus disease (COVID-19), the disease caused by infection with severe acute respiratory syndrome coronavirus 2 (SARS-CoV-2), were documented in institutions of higher education (IHEs; e.g., colleges and universities) across the United States (*1*–*5*). Before students returned to campus, IHEs implemented measures to reduce the spread of SARS-CoV-2 on campus (*6*–*8*). The congregate nature of on-campus residence halls might increase the odds of contracting SARS-CoV-2 because of close-contact exposure, but the association has not been well studied. We describe characteristics of on-campus students associated with having a SARS-CoV-2 infection, including if they shared living spaces, during the fall semester at a Wisconsin, USA, university.

The Study

The Centers for Disease Control and Prevention (CDC) partnered with the Wisconsin Division of Health Services (WDHS; Madison, WI, USA) and University of Wisconsin—Oshkosh to investigate COVID-19 among on-campus residents during the fall 2020 semester (September 2–December 19). On-campus residents were housed in 8 dormitories (dorms A–H). In 7 dormitories, students resided in double-occupancy rooms (dorm C included 4 triple-occupancy rooms) and shared bathrooms along with a common area per floor. Dorm D was the only dormitory made up of suites in which ≤4 students lived in either 4 single-occupancy or 2 double-occupancy bedrooms with the suite's own bathroom, common area, and kitchen. Not all bedrooms were occupied at their full capacity. After a positive COVID-19 diagnosis, on-campus residents were housed in an isolation dormitory. Students who might have been exposed were housed in a separate quarantine dormitory (*9*,*10*). (Appendix, https://wwwnc.cdc.gov/EID/article/27/11/21-1000-App1.pdf).

Data provided by the university included the number of available rooms, dormitory room types, student housing contracts, serial testing records, and a list of all student COVID-19 cases. For our study, we defined students sharing a bedroom with another student at the start of the semester as having a shared bedroom. Students sharing a suite or defined as having a shared bedroom were classified as having a shared living space. In addition, we defined dormitory floor-level occupancy as the number of occupied rooms divided by the number of rooms per floor. We defined a laboratory-confirmed case as a positive SARS-CoV-2 antigen or reverse transcription PCR test result for any on-campus student during the fall semester (*11*).

All data were analyzed using R version 4.0.2 (R Foundation for Statistical Computing, https://www.r-project.org). We used χ^2 tests, Fisher exact tests, and t-tests to determine differences between COVID-19 cases and noncases. We modeled the association between student characteristics and a laboratory-confirmed COVID-19 case using univariable and multivariable logistic regression; covariates were age, sex, race, ethnicity, all dormitories, and dormitory floor level occupancy. The dormitory with the

Author affiliations: Centers for Disease Control and Prevention, Atlanta, Georgia, USA (J.P. Bigouette, L. Ford, H.E. Segaloff, J.E. Tate, H.L. Kirking, M.E. Killerby); Wisconsin Department of Health Services, Madison, Wisconsin, USA (H.E. Segaloff, R.P. Westergaard); University of Wisconsin–Oshkosh, Oshkosh, Wisconsin, USA (K. Langolf, J. Kahrs, T. Zochert); Winnebago County Health Department, Oshkosh (D. Gieryn)

DOI: https://doi.org/10.3201/eid2711.211000

Table 1. Demographics of on-campus university students in study of coronavirus disease transmission, Wisconsin, USA, September 2–December 19, 2020

Characteristic	Overall	COVID-19 cases*	Non–COVID-19 cases	p value
Total no. persons	2,187	528	1,659	
Age, y, mean (SD)	19.3 (1.1)	19.3 (1.2)	19.2 (0.9)	<0.001
Sex, no. (%)				
F	1,326 (60.6)	324 (61.3)	1,002 (60.4)	0.641
M	820 (37.5)	192 (36.4)	628 (37.8)	
Unknown	41 (1.9)	12 (2.3)	29 (1.8)	
Race, no. (%)				0.017
Alaska Native or Native American	13 (0.6)	5 (0.9)	8 (0.5)	
Asian	86 (3.9)	13 (2.5)	73 (4.4)	
Black or African American	99 (4.5)	20 (3.8)	79 (4.8)	
Native Hawaiian or other Pacific Islander	33 (1.5)	1 (0.2)	32 (1.9)	
White	1,737 (79.4)	434 (82.2)	1,303 (78.5)	
Other	23 (1.1)	2 (0.4)	21 (1.3)	
Unknown/declined	196 (9.0)	53 (10.0)	143 (8.6)	
Ethnicity, no. (%)				0.014
Hispanic or Latino	127 (5.8)	17 (3.2)	110 (6.6)	
Not Hispanic or Latino	1,744 (79.7)	431 (81.6)	1,313 (79.2)	
Unknown/declined	316 (14.5)	80 (15.2)	236 (14.2)	
Dormitory, no. (%)				<0.001
Dorm A	176 (8.1)	33 (6.2)	143 (8.6)	
Dorm B†	206 (9.4)	40 (7.6)	166 (10.0)	
Dorm C	313 (14.3)	78 (14.8)	235 (14.2)	
Dorm D‡	269 (12.3)	83 (15.7)	186 (11.2)	
Dorm E	264 (12.1)	45 (8.5)	219 (13.2)	
Dorm F†	405 (18.5)	126 (23.9)	279 (16.8)	
Dorm G†	204 (9.3)	53 (10.0)	151 (9.1)	
Dorm H	350 (16.0)	70 (13.3)	280 (16.9)	
Shared bedroom, no. (%)§				0.001
Yes	1,630 (74.5)	423 (80.1)	1,207 (72.8)	
No	557 (25.5)	105 (19.9)	452 (27.2)	
Shared living space, no. (%)†				<0.001
Yes	1,787 (81.7)	472 (89.4)	1,315 (79.3)	
No	400 (18.3)	56 (10.6)	344 (20.7)	

*A laboratory-confirmed case was defined as a positive SARS-CoV-2 antigen or reverse transcription PCR test result for any on-campus student during the fall semester.
†First-year student dormitories.
‡Only suite-style dormitory made up of suites where ≤4 students were housed in either 4 single-occupancy or 2 double-occupancy bedrooms with the suite's own bathroom, common area, and kitchen.
§Students who share a bedroom with ≥1 students.

Table 2. Characteristics of living situations for on-campus students at a university in study of coronavirus disease transmission, Wisconsin, USA, September 2–December 19, 2020

	Dormitory*								
Characteristic	A	B†	C	D‡	E	F†	G†	H	Overall
Suite-style dormitory‡	No	No	No	Yes	No	No	No	No	NA
No. occupied floors	4	4	4	5	7	8	4	4	40
No. rooms	122	120	234	264	259	240	115	253	1,607
No. occupied bedrooms	107	110	202	216	186	218	108	223	1,307
Overall dormitory occupancy rate, %	87.7	91.7	86.3	81.8	71.8	90.8	93.9	88.1	81.3
Dormitory floor occupancy rate,§ mean % (SD)	87.7 (0.5)	90.1 (15.9)	86.3 (6.0)	82.1 (6.7)	72.2 (14.9)	86.8 (9.3)	89.9 (7.7)	88.1 (2.9)	85.4 (8.0)
No. student population	176	206	313	269	264	405	204	350	2,187
Students per dormitory floor, mean (SD)	44.0 (6.6)	51.5 (15.2)	78.3 (14.1)	53.8 (5.9)	37.7 (10.6)	50.6 (12.0)	51.0 (12.7)	87.5 (14.8)	54.7 (11.5)
No. COVID-19 cases¶	33	40	78	83	45	126	53	70	528
% Students positive	18.8	19.4	24.9	30.9	17.0	31.1	26.0	20.0	24.1

*Each dormitory floor had a shared common space and bathrooms except dorm D.
†First-year student dormitories.
‡Only suite-style dormitory comprised of suites where ≤4 students were housed in either 4 single- or 2 double-occupancy bedrooms with the suite's own bathroom, common area, and kitchen.
§Dormitory floor-level occupancy was defined as the number of occupied rooms divided by the number of rooms per floor.
¶A laboratory-confirmed case was defined as a positive severe acute respiratory syndrome coronavirus 2 antigen or reverse transcription PCR test result for any on-campus student during the fall semester.

lowest COVID-19 positivity for the semester was the reference group. Sharing a bedroom or living space were analyzed in separate models. We conducted our investigation consistent with applicable federal laws and CDC policy (e.g., 45 C.F.R. part 46.102(l)(2), 21 C.F.R. part 56; 42 U.S.C. §241(d); 5 U.S.C. 145 §552a; 44 U.S.C. §3501 et seq.). CDC and WDHS reviewed the investigation; in addition, the university's ethics review board determined the activities to be nonresearch public health surveillance.

At the start of the fall semester, 2,187 students had on-campus housing contracts. The median age of on-campus students was 19 years; 60.5% were female, 79.4% White, and 79.7% non-Hispanic/Latino (Table 1). Dormitory student populations range was 176–405 students per dormitory, with a mean of 55 students per occupied dormitory floor and a mean floor occupancy of 85% (Table 2) at semester start. Overall, 74.5% of students shared a bedroom and 81.7% of students shared a living space.

During the semester, 528 (24.1%) COVID-19 cases were identified among on-campus students. The percentage of students diagnosed with COVID-19 was 17.0%–31.1% across dormitories for the fall semester; the lowest percent positivity was in dorm E. All dormitories saw a rise in cases in mid- to late September (Figure 1).

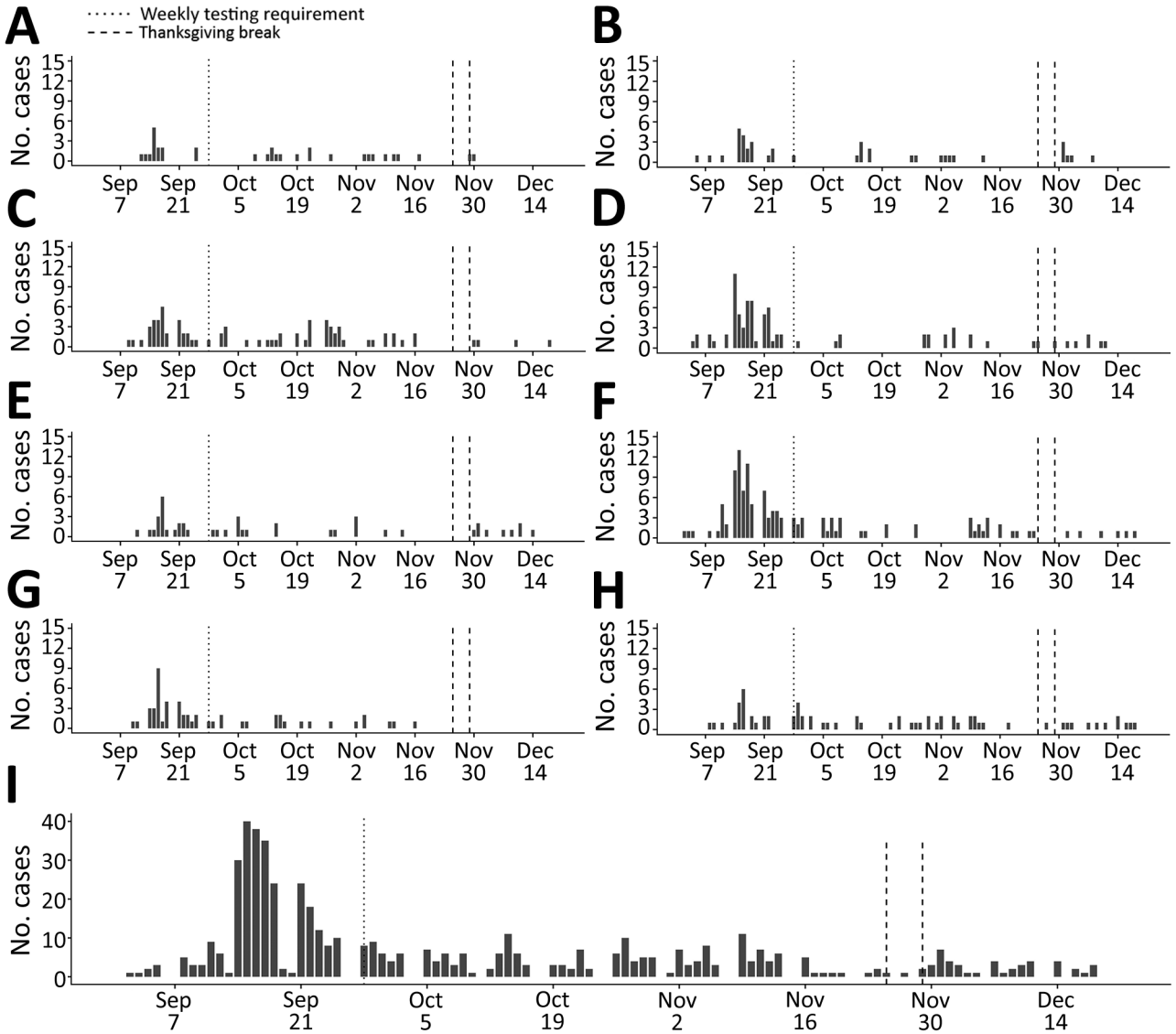

Figure 1. Epidemic curves of daily coronavirus disease cases in each of 8 dormitories (A–H) and overall (I) for a total of 528 cases at a university in Wisconsin, USA, September 2–December 19, 2020. Vertical dotted lines indicate the change in testing requirement from biweekly to weekly. On-campus students returning after the Thanksgiving break (November 25–29, 2020; vertical dashed lines) were required to test before leaving campus and twice >48 hours apart upon returning to campus. Dorms A, B, F, and G house first-year students. Dorm D is made up of suites of 4 single- or 2 double-occupancy bedrooms with a shared bathroom, common area, and kitchen.

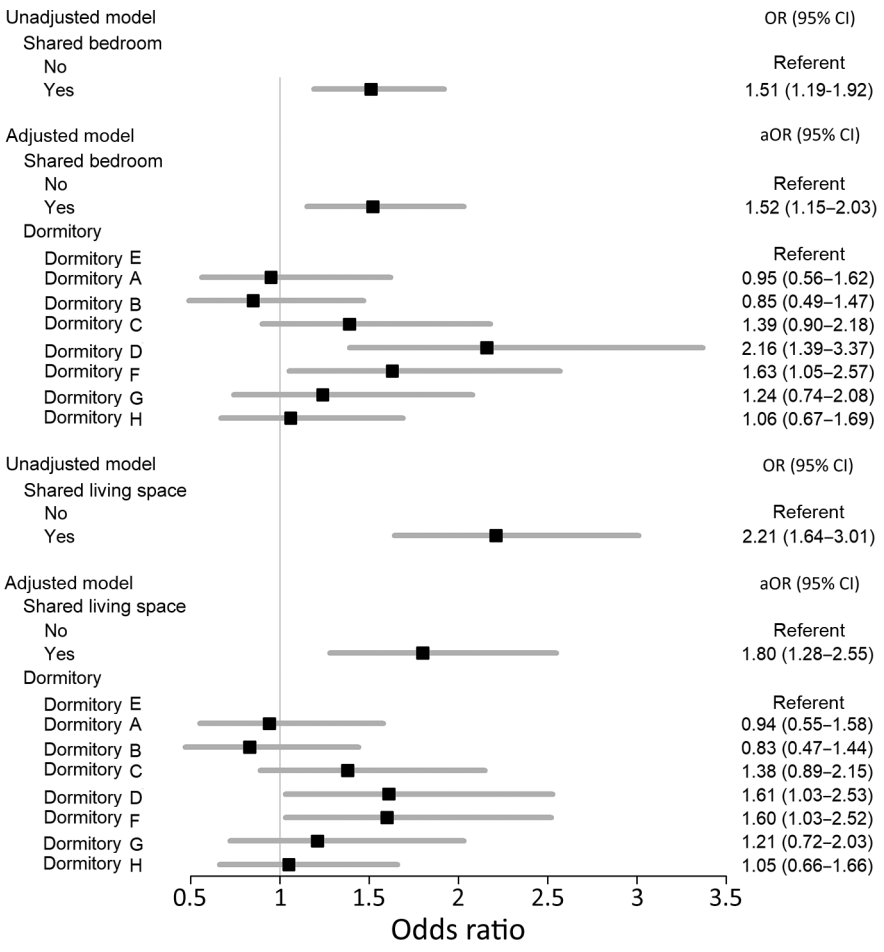

Figure 2. Associations between shared living spaces and coronavirus disease (COVID-19) at a university (N = 2,187), Wisconsin, USA, September 2–December 19, 2020. Black boxes indicate odds ratios; gray bars indicate 95% CIs. Models were adjusted for age, sex, race, ethnicity, dormitories, and floor level occupancy (%). Shared living space was defined as one in which >2 students share either a bedroom or suite. Dorms A, B, F, and G housed first-year students. Dorm E was selected as the reference group because it had the lowest semester COVID-19 positivity among on-campus residents. Dorm D is composed of suites of 4 single-occupancy or 2 double-occupancy bedrooms with a shared bathroom, common area, and kitchen. aOR, adjusted odds ratio; OR, odds ratio.

Using a univariable regression model, we found that students who shared a bedroom had 1.52 (95% CI 1.19–1.92) times the odds of receiving a COVID-19 diagnosis as students who lived alone (Figure 2). The effect estimate remained unchanged in the adjusted multivariable regression model (Appendix Table 1). However, in the adjusted model, students with a shared living space (e.g., suites and bedrooms) had 1.80 (95% CI 1.28–2.55) times the odds of testing positive for COVID-19 compared with students living alone. After controlling for shared living status, students from 2 dormitories, dorms D and F, had higher odds for COVID-19 than dorm E students in both models.

CDC has provided guidance on prevention measures to reduce the transmission of SARS-CoV-2 at IHEs (*6*,*8*). Similar to other IHE outbreak reports from the United States, the university saw a surge in cases during September (*1*,*3*–*5*). After the surge, the university updated their COVID-19 prevention plan such that residential students were tested weekly instead of biweekly for SARS-CoV-2, messaging on COVID-19 prevention measures increased, and on-campus dining was limited to takeout only for 2 weeks.

Conclusions

Despite this university's updated COVID-19 prevention plan, students sharing a suite or bedroom had higher odds of being diagnosed with COVID-19. SARS-CoV-2 household transmission studies have shown that households are a significant transmission source for both symptomatic and asymptomatic persons (*12*,*13*). For example, a meta-analysis found that the household SARS-CoV-2 secondary attack rate was 16.6% (*8*,*12*). Reducing the number of students with roommates or those in suite-style units is needed to limit SARS-CoV-2 transmission.

After adjusting for sharing bedrooms or living spaces, students from 2 dormitories still had higher odds of having COVID-19 than students from the dormitory with the lowest percentage of positive students. This finding could be associated with differing student attitudes and social behaviors towards COVID-19 (*14*).

Racial and ethnic disparities in COVID-19 incidence have been found in persons <25 years of age in the United States (*15*). However, we found that Native Hawaiian or other Pacific Islander students had lower odds of having COVID-19 compared with White students, and Hispanic students had lower odds than non-Hispanic students: adjusted odds ratio for Native Hawaiian or other Pacific Islander students was 0.13 (95% CI 0.01–0.63) and for Hispanic students it was 0.56 (95% CI 0.31–0.96). We observed no other associations by age, sex, race category, and dormitory floor occupancy. These results should be interpreted with caution; our findings could be the result of low sample sizes in some groups or residual confounding.

The first limitation of our study is that findings from this IHE may not be generalizable for all IHEs. Second, these results characterize an association between sharing a living space and COVID-19 and do not necessarily indicate roommate transmission. Third, students may have moved out of the dormitory during the semester, causing an underestimation of attack rates and misclassification of those students with roommates or suitemates for the term. Last, because this investigation was cross-sectional in design, a causal relationship cannot be determined.

In summary, sharing a living space or bedroom was associated with increased odds of having COVID-19 even with COVID-19 prevention policies at a Wisconsin university. Reducing the number of students sharing living spaces could further prevent the spread of SARS-CoV-2 on-campus as part of COVID-19 prevention practices at IHEs.

About the Author

Dr. Bigouette is an Epidemic Intelligence Service Officer in the Polio Eradication Branch, Global Immunization Division, Center for Global Health, Centers for Disease Control and Prevention. His primary research interests include infectious disease and disaster epidemiology, emergency management and response, and vaccine-preventable disease work.

References

1. Fox MD, Bailey DC, Seamon MD, Miranda ML. Response to a COVID-19 outbreak on a university campus—Indiana, August 2020. MMWR Morb Mortal Wkly Rep. 2021;70:118–22. https://doi.org/10.15585/mmwr.mm7004a3
2. Pray IW, Kocharian A, Mason J, Westergaard R, Meiman J. Trends in outbreak-associated cases of COVID-19—Wisconsin, March–November 2020. MMWR Morb Mortal Wkly Rep. 2021;70:114–7. https://doi.org/10.15585/mmwr.mm7004a2
3. Vang KE, Krow-Lucal ER, James AE, Cima MJ, Kothari A, Zohoori N, et al. Participation in fraternity and sorority activities and the spread of COVID-19 among residential university communities—Arkansas, August 21–September 5, 2020. MMWR Morb Mortal Wkly Rep. 2021;70:20–3. https://doi.org/10.15585/mmwr.mm7001a5
4. Wilson E, Donovan CV, Campbell M, Chai T, Pittman K, Seña AC, et al. Multiple COVID-19 clusters on a university campus—North Carolina, August 2020. MMWR Morb Mortal Wkly Rep. 2020;69:1416–8. https://doi.org/10.15585/mmwr.mm6939e3
5. Leidner AJ, Barry V, Bowen VB, Silver R, Musial T, Kang GJ, et al. Opening of large institutions of higher education and county-level COVID-19 incidence—United States, July 6–September 17, 2020. MMWR Morb Mortal Wkly Rep. 2021;70:14–9. https://doi.org/10.15585/mmwr.mm7001a4
6. Centers for Disease Control and Prevention. Coronavirus disease 2019 (COVID-19): testing, screening, and outbreak response for institutions of higher education (IHEs). 2020 [cited 2021 Feb 20]. https://www.cdc.gov/coronavirus/2019-ncov/community/colleges-universities/ihe-testing.html
7. Walke HT, Honein MA, Redfield RR. Preventing and responding to COVID-19 on college campuses. JAMA. 2020;324:1727–8. https://doi.org/10.1001/jama.2020.20027
8. Centers for Disease Control and Prevention. Coronavirus disease 2019 (COVID-19): considerations for institutions of higher education. 2020 [cited 2021 Feb 23]. https://www.cdc.gov/coronavirus/2019-ncov/community/colleges-universities/considerations.html
9. Centers for Disease Control and Prevention. Coronavirus disease 2019 (COVID-19): when to quarantine. 2021 [cited 23 Feb 2021]. https://www.cdc.gov/coronavirus/2019-ncov/if-you-are-sick/quarantine.html
10. Centers for Disease Control and Prevention. Coronavirus disease 2019 (COVID-19): isolate if you are sick. 2021 [cited 2021 Feb 22]. https://www.cdc.gov/coronavirus/2019-ncov/if-you-are-sick/isolation.html
11. Council of State and Territorial Epidemiologists. Coronavirus disease 2019 (COVID-19) 2020 interim case definition. 2020 [cited 2021 Feb 23]. https://wwwn.cdc.gov/nndss/conditions/coronavirus-disease-2019-covid-19/case-definition/2020/08/05/
12. Madewell ZJ, Yang Y, Longini IM, Jr, Halloran ME, Dean NE. Household transmission of SARS-CoV-2: a systematic review and meta-analysis. JAMA Network Open. 2020;3:e2031756. https://doi.org/10.1001/jamanetworkopen.2020.31756
13. Grijalva CG, Rolfes MA, Zhu Y, McLean HQ, Hanson KE, Belongia EA, et al. Transmission of SARS-COV-2 infections in households —Tennessee and Wisconsin, April–September 2020. MMWR Morb Mortal Wkly Rep. 2020;69:1631–4. https://doi.org/10.15585/mmwr.mm6944e1
14. Cohen AK, Hoyt LT, Dull B. A descriptive study of COVID-19–related experiences and perspectives of a national sample of college students in spring 2020. J Adolesc Health. 2020;67:369–75. https://doi.org/10.1016/j.jadohealth.2020.06.009
15. Van Dyke ME, Mendoza MCB, Li W, Parker EM, Belay B, Davis EM, et al. Racial and ethnic disparities in COVID-19 incidence by age, sex, and period among persons aged <25 years—16 US jurisdictions, January 1–December 31, 2020. MMWR Morb Mortal Wkly Rep. 2021;70:382–388. http://dx.doi.org/10.15585/mmwr.mm7011e1

Address for correspondence: John Paul Bigouette, Centers for Disease Control and Prevention, 1600 Clifton Rd NE, Mailstop H24-2, Atlanta, GA 30329-4027, USA; email: JBigouette@cdc.gov

Correlation of SARS-CoV-2 Subgenomic RNA with Antigen Detection in Nasal Midturbinate Swab Specimens

Katherine Immergluck,[1] Mark D. Gonzalez, Jennifer K. Frediani, Joshua M. Levy, Janet Figueroa, Anna Wood, Beverly B. Rogers, Jared O'Neal, Roger Elias-Marcellin, Allie Suessmith, Julie Sullivan, Raymond F. Schinazi, Ahmed Babiker, Anne Piantadosi, Miriam B. Vos, Greg S. Martin, Wilbur A. Lam, Jesse J. Waggoner

Among symptomatic outpatients, subgenomic RNA of severe acute respiratory syndrome coronavirus 2 in nasal midturbinate swab specimens was concordant with antigen detection but remained detectable in 13 (82.1%) of 16 nasopharyngeal swab specimens from antigen-negative persons. Subgenomic RNA in midturbinate swab specimens might be useful for routine diagnostics to identify active virus replication.

Accurate detection of severe acute respiratory syndrome coronavirus 2 (SARS-CoV-2) infection is critical for patient management and infection control (*1*). Molecular diagnostics are highly sensitive in the acute phase of coronavirus diseases (COVID-19), but viral RNA remains detectable long after replicating virus can be isolated from respiratory samples (*1*–*5*). Antigen diagnostics, though often less sensitive, are touted as providing accurate detection during peak infectivity, thereby identifying persons most likely to transmit SARS-CoV-2 (*6*,*7*).

Prolonged SARS-CoV-2 RNA detection has led to evaluation of molecular assays to detect subgenomic RNA (sgRNA) or negative-strand RNA, which are produced during active viral replication (*2*–*5*,*8*–*10*). sgRNA detection has predominantly been studied in hospitalized adults who have COVID-19 (*2*,*3*,*5*,*8*,*9*); published reports have not compared sgRNA and antigen detection, which should be highly correlated. We compared real-time reverse transcription PCR (rRT-PCR) detection of nucleocapsid sgRNA, the most abundant sgRNA in SARS-CoV-2–infected cells (*2*), with nucleocapsid antigen detection among symptomatic outpatients who had SARS-CoV-2 infections.

The Study

We obtained 88 nasal midturbinate and 39 nasopharyngeal swab specimens (PurFlock Ultra Flocked Swabs; Puritan Medical Products, https://www.puritanmedproducts.com) from 127 persons who came to COVID-19 testing centers affiliated with Emory University and Children's Healthcare of Atlanta (Atlanta, GA, USA) during January 2021. Inclusion criteria were a symptomatic respiratory illness for ≤7 days and a positive, routine-care SARS-CoV-2 molecular test (nasopharyngeal swab specimen). The study was approved by the Emory University Institutional Review Board and Children's Healthcare of Atlanta.

We extracted total nucleic acids from 500 µL of sample and eluted them into a volume of 50 µL by using an EMAG Instrument (bioMérieux, https://www.biomerieux.com). We tested eluates side-by-side in rRT-PCRs for sgRNA and total SARS-CoV-2 RNA (genomic plus sgRNA). For sgRNA, we combined a forward primer in the leader sequence (5′-CGATCTCTTGTAGATCTGTTCTC-3′) with the nucleocapsid 2 (N2) target reverse primer and probe (*11*).

Author affiliations: Emory University, Atlanta, Georgia, USA (K. Immergluck, M.D. Gonzalez, J.K. Frediani, J.M. Levy, J. Figueroa, A. Wood, B.B. Rogers, J. O'Neal, R. Elias-Marcellin, A. Suessmith, J. Sullivan, R.F. Schinazi, A. Babiker, A. Piantadosi, M.B. Vos, G.S. Martin, W.A. Lam, J.J. Waggoner); The Atlanta Center for Microsystems-Engineered Point-of-Care Technologies, Atlanta (K. Immergluck, M.D. Gonzalez, J.K. Frediani, J.M. Levy, J. Figueroa, A. Wood, B.B. Rogers, J. O'Neal, A. Suessmith, J. Sullivan, R.F. Schinazi, M.B. Vos, G.S. Martin, W.A. Lam, J.J. Waggoner); Children's Healthcare of Atlanta, Atlanta (M.D. Gonzalez, M.B. Vos)

DOI: https://doi.org/10.3201/eid2711.211135

[1]Current affiliation: Pomona College, Claremont, California, USA.

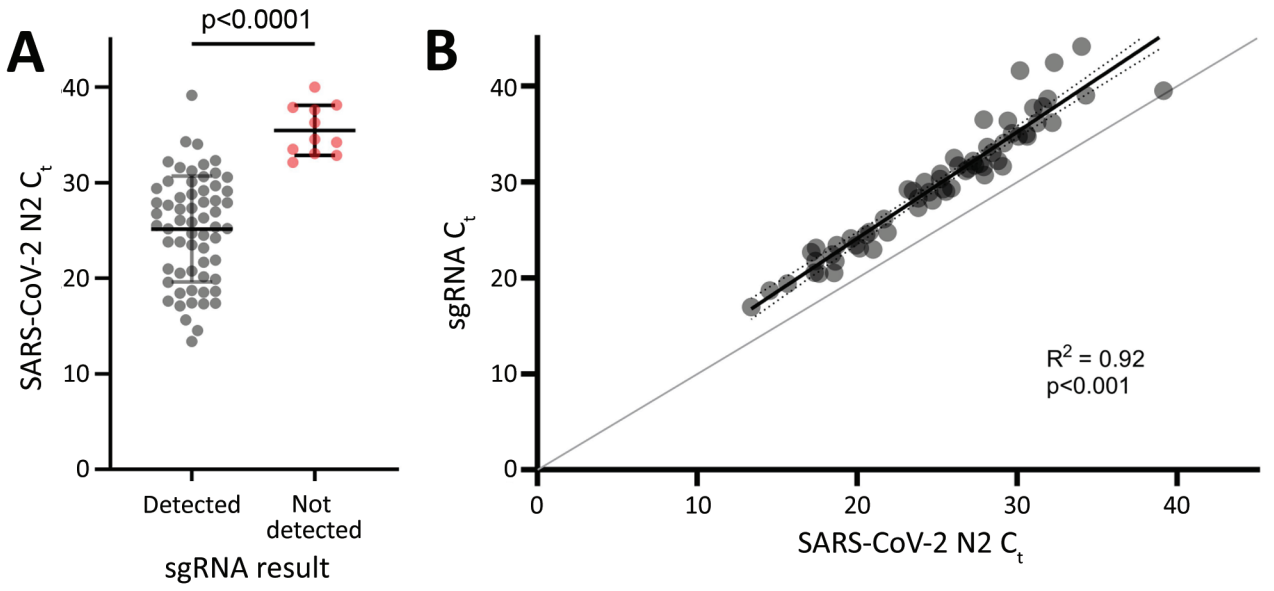

Figure 1. Correlation of sgRNA levels with total SARS-CoV-2 RNA in samples from study participants in Atlanta, Georgia, USA. A) N2 C_t values for samples in which sgRNA was detectable (gray dots) or not detectable (red dots). Horizontal bars indicate means, and error bars indicate SDs. B) sgRNA C_t values versus corresponding C_t values for the N2 target. Results of simple linear regression (black line) and error bars (dotted lines) are shown. Line of identity (gray line) is shown for reference. C_t, cycle threshold; N2, nucleocapsid 2; SARS-CoV-2, severe acute respiratory syndrome coronavirus 2; sgRNA, subgenomic RNA.

We performed the sgRNA assay in 20-μL reactions using the Luna Probe One-Step RT-qPCR Kit (New England Biolabs, https://www.neb.com) with 500 nmol/L of each primer, 250 nmol/L of probe, and 5 μL of eluate by using the following conditions: 55°C for 15 min, 95°C for 2 min, and 45 cycles of 95°C for 15 s and 60°C for 60 s. We detected total SARS-CoV-2 RNA by using a duplex N2-RNase P rRT-PCR performed as described (*12*). We obtained an anterior nares swab specimen for nucleocapsid antigen detection with the Abbott BinaxNOW COVID-19 Ag Card (swabs supplied with the BinaxNOW kit; Abbott Laboratories, https://www.abbott.com) performed per the package insert.

The first 73 participants had a midturbinate swab specimen available for molecular testing (evaluation group) and have been described (*13*). The subsequent 54 participants had dedicated midturbinate (n = 15) or residual nasopharyngeal (n = 39) swab specimens for molecular testing and available antigen test results (antigen testing group) (Appendix Figure 1, https://wwwnc.cdc.gov/EID/article/27/11/21-1135-App1.pdf).

We estimated nucleocapsid sgRNA as a percentage of total RNA by calculating copies per microliter of sgRNA and total RNA for each sample based on a standard curve for each target and then calculating the percentage of sgRNA. We used unpaired t-tests to compare continuous variables and the Fisher exact test for testing categorical variables. We performed simple linear regression to compare cycle threshold (C_t) values for sgRNA and total RNA. We conducted

Table 1. Demographic and clinical variables of study participants who had MT swab specimens in antigen-testing group analyzed for SARS-CoV-2 subgenomic RNA, Atlanta, Georgia, USA*

Variable	Overall, n = 15	Antigen positive, n = 8	Antigen negative, n = 7	p value
Mean age, y (SD)	54.35 (14.49)	53.98 (16.12)	54.78 (13.65)	0.921
Female sex	9 (60.00)	5 (62.50)	4 (57.14)	1.000
Mean days after symptom onset (SD)†	4.14 (2.44)	3.88 (2.23)	4.50 (2.88)	0.655
MT swab specimen, rRT-PCR positive	12 (80.0)	8 (100.0)	4 (57.1)	0.077
Race‡				
White	2 (14.3)	0	3 (33.3)	0.026
Black/African American	11 (78.6)	8 (100.0)	3 (50.0)	NA
Asian	11 (78.6)	8 (100.0)	3 (50.0)	NA

*Values are no. (%) unless indicated otherwise. MT, nasal midturbinate; NA, not available; rRT-PCR, real-time reverse transcription PCR; SARS-CoV-2, severe acute respiratory syndrome coronavirus 2.
†Day sample was collected.
‡One participant did not identify race; none identified as Hispanic.

Table 2. Correlation of SARS-CoV-2 subgenomic RNA with nucleocapsid detection in NP specimens from study participants analyzed for SARS-CoV-2 subgenomic RNA, Atlanta, Georgia, USA *

Variable	Overall, n = 39	Antigen positive, n = 20	Antigen negative, n = 19	p value
Mean age, y (SD)	8.6 (5.8)	9.8 (5.6)	7.4 (5.8)	0.148
Female sex	16 (41.0)	8 (40.0)	8 (42.1)	0.894
Mean days after symptom onset (SD)†	3.7 (2.2)	3.0 (1.4)	4.5 (2.7)	0.227
Repeat NP swab specimen, rRT-PCR positive	36 (92.3)	20 (100.0)	16 (84.2)	0.106
Race				
White	26 (66.67)	13 (65.0)	13 (68.42)	0.077
Black/African American	6 (15.38)	3 (15.0)	3 (15.79)	NA
Asian	4 (10.26)	4 (20.0)	0	NA
Biracial	3 (7.69)	0	3 (15.79)	NA
Hispanic ethnicity	19 (48.72)	6 (30.0)	13 (68.42)	0.016

*Values are no. (%) unless indicated otherwise. NA, not available; NP, nasopharyngeal; rRT-PCR, real-time reverse transcription PCR; SARS-CoV-2, severe acute respiratory syndrome coronavirus 2.
†Day sample was collected. One participant was asymptomatic (did not report symptoms in the past 14 days).

analyses by using GraphPad version 9.02 (https://www.graphpad.com) and SAS version 9.4 (https://support.sas.com).

The evaluation group included midturbinate swab specimens from 36 adults and 37 children. All samples (73/73) were positive for SARS-CoV-2 by rRT-PCR. Samples with detectable sgRNA (62/73, 84.9%) had significantly lower C_t values, indicative of higher viral loads, than samples without detectable sgRNA (mean C_t 25.1, SD 5.5, vs. mean C_t 35.5, SD 2.6; p<0.0001) (Figure 1, panel A). sgRNA was detectable in all samples (49/49) that had N2 C_t values <30 compared with 13 (54.2%) of 24 samples that had C_t values ≥30 (p<0.0001). Although sgRNA rRT-PCR amplification efficiency was slightly lower than that for the N2 assay, there was a strong linear correlation between sgRNA and N2 C_t values (Figure 1, panel B), and the assay provided linear sgRNA detection across the range of N2 C_t values observed in this study (Appendix Figure 2). sgRNA C_t values were a mean of 4.8 (SD 1.8) cycles higher than corresponding N2 C_t values, and nucleocapsid gene sgRNA accounted for a mean of 1.4% (SD 1.1%) of SARS-CoV-2 RNA. Samples from children had higher viral loads than samples from adults, although the relative amount of sgRNA did not differ (Appendix Figure 3).

We complied characteristics of participants in the antigen-testing group who had midturbinate (n = 15) swab specimens (Table 1) and nasopharyngeal (n = 39) swab specimens (Table 2). All midturbinate swab specimens from participants who had detectable antigen (n = 8) were also positive for sgRNA, whereas 0/4 samples from antigen-negative persons were positive (κ 1.0). Samples that had detectable sgRNA had significantly lower C_t values (mean 25.8, SD 2.7) than samples that did not have detectable sgRNA (mean 36.3, SD 1.8; p = 0.002) (Figure 2).

All (20/20) nasopharyngeal swab specimens from antigen-positive participants were positive for sgRNA. N2 C_t values were significantly lower among antigen-positive participants (mean 18.2, SD 5.0) than antigen-negative participants (mean 27.8, SD 4.5; p<0.0001) (Figure 2). sgRNA was detectable in 13 (81.2%) of 16 nasopharyngeal swab specimens from antigen-negative persons. Days after symptom onset (when the sample was collected) did not differ significantly between antigen-positive and sgRNA-positive/antigen-negative participants (mean 3.4, SD 1.9 days, vs. mean 3.8, SD 2.4 days; p = 0.6).

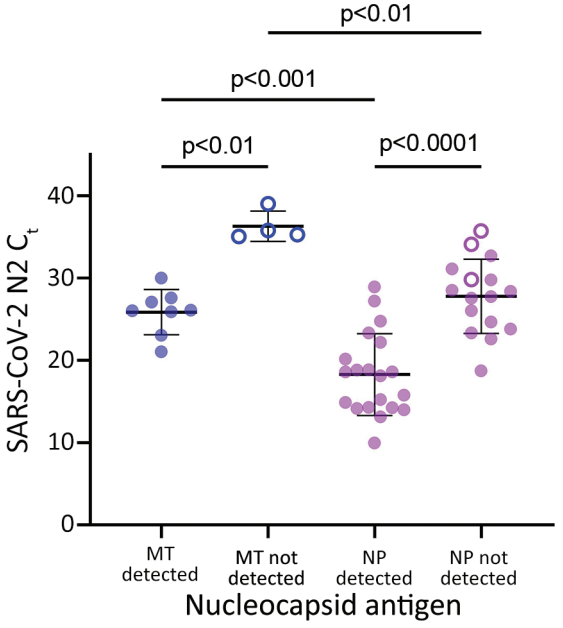

Figure 2. Concordance of SARS-CoV-2 sgRNA with nucleocapsid antigen detection in MT swab specimens, but not NP swab specimens, from study participants in Atlanta, Georgia, USA. sgRNA remains detectable in NP swab specimens for persons who showed negative results for nucleocapsid antigen. Symbols represent MT (blue) and NP (purple) swab specimens for persons with (filled circles) and without (open circles) detectable sgRNA. Horizontal bars indicate means, and error bars indicate SDs. C_t, cycle threshold; MT, nasal midturbinate; NP, nasopharyngeal; N2, nucleocapsid 2; SARS-CoV-2, severe acute respiratory syndrome coronavirus 2; sgRNA, subgenomic RNA.

Nucleocapsid gene sgRNA accounted for a smaller percentage of total SARS-CoV-2 RNA in antigen-negative participants (mean 0.6%, SD 0.4%) vs. antigen-positive participants (mean 1.0%, SD 0.5%; p = 0.012) (Appendix Figure 4). Compared with midturbinate swab specimens, nasopharyngeal swab specimens had lower C_t values for RNase P (Appendix Figure 5).

Conclusions

SARS-CoV-2 sgRNA was detected in all samples from antigen-positive participants (28/28 total), consistent with identification of active viral replication and potential shedding (*4*,*5*,*8*). However, among antigen-negative participants, sgRNA detection varied between SARS-CoV-2 RNA-positive midturbinate (0/4) and nasopharyngeal (13/16) swab specimens. Although nasopharyngeal swab specimens are expected to have higher viral loads (*14*), this difference did not appear to be the sole explanation. sgRNA represented a smaller proportion of total SARS-CoV-2 RNA in discordant nasopharyngeal swab specimens, and overall, nasopharyngeal swab specimens had higher amounts of human cellular material (lower RNase P C_t values) than midturbinate swab specimens. Therefore, discordant sgRNA and antigen results in nasopharyngeal swab specimens probably resulted from persistent detection of waning SARS-CoV-2 infections with low levels of detectable sgRNA, which is only found in infected cells but insufficient viral replication to yield detectable nucleocapsid antigen in the anterior nares.

Nucleocapsid antigen was detected by using the widely available BinaxNOW COVID-19 Ag Card. This card demonstrates similar performance to other rapid antigen tests, which commonly detect nucleocapsid protein, and maintains analytical sensitivity against SARS-CoV-2 variants (*7*). Therefore, it provided a useful and relevant comparator for sgRNA detection.

Limitations of our study include a relatively small number of midturbinate swab specimens tested in the antigen-testing group, which was affected by the need for multiple swab specimens at a single time point. The race/ethnicity makeup of groups that had midturbinate and nasopharyngeal swab specimens differed (Tables 1, 2), although this limitation is not expected to have affected our findings (*15*).

In conclusion, sgRNA detection in midturbinate swab specimens correlates with nucleocapsid antigen and could be implemented as a molecular test to evaluate infectivity. Given the strong correlation between sgRNA, nucleocapsid antigen, and total SARS-CoV-2 RNA, these data also support use of antigen testing or establishment of rRT-PCR C_t values as markers of active replication.

Acknowledgments

We thank the staff of the Atlanta Center for Microsystems Engineered Point-of-Care Technologies for their contributions and efforts, and study participants and family members for providing samples and clinical information.

This study was supported by the National Institutes of Health/National Institute of Biomedical Imaging and Bioengineering (grants U54 EB027690 02S1 and UL1 TR002378).

About the Author

At the time of this study, Ms. Immergluck was a research specialist in the Division of Infectious Diseases, Emory University School of Medicine, Atlanta, GA. She is currently completing her final year at Pomona College, Claremont, CA. Her research interest is development of new molecular methods for the detection of RNA viruses.

References

1. Centers for Disease Control and Prevention. Healthcare workers: information on COVID-19. 2021, March 31, 2021 [cited 2021] Apr 21 https://www.cdc.gov/coronavirus/2019-ncov/hcp
2. Dimcheff DE, Valesano AL, Rumfelt KE, Fitzsimmons WJ, Blair C, Mirabelli C, et al. SARS-CoV-2 total and subgenomic RNA viral load in hospitalized patients. J Infect Dis. 2021 Apr 19 [Epub ahead of print]. https://doi.org/10.1093/infdis/jiab215
3. Hogan CA, Huang C, Sahoo MK, Wang H, Jiang B, Sibai M, et al. Strand-specific reverse transcription PCR for detection of replicating SARS-CoV-2. Emerg Infect Dis. 2021;27:632–5. https://doi.org/10.3201/eid2702.204168
4. Perera RA, Tso E, Tsang OT, Tsang DN, Fung K, Leung YW, et al. SARS-CoV-2 virus culture and subgenomic RNA for respiratory specimens from patients with mild coronavirus disease. Emerg Infect Dis. 2020;26:2701–4. https://doi.org/10.3201/eid2611.203219
5. van Kampen JJ, van de Vijver DA, Fraaij PL, Haagmans BL, Lamers MM, Okba N, et al. Duration and key determinants of infectious virus shedding in hospitalized patients with coronavirus disease-2019 (COVID-19). Nat Commun. 2021;12:267.https://doi.org/10.1038/s41467-020-20568-4
6. Mina MJ, Parker R, Larremore DB. Rethinking COVID-19 test sensitivity: a strategy for containment. N Engl J Med. 2020;383:e120.https://doi.org/10.1056/NEJMp2025631
7. Frediani JK, Levy JM, Rao A, Bassit L, Figueroa J, Vos MB, et al. Multidisciplinary assessment of the Abbott BinaxNOW SARS-CoV-2 point-of-care antigen test in the context of emerging viral variants and self-administration. Sci Rep. 2021;11:14604.https://doi.org/10.1038/s41598-021-94055-1
8. Rodríguez-Grande C, Adán-Jiménez J, Catalán P, Alcalá L, Estévez A, Muñoz P, et al. Inference of active viral replication

in cases with sustained positive reverse transcription-PCR results for SARS-CoV-2. J Clin Microbiol. 2021;59:e02277–20. https://doi.org/10.1128/JCM.02277-20
9. Wölfel R, Corman VM, Guggemos W, Seilmaier M, Zange S, Müller MA, et al. Virological assessment of hospitalized patients with COVID-2019. Nature. 2020; 581:465–9. https://doi.org/10.1038/s41586-020-2196-x
10. Dagotto G, Mercado NB, Martinez DR, Hou YJ, Nkolola JP, Carnahan RH, et al. Comparison of subgenomic and total RNA in SARS-CoV-2 challenged rhesus macaques. J Virol. 2021 Jan 20 [Epub ahead of print]. https://doi.org/10.1128/JVI.02370-20
11. Centers for Disease Control and Prevention. Real-time RT-PCR panel for detection 2019-novel coronavirus, instructions for use, 2020 [cited 2021 Aug 17]. https://www.cdc.gov//coronavirus/2019-ncov/lab/rt-pcr-panel-primer-probes.html
12. Waggoner JJ, Stittleburg V, Pond R, Saklawi Y, Sahoo MK, Babiker A, et al. Triplex real-time RT-PCR for severe acute respiratory syndrome coronavirus 2. Emerg Infect Dis. 2020;26:1633–5.https://doi.org/10.3201/eid2607.201285
13. Levy JM, Frediani JK, Tyburski EA, Wood A, Figueroa J, Kempker RR, et al. Impact of repeated nasal sampling on detection and quantification of SARS-CoV-2. Sci Rep. 2021;11:14903.https://doi.org/10.1038/s41598-021-94547-0
14. Pinninti S, Trieu C, Pati SK, Latting M, Cooper J, Seleme MC, et al. Comparing nasopharyngeal and midturbinate nasal swab testing for the identification of severe acute respiratory syndrome coronavirus 2. Clin Infect Dis. 2021;72:1253–5. https://doi.org/10.1093/cid/ciaa882
15. Kociolek LK, Muller WJ, Yee R, Dien Bard J, Brown CA, Revell PA, et al. Comparison of upper respiratory viral load distributions in asymptomatic and symptomatic children diagnosed with SARS-CoV-2 infection in pediatric hospital testing programs. J Clin Microbiol. 2020;59:e02593–20.https://doi.org/10.1128/JCM.02593-20

Address for correspondence: Jesse J. Waggoner, Division of Infectious Diseases, Emory University School of Medicine, 1760 Haygood Dr NE, Rm E-169, Atlanta, GA 30322, USA; email: jjwaggo@emory.edu

etymologia

Prototheca [pro″to-the′kə]

Rüdiger D. Ollhoff, Fábio P. Sellera, Fabio C. Pogliani

From the Greek *proto-* (first) + *thēkē* (sheath), *Prototheca* is a genus of variably shaped spherical cells of achloric algae in the family *Chlorellaceae*. Wilhelm Krüger, a German expert in plant physiology and sugar production, reported *Prototheca* microorganisms in 1894, shortly after spending 7 years in Java studying sugarcane. He isolated *Prototheca* species from the sap of 3 tree species. Krüger named these organisms as *P. moriformis* and *P. zopfii*, the second name as a tribute to Friedrich Wilhelm Zopf, a renowned botanist, mycologist, and lichenologist.

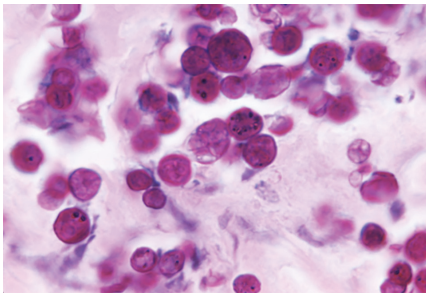

Figure 1. Periodic acid–Schiff–stained tissue sample from a case-patient who had protothecosis, showing several sphere-like cells of *Prototheca* spp. Source: Dr. Jerrold Kaplan, Centers for Disease Control, 1971.

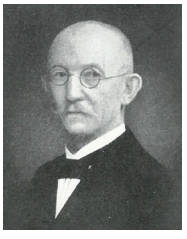

Figure 2. Wilhelm Krüger (1857–1947). Source: Institute for Sugar Beet Research (http://www.ifz-goettingen.de).

Protothecosis affects humans and wild and domestic animals, primarily causing mastitis in cows. Human protothecosis was reported in 1964 from a skin lesion in a farmer from Sierra Leone. There are increasing reports of infections in immunocompromised patients. Debates regarding *Prototheca* taxonomy persist.

Sources

1. Davies RR, Spencer H, Wakelin PO. A case of human protothecosis. Trans R Soc Trop Med Hyg. 1964;58:448–51. https://doi.org/10.1016/0035-9203(64)90094-X
2. Dorland's illustrated medical dictionary. 32nd ed. Philadelphia: Elsevier Saunders; 2012.
3. Kano R. Emergence of fungal-like organisms: Prototheca. Mycopathologia. 2020;185:747–54. https://doi.org/10.1007/s11046-019-00365-4
4. Krüger W. Brief characteristics of some lower organisms in the sap flow of deciduous trees [in German]. Hedwigia. 1894;33:241–66.
5. Todd JR, Matsumoto T, Ueno R, Murugaiyan J, Britten A, King JW, et al. Medical phycology 2017. Med Mycol. 2018;56(suppl 1):S188–204. https://doi.org/10.1093/mmy/myx162

Address for correspondence: Rüdiger D. Ollhoff, Programa de Pós-Graduação em Ciência Animal da Pontifícia Universidade Católica do Paraná, Rua Imaculada Conceição, 1155 Prado Velho, Curitiba 80215 901, Paraná, Brazil; email: daniel.ollhoff@pucpr.br

DOI: https://doi.org/10.3201/eid2801.211554

Author affiliations: Pontifícia Universidade Católica do Paraná, Curitiba, Brazil (R.D. Ollhoff); Universidade de São Paulo, São Paulo, Brazil (F.P. Sellera, F.C. Pogliani); Universidade Metropolitana de Santos, Santos, Brazil (F.P. Sellera)

Multinational Observational Cohort Study of COVID-19–Associated Pulmonary Aspergillosis[1]

Nico A.F. Janssen, Rémy Nyga, Lore Vanderbeke, Cato Jacobs, Mehmet Ergün, Jochem B. Buil, Karin van Dijk, Josje Altenburg, Catherine S.C. Bouman, Hans I. van der Spoel, Bart J.A. Rijnders, Albert Dunbar, Jeroen A. Schouten, Katrien Lagrou, Marc Bourgeois, Marijke Reynders, Niels van Regenmortel, Lynn Rutsaert, Piet Lormans, Simon Feys, Yves Debavaye, Fabienne Tamion, Damien Costa, Julien Maizel, Hervé Dupont, Taieb Chouaki, Saad Nseir, Boualem Sendid, Roger J.M. Brüggemann, Frank L. van de Veerdonk, Joost Wauters,[2] Paul E. Verweij[2]

We performed an observational study to investigate intensive care unit incidence, risk factors, and outcomes of coronavirus disease–associated pulmonary aspergillosis (CAPA). We found 10%–15% CAPA incidence among 823 patients in 2 cohorts. Several factors were independently associated with CAPA in 1 cohort and mortality rates were 43%–52%.

Incidence of coronavirus disease (COVID-19)–associated pulmonary aspergillosis (CAPA) in hospital intensive care units (ICUs) is 3.8%–33.3% (*1*–*9*). Variations might be explained by differences in patient populations and CAPA definitions used, complicating direct comparisons between studies.

Author affiliations: Radboud University Medical Center, Nijmegen, the Netherlands (N.A.F Janssen, M. Ergün, J.B. Buil, J.A. Schouten, R.J.M. Brüggemann, F.L. van de Veerdonk, P.E. Verweij); Amiens University Hospital, Amiens, France (R. Nyga, J. Maizel, H. Dupont, T. Chouaki); University Hospitals Leuven, Leuven, Belgium (L. Vanderbeke, C. Jacobs, K. Lagrou, Y. Debavaye, J. Wauters); Katholieke Universiteit Leuven, Leuven (L. Vanderbeke, K. Lagrou, J. Wauters); Amsterdam University Medical Centers, Amsterdam, the Netherlands (K. van Dijk, J. Altenburg, C.S.C. Bouman, H. van der Spoel); Erasmus Medical Center, Rotterdam, the Netherlands (B.J.A. Rijnders, A. Dunbar); AZ Sint-Jan Brugge-Oostende, Brugge, Belgium (M. Bourgeois, M. Reynders); ZNA Campus Stuivenberg, Antwerpen, Belgium (N. van Regenmortel, L. Rutsaert); AZ Delta Hospital, Roeselare, Belgium (P. Lormans, S. Feys); Rouen University Hospital, Rouen, France (F. Tamion, D. Costa); Lille University Hospital, Lille, France (S. Nseir, B. Sendid); University of Lille, Lille (S. Nseir, B. Sendid)

DOI: https://doi.org/10.3201/eid2711.211174

Diagnosing CAPA is complex because cases frequently lack typical radiologic features and European Organization for Research and Treatment of Cancer and the Mycoses Study Group Education and Research Consortium (EORTC/MSGERC) host factors (*10*) and because mycologic evidence is difficult to obtain. Serum galactomannan (GM) detection has low sensitivity in CAPA (*7*,*10*).

The European Confederation of Medical Mycology and International Society for Human and Animal Mycology (ECMM/ISHAM) published consensus criteria for a CAPA definition (*11*). We used these criteria to perform an observational cohort study to assess CAPA incidence in patients with COVID-19 admitted to ICUs during the first wave of the COVID-19 pandemic.

The Study

We collected partially prospective and partially retrospective data for 823 patients in 2 cohorts. The discovery cohort comprised patients with PCR-confirmed or clinically presumed COVID-19 admitted to 4 ICUs in the Netherlands and 4 ICUs in Belgium during February 28–May 27, 2020. The validation cohort comprised patients with PCR-confirmed COVID-19 admitted because of respiratory insufficiency to 3 participating ICUs in France during April 7–May 31, 2020 (Appendix Methods, Table 1, https://wwwnc.cdc.gov/EID/article/27/11/21-1174-App1.pdf).

[1]The results of this study were presented at the Scientific Spring Meeting of the Dutch Society of Medical Microbiology (NVMM) and the Royal Dutch Society of Microbiology (KNVM), held online March 30–31, 2021; and at the 31st European Congress of Clinical Microbiology & Infectious Diseases (ECCMID), held online from July 9–12, 2021.

[2]These authors were co–principal investigators.

Table 1. Demographic, clinical, and mycologic characteristics of the discovery cohort in a multinational observational study of COVID-19–associated pulmonary aspergillosis in 3 countries in Europe, 2020*

Characteristics	Total population, n = 519	CAPA, n = 42	CAPA excluded, n = 237	p value
Age, y	64 (55–72)	68 (61–73)	65 (57–71)	0.12
Sex				
F	141 (27)	8 (19)	58 (24)	
M	378 (73)	34 (81)	179 (76)	0.56
BMI, kg/m^2	27.2 (24.4–31.0); n = 507	27.4 (23.6–30.2); n = 40	26.9 (24.4–30.9); n = 231	0.72
Underlying conditions				
Cardiovascular disease†	291 (56)	25 (60)	130 (55)	0.62
Diabetes mellitus	139 (27)	9 (21)	61 (26)	0.70
Asthma	37 (7)	1 (2)	19 (8)	0.33
COPD	44 (9)	8 (19)	19 (8)	**0.042**
Liver cirrhosis	6 (1)	0	2 (0.8)	1.00
Rheumatological disease	31 (6)	5 (12)	14 (6)	0.18
HIV/AIDS	6 (1)	3 (7)	1 (0.4)	**0.011**
Solid organ malignancy	28 (5)	3 (7)	11 (5)	0.45
EORTC/MSGERC host factors				
Any‡	70 (16); n = 426	13 (33); n = 39	31 (19); n = 166	0.053
Recent neutropenia§	7 (2); n = 413	1 (3); n = 38	5 (3); n = 156	1.00
Hematologic malignancy	18 (4)	4 (10)	9 (4)	0.11
Receipt of allogeneic SCT	4 (0.8); n = 516	0	3 (1); n = 236	1.00
Receipt of SOT	6 (1)	1 (2)	2 (0.8)	0.39
Systemic corticosteroids ≤30 d before ICU admission, any dose	38 (9); n = 430	7 (18); n = 39	14 (9); n = 160	0.14
T or B cell immunosuppressants other than corticosteroids ≤90 d before ICU admission	31 (6); n = 514	7 (17)	12 (5); n = 233	**0.014**
Inherited severe immunodeficiency	0; n = 517	0	0; n = 236	NA
ICU treatment data				
Invasive mechanical ventilation	423 (82); n = 517	40 (98); n = 41	225 (95)	0.70
No. invasive ventilation days¶	14 (9–24); n = 395	16 (13–27); n = 37	18 (11–30); n = 212	0.98
RRT during ICU admission	93 (18); n = 516	17 (41)	44 (19); n = 236	**0.004**
Systemic corticosteroids during ICU admission	216 (42); n = 516	20 (48)	131 (56); n = 236	0.40
Outcome data				
ICU death	154 (30); n = 518	22 (52)	81 (34)	**0.036**
ICU LOS, d#	14 (8–24); n = 491	18 (12–27); n = 39	20 (12–32); n = 222	0.84
Mycologic diagnostic tests				
Serum GM OD >0.5, no. positive (%); no. values reported/no. performed	3 (2); 134/176	3 (11); 28/28	0; 106/148	NA
Serum GM OD**	0.10 (0.10–0.10); n = 134	0.10 (0.06–0.14); n = 28	0.10 (0.10–0.10); n = 106	0.95
Positive BALF/BL culture	17 (10); n = 166	17 (42); n = 41	0; n = 125	NA
BALF/BL GM OD ≥1.0, no. positive (%); no. OD values reported/no. BL/BALF performed	32 (19); 90/166	32 (78); 34/41	0; 55/125	NA
BALF/BL GM OD**	0.20 (0.10–1.50); n = 90	1.80 (1.00–3.90); n = 35	0.10 (0.10–0.20); n = 55	**<0.001**
Positive BALF/BL PCR, any C_t, no. positive (%); no. reported/no. tested	9 (5); 11/166	7 (17); 7/41	2 (2); 4/125††	NA
Days between ICU admission and first positive mycologic test‡‡	NA	6 (3–9); n = 41	NA	NA

*Data are presented as no. (%) or median (IQR) unless otherwise indicated. Continuous variables were compared by Mann-Whitney U test, categorical variables by Fisher exact test with omission of missing data, unless stated otherwise. Total percentages might not equal 100% because of rounding. Bold text indicates statistical significance. BAL, bronchoalveolar lavage; BALF, BAL fluid; BL, bronchial lavage; BMI, body mass index; CAPA, COVID-19–associated pulmonary aspergillosis; COPD, chronic obstructive pulmonary disease; COVID-19, coronavirus disease; C_t, cycle threshold; CT, computed tomography; ECMO, extracorporeal membrane oxygenation; EORTC/MSGERC, European Organization for Research and Treatment of Cancer and the Mycoses Study Group Education and Research Consortium; GM, galactomannan; ICU, intensive care unit; IQR, interquartile range; LOS, length of stay; NA, not applicable; NBL, nonbronchoscopic lavage; OD, optical density; RRT, renal replacement therapy; SCT, stem cell transplantation; SOT, solid organ transplant.

†Includes hypertension

‡Includes any use of systemic corticosteroids before ICU admission; If data on one or more EORTC host factors were missing, then data were regarded as missing for this variable.

§Neutropenia includes absolute neutrophil count of <0.5 × 10^9 cells/L for >10 d.

¶If transferred to another hospital from ICU and still on ventilatory support of any kind, duration of invasive mechanical ventilatory support was regarded as missing data and not included in the analyses. The same holds true for those who received a tracheostomy for a prolonged weaning trajectory.

#Data on ICU LOS were regarded as missing if transfer to another hospital was the reason for ICU discharge because exact ICU LOS was unknown.

**When multiple values were reported for 1 patient, the median of these values was used for further calculations.

††Positive PCR with C_t values ≥36 as only positive mycologic criterion.

‡‡Mycologic test considered a criterion for proven, probable, or possible CAPA according to the 2020 European Confederation for Medical Mycology/International Society for Human and Animal Mycology classification (*11*).

We applied ECMM/ISHAM classification criteria for CAPA (*11*). We considered bronchial lavage (BL) equivalent to bronchoalveolar lavage (BAL). We assumed all CAPA classified patients demonstrated clinical factors and radiographic abnormalities. We defined 3 patient groups: CAPA, CAPA-excluded, and CAPA not classifiable (Figure 1; Appendix).

We included 519 patients in the discovery cohort; median age was 64 years, 73% were male, and 82% required invasive mechanical ventilation during ICU admission (Table 1; Appendix Table 2, 3, 4). Among patients in the discovery cohort, 279 (54%) were classifiable: 6 (2%) as CAPA proven, 32 (12%) as probable CAPA, and 4 (1%) as possible CAPA (Figure 1, panel A; Appendix Results, Tables 5, 6). CAPA incidence among classifiable patients was 15% (42/279); 85% were CAPA-excluded. Among patients in the discovery cohort, 46% (240/519) were not classifiable, including 3 who did not fulfill the criteria for possible CAPA (Figure 1, panel A). In patients with any EORTC/MSGERC host factor, CAPA incidence was 30% (13/44), compared with 16% (26/161) in patients with no host factors (p = 0.053).

Chronic obstructive pulmonary disease (COPD; p = 0.04) and HIV/AIDS (p = 0.01) were more prevalent in CAPA patients (Table 1; Appendix Table 2). Among CAPA patients, 33% had ≥1 EORTC/MSGERC host factor, compared with 19% of CAPA-excluded patients (p = 0.053). Corticosteroid use was not more prevalent in the CAPA group (p = 0.14), in contrast to other immunosuppressant drugs (p = 0.01). In logistic regression analysis, corticosteroid use at any dose before or during ICU admission was not independently associated with CAPA development. However, COPD, HIV/AIDS, and use of other immunosuppressant drugs before ICU admission were associated with CAPA (Appendix Figure 1, panel A).

Among CAPA patients who underwent BAL or BL, *Aspergillus* culture was positive in 42%, GM was positive (optical density [OD] ≥1.0) in 78%, and *Aspergillus* PCR was positive in 17%. Among CAPA patients who underwent nonbronchoscopic lavage, 67% had positive cultures. Serum GM was positive in 11% of tested CAPA patients. Median time between ICU admission and first positive mycologic test was 6 (interquartile range [IQR] 3–9) days (Table 1; Appendix Table 7).

The proportion of patients receiving systematic corticosteroid treatment in ICUs was not

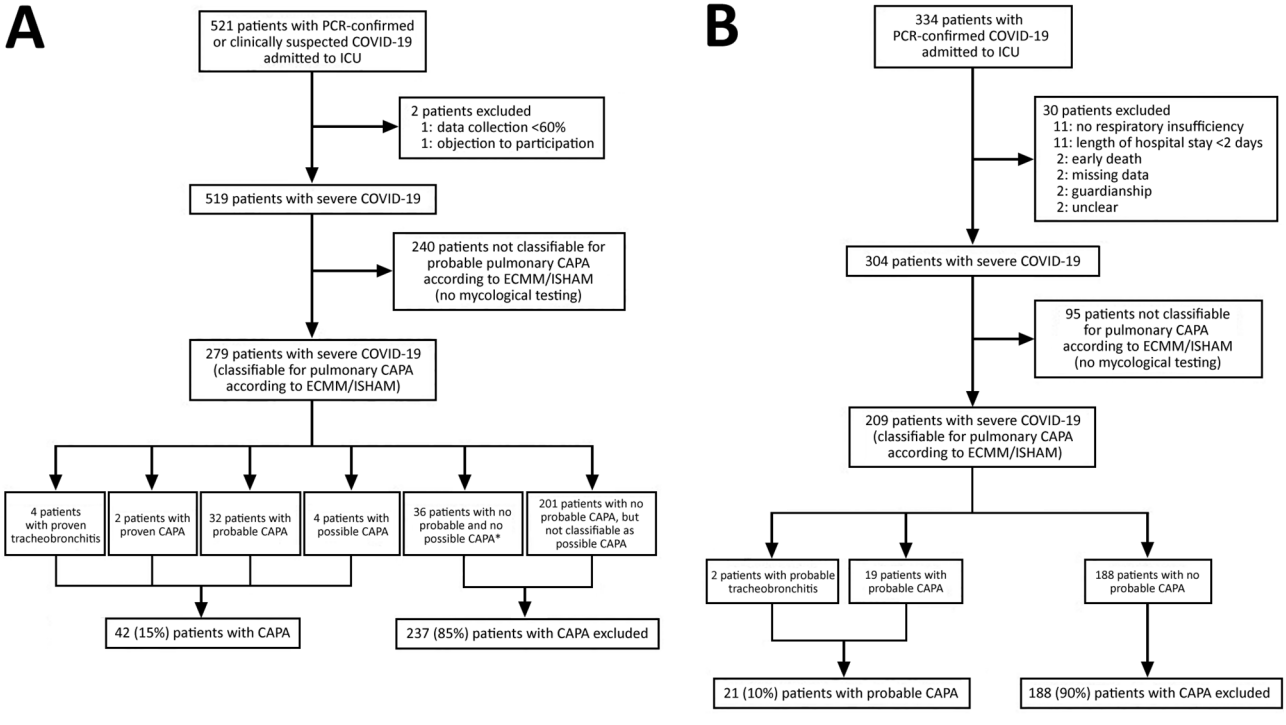

Figure 1. Flowchart of the study inclusion process for a multinational observational study of CAPA in 3 countries in Europe, 2020. A) Discovery cohort; B) validation cohort. For further analyses, patients with proven, probable, and possible CAPA were designated to the CAPA group. Patients were classified to the CAPA excluded group when they had ≥1 negative mycological test according to 2020 ECMM/ISHAM classification consensus criteria (*11*). Patients who did not undergo any of the mycological tests were designated to the CAPA not classifiable group. *Value includes 6 patients in whom CAPA was excluded at the time of autopsy. CAPA, COVID-19–associated pulmonary aspergillosis; COVID-19, coronavirus disease; ECMM/ISHAM, European Confederation for Medical Mycology/International Society for Human and Animal Mycology; ICU, intensive care unit.

significantly different between CAPA and CAPA-excluded groups (p = 0.40), nor was corticosteroid dose (p = 0.88) (Table 1; Appendix Table 4). Antifungal treatment was administered to 16% (83/519) of patients, 88% of CAPA patients, and 15% of CAPA-excluded patients (Appendix Table 8). ICU mortality rates were significantly higher in CAPA patients (52%) than in CAPA-excluded patients (34%) (p = 0.04; Table 1; Appendix Table 4); mortality rates were 67% for patients with positive serum GM. CAPA patients demonstrated reduced survival (p = 0.02) (Figure 2, panel A); estimated median survival was 42 days after ICU admission. When correcting for covariates, CAPA was not independently associated with ICU mortality rates, but older age and acute kidney injury (AKI) during ICU stay were (Appendix Figure 1, panel B).

We included 304 patients in the validation cohort (Figure 1, panel B); median age was 63 years, 25% were male, and 76% required invasive mechanical ventilation (Table 2; Appendix Tables 9, 10). Ultimately, 209/304 (69%) patients were classifiable for CAPA: 21 (10%) probable CAPA and 188 (90%) CAPA excluded (Figure 1, panel B; Appendix Results, Tables 5, 11). Among patients with EORTC/MSGERC host factors, CAPA incidence was 13% (3/23), compared with 10% (18/186) among patients without host factors (p = 0.71).

All 21 probable CAPA patients were female; cardiovascular disease, excluding hypertension (p = 0.02), and bronchiectasis (p = 0.03) were more prevalent in this group (Table 2; Appendix Table 9). Use of corticosteroids before or during ICU admission or other immunosuppressant drugs before ICU admission were not independently associated with CAPA (Appendix Figure 1, panel C). In the validation cohort, 19% received antifungal treatment; 57% of the CAPA group received antifungal treatment (Appendix Table 8).

Corticosteroid use during ICU stay was not significantly different between the CAPA and CAPA-excluded groups (p = 0.82) in the validation cohort. ICU mortality rates were higher in the CAPA group than the CAPA-excluded group (43% vs. 25%; p = 0.12) (Table 2; Figure 2, panel B; Appendix Table 10). The ICU mortality rate was 50% in patients with positive serum GM. CAPA was not independently associated with ICU death, but older age and AKI during ICU admission were (Appendix Table 10, Figure 1, panel D).

Conclusions

We found CAPA incidence was 10%–15%, corresponding to the 14%–19% reported in other studies (*8*,*9*). Discovery cohort CAPA incidence was similar to influenza-associated pulmonary aspergillosis (IAPA) incidence in ICUs (*12*,*13*). CAPA seems to develop later after ICU admission than IAPA. Median time to first positive mycologic test in our study was 6 days after ICU admission, similar to other studies reporting 4–8 days (*7*–*9*) but in contrast to the median 3 days reported for IAPA (*12*,*14*).

Corticosteroids were not associated with CAPA in our study, consistent with previous reports (*7*–*9*), but contrasting associations seen with invasive pulmonary aspergillosis (IPA) and IAPA (*12*). This finding might be explained by possible dual effects of corticosteroids in COVID-19, impairing anti-*Aspergillus* immunity while simultaneously ameliorating the hyperinflammatory immune dysregulation and associated tissue damage conducive to IPA.

We found CAPA ICU mortality rates were 43%–52%, in line with previous reports (*7*–*9*) and

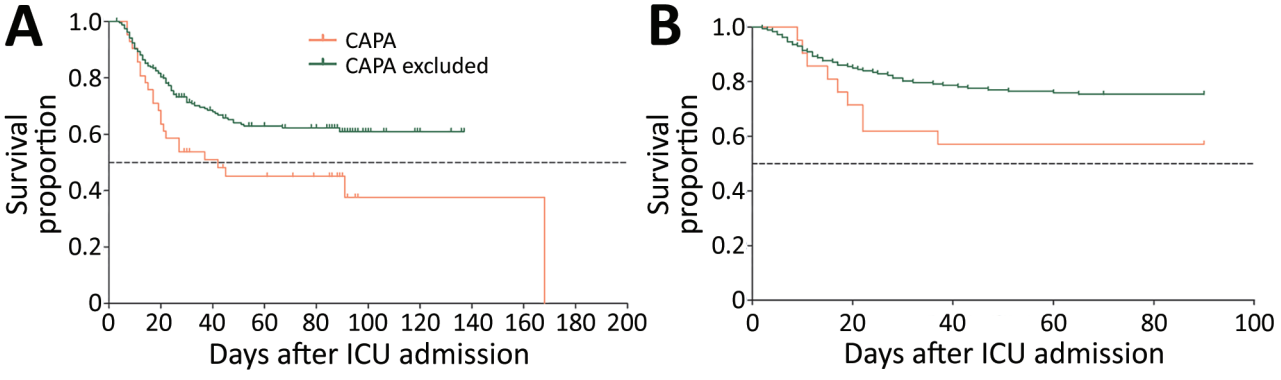

Figure 2. Kaplan-Meier survival curves comparing patients with CAPA and those classified as CAPA excluded in a multinational observational study. A) Discovery cohort; B) validation cohort. Survival analysis performed by using Mantel-Cox log rank test. Survival over time differs significantly in the discovery cohort (n = 279); median estimated survival in the CAPA group is 42.0 days (p = 0.015 by log rank test). In the validation cohort (n = 209), survival over time is not significantly different between the 2 groups (p = 0.065 by log rank test). CAPA, COVID-19–associated pulmonary aspergillosis; COVID-19, coronavirus disease; ICU, intensive care unit.

comparable to those for IAPA (*12*). We could not assess antifungal treatment effects on mortality rates, but CAPA patients in the validation cohort who received antifungal treatment demonstrated a trend toward improved survival (Appendix Figure 2).

Table 2. Demographic, clinical, and mycologic characteristics of the validation cohort in a multinational observational study of COVID-19–associated pulmonary aspergillosis in 3 countries in Europe, 2020*

Characteristics	Total population, n = 304	CAPA, n = 21	CAPA excluded, n = 188	p value
Age, y	63 (55–71)	67 (59–75)	62 (53–69)	0.06
Sex				
F	227 (75)	21 (100)	141 (75)	
M	77 (25)	0	47 (25)	**0.005**
BMI, kg/m^2	30.0 (26.0–34.4); n = 296	30.2 (26.1–32.8); n = 20	30.0 (26.4–34.5); n = 185	0.84
Underlying conditions				
Active hematologic malignancy	10 (3)	0	6 (3)	1.00
Cardiovascular disease†	185 (61)	17 (81)	112 (60)	0.06
Diabetes mellitus	92 (30)	9 (43)	62 (33)	0.47
Asthma	22 (7)	2 (10)	12 (6)	0.64
COPD	20 (7)	2 (10)	12 (6)	0.64
Liver cirrhosis‡	5 (2)	2 (10)	2 (1)	0.051
Autoimmune disease	16 (5)	2 (10)	11 (6)	0.63
HIV/AIDS	3 (1)	0	1 (0.5)	1.00
Active solid organ malignancy	4 (1)	1 (5)	3 (2)	0.35
Bronchiectasis	5 (2)	2 (10)	1 (0.5)	**0.027**
EORTC/MSGERC host factors				
Any§	35 (12)	3 (14)	20 (11)	0.71
Recent neutropenia¶	0; n = 303	0	0; n = 187	NA
Hematological malignancy	10 (3)	0	6 (3)	1.00
Receipt of SOT	9 (3)	1 (5)	5 (3)	0.48
Corticosteroids ≥0.3 mg/kg for ≥3 wks within previous 60 d	17 (6)	2 (10)	10 (5)	0.34
Other immunosuppressants ≤90 d before ICU admission	23 (8)	2 (10)	16 (9)	0.70
ICU treatment data				
Invasive mechanical ventilation	228 (76); n = 302	19 (95); n = 20	168 (89)	0.70
No. invasive ventilation days	15 (9–25); n = 212	18 (13–25); n = 17	15 (9–25); n = 157	0.21
RRT	64 (21); n = 303	11 (55); n = 20	47 (25)	**0.008**
Systemic corticosteroids during ICU admission	147 (49); n = 303	11 (52)	106 (57); n = 187	0.82
Outcome data				
ICU death	69 (23); n = 299	9 (43)	46 (25); n = 185	0.12
ICU LOS, d#	14 (8–26); n = 295	22 (12–35); n = 20	18 (10–28); n = 183	0.27
Mycologic diagnostic tests				
Serum GM OD >0.5	4 (2); n = 172**	4 (22); n = 18	0; n = 154††	NA
Serum GM OD	0.07 (0.04–0.12); n = 172**	0.10 (0.06–0.34); n = 18	0.06 (0.04–0.11); n = 154††	**0.008**
Positive BALF culture	11 (8); n = 135	11 (52) n = 21	0; n = 114	NA
BALF GM OD ≥1.0	13 (11); n = 123	13 (62) n = 21	0; n = 102	NA
BALF GM OD‡‡	0.12 (0.05–0.32); n = 123	1.10 (0.12–3.06); n = 21	0.11 (0.05–0.18); n = 102	**<0.001**
Positive BALF PCR, any C_t	8 (13); n = 64	8 (53); n = 15	0; n = 49	NA
Serum β-D-glucan value ≥80 pg/mL	37 (20); n = 184	8 (42); n = 19	29 (18); n = 160	**0.030**
Serum β-D-glucan value§§	31 (13–60); n = 184	34 (31–156); n = 19	31 (10–59); n = 160	0.055

*Data are presented as no. (%) or median (IQR), unless stated otherwise. Continuous variables were compared by Mann-Whitney U test, categorical variables by Fisher exact test with omission of missing data, unless stated otherwise. Total percentages might not equal 100% because of rounding. Bold text indicates statistical significance. BAL, bronchoalveolar lavage; BALF, BAL fluid; BL, bronchial lavage; BMI, body mass index; CAPA, COVID-19–associated pulmonary aspergillosis; COPD, chronic obstructive pulmonary disease; COVID-19, coronavirus disease; Ct, cycle threshold; CT, computed tomography; ECMO, extracorporeal membrane oxygenation; EORTC/MSGERC, European Organization for Research and Treatment of Cancer and the Mycoses Study Group Education and Research Consortium; ICU, intensive care unit; IQR, interquartile range; GM, galactomannan; LOS, length of stay; NA, not applicable; OD, optical density; RRT, renal replacement therapy; SAPS, simplified acute physiology score; SOT, solid organ transplant; TBA, tracheobronchial aspirate.
†Includes Factor V Leiden mutation and hypertension.
‡Includes hemochromatosis.
§Includes use of any systemic corticosteroids. We did not assess receipt of an allogeneic stem cell transplant, presence of an inherited severe immunodeficiency, and presence of acute graft-versus-host disease.
¶Neutropenia includes absolute neutrophil count of <0.5 × 10^9/L for >10 d.
#Data on ICU LOS were regarded as missing if still admitted at the time of data entry or if transfer to another hospital was the reason for ICU discharge.
**Serum GM performed in 173 patients, including 1 patient with an unknown result.
††Serum GM values known for 154 patients, unknown value in 1 patient.
‡‡One value of >6.0 entered as 6.0.
§§One value of >500 pg/mL entered as 500 pg/mL.

The first limitation of our study is that assuming clinical and imaging factors were available for all patients classified with CAPA possibly led to overreporting of CAPA. Excluding CAPA based on 1 negative mycologic test might have led to underreporting. Another limitation was that patients undergoing mycologic workup were likely more severely ill, which becomes apparent when comparing baseline and outcome data of the CAPA not classifiable group to the other 2 groups (Appendix Tables 5–12). Several classifications have been published or updated after we initiated this study; therefore, not all diagnostic modalities were evaluated, and we used some terms, such as BAL and BL, interchangeably (*11*,*15*).

In conclusion, we report CAPA incidence of 10%–15% in COVID-19 patients admitted to ICUs, CAPA ICU mortality rates of 43%–52%, and decreased survival over time. Clinicians should be aware of CAPA and that underlying factors, including COPD, immunosuppressant drugs other than corticosteroids, and HIV/AIDS, can increase the risk for CAPA.

Acknowledgments

We sincerely thank all the patients included in this study. We thank all colleagues in the participating centers for submitting their data. We thank Maeve van den Aakster, Burak Atasever, Aleid Breuning, Elena Decat, Joke Denolf, Ruben De Rouck, Laura De Velder, Willemijn van der Kleij, Gideon Saelman, Evi Smeyers, Manon Vanbellinghen, and Lauren Van der Sloten for their support in data entry.

L.V. reports grants from the Research Foundation Flanders during the study period and nonfinancial support from Gilead Sciences and Pfizer for work outside the submitted study. J.B.B. reports grants from F2G, Gilead Sciences, and Thermo Fisher Scientific for work outside the submitted study. B.J.A.R. reports grants from Gilead Sciences for work outside the submitted study. K.L. reports nonfinancial support from Pfizer and personal fees from SMB Laboratoires, Gilead Sciences, FUJIFILM Wako, Thermo Fisher Scientific, and MSD for work outside the submitted study. S.N. reports personal fees from MSD, Pfizer, Gilead, bioMérieux, and Bio-Rad for work outside the submitted study. K.L. received consultancy fees from MSD, SMB Laboratoires Brussels, and Gilead; nonfinancial support from Pfizer and MSD, speaker fees from Gilead Sciences, FUJIFILM WAKO, and Pfizer; and a grant from Thermo Fisher Scientific, for work outside the submitted study. R.J.M.B. has served as a consultant to Astellas Pharma, Inc., F2G, Amplyx, Gilead Sciences, Merck Sharp & Dohme Corp., Mundipharma, and Pfizer, Inc., and has received unrestricted and research grants from Astellas Pharma, Inc., Gilead Sciences, Merck Sharp & Dohme Corp., and Pfizer, Inc., for work outside the submitted study; all contracts were through Radboudumc, and all payments were invoiced by Radboudumc. J.W. reports grants from Gilead during the study period, grants and nonfinancial support from MSD, and grants from Pfizer for work outside the submitted study. P.E.V. reports grants from Mundipharma, F2G, Pfizer, Thermofisher, Gilead Sciences, and Cidara and nonfinancial support from IMMY for work outside the submitted study.

F.L.v.d.V. is supported by a Vidi grant of the Netherlands Association for Scientific Research.

Authors' contributions: N.A.F.J., R.N., F.T., J.M., H.D., S.N., R.J.M.B., F.L.v.d.V., J.W., and P.E.V. came up with study concept and design. N.A.F.J., R.N., L.V., C.J., M.E., J.B.B., K.v.D., J.A., C.S.C.B., H.I.v.d.S., B.J.A.R., A.D., J.A.S., K.L., M.B., M.R., N.v.R., L.R., P.L., S.F., Y.D., F.T., D.C., J.M., H.D., T.C., S.N., B.S., R.J.M.B., F.L.v.d.V., J.W., and P.E.V. acquired data. N.A.F.J., R.J.M.B., F.L.v.d.V., J.W., and P.E.V. analyzed and interpreted data. N.A.F.J., R.J.M.B., F.L.v.d.V., J.W., and P.E.V. drafted the manuscript. R.N., L.V., C.J., M.E., J.B.B., K.v.D., J.A., C.S.C.B., H.I.v.d.S., B.J.A.R., A.D., J.A.S., K.L., M.B., M.R., N.v.R., L.R., P.L., S.F., Y.D., F.T., D.C., J.M., H.D., T.C., S.N., and B.S. provided critical revision of manuscript.

About the Author

Dr. Janssen is an infectious disease clinician and PhD candidate at the Radboud University Medical Center, Nijmegen, the Netherlands. His primary research interests are fungal diseases, including viral pneumonitis-associated invasive aspergillosis and chronic pulmonary aspergillosis.

References

1. Koehler P, Cornely OA, Böttiger BW, Dusse F, Eichenauer DA, Fuchs F, et al. COVID-19 associated pulmonary aspergillosis. Mycoses. 2020;63:528–34. https://doi.org/10.1111/myc.13096
2. van Arkel ALE, Rijpstra TA, Belderbos HNA, van Wijngaarden P, Verweij PE, Bentvelsen RG. COVID-19–associated pulmonary aspergillosis. Am J Respir Crit Care Med. 2020;202:132–5. https://doi.org/10.1164/rccm.202004-1038LE
3. Rutsaert L, Steinfort N, Van Hunsel T, Bomans P, Naesens R, Mertes H, et al. COVID-19-associated invasive pulmonary aspergillosis. Ann Intensive Care. 2020;10:71. https://doi.org/10.1186/s13613-020-00686-4
4. Wang J, Yang Q, Zhang P, Sheng J, Zhou J, Qu T. Clinical characteristics of invasive pulmonary aspergillosis in patients with COVID-19 in Zhejiang, China: a retrospective case series. Crit Care. 2020;24:299. https://doi.org/10.1186/s13054-020-03046-7
5. Alanio A, Dellière S, Fodil S, Bretagne S, Mégarbane B. Prevalence of putative invasive pulmonary aspergillosis in critically ill patients with COVID-19. Lancet Respir Med. 2020;8:e48–9. https://doi.org/10.1016/S2213-2600(20)30237-X

6. Lamoth F, Glampedakis E, Boillat-Blanco N, Oddo M, Pagani JL. Incidence of invasive pulmonary aspergillosis among critically ill COVID-19 patients. Clin Microbiol Infect. 2020;26:1706–8. https://doi.org/10.1016/j.cmi.2020.07.010
7. Bartoletti M, Pascale R, Cricca M, Rinaldi M, Maccaro A, Bussini L, et al.; PREDICO study group. Epidemiology of invasive pulmonary aspergillosis among COVID-19 intubated patients: a prospective study. Clin Infect Dis. 2020 Jul 28 [Epub ahead of print]. https://doi.org/10.1093/cid/ciaa1065
8. White PL, Dhillon R, Cordey A, Hughes H, Faggian F, Soni S, et al. A national strategy to diagnose COVID-19–associated invasive fungal disease in the intensive care unit. Clin Infect Dis. 2020 Aug 29 [Epub ahead of print]. https://doi.org/10.1093/cid/ciaa1298
9. Dellière S, Dudoignon E, Fodil S, Voicu S, Collet M, Oillic PA, et al. Risk factors associated with COVID-19–associated pulmonary aspergillosis in ICU patients: a French multicentric retrospective cohort. Clin Microbiol Infect. 2020;27:790.e1–5. https://doi.org/10.1016/j.cmi.2020.12.005
10. Verweij PE, Gangneux JP, Bassetti M, Brüggemann RJM, Cornely OA, Koehler P, et al.; European Confederation of Medical Mycology; International Society for Human and Animal Mycology; European Society for Clinical Microbiology and Infectious Diseases Fungal Infection Study Group; ESCMID Study Group for Infections in Critically Ill Patients. Diagnosing COVID-19–associated pulmonary aspergillosis. Lancet Microbe. 2020;1:e53–5. https://doi.org/10.1016/S2666-5247(20)30027-6
11. Koehler P, Bassetti M, Chakrabarti A, Chen SCA, Colombo AL, Hoenigl M, et al.; European Confederation of Medical Mycology; International Society for Human Animal Mycology; Asia Fungal Working Group; INFOCUS LATAM/ISHAM Working Group; ISHAM Pan Africa Mycology Working Group; European Society for Clinical Microbiology; Infectious Diseases Fungal Infection Study Group; ESCMID Study Group for Infections in Critically Ill Patients; Interregional Association of Clinical Microbiology and Antimicrobial Chemotherapy; Medical Mycology Society of Nigeria; Medical Mycology Society of China Medicine Education Association; Infectious Diseases Working Party of the German Society for Haematology and Medical Oncology; Association of Medical Microbiology; Infectious Disease Canada. Defining and managing COVID-19–associated pulmonary aspergillosis: the 2020 ECMM/ISHAM consensus criteria for research and clinical guidance. Lancet Infect Dis. 2021;21;e149–62. https://doi.org/10.1016/S1473-3099(20)30847-1
12. Schauwvlieghe AFAD, Rijnders BJA, Philips N, Verwijs R, Vanderbeke L, Van Tienen C, et al.; Dutch-Belgian Mycosis study group. Invasive aspergillosis in patients admitted to the intensive care unit with severe influenza: a retrospective cohort study. Lancet Respir Med. 2018;6:782–92. https://doi.org/10.1016/S2213-2600(18)30274-1
13. van de Veerdonk FL, Kolwijck E, Lestrade PP, Hodiamont CJ, Rijnders BJ, van Paassen J, et al.; Dutch Mycoses Study Group. Influenza-associated aspergillosis in critically ill patients. Am J Respir Crit Care Med. 2017;196:524–7. https://doi.org/10.1164/rccm.201612-2540LE
14. Wauters J, Baar I, Meersseman P, Meersseman W, Dams K, De Paep R, et al. Invasive pulmonary aspergillosis is a frequent complication of critically ill H1N1 patients: a retrospective study. Intensive Care Med. 2012;38:1761–8. https://doi.org/10.1007/s00134-012-2673-2
15. Donnelly JP, Chen SC, Kauffman CA, Steinbach WJ, Baddley JW, Verweij PE, et al.; Revision and Update of the Consensus Definitions of Invasive Fungal Disease from the European Organization for Research and Treatment of Cancer and the Mycoses Study Group Education and Research Consortium. Revision and update of the consensus definitions of invasive fungal disease from the European Organization for Research and Treatment of Cancer and the Mycoses Study Group Education and Research Consortium. Clin Infect Dis. 2020;71:1367–76. https://doi.org/10.1093/cid/ciz1008

Address for correspondence: P.E. Verweij, Department of Medical Microbiology, Radboud University Medical Center, Geert Grooteplein-Zuid 10,6525 GA Nijmegen, the Netherlands; email: paul.verweij@radboudumc.nl

Mutations Associated with SARS-CoV-2 Variants of Concern, Benin, Early 2021

Anna-Lena Sander,[1] Anges Yadouleton,[1] Edmilson F. de Oliveira Filho, Carine Tchibozo, Gildas Hounkanrin, Yvette Badou, Praise Adewumi, Keke K. René, Dossou Ange, Salifou Sourakatou, Eclou Sedjro, Melchior A. Joël Aïssi, Hinson Fidelia, Mamoudou Harouna Djingarey, Michael Nagel, Wendy Karen Jo, Andres Moreira-Soto, Christian Drosten, Olfert Landt, Victor Max Corman, Benjamin Hounkpatin, Jan Felix Drexler

Intense transmission of severe acute respiratory syndrome coronavirus 2 (SARS-CoV-2) in Africa might promote emergence of variants. We describe 10 SARS-CoV-2 lineages in Benin during early 2021 that harbored mutations associated with variants of concern. Benin-derived SARS-CoV-2 strains were more efficiently neutralized by antibodies derived from vaccinees than patients, warranting accelerated vaccination in Africa.

Genomic surveillance is key to elucidate coronavirus disease (COVID-19) transmission chains and to monitor emerging severe acute respiratory syndrome coronavirus 2 (SARS-CoV-2) variants associated with partial or complete immune escape (*1*). Intense transmission likely promotes the emergence of variants, including mutations in the gene encoding the spike (S) protein, which is a major component of all available COVID-19 vaccines (*2*). Genomic surveillance is notoriously weak in sub-Saharan Africa (Appendix Figure, panel A, https://wwwnc.cdc.gov/EID/article/27/11/21-1353-App1.pdf). A total of 55 SARS-CoV-2 lineages were described in West Africa as of May 25, 2021, considerably fewer than the >350 lineages in affluent regions (Appendix Figure, panel B). We previously described 2 diverse lineages (A.4 and B.1) in Benin early in the pandemic (*3*). In this study, we analyzed SARS-CoV-2 genomic diversity in Benin ≈1 year later and assessed the ability of vaccinee-derived and patient-derived serum samples to neutralize SARS-CoV-2 variants.

The Study

We used 378 SARS-CoV-2–positive diagnostic respiratory samples tested at the reference laboratory in Benin during January 30–April 2, 2021, for genomic surveillance. All samples with cycle threshold ≤36 (Sarbeco E-gene assay; TIB Molbiol, https://www.tib-molbiol.de) were used for this study. To enable rapid prescreening of mutations known to affect the viral phenotype, we used 4 reverse transcription PCR (RT-PCR)–based single-nucleotide polymorphism (SNP) assays (VirSNiP; TIB Molbiol) targeting 9 hallmark mutations in 7 S codons of variants of concern (VOCs): B.1.1.7 (Alpha), B.1.351 (Beta), P.1 (Gamma), and B.1.617.2 (Delta) (Table 1). A total of 374 (98.9%) samples selected for the study tested positive for ≥1 mutation. Of those, ≈67.5% (255/378) showed the

Author affiliations: Charité-Universitätsmedizin Berlin, corporate member of Freie Universität Berlin, Humboldt-Universität zu Berlin, Institute of Virology, Berlin, Germany (A.-L. Sander, E.F. de Oliveira Filho, W.K. Jo, A. Moreira-Soto, C. Drosten, V.M. Corman, J.F. Drexler); Ecole Normale Supérieure de Natitingou, Natitingou, Benin (A. Yadouleton); Université Nationale des Sciences, Technologies, Ingénierie et Mathématiques (UNSTIM), Cotonou, Benin (A. Yadouleton); Laboratoire des Fièvres Hémorragiques Virales du Benin, Cotonou (A. Yadouleton, C. Tchibozo, G. Hounkanrin, Y. Badou, P. Adewumi); Ministry of Health, Cotonou (K.K. René, D. Ange, S. Sourakatou, B. Hounkpatin); Conseil National de Lutte contre le VIH-Sida, la Tuberculose, le Paludisme, les IST et les Epidémies, Cotonou (E. Sedjro, M.A. Joël Aïssi, H. Fidelia); World Health Organization Regional Office for Africa, Health Emergencies Programme, Brazzaville, Democratic Republic of the Congo (M.H. Djingarey); Deutsche Gesellschaft für Internationale Zusammenarbeit, Bonn, Germany (M. Nagel); German Centre for Infection Research (DZIF), associated partner Charité-Universitätsmedizin Berlin, Berlin (C. Drosten, V.M. Corman, J.F. Drexler); TIB Molbiol Syntheselabor GmbH, Berlin (O. Landt)

DOI: https://doi.org/10.3201/eid2711.211353

[1]These first authors contributed equally to this article.

Table 1. Screened mutations, potential effects, and occurrence in severe acute respiratory syndrome coronavirus 2 variants, Benin, 2021

SNP assay	Spike protein variation	Potential effects	SARS-CoV-2 variant						
			B.1.1.7 Alpha†	B.1.525	B.1.351 Beta†	P.1 Gamma†	P.2	P.3	B.1.617.2 Delta†
1	del HV69/70	Immune escape and enhanced viral infectivity (*4*)	x	x					
	E484K	Antibody resistance (*4*)		x	x	x	x	x	
	N501Y	Increased transmission (*4*)	x		x	x		x	
2	V1176F	Higher mortality rates‡				x	x		
3	L452R	Antibody resistance (*4*)							x
4	K417T	No data				x			
	K417N	Immune escape (*5*)			x				
	P681H	No data	x						
	P681R	No data							x

*SARS-CoV-2, severe acute respiratory syndrome coronavirus 2; SNP single-nucleotide polymorphism.
†Variants of concern according to the World Health Organization.
‡G. Hahn et al., unpub. data, https://www.biorxiv.org/content/10.1101/2020.11.17.386714v2.

69/70 deletion, 58.9% (223/378) the E484K mutation, 33.9% (128/378) the N501Y mutation, 30.4% (115/378) the P681H mutation, 14.8% (56/378) the L452R mutation, and 0.3% (1/378) the K417N or P681R mutation. The K417T or V1176F mutations associated with the Beta and Gamma VOCs were not detected. Approximately 22.2% (84/378) of samples were typeable to 1 of the lineages covered by the VirSNiP assays. According to SNP-based analyses, 14.8% (56/378) of the overall samples showed the mutation pattern of the Alpha variant, B.1.1.7, and 7.4% (28/378) of the B.1.525 variant. Frequent occurrence of the mutations under study suggests that earlier SARS-CoV-2 lineages not carrying those mutations have been replaced in Benin.

Definite lineage designation relies on the full genome sequence. We selected 68 (9 typeable and 59 nontypeable) samples according to unique mutational patterns covering the complete period of the study for a NimaGen/Illumina-based whole-genome sequencing workflow (Appendix Table 1). All near-full genomes generated within this study were deposited into GISAID (https://www.gisaid.org; accession nos. EPI_ISL_2932532–84 and EPI_ISL_2958658–72). Lineage assignment using the Pangolin COVID-19 Lineage Assigner version 3.0.2 (https://pangolin.cog-uk.io) confirmed SNP-based lineage prediction in all 9 typeable samples selected for whole-genome sequencing (Appendix Table 2). Despite robust lineage prediction based on unambiguous SNP-based results, our data demonstrate the limited use of VirSNiP assays for strain designation; however, these assays can detect relevant mutations of currently circulating variants. The 68 Benin-derived near-complete genomes were designated to 10 unique lineages, suggesting higher genetic diversity in Benin than ≈1 year before (*3*). During early 2021, lineages B.1.1.7 (22%), A.27 (19.1%), B.1.525 (17.6%), and B.1.1.318 (16.2%) were most prominent in Benin (Appendix Table 3). Despite presence of the mutation P681R (associated with the Delta VOC) in 1 sequence, that strain was typed as A.23.1, and no Delta variant was found.

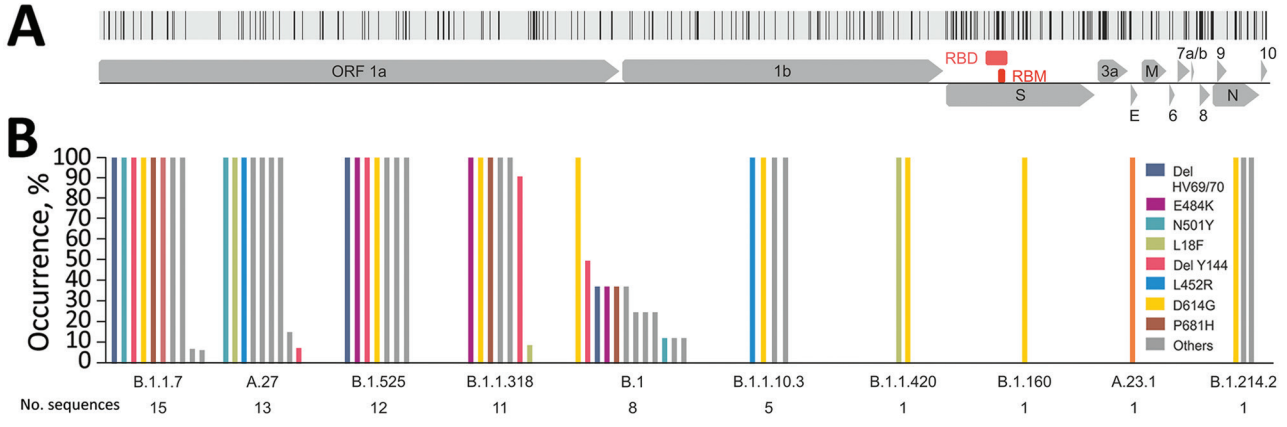

Figure 1. Genomic surveillance of severe acute respiratory syndrome coronavirus 2 (SARS-CoV-2) lineages in Benin, 2021. A) Nonsynonymous mutations of Benin-derived SARS-CoV-2 sequences across the full genome. B) Spike mutations occurring in the SARS-CoV-2 lineages circulating in Benin. Hallmark mutations of variants of concern are shown in color. Other mutations occurring in the Benin-derived sequences are depicted in gray and summarized as others. ORF, open reading frame; RBD, receptor-binding domain.

These data are consistent with recent online sequence reports from West Africa (A.E. Augustin, unpub. data, https://www.medrxiv.org/content/10.1101/2021.05.06.21256282v1; E.A. Ozer et al., unpub. data, https://www.medrxiv.org/content/10.1101/2021.04.09.21255206v3). A 100% consensus sequence of all 68 Benin-derived sequences showed 229 nonsynonymous nucleotide substitutions across the whole genome; 57 (24.9%) occurred in the S protein (Figure 1, panel A). Of note, variants with mutations in the S protein might alter the transmissibility and antigenicity of the virus (4). Internationally recognized VOCs to date share 16 S mutations in unique combinations (https://covariants.org/shared-mutations). The Benin-derived SARS-CoV-2 strains shared 10 unique S mutations reported in VOCs, although most of those strains were not defined as any VOC other than Alpha (Figure 1, panel B), suggesting convergent evolution of key mutations across different lineages (D.P. Martin et al., unpub. data, https://www.medrxiv.org/content/10.1101/2021.02.23.21252268v3; S. Cherian, unpub. data, https://www.biorxiv.org/content/10.1101/2021.04.22.440932v2). Putative higher fitness mediated by genomic change was consistent with more mutations in predominant lineages than in lineages found at lower frequencies (Figure 1, panel B).

Because S mutations, individually or in combination, have been shown to afford viral escape to antibody-mediated immune responses, the high prevalence of variants with large numbers of these mutations circulating in Benin was cause for concern. To investigate whether and to what extent

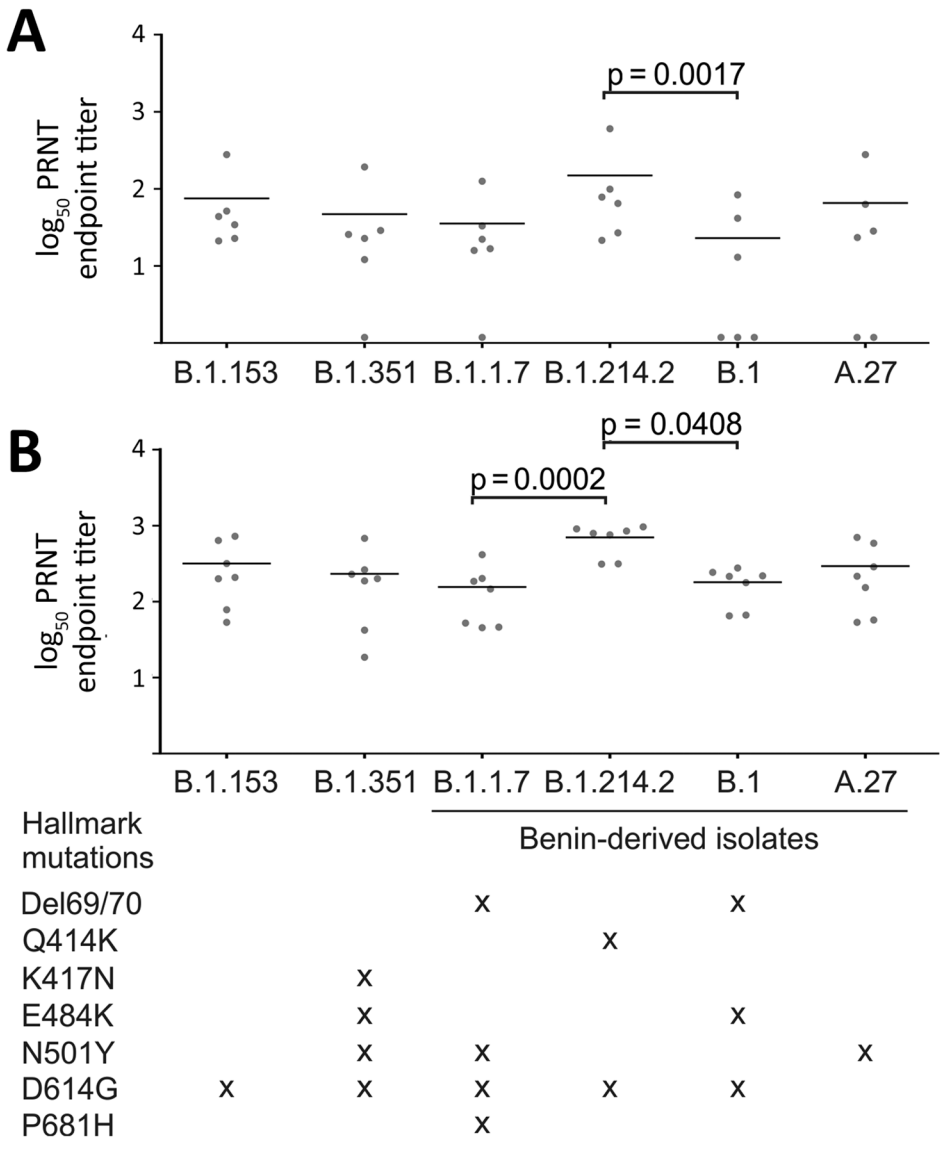

Figure 2. PRNT results of severe acute respiratory syndrome coronavirus 2 (SARS-CoV-2) variants from Benin, 2021. Graphs compare results of neutralization tests for naturally infected persons (A) and persons who received the Pfizer-BioNTech vaccine (BNT162b2; https://www.pfizer.com) (B) against the B.1.153 lineage from January 2020 (Munich/ChVir929/2020 strain; GISAID [http://www.gisaid.org] accession no. EPI_ISL_406862; Pangolin version 2021–05–19), the Beta strain (Baden-Wuertemberg/ChVir22131/2021; accession no. EPI_ISL_862149; B.1.351; Pangolin version 2021–05–19) and the B.1.1.7, B.1.214.2, B.1, and A.27 lineages isolated from patients from Benin. Lines denote the mean $PRNT_{50}$ endpoint titer. Statistical significance was determined by the Dunn's multiple comparisons test. Nonsignificant values are not shown for clarity of presentation. $PRNT_{50}$, 50% plaque reduction neutralization test.

Table 2. Hallmark mutations and $PRNT_{50}$ results of Benin-derived severe acute respiratory syndrome coronavirus 2 lineages, Benin, 2021

Sample no.	251307	314235	251455	312541
Lineage	B.1	B.1.1.7	A.27	B.1.214.2
Mutations	Q52R, Del HV69/70, Del Y144, E484K, D614G, Q677H, F888L	Del HV69/70, Del Y144, F490S, N501Y, A570D, D614G, P681H, T716I, S982A, D1118H	L18F, L452R, N501Y, A653V, H655Y, D796Y, G1219V	Ins R214TDR, Q414K, D614G, T716I
Patient-derived samples				
Mean titer (95% CI)	23 (–12.4 to 58.4)	35.5 (–12 to 83)	65.6 (–46.6 to 177.7)	148.9 (–86.59 to 384.3)
No. (%) neutralized	3/6 (50)	5/6 (83.3)	4/6 (66.7)	6/6 (100)
Titer difference†	52.2 (1.5-fold)	39.7	9.7	–73.6‡
Vaccinee-derived samples				
Mean titer (95% CI)	180.5 (102.8–258.1)	156.2 (33.6–278.7)	293.7 (57.1–530.2)	698.3 (446.8–949.9)
No. (%) neutralized	7/7 (100)	7/7 (100)	7/7 (100)	7/7 (100)
Titer difference†	136.7	161	23.5	–381.1‡

*$PRNT_{50}$, 50% plaque reduction neutralization test.
†Compared to variant B.1.153.
‡Lower titers against the early isolate compared with this Benin-derived isolate.

SARS-CoV-2 variants circulating in Benin and West Africa (*5*) evade neutralizing antibody responses, we isolated 4 lineages with unique mutational patterns (Table 2): an A.27 lineage isolate harboring the N501Y mutation; a B.1 isolate harboring the 69/70 deletion and the E484K and D614G mutations; a B.1.1.7 lineage isolate harboring the 69/70 deletion and the N501Y, D614G, and P681H mutations; and a B.1.214.2 lineage harboring the Q414K and D614G mutations (Figure 2). Additional isolation attempts of strains belonging to the frequently detected B.1.525 and B.1.318 lineages failed, likely because of degradation after repeated freeze-thaw cycles under tropical conditions. We tested neutralization potency of 6 serum samples from patients in Benin taken ≈8 days after RT-PCR–confirmed SARS-CoV-2 infection during early 2020 (*6*) and another 7 serum samples from persons in Europe 4 weeks after receiving the second dose of the Pfizer/BioNTech vaccine (BNT162b2; https://www.pfizer.com) (Appendix Table 4). Sampling was approved by the ethics committee of the Benin Ministry of Health (approval no. 030/MS/DC/SGM/DNSP/CJ/SA/027SGG2020) and of Charité-Universitätsmedizin Berlin (approval nos. EA1/068/20 and EA4/245/20). We compared neutralization titers with a SARS-CoV-2 strain (B.1.153) from January 2020 and the Beta strain (B.1.351) known to evade antibody-mediated neutralization (*7*). Despite the early sampling time after RT-PCR confirmation of SARS-CoV-2 infection, all 6 serum specimens from patients in Benin efficiently neutralized the early SARS-CoV-2 isolate carrying only the D614G mutation. In contrast, only 3 of those 6 serum specimens neutralized the B.1 isolate, the only isolate with the E484K mutation (Figure 2, panel A). Among the serum specimens from vaccinated persons, all neutralized the B.1 isolate, albeit at 1.5-fold lower titers than the early lineage B.1.153 isolate (by Friedman test and Dunn's multiple comparisons test; $p>0.99$) (Figure 2, panel B). Those data were consistent with a recent report describing efficient neutralization of a B.1.525 strain from Nigeria by vaccinee-derived serum specimens (*8*). Of note, another strain classified as B.1.214.2 was neutralized more efficiently than all other tested lineages (Figure 2), highlighting that not every mutation in circulating lineages affords reduced antibody-mediated neutralization. Other hypothetically present fitness advantages of such strains will require detailed virologic investigation.

Our study is limited by patient-derived samples taken an average of 8 days after infection (*7*), which could imply incomplete maturation of antibodies. However, similar neutralization patterns between patient-derived and vaccinee-derived serum specimens suggest robustness of our data. Another limitation is that vaccinee-derived serum samples originated exclusively from Europe. Vaccine responses vary between populations, possibly influenced by genetic background and immune-modulating diseases (e.g., malaria or HIV) (*9*), highlighting the importance of testing serum samples from vaccinees in Africa for future studies. Of note, the efficacy trial of the Pfizer/BioNTech vaccine enrolled ≈40,000 participants, only ≈800 of whom were from Africa, and all of those from South Africa (*10*).

Conclusions

Our data highlight the importance of ongoing monitoring of population immunity to emerging SARS-CoV-2 variants in Africa and of using serum specimens from local settings for phenotypic characterizations. Vaccination programs in Africa should be accelerated urgently, emphasizing the importance of global access to vaccines.

Acknowledgments

We thank Sebastian Brünink, Arne Kühne, Ben Wulf, and Antje Kamprad for support.

This work was funded by the Deutsche Gesellschaft für Internationale Zusammenarbeit (GIZ) GmbH (project number 81263623). This study is also based on research funded in part by the Bill & Melinda Gates Foundation (grant ID INV-005971). The findings and conclusions contained within are those of the authors and do not necessarily reflect positions or policies of the Bill & Melinda Gates Foundation.

O.L. is the owner of TIB Molbiol, the company developing and marketing SARS VirSNiP assays.

About the Author

Ms. Sander is a PhD student at the Institute of Virology at Charité-Universitätsmedizin, Berlin, Germany; her main research interest is the evolution of newly emerging viruses. Dr. Yadouleton is a medical entomologist in the Centre de Recherche Entomologique de Cotonou, Benin, head of the Laboratoire des Fièvres Hémorragiques in Cotonou, and a teacher at the University of Natitingou, Benin; his research interests include mosquito control and the diagnosis of viral hemorrhagic fevers.

References

1. Warmbrod KL, West R, Frieman M, George D, Martin E, Rivers C. Staying ahead of the variants: policy recommendations to identify and manage current and future variants of concern. Baltimore (MD): Johns Hopkins Center for Health Security; 2021 Feb 16 [cited 2021 May 28]. https://www.centerforhealthsecurity.org/our-work/publications/staying-ahead-of-the-variants
2. Jo WK, Drosten C, Drexler JF. The evolutionary dynamics of endemic human coronaviruses. Virus Evol. 2021;7:veab020.
3. Sander AL, Yadouleton A, Moreira-Soto A, Tchibozo C, Hounkanrin G, Badou Y, et al. An observational laboratory-based assessment of SARS-CoV-2 molecular diagnostics in Benin, Western Africa. MSphere. 2021;6:e00979–20. https://doi.org/10.1128/mSphere.00979-20
4. Harvey WT, Carabelli AM, Jackson B, Gupta RK, Thomson EC, Harrison EM, et al.; COVID-19 Genomics UK (COG-UK) Consortium. SARS-CoV-2 variants, spike mutations and immune escape. Nat Rev Microbiol. 2021;19:409–24. https://doi.org/10.1038/s41579-021-00573-0
5. Zhou D, Dejnirattisai W, Supasa P, Liu C, Mentzer AJ, Ginn HM, et al. Evidence of escape of SARS-CoV-2 variant B.1.351 from natural and vaccine-induced sera. Cell. 2021;184:2348–2361.e6. https://doi.org/10.1016/j.cell.2021.02.037
6. Sanyang B, Kanteh A, Usuf E, Nadjm B, Jarju S, Bah A, et al. COVID-19 reinfections in The Gambia by phylogenetically distinct SARS-CoV-2 variants-first two confirmed events in west Africa. Lancet Glob Health. 2021;9:e905–7. https://doi.org/10.1016/S2214-109X(21)00213-8
7. Yadouleton A, Sander AL, Moreira-Soto A, Tchibozo C, Hounkanrin G, Badou Y, et al. Limited specificity of serologic tests for SARS-CoV-2 antibody detection, Benin, Western Africa. Emerg Infect Dis. 2021;27:2020. 10.3201/eid2701.203281 https://doi.org/10.3201/eid2701.203281
8. Liu J, Liu Y, Xia H, Zou J, Weaver SC, Swanson KA, et al. BNT162b2-elicited neutralization of B.1.617 and other SARS-CoV-2 variants. Nature. 2021. https://doi.org/10.1038/s41586-021-03693-y
9. Kollmann TR. Variation between populations in the innate immune response to vaccine adjuvants. Front Immunol. 2013;4:81. https://doi.org/10.3389/fimmu.2013.00081
10. Polack FP, Thomas SJ, Kitchin N, Absalon J, Gurtman A, Lockhart S, et al.; C4591001 Clinical Trial Group. Safety and efficacy of the BNT162b2 mRNA Covid-19 vaccine. N Engl J Med. 2020;383:2603–15. https://doi.org/10.1056/NEJMoa2034577

Address for correspondence: Jan Felix Drexler, Helmut-Ruska-Haus, Institute of Virology, Campus Charité Mitte, Charitéplatz 1, 10098 Berlin, Germany; email: felix.drexler@charite.de

Bordetella hinzii Pneumonia and Bacteremia in a Patient with SARS-CoV-2 Infection

Michele Maison-Fomotar, Geetha Sivasubramanian

Patients with severe acute respiratory syndrome coronavirus 2 infection may have bacterial co-infections, including pneumonia and bacteremia. *Bordetella hinzii* infections are rare, may be associated with exposure to poultry, and have been reported mostly among immunocompromised patients. We describe *B. hinzii* pneumonia and bacteremia in a severe acute respiratory syndrome coronavirus 2 patient.

Since the December 2019 beginning of the coronavirus disease (COVID-19) pandemic, caused by severe acute respiratory syndrome coronavirus (SARS-CoV-2), there have been >180 million cases and >3.9 million deaths worldwide (*1*). Severe bacterial and fungal co-infections are a major concern with COVID-19 and increase disease mortality (*2*).

The genus *Bordetella* comprises >10 known species of small, gram-negative coccobacilli, the most common of which is *Bordetella pertussis* (*3*). *Bordetella hinzii* was first identified as a cause of respiratory infection in poultry and more rarely in rodents (*4*). It was first reported as a human infection in a patient with HIV infection in 1994 as a cause of bacteremia (*5*) and has subsequently been identified as a cause of soft tissue infections, pneumonia, cholangitis, urinary tract infections, bacteremia, and endocarditis, most often in immunocompromised patients (*4*–*15*; Appendix references *16*,*17*, https://wwwnc.cdc.gov/EID/article/27/11/21-1468-App1.pdf). We report a case of *B. hinzii* pneumonia and bacteremia in a patient with SARS-CoV-2 infection.

The Study

A 77-year-old man with medical history notable for uncontrolled type 1 diabetes mellitus and coronary artery disease and who was receiving hemodialysis for end-stage renal disease sought treatment with worsening shortness of breath and 3 days of chest pain. He also reported cough, nausea, fever, and back pain. He lived at a nursing home and had no known poultry or pet exposure. At initial examination, he was afebrile; had a blood pressure of 165/83 mm Hg; heart rate of 92 beats/min, and respiratory rate of 18 breaths/min; was severely hypoxic with oxygen saturation of 50% on room air, requiring a nonrebreather mask; and had decreased breath sounds on chest auscultation. Blood test results (reference ranges) showed hemoglobin, 10 g/dL (12–16 g/dL); leukocytes, 4,300 cells/mm^3 (4,000–11,000 cells/mm^3), 78% neutrophils; platelets, 238,000/mm^3 (140,000–440,000/mm^3); serum creatinine level, 4.3 mg/dL (0.5–1.1 mg/dL); procalcitonin, 3.3 ng/mL (0.00–0.30 ng/mL); lactate dehydrogenase, 169 U/L (100–230 U/L); C-reactive protein, 213 mg/L (0.0–3.0 mg/L); and ferritin, 2,492 ng/mL (22.0–322.0 ng/mL). A SARS-CoV-2 nasopharyngeal swab sample test was positive by PCR. A computed tomography scan of his chest revealed multiple rib fractures, a large right-side pleural effusion, and right upper-lobe pulmonary infiltrate.

We started the patient on dexamethasone. We considered remdesivir therapy but did not start it because of his renal disease. We also empirically initiated treatment with piperacillin/tazobactam and levofloxacin for bacterial pneumonia. We performed right-side thoracentesis and drained 725 mL of transudative fluid; fluid culture was negative for growth of bacteria. He was intubated on day 7 after admission because of worsening hypoxemia but subsequently extubated on day 9. On day 13, acute respiratory failure (oxygen saturation ≈70%) and bradycardia (heart rate ≈40 beats/min) developed, and he was hypotensive with agonal breathing. He was emergently reintubated and given atropine, which improved his heart rate. We initiated broad-spectrum antimicrobial treatment with intravenous vancomycin and cefepime.

Author affiliation: University of California, San Francisco, Fresno, California, USA

DOI: https://doi.org/10.3201/eid2711.211468

Blood cultures drawn on day 13 after admission grew gram-negative rods in routine blood, chocolate, and MacConkey agar media. A computed tomography scan of the chest revealed bilateral patchy ground glass opacities, dense consolidations in both lung bases, and a small right pleural effusion (Figure). The patient underwent a bronchoalveolar lavage (BAL) on day 14; the BAL fluid grew >100,000 CFUs of the same gram-negative bacilli, which we had not yet identified, along with 20,000–50,000 CFUs of *Klebsiella pneumoniae*. Gram stain of the BAL fluid showed many leukocytes and few gram-negative rods. We continued treatment with vancomycin and cefepime. On day 17, we extubated then reintubated him the same day because of ongoing hypotension and poor mentation. Because of worsening hemodynamic status, continued poor mentation, and overall poor prognosis, we changed goals of care to comfort measures only, and the patient died soon after.

On day 18 after the patient's admission, we identified the gram-negative rod in the blood culture and BAL fluid as *Bordetella hinzii* on the basis of an excellent score (2.43) in matrix-assisted laser desorption/ionization-time of flight mass spectrometry testing. We measured antimicrobial sensitivities by broth microdilution using the Vitek 2 system (bioMérieux; https://www.biomerieux.com) and MIC, interpreting breakpoints using Clinical and Laboratory Standards Institute (https://clsi.org) guidelines. The isolate was sensitive only to meropenem, levofloxacin, amikacin, and gentamicin and showed high MICs of 32 μg/mL to ceftazidime and 64 μg/mL to cefepime (Table 1).

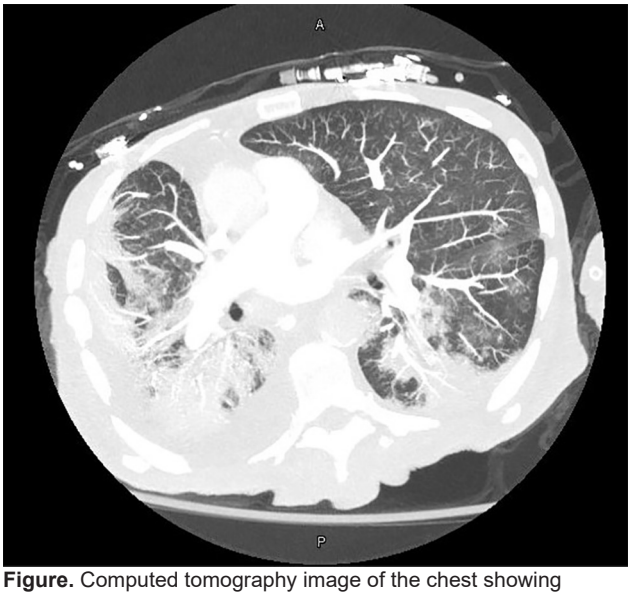

Figure. Computed tomography image of the chest showing bilateral dense consolidations and right-sided pleural effusion in 77-year-old man with severe acute respiratory syndrome coronavirus 2 who was later found to be co-infected with *Bordetella hinzii*. A, anterior; P, posterior

Conclusions

B. hinzii is a strictly aerobic gram-negative bacillus that was first identified as a cause of respiratory illnesses, mostly rhinotracheitis, in poultry (*3*). Manifestations from reported human cases include skin infection, urinary tract infection, pneumonia, and infective endocarditis, with or without bacteremia (*4*–*15*; Appendix references *16*,*17*) (Table 2). Human infection with *B. hinzii* is very uncommon; the 18 cases thus far reported suggest that *B. hinzii* behaves like an opportunistic pathogen in humans. Underlying conditions in patients from those cases included HIV, malignancy, liver disease, ulcerative colitis, diabetes, and liver transplantation; 3 of the patients had no underlying medical conditions. There was often known poultry exposure, unlike in this case. It is possible that this pathogen colonizes the respiratory tract then is activated to cause infection later when the host becomes immunocompromised (*7*; Appendix reference *16*). *B. hinzii* was isolated from wild rodents in Southeast Asia, raising the possibility that they might serve as reservoirs that could transmit the pathogen to humans or pets (Appendix reference *18*). Most patients recovered when treated with appropriate antimicrobial drugs, but this infection can lead to death, especially in severely immunocompromised patients (*10*,*13*).

B. hinzii is frequently resistant to many antimicrobial drugs, including β-lactams, cephalosporins, and quinolones. Reported isolates have been susceptible to piperacillin/tazobactam, ceftazidime, tigecycline, and meropenem (*4*–*11*). The interpretation of antimicrobial sensitivity testing is not established. Choice of antimicrobial drugs and treatment duration are also not standardized. The cases of bacteremia and endocarditis identified were treated with

Table 1. Antimicrobial susceptibility of *Bordetella hinzii* isolate by broth dilution

Drug	MIC*	Interpretation
Amikacin	8 μg/mL	Sensitive
Aztreonam	≥64 μg/mL	Resistant
Cefepime	≥64 μg/mL	Resistant
Ceftazidime	≥32 μg/mL	Resistant
Ciprofloxacin	≥8 μg/ml	Resistant
Gentamicin	4 μg/mL	Sensitive
Levofloxacin	2 μg/mL	Sensitive
Meropenem	2 μg/mL	Sensitive
Piperacillin/tazobactam	≥128/4 μg/mL	Resistant
Ticarcillin/clavulanic acid	≥256/2 μg/mL	Resistant
Tobramycin	16 μg/mL	Resistant

*MIC breakpoints were interpreted using CLSI guidelines (https://clsi.org).

Table 2. Characteristics of previously reported *Bordetella hinzii* infections*

Ref.†	Type of infection	Age, y	Underlying conditions	Animal exposure	Antimicrobial drugs	Patient outcome
(*5*)	Bacteremia	24	HIV/AIDS	None	Ceftazidime	Recovered
(*4*)	Pneumonia	NA	HIV/AIDS	None	NA	NA
(*6*)	Bacteremia and cholangitis	69	None	None	Ticarcillin/sulbactam, ciprofloxacin	Died
(*7*)	Cholangitis	29	Primary sclerosing cholangitis, liver transplant recipient	None	Meropenem	Died
(*8*)	Bacteremia	79	Myelodysplastic syndrome	None	Ceftazidime	Recovered
(*9*)	Bacteremia	36	EBV associated diffuse large cell lymphoma	None	Meropenem	Died
(*10*)	Pneumonia	43	AML, transplant, diabetes bronchiectasis	Poultry	Piperacillin/tazobactam, ciprofloxacin	Recovered
(*10*)	Pneumonia	74	Laryngeal cancer, prostate cancer, diabetes, COPD	None	Piperacillin/tazobactam	Recovered
(*11*)	Urinary tract infection	55	None	Possible poultry	Trimethoprim/ sulfamethoxazole	Recovered
(*11*)	Liver abscess	58	Hypothyroidism, cholecystectomy	None	None	Recovered
(*12*)	Bacteremia and infective endocarditis	79	Aortic valve replacement, diabetes, cirrhosis, colon cancer, kidney disease	None	Meropenem	Recovered
(*13*)	Bacteremia and infective endocarditis	53	Ulcerative colitis	None	Ceftazidime	Recovered
(*14*)	Soft tissue abscess	63	None	None	Sitafloxacin	Recovered
(*15*)	Pancreatic abscess	42	Alcoholic liver disease	None	Tigecycline	Recovered
(*16*)	Urinary tract infection	37	Chronic alcohol use	None	Trimethoprim/ sulfamethoxazole	Recovered
(*17*)	Pneumonia	67	Diabetes mellitus	None	Cefmetazole	Recovered

*AML, Acute myeloid leukemia; COPD, chronic obstructive pulmonary disease; EBV, Epstein-Barr virus; NA, not available; ref., reference.
†References *16,17* in Appendix, https://wwwnc.cdc.gov/EID/article/27/11/21-1468-App1.pdf.

ceftazidime and ticarcillin/clavulanate. The patient we describe had received only a short course of vancomycin and cefepime before we identified *B. hinzii* in cultures from samples he provided. The isolate of *B. hinzii* identified had a high MIC to cefepime, 64 μg/mL, suggesting inadequate antimicrobial coverage before his death. This high MIC to third- and fourth-generation cephalosporins had been reported in only 1 previous case (*11*).

The cause of death in this case was likely multifactorial and included respiratory infection with SARS-COV-2 and the hemodynamic compromise that ensued. The role of *Klebsiella* isolated from BAL fluid seems unclear, but this bacterium was found only in very small quantities from the respiratory tract and was treated with appropriate antimicrobial drugs.

In summary, *B. hinzii* has multiple clinical manifestations and outcomes in both immunocompetent and immunocompromised patients. Reports of patients with *B. hinzii* infections seem to be increasing in recent years, which may be because of the availability of better identification methods, such as matrix-assisted laser desorption/ionization-time of flight mass spectrometry and gene sequencing, as well as an increase in the number of immunocompromised persons who have underlying conditions such as HIV, malignancy, or transplantation or who are taking immunosuppressive agents. Our patient likely had untreated lung *B. hinzii* infection that led to bacteremia. He had uncontrolled diabetes and received dexamethasone as part of his treatment, which may have resulted in dissemination through bacteremia. In addition, SARS-CoV-2 co-infection rendered him more susceptible to infection. Our findings add to the growing knowledge of emerging secondary infectious complications, including from opportunistic pathogens, concurrent with or after SARS-CoV-2 infection. The increasing case reports of invasive *B. hinzii* may indicate its emergence as a pathogen in humans.

About the Author

Dr. Maison-Fomotar is a graduating second-year infectious diseases fellow at the University of California San Francisco, Fresno, California. Her primary interests are HIV, central nervous system infections, and infectious disease issues in underserved populations.

Dr. Sivasubramanian is an assistant professor of infectious diseases at University of California San Francisco, Fresno, California. Her primary interests are fungal infections and infections in critically ill patients.

References

1. WHO. COVID-19 dashboard [cited 2021 Jun 28]. https://covid19.who.int
2. Chen X, Liao B, Cheng L, Peng X, Xu X, Li Y, et al. The microbial coinfection in COVID-19. Appl Microbiol Biotechnol. 2020;104:7777–85. https://doi.org/10.1007/s00253-020-10814-6
3. Mattoo S, Cherry JD. Molecular pathogenesis, epidemiology, and clinical manifestations of respiratory infections due to *Bordetella* pertussis and other Bordetella subspecies. Clin Microbiol Rev. 2005;18:326–82. https://doi.org/10.1128/CMR.18.2.326-382.2005
4. Gadea I, Cuenca-Estrella M, Benito N, Blanco A, Fernández-Guerrero ML, Valero-Guillén PL, et al. *Bordetella hinzii*, a "new" opportunistic pathogen to think about. J Infect. 2000;40:298–9. https://doi.org/10.1053/jinf.2000.0646
5. Cookson BT, Vandamme P, Carlson LC, Larson AM, Sheffield JV, Kersters K, et al. Bacteremia caused by a novel *Bordetella* species, "*B. hinzii*." J Clin Microbiol. 1994;32:2569–71. https://doi.org/10.1128/jcm.32.10.2569-2571.1994
6. Kattar MM, Chavez JF, Limaye AP, Rassoulian-Barrett SL, Yarfitz SL, Carlson LC, et al. Application of 16S rRNA gene sequencing to identify *Bordetella hinzii* as the causative agent of fatal septicemia. J Clin Microbiol. 2000;38:789–94. https://doi.org/10.1128/JCM.38.2.789-794.2000
7. Arvand M, Feldhues R, Mieth M, Kraus T, Vandamme P. Chronic cholangitis caused by *Bordetella hinzii* in a liver transplant recipient. J Clin Microbiol. 2004;42:2335–7. https://doi.org/10.1128/JCM.42.5.2335-2337.2004
8. Fry NK, Duncan J, Edwards MT, Tilley RE, Chitnavis D, Harman R, et al. A UK clinical isolate of *Bordetella hinzii* from a patient with myelodysplastic syndrome. J Med Microbiol. 2007;56:1700–3. https://doi.org/10.1099/jmm.0.47482-0
9. Hristov AC, Auwaerter PG, Romagnoli M, Carroll KC. *Bordetella hinzii* septicemia in association with Epstein-Barr virus viremia and an Epstein-Barr virus-associated diffuse large B-cell lymphoma. Diagn Microbiol Infect Dis. 2008;61:484–6. https://doi.org/10.1016/j.diagmicrobio.2008.03.013
10. Fabre A, Dupin C, Bénézit F, Goret J, Piau C, Jouneau S, et al. Opportunistic pulmonary *Bordetella hinzii* infection after avian exposure. Emerg Infect Dis. 2015;21:2122–6. https://doi.org/10.3201/eid2112.150400
11. Almuzara M, Barberis C, Traglia GM, Sly G, Procopio A, Vilches V, et al. Isolation of *Bordetella* species from unusual infection sites. JMM Case Rep. 2015;2:e000029. https://doi.org/10.1099/jmmcr.0.000029
12. González MM, Romano MPC, de Guzmán García Monge MT, Martín BB, García AS. *Bordetella hinzii* endocarditis, a clinical case not previously described. Eur J Case Rep Intern Med. 2019;6:000994.
13. Zohourian H, Sorokin AV, Ladna JM, Mushtaq F. *Bordetella hinzii*: an unexpected pathogen in native valve endocarditis. Can J Cardiol. 2019;35:1604.e17–9. https://doi.org/10.1016/j.cjca.2019.08.016
14. Negishi T, Matsumoto T, Shinagawa J, Kasuga E, Horiuchi K, Natori T, et al. A case of cervical subcutaneous abscess due to *Bordetella hinzii*. Diagn Microbiol Infect Dis. 2019;95:114865. https://doi.org/10.1016/j.diagmicrobio.2019.07.003
15. Kampmeier S, Rennebaum F, Schmidt H, Riegel A, Herrmann M, Schaumburg F. Peripancreatic abscess supported by *Bordetella hinzii*. New Microbes New Infect. 2020;34:100650. https://doi.org/10.1016/j.nmni.2020.100650

Address for correspondence: Geetha Sivasubramanian, Division of Infectious Diseases, Department of Internal Medicine, UCSF Fresno, 155 N Fresno St, Ste 307, Fresno, CA 93701, USA; email: geetha.sivasubramanian@ucsf.edu

COVID-19 Vaccination Coverage, Intent, Knowledge, Attitudes, and Beliefs among Essential Workers, United States

Kimberly H. Nguyen, David Yankey, Kelsey C. Coy, Kathryn A. Brookmeyer, Neetu Abad, Rebecca Guerin, Girija Syamlal, Peng-jun Lu, Brittney N. Baack, Hilda Razzaghi, Andrea Okun, James A. Singleton

We assessed coronavirus disease vaccination and intent and knowledge, attitudes, and beliefs among essential workers during March–June 2021. Coverage was 67%; 18% reported no intent to get vaccinated. Primary concerns were potential side effects, safety, and lack of trust in vaccines, highlighting the importance of increasing vaccine confidence in this population.

Essential workers, who conduct a range of operations and services to ensure the continuity and viability of critical infrastructure functions, have more coronavirus disease (COVID-19) exposures and experience greater risk for severe illness and death than do nonessential workers (*1*–*4*). In December 2020, the US Advisory Committee on Immunization Practices issued recommendations prioritizing healthcare personnel (HCP), nonhealthcare frontline essential workers, and other essential workers for COVID-19 vaccination (*5*) (Appendix, https://wwwnc.cdc.gov/EID/article/27/11/21-1557-App1.pdf). Previous findings indicate that <50% of essential workers intended to get vaccinated: 37.1% in September 2020 and 49.1% in December 2020 (*6*,*7*). Assessing vaccination coverage and intent among essential workers, who continue to face increased risk because of their public-facing roles can help tailor messages and strategies to increase vaccination uptake and confidence among this high-risk group. We analyzed data from surveys to assess COVID-19 vaccine coverage and intent and knowledge, attitudes, and beliefs (KABs) among essential workers.

Author affiliations: Centers for Disease Control and Prevention, Atlanta, Georgia, USA (K.H. Nguyen, D. Yankey, K.C. Coy, K.A. Brookmeyer, N. Abad, R. Guerin, G. Syamlal, P. Lu, B. Baack, H. Razzaghi, A. Okun, J.A. Singleton); Leidos, Inc., Atlanta (K.C. Coy)

DOI: https://doi.org/10.3201/eid2711.211557

The Study

We analyzed data from 2 nationally representative household surveys collected over 6 COVID-19 waves during March 5–June 2, 2021, Ipsos KnowledgePanel (*8*) and NORC AmeriSpeak (*9*) (Appendix). Because of the small sample sizes, to bolster the strength of the study's estimates and increase the reliability of results, we combined data for analysis from each survey during the 6 waves of data collection.

The total sample size was 7,734 respondents; 5,303 were essential workers and 2,426 nonessential workers. We used the American Association for Public Opinion Research definition for cooperation rates (*10*), the proportion of all respondents interviewed of all eligible units ever contacted. Among respondents, cooperation rates were 20.3%–60.1%.

We categorized respondents as essential or nonessential workers. The essential worker category comprised the HCP, nonhealthcare frontline, and other essential worker groups (Appendix). We examined sociodemographic characteristics, including age group, sex, race and ethnicity, annual household income, health insurance status, marital status, urban versus rural status, and underlying conditions (Appendix).

We assessed vaccination status, intent, and KABs by worker group (Appendix). We categorized respondents as reachable or reluctant; reachable respondents said they probably would get or were unsure about getting a vaccine, whereas reluctant respondents said they probably or definitely would not get a vaccine. We assessed the following KABs about COVID-19 vaccination: reasons for not getting vaccinated, barriers to getting vaccinated, motivators for getting vaccinated, concerns about getting vaccinated, and concerns about vaccine side effects.

We weighted all surveys to ensure US population representation (Appendix). We used contrast

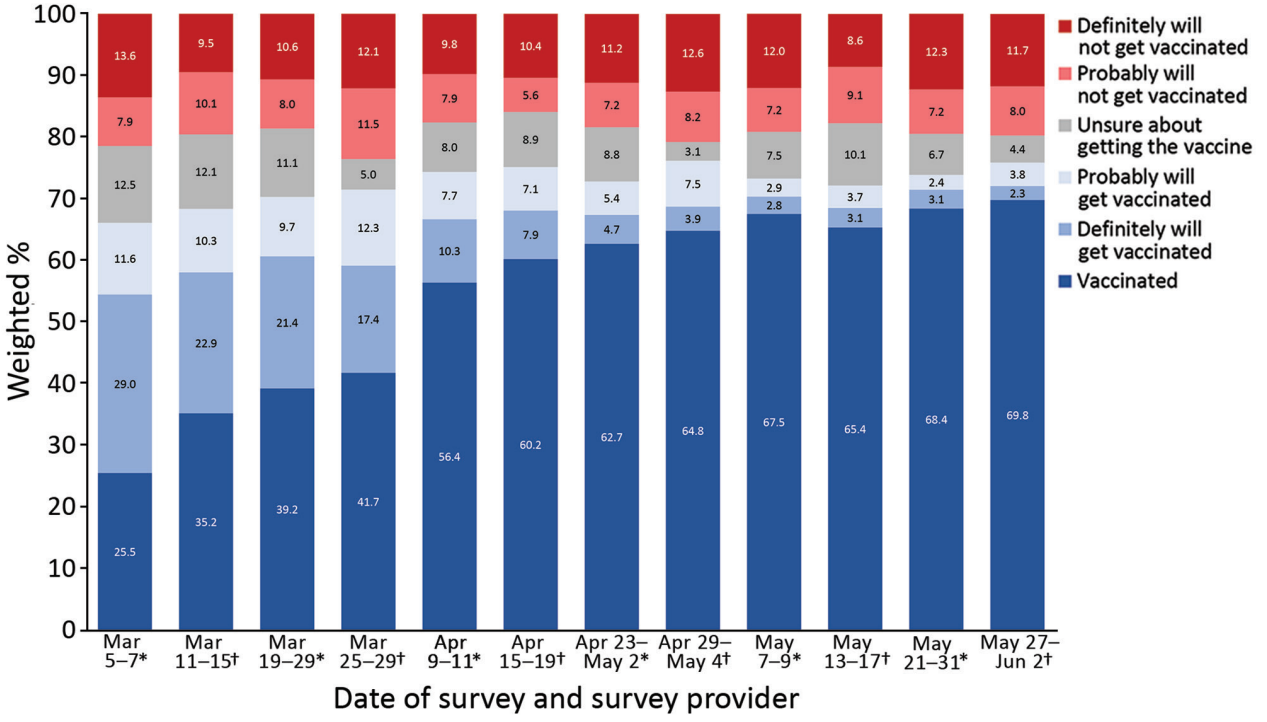

Figure 1. Trends in COVID-19 vaccination status and intent among essential workers, United States, March 5–June 2, 2021. *Data collected by Ipsos KnowledgePanel (*8*). †Data collected by NORC AmeriSpeak (*9*). COVID-19, coronavirus disease.

tests for differences in percentages to compare reachable versus reluctant groups among each of the worker categories. This activity was reviewed by the Centers for Disease Control and Prevention and was conducted consistent with applicable federal law and Centers for Disease Control and Prevention policy (Appendix).

Vaccination coverage among essential workers increased from 25.5% in March 2021 to 69.8% in June 2021 (Figure 1). Average vaccination coverage during the

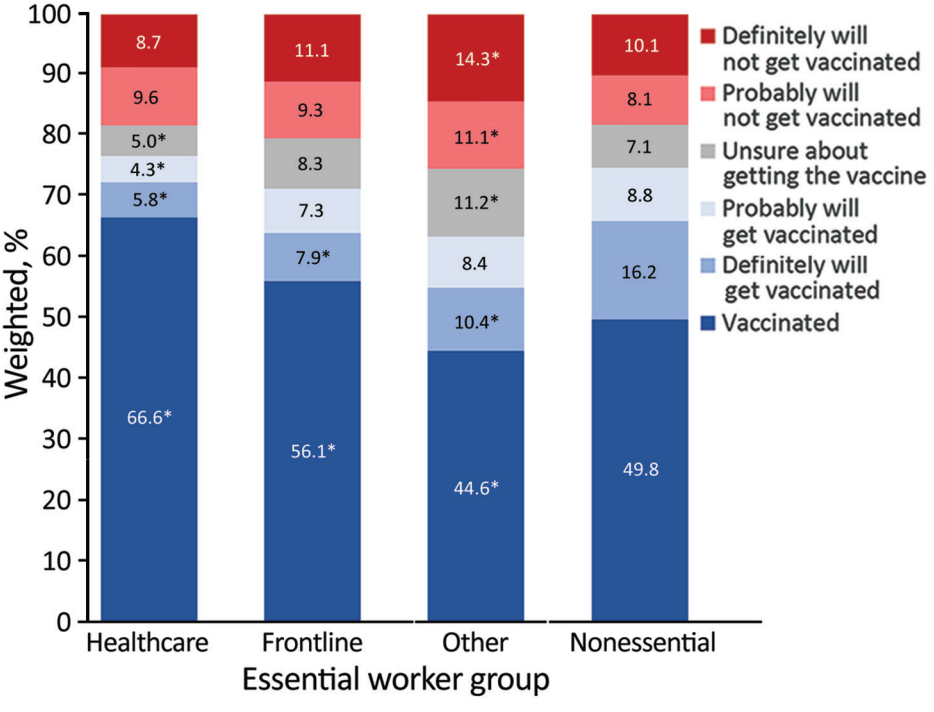

Figure 2. Average prevalence of COVID-19 vaccination status and intent by essential and nonessential worker groups, United States, March 5–June 2, 2021. Asterisk (*) indicates statistically significant ($p<0.05$) differences between vaccination coverage and intent among each essential worker group versus vaccination coverage and vaccination intent among nonessential workers. COVID-19, coronavirus disease.

study period was higher for HCP (66.6%) and frontline essential workers (56.1%) and lower for other essential workers (44.6%) and nonessential workers (49.8%) (Figures 1, 2). The percentage of reluctant persons was lowest among HCP (18.3%) and highest among other essential workers (25.5%) (Figure 2). In addition, the percentage of reluctant adults was highest (25.0%) among persons 18–34 years of age; those who had a high school education or less (28.1%), income <$25,000 (26.3%), or no health insurance (32.3%); and those who lived in rural areas (29.3%) (Appendix Table 1).

Among all unvaccinated essential workers, reasons for not getting vaccinated included concern for possible side effects (58.0%), vaccine safety (42.9%), and distrust of the vaccine (41.9%) (Table 1). Higher percentages of the reachable group than the reluctant group planned to wait to see if the vaccine is safe (54.4% vs. 35.2%) and believed that other persons need the vaccine more (28.7% vs. 12.2%). A higher percentage of the reluctant group reported a lack of trust in COVID-19 vaccines compared with the reachable group (56.2% vs. 22.3%). More respondents in the reluctant group also did not believe a vaccine is needed (36.6% vs. 10.5% of reachable group), did not think COVID-19 is much of a threat (25.9% vs. 8.6%), and did not know whether a vaccine will work (27.8% vs. 19.9%).

Concern about COVID-19 disease was lower (38.5%) than concern about side effects from the vaccine (46.4%) among all essential workers (Appendix Table 2). Among reachable groups, 42.5% reported concern about getting COVID-19 compared with 21.8% of those in reluctant groups. Among HCP,

Table 1. Reasons for not getting a COVID-19 vaccine, by essential worker group and vaccination intent, United States, March–June 2021*

	All groups, n = 5,308			Healthcare personnel, n = 1,308			Frontline workers, n = 2,300			Other workers, n = 1,700		
Reason	Total	R, n = 714	RL, n = 1,059	Total	R, n = 121	RL, n = 197	Total	R, n = 316	RL, n = 437	Total	R, n = 277	RL, n = 425
Possible side effects	58.0 (55.0–60.9)	59.5 (54.7–64.2)	57.3 (53.4–61.1)	58.3 (50.6–65.7)	55.5 (44.1–66.4)	60.4 (50.2–69.9)	57.9 (53.3–62.3)	58.4 (51.0–65.5)	57.6 (51.5–63.5)	58.0 (53.3–62.6)	62.3 (54.5–69.7)	55.1 (49.2–60.9)
Wait and see if it is safe	42.9 (40.1–45.8)	**54.4 (49.5–59.3)**	35.2 (31.6–38.9)	46.3 (39.1–53.7)	**57.7 (46.3–68.5)**	41.0 (31.6–50.9)	41.4 (37.3–45.7)	**50.4 (43.5–57.3)**	35.0 (29.9–40.4)	**43.0 (38.2–47.9)**	57.6 (49.2–65.7)	32.1 (26.9–37.8)
Do not trust the vaccine	41.9 (39.0–44.8)	**22.3 (18.6–26.4)**	56.2 (52.3–59.9)	45.2 (37.7–52.8)	**21.2 (13.3–31.1)**	57.9 (48.2–67.2)	41.3 (37.0–45.6)	**24.9 (19.1–31.5)**	54.2 (48.2–60.2)	**41.0 (36.6–45.5)**	19.8 (14.4–26.3)	57.3 (51.4–63.0)
Vaccine is not needed	25.7 (23.1–28.5)	**10.5 (7.8–13.7)**	36.6 (32.8–40.5)	23.7 (17.3–31.1)	**8.5 (4.2–15.0)**	31.8 (22.6–42.1)	24.2 (20.5–28.2)	**10.8 (7.1–15.6)**	34.4 (29.0–40.2)	**28.3 (24.1–32.8)**	10.9 (6.3–17.2)	41.8 (36.0–47.7)
Concern about allergic reaction	25.0 (22.6–27.5)	26.7 (22.8–31.0)	23.9 (20.8–27.2)	23.0 (17.7–29.0)	**32.6 (22.5–44.1)**	17.3 (11.9–24.0)	26.1 (22.4–30.0)	23.5 (18.3–29.4)	28.4 (23.2–33.9)	24.9 (20.8–29.2)	28.1 (21.3–35.8)	22.6 (18.0–27.7)
Vaccine might not work	24.3 (21.8–27.0)	**19.9 (16.3–23.9)**	27.8 (24.2–31.5)	28.5 (21.6–36.2)	**17.7 (11.1–26.3)**	34.3 (24.8–44.8)	22.6 (19.3–26.3)	**17.1 (12.3–22.9)**	27.1 (22.3–32.4)	24.2 (20.2–28.6)	23.8 (17.6–30.9)	24.8 (19.6–30.5)
Others need vaccine more	19.0 (16.8–21.4)	**28.7 (24.8–32.9)**	12.2 (9.8–14.9)	14.9 (9.8–21.3)	19.7 (11.9–29.8)	12.6 (6.3–21.7)	18.2 (15.1–21.6)	**26.0 (20.1–32.5)**	12.4 (9.2–16.1)	**21.8 (18.1–26.0)**	35.1 (27.9–42.9)	11.8 (8.3–16.2)
COVID-19 is not a threat	18.7 (16.5–21.0)	**8.6 (5.9–12.0)**	25.9 (22.9–29.2)	16.3 (11.0–22.8)	**3.1 (0.8–7.9)**†	23.3 (15.5–32.6)	17.6 (14.6–21.0)	**10.4 (6.2–16.1)**	23.2 (18.9–28.0)	**21.0 (17.4–24.9)**	8.6 (4.3–15.0)	30.4 (25.3–35.9)
Do not like needles	10.4 (8.6–12.5)	12.3 (9.1–16.1)	9.2 (6.9–11.9)	8.7 (4.5–14.8)	6.6 (1.7–16.7)†	9.8 (4.3–18.4)†	11.2 (8.5–14.5)	14.7 (9.9–20.6)	8.8 (5.6–13.0)	10.4 (7.5–13.9)	11.8 (7.0–18.3)	9.3 (6.1–13.6)
Obstacles prevent vaccination	5.1 (3.8–6.8)	6.7 (4.4–9.6)	4.0 (2.4–6.3)	6.5 (2.8–12.6)†	7.5 (3.2–14.5)†	6.0 (1.4–15.9)†	4.9 (3.2–7.2)	6.2 (3.7–9.7)	3.8 (1.7–7.2)†	4.7 (2.7–7.6)	6.8 (3.0–13.1)†	3.1 (1.6–5.5)
Concerned about cost	4.6 (3.2–6.5)	**7.2 (4.5–10.8)**	2.8 (1.5–5.0)	3.8 (1.4–8.0)†	7.0 (1.6–18.2)†	2.1 (0.4–6.2)†	3.6 (2.0–6.0)	5.8 (3.0–10.1)	2.0 (0.5–5.3)	6.2 (3.4–10.2)	8.8 (3.9–16.7)†	4.2 (1.5–9.1)†
Community members are not getting vaccinated	3.1 (2.2–4.2)	2.6 (1.6–4.1)	3.4 (2.2–5.1)	1.2 (0.3–3.2)	1.3 (0.1–5.5)†	1.2 (0.2–3.9)	4.0 (2.5–6.1)	2.9 (1.3–5.4)	4.9 (2.6–8.4)	2.9 (1.7–4.6)	2.9 (1.3–5.6)	3.0 (1.3–5.6)

*Values are reported as % respondents (95% CI). n values indicate unweighted sample size/denominator. Bold text indicates statistical significance (p<0.05) between reachable and reluctant groups; reluctant group is the referent. R respondents were defined as adults who probably would or were unsure about getting a COVID-19 vaccine. RL respondents were defined as adults who probably or definitely would not get a COVID-19 vaccine. COVID-19, coronavirus disease; R, reachable; RL, reluctant.
†Estimates do not meet the National Center for Health Statistics standards of reliability (https://www.cdc.gov/nchs/data/series/sr_02/sr02_175.pdf).

Table 2. Motivators for getting a COVID-19 vaccine, by essential worker group and vaccination intent, United States, March–June 2021*

	All groups, n = 5,308			Healthcare personnel, n = 1,308			Frontline workers, n = 2,300			Other workers, n = 1,700		
Reason	Total†	R, n = 714	RL, n = 1,059	Total	R, n = 121	RL, n = 197	Total	R, n = 316	RL, n = 437	Total	R, n = 277	RL, n = 425
Prevent COVID-19 spread to family and friends	51.4 (49.6–53.2)	**26.0 (22.0–30.3)**	4.7 (3.1–6.9)	58.0 (54.4–61.4)	**30.5 (20.3–42.3)**	7.7 (2.5–17.2)†	50.5 (47.7–53.3)	**30.7 (24.4–37.5)**	4.1 (2.2–6.8)	47.6 (44.7–50.5)	**19.1 (13.7–25.4)**	3.7 (2.0–6.3)
More information on vaccine effectiveness	44.4 (42.7–46.2)	**31.1 (26.7–35.7)**	14.1 (11.6–16.9)	46.0 (42.6–49.4)	**26.4 (17.6–36.8)**	13.7 (8.5–20.5)	44.9 (42.3–47.5)	**29.1 (23.5–35.2)**	17.1 (13.1–21.7)	42.6 (39.7–45.6)	**35.0 (27.7–42.9)**	11.0 (7.4–15.6)
Reduce COVID-19 spread in community	41.9 (40.2–43.6)	**19.4 (15.9–23.2)**	2.9 (1.7–4.7)	45.8 (42.3–49.4)	**14.5 (8.3–23.0)**	3.0 (1.1–6.5)†	42.5 (39.8–45.2)	**20.9 (16.0–26.6)**	3.2 (1.0–7.3)†	37.9 (35.0–40.9)	**19.4 (13.5–26.4)**	2.6 (1.1–5.2)
Ability to resume social activities	36.7 (35.0–38.3)	**15.5 (12.3–19.2)**	2.2 (1.3–3.3)	38.5 (35.1–42.0)	**9.0 (4.5–15.7)**	1.2 (0.2–3.8)	37.7 (35.3–40.2)	**14.3 (9.9–19.6)**	3.6 (1.9–6.1)	33.8 (31.1–36.5)	**19.3 (13.4–26.3)**	1.2 (0.4–2.8)
More severe COVID-19 cases	33.4 (31.8–35.0)	**13.7 (10.8–17.0)**	4.8 (3.4–6.6)	36.2 (32.9–39.5)	**14.4 (7.8–23.6)**	2.2 (0.7–5.4)	33.6 (31.2–36.1)	**13.1 (9.1–18.1)**	6.2 (3.5–10.0)	30.9 (28.3–33.6)	**14.0 (9.3–19.9)**	4.7 (2.7–7.5)
Ability to travel	31.3 (29.8–32.8)	**16.9 (13.8–20.5)**	6.9 (5.1–9.1)	32.5 (29.2–35.9)	15.0 (8.1–24.5)	7.4 (3.2–14.2)†	32.4 (30.1–34.7)	**16.4 (12.1–21.6)**	6.4 (4.1–9.4)	28.8 (26.2–31.4)	**18.3 (12.7–24.9)**	7.1 (4.3–10.8)
Someone I know became seriously ill or died from COVID-19	22.1 (20.8–23.5)	9.4 (6.8–12.6)	6.4 (4.6–8.5)	24.1 (21.4–27.0)	**11.7 (5.6–21.0)**†	2.7 (0.8–6.6)†	21.7 (19.7–23.9)	11.5 (6.9–17.8)	8.0 (5.2–11.6)	21.0 (18.7–23.4)	6.1 (3.6–9.6)	6.6 (3.9–10.4)
Recommend by a healthcare provider	17.2 (16.0–18.5)	**14.1 (10.9–17.9)**	3.6 (2.2–5.5)	19.9 (17.4–22.6)	**13.5 (6.3–24.2)**†	3.9 (0.8–11.0)†	16.8 (14.9–18.7)	**15.5 (10.8–21.2)**	4.2 (2.2–7.4)	15.7 (13.7–17.9)	**12.9 (7.7–19.8)**	2.8 (1.2–5.5)
Workplace or school requirement	14.9 (13.8–16.1)	**29.1 (25.0–33.5)**	14.2 (11.8–17.0)	19.9 (17.2–22.9)	**39.5 (28.6–51.2)**	10.8 (6.5–16.7)	13.7 (12.0–15.4)	**27.2 (21.6–33.5)**	17.1 (13.0–21.9)	12.8 (10.8–15.0)	**27.4 (20.9–34.7)**	13.0 (9.4–17.4)
Vaccine safety information available	14.8 (13.4–16.3)	**39.8 (35.4–44.5)**	20.8 (17.9–24.1)	11.7 (9.3–14.6)	**46.6 (35.6–57.9)**	21.2 (14.7–28.9)	14.2 (12.2–16.4)	**36.8 (30.5–43.3)**	21.7 (17.1–26.8)	18.0 (15.2–21.1)	**40.7 (33.3–48.6)**	19.7 (15.1–25.1)
Enables children back to school	14.8 (13.6–16.0)	**8.1 (5.9–10.9)**	1.5 (0.7–2.8)	16.5 (13.9–19.3)	**12.6 (5.6–23.3)**†	2.0 (0.6–5.1)	16.0 (14.2–17.8)	**8.5 (5.4–12.4)**	2.2 (0.6–5.2)	11.8 (10.0–13.8)	**6.1 (3.3–10.1)**	0.4 (0.0–1.6)
Enables me to get back to work or school	12.4 (11.2–13.7)	**4.8 (3.2–7.0)**	1.4 (0.7–2.7)	14.3 (11.7–17.3)	2.2 (0.4–6.7)†	1.7 (0.4–4.6)	14.9 (13.0–16.8)	**6.4 (3.7–10.3)**	2.0 (0.5–5.1)	7.5 (6.1–9.2)	**4.1 (1.9–7.5)**†	0.7 (0.1–2.1)
Recommended by a family member or friend	11.9 (10.8–13.0)	**5.4 (3.7–7.7)**	1.3 (0.6–2.4)	11.2 (9.0–13.7)	7.6 (2.3–17.8)†	2.2 (0.6–5.3)	13.0 (11.4–14.8)	**5.9 (3.4–9.4)**	1.7 (0.5–4.4)	10.8 (9.1–12.6)	**4.2 (2.1–7.2)**	0.3 (0.0–1.3)
See community members getting vaccinated	10.3 (9.1–11.5)	**5.2 (3.4–7.5)**	2.6 (1.3–4.6)	10.5 (8.2–13.2)	10.2 (3.7–21.3)†	2.1 (0.6–5.2)	11.7 (9.8–13.8)	5.3 (3.0–8.6)	4.5 (1.7–9.4)†	8.2 (6.7–9.9)	**3.2 (1.4–6.0)**	0.7 (0.1–2.2)
Large increase in COVID-19 cases in my area	3.1 (2.5–3.9)	**10.1 (7.7–13.0)**	3.2 (2.0–4.9)	2.3 (1.2–4.1)	**13.5 (6.4–24.1)**†	2.1 (0.5–5.3)	3.2 (2.2–4.4)	7.8 (5.1–11.4)	5.1 (2.6–8.8)	3.7 (2.5–5.4)	**11.4 (7.2–17.1)**	1.8 (0.7–3.7)
None of the above	19.9 (18.3–21.5)	**14.1 (11.1–17.6)**	55.9 (52.1–59.6)	15.6 (12.3–19.4)	**10.7 (5.8–17.7)**	54.1 (44.3–63.6)	17.7 (15.4–20.1)	**11.9 (8.1–16.7)**	52.7 (46.6–58.7)	26.2 (23.3–29.2)	**17.8 (12.1–24.9)**	60.5 (54.5–66.3)

*Values are reported as % respondents (95% CI). n values indicate unweighted sample size/denominator. Bold text indicates statistical significance ($p<0.05$) between reachable and reluctant groups; reluctant group is the referent. R respondents were defined as adults who probably would or were unsure about getting a COVID-19 vaccine. RL respondents were defined as adults who probably or definitely would not get a COVID-19 vaccine. COVID-19, coronavirus disease; R, reachable; RL, reluctant.
†Estimates do not meet the National Center for Health Statistics standards of reliability (https://www.cdc.gov/nchs/data/series/sr_02/sr02_175.pdf).

85.5% of reachable respondents were concerned about vaccine side effects compared with 68.8% of those in reluctant groups.

Among all essential workers, the main motivators for getting vaccinated were protection from spreading COVID-19 to family and friends (51.4%), receiving more information on effectiveness of COVID-19 vaccines (44.4%), and reducing spread of COVID-19 in the community (41.9%) (Table 2). Motivators that were higher among the reachable than the reluctant groups were increased information on vaccine safety (39.8% vs. 20.8%) and effica-

cy (31.1% vs. 14.1%), requirement by workplace or school (29.1% vs. 14.2%), and protection for family and friends (26.0% vs. 4.7%).

Conclusions

Despite their increased risk for COVID-19 exposure, only about 70% of essential workers included in the sample received ≥1 vaccine dose by early June 2021, similar to the 69% of all adults in the sample population during the same time period (data not shown). Over the 6 waves of data collection, HCP had the highest vaccination coverage (66.6%); those in the other essential worker group had the lowest vaccination coverage (45%) during March–June 2021, and one quarter were reluctant to get COVID-19 vaccinations. Consistent with another study (*11*), we found that younger adults and those who have lower education or income levels are more vaccine hesitant.

The first limitation of our study is that although the panel recruitment survey methodology and data weighting were designed to produce nationally representative results, respondents might not be fully representative of the general US adult population. Vaccination coverage among respondents was self-reported and could be subject to recall or social desirability bias. Data were combined across multiple survey waves, which might overaverage any recent changes in vaccination coverage and intent. Finally, state-specific vaccine prioritization varied during the data collection period, which might have affected vaccination coverage responses to items related to attitudes, behaviors, and perceptions.

Among essential workers in this sample, predominant motivators for getting vaccinated were protecting family and friends, gaining more information about the safety and effectiveness of vaccinates, and preventing community spread. These data suggest that clear, consistent messages from healthcare providers, public health officials, and immunization partners about the safety and effectiveness of the vaccine could increase vaccination coverage and vaccine confidence more broadly (*12*). In addition, framing messages in terms of benefits such as protecting family and friends; being able to travel; and resuming work, school, and social activities might further boost immunization coverage and confidence (*12*).

Among unvaccinated essential workers, nearly 60% were worried about vaccine side effects. Connecting employers and employees to credible resources on vaccine safety and expected side effects might improve vaccination coverage among essential workers. Implementing interventions to mitigate barriers to vaccination, such as flexible scheduling, paid time off for vaccination and illness resulting from side effects, on-site vaccination, and walk-in clinics, also could improve vaccination coverage.

In conclusion, our findings suggest public health officials and other leaders should differentiate between continued challenges in accessing vaccines for all populations from behavioral factors associated with vaccination. To reach vaccination goals for essential workers and everyone in the community, healthcare providers, public health officials, and immunization partners should consider KABs when tailoring messages and strategies to increase vaccination uptake and confidence, especially at local community levels.

About the Author

Dr. Nguyen is an epidemiologist in the Immunization Services Division, National Center for Immunization and Respiratory Diseases, Centers for Disease Control and Prevention (CDC), Atlanta, Georgia, USA. She is working with the CDC COVID-19 Vaccine Task Force. Her research interests include investigating gaps in COVID-19 vaccination coverage and developing strategies to increase vaccination uptake and confidence.

References

1. Cybersecurity and Infrastructure Security Agency. Guidance on the essential critical infrastructure workforce [cited 2021 May 9]. https://www.cisa.gov/publication/guidance-essential-critical-infrastructure-workforce
2. Centers for Disease Control and Prevention. Interim list of categories of essential workers mapped to standardized industry codes and titles [cited 2021 May 12]. https://www.cdc.gov/vaccines/covid-19/categories-essential-workers.html
3. The Lancet. The plight of essential workers during the COVID-19 pandemic. Lancet. 2020;395:1587. https://doi.org/10.1016/S0140-6736(20)31200-9
4. Mutambudzi M, Niedzwiedz C, Macdonald EB, Leyland A, Mair F, Anderson J, et al. Occupation and risk of severe COVID-19: prospective cohort study of 120 075 UK Biobank participants. Occup Environ Med. 2021;78:307–14. https://doi.org/10.1136/oemed-2020-106731
5. Centers for Disease Control and Prevention. COVID-19 ACIP vaccine recommendations [cited 2021 Apr 21]. https://www.cdc.gov/vaccines/hcp/acip-recs/vacc-specific/covid-19.html
6. Nguyen KH, Srivastav A, Razzaghi H, Williams W, Lindley MC, Jorgensen C, et al. COVID-19 vaccination intent, perceptions, and reasons for not vaccinating among groups prioritized for early vaccination—United States, September and December 2020. MMWR Morb Mortal Wkly Rep. 2021;70:217–22. https://doi.org/10.15585/mmwr.mm7006e3
7. Nguyen KH, Kahn K, Hoehner J, Hendrich M, Pedraza O, Fisun H, et al. COVID-19 vaccination intent, perceptions, and reasons for not vaccinating among groups prioritized for early vaccination, United States, September 2020 [cited 2021 Mar 29]. https://www.cdc.gov/vaccines/imz-managers/coverage/adultvaxview/pubs-resources/COVID-online-report2020.html
8. Ipsos. KnowledgePanel: a methodological overview [cited 2021 Mar 30]. https://www.ipsos.com/sites/default/files/ipsosknowledgepanelmethodology.pdf

9. NORC. Amerispeak omnibus [cited 2021 Mar 30]. https://amerispeak.norc.org/our-capabilities/Pages/AmeriSpeak-Omnibus.aspx
10. American Association for Public Opinion Research. Standard definitions: final dispositions of case codes and outcome rates for surveys [cited 2021 Apr 4]. https://www.aapor.org/AAPOR_Main/media/publications/Standard-Definitions20169theditionfinal.pdf
11. Biswas N, Mustapha T, Khubchandani J, Price JH. The nature and extent of COVID-19 vaccination hesitancy in healthcare workers. J Community Health. 2021 Apr 21 [Epub ahead of print]. https://doi.org/10.1007/s10900-021-00984-3
12. Centers for Disease Control and Prevention. Building confidence in COVID-19 vaccines [cited 2021 May 15]. https://www.cdc.gov/vaccines/covid-19/vaccinate-with-confidence.html

Address for correspondence: Kimberly Nguyen, Centers for Disease Control and Prevention, 1600 Clifton Rd NE, Mailstop H24-4, Atlanta, GA 30329-4027; email: uxp1@cdc.gov

Fatal Multisystem Inflammatory Syndrome in Adult after SARS-CoV-2 Natural Infection and COVID-19 Vaccination

Heather N. Grome, Michael Threlkeld, Steve Threlkeld, Charles Newman, Roosecelis Brasil Martines, Sarah Reagan-Steiner, Michael A. Whitt, Maria Gomes-Solecki, Nisha Nair, Mary-Margaret Fill, Timothy F. Jones, William Schaffner, John Dunn

We describe a fatal case of multisystem inflammatory syndrome in an adult with onset 22 days after a second dose of mRNA coronavirus disease vaccine. Serologic and clinical findings indicated severe acute respiratory syndrome coronavirus 2 infection occurred before vaccination. The immunopathology of this syndrome, regardless of vaccination status, remains poorly understood.

A multisystem inflammatory syndrome in children (MIS-C) and adults (MIS-A) occurring after coronavirus disease (COVID-19) has been identified; onset is ≈4–6 weeks after severe acute respiratory syndrome coronavirus 2 (SARS-CoV-2) infection (*1*–*3*). A case definition for MIS-A has been developed by the Centers for Disease Control and Prevention (CDC) (*4*); MIS-A after vaccination is rare and remains of great clinical and public health interest (*5*). We report a case study and histopathologic findings from a fatal MIS-A case after SARS-CoV-2 infection and subsequent complete COVID-19 vaccination.

Author affiliations: Centers for Disease Control and Prevention, Atlanta, Georgia, USA (H.N. Grome, R.B. Martines, S. Reagan-Steiner); Tennessee Department of Health, Nashville, Tennessee, USA (H.N. Grome, M.-M. Fill, T.F. Jones, J. Dunn); Baptist Memorial Health Care, Memphis, Tennessee, USA (M. Threlkeld, S. Threlkeld); Methodist LeBonheur Healthcare, Memphis (M. Threlkeld, S. Threlkeld); Pathology Group of the MidSouth, Germantown, Tennessee, USA (C. Newman); Trumbull Laboratories, Germantown (C. Newman); University of Tennessee Health Science Center, Memphis (M.A. Whitt, M. Gomes-Solecki, N. Nair); Vanderbilt University School of Medicine, Nashville (W. Schaffner)

DOI: https://doi.org/10.3201/eid2711.211612

The Patient

The patient was a healthcare worker in his 30s with no notable medical history. In December 2020, he experienced mild COVID-19–like illness symptoms, including fatigue and loss of taste and smell. He did not undergo testing for SARS-CoV-2 at that time and was unaware of the need for isolation. Six days after onset of COVID-19–like symptoms, and when fully recovered, the patient received the first dose of Pfizer/BioNTech (https://www.pfizer.com) mRNA COVID-19 vaccine. He received the second dose 20 days later. After the second dose, he reported fatigue and malaise, which resolved within 2 days.

Twenty-two days after receiving the second dose of the COVID-19 vaccine, he had onset of new fever, malaise, headache, and odynophagia. He was examined by an outpatient medical provider. Diagnostic testing was notable for a negative COVID-19 test by reverse transcription PCR (RT-PCR), negative rapid influenza antigen, and negative rapid antigen detection for group A *Streptococcus*. Four days later, the patient visited an emergency department because of worsening symptoms. Assessment of vital signs revealed a temperature of 37.2°C, heart rate 113 beats/min, and blood pressure of 117/66 mmHg. Physical examination identified right-sided cervical lymphadenopathy, marked bilateral conjunctival erythema, and a faint papular rash on the pelvis and left flank. Laboratory testing revealed a peripheral-blood leukocyte count of 11,000 cells/μL, 93.5% segmented neutrophils, and thrombocytopenia with a platelet count of 110,000/μL (Table). Portable chest radiograph results were without notable findings.

On hospital day 2, the patient remained febrile and tachycardic (heart rate 90–135 beats/min) and

had a blood pressure of 92/56 mmHg. Diagnostic evaluation revealed a negative SARS-CoV-2 RT-PCR test but a positive serologic test for SARS-CoV-2 nucleocapsid IgG. Additional diagnostic tests were conducted (Table). Inflammatory markers showed elevated C-reactive protein at 284.0 mg/L, serum ferritin at 1434.9 ng/mL, and troponin-I at 18.0 ng/mL. On the evening of hospital day 2, the patient received 75 g of intravenous immune globulin (IVIG).

Early morning on hospital day 3, the patient had an acute change in mental status, including confusion and global aphasia. An emergent computed tomography scan of the head was negative for cerebrovascular accident and showed normal brain parenchyma and no evidence of acute infarction, mass, or hemorrhage. On completion of the scan, the patient was found nonresponsive and without a pulse. He underwent multiple rounds of advanced cardiac life support, resulting in return of spontaneous circulation. A chest radiograph showed an enlarged cardiac silhouette, and an echocardiogram showed severe biventricular dysfunction, severe global hypokinesis of the left ventricle, and left ventricular ejection fraction of 20%. The patient received a second dose of IVIg and intravenous steroids and extracorporeal membrane oxygenation support was initiated. On hospital day 4, severe multisystem organ failure continued to progress. The patient died on hospital day 4.

Table. Results of pertinent laboratory testing completed during the 4-day hospitalization of a patient with fatal multisystem inflammatory syndrome in adult, Tennessee, USA, 2021*

Variable	Hospital day				Reference range
	Day 1	Day 2	Day 3†	Day 4†	
Hematologic testing					
Peripheral leukocyte count, 1,000/μL	11.0	14.4	28.1	8.8	4.2–10.2
Hemoglobin, g/dL	13.7	11.7	10.8	9.5	12.8–16.4
Hematocrit, %	39.6	33.8	34.3	27.7	38.8–48.1
Platelets, 1,000/μL	110.0	86.0	45.0	17.0	150–400
Absolute neutrophils, 1,000/μL	10.5	13.7	23.9		1.8–7.1
Absolute lymphocytes, 1,000/μL	0.4	0.4	5.0		1.3–5.9
Segmented neutrophil, %	95.3	95.3	76.6		40.0–76.0
Lymphocytes, %	3.8	2.8	15.9		14.0–46.0
Monocytes, %	1.9	0.9	0.9		4.0–12.0
Chemical testing					
Creatinine, mg/dL	1.2	1.3	3.4	1.9	0.70–1.30
AST, U/L		78.0	5,938.0	8,861.0	15–37
ALT, U/L		61.0	3,386.0	3,421.0	16–61
Total bilirubin, mg/dL	1.9	1.4	1.6		0.2–1.0
Alkaline phosphatase, U/L	76.0	74.0	295.0	202.0	45–117
Ferritin, serum, mg/dL		1434.9	>40,000.0		26.0–388.0
Coagulation					
aPTT, s	29.3		54.2	80.9	23.2–34.1
PT, s	13.9		39.6		11.7–14.5
INR	1.1		4.2	3.6	0.9–1.0
Fibrinogen, mg/dL	642.0		750.0		208–475
D-Dimer, μg FEU/mL	5.2	4.3	12.2		0.0–0.44
Cardiac					
Troponin-I, ng/mL		18.0	15.5		0.0–0.045
Immunochemical testing					
ESR, mm/h	40.0				0–15
C-reactive protein, mg/L		284.0	174.0		≤3.0
Procalcitonin level, ng/mL		4.9			0.50–2.0
Microbiologic testing					
SARS-CoV-2 RT-PCR, index value	Negative				Negative
SARS-CoV-2 IgG antibody,‡ index value	4.96				≤1.39
Adenovirus DNA PCR, qualitative	Not detected				Not detected
CMV PCR, quantitative	Negative				Negative
Mononucleosis screen	Negative				Negative
Ehrlichia chaffeensis DNA PCR	Not detected				Not detected
HIV-1 p24 Ag	Nonreactive				Nonreactive
Peripheral blood culture, 2 sets	No growth	No growth	No growth	No growth	No growth

*Laboratory values represent pertinent laboratory results during the patient's hospitalization. Not all laboratory studies completed during hospitalization are represented in this table. Blank cells indicate test not done. ALT, alanine aminotransferase; AST, aspartate aminotransferase; aPTT, activated partial thromboplastin time; CMV, cytomegalovirus; ESR, erythrocyte sedimentation rate; FEU, fibrinogen equivalent units; INR, international normalized ratio; PT: prothrombin time; RT-PCR, reverse transcription PCR; SARS-CoV-2, severe acute respiratory syndrome coronavirus 2.
†Laboratory values indicate studies after cardiac arrest, which occurred at ≈3 a.m. on hospital day 3. Note patient was initiated on extracorporeal membrane oxygenation shortly after return of spontaneous circulation; anticoagulation treatments affect laboratory values.
‡SARS-CoV-2 IgG test specific for nucleocapsid protein antibody.

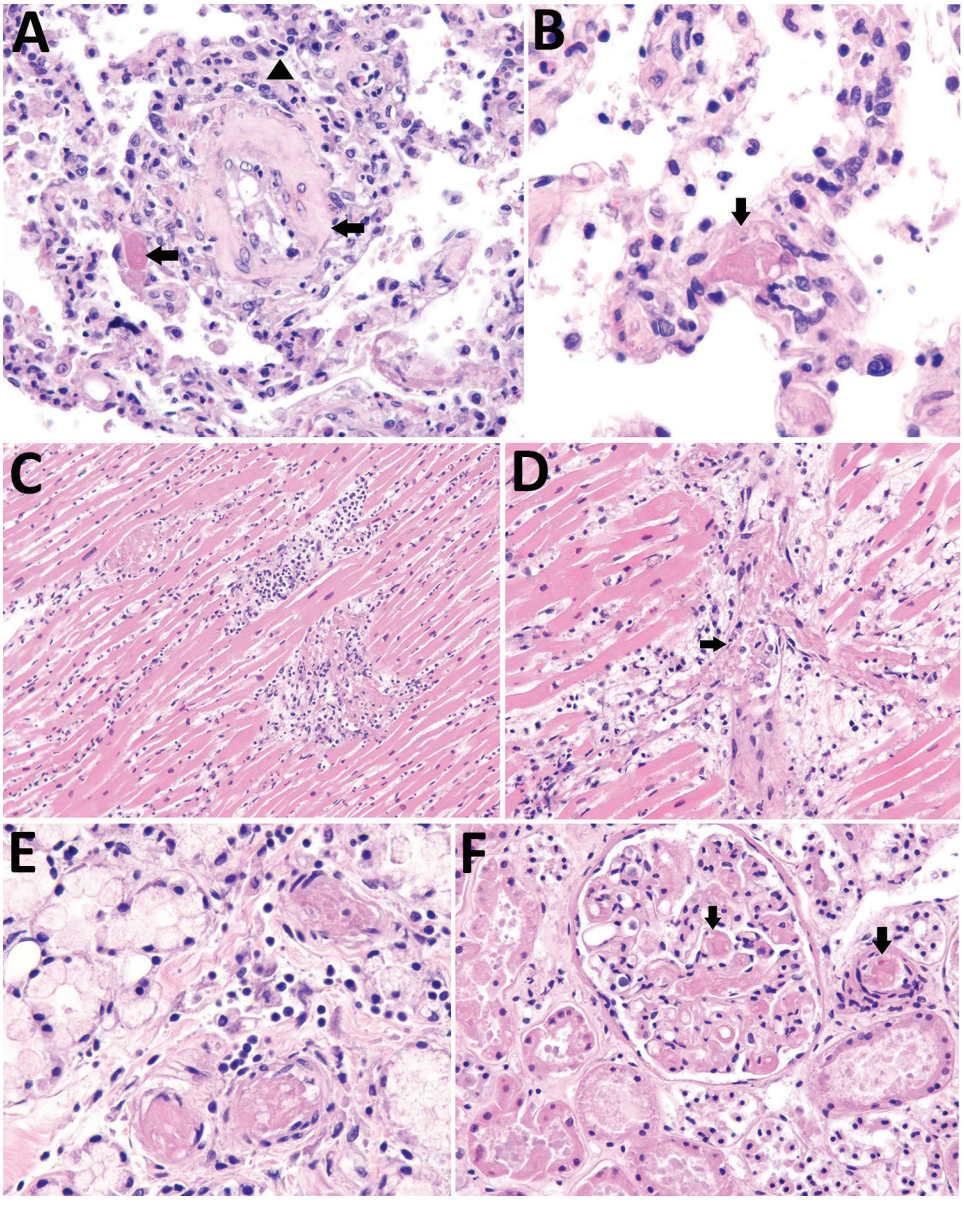

Figure. Histopathologic findings in a fatal case of multisystem inflammatory syndrome in adult after natural severe acute respiratory syndrome coronavirus 2 infection and coronavirus disease vaccination, Tennessee, USA, 2021. A) Lung tissue shows capillaritis characterized by neutrophilic inflammation and necrosis within interalveolar septa (arrowhead). Fibrin and organizing intraluminal microthrombi in small arteries are also seen (arrows). Original magnification 20×. B) Higher magnification of fibrin microthrombus within a lung vessel (arrow). Original magnification 63×. C) Heart tissue shows myocarditis with myocyte necrosis and mixed inflammatory infiltrate. Original magnification 20×. D) Higher magnification cardiac vessel showing microthrombus and perivascular mononuclear inflammatory infiltrate (arrow). Original magnification 40×. E) Stomach tissue shows submucosal microthrombi with perivascular lymphocytic infiltrate. Original magnification 63×. F) Kidney tissue shows multiple fibrin thrombi in glomerular (arrow) and interstitial capillaries (arrow). Original magnification 40×.

We reviewed the patient's medical history and clinical chart. We assessed serum samples collected during the hospital course before and after IVIg, and we determined endpoint titers to SARS-CoV-2 nucleocapsid (IgM and IgG) and spike receptor binding domain with neutralization functions against spike protein (*6*,*7*). The endpoint titer was a modified protocol based on Stadlbauer et al. (*8*). We completed an autopsy and sent formalin-fixed, paraffin-embedded tissues to CDC. Microscopic examination of lung, airways, pulmonary lymph node, liver, heart, spleen, kidneys and stomach tissue samples was performed; LT-Gram stain was performed on lungs and heart. An RT-PCR assay for SARS-CoV-2 was performed on RNA extracted from formalin-fixed, paraffin-embedded tissues from lungs, airways, and heart by methods previously published (*9*). This activity was reviewed by CDC and was conducted consistent with applicable federal law and CDC policy.

Serum antibody results drawn before IVIg infusion were negative for SARS-CoV-2 IgM but positive for IgG. Serum results had a high titer of anti-spike receptor binding domain antibody both before and after IVIg (1:75,000) compared with a naturally infected SARS-CoV-2–positive control (1:4,000). In addition, the pre-IVIG sample serum results demonstrated neutralizing function.

Notable findings on gross internal autopsy examination included a 525-mL pericardial effusion and cardiac enlargement, as well as a 5-L hemoperitoneum and a 20-cm diameter perisplenic hematoma. Microscopic examination of the lungs showed diffuse congestion, increased intra-alveolar macrophages, multifocal hemorrhage, capillaritis, and microthrombi throughout (Figure, panels A, B). We observed no viral inclusions or diffuse alveolar damage. Trachea and bronchi showed mild tracheobronchitis. Sections of the heart showed multifocal myocarditis with mixed inflammatory infiltrate, myocyte necrosis, and numerous microthrombi. We also identified disseminated microvascular thrombosis in the heart, stomach, kidneys, and liver (Figure, panels C–F). Gram stain results were negative on lung and heart tissue. SARS-CoV-2 RT-PCR was negative on lungs, trachea, bronchi, and heart.

Conclusions

This fatal case of MIS-A occurred after full COVID-19 vaccination in a patient with prior natural SARS-CoV-2 infection suspected 6 weeks before MIS-A symptom onset. Serum antibody results before IVIg infusion indicated the patient was previously infected with SARS-CoV-2 and was vaccinated with a COVID-19 vaccine. Antibodies to the nucleocapsid protein are the most sensitive target for serologic diagnosis for natural infection (P.D. Burbelo et al., unpub. data, https://doi.org/10.1101/2020.04.20.20071423), and these antibodies are not present following COVID-19 vaccination alone. In addition, clinical history was compatible with natural infection beginning 6 days before the first mRNA vaccine dose and consistent with negative SARS-CoV-2 nucleocapsid IgM on testing during hospitalization.

The patient demonstrated similar clinical findings to previously reported MIS-A cases, including fever for 3 consecutive days, laboratory evidence of inflammation, neurologic and mucocutaneous clinical findings, and severe cardiac illness that included systemic hypotension progressing to cardiogenic shock (*1*,*5*). These criteria meet the CDC case definition for MIS-A, as well as a definitive case at level 1 of diagnostic certainty by the Brighton collaboration case definition for MIS-A and MIS-C (*10*). In addition, the histopathologic findings of capillaritis and multiorgan microvascular thrombosis in association with clinical symptoms and laboratory findings are compatible with MIS-A (*1*,*11*). Substantial blood loss on gross examination may represent a diffuse intravascular coagulation–type picture in which diffuse microthrombosis depleted platelets and clotting factors. The etiology for clinical deterioration was likely multifactorial, although considerable cardiac compromise in the setting of high fluid volumes and intraperitoneal hemorrhage may have contributed to multiorgan failure

Whether mRNA COVID-19 vaccination contributed to MIS-A onset in this case is unclear, and future epidemiologic studies are needed to understand whether an association exists. The immunopathology leading to hyperinflammation causing MIS-A after SARS-CoV-2 infection remains unknown, although postinfection immune dysregulation is consistent among reported cases. Notably, MIS-A has not been reported among adult participants of COVID-19 vaccine trials (*10*), and no direct evidence exists to support vaccine alone as the primary etiology in this case. This article further emphasizes the importance of COVID-19 prevention, for which infection prevention strategies and vaccination remain our greatest defense.

This work was supported by the National Institutes of Health (grant nos. R43 AI155211 and R01 AI139267 awarded to M.G.S.).

About the Author

Dr. Grome is an infectious diseases physician and Epidemic Intelligence Service Officer for the Centers for Disease Control and Prevention, Atlanta, Georgia. She is currently assigned as a field officer at the Tennessee Department of Health in Nashville, Tennessee.

References

1. Morris SB, Schwartz NG, Patel P, Abbo L, Beauchamps L, Balan S, et al. Case series of multisystem inflammatory syndrome in adults associated with SARS-CoV-2 infection—United Kingdom and United States, March–August 2020. MMWR Morb Mortal Wkly Rep. 2020;69:1450–6. https://doi.org/10.15585/mmwr.mm6940e1
2. Tenforde MW, Morris SB. Multisystem inflammatory syndrome in adults: coming into focus. Chest. 2021;159:471–2. https://doi.org/10.1016/j.chest.2020.09.097
3. Godfred-Cato S, Bryant B, Leung J, Oster ME, Conklin L, Abrams J, et al.; California MIS-C Response Team. COVID-19-associated multisystem inflammatory syndrome in children—United States, March–July 2020. MMWR Morb Mortal Wkly Rep. 2020;69:1074–80. https://doi.org/10.15585/mmwr.mm6932e2
4. National Center for Immunization and Respiratory Diseases, Centers for Disease Control and Prevention. Multisystem inflammatory syndrome in adults (MIS-A) case definition information for healthcare providers 2021 [cited 2021 Jul 1]. https://www.cdc.gov/mis/mis-a/hcp.html
5. Salzman MB, Huang CW, O'Brien CM, Castillo RD. Multisystem inflammatory syndrome after SARS-CoV-2 infection and COVID-19 vaccination. Emerg Infect Dis. 2021;27:1944–8. https://doi.org/10.3201/eid2707.210594
6. McAndrews KM, Dowlatshahi DP, Dai J, Becker LM, Hensel J, Snowden LM, et al. Heterogeneous antibodies

against SARS-CoV-2 spike receptor binding domain and nucleocapsid with implications for COVID-19 immunity. JCI Insight. 2020;5:142386. https://doi.org/10.1172/jci.insight.142386
7. Condor Capcha JM, Lambert G, Dykxhoorn DM, Salerno AG, Hare JM, Whitt MA, et al. Generation of SARS-CoV-2 spike pseudotyped virus for viral entry and neutralization assays: a 1-week protocol. Front Cardiovasc Med. 2021;7:618651. https://doi.org/10.3389/fcvm.2020.618651
8. Stadlbauer D, Amanat F, Chromikova V, Jiang K, Strohmeier S, Arunkumar GA, et al. SARS-CoV-2 seroconversion in humans: a detailed protocol for a serological assay, antigen production, and test setup. Curr Protoc Microbiol. 2020;57:e100. https://doi.org/10.1002/cpmc.100
9. Bhatnagar J, Gary J, Reagan-Steiner S, Estetter LB, Tong S, Tao Y, et al. Evidence of severe acute respiratory syndrome coronavirus 2 replication and tropism in the lungs, airways, and vascular endothelium of patients with fatal coronavirus disease 2019: an autopsy case series. J Infect Dis. 2021;223:752–64. https://doi.org/10.1093/infdis/jiab039
10. Vogel TP, Top KA, Karatzios C, Hilmers DC, Tapia LI, Moceri P, et al. Multisystem inflammatory syndrome in children and adults (MIS-C/A): case definition & guidelines for data collection, analysis, and presentation of immunization safety data. Vaccine. 2021;39:3037–49. https://doi.org/10.1016/j.vaccine.2021.01.054
11. Magro C, Mulvey JJ, Berlin D, Nuovo G, Salvatore S, Harp J, et al. Complement associated microvascular injury and thrombosis in the pathogenesis of severe COVID-19 infection: a report of five cases. Transl Res. 2020;220:1–13. https://doi.org/10.1016/j.trsl.2020.04.007

Address for correspondence: Heather N. Grome, Tennessee Department of Health, Communicable Diseases and Emergency Preparedness Division, 710 James Robertson Pkwy, Nashville, TN 37243, USA; email: qds9@cdc.gov

Effectiveness of BNT162b2 Vaccine in Adolescents during Outbreak of SARS-CoV-2 Delta Variant Infection, Israel, 2021

Aharona Glatman-Freedman, Yael Hershkovitz, Zalman Kaufman, Rita Dichtiar, Lital Keinan-Boker, Michal Bromberg

In Israel, the BNT162b2 vaccine against severe acute respiratory syndrome coronavirus 2 was approved for use in adolescents in June 2021, shortly before an outbreak of B.1.617.2 (Delta) variant–dominant infection. We evaluated short-term vaccine effectiveness and found the vaccine to be highly effective among this population in this setting.

In May 2021, the US Food and Drug Administration and the European Medicines Agency expanded existing authorization for BNT162b2 vaccine (Pfizer-BioNTech, https://www.pfizer.com) against severe acute respiratory syndrome coronavirus 2 (SARS-CoV-2) to include its use in adolescents 12–15 years of age (*1*,*2*). On June 2, 2021, the Israel Ministry of Health declared the availability of BNT162b2 vaccine for adolescents 12–15 years of age (*3*) as a 2-dose regimen, given 21 days apart. By August 26, 2021, a total of 277,218 adolescents (46.1% of those eligible) had received 1 dose of the vaccine and 187,707 (31.2%) had received 2 doses (Figure 1, panel A). In mid-June 2021, after a month of extremely low SARS-CoV-2 activity in Israel, 2 local outbreaks erupted (*4*–*6*). These outbreaks marked the beginning of a new widespread SARS-CoV-2 outbreak in Israel (Figure 1, panel B), dominated by the B.1.617.2 (Delta) variant, which accounted for 93%–99% of the sequenced viruses during July and August 2021 (*7*). We analyzed effectiveness of this vaccine among adolescents who had been vaccinated in the early stages of this outbreak in Israel.

Author affiliations: The Israel Center for Disease Control, Ramat Gan, Israel (A. Glatman-Freedman, Y. Hershkovitz, Z. Kaufman, R. Dichtiar, L. Keinan-Boker, M. Bromberg); Tel Aviv University, Tel Aviv, Israel (A. Glatman-Freedman, M. Bromberg); Haifa University, Haifa, Israel (L. Keinan-Boker)

DOI: https://doi.org/10.3201/eid2711.211886

The study was approved by the superior ethical committee of the Israel Ministry of Health and included exemption from informed consent.

The Study

We performed a nationwide retrospective cohort study to estimate vaccine effectiveness against PCR-confirmed SARS-CoV-2 infections among adolescent Israel residents 12–15 years of age who had received the second vaccine dose during July 1–24, 2021. The data sources used are described in detail elsewhere (*8*). We estimated vaccine effectiveness and 95% CIs by using (1 – incidence rate ratio) × 100 for 1–7, 8–14, 15–21, and 22–28 days after the second vaccine dose. Incidence rate ratio denotes the ratio of the rate of PCR-confirmed SARS-CoV-2 infections in the vaccinated and unvaccinated groups.

We excluded from analysis adolescents who had had a documented SARS-CoV-2–positive PCR result before the evaluation periods, regardless of their vaccination status. When several positive SARS-CoV-2 test results were documented for the same person during the study period, we included only the first result in our analysis.

We determined the number of unvaccinated controls for each date during July 1–24, 2021, by omitting the number of fully vaccinated adolescent Israel residents 12–15 years of age who had received the second BNT162b2 vaccine dose on a particular date from the total number of Israel residents who did not have a documented SARS-CoV-2–positive test result and had not received only a single vaccine dose by that date. We expressed the denominators of the vaccinated and unvaccinated groups in person-days.

After administration of the second vaccine dose, crude vaccine effectiveness against laboratory-confirmed SARS-CoV-2 infection was 55.3% (95% CI

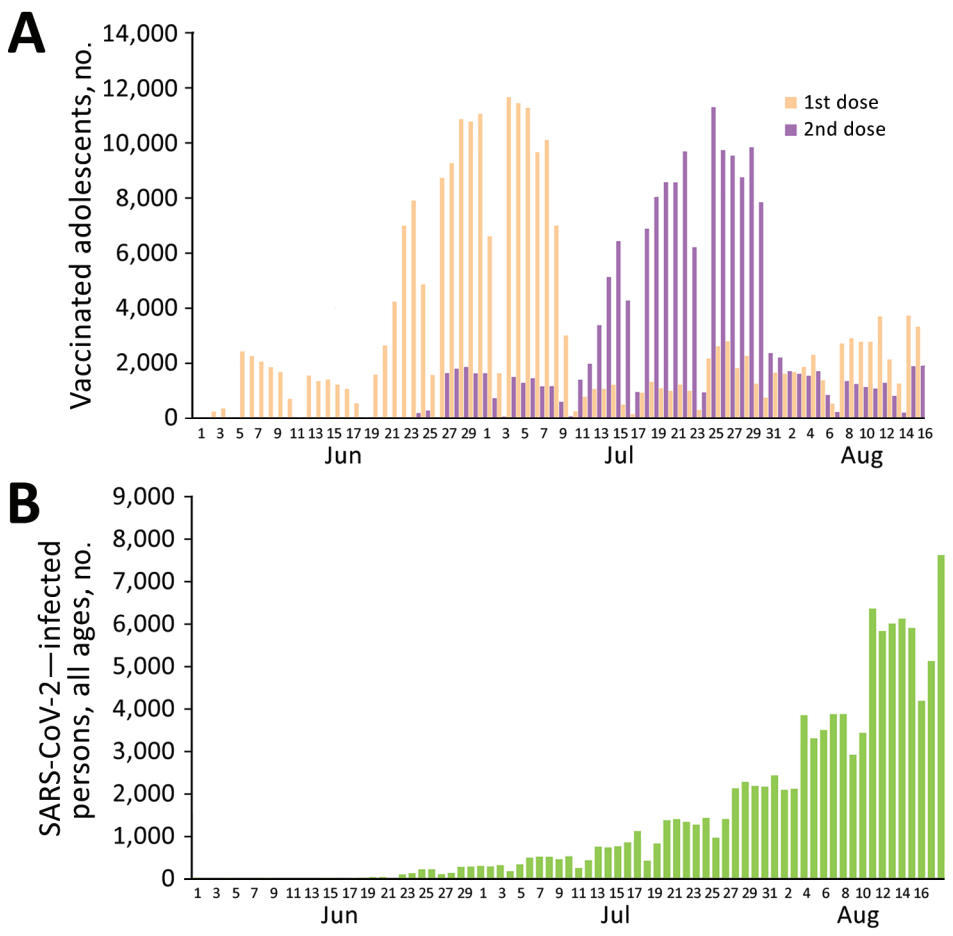

Figure 1. Vaccine doses among adolescents and total severe acute respiratory syndrome coronavirus 2 infections, Israel, June 1–August 26, 2021. A) Daily frequency of administration of first and second dose of BNT162b2 vaccine (Pfizer-BioNTech, https://www.pfizer.com) among adolescents 12–15 years of age. B) Daily cases of severe acute respiratory syndrome coronavirus 2 infection in persons of all ages.

41.3%–66.0%) in the first week, 87.1% (95% CI 81.0%–91.2%) in the second week, 91.2% (87.4%–93.8%) in the third week, and 88.2% (95% CI 85.0%–90.7%) in the fourth week (Table; Figure 2). Vaccine effectiveness differed significantly between the first and subsequent weeks, but we found no statistically significant differences in vaccine effectiveness among the second, third, and fourth weeks. Because of the small number of cases of SARS-CoV-2 infection among vaccinated adolescents, we could not adjust for weekly vaccine effectiveness evaluation. However, adjustments for sex and epidemiologic week for days 8–28 after the second dose combined demonstrated adjusted vaccine effectiveness of 91.5% (95% CI 88.2%–93.9%) against SARS-CoV-2 infection (Table). We did not estimate vaccine effectiveness against symptomatic diseases because epidemiologic investigation was performed for 42% of vaccinated and 40% of unvaccinated adolescents in our cohort.

As of August 26, 2021, none of the vaccinated adolescents who became SARS-CoV-2–positive on days 1–28 after the the second vaccine dose had been hospitalized. By that same date, among unvaccinated adolescents, 7 (0.38%) of 1,825 who tested positive for SARS-CoV-2 on days 1–7 after vaccinated adolescents had received their second vaccine dose and 26 (0.32%)

Table. Effectiveness of BNT162B2 vaccine against PCR-confirmed SARS-CoV-2 infection in adolescents 12–15 years of age after receipt of second dose, Israel, 2021*

Period	Days after second dose	Unvaccinated, SARS-CoV-2–positive, no.	Unvaccinated person-days	Vaccinated, SARS-CoV-2–positive, no.	Vaccinated person-days	Crude vaccine effectiveness (95% CI)	Adjusted vaccine effectiveness (95% CI)
Week 1	1–7	1,825	10,148,829	53	673,129	55.3 (41.3–66.0)	NA
Week 2	8–14	2,923	9,750,816	26	672,790	87.1 (81.0–91.2)	NA
Week 3	15–21	4,906	9,386,429	31	672,624	91.2 (87.4–93.8)	NA
Week 4	22–28	7,510	8,905,457	67	672,328	88.2 (85.0–90.7)	NA
Weeks 2–4	8–28	8,144	13,623,714	124	2,034,591	89.8 (87.8–91.5)	91.5 (88.2–93.9)

*BNT162B2 vaccine, Pfizer-BioNTech (https://www.pfizer.com) NA, not applicable; SARS-CoV-2, severe acute respiratory syndrome coronavirus 2.

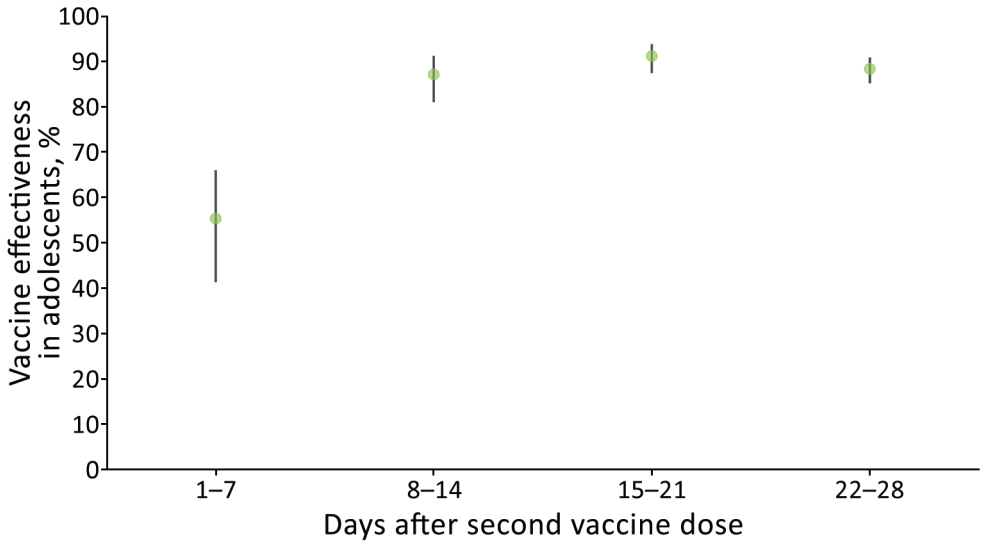

Figure 2. Vaccine effectiveness against severe acute respiratory syndrome coronavirus 2 infection in adolescents 12–15 years of age, by time after second dose of BNT162b2 vaccine (Pfizer-BioNTech, https://www.pfizer.com), Israel, 2021. Error bars indicate 95% CIs.

of 8,144 who tested positive on days 8–28 were hospitalized. Also by August 26, no vaccinated or unvaccinated SARS-CoV-2–positive adolescents had died.

Conclusions

The BNT162b2 vaccination campaign for adolescents 12–15 years of age in Israel coincided with the outbreak of the SARS-CoV-2 Delta variant. As such, the timing enabled estimation of vaccine effectiveness against SARS-CoV-2 infection for this age group during predominant circulation of the Delta variant.

Our results demonstrate high vaccine effectiveness against SARS-CoV-2 infection in this population starting the second week after the second vaccine dose. These estimates are somewhat lower than those that had been estimated for persons 16–39 years of age during the same time intervals after the second vaccine dose during circulation of the SARS-CoV-2 Alpha variant and wild-type virus in Israel (*8*). Specifically, adjusted vaccine effectiveness against SARS-CoV-2 infection for persons 16–39 years of age was 93.2% (95% CI 91.9%–94.2%) at 8–14 days, 96.7% (95% CI 95.8%–97.4%) at 15–21 days, and 96.6 (95% CI 95.7%–97.3%) at 22–28 days after receipt of the second vaccine dose. Although vaccine effectiveness estimates and 95% CIs during the circulation of the Alpha variant and the wild-type virus were adjusted for age, sex, and epidemiologic week, only minor differences in point estimates and 95% CIs were noted between crude and adjusted vaccine effectiveness (*8*).

The effectiveness estimate of 55.3% in the first week after the second dose probably reflects the effect of the first vaccine dose. This estimate is consistant with previous estimates of vaccine effectiveness 14–20 days after the first dose (*8*–*10*).

Our findings are consistent with those of a recent study from the United Kingdom, which demonstrated vaccine effectiveness of 88.0% (95% CI 85.3%–90.1%) against symptomatic disease caused by the SARS-CoV-2 Delta variant (*11*), compared with vaccine effectiveness of 93.7% (95% CI 91.6%–95.3%) against disease caused by the Alpha variant among persons ≥16 years of age who had received 2 doses of BNT162b2 (*11*). However, that study addressed neither the interval between the 2 doses nor the exact interval between assessment of vaccine effectiveness and the date of the second dose (*11*).

As of September 2021, two controlled studies had assessed vaccine efficacy in adolescents, without specifying the SARS-CoV-2 variant (*12*,*13*). One study reported BNT162b2 vaccine efficacy of 100% against laboratory-confirmed COVID-19 ≥7 days after receipt of the second vaccine dose at 21 days after the first dose (*12*). The other study reported that vaccine efficacy of the mRNA-1273 vaccine 14 days after the second dose was difficult to assess because of the low incidence of laboratory-confirmed COVID-19 in the trial population (4 cases in the placebo group and 0 cases in the mRNA-1273 group) (*13*). Of note, the geometric mean ratio of neutralizing antibodies in adolescents receiving those vaccines was similar to or greater than that of young adults after receipt of 2 doses (*12*,*13*).

Behavioral and testing policy factors can potentially affect estimations of vaccine effectiveness. Behaviors that increase exposure to SARS-CoV-2 may be assumed by vaccinated or unvaccinated adolescents for different reasons and are difficult to measure. During the study period, SARS-CoV-2 testing was available in Israel regardless of vaccination status.

The recent rise in SARS-CoV-2 cases in Israel raised 2 concerns. The first concern was that BNT162b2 vaccine–elicited immunity was waning. Waning of spike protein antibody levels was detected over time after receipt of a second dose of SARS-CoV-2 vaccines (*14*). The second concern was that the vaccine was not effective against the SARS-CoV-2 Delta variant. However, our findings indicate that the BNT162b2 vaccine provides adolescents with highly effective short-term protection against the SARS-CoV-2 Delta variant.

A.G.-F. conceived and designed the study, led data analysis, and wrote the first draft of the manuscript. M.B. oversaw the study design and analysis. Y.H. and R.D. retrieved the data. Y.H. and R.D. performed data analysis. Z.K. performed comparative evaluation with previous data. A.G.-F., Z.K., L.K.-B., and M.B. interpreted the data and edited the final manuscript. All authors revised the manuscript critically for important intellectual content and approved the final version of the manuscript.

About the Author

Dr. Glatman-Freedman is the director of the Infectious Diseases Unit in the Israel Center for Disease Control. She is affiliated academically with the School of Public Health at Tel Aviv University. Her primary research interests are the epidemiology of respiratory viruses, syndromic surveillance, and vaccine effectiveness.

References

1. Food and Drug Administration. Coronavirus (COVID-19) update: FDA authorizes Pfizer-BioNTech COVID-19 vaccine for emergency use in adolescents in another important action in fight against pandemic [cited 2021 Aug 23]. https://www.fda.gov/news-events/press-announcements/coronavirus-covid-19-update-fda-authorizes-pfizer-biontech-covid-19-vaccine-emergency-use
2. European Medicines Agency. First COVID-19 vaccine approved for children aged 12 to 15 in EU [cited 2021 Aug 23]. https://www.ema.europa.eu/en/news/first-covid-19-vaccine-approved-children-aged-12-15-eu
3. Israel Ministry of Health. Ministry of Health's position regarding the expansion of the vaccination operation to ages 12–16 years [cited 2021 Aug 23]. https://www.gov.il/en/departments/news/02062021-01
4. Israel Ministry of Health. Coronavirus outbreak in Binyamina [cited 2021 Aug 23]. https://www.gov.il/en/departments/news/19062021-02
5. Israel Ministry of Health. Effective today (20.6.2021)—masking requirement at all schools in Modi'in and Binyamina [cited 2021 Aug 23]. https://www.gov.il/en/departments/news/20062021-01
6. Israel Ministry of Health. Home Front Command coronavirus testing points closed [cited 2021 Aug 23]. https://www.gov.il/en/departments/news/02062021-03
7. Our World in Data. SARS-CoV-2 variants in analyzed sequences, Israel [cited 2021 Aug 18]. https://ourworldindata.org/grapher/covid-variants-area?country=~ISR
8. Glatman-Freedman A, Bromberg M, Dichtiar R, Hershkovitz Y, Keinan-Boker L. The BNT162b2 vaccine effectiveness against new COVID-19 cases and complications of breakthrough cases: a nation-wide retrospective longitudinal multiple cohort analysis using individualised data. EBioMedicine. 2021;72:103574. https://doi.org/10.1016/j.ebiom.2021.103574
9. Dagan N, Barda N, Kepten E, Miron O, Perchik S, Katz MA, et al. BNT162b2 mRNA Covid-19 vaccine in a nationwide mass vaccination setting. N Engl J Med. 2021;384:1412–23.
10. Chodick G, Tene L, Patalon T, Gazit S, Ben Tov A, Cohen D, et al. Assessment of effectiveness of 1 dose of BNT162b2 vaccine for SARS-CoV-2 infection 13 to 24 days after immunization. JAMA Netw Open. 2021;4:e2115985. https://doi.org/10.1001/jamanetworkopen.2021.15985
11. Lopez Bernal J, Andrews N, Gower C, Gallagher E, Simmons R, Thelwall S, et al. Effectiveness of Covid-19 vaccines against the B.1.617.2 (Delta) variant. N Engl J Med. 2021;385:585–94. https://doi.org/10.1056/NEJMoa2108891
12. Frenck RW, Jr., Klein NP, Kitchin N, Gurtman A, Absalon J, Lockhart S, et al. Safety, immunogenicity, and efficacy of the BNT162b2 Covid-19 vaccine in adolescents. N Engl J Med. 2021;385:239–50.
13. Ali K, Berman G, Zhou H, Deng W, Faughnan V, Coronado-Voges M, et al. Evaluation of mRNA-1273 SARS-CoV-2 vaccine in adolescents. N Engl J Med. 2021 Aug 11 [Epub ahead of print]. https://doi.org/10.1056/NEJMoa2109522
14. Shrotri M, Navaratnam AMD, Nguyen V, Byrne T, Geismar C, Fragaszy E, et al.; Virus Watch Collaborative. Spike-antibody waning after second dose of BNT162b2 or ChAdOx1. Lancet. 2021;398:385–7. https://doi.org/10.1016/S0140-6736(21)01642-1

Address for correspondence: Aharona Glatman-Freedman, The Israel Center for Disease Control, Israel Ministry of Health Gertner Institute Building, Tel Hashomer, Ramat Gan 5265601, Israel; email: aharona.freedman@moh.gov.il

Influenza and SARS-CoV-2 Co-infections in California, USA, September 2020–April 2021

Kyle R. Rizzo, Cora Hoover, Seema Jain, Monica Sun, Jennifer F. Myers, Brooke Bregman, Deniz M. Dominguez, Allison Jacobsen, Garrett J. Jenkins, Tamara Hennessy-Burt, Erin L. Murray

During September 1, 2020–April 30, 2021, the California Department of Public Health, Richmond, California, USA, received 255 positive influenza molecular test results that matched with severe acute respiratory syndrome coronavirus 2 molecular test results; 58 (23%) persons were co-infected. Influenza activity was minimal in California, and co-infections were sporadic.

The public health community anticipated widespread co-circulation of influenza and severe acute respiratory syndrome coronavirus 2 (SARS-CoV-2), the virus that causes coronavirus disease (COVID-19), during the 2020–21 influenza season. However, influenza activity in California was unusually low (*1*). The California Department of Public Health (CDPH; Richmond, California, USA) matched positive influenza test results with SARS-CoV-2 test results to assess the occurrence of influenza and SARS-CoV-2 co-infections in California.

The Study

California laboratories and medical providers must report all positive and nonpositive (i.e., negative, inconclusive, or invalid) SARS-CoV-2 laboratory results to their local health jurisdictions (LHJs) (*2*). For influenza, only positive results that can be submitted electronically by laboratories are reportable. Most data are reported directly to CDPH's web-based platform, California Reportable Diseases Information Exchange (CalREDIE). CalREDIE assigns electronic laboratory reports a unique identifier, personID, that can be used to link the same person across different disease reports. CalREDIE is used by 59 of California's 61 LHJs for disease tracking and reporting. Two LHJs, Los Angeles and San Diego, which represent one third of California's population, do not use CalREDIE directly; we excluded data from those LHJs.

We matched positive molecular influenza test results reported during September 1, 2020–April 30, 2021, with positive and nonpositive molecular SARS-CoV-2 test results to identify co-infections. We matched positive influenza results with nonpositive SARS-CoV-2 results to determine whether persons infected with influenza were negative for SARS-CoV-2 or were potentially not tested for SARS-CoV-2. We deduplicated all positive influenza tests results and excluded antigen test results.

We matched laboratory results first using CalREDIE personID, then by name and date of birth, and finally by manual record review if positive influenza results did not match to SARS-CoV-2 results by personID or name and date of birth (Figure 1). If a person had both positive and nonpositive SARS-CoV-2 results within 7 days of a positive influenza result, we used the positive SARS-CoV-2 result in the analysis. Persons with both positive influenza and SARS-CoV-2 test results with ≤7 days between specimen collection dates met criteria for influenza and SARS-CoV-2 co-infection. We analyzed co-infection data by week of illness onset and geographic distribution. We summarized co-infected persons by age, race and ethnicity, sex, hospitalization, and survival status. We completed all analyses using SAS version 9.4 (SAS Institute, http://www.sas.com). This study received a nonresearch determination from the California Committee for the Protection of Human Subjects.

CDPH received 258 positive influenza test results during September 1, 2020–April 30, 2021, and >21.1 million SARS-CoV-2 total test results. Among positive influenza results, 255 (99%) matched with a SARS-CoV-2 test result (positive or nonpositive). From these matches, 58 (23%) persons were co-infected

Author affiliation: California Department of Public Health, Richmond, California, USA

DOI: https://doi.org/10.3201/eid2711.21129

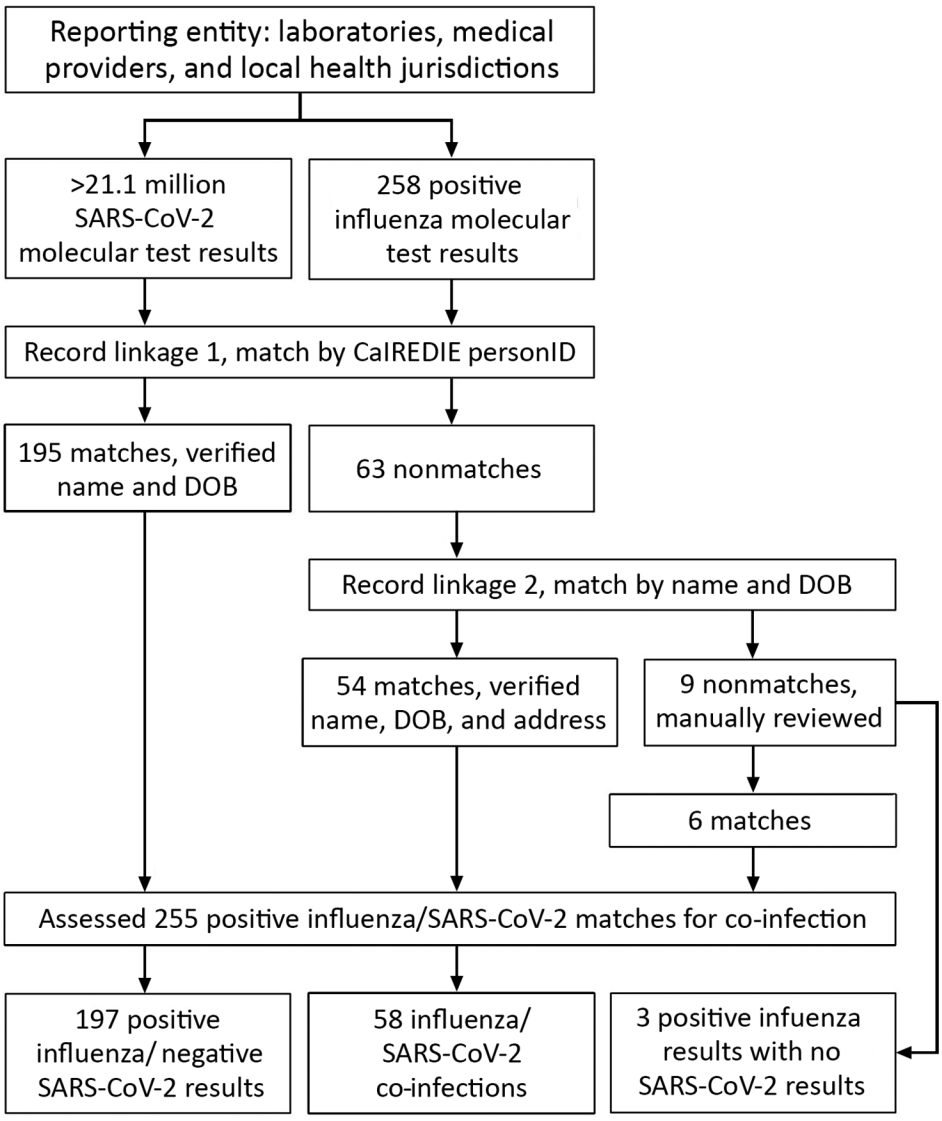

Figure 1. Matching process of influenza and SARS-CoV-2 molecular test results submitted to CalREDIE, California, USA, September 1, 2020–April 30, 2021. CalREDIE, California Reportable Diseases Information Exchange; DOB, date of birth; personID, CalREDIE individual identification code; SARS-CoV-2, severe acute respiratory syndrome coronavirus 2

with influenza and SARS-CoV-2 and 197 (77%) were positive for influenza and negative for SARS-CoV-2 (Figure 1). Co-infections occurred sporadically in California beginning in mid-November 2020 (Figure 2). At least 1 positive influenza result was received from 35 (59%) of 59 reporting LHJs, and ≥1 co-infections were identified in 21 (36%) LHJs throughout all regions in California. Among the 258 persons with positive influenza tests, 170 (66%) had influenza B and 88 (34%) influenza A. Influenza B was predominant (n = 39; 67%) among co-infected persons. Fifty-two (90%) co-infected persons had influenza and SARS-CoV-2 test specimens collected on the same date.

Age distribution among co-infected persons was 5 (9%) who were 0–17 years, 23 (40%) 18–49 years, 12 (21%) 50–64 years, and 18 (31%) ≥65 years of age. Twenty-two (38%) persons were female and 35 (60%) were male; sex was unknown for 1 (2%) co-infected person. The racial/ethnic distribution of co-infected persons was 20 (34%) Latino, 20 (34%) White, 5 (9%) Asian, 3 (5%) African American, 1 (2%) American Indian or Alaskan Native, 1 (2%) Native Hawaiian or Pacific Islander, 2 (3%) other, 2 (3%) multirace, and 4 (7%) unknown. Among 28 (48%) co-infected persons with available hospitalization status data, 11 (39%) were hospitalized. Five (9%) co-infected persons died, including 2 who were hospitalized; all who died were >50 years of age.

Conclusions

Influenza activity was minimal during the 2020–21 influenza season in the United States and Northern Hemisphere, after low levels were reported in the Southern Hemisphere during the 2020 season there

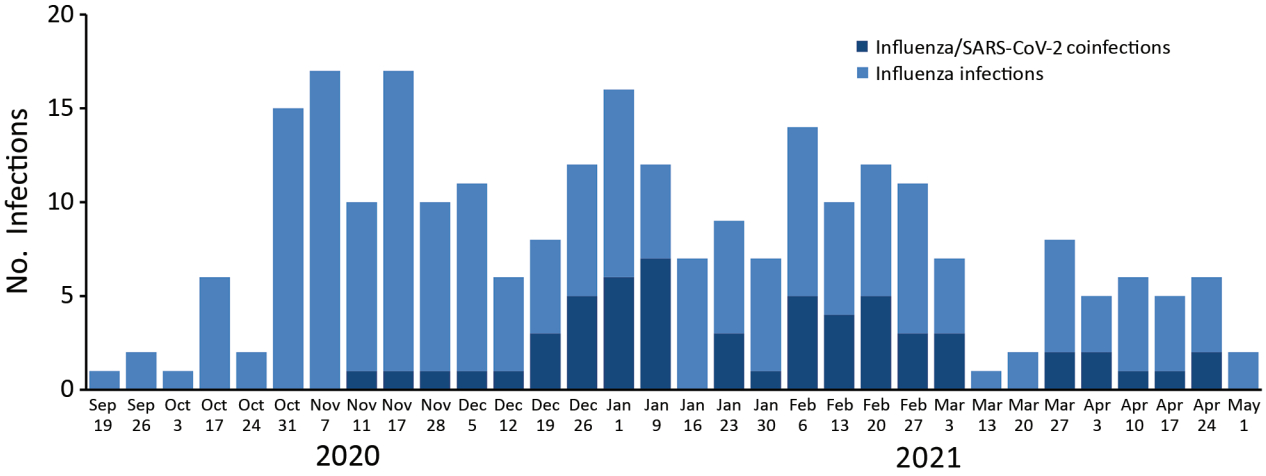

Figure 2. Number of influenza infections (n = 258) and co-infections with SARS-CoV-2 (n = 58) by week of onset, California, USA, September 1, 2020–April 30, 2021. SARS-CoV-2, severe acute respiratory syndrome coronavirus 2.

(*3*,*4*). Only 258 positive influenza test results were reported to CDPH during September 1, 2020–April 30, 2021, in contrast to the >1.77 million COVID-19 cases reported by the 59 LHJs included in this analysis. The low numbers of influenza infections in this report are consistent with California sentinel laboratory data and national trends (*1*,*3*). In addition, influenza activity in California during 2020–21 was at a historic low based on clinical sentinel laboratory data collected from 2009–2020 (*5*). Less than 1% of specimens tested were positive for influenza at California clinical sentinel laboratories throughout the 2020–21 influenza season, compared with peaks in influenza specimen positivity of 24%–41% in prior seasons. Overall, 58 (23%) of 255 persons with a positive influenza test result and a matching SARS-CoV-2 test result met our case definition for a co-infection.

Multiple factors likely account for the 2020–21 influenza season trends we observed in California. Travel was substantially affected by shelter-in-place policies, and reduced travel might have interrupted traditional influenza transmission patterns in which travelers carry influenza viruses between regions. Adopting COVID-19 mitigation practices, including social distancing, wearing face coverings, and closing schools and businesses, might also have helped prevent the transmission of influenza in communities. Factors such as viral interference might have contributed to the uncharacteristically low influenza activity reported (*6*). It is not yet clear how much influenza vaccination contributed to the minimal levels of influenza activity reported. Preliminary data from the Centers for Disease Control and Prevention indicate that overall, ≈53% of US adults had received the 2020–21 seasonal influenza vaccine by January 2021, compared with 45% of adults who had received the 2019–20 vaccine by January 2020. However, vaccination percentages were lower among children, especially Black and Hispanic children, and pregnant women in 2021 (*7*).

The first limitation of our analysis is that the lack of influenza laboratory data from Los Angeles and San Diego LHJs likely underestimates the number of influenza infections and co-infections with SARS-CoV-2 in California. However, Los Angeles and San Diego LHJs reported similarly low levels of influenza activity, and thus, including data from those LHJs is unlikely to have changed the main findings of this analysis (*8*,*9*). We could not assess whether medical providers and patients sought influenza testing during this surveillance period as routinely as they did in years past because nonpositive influenza test results are not reportable to CDPH. It is possible that SARS-CoV-2 testing was prioritized over influenza virus testing, and infrequent or inaccessible influenza testing might have contributed to underestimates of influenza transmission in California. Finally, we did not require that test results reported by laboratories and medcal providers undergo confirmatory testing by public health laboratories for inclusion in this analysis.

Ongoing public health surveillance is needed to assess the burden of SARS-CoV-2 infection and interactions with other respiratory viruses, including influenza. Healthcare providers should consider testing patients for influenza and SARS-CoV-2 on the basis of the local epidemiology of these infections and public health guidance. Safe and effective vaccines are

available throughout the United States to prevent against both influenza and COVID-19 (*10*,*11*). Healthcare providers should encourage influenza and COVID-19 vaccination as a primary prevention strategy for all community members, especially among persons of color and low-income residents, who are disproportionately affected by both diseases.

Acknowledgements

CDPH greatly appreciates the work of healthcare providers, laboratorians, researchers, and local health departments for their tireless efforts during the COVID-19 pandemic.

Aspects of this work were supported by funds from Centers for Disease Control and Prevention epidemiology and laboratory capacity grants and immunization grants and from the Coronavirus Aid, Relief, and Economic Security (CARES) Act.

About the Author

Mr. Rizzo is a research scientist with the Immunization Branch at the California Department of Public Health. His work focuses on vaccine-preventable diseases.

References

1. Immunization Branch, California Department of Public Health. Influenza surveillance program: flu reports [cited 2021 Feb 24]. https://www.cdph.ca.gov/Programs/CID/DCDC/pages/immunization/flu-reports.aspx
2. California Code of Regulations. Notification by laboratories 17 CA ADC § 2505 [cited 2021 Mar 1]. https://www.cdph.ca.gov/Programs/CID/DCDC/CDPH%20Document%20Library/LabReportableDiseases.pdf
3. Centers for Disease Control and Prevention. Weekly U.S. influenza surveillance report [cited 2021 Feb 4]. https://www.cdc.gov/flu/weekly/index.htm
4. World Health Organization. Influenza laboratory surveillance information [cited 2021 Feb 4]. https://apps.who.int/flumart/Default?ReportNo=5&Hemisphere=Northern
5. California Open Data Portal. Clinical sentinel laboratory influenza and other respiratory virus surveillance data by region and influenza season [cited 2021 Jul 13]. https://data.ca.gov/dataset/influenza-surveillance/resource/d2207905-14eb-4264-9a02-8b6ac15ddc39
6. Peng JY, Shin DL, Li G, Wu NH, Herrler G. Time-dependent viral interference between influenza virus and coronavirus in the infection of differentiated porcine airway epithelial cells. Virulence. 2021;12:1111–21. https://doi.org/10.1080/21505594.2021.1911148
7. Centers for Disease Control and Prevention. Weekly national flu vaccination dashboard [cited 2021 Feb 24]. https://www.cdc.gov/flu/fluvaxview/dashboard/vaccination-dashboard.html
8. Acute Communicable Disease Control, County of Los Angeles Public Health [cited 2021 Feb 24]. Influenza in Los Angeles County. http://publichealth.lacounty.gov/acd/FluData.htm
9. Epidemiology Unit. San Diego County Health & Human Services Agency. Influenza [cited 2021 Feb 24]. https://www.sandiegocounty.gov/hhsa/programs/phs/community_epidemiology/dc/influenza.html#Surveillance
10. Centers for Disease Control and Prevention. Who needs a flu vaccine and when [cited 2021 Mar 8]. https://www.cdc.gov/flu/prevent/vaccinations.htm
11. Centers for Disease Control and Prevention. Different COVID-19 vaccines [cited 2021 Mar 8]. https://www.cdc.gov/coronavirus/2019-ncov/vaccines/different-vaccines.html

Address for correspondence: Kyle Rizzo, California Department of Public Health, Immunization Branch, 850 Marina Bay Pkwy, Bldg P, 2nd Fl, Richmond, CA 94804, USA; email: kyle.rizzo@cdph.ca.gov

Emergence of *Vibrio cholerae* O1 Sequence Type 75, South Africa, 2018–2020

Anthony M. Smith, François-Xavier Weill, Elisabeth Njamkepo, Hlengiwe M. Ngomane, Ntsieni Ramalwa, Phuti Sekwadi, Juno Thomas

We describe the molecular epidemiology of cholera in South Africa during 2018–2020. *Vibrio cholerae* O1 sequence type (ST) 75 recently emerged and became more prevalent than the *V. cholerae* O1 biotype El Tor pandemic clone. ST75 isolates were found across large spatial and temporal distances, suggesting local ST75 spread.

The seventh cholera pandemic, caused by *Vibrio cholerae* O1 biotype El Tor (7PET), arrived in Africa during 1970 and became endemic in many countries on the continent (*1*). Cholera was first reported in South Africa in 1974 (*2*). However, South Africa is not considered a cholera-endemic area; outbreaks typically are associated with importation, particularly from neighboring countries. The last cholera outbreak in South Africa was triggered by imported cases from an outbreak in Zimbabwe during 2008; South Africa reported 12,706 cases during November 2008–April 2009 (*3*).

Globally, 7PET isolates are genetically homogeneous and linked to the Bay of Bengal in South Asia (*4*,*5*). Most 7PET isolates are multidrug-resistant sequence type (ST) 69 (*6*). Rarely, 7PET has a single-locus variant, ST515, in isolates from Africa belonging to lineage T10 (*7*). As of September 2021, all cholera isolates from South Africa have been characterized as 7PET ST69 by multilocus sequence typing (MLST).

South Africa actively surveils for cholera. Since the 2008–2009 outbreak, few cases have been identified: 5 during 2010–2014, most of which were imported, and none during 2015–2017. During 2008–2009, large outbreaks occurred in 3 provinces, Mpumalanga, Limpopo, and KwaZulu-Natal (*3*), but all were caused by imported cases from neighboring Zimbabwe and Mozambique. Therefore, given their experience, healthcare workers and laboratorians in these provinces typically will test for cholera in all cases of acute watery diarrhea.

In South Africa, the National Institute for Communicable Diseases (NICD) is notified of suspected cholera cases. NICD's Centre for Enteric Diseases supports case investigations and receives all human and environmental *V. cholerae* isolates for further investigation. The case definition for confirmed cholera is isolation of *V. cholerae* O1 or O139 from a person with diarrhea. We investigated the molecular epidemiology of *V. cholerae* in South Africa during 2018–2020.

The Study

During February 2018–January 2020, NICD received 102 *V. cholerae* isolates for testing; 9 were identified as *V. cholerae* O1. We characterized the bacteria by whole-genome sequencing, comparative genomics, and phylogenetic analysis (Appendix 1, https://wwwnc.cdc.gov/EID/article/27/11/21-1144-App1.pdf). The Human Research Ethics Committee of the University of the Witwatersrand (Johannesburg, South Africa) provided ethics approval for this study (protocol no. M160667).

Of 9 *V. cholerae* O1 isolates tested, we identified 2 ST69 (7PET) and 7 ST75 isolates. The ST69 isolates were collected in October 2018 from 2 cholera patients in a family cluster. The index case-patient had traveled to Zimbabwe, where an outbreak was ongoing (*8*), within the 7-day cholera incubation period before symptom onset. We confirmed these ST69 isolates belonged to the previously described highly antimicrobial-resistant Zimbabwe outbreak strain (*8*). The 7 ST75 isolates originated from KwaZulu-Natal and Limpopo Provinces. Five isolates were collected

Author affiliations: National Institute for Communicable Diseases, Johannesburg, South Africa (A.M. Smith, H.M. Ngomane, N. Ramalwa, P. Sekwadi, J. Thomas); University of Pretoria, Pretoria, South Africa (A.M. Smith, N. Ramalwa); Institut Pasteur, Paris, France (F.-X. Weill, E. Njamkepo)

DOI: https://doi.org/10.3201/eid2711.211144

Table 1. Clinical and demographic characteristics of 5 patients hospitalized with *Vibrio cholerae* O1 ST75 diagnosed from stool cultures and risk factors for *V. cholerae* infection, South Africa, 2018–2020*

Isolate no.	Province	Sample collection date	Patient age, y/sex	Clinical manifestations	Source of drinking water	Sanitation	Linked environmental samples	Type of environmental sample, isolate no.
YA00085869	KwaZulu-Natal	2018 Feb 8	37/F	Acute watery diarrhea, dehydration	Untreated river water	NA	N	NA
YA00132994	Limpopo	2018 Nov 9	38/M	Acute watery diarrhea, vomiting, dehydration	Untreated borehole water	Pit latrine and open defecation	N	NA
YA00134463	Limpopo	2018 Nov 20	45/M	Acute watery diarrhea, dehydration	Untreated borehole water	Flush toilets	Y	Sewage, OA01603367
YA00192016	KwaZulu-Natal	2019 Dec 29	49/M	Acute watery diarrhea, abdominal cramps, dehydration	Untreated river water	Pit latrine	Y	River water, CF00214281
YA00193061	KwaZulu-Natal	2020 Jan 12	57/F	Acute watery diarrhea, dehydration	NA	NA	N	NA

*All cases were diagnosed from stool cultures. All patients survived. NA, Not available; ST, sequence type.
†Environmental samples tested positive for *V. cholerae* O1 ST75.

from patients with cholera, all adults 37–57 years of age; 2 isolates were from environmental samples collected during case investigations, 1 from sewage in Limpopo Province and 1 from river water in KwaZulu-Natal Province (Table 1). The 3 KwaZulu-Natal cases occurred ≈200–600 km apart; the first occurred in February 2018 and the last in January 2020. The 2 Limpopo cases occurred ≈70 km apart in the same district during November 2018. The Limpopo cases were ≥900 km from the KwaZulu-Natal cases. Epidemiologic investigations involved interviewing case-patients by using a standard case investigation form; visiting case-patients' residences to inspect water and sanitation services and interview other household members; collecting stool samples from household members; and collecting environmental samples when indicated. Investigators found no evidence of importation from another country, epidemiologic links between cases, or secondary transmission.

The 7 ST75 isolates showed notable features (Table 2). In particular, all carried the cholera toxin (CTX) prophage resembling CTX-2 with *ctxB1* genotype; *Vibrio* pathogenicity island 1 (VPI-1) encoding the toxin co-regulated pilus; and a variant form of *Vibrio* pathogenicity island 2 (VPI-2). However, isolates did not contain *Vibrio* seventh pandemic island I (VSP-I) and VSP-II. We noted several genomic islands (GIs), including VC-GI 119, but GI-05 was not present (Appendix 2, https://wwwnc.cdc.gov/EID/article/27/11/21-1144-App2.xlsx).

The only antimicrobial-resistance determinant found in all ST75 isolates was the *qnrVC4* gene, located in the chromosomal superintegron. Various *qnrVC* alleles previously have been reported in the *Vibrionaceae* family and sometimes are associated with fluoroquinolone resistance (*10*,*11*). However, all ST75 isolates we analyzed showed fluoroquinolone susceptibility, MIC of ciprofloxacin 0.06 μg/mL, and susceptibility to all other tested antimicrobial drugs. This pansusceptibility sharply contrasts antimicrobial resistance trends observed in 7PET isolates from Africa, which reportedly became increasingly antimicrobial resistant over time; after the 2000s, none were susceptible to antimicrobial agents (*5*).

Table 2. Features of *Vibrio cholerae* O1 ST75 isolates, South Africa, 2018–2020*

Strain no.	Serotype	Biotype	AMR phenotype	AMR gene	Plasmids	*ctxB* allele	*tcpA*	*wbeT* mutation†	Lineage‡
YA00085869	Ogawa	El Tor	Pansusceptible	*qnrVC4*	None	*ctxB1*	*tcpA*^{N16961}	WT	L3b.1
YA00132994	Inaba	El Tor	Pansusceptible	*qnrVC4*	None	*ctxB1*	*tcpA*^{N16961}	B08	L3b.1
YA00134463	Inaba	El Tor	Pansusceptible	*qnrVC4*	None	*ctxB1*	*tcpA*^{N16961}	B08	L3b.1
OA01603367	Inaba	El Tor	Pansusceptible	*qnrVC4*	None	*ctxB1*	*tcpA*^{N16961}	B08	L3b.1
YA00192016	Ogawa	El Tor	Pansusceptible	*qnrVC4*	None	*ctxB1*	*tcpA*^{N16961}	WT	L3b.1
CF00214281	Ogawa	El Tor	Pansusceptible	*qnrVC4*	None	*ctxB1*	*tcpA*^{N16961}	WT	L3b.1
YA00193061	Ogawa	El Tor	Pansusceptible	*qnrVC4*	None	*ctxB1*	*tcpA*^{N16961}	WT	L3b.1

*AMR, antimicrobial resistance; ST, sequence type; WT, wild-type.
†Nomenclature according to F.-X. Weill et al. (*5*).
‡Nomenclature according to H. Wang et al. (*9*).

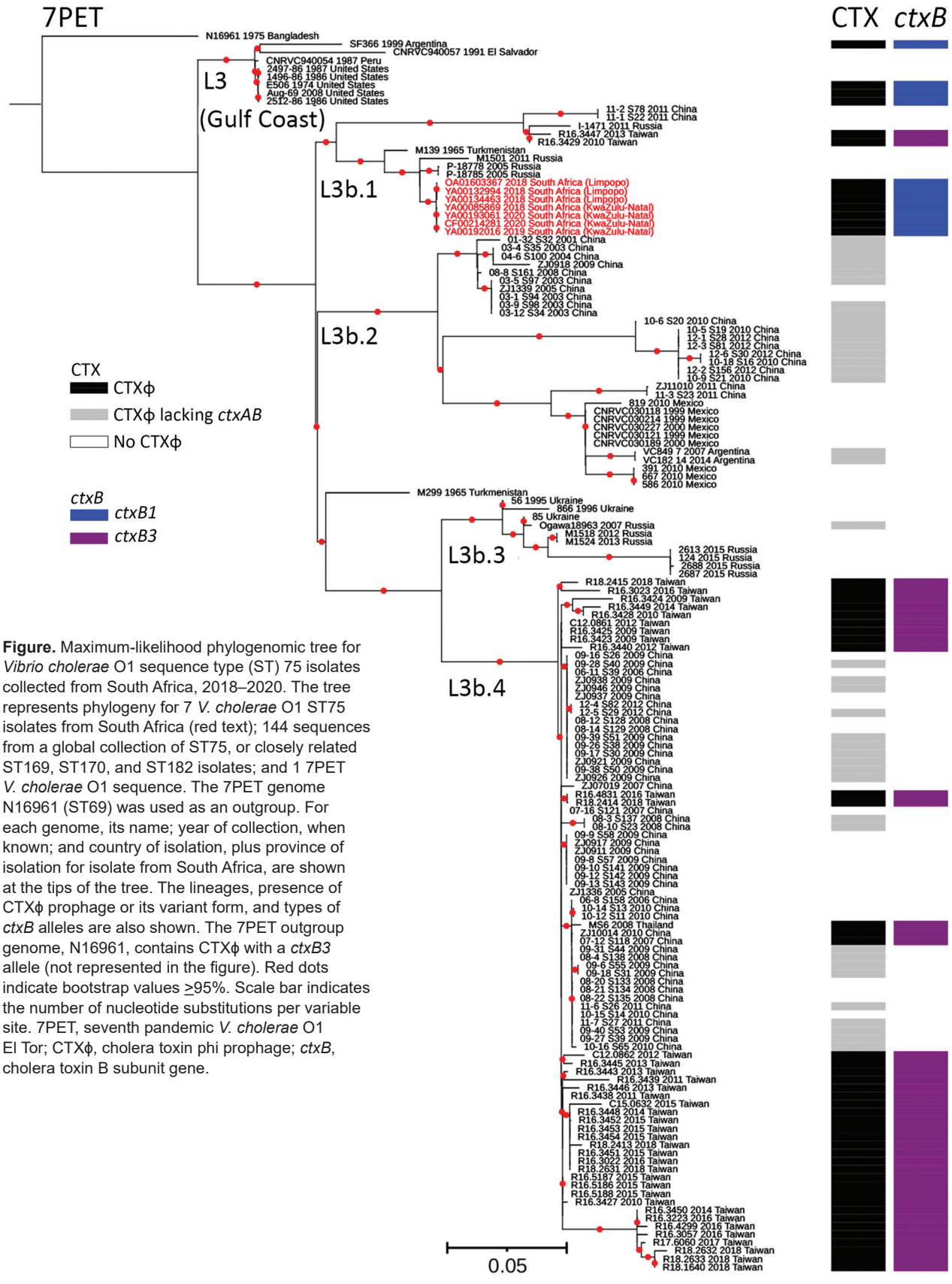

Figure. Maximum-likelihood phylogenomic tree for *Vibrio cholerae* O1 sequence type (ST) 75 isolates collected from South Africa, 2018–2020. The tree represents phylogeny for 7 *V. cholerae* O1 ST75 isolates from South Africa (red text); 144 sequences from a global collection of ST75, or closely related ST169, ST170, and ST182 isolates; and 1 7PET *V. cholerae* O1 sequence. The 7PET genome N16961 (ST69) was used as an outgroup. For each genome, its name; year of collection, when known; and country of isolation, plus province of isolation for isolate from South Africa, are shown at the tips of the tree. The lineages, presence of CTXϕ prophage or its variant form, and types of *ctxB* alleles are also shown. The 7PET outgroup genome, N16961, contains CTXϕ with a *ctxB3* allele (not represented in the figure). Red dots indicate bootstrap values ≥95%. Scale bar indicates the number of nucleotide substitutions per variable site. 7PET, seventh pandemic *V. cholerae* O1 El Tor; CTXϕ, cholera toxin phi prophage; *ctxB*, cholera toxin B subunit gene.

We further compared the ST75 isolates from South Africa with a larger global collection of 144 ST75, or closely related ST169, ST170, and ST182, genomes (Appendix 2), and constructed a maximum-likelihood phylogeny by using 49,540 SNPs (Figure). Our phylogenetic analysis showed that the 7 isolates from South Africa clustered in the L3b.1 clade, defined by H. Wang et al. (*9*), with a maximum pairwise distance of 22 SNPs. Isolates from Limpopo Province had a maximum pairwise distance of 1–6, but KwaZulu-Natal Province isolates had no SNP differences. Core-genome MLST showed Limpopo Province isolates differed from the KwaZulu-Natal Province isolates by 4–5 alleles (Appendix 1 Figure). The closest related isolates were collected in Russia from Rostov Oblast in 2005 and Republic of Kalmykia in 2011 and from Turkmenistan in Central Asia in 1965, but none of those isolates contained the CTX prophage. L3b.1 isolates from Taiwan containing the CTX prophage *ctxB3* allele were more distant.

Emergence of ST75 L3b.1 clade in South Africa is cause for concern. Recent studies on *V. cholerae* O1 isolated in Taiwan (*12*) and China (*13*) reported emerging and potential toxigenic ST75. Genomic signatures of these ST75 isolates closely resembled the US Gulf Coast *V. cholerae* O1 clone that emerged in 1973 (*14*). In particular, an investigation of *V. cholerae* O1 isolated during 2002–2018 in Taiwan showed that ST75 emerged there in 2009 and now is more prevalent than the ST69 pandemic clone (*12*). Our findings from South Africa align with the findings from Taiwan, showing that ST75 isolates outnumber ST69 isolates.

One limitation of our study is that we used reference laboratory data and a review of published *V. cholerae* O1 data to conclude that all previous cholera isolates in South Africa characterized by MLST were *V. cholerae* O1 biotype El Tor ST69. However, we cannot exclude the possibility that *V. cholerae* O1 isolates not characterized by MLST, particularly those from environmental samples, could have been non-ST69.

Epidemic 7PET lineage cholera demands an aggressive public health response to prevent outbreaks. In contrast, sporadic *V. cholerae* O1 infections mediated by other lineages, including those carrying toxin co-regulated pilus and CTX genes, typically are not epidemic-prone; most are associated with sporadic cases that rarely lead to secondary transmission (*15*). Tailoring the public health response to the degree of epidemic risk would be invaluable, especially in resource-limited settings. In countries that are not cholera-endemic but are at high risk for cholera introductions, conventional laboratory determination of *V. cholerae* O1, even complemented by identifying *ctxA* or *ctxB* genes, might be insufficient. Typing resolution of genomics, which distinguishes between 7PET and nonepidemic lineages, can elucidate the local and global epidemiology of cholera and inform public health decisions.

Conclusions

The emergence and dominance of nonepidemic, non-7PET, *V. cholerae* ST75 L3b.1 in South Africa requires close monitoring. The spatiotemporal pattern suggests local spread, possibly indicating a geographically widespread risk for sporadic disease from this strain. South Africa should strengthen its disease and environmental surveillance systems to identify nonpandemic ST75 strains, define local epidemiology, and inform an appropriate public health response.

Acknowledgments

We thank the following departments and divisions for their assistance during our study: the KwaZulu-Natal Provincial Centre for Disease Control and Prevention Directorate; health officials in King Cetshwayo, Ugu, and Umkhanyakude districts in KwaZulu-Natal Province; the Limpopo Province Department of Health; health officials in Capricorn District, Limpopo Province; National Health Laboratory Service laboratories and personnel, KwaZulu-Natal and Limpopo Provinces; Ampath Laboratories, KwaZulu-Natal Province; and Division of Public Health Surveillance and Response, National Institute for Communicable Diseases.

This study was funded by the United Kingdom Department of Health and Social Care, managed by the Fleming Fund, and performed under the auspices of the SEQAFRICA project. The Fleming Fund is a £265 million aid program supporting ≤24 low- and middle-income countries to generate, share, and use data on antimicrobial resistance. The Fleming Fund works in partnership with Mott MacDonald, the Management Agent for the Country and Regional Grants and Fellowship Programme.

About the Author

Dr. Smith is a principal medical scientist at the Centre for Enteric Diseases, National Institute for Communicable Diseases, Johannesburg, South Africa. He also holds an extraordinary professor appointment at the University of Pretoria, Pretoria, South Africa. His research interests include surveillance and epidemiology of enteric bacterial pathogens in South Africa.

References

1. Mintz ED, Tauxe RV. Cholera in Africa: a closer look and a time for action. J Infect Dis. 2013;208:S4–7. https://doi.org/10.1093/infdis/jit205
2. Küstner HG, Gibson IH, Carmichael TR, Van Zyl L, Chouler CA, Hyde JP, et al. The spread of cholera in South Africa. S Afr Med J. 1981;60:87–90.
3. Ismail H, Smith AM, Tau NP, Sooka A, Keddy KH; Group for Enteric, Respiratory and Meningeal Disease Surveillance in South Africa. Cholera outbreak in South Africa, 2008–2009: laboratory analysis of *Vibrio cholerae* O1 strains. J Infect Dis. 2013;208:S39–45. https://doi.org/10.1093/infdis/jit200
4. Mutreja A, Kim DW, Thomson NR, Connor TR, Lee JH, Kariuki S, et al. Evidence for several waves of global transmission in the seventh cholera pandemic. Nature. 2011;477:462–5. https://doi.org/10.1038/nature10392
5. Weill FX, Domman D, Njamkepo E, Tarr C, Rauzier J, Fawal N, et al. Genomic history of the seventh pandemic of cholera in Africa. Science. 2017;358:785–9. https://doi.org/10.1126/science.aad5901
6. Ramamurthy T, Mutreja A, Weill FX, Das B, Ghosh A, Nair GB. Revisiting the global epidemiology of cholera in conjunction with the genomics of *Vibrio cholerae*. Front Public Health. 2019;7:203. https://doi.org/10.3389/fpubh.2019.00203
7. Irenge LM, Ambroise J, Mitangala PN, Bearzatto B, Kabangwa RKS, Durant JF, et al. Genomic analysis of pathogenic isolates of *Vibrio cholerae* from eastern Democratic Republic of the Congo (2014–2017). PLoS Negl Trop Dis. 2020; 14:e0007642. https://doi.org/10.1371/journal.pntd.0007642
8. Mashe T, Domman D, Tarupiwa A, Manangazira P, Phiri I, Masunda K, et al. Highly resistant cholera outbreak strain in Zimbabwe. N Engl J Med. 2020;383:687–9. https://doi.org/10.1056/NEJMc2004773
9. Wang H, Yang C, Sun Z, Zheng W, Zhang W, Yu H, et al. Genomic epidemiology of *Vibrio cholerae* reveals the regional and global spread of two epidemic non-toxigenic lineages. PLoS Negl Trop Dis. 2020;14:e0008046. https://doi.org/10.1371/journal.pntd.0008046
10. Fonseca EL, Dos Santos Freitas F, Vieira VV, Vicente ACP. New *qnr* gene cassettes associated with superintegron repeats in *Vibrio cholerae* O1. Emerg Infect Dis. 2008;14:1129–31. https://doi.org/10.3201/eid1407.080132
11. Fonseca EL, Vicente ACP. Epidemiology of *qnrVC* alleles and emergence out of the *Vibrionaceae* family. J Med Microbiol. 2013;62:1628–30. https://doi.org/10.1099/jmm.0.062661-0
12. Tu YH, Chen BH, Hong YP, Liao YS, Chen YS, Liu YY, et al. Emergence of *Vibrio cholerae* O1 sequence type 75 in Taiwan. Emerg Infect Dis. 2020;26:164–6. https://doi.org/10.3201/eid2601.190934
13. Luo Y, Octavia S, Jin D, Ye J, Miao Z, Jiang T, et al. US Gulf-like toxigenic O1 *Vibrio cholerae* causing sporadic cholera outbreaks in China. J Infect. 2016;72:564–72. https://doi.org/10.1016/j.jinf.2016.02.005
14. Wachsmuth IK, Bopp CA, Fields PI, Carrillo C. Difference between toxigenic *Vibrio cholerae* O1 from South America and US Gulf Coast. Lancet. 1991;337:1097–8. https://doi.org/10.1016/0140-6736(91)91744-F
15. Domman D, Quilici ML, Dorman MJ, Njamkepo E, Mutreja A, Mather AE, et al. Integrated view of *Vibrio cholerae* in the Americas. Science. 2017;358:789–93. https://doi.org/10.1126/science.aao2136

Address for correspondence: Anthony Smith, Centre for Enteric Diseases, National Institute for Communicable Diseases, Private Bag X4, Sandringham, 2131, Johannesburg, South Africa; email: anthonys@nicd.ac.za

Toward Cholera Elimination, Haiti

Stanislas Rebaudet, Patrick Dély, Jacques Boncy, Jean Hugues Henrys, Renaud Piarroux

This study describes the apparent discontinuation of cholera transmission in Haiti since February 2019. Because vulnerabilities persist and vaccination remains limited, our findings suggest that case-area targeted interventions conducted by rapid response teams played a key role. We question the presence of environmental reservoirs in Haiti and discuss progress toward elimination.

After cholera was reintroduced into Haiti in 2010 (*1*), the country experienced an epidemic of unparalleled magnitude: the 9,789 recorded casualties represent the largest number for a single epidemic in the past 20 years (http://apps.who.int/gho/data/node.main.174). Unfortunately, vulnerabilities of people in Haiti to fecal–oral diseases such as cholera have barely been reduced over the past decade. The National Plan for the Elimination of Cholera 2013–2022 aimed to improve access to drinking water to ≥85% of the population, access to sanitation to ≥90% of the population, and access to healthcare to ≥80% of the population (*2*). However, these indicators improved very slowly or even deteriorated during 2012–2017 (*3*). The country still faces a deep economic and social crisis and has also endured several natural disasters, such as Hurricane Matthew in October 2016. In addition, the Multi-Partner Trust Fund set in December 2016 by the United Nations to support the response to cholera in Haiti gathered only US $20.8 million during 2016–2020 (http://mptf.undp.org/factsheet/fund/CLH00).

To alleviate these persisting vulnerabilities and eliminate cholera transmission, experts and public health institutions have appealed to expand mass use of oral cholera vaccines (OCV) (*4*,*5*). Meanwhile, a nationwide coordinated rapid response strategy structured around case-area targeted interventions was gradually implemented beginning in July 2013 by the Ministry of Public Health and Population of Haiti (MOH), UNICEF, and other partners (*6*). Analogous to forest fire management, the strategy aimed to rapidly detect local outbreaks and send rapid response teams, mostly composed of nongovernmental organization and MOH staff, to the households and neighbors of infected persons (Appendix, https://wwwnc.cdc.gov/EID/article/27/11/20-3372-App1.pdf). This study aims to describe and decipher the progress of cholera control in Haiti.

The Study

We analyzed cholera surveillance data routinely collected since 2010 by the MOH with support of the Pan American Health Organization and the Centers for Disease Control and Prevention, including results of stool cultures searching for *Vibrio cholerae* O1 (Appendix). The study was approved by the Bioethics National Committee of the MOH (authorization no. 1819-41). Suspected cholera cases stagnated during 2013–2016; the median was 38,733 annual cases (incidence rate 6.9/100,000 person-weeks). Incidence then dramatically decreased to 13,681 cases (incidence rate 2.2/100,000 person-weeks) in 2017, to 3,777 cases (incidence rate 0.6/100,000 person-weeks) in 2018, and to 720 cases in 2019 (incidence rate 0.1/100,000 person-weeks). The last cluster of suspected cholera cases and the last cholera-associated death were observed in the commune of L'Estère, Artibonite department, in February 2019. As of July 1, 2021, a total of 92 (67%) of the 140 communes have not notified a case for ≥3 years (Figure 1, panel A). Of note, the last stool culture positive for *V. cholerae* O1 was also sampled in L'Estère on February 4, 2019; none of the

Author affiliations: Hôpital Européen, Marseille, France (S. Rebaudet); Aix Marseille Univ, Institut National de la Santé et de la Recherche Médicale, Institut de Recherche pour le Développement, Sciences Économiques et Sociales de la Santé et Traitement de L'information Médicale, ISSPAM, Marseille (S. Rebaudet); Institut Pierre-Louis d'Epidémiologie et de Santé Publique, Sorbonne Université, Institut National de la Santé et de la Recherche Médicale, Paris, France (S. Rebaudet, R. Piarroux); Direction d'Epidémiologie des Laboratoires et de la Recherche, Ministère de la Santé Publique et de la Population, Delmas, Haiti (P. Dély); Faculté de Médecine et de Pharmacie, Université d'Etat d'Haïti, Port-au-Prince, Haiti (P. Dély); Laboratoire National de Santé Publique, Ministère de la Santé Publique et de la Population, Delmas (J. Boncy); Equipe de recherche sur l'écologie des maladies infectieuses et tropicales (EREMIT), Université Quisqueya, Port-au-Prince (J.H. Henrys); AP-HP, Hôpital Pitié-Salpêtrière, Paris (R. Piarroux)

DOI: https://doi.org/10.3201/eid2711.203372

5,223 consecutive stool specimens sampled from diarrheic patients across the country, including 2,255 specimens sampled in 2021, have tested positive since 2019 (Figure 1, panel B). Reports of cholera have thus halted for ≥3 years in 112 (80%) of communes in Haiti (Figure 1, panel A).

To analyze factors associated with this apparent discontinuation of cholera transmission in February 2019, we compiled data from mass OCV campaigns implemented across Haiti (Appendix). During 2012–2018, the MOH recorded 33 campaigns targeting 31 communes and 16 prisons (Table 1; Figure 2, panel A). A total of 1,576,209 persons received ≥1 dose. The 2-dose regimen was completed for 74% of these persons, with marked heterogeneity (Figure 2, panel A). Overall, <10% of the population in Haiti has been fully vaccinated (Table 1). Considering the duration of protection of 1-dose and 2-dose regimens of OCVs (*7*), only 2.4% of persons in Haiti were likely still protected in 2019 (Table 1).

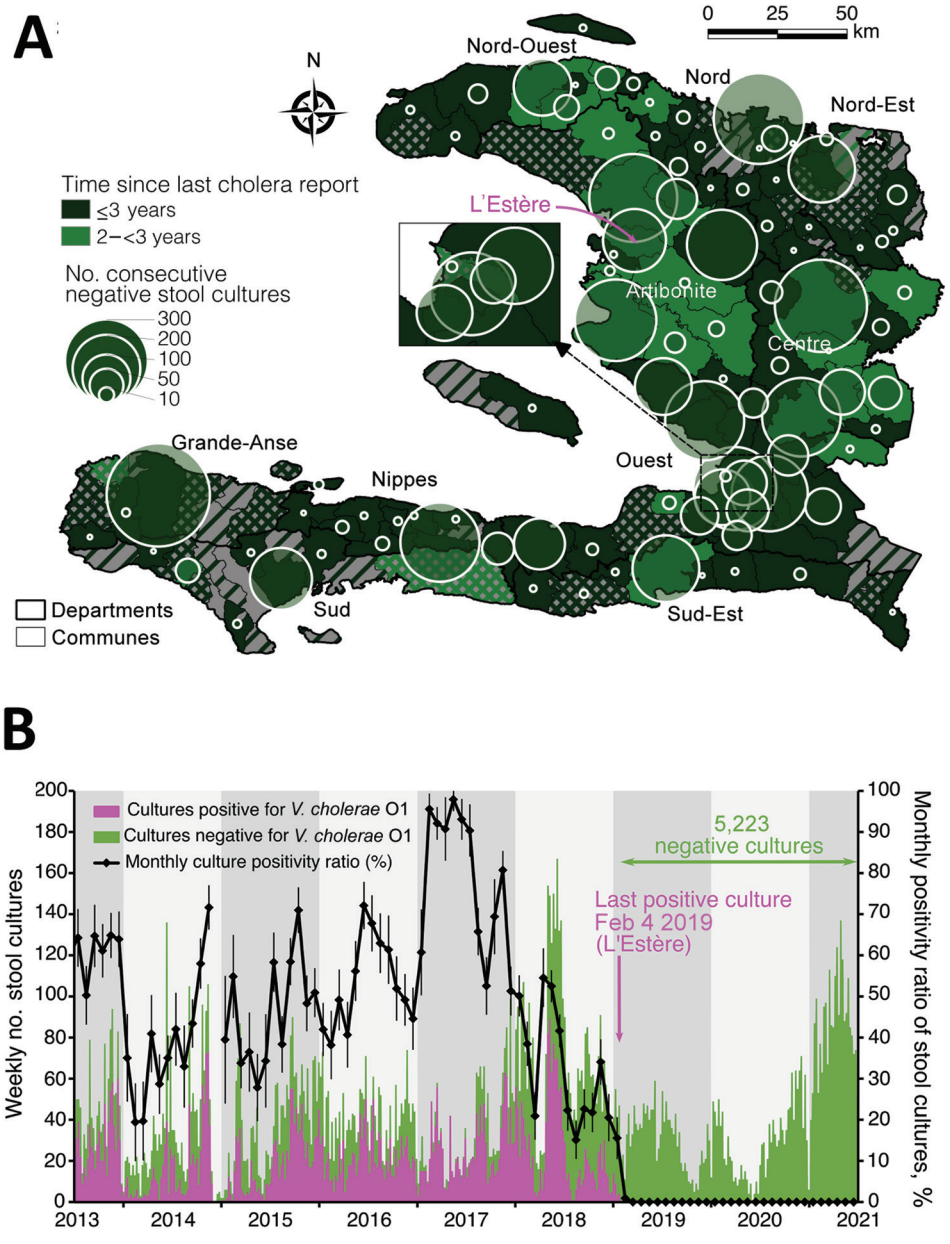

Figure 1. Cholera elimination progress and surveillance effort in Haiti as of July 1, 2021. A) Time elapsed since the last cholera report (i.e., number of years since the last positive culture or last reported suspected cholera case [choropleth colors and patterns]) and of the number of consecutive negative cultures (proportional circles), by commune. Communes with ≥1 negative culture since the last positive culture or the last reported death are colored with solid green, with elimination time calculated since the last positive culture or suspected cholera death; communes with no stool sampled for culture since the last positive culture or the last reported death are colored with green cross-hatching, with elimination time calculated since the last reported suspected cholera case or death; communes with no history of stool sampling for cholera culture but with reported cases are colored with green diagonal hatching, with elimination time calculated since the last reported suspected cholera case or death; and communes with no history of stool sampling and no reported cases are colored in solid gray. Communes are colored according to the time elapsed since possible elimination (i.e., number of years since the last positive culture or the last reported suspected cholera case). The magenta arrow localizes the commune of the last positive stool sample in Haiti. B) Plot of the weekly number of positive (magenta) and negative (green) stool cultures for *Vibrio cholerae* O1 and monthly culture-positivity ratio. Data source: Ministry of Public Health and Population of Haiti (pers. comm., 2021 Jul 20; see also Appendix, https://wwwnc.cdc.gov/EID/article/27/11/20-3372-App1.pdf). *V. cholerae* O1, *Vibrio cholerae* O1.

Table 1. Summary of killed whole-cell oral cholera vaccine campaigns, Haiti, 2012–2019*

Year	Population in Haiti	No. (%) targeted communes	No. persons who received ≥1 OCV dose	No. persons who received 2nd OCV dose (%)	Percentage of fully vaccinated population†	Percentage of population with residual vaccine immunity‡
2012	10,644,927	3	97,774	88,762	0.8%	0.5%
2013	10,937,675	2	113,045	102,250	0.9%	1.0%
2014	11,239,398	8	197,147	188,909	1.7%	1.8%
2015	11,550,392	0	0	0	0.0%	1.5%
2016	11,870,966	18	885,210	106,054	0.9%	1.5%
2017	12,201,437	3	215,358	628,049	5.1%	5.1%
2018	12,542,135	1	67,675	59,537	0.5%	3.9%
2019	12,893,402	0	0	0	0.0%	2.4%
Total	NA	31 (22)	1,576,209	1,173,561 (74)	9.1%	NA

*Data source: Ministry of Public Health and Population of Haiti (pers. comm., 2021 Jul 20; see also Appendix, https://wwwnc.cdc.gov/EID/article/27/11/20-3372-App1.pdf). NA, not applicable; OCV, oral cholera vaccine.
†The proportion of fully vaccinated population was calculated by dividing the number of persons who received the 2nd OCV dose by the population of Haiti.
‡Percentage of the population with residual vaccine immunity was estimated taking into account the number of vaccinated persons, the percentage of fully vaccinated persons, and the published protection duration after a 1-dose and 2-dose regimen (Appendix).

We compiled a total of 48,710 case-area targeted interventions recorded by UNICEF during July 2013–December 2019 that were implemented across 139 administrative communes (Table 2; Figure 2, panel B). Of those interventions, ≈71% involved a complete package: house decontamination by chlorine spraying, health education about cholera, distribution of soap and chlorine tablets for household water treatment, and distribution of antibiotic prophylaxis to close contacts of cholera cases. Progress from 2013 to 2019 was strong (Table 2), and spatial heterogeneity was marked (Figure 2, panel B). The overall number of case-area targeted interventions per suspected cholera case was 0.3; this ratio improved markedly during 2013–2019 (Table 2).

Conclusions

As confirmed by an extensive laboratory-based surveillance effort, despite sociopolitical turmoil, the cholera epidemic in Haiti seems to be ending. However, a high-coverage national 2-dose cholera vaccination campaign could not be implemented, because neither the required stockpile nor the funds, estimated at US $66 million (*5*), have been available. Although OCV campaigns proved effective in some targeted areas (*8*), these limited and incomplete campaigns were insufficient to compensate for the global waning of the herd immunity built up during the initial incidence peaks of 2010–2012. In the absence of major progress in water, sanitation, and hygiene indicators, most of the fight against cholera transmission has thus been conducted through the nationwide rapid response strategy, which was gradually implemented beginning in mid-2013 (*6*) and was shown to effectively shorten and mitigate cholera outbreaks in Haiti (*9*).

According to observational and experimental results from Bangladesh, vibriophages might play a role in the natural control of cholera epidemics (*10*). Although a single phage isolation was reported in Haiti in 2013 (*11*), vibriophages might have influenced the seasonal dynamic of cholera. Whether they have also contributed to the epidemic collapse requires further investigation.

Because reports of long-term carriers of cholera are anecdotal and they have not been shown to trigger outbreaks (*12*), the critical issue now is whether the epidemic strain of *V. cholerae* O1 has settled in Haiti and could lead to the reemergence of cholera in the near future (*13*). This scenario explicitly informed the Elimination Plan, which required substantial progress in human development to limit the annual incidence rate of cholera to 0.01% of the population (*2*). According to the published literature (*13*,*14*), no epidemic strain seems to have been isolated in surface waters in Haiti since November 2015. Until then, environmental isolates had remained sporadic and usually concomitant to local cholera cases; therefore, differentiating a true environmental reservoir from a recent fecal contamination remains controversial (*13*,*14*). Cholera recurrence after lull periods might simply come from a low-grade and underreported persistent interhuman transmission (*14*) rather than from aquatic reservoirs (*13*).

Because cholera has not been reported in the neighboring Dominican Republic since 2018 (http://digepisalud.gob.do/documentos), the island of Hispaniola might now be located thousands of kilometers away from current transmission foci. In the past, numerous countries in Africa have experienced severe epidemics and prolonged remissions, despite low human development indices, and have remained free from cholera for years (e.g., 8 years for Guinea and 19 years for Madagascar). Similarly, the absence of cholera outbreaks in South America since the early

2000s, despite a large epidemic wave in the 1990s, is reason for optimism.

Until the certification of cholera elimination by the World Health Organization, systematic bacteriologic testing of every case of severe acute watery diarrhea, combined with environmental monitoring, should be maintained in Haiti. However, achieving 2.5 years with no deaths from cholera or confirmed cholera cases in a country where the disease was considered impregnable is already a victory. This achievement should be considered a springboard to further understand cholera epidemics and improve control strategies worldwide. This success should foster investments in water, sanitation, and hygiene infrastructure, which will protect Haiti against possible future cholera epidemics and against other remaining waterborne diseases.

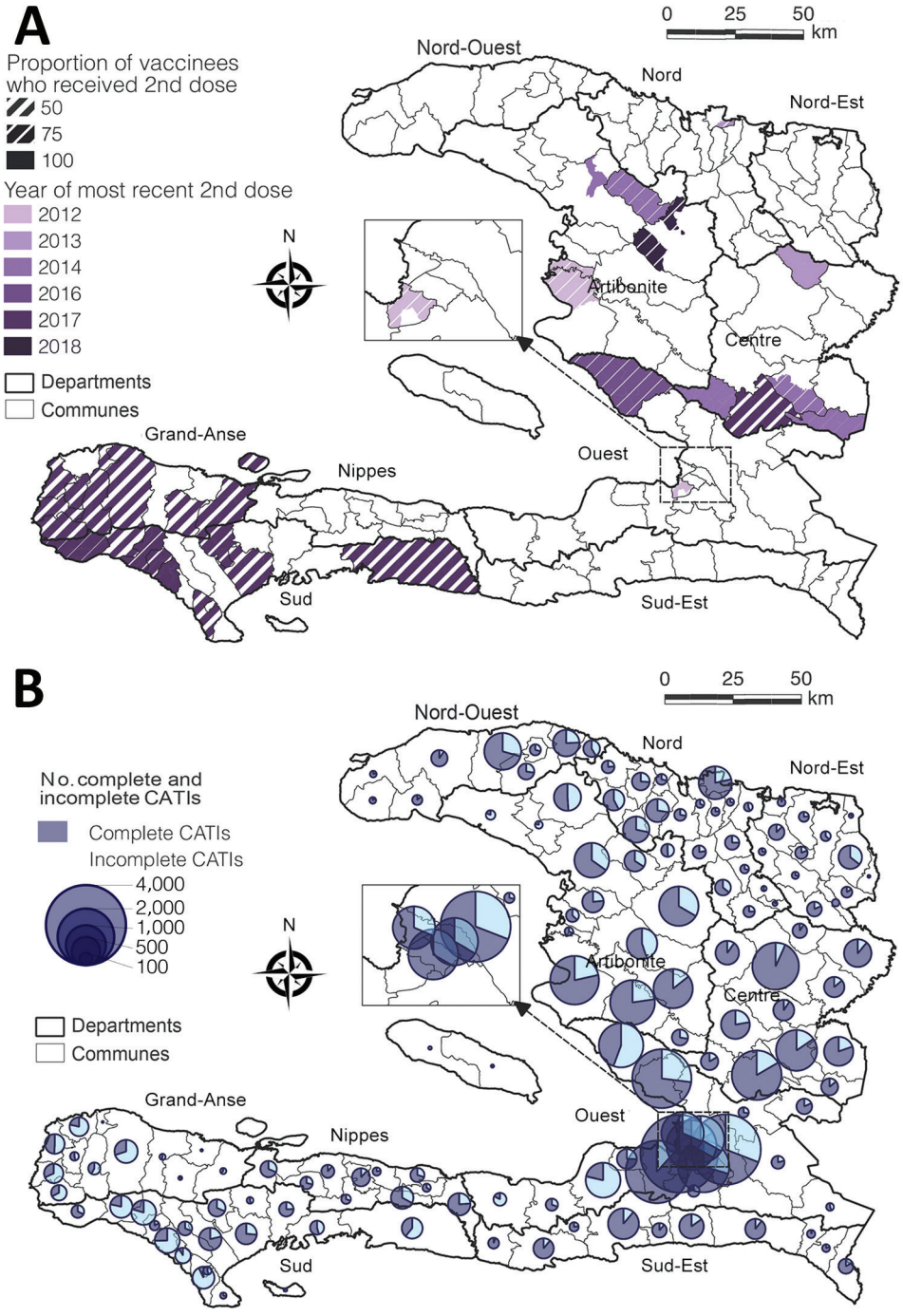

Figure 2. Cholera control in Haiti, 2012–2019. A) Oral cholera vaccine campaigns during 2012–2018 by subcommune; B) complete and incomplete CATIs conducted during July 2013–December 2019 by commune. Complete CATIs are defined by house decontamination, education, soap and chlorine distribution, and distribution of antibiotics to close contacts of cholera case-patients. Data source: Ministry of Public Health and Population of Haiti (pers. comm., 2021 Jul 20); UNICEF (pers. comm., 2020 Jan 20; see also Appendix, https://wwwnc.cdc.gov/EID/article/27/11/20-3372-App1.pdf). CATI, case-area targeted interventions.

Table 2. Suspected cholera cases and case-area targeted interventions, Haiti, 2012–2019*

Year	Total no. suspected cholera cases	No. CATIs	No. (%)		CATIs/case ratio‡
			Complete CATIs†	Targeted communes	
2012	101,503	ND	ND	ND	ND
2013	58,574	3,599	4 (0)	87 (62)	0.1
2014	27,392	3,241	434 (13)	125 (89)	0.1
2015	36,045	8,091	5,500 (68)	131 (94)	0.2
2016	41,421	13,031	10,869 (83)	138 (99)	0.3
2017	13,681	12,244	10,739 (88)	129 (92)	0.9
2018	3,777	6,561	5,525 (84)	83 (59)	1.7
2019	458	1,943	1,683 (87)	42 (30)	4.2
Total	181,348	48,710	34,754 (71)	139 (99)	0.3

*Data source: UNICEF (pers. comm., 2020 Jan 20; see also Appendix, https://wwwnc.cdc.gov/EID/article/27/11/20-3372-App1.pdf). Exhaustive recording of CATIs by UNICEF started in July 2013 with the launch of the nationwide coordinated rapid response strategy. CATI, case-area targeted interventions; ND, no data.
†CATI with house decontamination, education, soap and chlorine distribution, and distribution of antibiotic drugs to contacts.
‡Ratio of the total number of CATIs by the total number of suspected cholera cases, per year.

Acknowledgments

We are grateful to the staff of the MOH, UNICEF, Pan American Health Organization, Centers for Disease Control and Prevention, Direction Nationale de l'Eau Potable et de l'Assainissement, nongovernmental organizations, and others, who took part in patients' care, field responses, stool specimens sampling and analysis, and compiling epidemiological and intervention data.

The study was partly funded by UNICEF, Assistance Publique Hôpitaux de Marseille, Assistance Publique Hôpitaux de Paris, and Sorbonne University.

About the Author

Dr. Rebaudet is an infectious diseases physician and epidemiologist working in Marseille, France. His primary research interests are the epidemiology and control of cholera and antimicrobial stewardship.

References

1. Piarroux R, Barrais R, Faucher B, Haus R, Piarroux M, Gaudart J, et al. Understanding the cholera epidemic, Haiti. Emerg Infect Dis. 2011;17:1161–8. https://doi.org/10.3201/eid1707.110059
2. Republic of Haiti, Ministry of Public Health and Population, National Directorate for Water Supply and Sanitation. National plan for the elimination of cholera in Haiti 2013–2022. Port-au-Prince, Haiti; 2013 [cited 2021 Sep 23]. http://www.paho.org/hq/index.php?option=com_docman&task=doc_view&gid=20326&Itemid=270&lang=en
3. Institut Haïtien de l'Enfance (IHE) and ICF. Haiti mortality, morbidity and service utilization survey (EMMUS-VI) 2016–2017 [in French]. Pétionville, Haiti, and Rockville, MD, USA: Institut Haïtien de l'Enfance and ICF; 2018 [cited 2021 Sep 23]. https://haiti.un.org/sites/default/files/2019-04/Emmus%20VI%20Juillet%202018%20Haiti.pdf
4. Date KA, Vicari A, Hyde TB, Mintz E, Danovaro-Holliday MC, Henry A, et al. Considerations for oral cholera vaccine use during outbreak after earthquake in Haiti, 2010-2011. Emerg Infect Dis. 2011;17:2105–12. https://doi.org/10.3201/eid1711.110822
5. Ivers LC. Eliminating cholera transmission in Haiti. N Engl J Med. 2017;376:101–3. https://doi.org/10.1056/NEJMp1614104
6. Rebaudet S, Bulit G, Gaudart J, Michel E, Gazin P, Evers C, et al. The case-area targeted rapid response strategy to control cholera in Haiti: a four-year implementation study. PLoS Negl Trop Dis. 2019;13:e0007263. https://doi.org/10.1371/journal.pntd.0007263
7. Bi Q, Ferreras E, Pezzoli L, Legros D, Ivers LC, Date K, et al.; Oral Cholera Vaccine Working Group of The Global Task Force on Cholera Control. Protection against cholera from killed whole-cell oral cholera vaccines: a systematic review and meta-analysis. Lancet Infect Dis. 2017;17:1080–8. https://doi.org/10.1016/S1473-3099(17)30359-6
8. Ivers LC, Hilaire IJ, Teng JE, Almazor CP, Jerome JG, Ternier R, et al. Effectiveness of reactive oral cholera vaccination in rural Haiti: a case-control study and bias-indicator analysis. Lancet Glob Health. 2015;3:e162–8. https://doi.org/10.1016/S2214-109X(14)70368-7
9. Michel E, Gaudart J, Beaulieu S, Bulit G, Piarroux M, Boncy J, et al. Estimating effectiveness of case-area targeted response interventions against cholera in Haiti. eLife. 2019;8:e50243. https://doi.org/10.7554/eLife.50243
10. Faruque SM. Role of phages in the epidemiology of cholera. Curr Top Microbiol Immunol. 2013;379:165–80. https://doi.org/10.1007/82_2013_358
11. Seed KD, Yen M, Shapiro BJ, Hilaire IJ, Charles RC, Teng JE, et al. Evolutionary consequences of intra-patient phage predation on microbial populations. eLife. 2014;3:e03497. https://doi.org/10.7554/eLife.03497
12. Azurin JC, Kobari K, Barua D, Alvero M, Gomez CZ, Dizon JJ, et al. A long-term carrier of cholera: cholera Dolores. Bull World Health Organ. 1967;37:745–9.
13. Mavian C, Paisie TK, Alam MT, Browne C, Beau De Rochars VM, Nembrini S, et al. Toxigenic *Vibrio cholerae* evolution and establishment of reservoirs in aquatic ecosystems. Proc Natl Acad Sci U S A. 2020;117:7897–904. https://doi.org/10.1073/pnas.1918763117
14. Rebaudet S, Moore S, Rossignol E, Bogreau H, Gaudart J, Normand A-C, et al. Epidemiological and molecular forensics of cholera recurrence in Haiti. Sci Rep. 2019;9:1164. https://doi.org/10.1038/s41598-018-37706-0

Address for correspondence: Stanislas Rebaudet, Hôpital Européen, 6, rue Désirée Clary, 13003, Marseille, France; email: stanreb@gmail.com

Acute Chagas Disease Manifesting as Orbital Cellulitis, Texas, USA

F. Parker Hudson, Natalie Homer, Aliza Epstein, Kristin Mondy

We report a case of acute, vectorborne Chagas disease, acquired locally in central Texas, USA, manifesting as Romaña's sign, which was initially mistaken for orbital cellulitis. After the infection failed to respond to antibiotics, DNA-based next generation sequencing on plasma yielded high levels of *Trypanasoma cruzi*; results were confirmed by PCR.

Infection with *Trypanosoma cruzi*, or Chagas disease, is endemic in Latin America. An estimated ≥300,000 cases of chronic Chagas disease exist in the United States, predominantly in immigrants who acquired it through vectorborne transmission from triatomine insects in their countries of origin (*1*). Multiple triatomine species also exist in the southern United States, and enzootic transmission to dogs or small rodents is common (*1*–*3*). However, local cases of vectorborne *T. cruzi* transmission to humans is rare. In a 2009 review, the number of acute, autochthonous, vectorborne infections acquired in the United States since 1955 was only 7; of these, 4 occurred in Texas (*4*). During 2013–2018, a total of 26 locally acquired Chagas cases were reported in Texas, but only 1 was an acute case (*5*). Most persons with acute Chagas are asymptomatic, but some have nonspecific constitutional symptoms or Romaña's sign, a painless periorbital and conjunctival injection attributed to triatomine feces deposited or inadvertently rubbed into the eye.

Acute Chagas disease may be overlooked in areas outside of Latin America, despite the existence of *T. cruzi*–infected triatomine reservoirs (*6*). We describe a case of locally acquired, vectorborne, acute Chagas disease in a patient who manifested Romaña's sign; the infection was initially mistaken for orbital cellulitis. We also describe the use of next-generation sequencing (NGS) as a helpful diagnostic tool and review potential vector transmission risk in the southern United States.

Author affiliations: University of Texas Austin Dell Medical School, Austin, Texas, USA (F.P. Hudson, K. Mondy); Texas Oculoplastics Consultants, Austin (N. Homer, A. Epstein)

DOI: https://doi.org/10.3201/eid2711.203698

The Patient

A previously healthy 41-year-old man from central Texas with no medical or travel history described an ocular foreign-body sensation after working outdoors at his ranch. Over the next 2 days he experienced mild conjunctival injection with periorbital erythema and edema (Figure 1). He described mildly blurry vision but no fever, chills, or constitutional symptoms. On day 3 of illness, his primary care provider prescribed oral trimethoprim/sulfamethoxazole and ophthalmic ciprofloxacin drops. The patient's eye symptoms worsened, and on day 5 of illness an ophthalmologist hospitalized him for orbital cellulitis. The patient had normal visual acuity. A computed tomography scan demonstrated nonspecific preseptal and postseptal inflammatory changes, consistent with mild orbital cellulitis. The patient was initiated on intravenous vancomycin and piperacillin/tazobactam.

Results of testing for HIV, syphilis, and methicillin-resistant *Staphylococcus aureus* nasal colonization were negative. On the eighth day of illness, the patient had onset a palpable, left preauricular lymph node. Given the suspicion for oculoglandular syndrome, the patient was switched to intravenous rifampin and doxycycline for possible *Bartonella* infection. However, results of *Bartonella* serologic testing and blood cultures were negative.

On day 11 of illness, the patient had onset of fever. His periorbital edema and lymphadenopathy persisted. His antibiotics were broadened to include vancomycin, cefepime, and acyclovir. He remained febrile, and on day 15 he was transferred to a tertiary care center for evaluation by infectious diseases, oculoplastic surgery, and rheumatology specialists. Further history revealed that he frequently stayed at a local ranch with horses and small mammals, including rabbits, squirrels, and stray cats. He otherwise resided at his suburban residence with his family and two dogs and worked indoors at a nearby university. A magnetic resonance imaging scan demonstrated persistent enhancement of left medial

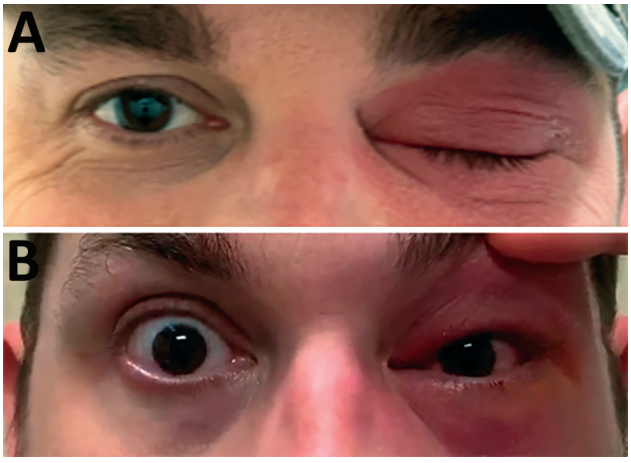

Figure 1. Patient with acute Chagas disease manifesting as orbital cellulitis, Texas, USA, on the day he first accessed care. A) Left periorbital edema and erythema. B) Conjunctival injection.

and inferior rectus muscles, compatible with orbital myositis. However, the patient never experienced pain or limitations of extraocular movements. Results of additional tests for toxoplasmosis, tularemia, and adenovirus were negative.

We sent plasma to Karius, Inc. (https://kariusdx.com; Redwood City, California, USA), to undergo the Karius Test, which uses next-generation sequencing to detect foreign pathogens. On day 16, the patient was started on steroids for possible noninfectious etiologies, including IgG4-related disease, sarcoidosis, or vasculitis. His fever subsequently abated, and the periorbital edema and erythema slightly improved. On day 19, he was discharged on a tapering course of oral steroids and an additional 7 days of oral antibiotics. After discharge, results of the Karius Test were positive for *T. cruzi* at a high level of 505 DNA molecules/μL (Figure 2). Additional testing through the Texas Department of State Health Services and the Centers for Disease Control and Prevention yielded a positive *T. cruzi* PCR test, confirming acute infection. The patient received benznidazole (200 mg 2×/d for 60 d), and steroids were discontinued. He reported some initial general malaise during the first week of therapy but thereafter had only mild generalized itchiness but no rash. He had complete resolution of clinical disease by the fifth week of treatment.

Conclusions

Human acquisition of Chagas disease in the United States remains rare, but this rarity may be attributable in part to the protean manifestations of acute disease, resulting in missed diagnoses. The World Health Organization estimates that <50% of symptomatic persons with acute infection will have a visible sign of a triatomine bite (chagoma) or the classic Romaña's sign (*7*). We found NGS testing to be useful in diagnosing acute Chagas. This patient continued to have ocular manifestations and fever despite broad-spectrum antibiotics and an extensive work-up for the broad differential of oculoglandular diseases.

The Karius Test is a commercially available NGS test for which detailed methodology has been previously described (*8*,*9*). The Karius laboratory extracts and subsequently sequences microbial cell-free DNA from a plasma sample. Within 48 hours, the test indicates bacteria, fungi, DNA viruses, and parasites present at levels greater than a predefined threshold, after removal of human sequences. NGS testing may be a particularly useful tool in atypical febrile syndromes such as in this case, where a very broad range of differential diagnoses were considered (*8*). Such cases require numerous serologic tests, some

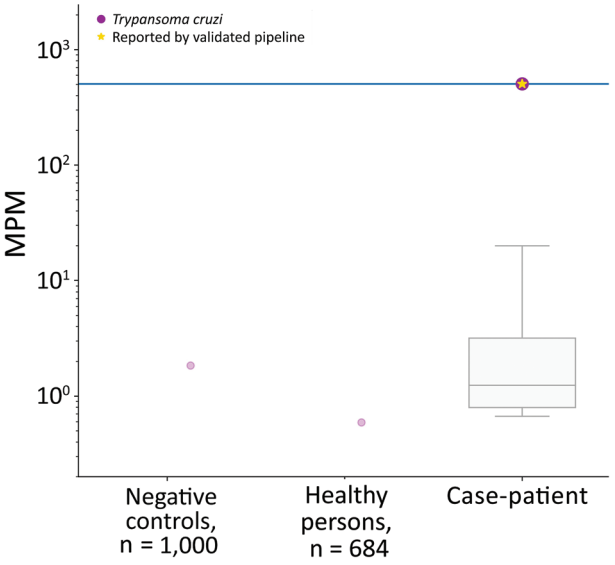

Figure 2. Results of next-generation sequencing on a plasma sample of a patient with acute Chagas disease manifesting as orbital cellulitis, Texas, USA, showing the very high detection of *Trypanosoma cruzi* (505.61 MPM) (right). The comparison with 1,000 aggregated negative controls (buffer/reagents) show a very low microbial cell-free DNA (mcfDNA) signal, which aligned to *T. cruzi* in 1 sample (left). A cohort of 684 healthy controls had a very low mcfDNA signal, which aligned to *T. cruzi* in 1 person (middle). The purple dots indicate any mcfDNA that aligsn to *T. cruzi*; the gold star indicates an mcfDNA detection that represents a positive result for *T. cruzi* identified by the Karius Test (Karius, Inc., https://kariusdx.com). The other detected but not clinically or statistically significant mcfDNA in the case patient's sample are also shown in the gray box and whisker plot on the log scale; horizontal line within box indicates median, box top and bottom indicate interquartile range (Q1–Q3), and error bars indicate range. MPM, molecules/μL.

of which may have variable sensitivity and specificity, costs, and delays in diagnosis and hospital discharge. Otherwise, acute Chagas is typically diagnosed by either identifying the parasite on a blood smear or sending a blood sample to the Centers for Disease Control and Prevention for PCR testing. Such tests would probably not be ordered outside of a known endemic area.

Our case suggests that the extent of domestic-transmission cycles between triatomine vectors and humans is underrecognized in southern US states. In endemic regions, the primary risk for insect-to-human transmission has been related to efficiency with which local vector species can invade and colonize homes (typically in rural areas with impoverished housing conditions such as adobe, wood, and thatch) (*1*). In a study conducted in south Texas, however, large infestations of triatomine insects were found under solid foundations, including cement patios connected to houses and car garages, and >50% of the insects were infected with *T. cruzi* (*2*). In another study of multiple residential sites in central Texas, a high proportion of the triatomine specimens found were infected *T. cruzi*, including 69% of those found inside houses, 81% of those found outside houses, and 82% of those found in dog kennels (*3*). Finally, prolonged periods outdoors, especially while hunting and camping, have been hypothesized to contribute to transmission (*10*). Although the vector and pathogen are quite ubiquitous, the contact between vectors and humans while sleeping and the inefficiency of transmission may account for lower rates of acute infection in Texas compared with Latin America.

In light of our findings, physicians need to be aware of the risk for vectorborne transmission of Chagas disease in and around residential areas, particularly in southern areas of the United States such as Texas. Prompt recognition and treatment of acute Chagas can lead to cure as well as prevention of the illness and risk for death associated with chronic Chagas disease, unnecessary hospitalization, or worsening of the patient's condition from the use of immunosuppressive agents.

Acknowledgments

We thank Asim Ahmed and Martin Lindner for their help with the next-generation sequencing and Figure 2.

About the Author

Dr. Hudson is an assistant professor in the Department of Infectious Diseases and is the Internal Medicine Residency Program Director at the University of Texas at Austin's Dell Medical School. His work has focused on HIV, coronavirus, and medical education.

References

1. Bern C, Kjos S, Yabsley MJ, Montgomery SP. *Trypanosoma cruzi* and Chagas' disease in the United States. Clin Microbiol Rev. 2011;24:655–81. https://doi.org/10.1128/CMR.00005-11
2. Beard CB, Pye G, Steurer FJ, Rodriguez R, Campman R, Peterson AT, et al. Chagas disease in a domestic transmission cycle, southern Texas, USA. Emerg Infect Dis. 2003;9:103–5. https://doi.org/10.3201/eid0901.020217
3. Kjos SA, Marcet PL, Yabsley MJ, Kitron U, Snowden KF, Logan KS, et al. Identification of bloodmeal sources and *Trypanosoma cruzi* infection in triatomine bugs (Hemiptera: Reduviidae) from residential settings in Texas, the United States. J Med Entomol. 2013;50:1126–39. https://doi.org/10.1603/ME12242
4. Bern C, Montgomery SP. An estimate of the burden of Chagas disease in the United States. Clin Infect Dis. 2009;49:e52–4. https://doi.org/10.1086/605091
5. Texas Department of State Health Services. Chagas disease data [cited 2020 Apr 28]. https://www.dshs.texas.gov/IDCU/disease/chagas/Chagas-Disease-Data.aspx
6. Garcia MN, Woc-Colburn L, Aguilar D, Hotez PJ, Murray KO. Historical perspectives on the epidemiology of human Chagas disease in Texas and recommendations for enhanced understanding of clinical Chagas disease in the southern United States. PLoS Negl Trop Dis. 2015;9:e0003981. https://doi.org/10.1371/journal.pntd.0003981
7. World Health Organization. Chagas disease [cited 2020 Apr 28] https://www.who.int/chagas/disease/home_symptoms_more
8. Rossoff J, Chaudhury S, Soneji M, Patel SJ, Kwon S, Armstrong A, et al. Noninvasive diagnosis of infection using plasma next-generation sequencing: a single-center experience. Open Forum Infect Dis. 2019;6:1–3. https://doi.org/10.1093/ofid/ofz327
9. Vudatha V, Ranson M, Blair L, Ahmed AA. Rapid detection of bacille Calmette-Guérin-associated mycotic aortic aneurysm using novel cell-free DNA assay. J Vasc Surg Cases Innov Tech. 2019;5:143–8. https://doi.org/10.1016/j.jvscit.2018.11.006
10. Garcia MN, Hotez PJ, Murray KO. Potential novel risk factors for autochthonous and sylvatic transmission of human Chagas disease in the United States. Parasit Vectors. 2014;7:311. https://doi.org/10.1186/1756-3305-7-311

Address for correspondence: Parker Hudson, University of Texas at Austin Dell Medical School, 1701 Trinity St, DMS HDB 7.810, Stop Z0900, Austin, TX 78712-1876, USA; email: parker.hudson@austin.utexas.edu

Genetically Divergent Highly Pathogenic Avian Influenza A(H5N8) Viruses in Wild Birds, Eastern China

Guimei He, Le Ming, Xiang Li, Yuhe Song, Ling Tang, Min Ma, Jie Cui, Tianhou Wang

In late 2020, we detected 32 highly pathogenic avian influenza A(H5N8) viruses in migratory ducks in Shanghai, China. Phylogenetic analysis of 5 representative isolates identified 2 sublineages of clade 2.3.4.4b. Each sublineage formed separate clusters with isolates from East Asia and Europe.

Highly pathogenic avian influenza (HPAI) A(H5Nx) clade 2.3.4.4 viruses, which originated from the HPAI A(H5N1) clade 2.3.4 of the A/Goose/Guangdong/1/96-lineage in China, have spread globally, causing severe disease in poultry and wild birds (*1*–*4*). According to the World Health Organization, clade 2.3.4.4 viruses have evolved into 8 subclades, designated as clades 2.3.4.4a–h (https://www.who.int/influenza/vaccines/virus/202002_zoonotic_vaccinevirusupdate.pdf). In 2013, a novel reassortant A(H5N8) clade 2.3.4.4b virus was isolated from domestic ducks in eastern China (*2*); this virus was later detected in Korea and Japan (*3*). Since 2014, clade 2.3.4.4b viruses have spread to Europe and Africa along the migratory flyways of birds (*4*,*5*). These introductions caused large HPAI outbreaks in wild and domestic birds in Europe during the winter of 2016–17 (*6*). At the same time, wild birds carried clade 2.3.4.4c viruses to North America (*4*).

In early 2020, outbreaks of clade 2.3.4.4b viruses mainly occurred in Europe (*7*). Beginning in July 2020, several outbreaks of H5N8 viruses in poultry and wild birds were reported in Eurasia, including Kazakhstan, Russia, Poland, England, Netherlands, Korea, and Japan (*7*–*10*); outbreaks were not reported in China until October 2020, when clade 2.3.4.4b viruses related to those circulating in Eurasia were detected in 2 dead swans in Mongolia (*11*). Because eastern China is a major bird migration destination, migratory birds might carry HPAI viruses to this region. We detected 32 H5N8 viruses of 2 genetically distinct lineages in wild birds in eastern China.

The Study

On October 31, 2020, we began annual surveillance for avian influenza viruses (AIVs) in migratory birds. As of December 2, 2020, we had collected 612 cloacal and tracheal swab samples from migratory ducks in the Jiuduansha wetland (31°06′–31°14′N, 121°46′–122°15′E). This wetland is located at the Yangtze River Estuary and is a major stopover site for migratory birds traveling along the East Asian–Australasian flyway. The birds showed no signs of illness. Reverse transcription PCR detected 32 H5N8 viruses by described procedures (*12*). We determined the prevalence of H5N8 viruses to be 5.2%. These H5N8-positive bird species comprised the common teal (*Anas crecca*), spot-billed duck (*Anas poecilorhyncha*), northern pintail (*Anas acuta*), falcated teal (*Anas falcata*), and mallard (*Anas platyrhynchos*). We determined the sequences of the hemagglutinin (HA) and neuraminidase (NA) gene segments of these isolates. We found that 31 isolates had nearly identical HA and NA segments, sharing 99.7%–100% nucleotide sequence identity. We then determined the entire genomic sequences of 5 representative isolates from 5 different host species. We designated these 5 isolates as A/common teal/Shanghai/JDS20103116/2020-H5N8 (GenBank accession nos. MW269587–94), A/northern pintail/Shanghai/JDS20843/2020-H5N8

Author affiliations: East China Normal University, Shanghai, China (G. He, L. Ming, L. Tang, M. Ma, T. Wang); CAS Key Laboratory of Molecular Virology & Immunology, Institut Pasteur, Center for Biosafety Mega-Science, Chinese Academy of Sciences, Shanghai (X. Li, Y. Song, J. Cui)

DOI: https://doi.org/10.3201/eid2711.204893

(GenBank accession nos. MW362179–86), A/falcated teal/Shanghai/JDS20857/2020-H5N8 (GenBank accession nos. MW362170–7), A/spot-billed duck/Shanghai/JDS20867/2020-H5N8 (GenBank accession nos. MW362161–8), and A/mallard/ Shanghai/JDS20876/2020-H5N8 (GenBank accession nos. MW357308–15).

Whole-genome sequencing of these 5 H5N8 viruses revealed that isolate JDS20103116-H5N8 shared a relatively low nucleotide sequence identity (92.4%–97.8%) with the other 4 isolates, indicating that these viruses are genetically divergent. BLAST analysis (https://blast.ncbi.nlm.nih.gov/Blast.cgi) showed that these 5 H5N8 isolates shared the highest sequence identity (99.3%–100.0%) with H5N8 viruses isolated in late 2020 from poultry and wild birds in South Korea, Japan, and Europe (including Russia, Netherlands, and England) (Table). To further characterize these 5 isolates, we constructed phylogenetic trees by comparing the sequences of all 8 genomic segments with those in the GISAID database (https://www.gisaid.org) using IQ-TREE (*13*). We used the general time reversible (GTR) plus F plus G4 model for the HA and polymerase basic 2 protein segments, the transversion e plus G4 model for the matrix protein segment, the K3Pu plus F plus G4 model for the nonstructural protein and NA segments, the transversion plus F plus G4 model for the polymerase acidic protein segment, the GTR plus F plus invariant sites plus G4 model for the polymerase basic 1 protein segment, and the transition 2 plus F plus invariant sites plus G4 model for the nucleoprotein segment. We set parameters to –m (model selection), MFP (model find program), –B (ultrafast bootstrap value), 1,000 bootstraps, –T (threads for used for tree building), and AUTO (automatically selected number of threads).

Results showed that the isolates belonged to clade 2.3.4.4b and formed 2 distinct genetic sublineages (Figure, https://wwwnc.cdc.gov/EID/article/27/11/20-4893-F1.htm). The isolate JDS20103116-H5N8 clustered with the isolates found in East Asia (including South Korea and Japan) in late 2020, as well as the isolates found in Europe in late 2019 and early 2020 (*14*). The other 4 H5N8 isolates clustered with the viruses found in poultry and wild birds in Eurasia (including South Korea, Japan, China, and Europe) in late 2020. The cluster showed high bootstrap support; we proposed the clade to be a novel genotype of the 2.3.4.4b clade (Figure). The topologic structure of trees based on the other gene segments were identical to that of the tree based on the HA gene segment (Appendix Figure, https://wwwnc.cdc.gov/EID/article/27/11/20-4893-App1.pdf).

The novel genotype of the 2.3.4.4b clade also was closely related to viruses detected in poultry in Iraq in May 2020 and in Egypt in 2019, suggesting that these viruses might be the source of the novel

Table. Nucleotide sequence identity of 5 representative avian influenza A(H5N8) isolates from 5 different host species, Shanghai, China, 2020

Isolates	Gene segment	Homologous strains*	GISAID accession no.	Identity, %
JDS20103116	Polymerase basic 2 protein	A/duck/Korea/H439/2020 (A/H5N8)	EPI1845982	99.9
	Polymerase basic 1 protein	A/duck/Korea/H439/2020 (H5N8)	EPI1845983	99.9
	Polymerase acidic protein	A/northern pintail/Hokkaido/M13/2020(H5N8)	EPI1818401	99.7
	Hemagglutinin	A/duck/Korea/H439/2020 (A/H5N8)	EPI1845985	99.8
	Nucleoprotein	A/duck/Korea/H439/2020 (A/H5N8)	EPI1845978	99.3
	Neuraminidase	A/ duck/Korea/H439/2020 (A/H5N8)	EPI1845984	99.9
	Matrix protein	A/chicken/Kagawa/11C/2020(H5N8)	EPI1815028	99.8
	Nonstructural protein	A/chicken/Kagawa/11C/2020(H5N8)	EPI1815027	99.4
JDS20843,	Polymerase basic 2 protein	A/wild duck/Korea/H331/2020 (H5N8)	EPI1846695	99.6
JDS20843,		A/spot-billed duck/Korea/WA1000/2020 (H5N8)	EPI1846695	99.6
JDS20867,	Polymerase basic 1 protein	A/quail/Korea/H440/2020 (H5N8)	EPI1846512	99.7
JDS20876		A/chicken/Korea/H440/2020 (H5N8)	EPI1845991	99.7
	Polymerase acidic protein	A/chicken/Omsk/0119/2020 (H5N8)	EPI1813381	99.9
		A/domestic duck/kazakhstan/1–274–20-B/2020 (H5N8)	EPI1811610	99.9
	Hemagglutinin	A/chicken/Korea/H544/2020 (H5N8)	EPI1850622	100.0
		A/chicken/Korea/H001/2021 (H5N8)	EPI1846522	100.0
	Nucleoprotein	A/mallard/Kagoshima/ KU-d89/2021 (H5N8)	EPI1846675	99.9
		A/spot-billed duck/Korea/Wa1000/2020 (H5N8)	EPI1846697	99.9
	Neuraminidase	A/wild duck/Korea/H331/2020 (H5N8)	EPI1850682	99.9
		A/chicken/Korea/H002/2021 (H5N8)	EPI1846529	99.9
	Matrix protein	A/wild bird/Korea/H496–3/2020 (H5N8)	EPI1857465	100.0
		A/chicken/Korea/H544/2020 (H5N8)	EPI1850662	100.0
	Nonstructural protein	A/Greylag_goose/England/033100/2020 (A/H5N8)	EPI1837929	99.8
		A/turkey/Omsk/0003/2020 (H5N8)	EPI1846695	99.8

*List comprises the most or the 2 most homologous viruses available in GISAID (https://www.gisaid.org) for each gene segment.

genotype. After the outbreaks in Iraq, clade 2.3.4.4b viruses were detected in backyard poultry in Russia in late July 2020 and in wild birds in Russia and Kazakhstan in September 2020. In October 2020, those viruses were also prevalent among birds traveling along various migratory flyways of Europe and Asia (*7*–*10*). We speculate that these viruses circulated among domestic birds in Egypt and then among migratory birds in Russia before emerging in Eurasia in late 2020. Because of the lack of surveillance data at breeding sites in 2019 and early 2020, the transmission routes of these viruses remain unclear. In February 2021, an avian influenza H5N8 infection was reported in a person in Russia. The causative virus, designated A/Astrakhan/3212/2020H5N8, belonged to the 2.3.4.4b clade. These observations suggest that the H5N8 viruses in this novel genotype of 2.3.4.4b clade could infect a wide range of hosts and might spread globally, as did previous H5N8 outbreaks that spread from Asia to Europe and North America in 2014 (*15*).

Molecular analysis of HA cleavage sites demonstrated that the 5 H5N8 isolates contain multiple basic amino acids, PLREKRRKR/GL, which are characteristic of HPAI viruses. The HA1 receptor-binding sites of all 5 H5N8 isolates have amino acid residues Q226 and G228 (H3 numbering), indicative of an avian-like (a2, 3-SA) receptor-binding preference. We documented 2 new amino acid substitutions, T140A and N236D (H3 numbering), in the HA protein of the novel genotype of the 2.3.4.4b clade. The significance of these 2 new mutations remains undetermined. We did not find the E627K and D701N residues in the polymerase basic 2 protein, suggesting that the viruses have not adapted to mammal hosts.

Conclusions

During our annual surveillance, we detected 32 H5N8 HPAI viruses from migratory ducks without signs of illness in Shanghai, China. Results of phylogenetic analyses of 5 representative isolates showed that they belonged to 2 sublineages of H5N8 viruses circulating in this region. Some isolates clustered with a novel genotype of 2.3.4.4b clade that was identified in Europe and East Asia in late 2020. The detection of these H5N8 AIVs in asymptomatic migratory birds support the hypothesis that free-living wild birds play a crucial role in the dissemination of these viruses. More active surveillance is needed to detect new AIVs, especially in the breeding grounds and migratory sites of various birds. Because of their high genetic diversity, new AIVs might pose a substantial threat to global health.

Acknowledgments

We thank Shanghai Forestry Station for assistance in field sampling and all investigators who submitted avian influenza sequences to the GISAID database (https://www.gisaid.org), making this study possible. We greatly appreciate Ron A.M. Fouchier, Bianca Zecchin, Elliot Whittard, Ivan Sobolev, Ivan M. Susloparov, Vasily Evseenko, Katalin Szentpáli-Gavallér, Edyta Swieton, and Jacqueline King for permission to use the sequences they submitted to GISAID.

This work was supported by grants from the National Key Research and Development Program (grant no. 2016YFD0500201), Shanghai Science and Technology Committee (grant no. 18DZ2293800), and Shanghai Wildlife-Borne Infectious Disease Monitoring Program.

About the Author

Dr. He is an associate professor at East China Normal University, Shanghai, China. Her primary research interests are molecular epidemiology of avian influenza viruses in wild birds and pathogenesis of acute lung injury induced by influenza viruses.

References

1. Gu M, Liu W, Cao Y, Peng D, Wang X, Wan H, et al. Novel reassortant highly pathogenic avian influenza (H5N5) viruses in domestic ducks, China. Emerg Infect Dis. 2011;17:1060–3. https://doi.org/10.3201/eid/1706.101406
2. Wu H, Peng X, Xu L, Jin C, Cheng L, Lu X, et al. Novel reassortant influenza A(H5N8) viruses in domestic ducks, eastern China. Emerg Infect Dis. 2014;20:1315–8. https://doi.org/10.3201/eid2008.140339
3. Lee YJ, Kang HM, Lee EK, Song BM, Jeong J, Kwon YK, et al. Novel reassortant influenza A(H5N8) viruses, South Korea, 2014. Emerg Infect Dis. 2014;20:1087–9. https://doi.org/10.3201/eid2006.140233
4. Lee DH, Torchetti MK, Winker K, Ip HS, Song CS, Swayne DE. Intercontinental spread of Asian-origin H5N8 to North America through Beringia by migratory birds. J Virol. 2015;89:6521–4. https://doi.org/10.1128/JVI.00728-15
5. Bouwstra R, Heutink R, Bossers A, Harders F, Koch G, Elbers A. Full-genome sequence of influenza A(H5N8) virus in poultry linked to sequences of strains from Asia, the Netherlands, 2014. Emerg Infect Dis. 2015;21:872–4. https://doi.org/10.3201/eid2105.141839
6. Napp S, Majó N, Sánchez-Gónzalez R, Vergara-Alert J. Emergence and spread of highly pathogenic avian influenza A(H5N8) in Europe in 2016–2017. Transbound Emerg Dis. 2018;65:1217–26. https://doi.org/10.1111/tbed.12861
7. Lewis NS, Banyard AC, Whittard E, Karibayev T, Al Kafagi T, Chvala I, et al. Emergence and spread of novel H5N8, H5N5 and H5N1 clade 2.3.4.4 highly pathogenic avian influenza in 2020. Emerg Microbes Infect. 2021;10:148–51. https://doi.org/10.1080/22221751.2021.1872355
8. Isoda N, Twabela AT, Bazarragchaa E, Ogasawara K, Hayashi H, Wang ZJ, et al. Re-invasion of H5N8 high pathogenicity avian influenza virus clade 2.3.4.4b in Hokkaido, Japan, 2020. Viruses. 2020;12:1439.

https://doi.org/10.3390/v12121439
9. Jeong S, Lee DH, Kwon JH, Kim YJ, Lee SH, Cho AY, et al. Highly pathogenic avian influenza clade 2.3.4.4b subtype H5N8 virus isolated from mandarin duck in South Korea, 2020. Viruses. 2020;12:1389. https://doi.org/10.3390/v12121389
10. Baek YG, Lee YN, Lee DH, Shin JI, Lee JH, Chung DH, et al. Multiple reassortants of H5N8 clade 2.3.4.4b highly pathogenic avian influenza viruses detected in South Korea during the winter of 2020–2021. Viruses. 2021;13:490. https://doi.org/10.3390/v13030490
11. Li X, Lv X, Li Y, Peng P, Zhou R, Qin S, et al. Highly pathogenic avian influenza A (H5N8) virus in swans, China, 2020. Emerg Infect Dis. 2021;27:1732–4. https://doi.org/10.3201/eid2706.204727
12. Tang L, Tang W, Ming L, Gu J, Qian K, Li X, et al. Characterization of avian influenza virus H10–H12 subtypes isolated from wild birds in Shanghai, China from 2016 to 2019. Viruses. 2020;12:1085. https://doi.org/10.3390/v12101085
13. Minh BQ, Schmidt HA, Chernomor O, Schrempf D, Woodhams MD, von Haeseler A, et al. IQ-TREE 2: new models and efficient methods for phylogenetic inference in the genomic era. Mol Biol Evol. 2020;37:1530–4. https://doi.org/10.1093/molbev/msaa015
14. Świętoń E, Fusaro A, Shittu I, Niemczuk K, Zecchin B, Joannis T, et al. Sub-Saharan Africa and Eurasia ancestry of reassortant highly pathogenic avian influenza A(H5N8) virus, Europe, December 2019. Emerg Infect Dis. 2020;26:1557–61. https://doi.org/10.3201/eid2607.200165
15. Global Consortium for H5N8 and Related Influenza Viruses. Role for migratory wild birds in the global spread of avian influenza H5N8. Science. 2016;354:213–7. https://doi.org/10.1126/science.aaf8852

Address for correspondence: Tianhou Wang, School of Life Sciences, East China Normal University, no. 3663, North Zhongshan Rd, Shanghai, China; email: thwang@bio.ecnu.edu.cn; Jie Cui, CAS Key Laboratory of Molecular Virology & Immunology, Institute Pasteur, Center for Biosafety Mega-Science, Chinese Academy of Sciences, Shanghai, China; email: jcui@ips.ac.cn

Isolation of Novel *Mycobacterium* Species from Skin Infection in an Immunocompromised Person

You-Ming Mei,[1] Qian Zhang,[1] Wen-Yue Zhang,[1] Hai-Qin Jiang, Ying Shi, Jing-Shu Xiong, Le Wang, Yan-Qing Chen, Si-Yu Long, Chun Pan, Gai Ge, Zhen-Zhen Wang, Zi-Wei Wu, Yan Wang, Yi-Qun Jiang, Hong-Sheng Wang

We investigated a case of cutaneous infection in an immunocompromised patient in China that was caused by a novel species within the *Mycobacterium gordonae* complex. Results of whole-genome sequencing indicated that some strains considered to be *M. gordonae* complex are actually polyphyletic and should be designated as closely related species.

Mycobacterium gordonae was first described 50 years ago as a slow-growing scotochromogenic nontuberculous mycobacterium. Previous research revealed vague molecular typing results for *M. gordonae*–like strains. For example, the RNA polymerase-β (*rpoB*) PCR restriction analysis discriminates *M. gordonae* into 4 clusters even though cluster D does not hybridize well with the type strain (*1*). Two novel species, *M. paragordonae* and *M. vicinigordonae*, share >99% 16S rRNA gene similarity with *M. gordonae*, which might also lead to confusion about their classification (*2*,*3*).

M. gordonae is frequently isolated from water systems and clinical samples as a potential opportunistic pathogen (*4*,*5*); clinical infections ranging from skin and lung infections to disseminated systemic infections have been reported, especially in immunosuppressed patients (*6*,*7*). Both the *M. paragordonae* and *M. vicinigordonae* strains were first isolated as nonpathogenic organisms from pneumonia patients (*2*,*3*). *M. paragordonae* is often isolated from hospital water systems and devices, but only 1 case of iatrogenic *M. paragordonae* infection has been reported (*8*,*9*). These reports reveal the dissimilar effects produced by different *M. gordonae*–like strains.

Author affiliation: Chinese Academy of Medical Sciences and Peking Union Medical College, Institute of Dermatology, Nanjing, China

DOI: https://doi.org/10.3201/eid2711.210426

The advent of whole-genome sequencing has brought genomewide analyses into common use to delineate species (*10*–*12*). The widely accepted cutoffs adopted for the average nucleotide identity (ANI) and in silico DNA–DNA hybridization (isDDH), 95%–97% for ANI and 70% for isDDH, strongly correlate with traditional DDH division values, providing more robust resolution than phenotyping or mycolic acid analysis for determining mycobacterial taxonomy (*11*,*12*). We report a case of cutaneous infection in Jiangsu Province, China, caused by a previously undescribed novel species belonging to the *M. gordonae* group.

The Study

A 63-year-old man was admitted to the hospital for a 5-year history of a nodule on his left shin. The asymptomatic lesion initially appeared as a papule and gradually developed into a dull red verrucous nodule with scales (Figure 1, panel A). No trauma history before the onset was reported. The patient had received a diagnosis of lupus erythematosus 30 years earlier and had taken oral prednisone (20 mg/d) over the previous year. Laboratory test results indicated no remarkable findings. Histologic examination of a skin sample showed irregular epithelial hyperplasia and granulomatous infiltrations of a large number of epithelioid histocytes, neutrophil cells, plasma cells, and lymphocytes in the dermal layer. After 19 days of culture, orange colonies were observed on modified Löwenstein–Jensen slants at 32°C (Figure 1, panel B). The organism was scotochromogenic with a smooth appearance and grew well at 32°C and 37°C on both Löwenstein–Jensen slants and Middlebrook 7H9 with oleic acid dextrose citrate. The colonies were confirmed to be rod-shaped, acid-fast bacterium.

[1]These first authors contributed equally to this article.

We extracted DNA from the colonies for PCR analysis and compared the sequences using BLAST (https://blast.ncbi.nlm.nih.gov/Blast.cgi). The 16S rRNA (1452 bp) gene shared greatest similarity (99.51%) with *M. gordonae ASCr-1.2*; gene sequencing showed *rpoB* (365 bp) shared 97.53% and *hsp65* (765 bp) 95.53% similarity with *M. paragordonae* 49061. On the basis of these results, we diagnosed infection with a member of the *M. gordonae* complex. Drug sensitivity analysis revealed the bacterium to be sensitive to moxifloxacin, levofloxacin, ethambutol, and amikacin and resistant to clarithromycin, isoniazid, and rifampicin; we therefore prescribed a moxifloxacin regimen for the patient. Because the lesion had not healed over several years, we surgically resected it and applied photodynamic therapy after 2 months of antimicrobial drug treatment. One month later, the patient reported that the lesion had recovered well and refused further oral antimicrobial drugs. No recurrence was observed in the following year.

To accurately identify the pathogen to the species level, we performed whole-genome sequencing (8,509,558 reads, 110×) of the isolate X7091 using the Illumina Hiseq 4000 (https://www.illumina.com) and PacBio RS II (https://www.pacb.com) platforms at the Beijing Genomics Institute. Sequence data indicated a 7.1-Mb genome (7,319,570 bp) including a plasmid (216,348 bp) with a guanine-cytosine content of 64.6% (Genbank accession no. GCA_017086405.1). The complete genome had a guanine-cytosine content of 66.7%, similar to *M. gordonae* (66.8%) and *M. paragordonae* (67.0%). Functional annotation obtained through multiple databases revealed 6,704 coding sequences, 48 tRNA, 3 rRNA, and 35 small RNA genes.

We compared this isolate with all available genomes of the *M. gordonae* group using whole-genome-based computational strategies. ANI calculated by FastANI (https://github.com/ParBLiSS/FastANI) revealed that the closest matches, with *M. gordonae* HMC_M15 (87.80%) and *M. gordonae* DSM 44160 (87.79%), were well below the threshold for species delineation (Appendix Table, https://wwwnc.cdc.gov/EID/article/27/11/21-0426-App1.pdf) (*11*). Evaluating isDDH using the Type Strain Genome Server (https://tygs.dsmz.de) showed weak relations with *M. gordonae* DSM 44160 (34.5%) and *M. paragordonae* 49061 (31.3%) (*13*) (Appendix Table); we found no closely related genome in the database. For *M. paragordonae* strains, ANI was 97.8%–98.6% and isDDH 80.4%–99.9%; for *M. gordonae* strains, ANI was 99.1%–99.9% and isDDH 93.0%–99.3%.

The core-genome phylogeny of the *M. gordonae* complex, constructed using a previously described method, suggested that the isolated strain is a branch within the cluster but distant from other *M. gordonae*-like strains (*14*,*15*) (Figure 2, panel B). Integration of these highly concordant results strongly suggested that the isolate is distinct from present *M. gordonae*–like strains and represents a novel species within the *M. gordonae* complex. We proposed *Mycobacterium camsnse* sp. nov. as the name for this strain.

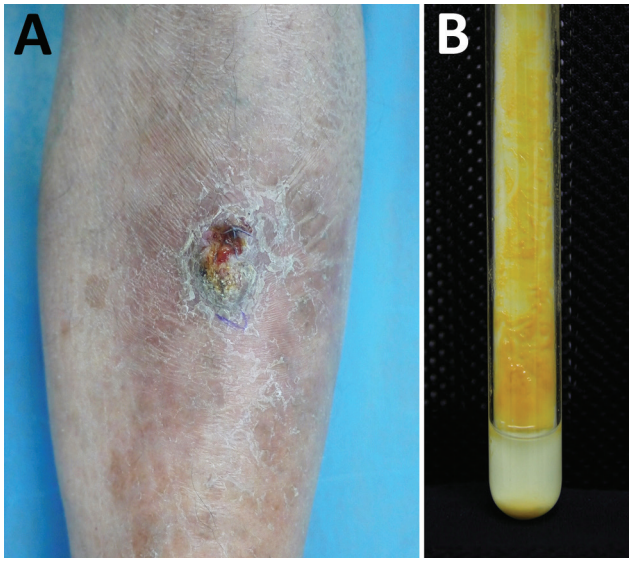

Figure 1. Novel *Mycobacterium gordonae*–like infection in a 63-year-old man in China. A) Verrucous dull nodule on the left shin of the patient. B) *Mycobacterium* colonies grown on Löwenstein–Jensen medium.

When comparing the similarity index of all available genomes of the *M. gordonae* group, we found clear demarcations among the *M. camsnse* X7091, *M. gordonae* CTRI 14-8773, *M. vicinigordonae* 24, 7 *M. paragordonae*, and 3 *M. gordonae* strains including the type strain DSM 44160 (Figure 2). Two strains recorded as *M. gordonae* ssp. in the cluster of *M. paragordonae* may have previously been misclassified. *M. gordonae* CTRI 14-8773, isolated in Russia, also represents a novel species of the *M. gordonae* group. These results confirmed the genomic diversity of *M. gordonae*–like strains, corroborating that the *M. gordonae* group is polyphyletic and should be divided into ≥5 closely related species.

Conclusions

M. gordonae is generally considered a minimally pathogenic mycobacteria. Nonetheless, clinical infections have been reported, even in immunocompetent individuals (*6*,*7*). We isolated a distinct strain within the *M. gordonae* group from a skin infection using whole genome–level approaches based on ANI, isDDH, and core gene phylogeny. We proposed the

name *Mycobacterium camsnse* sp. nov. for this strain. We also provided genomic insights into the heterogeneity of the *M. gordonae*–like strains, including finding 2 strains potentially misclassified as *M. gordonae* ssp., and demonstrated that the present *M. gordonae* group should be designated as 5 closely related species.

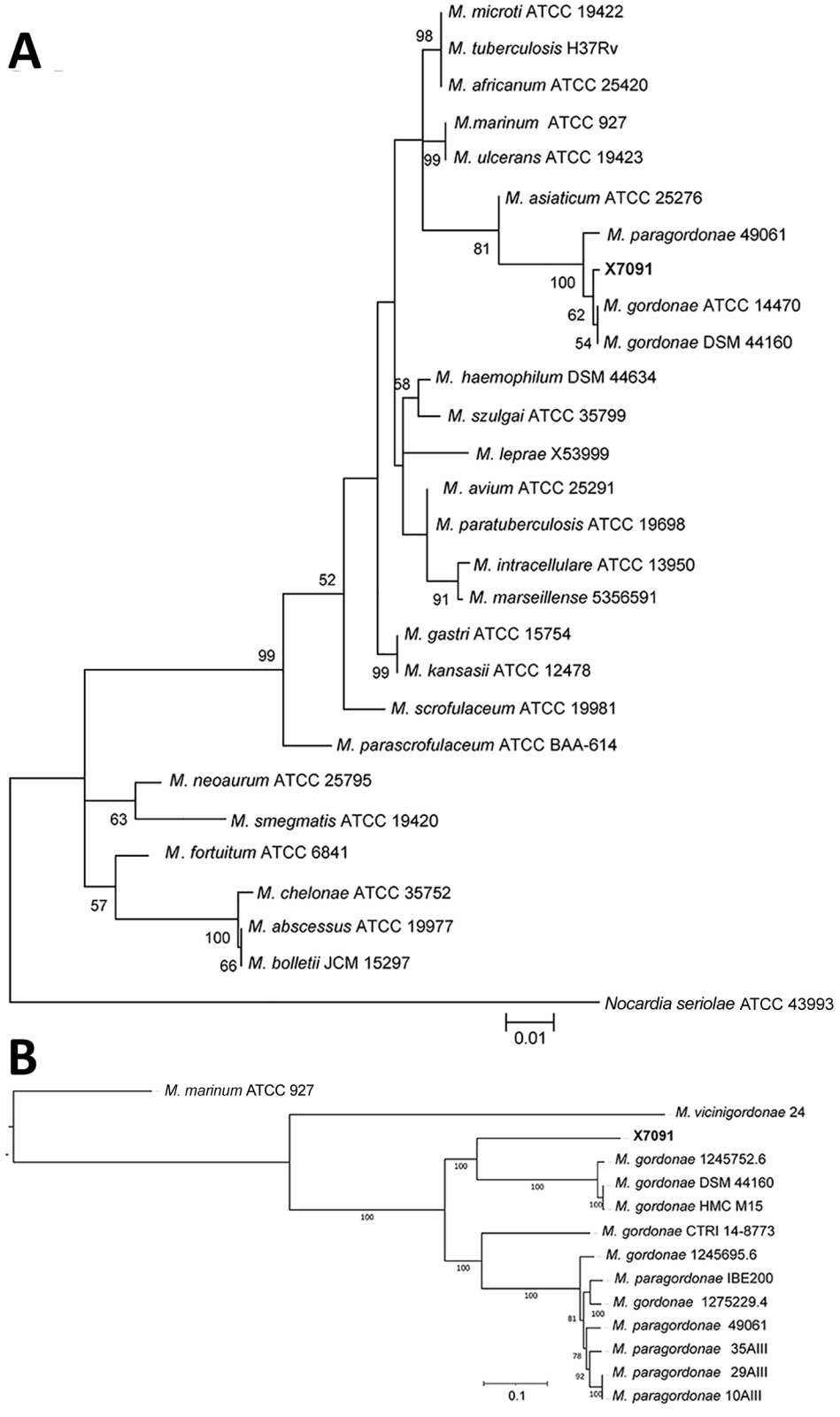

Figure 2. Phylogenetic trees of isolate from novel *Mycobacterium gordonae*–like infection in a 63-year-old man in China (X7091) and reference isolates. A) Evolutionary tree involving *16S rRNA* gene (1,067 positions) of isolate X7091 and 26 *Mycobacterium* strains. Tree constructed using the maximum-likelihood method and Tamura-Nei model with 500 bootstrap replications in MEGA X (https://www.megasoftware.net). We selected *Norcadia seriolae* ATCC 43993 as the outgroup. B) Core genome–based maximum-likelihood phylogeny of isolate X7091 and other *M. gordonae*–like strains analyzed by Roary (https://sanger-pathogens.github.io/Roary) and constructed with a general time-reversible plus gamma maximum model (500 bootstrap replications) using the RaxML tool (*14*). We selected *Mycobacterium marinum* ATCC 927 as the outgroup. Scale bars indicate the number of nucleotide substitutions per site.

Conventional routines for describing species, such as wet-lab DDH and phenotypic tests, which are tedious and restricted by laboratory capacity, often do not delineate closely related species. Genome-based analysis affords a more accurate alternative for delineating species. Although digital gene-expression analyses might not have provided enough conclusive authentication data, the low genomewide similarity between the strain X7091 and *M. gordonae* group strongly support it as a novel species. Only a few *M. gordonae* assembly models are available, and large-scale investigations are needed to better understand species diversity, geographic distribution, and clinical significance of *M. camsnse* sp. nov. infections.

The persistent but limited nonpurulent lesion of the immunosuppressed patient in our study reflects the attenuated nature of the pathogen. The various drug resistance properties of X7091 and other *M. gordonae*–like strains indicate the need for drug sensitivity testing before initiating drug treatment for *M. gordonae*–like strain infections (*6*,*7*). Our patient responded well, indicating that operation combined with antimicrobial therapy could be a good option for treating environmental *Mycobacterium*-induced skin infections.

This study was supported by grants from the Chinese Academy of Medical Sciences Innovation Fund for Medical Sciences (2016-I2M-1-005, 2017-I2M-B&R-14) and the National Natural Science Foundation of China (81972950).

About the Author

Dr. Mei is a dermatologist at the Institute of Dermatology, Chinese Academy of Medical Sciences and Peking Union Medical College in Nanjing, China. Her primary research interest is mycobacterial infectious diseases.

References

1. Itoh S, Kazumi Y, Abe C, Takahashi M. Heterogeneity of RNA polymerase gene (rpoB) sequences of *Mycobacterium gordonae* clinical isolates identified with a DNA probe kit and by conventional methods. J Clin Microbiol. 2003;41:1656–63. https://doi.org/10.1128/JCM.41.4.1656-1663.2003
2. Kim BJ, Hong SH, Kook YH, Kim BJ. *Mycobacterium paragordonae* sp. nov., a slowly growing, scotochromogenic species closely related to *Mycobacterium gordonae.* Int J Syst Evol Microbiol. 2014;64:39–45. https://doi.org/10.1099/ijs.0.051540-0
3. Liu G, Yu X, Luo J, Hu Y, Dong L, Jiang G, et al. *Mycobacterium vicinigordonae* sp. nov., a slow-growing scotochromogenic species isolated from sputum. Int J Syst Evol Microbiol. 2021;71:71. https://doi.org/10.1099/ijsem.0.004796
4. Loret JF, Dumoutier N. Non-tuberculous mycobacteria in drinking water systems: a review of prevalence data and control means. Int J Hyg Environ Health. 2019;222:628–34. https://doi.org/10.1016/j.ijheh.2019.01.002
5. Barber TW, Craven DE, Farber HW. *Mycobacterium gordonae*: a possible opportunistic respiratory tract pathogen in patients with advanced human immunodeficiency virus, type 1 infection. Chest. 1991;100:716–20. https://doi.org/10.1378/chest.100.3.716
6. Al-Busaidi I, Wong D, Boggild AK. Cutaneous *Mycobacterium gordonae* infection in an elderly diabetic returned traveller. J Travel Med. 2017;24:24. https://doi.org/10.1093/jtm/tax019
7. Chen Y, Jiang J, Jiang H, Chen J, Wang X, Liu W, et al. *Mycobacterium gordonae* in patient with facial ulcers, nosebleeds, and positive T-SPOT.TB test, China. Emerg Infect Dis. 2017;23:1204–6. https://doi.org/10.3201/eid2307.162033
8. Cheung CY, Cheng NHY, Ting WM, Chak WL. *Mycobacterium paragordonae*: a rare cause of peritonitis in a peritoneal dialysis patient. Clin Nephrol. 2017;88:371–2. https://doi.org/10.5414/CN109272
9. Takajo I, Iwao C, Aratake M, Nakayama Y, Yamada A, Takeda N, et al. Pseudo-outbreak of *Mycobacterium paragordonae* in a hospital: possible role of the aerator/rectifier connected to the faucet of the water supply system. J Hosp Infect. 2020;104:545–51. https://doi.org/10.1016/j.jhin.2019.11.014
10. Jagielski T, Borówka P, Bakuła Z, Lach J, Marciniak B, Brzostek A, et al. Genomic insights into the *Mycobacterium kansasii* complex: an update. Front Microbiol. 2020;10:2918. https://doi.org/10.3389/fmicb.2019.02918
11. Jain C, Rodriguez-R LM, Phillippy AM, Konstantinidis KT, Aluru S. High throughput ANI analysis of 90K prokaryotic genomes reveals clear species boundaries. Nat Commun. 2018;9:5114. https://doi.org/10.1038/s41467-018-07641-9
12. Zong Z. Genome-based taxonomy for bacteria: a recent advance. Trends Microbiol. 2020;28:871–4. https://doi.org/10.1016/j.tim.2020.09.007
13. Meier-Kolthoff JP, Göker M. TYGS is an automated high-throughput platform for state-of-the-art genome-based taxonomy. Nat Commun. 2019;10:2182. https://doi.org/10.1038/s41467-019-10210-3
14. Stamatakis A. RAxML version 8: a tool for phylogenetic analysis and post-analysis of large phylogenies. Bioinformatics. 2014;30:1312–3. https://doi.org/10.1093/bioinformatics/btu033
15. Luo T, Xu P, Zhang Y, Porter JL, Ghanem M, Liu Q, et al. Population genomics provides insights into the evolution and adaptation to humans of the waterborne pathogen *Mycobacterium kansasii.* Nat Commun. 2021;12:2491. https://doi.org/10.1038/s41467-021-22760-6

Address for correspondence: Hong-sheng Wang, Institute of Dermatology, Chinese Academy of Medical Sciences and Peking Union Medical College, St.12 Jiangwangmiao, Nanjing, Jiangsu, 210042, China; email: whs33@vip.sina.com

Co-Infection with 4 Species of Mycobacteria Identified by Using Next-Generation Sequencing

Lulan Wang,[1] Dakai Liu,[1] Lok Yung, George David Rodriguez, Nishant Prasad, Sorana Segal-Maurer, Vishnu Singh, Ellee Vikram, Angela Zou, Genhong Cheng, William Harry Rodgers

Author affiliations: University of California, Los Angeles, California, USA (L. Wang, E. Vikram, A. Zou, G. Cheng); New York-Presbyterian Queens Hospital, Flushing, New York, USA (D. Liu, L. Yung, G.D. Rodriguez, N. Prasad, S. Segal-Maurer, V. Singh, W.H. Rodgers); Weil Cornell Medical College, New York (W.H. Rodgers)

DOI: https://doi.org/10.3201/eid2711.203458

We identified co-infection with 4 species of mycobacteria in a woman in New York, New York, USA, by using next-generation sequencing. This procedure is useful for identifying co-infections with multiple mycobacteria, tracing the geographic origin of strains, investigating transmission dynamics in susceptible populations, and gaining insight into prevention and control.

Mycobacteria are major human pathogens; ≈13 million persons in the United States live with *Mycobacterium tuberculosis* complex (MTBC) infection, and incidence of nontuberculous mycobacterial (NTM) pulmonary disease is increasing worldwide. The challenges of managing MTBC and *M. avium* complex (MAC) co-infection are well described, including the risk for falsely interpreted Xpert RIF (rifampin) results (*1*,*2*). MTBC and *M. abscessus* co-infection has been described in case reports only (*3*,*4*). We describe co-infection with 4 species of mycobacteria.

In July 2019, an 82-year-old Asian woman was hospitalized in Flushing, New York, USA, for persistent fever associated with worsening weakness. Computed tomography of her chest showed near-complete atelectasis of the left upper lobe, hyperinflation in other areas, and a small left-sided pleural effusion. Scattered nodular opacities in a tree-in-bud pattern and pulmonary granulomas were present throughout the lungs, and discontinuity of the left upper lobe bronchus was noted. Cultures of blood, urine, stool, and respiratory specimens yielded negative results for nonmycobacteria.

In a sputum sample collected for routine mycobacterial testing, fluorochrome staining exhibited rare acid-fast bacilli, and MTBC was detected by using Xpert MTB/RIF (Cepheid, https://www.cepheid.com). We then inoculated a Lowenstein-Jensen Gruft slant with sputum, incubated it at 37°C, and inoculated VersaTREK Myco bottles containing Modified Middlebrook 7H9 Broth with Sponges (Thermo Fisher, https://www.thermofisher.com) and incubated them at 35°C. No isolate was recovered from the Lowenstein-Jensen Gruft slant. Only MAC was detected by AccuProbe (Hologic, https://www.hologic.com) in Kinyoun-positive culture from the Myco bottles. One week later, another sputum sample with Kinyoun-positive growth from the Myco bottles was negative for MAC, MTBC, *M. gordonae*, and *M. kansasii*. *M. abscessus* was identified on the Lowenstein-Jensen Gruft slant.

Considering the sensitivity limit and narrow species coverage of AccuProbe and the difficulty of identifying mycobacteria by culturing and because of growth interference among different mycobacteria, we conducted next-generation sequencing (NGS) by using Hiseq3000 (Illumina, https://www.illumina.com) on the supernatant of the first sputum culture. NGS yielded ≈175 million reads, each with a quality score of >35. We checked NGS data for quality control by using FastQC (Galaxy, https://usegalaxy.org). All steps and programs used the data processing pipeline from Galaxy, an open-source, web-based platform for data-intensive biomedical research. Each read identified had a quality control score of 39.4 and an average guanine-cytosine content of 68%. Only 0.69% of bases resulted in no hits and were not identifiable. We performed De Novo classification by using De Novo Assembly Unicycler, Quast QC, and Kraken Classification (Galaxy) and generated coverage and depth data by using BWA Aligner and SAMtools Depth (Galaxy). We aligned the reads, visualized onto bacteria reference genomes by using Bowtie2 (Galaxy) and converted into BED (Browser Extensible Data) files followed by Bedtools Merge, Multicov (https://bedtools.readthedocs.io).

The genome visualization pipeline confirmed 4 genomic traces of *Mycobacterium* strains (Figure): *M. yongonense* strain 05-1390 (GenBank accession no. NC_021715.1), *M. tuberculosis* strain FDAARGOS_757 (GenBank accession no. CP054013.1), *Mycobacterium* sp. MOTT36Y (GenBank accession no. NC_017904.1), and *M. abscessus* ATCC 19977 (GenBank accession no. CU458896.1). *M. yongonense* was identified with a genome coverage of 88.73% (4.9 Mb mapped of 5.5-Mb genome) and a read depth of 1,224×. *M. tuberculosis* was identified with a genome

[1]These first authors contributed equally to this article.

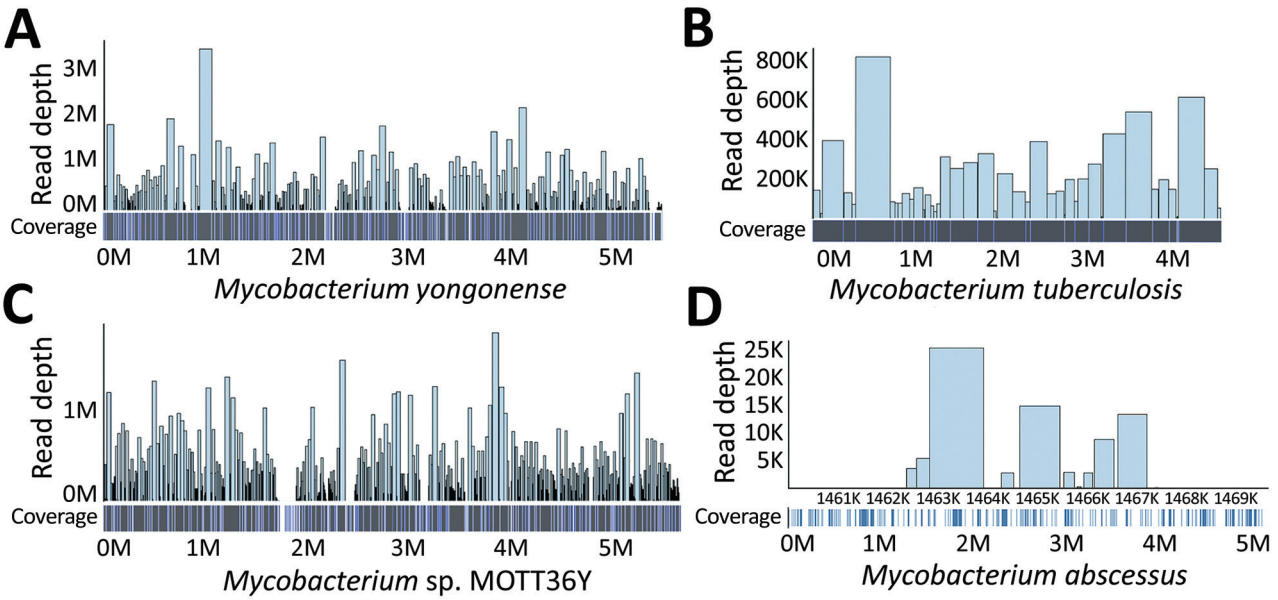

Figure. Genomic coverage and depth map of 4 *Mycobacterium* strains identified by using next-generation sequencing on isolates from a woman in New York, New York, USA. The reads were aligned by using bacteria reference genomes with Bowtie 2 and visualized by using aligned BED file (https://bedtools.readthedocs.io). A) *M. yongonense*; B) *M. tuberculosis*; C) *Mycobacterium* sp. MOTT36Y; D) *M. abscessus*.

coverage of 99.99% (4.4 Mb mapped of 4.4-Mb genome) and a read depth of 63×. *Mycobacterium* sp. was identified with a genome coverage of 94.41% (5.3 Mb mapped of 5.6-Mb genome) and a read depth of 1210×. *M. abscessus* was identified with a genome coverage of only 2.75% (0.14 Mb mapped of 5.1-Mb genome) and a read depth of 8× (Table). The mycobacteria identified by NGS were verified by various mycobacteria tests.

We obtained the consensus sequence for 4 strains of bacteria by using MEGAHIT (Galaxy) and generated a BLAST (https://blast.ncbi.nlm.nih.gov/Blast.cgi) tree based on minimum evolution at the species level by using ≥15 kbp from each sequence. Assembly on MTBC sequencing data yielded a total consensus sequence of 4,376,826 bp and 78,208 single-nucleotide polymorphism sites (1.79%). Analysis by BLAST and Mykrobe (https://www.mykrobe.com) revealed that the MTBC isolate belongs to sublineage 2.2.

The patient received RIPE therapy (rifampin, isoniazid, pyrazinamide, and ethambutol), along with amikacin, tigecycline, and azithromycin. At 6 months, RIPE therapy was completed. At 9 months, sputum culture was negative. The patient continues to take amikacin, tigecycline, and azithromycin as an outpatient with close follow-up.

Identification of co-infection with mycobacteria is necessary for diagnosis and treatment (*5*). Treatment regimens and duration remain species specific because of unique resistance mechanisms. To achieve the greatest potential for success while minimizing toxicities, early empiric treatment should account for clinical characteristics of MTBC and NTM co-infection and strain identification.

Our report highlights the value of NGS for identifying multiple mycobacteria co-infections in populations with high susceptibility to and prevalence of MTB and NTM (i.e., immigrants, immunocompromised patients, and international travelers). NGS can trace the geographic origin of the *Mycobacterium* strain. These features, in combination with a patient's epidemiologic exposure and travel history, could elucidate the potential time and location of infection acquisition. NGS could also be used to identify drug-resistance genes to guide targeted therapy.

Table. Classification and coverage of multiple *Mycobacterium* strains identified by using next-generation sequencing of isolates from a woman in New York, New York, USA

Strain	Genome size, bp	Coverage, bp	Coverage, %	Read depth	Quality
Mycobacterium avium complex sp YG	5,521,023	4,900,000	88.752	1223.91×	39.4
M. tuberculosis complex	4,405,981	4,405,474	99.999	63.32×	39.4
Mycobacterium sp. Mott36Y	5,613,626	5,300,000	94.413	1209.57×	39.4
M. abscessus	5,090,491	139,997	2.750	7.66×	39.4

Acknowledgments

We thank Jun Young Choi, Debra Harragan Jokisch, Eric Konadu, Marian Memmer, Joseph Pilz, Huimin Wu for their technical assistance and Carl Urban for manuscript review.

The sequenced isolate in this manuscript was submitted to GenBank (accession no. CP074075). Details of submission are SUBID SUB9558401; BioProject PRJNA726345: BioSample SAMN18928235; Organism Mycobacterium tuberculosis 2.2.

About the Authors

Dr. Wang is a postdoctoral fellow working in the Department of Microbiology, Immunology and Molecular Genetics, University of California, Los Angeles. His research focuses on immunology, virology, and molecular diagnostics. Dr. Liu is the laboratory director for Microbiology, Immunology and Molecular Diagnostics, Department of Pathology and Clinical Laboratories, New York-Presbyterian Queens Hospital. His research focus is developing rapid molecular assays for pathogen diagnosis.

References

1. Bazzi AM, Abulhamayel Y, Rabaan AA, Al-Tawfiq JA. The impact of the coexistence of *Mycobacterium avium* with *Mycobacterium tuberculosis* on the result of GeneXpert and MGIT susceptibility test. J Infect Public Health. 2020;13:827–9. PubMed https://doi.org/10.1016/j.jiph.2020.01.006
2. Sarro YDS, Kone B, Diarra B, Kumar A, Kodio O, Fofana DB, et al. Simultaneous diagnosis of tuberculous and non-tuberculous mycobacterial diseases: time for a better patient management. Clin Microbiol Infect Dis. 2018;3:1–8. https://doi.org/10.15761/CMID.1000144
3. Sohn S, Wang S, Shi H, Park S, Lee S, Park KT. Mixed infection of *Mycobacterium abscessus* subsp. *abscessus* and *Mycobacterium tuberculosis* in the lung. Korean J Thorac Cardiovasc Surg. 2017;50:50–3. https://doi.org/10.5090/kjtcs.2017.50.1.50
4. Ishiekwene C, Subran M, Ghitan M, Kuhn-Basti M, Chapnick E, Lin YS. Case report on pulmonary disease due to coinfection of *Mycobacterium tuberculosis* and *Mycobacterium abscessus*: difficulty in diagnosis. Respir Med Case Rep. 2017;20:123–4. https://doi.org/10.1016/j.rmcr.2017.01.011
5. Feng Z, Bai X, Wang T, Garcia C, Bai A, Li L, et al. Differential responses by human macrophages to infection with *Mycobacterium tuberculosis* and non-tuberculous mycobacteria. Front Microbiol. 2020;11:116. https://doi.org/10.3389/fmicb.2020.00116

Address for correspondence: Dakai Liu and William H. Rodgers, Department of Pathology and Clinical Laboratories, New York Presbyterian Queens Hospital, 56-45 Main St., Flushing, NY 11355, USA; email: dal9165@nyp.org and whr9001@nyp.org; Genhong Cheng, Department of Microbiology, Immunology & Molecular Genetics, University of California, Los Angeles, 615 Charles Young Dr S, Los Angeles, CA 90095, USA; email: gcheng@mednet.ucla.edu

Fatal Co-infections with SARS-CoV-2 and *Legionella pneumophila*, England

Victoria J. Chalker, Hugh Adler, Robert Ball, Falguni Naik, Jessica Day, Baharak Afshar, Amit K. Amin

Author affiliations: United Kingdom Health Security Agency, London, UK (V.J. Chalker, F. Naik, B. Afshar); St. Helen's & Knowsley Teaching Hospitals National Health Service Trust, St. Helen's, UK (H. Adler, R. Ball); London Northwest University Healthcare National Health Service Trust, London (A.K. Amin)

DOI: https://doi.org/10.3201/eid2711.4121

Both *Legionella pneumophila* and severe acute respiratory syndrome coronavirus 2 (SARS-CoV-2) can cause pneumonia. *L. pneumophila* is acquired from water sources, sometimes in healthcare settings. We report 2 fatal cases of *L. pneumophila* and SARS-CoV-2 co-infection in England. Clinicians should be aware of possible *L. pneumophila* infections among SARS-CoV-2 patients.

Legionnaires' disease, caused by *Legionella* bacteria, is a factor in community and healthcare acquired pneumonia. *Legionella* infection occurs from manmade water sources, including water aerosolized from cooling towers, spa pools, and water features, and from plumbing in hotels, workplaces, and healthcare facilities (*1*), where patients can be more susceptible to infection (*1*).

Severe acute respiratory syndrome coronavirus 2 (SARS-CoV-2) causes coronavirus disease (COVID-19), which also can cause pneumonia. Clinically differentiating Legionnaires' disease from COVID-19 requires laboratory diagnostics, such as urine antigen testing, PCR, and culture. The clinical focus on SARS-CoV-2 potentially causes underdiagnosis of *L. pneumophila* because clinicians might not suspect or investigate the bacterium, but co-infections have been reported. Documented co-infections in COVID-19 patients include human metapneumovirus (*2*), influenza (*3*), *Chlamydia pneumoniae*, *Mycoplasma pneumoniae*, non–COVID-19 coronavirus, enterovirus, rhinovirus, parainfluenza, and respiratory syncytial virus (*4*), and *L. pneumophila* in a case associated with a cruise ship (*5*). Rapid identification of co-infections is essential for managing and treating severe COVID-19 cases (*6*). We describe 2 cases of SARS-CoV-2 and *L. pneumophila* co-infection in patients admitted to hospitals in the United Kingdom.

In February 2020, a female patient >65 years of age was admitted in Addisonian crisis. She was dis-

charged to home but was readmitted to the same ward 8 days later with pneumonia. Her chest radiograph demonstrated minor bibasal opacity. The patient was prescribed amoxicillin/clavulanate and clarithromycin at admission for suspected bacterial infection; only clarithromycin would be effective against *Legionella* infection. No *L. pneumophila* nor SARS-CoV-2 testing was performed at admission and blood culture showed no growth. After initial clinical improvement, the patient's respiratory status deteriorated on day 10 and her chest radiograph showed extensive bilateral infiltrates. She tested positive for *L. pneumophila* by BinaxNOW Legionella Urinary antigen test (Alere, https://immuview.com) and for SARS-CoV-2 by PCR of nose and throat swab samples. *L. pneumophila* was confirmed by using Legionella Urinary Antigen EIA (Bartels, https://www.trinitybiotech.com) and Rapid Test Kit BinaxNOW Enzyme Immunoassay (EIA; Alere) on urine. No confirmatory lower respiratory samples were obtained. Despite antimicrobial drug and supportive treatment, the patient did not improve and was transitioned to palliative measures. She died 20 days after admission. We used culture to test water from all outlets on the ward; all were negative for *L. pneumophila* serogroup 1. We could not determine whether *L. pneumophila* and SARS-CoV-2 co-infection occurred in the community before hospital admission or in the hospital setting.

Another co-infection occurred in a woman >80 years of age with a history of hypertension and chronic kidney disease who resided with her family in the community. She was admitted with dyspnea, hypoxia, and acute-on-chronic kidney injury in April 2020. Her chest radiograph demonstrated bilateral mid- and lower-zone consolidation, predominantly peripheral. The patient was prescribed amoxicillin/clavulanate and clarithromycin for suspected bacterial infection. The patient deteriorated over the subsequent 24 hours with progressive hypoxia despite maximal oxygen therapy. A nasal swab collected at admission tested positive for SARS-CoV-2 by PCR. Blood cultures collected at admission were negative. Per guidelines for testing for pneumonia, urine collected on day 2 after admission tested positive by BinaxNOW Legionella Urinary Antigen Test (Alere) and was confirmed with EIA as in the prior case; urinary pneumococcal antigen test was negative. No lower respiratory samples for confirmatory *Legionella* culture and typing were obtained. The treatment strategy was transitioned to palliative measures, and she died 5 days after admission. We assume this patient acquired both *L. pneumophila* and COVID-19 in the community, but she had no apparent epidemiologic risk for *L. pneumophila*, such as travel.

Our study is limited by the low number of cases and the lack of lower respiratory specimens, which prevented confirmation and identification of *L. pneumophila* infection by PCR or culture. Nonetheless, *Legionella* testing of patients and water systems should not be neglected during the SARS-CoV-2 pandemic. Healthcare facilities and clinicians should continue to adhere to recommended protocols for *L. pneumophila* infection prevention and diagnosis.

Even during the COVID-19 pandemic, patients are at risk for *L. pneumophila* infection in community and healthcare settings. Because periods of water system disuse can permit *Legionella* to grow and increase risk for infection (*1*), pandemic measures, such as temporary closure and reopening of buildings, could increase risk for *Legionella* exposure. Healthcare facilities should follow national guidance for managing *Legionella* during the COVID-19 pandemic and consider publications from the European Society for Clinical Microbiology and Infectious Disease European Study Group for *Legionella* Infections (*7*).

Hospital-acquired *L. pneumophila* cases and outbreaks can have higher fatality rates than community-acquired single cases (*8*). Recent data indicates bacterial co-infection in SARS-CoV-2 cases is uncommon in patients newly admitted to the hospital (*9*). However, effects of *L. pneumophila* co-infection on COVID-19 mortality rates is not yet known. Large outbreaks might be missed because of reduced testing or less consideration for *L. pneumophila* infection in differential diagnosis. Clinicians should maintain *Legionella* testing and conduct patient investigations where clinically indicated during the pandemic.

In conclusion, patients with SARS-CoV-2 might be at increased risk for other community- or healthcare-acquired infections. Clinicians should be aware of possible *L. pneumophila* infections among SARS-CoV-2 patients.

About the Author

Dr. Chalker is head of the Respiratory and Vaccine Preventable Bacteria Reference Laboratory in the United Kingdom Health Security Agency. Her research interests include molecular epidemiology and genomics of *Legionella* and other pathogens, clinical diagnostics, and outbreak analysis and control.

References

1. Phin N, Parry-Ford F, Harrison T, Stagg HR, Zhang N, Kumar K, et al. Epidemiology and clinical management of Legionnaires' disease. Lancet Infect Dis. 2014;14:1011–21. https://doi.org/10.1016/S1473-3099(14)70713-3

2. Touzard-Romo F, Tapé C, Lonks JR. Co-infection with SARS-CoV-2 and human metapneumovirus. R I Med J. 2020;103:75–6. PubMed
3. Wu X, Cai Y, Huang X, Yu X, Zhao L, Wang F, et al. Co-infection with SARS-CoV-2 and influenza A virus in patient with pneumonia, China. Emerg Infect Dis. 2020;26:1324–6. https://doi.org/10.3201/eid2606.200299
4. Richardson S, Hirsch JS, Narasimhan M, Crawford JM, McGinn T, Davidson KW, et al. Presenting characteristics, comorbidities, and outcomes among 5700 patients hospitalized with COVID-19 in the New York City area. JAMA. 2020;323:2052–59. https://doi.org/10.1001/jama.2020.6775
5. Arashiro T, Nakamura S, Asami T, Mikuni H, Fujiwara E, Sakamoto S, et al. SARS-CoV-2 and *Legionella* co-infection in a person returning from a Nile Cruise. J Travel Med. 2020;27:taaa053. PubMed https://doi.org/10.1093/jtm/taaa053
6. Cox MJ, Loman N, Bogaert D, O'Grady J. Co-infections: potentially lethal and unexplored in COVID-19. Lancet Microbe.2020;1:e11. https://doi.org/10.1016/S2666-5247(20)30009-4
7. ESCMID. ESCMID Study Group for Legionella Infections [cited 2020 Sep 24]. https://www.escmid.org/research_projects/study_groups/study_groups_g_n/legionella_infections
8. Public Health England. Legionnaires' disease in residents of England and Wales: 2016 [cited 2020 May 6]. https://www.gov.uk/government/publications/legionnaires-disease-in-residents-of-england-and-wales-2016
9. Adler H, Ball R, Fisher M, Mortimer K, Vardhan MS. Low rate of bacterial co-infection in patients with COVID-19. Lancet Microbe. 2020;1:e62. https://doi.org/10.1016/S2666-5247(20)30036-7

Address for correspondence: Vicki Chalker, United Kingdom Health Security Agency, 61 Colindale Ave, London NW9 5EQ, UK; email: Vicki.chalker@phe.gov.uk

Invasive Malaria Vector *Anopheles stephensi* Mosquitoes in Sudan, 2016–2018

Ayman Ahmed, Patricia Pignatelli, Arwa Elaagip, Muzamil M. Abdel Hamid, Omnia Fateh Alrahman, David Weetman

Author affiliations: Liverpool School of Tropical Medicine, Liverpool, UK (A. Ahmed, P. Pignatelli, D. Weetman); University of Khartoum, Khartoum, Sudan (A. Ahmed, A. Elaagip, M.M. Abdel Hamid, O. Fateh Alrahman)

DOI: https://doi.org/10.3201/eid2711.210400

Anopheles stephensi mosquitoes are urban malaria vectors in Asia that have recently invaded the Horn of Africa. We detected emergence of *An. stephensi* mosquitoes in 2 noncontiguous states of eastern Sudan. Results of mitochondrial DNA sequencing suggest the possibility of distinct invasions, potentially from a neighboring country.

Anopheles stephensi mosquitoes are efficient vectors of *Plasmodium vivax* and *P. falciparum*. Their native range centers on the Indian subcontinent, from which they are increasingly expanding their geographic distribution (*1*). Recent establishment in Ethiopia (*2*) and Djibouti (*3*) is especially worrying. We document the emergence of *An. stephensi* mosquitoes in Sudan.

Among study sites in a study originally investigating insecticide resistance in the dominant malaria vector in Sudan, *Anopheles arabiensis* mosquitoes, we selected 12 sites in the eastern half of the country to represent the different ecologic zones (Appendix Figure 1, https://wwwnc.cdc.gov/EID/article/27/11/21-0400-App1.pdf). We collected *Anopheles* spp. larvae from all sites in 2016 and from most again in late 2017 or early 2018 (Appendix Table 1). We reared the larvae to adults, checked them morphologically, and initially identified the species as *An. gambiae* s.l. We extracted DNA from a subset for molecular identification of the species by PCR (*3*). Of these, 149 DNA samples failed to amplify when we used the standard protocol for identification of the *An. gambiae* complex, and we investigated them further. We performed mitochondrial cytochrome oxidase 1 amplification and sequencing by using the universal primers C1-J-2183 and TL2-N-3014 on the first batch (*4*); to provide conformity with other studies in East Africa, we used Folmer primers LCO1490 and HCO2198 on a second batch (*4*). To confirm species identity, we performed BLAST (https://blast.ncbi.nlm.nih.gov/Blast.cgi) searches. We supplemented sequences generated for the mosquitoes from Sudan by using the Folmer primers with sequences from other studies downloaded from GenBank, assembled them by using Clustal within MEGAX (*5*), and displayed the results as a maximum-likelihood tree with 1,000 bootstraps.

Sequence analysis demonstrated that many of the samples failing diagnostic PCR were not *An. gambiae* s.l. mosquitoes; most samples identified by BLAST were *An. stephensi* mosquitoes (Appendix Table 1). The relative frequencies of *An. stephensi* mosquito detection were similarly high (>40%) among those

from the 2 Red Sea state sites, Port Sudan and Tokar, but seem much lower elsewhere; only 1 individual *An. stephensi* mosquito was detected at each site in Gedaref state, and none were detected at the other study sites (Appendix Table 1, Figure 2). Although sample site identifications were clear, year identification labels were unfortunately not preserved during sample shipment, and from these samples we cannot determine when *An. stephensi* mosquitoes were collected. However, sequencing of pools of additional samples from Tokar and Port Sudan from each collection year, which were preserved primarily for RNA analysis, confirmed their presence in both years.

Phylogenetic analysis of the sequences identified 3 haplotypes, which we named Sudan H1–3 (Figure). The most common Sudan haplotype was H3 (86%), detected at both of the Red Sea state sites (Tokar and Port Sudan); the relatively similar haplotype H2 was detected at lower frequency at Port Sudan only (Appendix Figure 1). H2 and H3 cluster with those collected in Ethiopia in 2016 (*2*) and with 2 of those collected in 2019, for which we retained the authors' haplotype notation (*6*). H1 was detected only in Abu Alnaja (Gedaref state) and clustered within a larger clade encompassing a broad range of locations, including a haplotype detected in both Djibouti and Ethiopia (Appendix Figure 1). The sample of

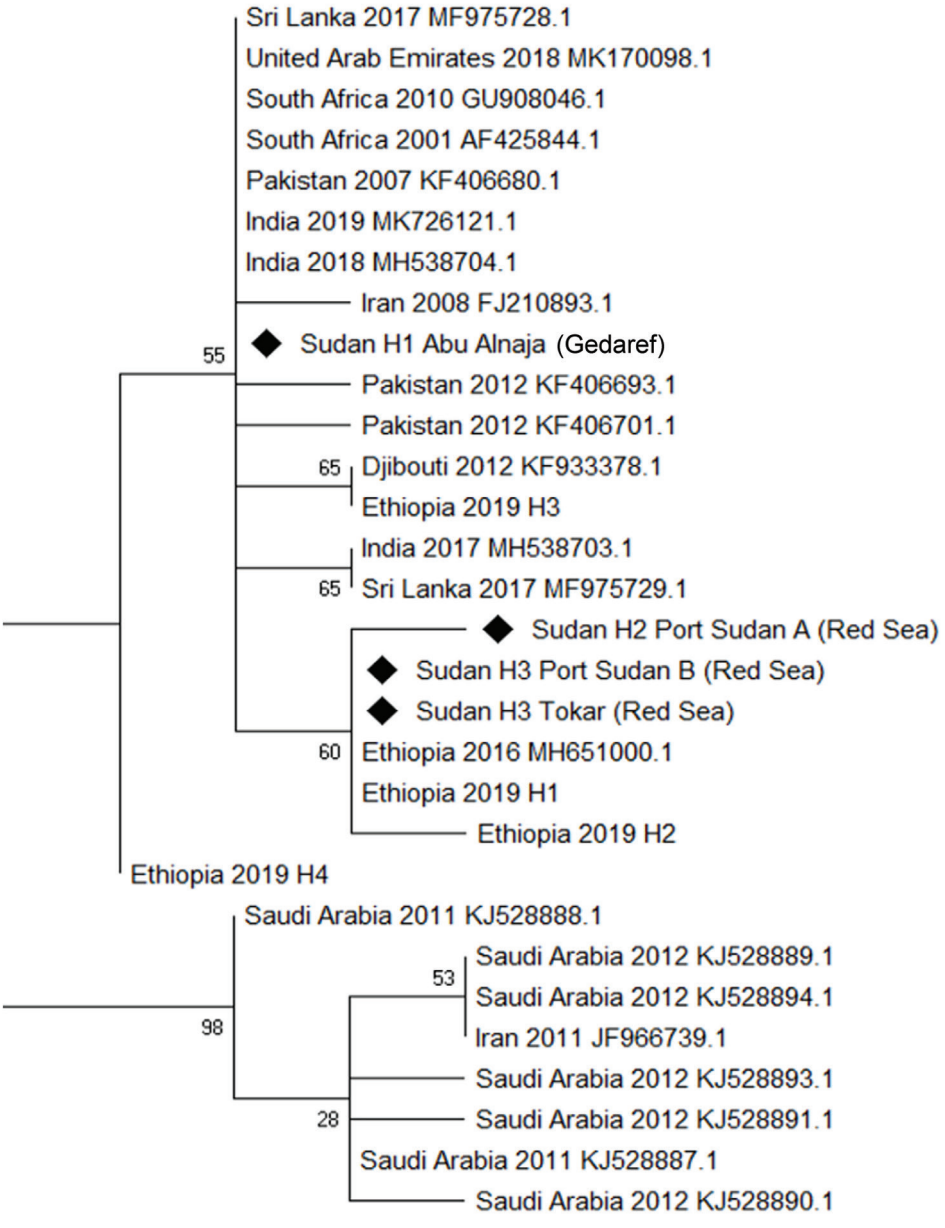

Figure. Phylogenetic analysis of *Anopheles stephensi* mosquitoes collected in Sudan, 2016–2018, and reference sequences. Maximum-likelihood tree was constructed by using mitochondrial cytochrome oxidase 1 sequences from Sudan (diamonds) and other countries from which data are available. GenBank accession numbers are provided for reference sequences.

An. stephensi mosquitoes from Daim Bakur failed to amplify after use of the Folmer primers and thus was not included in the tree. The initial origins of *An. stephensi* mosquitoes are currently difficult to ascertain because of a lack of geographic resolution in the phylogeny; the exception is the highly differentiated clade of samples from Saudi Arabia and Iran. However, the haplotypes detected in Sudan are similar to 3 of the 4 detected in Ethiopia and are thus potentially consistent with spread from Ethiopia or elsewhere in the Horn of Africa. The presence of haplotypes from different states in 2 distinct clades may also indicate separate introduction sources, although wider sampling is required for confirmation.

The emergence of *An. stephensi* mosquitoes in Sudan poses substantial concern for malaria control and elimination and potentially stark predictions for urban malaria in Africa if this species should spread farther (*7*). In Sudan and throughout much of Africa, local surveillance systems, as well as knowledge and expertise, focus mainly on the mosquito vector members of the predominant *An. gambiae* complex and *An. funestus* group (*8*). Although the actual epidemiologic effects of *An. stephensi* mosquito emergence is not known, temporal coincidence of their establishment and rising malaria rates in Djibouti suggest a substantial threat (*9*). Although little is known about *An. stephensi* mosquitoes in Sudan, we identified productive breeding sites in septic tanks, manholes, and the water-storage containers used for construction purposes in cities (Appendix Figure 3); these findings correspond with reports from Ethiopia (*6*). Information about the wider and local distribution of *An. stephensi* mosquitoes in Sudan, coupled with bionomic studies, can be used to guide rational control strategies.

Acknowledgments

We thank our colleagues at the Department of Medical Entomology, Sudan National Public Health Laboratory, who supported and helped us collect and rear the mosquito specimens. We are also grateful to Fitsum Tadesse for providing haplotype sequences from Ethiopia before their publication.

This work was supported by a Wellcome Trust Master's Fellowship in Public Health and Tropical Medicine awarded to A.A. (award no. 200068/Z/15/Z).

About the Author

Mr. Ahmed is a lecturer at the Institute of Endemic Diseases, University of Khartoum, Sudan, and a Wellcome Trust Master Fellow of Public Health and Tropical Medicine at Liverpool School of Tropical Medicine, UK. His interests are the research and control of the vectorborne diseases, with a particular focus on emerging and re-emerging diseases and invasive disease vectors.

References

1. Surendran SN, Sivabalakrishnan K, Sivasingham A, Jayadas TTP, Karvannan K, Santhirasegaram S, et al. Anthropogenic factors driving recent range expansion of the malaria vector *Anopheles stephensi*. Front Public Health. 2019;7:53 https://doi.org/10.3389/fpubh.2019.00053
2. Carter TE, Yared S, Gebresilassie A, Bonnell V, Damodaran L, Lopez K, et al. First detection of *Anopheles stephensi* Liston, 1901 (Diptera: culicidae) in Ethiopia using molecular and morphological approaches. Acta Trop. 2018;188:180–6. https://doi.org/10.1016/j.actatropica.2018.09.001
3. Scott JA, Brogdon WG, Collins FH. Identification of single specimens of the *Anopheles gambiae* complex by the polymerase chain reaction. Am J Trop Med Hyg. 1993;49:520–9. https://doi.org/10.4269/ajtmh.1993.49.520
4. Simon C, Frati F, Beckenbach A, Crespi B, Liu H, Flook P. Evolution, weighting, and phylogenetic utility of mitochondrial gene sequences and a compilation of conserved polymerase chain reaction primers. Ann Entomol Soc Am. 1994;87:651–701. https://doi.org/10.1093/aesa/87.6.651
5. Kumar S, Stecher G, Li M, Knyaz C, Tamura K. MEGA X: Molecular Evolutionary Genetics Analysis across computing platforms. Mol Biol Evol. 2018;35:1547–9. https://doi.org/10.1093/molbev/msy096
6. Tadesse FG, Ashine T, Teka H, Esayas E, Messenger LA, Chali W, et al. *Anopheles stephensi* mosquitoes as vectors of *Plasmodium vivax* and *falciparum*, Horn of Africa, 2019. Emerg Infect Dis. 2021;27:603–7. https://doi.org/10.3201/eid2702.200019
7. Sinka ME, Pironon S, Massey NC, Longbottom J, Hemingway J, Moyes CL, et al. A new malaria vector in Africa: predicting the expansion range of *Anopheles stephensi* and identifying the urban populations at risk. Proc Natl Acad Sci U S A. 2020;117:24900–8. https://doi.org/10.1073/pnas.2003976117
8. Takken W, Lindsay S. Increased threat of urban malaria from *Anopheles stephensi* mosquitoes, Africa. Emerg Infect Dis. 2019;25:1431–3. https://doi.org/10.3201/eid2507.190301
9. de Santi VP, Khaireh BA, Chiniard T, Pradines B, Taudon N, Larréché S, et al. Role of *Anopheles stephensi* mosquitoes in malaria outbreak, Djibouti, 2019. Emerg Infect Dis. 2021;27:1697–700. https://doi.org/10.3201/eid2706.204557

Address for correspondence: Ayman Ahmed, Institute of Endemic Diseases, University of Khartoum, Khartoum 11111, Sudan; email: ayman.ame.ahmed@gmail.com

Nonclonal *Burkholderia pseudomallei* Population in Melioidosis Case Cluster, Sri Lanka

Himali S. Jayasinghearachchi, Vaithehi R. Francis, Harindra D. Sathkumara, Shivankari Krishnananthasivam, Jayanthi Masakorala, Thilini Muthugama, Aruna D. De Silva, Enoka M. Corea

Author affiliations: General Sir John Kotelawala Defense University, Ratmalana, Sri Lanka (H.S. Jayasinghearachchi, T. Muthugama, A.D. De Silva); Eastern University, Vantharumoolai, Sri Lanka (V.R. Francis), Genetech Research Institute, Colombo, Sri Lanka (H.D. Sathkumara, S. Krishnananthasivam); University of Colombo, Colombo (J. Masakorala, E.M. Corea)

DOI: https://doi.org/10.3201/eid2711.210219

A melioidosis case cluster of 10 blood culture–positive patients occurred in eastern Sri Lanka after an extreme weather event. Four infections were caused by *Burkholderia pseudomallei* isolates of sequence type 594. Whole-genome analysis showed that the isolates were genetically diverse and the case cluster was nonclonal.

Melioidosis, an emerging tropical infection caused by the soil bacterium *Burkholderia pseudomallei*, is found most commonly in northern Australia and the tropical countries of Southeast Asia. Melioidosis is endemic in Sri Lanka and has a case-fatality rate of 24% (*1*). The primary route of acquisition is inoculation of contaminated surface water or soil through skin and mucous membranes. However, a high incidence of pneumonia with sepsis has been reported during extreme weather events, such as heavy rainfall, indicating that inhalation of aerosolized bacteria during cyclones and typhoons is a likely mode of transmission in this setting (*2*).

We identified a case cluster of 10 blood culture–positive cases of melioidosis in the Batticaloa District of the Eastern Province of Sri Lanka during November–December 2015, after a flooding event; 4 case-patients died (Appendix Table, https://wwwnc.cdc.gov/EID/article/27/11/21-0219-App1.pdf). Before this case cluster was identified, 1 case had been reported from Batticaloa in March 2015, and after this case cluster, 5 cases were found in 2016. We confirmed isolates as *B. pseudomallei* by real-time PCR to detect the *lpxo* gene (*3*). We identified 6 sequence types (STs) by multilocus sequence typing (MLST) (*4*); of the 10 isolates, 4 were ST594, belonging to the uncommon *B. thailandensis*–like flagellum and chemotaxis (BTFC) gene cluster. Although the monthly average rainfall for October in the Batticaloa District is usually 160 mm, ≈331.5 mm of rain was recorded in the 48 hours ending at 8:30 A.M. Previous evidence has shown that, in this setting, infections are usually caused by diverse strains because of widespread aerosolization of multiple clones (*2*). We performed whole-genome sequencing (WGS) to determine clonality among the isolates of identical ST. The Ethics Review Committee of the Faculty of Medicine, University of Colombo, (Colombo, Sri Lanka), approved this study.

We mapped the geographic location of the cases on Google Earth using ArcGIS version 10.1 (ESRI, https://www.esri.com) (Figure). We compared WGS data of 3 ST594 *B. pseudomallei* isolates (114, 122, and 133) using binary alignment files with Unipro UGENE version 33 (*5*). We determined the distribution of genomic islands (GIs) using the Island Viewer 4 web tool (*6*) and the National Center for

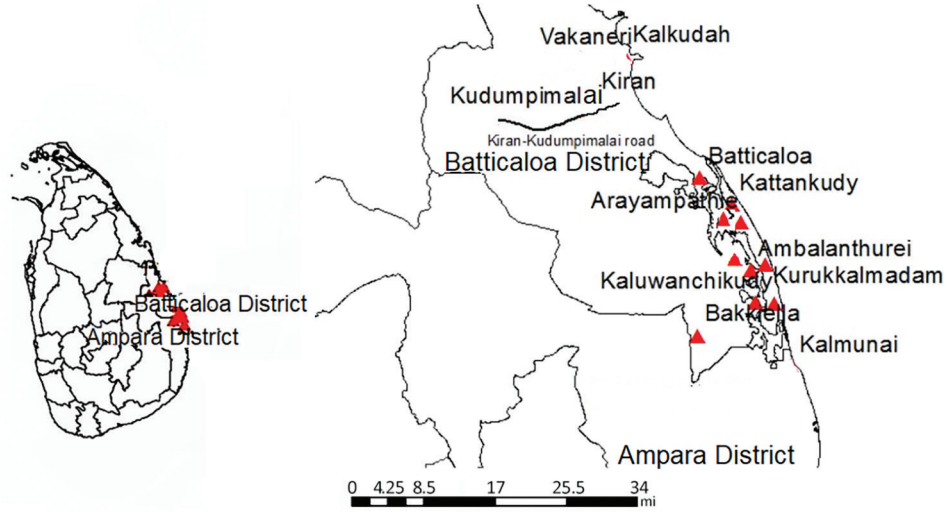

Figure. Location of melioidosis cases (red arrows) in the Batticaloa District of Sri Lanka during November–December 2015. Inset shows location of Batticaloa and Ampara Districts in Sri Lanka.

Table. Characteristics of *Burkholderia pseudomallei* isolates from cluster cases of melioidosis after heavy rain, Sri Lanka*

Characteristic	Isolate 114	Isolate 122	Isolate133
Sequence type	594	594	594
Clade	BTFC	BTFC	BTFC
BimA allele type	$BimA_{Bm}$	$BimA_{Bp}$	$BimA_{BP}$
No. prophages in chromosome 1	6	1	6
No. prophages in chromosome 2	1	1	1
No. intact phages	0	2	0
Presence or absence of intact prophage PHAGE_Burkho_phiE202_NC_009234	Absent	Present	Absent
GIs identified	GI1, GI4, GI5, GI6, GI7, GI8, GI9, GI8.i, GI8.ii, GI11, GI12, GI13, GI14, GI16	GI1. GI2, GI4, GI6, GI7, GI8, GI8.i, GI8.ii, GI11, GI12, GI13, GI14, GI16	GI1, GI4, GI6, GI7, GI8, GI8.i, GI8.ii, GI11, GI12, GI13, GI14, GI16
GIs located next to tRNA genes	GI7	GI2, GI4	GI7, GI8
GIs containing phage or site-specific integrases	GI4, GI7, GI15i	GI7, GI15i	GI4, GI7, GI15i
GIs containing prophage DNA	GI7, GI4, GI15i, GI13	GI2, GI7, GI15i, GI13	GI4, GI7, GI15i, GI13
No. transposable elements in GI8	7	6	6
New GI15i	GI15i	GI15i	GI15i
No. integrases	2	2	2

*BTFC, *B. thailandensis*–like flagellum and chemotaxis; GI, genomic island.

Biotechnology Information Multiple Sequence Alignment (https://www.ncbi.nlm.nih.gov/tools/msaviewer) and BLAST (https://blast.ncbi.nlm.nih.gov/Blast.cgi) tools. We used the PHAge Search Tool Enhanced Release (PHASTER) webserver to analyze the annotated bacterial genomes to locate prophage-specifying DNA regions (*7*). We manually searched the sequences identified by PHASTER and used the position of integrase and last phage–related genes to determine genome boundaries (*8*). We predicted and annotated all open reading frames (ORFs) of the prophages by PHASTER and BLASTp. We also determined the intracellular motility factor (*bimA*) allele type present in each strain as previously described (*9*).

WGS showed genetic diversity in terms of gene content, location, number and type of GIs, prophage DNA distribution, number of intact prophages and *bimA* allele type among the isolates of ST594 (Table). These results show that the case cluster was nonclonal in origin.

This case cluster after heavy rainfall and flooding in Sri Lanka confirmed that *B. pseudomallei* is present in the environment of eastern Sri Lanka. The case-fatality rate of the cluster (40%) was almost double that of sporadic infections in Sri Lanka (23%) (*1*). Six of the 10 isolates in our study belonged to diverse STs; 4 isolates were novel (ST1364, ST1442, ST1179, and ST1413). However, 4 isolates belonging to ST594 were from patients from different geographic locations. In addition, WGS analysis of prophage DNA distribution was able to discriminate between the isolates. GI variation in *B. pseudomallei* is known to be associated with genomic plasticity of the organism, and GIs appear to be a main source of genomic diversity within *B. pseudomallei* that can be useful in identifying genetically diverse strains (*10*). The strain-specific variations in the structure and distribution of GIs in the isolates in this case cluster indicate the presence of genetically diverse strains.

As weather patterns change globally and include more severe weather events and increased flooding, we may see more such case clusters of melioidosis. Physicians in tropical regions must be vigilant for such occurrences because of the high mortality rate associated with melioidosis in this setting. Primary prevention of melioidosis is difficult because of the saprophytic nature of *B. pseudomallei* and regular flooding during the rainy season. The predominance of diabetic patients in this cluster (Appendix Table) illustrates the importance of detection and control of diabetes in high-risk communities for primary prevention. Secondary prevention requires close coordination between clinicians and microbiologists to encourage patients to seek medical advice early in illness and to transfer febrile patients promptly to centers with blood culture facilities. Early suspicion of melioidosis will enable timely, effective antimicrobial treatment.

Acknowledgments

We thank K. Arulmoly, P. Mayurathan, S.A. Jauffar, S. Prasath, V. Jeyathas, and M.T.A. Rikarz, and other clinical staff of the Teaching Hospital, Batticaloa. We thank the staff of the Genetech Research Institute and the Department of Microbiology, Faculty of Medicine, University of Colombo, for laboratory assistance. We thank Sameera Fernando, Anjana Rahubaddha, Rajitha Fernando, Kasun de Soyza, Thanuka Gunawardana, and Shehan Dayarathna for assistance with sample and data collection.

This study was funded by US Army Medical Research Acquisition Activity (grant no. W81XWH14C0071) and partially funded by National Research Council, Sri Lanka (grant no. NRC 18079 to A.D.D.S.).

About the Author

Dr. Jayasinghearachchi is a senior lecturer at General Sir John Kotelawala Defense University, Ratmalana. Her research interests include molecular evolution of human pathogens and their epidemiology.

References

1. Corea EM, de Silva AD, Thevanesam V. Melioidosis in Sri Lanka. Trop Med Infect Dis. 2018;3:22. https://doi.org/10.3390/tropicalmed3010022
2. Ko WC, Cheung BM, Tang HJ, Shih HI, Lau YJ, Wang LR, et al. Melioidosis outbreak after typhoon, southern Taiwan. Emerg Infect Dis. 2007;13:896–8. https://doi.org/10.3201/eid1306.060646
3. Merritt A, Inglis TJ, Chidlow G, Harnett G. PCR-based identification of *Burkholderia pseudomallei*. Rev Inst Med Trop São Paulo. 2006;48:239–44. https://doi.org/10.1590/S0036-46652006000500001
4. Jayasinghearachchi HS, Corea EM, Krishnananthasivam S, Sathkumara HD, Francis VR, Abeysekere TR, et al. Whole-genome sequences of eight clinical isolates of *Burkholderia pseudomallei* from melioidosis patients in eastern Sri Lanka. Microbiol Resour Announc. 2019;8:e00645–19. https://doi.org/10.1128/MRA.00645-19
5. Okonechnikov K, Golosova O, Fursov M; UGENE team. Unipro UGENE: a unified bioinformatics toolkit. Bioinformatics. 2012;28:1166–7. https://doi.org/10.1093/bioinformatics/bts091
6. Bertelli C, Laird MR, Williams KP, Lau BY, Hoad G, Winsor GL, et al.; Simon Fraser University Research Computing Group. IslandViewer 4: expanded prediction of genomic islands for larger-scale datasets. Nucleic Acids Res. 2017;45(W1):W30–5. https://doi.org/10.1093/nar/gkx343
7. Arndt D, Grant JR, Marcu A, Sajed T, Pon A, Liang Y, et al. PHASTER: a better, faster version of the PHAST phage search tool. Nucleic Acids Res. 2016;44(W1):W16–21. https://doi.org/10.1093/nar/gkw387
8. Kearse M, Moir R, Wilson A, Stones-Havas S, Cheung M, Sturrock S, et al. Geneious Basic: an integrated and extendable desktop software platform for the organization and analysis of sequence data. Bioinformatics. 2012;15;28(12):1647–9. https://doi.org/10.1093/bioinformatics/bts199
9. Sitthidet C, Stevens JM, Chantratita N, Currie BJ, Peacock SJ, Korbsrisate S, et al. Prevalence and sequence diversity of a factor required for actin-based motility in natural populations of *Burkholderia* species. J Clin Microbiol. 2008;46:2418–22. https://doi.org/10.1128/JCM.00368-08
10. Holden MT, Titball RW, Peacock SJ, Cerdeño-Tárraga AM, Atkins T, Crossman LC, et al. Genomic plasticity of the causative agent of melioidosis, *Burkholderia pseudomallei*. Proc Natl Acad Sci U S A. 2004;101:14240–5. https://doi.org/10.1073/pnas.0403302101

Address for correspondence: Enoka M. Corea, Department of Microbiology, Faculty of Medicine, University of Colombo, Colombo, Sri Lanka; email: enokac@micro.cmb.ac.lk; Aruna D. De Silva, Department of Paraclinical Sciences, Faculty of Medicine, General Sir John Kotelawala Defense University, Ratmalana, Sri Lanka; email: dharshan_fom@kdu.ac.lk

Real-Time Genomic Surveillance for SARS-CoV-2 Variants of Concern, Uruguay

Natalia Rego,[1] Alicia Costábile,[1] Mercedes Paz,[1] Cecilia Salazar,[1] Paula Perbolianachis,[1] Lucía Spangenberg, Ignacio Ferrés, Rodrigo Arce, Alvaro Fajardo, Mailen Arleo, Tania Possi, Natalia Reyes, Ma Noel Bentancor, Andrés Lizasoain, María José Benítez, Viviana Bortagaray, Ana Moller, Gonzalo Bello, Ighor Arantes, Mariana Brandes, Pablo Smircich, Odhille Chappos, Melissa Duquía, Belén González, Luciana Griffero, Mauricio Méndez, Ma Pía Techera, Juan Zanetti, Bernardina Rivera, Matías Maidana, Martina Alonso, Cecilia Alonso, Julio Medina, Henry Albornoz, Rodney Colina, Veronica Noya, Gregorio Iraola, Tamara Fernández-Calero, Gonzalo Moratorio, Pilar Moreno

Author affiliations: Institut Pasteur, Montevideo, Uruguay (N. Rego, A. Costábile, M. Paz, C. Salazar, P. Perbolianachis, L. Spangenberg, I. Ferres, R. Arce, A. Fajardo, M. Brandes, B. Rivera, M. Maidana, M. Alonso, G. Iraola, T. Fernandez-Calero, G. Moratorio, P. Moreno); Universidad de la República, Montevideo, Uruguay (A. Costabile, P. Perbolianachis, R. Arce, A. Fajardo, A. Lizasoain, M.J. Benítez, V. Bortagaray, A. Moller, O. Chappos, M. Duquía, B. González, L. Griffero, M. Méndez, M.P. Techera, J. Zanetti, C. Alonso, R. Colina, G. Moratorio, P. Moreno); Sanatorio Americano, Montevideo (M. Arleo, T. Possi, N. Reyes, M.N. Bentancor, V. Noya); Instituto Oswaldo Cruz–Fiocruz, Rio de Janeiro, Brazil (G. Bello, I. Arantes); Instituto de Investigaciones Biológicas Clemente Estable, Montevideo (P. Smirnich); Ministerio de Salud Pública, Montevideo (J. Medina, H. Albornoz)

DOI: https://doi.org/10.3201/eid2711.211198

We developed a genomic surveillance program for real-time monitoring of severe acute respiratory syndrome coronavirus 2 (SARS-CoV-2) variants of concern (VOCs) in Uruguay. We report on a PCR method for SARS-CoV-2 VOCs, the surveillance workflow, and multiple independent introductions and community transmission of the SARS-CoV-2 P.1 VOC in Uruguay.

By late 2020, because of natural viral evolution, severe acute respiratory syndrome coronavirus 2 (SARS-CoV-2) genetic variants emerged, some of which show increased transmissibility and cause more severe coronavirus disease (COVID-19) (*1*). In

[1]These authors contributed equally to this article.

addition, these variants show reduced neutralization by antibodies generated during previous infection or vaccination, which can reduce effectiveness of treatments, vaccines, or diagnostic tests (*1*). By July 2021, a total of 4 variants of concern (VOCs) had been identified: B.1.1.7 (Alpha), B.1.351 (Beta), P.1 (Gamma), and B.1.617 (Delta) (*2*). Nonetheless, a robust surveillance workflow for early VOC identification is key to accelerating the pandemic response.

Brazil demonstrated a sharp increase in SARS-CoV-2 cases, hospitalizations, and deaths after the emergence of the P.1 VOC in Amazonas State in November 2020 (*3*; F. Naveca et al., unpub. data, https://doi.org/10.21203/rs.3.rs-275494/v1). P.1 displays higher transmissibility than previous local SARS-CoV-2 lineages and rapidly became the predominant strain in most states of Brazil during February–March 2021 (*3*,*4*; F. Naveca et al., unpub. data, https://doi.org/10.21203/rs.3.rs-275494/v1). P.1 also has spread worldwide; by July 2021, P.1 had been detected in ≥41 countries (*5*), where it might replicate the epidemic trajectory observed in Brazil. Uruguay, which shares 600 miles of dry border with Brazil, has experienced an exponential increase in COVID-19 cases since February 2021; by June 2021, Uruguay was among countries with the highest number of daily cases and deaths per million persons (*6*). Despite closing the Brazil–Uruguay border to tourism on March 13, 2020, evidence suggests a high viral flux between the countries (*7*,*8*). Therefore, P.1 could be introduced into Uruguay and the country needs an organized strategy to monitor VOC emergence.

In response to concerns over VOCs, the Ministry of Public Health, the Pasteur Institut of Montevideo (Uruguay), University of the Republic, and Zurgen-Sanatorio Americano formed a multidisciplinary workgroup to develop a genomic surveillance program for real-time monitoring for VOC emergence in Uruguay. The workgroup aimed to provide expertise and resources for large-scale sequencing, genomic analysis, and an affordable and decentralized inhouse PCR to detect known VOCs, including B.1.1.7, B.1.351, and P.1. Within a few weeks, the working group developed a PCR VOC detection method and a national sample processing workflow (Appendix 1 Figure 1, https://wwwnc.cdc.gov/EID/article/27/11/21-1198-App1.pdf). In addition, we identified multiple independent introductions of P.1 and community transmission in Uruguay.

The workgroup processes >3,000 nasopharyngeal samples daily, and around 100–300 SARS-CoV-2–positive samples are sent weekly for PCR VOC analysis and sequencing. During January 11–March 26, 2021, the working group collected and processed a total of 251 SARS-CoV-2–positive RNA samples from 15/19 departments in Uruguay (Appendix 1 Table 1). Cycle thresholds for initial diagnostic PCR were 9–34.7. Among patients with positive samples, 95 were male, 95 were female, and 61 were of unknown sex; ages ranged from 1–85 years. Results from PCR VOC assay showed that 67/251 (27%) samples corresponded to putative P.1/B.1.351 (Appendix 1 Figure 2).

To validate PCR VOC classification, we sequenced all VOC–positive samples, plus 31 additional samples, by applying the ARTIC Network protocol (J.R. Tyson et al., unpub. data, https://doi.org/10.1101/2020.09.04.283077) for the MinION sequencing platform (Oxford Nanopore Technologies, https://nanoporetech.com) (Appendix 1). For the final 74 high-quality consensus sequences that were assigned to SARS-CoV-2 lineages following Pango nomenclature (*9*), we achieved a 100% agreement between PCR VOC and genome sequencing results. Predictably, given Uruguay's proximity to Brazil, samples classified as P.1/B.1.351 by PCR VOC were assigned to lineage P.1 after genome sequencing. The PCR we developed is a feasible, precise, and scalable method for real-time surveillance of known VOCs and verified circulation of P.1 lineage in 15/19 departments in Uruguay (Appendix 1 Figures 2, 3).

To estimate geographic sources and the number of independent P.1 introductions into Uruguay, we combined P.1 sequences from Uruguay and 691 P.1 sequences from South America available from EpiCoV in GISAID (https://www.epicov.org/epi3; Appendix 1 Tables 2, 3; Appendix 2, https://wwwnc.cdc.gov/EID/article/27/11/21-1198-App2.xlsx). The maximum-likelihood phylogeographic analysis identified ≥12 independent P.1 introductions into Uruguay from Brazil and ≥6 local transmission clusters of 3–24 sequences (Figure; Appendix 1 Figure 4). We used Bayesian analysis to estimate the median time of most recent common ancestor of P.1 clades in Uruguay to be mid-February to early March 2021 (Appendix 1 Table 4, Figure 5), which coincides with increasing mobility and the beginning of the exponential surge in COVID-19 cases in the country (Appendix 1 Figure 6).

The rapid emergence of the SARS-CoV-2 lineage P.1 in South America justifies the need for increased screening for this highly transmissible virus. We elaborated a comprehensive genomic surveillance program and provide a clear example of how multidisciplinary

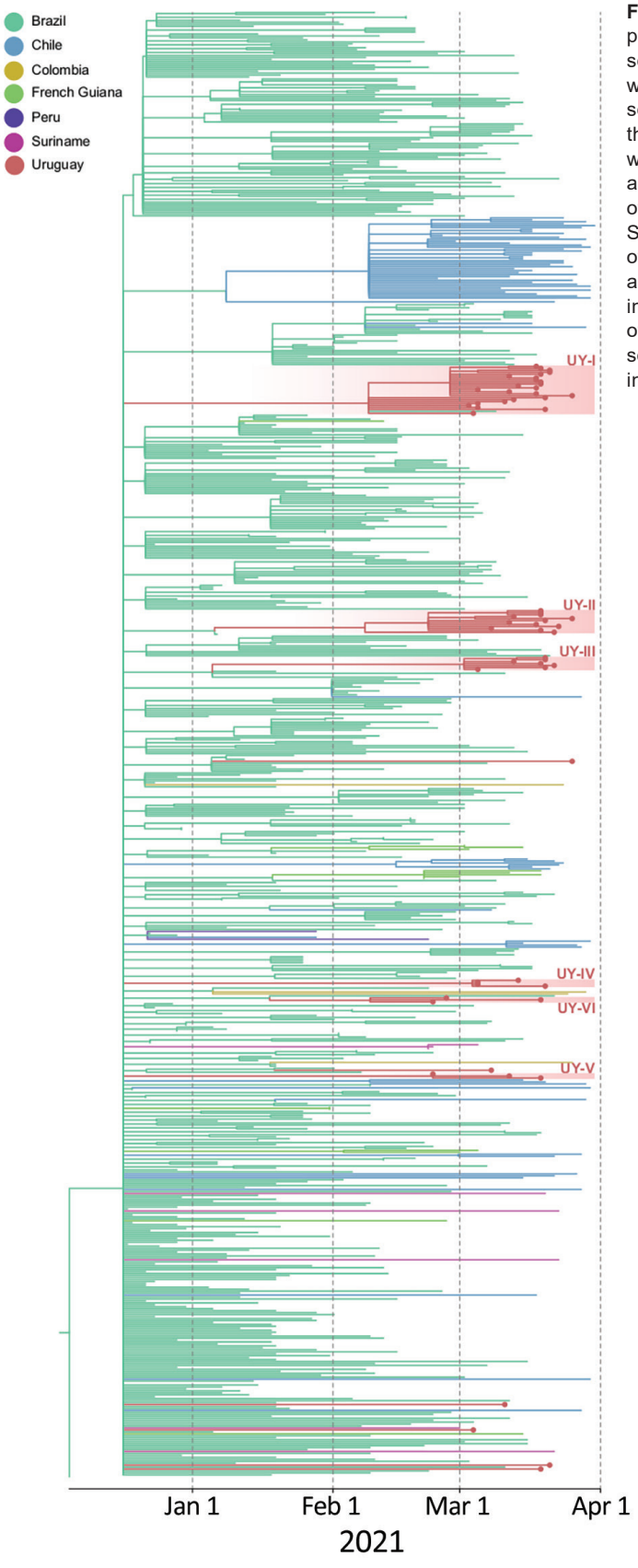

Figure. Time-scaled maximum likelihood Bayesian phylogeographic maximum clade credibility tree of 59 severe acute respiratory syndrome coronavirus 2 lineage P.1 whole-genome sequences from Uruguay and 691 reference sequences from South America. The tree was rooted with the EPI_ISL_833137 sequence from GISAID (https://www.gisaid.org), collected December 4, 2020. Branches are colored according to the most probable location state of their descendant nodes as indicated at the legend. Sequences from Uruguay are shown with dots at the end of the branch. Red shading indicates clades from Uruguay and their distribution along the P.1 tree demonstrates ≥12 independent introductions and locally transmitted clusters of 3–24 sequences. The tree suggests Brazil has been the source of P.1 dissemination to Uruguay and other countries in South America.

authorities manage the COVID-19 crisis. Our findings revealed that the P.1 VOC was introduced into Uruguay multiple times over a period of increasing mobility in binational cities along the Brazil–Uruguay border and in Uruguay between mid-February and early March 2021. The introduction of the highly transmissible P.1 VOC coupled with the increasing human mobility probably contributed to the rapid local spread of this variant and the worsening COVID-19 epidemic in Uruguay during January–July 2021.

This article was preprinted at https://www.medrxiv.org/content/10.1101/2021.05.20.21256969v1.

Acknowledgments

We thank the groups that contributed SARS-CoV-2 genomes to the EpiCoV GISAID initiative (Appendix 2). We thank Marcelo Fiori and María Inés Fariello for sharing mobility data from Uruguay and Christian Brandt from Institute for Infectious Diseases and Infection Control (Jena University Hospital), for adapting their poreCov Nextflow pipeline to our requirements and for clarifying doubts about its implementation. We thank Nicolas Nin and Javier Hurtado from Hospital Español for their work as medical doctors caring for patients included in this study.

This work was supported by FOCEM-Fondo para la Convergencia Estructural del Mercosur (COF03/11).

About the Author

Ms. Rego is a research biologist and trained in bioinformatics at Institut Pasteur de Montevideo, Uruguay. Her research interests include evolutionary biology, transcriptomics, host-pathogen interactions, and the epidemiology and phylogeny of coronaviruses.

References

1. Abdool Karim SS, de Oliveira T. New SARS-CoV-2 variants—clinical, public health, and vaccine implications. N Engl J Med. 2021;384:1866–8. https://doi.org/10.1056/NEJMc2100362
2. Centers for Disease Control and Prevention. SARS-CoV-2 variant classifications and definitions [cited 2021 Apr 10]. https://www.cdc.gov/coronavirus/2019-ncov/cases-updates/variant-surveillance/variant-info.html
3. Faria NR, Mellan TA, Whittaker C, Claro IM, Candido DDS, Mishra S, et al. Genomics and epidemiology of the P.1 SARS-CoV-2 lineage in Manaus, Brazil. Science. 2021;372:815–21. https://doi.org/10.1126/science.abh2644
4. Fiocruz Genomic Network. Frequency of the main SARS-CoV-2 lineages per month sampling [in Portuguese] [cited 2021 Apr 30]. http://www.genomahcov.fiocruz.br/frequencia-das-principais-linhagens-do-sars-cov-2-por-mes-de-amostragem
5. Outbreak.info. P.1 lineage report [cited 2021 Apr 30]. https://outbreak.info/situation-reports?pango=P.1&selected=BRA&loc=BRA&loc=USA&loc=USA_US-CA
6. Our World in Data. Daily new and confirmed COVID-19 cases per million people [cited 2021 Jun 30]. https://ourworldindata.org/explorers/coronavirus-data-explorer
7. Elizondo V, Harkins GW, Mabvakure B, Smidt S, Zappile P, Marier C, et al. SARS-CoV-2 genomic characterization and clinical manifestation of the COVID-19 outbreak in Uruguay. Emerg Microbes Infect. 2021;10:51–65. https://doi.org/10.1080/22221751.2020.1863747
8. Mir D, Rego N, Resende PC, Tort F, Fernández-Calero T, Noya V, et al. Recurrent dissemination of SARS-CoV-2 through the Uruguayan–Brazilian border. Front Microbiol. 2021;12:653986. https://doi.org/10.3389/fmicb.2021.653986
9. Rambaut A, Holmes EC, O'Toole Á, Hill V, McCrone JT, Ruis C, et al. A dynamic nomenclature proposal for SARS-CoV-2 lineages to assist genomic epidemiology. Nat Microbiol. 2020;5:1403–7. https://doi.org/10.1038/s41564-020-0770-5

Tamara Fernández-Calero, Gonzalo Moratorio, and Pilar Moreno, Laboratorio de Virología Molecular, Facultad de Ciencias, Universidad de la República, Mataojo 2055, Montevideo, Uruguay; email: tamfer@pasteur.edu.uy, moratorio@pasteur.edu.uy, and pmoreno@pasteur.edu.uy

Highly Pathogenic Avian Influenza A(H5N1) Virus in Wild Red Foxes, the Netherlands, 2021

Jolianne M. Rijks, Hanna Hesselink, Pim Lollinga, Renee Wesselman, Pier Prins, Eefke Weesendorp, Marc Engelsma, Rene Heutink, Frank Harders, Marja Kik, Harry Rozendaal, Hans van den Kerkhof, Nancy Beerens

Author affiliations: Dutch Wildlife Health Centre, Utrecht University, Utrecht, the Netherlands (J.M. Rijks, H. Hesselink, M. Kik); Stichting Faunavisie Wildlife Care, Westernieland, the Netherlands (P. Lollinga); Stichting Faunavisie Wildlife Care, Blijham, the Netherlands (R. Wesselman); Dierenkliniek Winsum, Winsum, the Netherlands (P. Prins); Wageningen Bioveterinary Research, Lelystad, the Netherlands (E. Weesendorp, M. Engelsma, R. Heutink, F. Harders, N. Beerens); Dutch Food and Consumer Products Safety Authority, Utrecht (H. Rozendaal); Coordination Centre for Communicable Disease Control, National Institute for Public Health and the Environment, Bilthoven, the Netherlands (H. van den Kerkhof)

DOI: https://doi.org/10.3201/eid2711.211281

We detected infection with highly pathogenic avian influenza A(H5N1) virus clade 2.3.4.4b in 2 red fox (*Vulpes vulpes*) cubs found in the wild with neurologic signs in the Netherlands. The virus is related to avian influenza viruses found in wild birds in the same area.

On May 10, a red fox *Vulpes vulpes* cub (cub 1) displaying abnormal behavior was found in Bellingwolde, the Netherlands, and taken into care of a wildlife rescue center. Upon entry, the 6- to 8-week-old cub was slightly dehydrated and showed at intervals of <30 minutes lip retraction, rapid opening and closing of mouth, excessive salivation, skin twitching, head shaking, and body tremors (Figure; Video, https://wwwnc.cdc.gov/EID/article/27/11/21-1281-V1.htm). The cub first seemed to improve, but on May 12 it reacted aggressively when touched. Subsequently, we observed difficult swallowing and labored breathing. The cub seemed blind and stopped eating. As the situation further deteriorated, we humanely euthanized the cub on May 16. On May 13, the center received another 6- to 8-week-old red fox cub (cub 2) found ≈900 m from cub 1. Cub 2 was hypothermic and dehydrated. It had seizures and died overnight.

Retrospectively, we concluded that the mother of the cubs was likely a vixen found walking circles on May 10, ≈975 m direct distance from cub 1 and ≈90 m from cub 2. The vixen reacted very aggressively to capture, responding to sound but blind. The vixen had a fresh elbow fracture, probably caused by a road traffic accident. We humanely euthanized her the same day and sent her carcass for destruction.

Although rabies lyssavirus is unlikely in the Netherlands, European bat 1 lyssavirus is endemic in serotine bats (*Eptesicus serotinus*) (*1*). To exclude lyssavirus infection in the fox cubs, we performed a direct fluorescent antibody test on smears of brain tissue in accordance with World Organisation for Animal Health (OIE) protocol (https://www.oie.int/fileadmin/Home/eng/Health_standards/tahm/3.01.17_RABIES.pdf). Test results were negative.

Subsequently, we tested brain samples for avian influenza virus by using a PCR detecting the influenza A virus matrix gene, followed by the subtype-specific H5-PCR on the hemagglutinin gene, as described previously (*2*). The samples from both cubs tested positive (Table), and we subtyped the virus as highly pathogenic avian influenza (HPAI) influenza virus A subtype H5N1. We isolated the HPAI H5N1 virus from the brain of cub 1 by inoculation of the samples into 10-day-old embryonated special pathogen–free chicken eggs.

During April–May 2021, large numbers of dead barnacle geese (*Branta leucopsis*) were reported in the northern part of the Netherlands, and later other species of waterfowl and birds of prey were also found dead. A selected number of dead wild birds were submitted for AI diagnostics and tested positive for HPAI H5N1 virus. We performed whole-genome sequencing of the HPAI H5N1 viruses found in wild birds and the 2 foxes as previously described (*3*) and conducted genetic and phylogenetic analyses to study the relationship between these viruses. Phylogenetic analysis of the gene segments (Appendix 1 Figure 1–8) showed the viruses detected in wild birds and the 2 foxes were in the same cluster and highly related. We classified the viruses as H5 clade 2.3.4.4b viruses, which were related to other HPAI H5N1 viruses detected in wild birds and poultry in Europe during 2020–2021. The HPAI H5N1 viruses detected in the foxes were not related to zoonotic H5N1 strains infecting humans in Asia and did not contain any known zoonotic mutations (data not shown). The sequences of the viruses detected in cub 1 (GISAID [https://www.gisaid.org] accession no. EPI_2194218) and cub 2 (GISAID accession no. EPI_2194219) were identical; the closest related virus was identified in a white-tailed eagle (*Haliaeetus albicilla*) near the village of Noordlaren. We observed only 6 aa differences: mutations A152T and T521I in polymerase basic

Figure. Salivating red fox (*Vulpes vulpes*) cub 1 during a fit, the Netherlands, 2021. Seizure started with retracting lips at 0 sec (A), followed by facial wrinkling with opening of mouth at 0.07 sec (B), closing of the jaws at 0.17 sec (C), then back to "normal" at 0.40 sec (D), before this sequence starts all over at 0.50 sec.

Table. Results of diagnostic tests of avian influenza viruses detected in 2 red fox (*Vulpes vulpes*) cubs, the Netherlands, 2021*

Red fox	Pooled samples of brain	M-PCR1 C_t value	M-PCR2 C_t value	H5-PCR C_t value
Cub 1	Ammon's horn and medulla oblongata	21.27	21.46	23.35
Cub 1	Cerebellum and cerebrum	19.31	20.79	21.65
Cub 2	Ammon's horn and medulla oblongata	25.72	25.92	26.44
Cub 2	Cerebellum and cerebrum	20.09	21.58	23.47

*C_t, cycle threshold; H5-PCR, subtype-specific PCR on the H5 gene; M-PCR1, PCR on the matrix gene of influenza A, repetition 1; M-PCR2, PCR on the matrix gene of influenza A, repetition 2

protein 2 (PB2); M644V in polymerase basic protein 1; A336T in nucleoprotein; L22S in neuraminidase protein; and D209N in nonstructural protein (Appendix 1 Figure 1–8). Whether these changes are associated with adaptation of the avian virus to mammal species remains unknown.

These 2 cases of infection with H5N1 clade 2.3.4.4b virus in wild red fox cubs underscore the need to raise awareness that HPAI viruses are not only zoonotic but also infect other mammal species. HPAI infection should be on the list of differential diagnoses for animals that have signs of respiratory or neurologic disease. The detection of virus in the brain suggests systemic infection of the cubs. The clinical signs were largely consistent with those reported in other natural infections of carnivores with HPAI H5 subtypes (*4*–*7*). Whether the fox cubs were infected through the parents or by eating infected bird carcasses is unclear (cubs start eating solid food at 4 weeks of age). Carnivores are known to be at risk for avian influenza virus infection upon ingesting infected birds (*4*,*5*,*8*). We did not test for virus shedding in these cubs, but virus shedding has been observed in experimental infection of 6- to 10-month-old red foxes with HPAI H5N1 clade 2.2 virus (*8*).

The United Kingdom reported infection of a red fox and seals in an animal shelter with a related HPAI H5N8 clade 2.3.4.4b virus (*9*), and Russia reported infection in poultry workers (*10*). These findings suggest that HPAI H5 clade 2.3.4.4b viruses may sporadically transmit from birds to mammals, including humans. Virus evolution and adaptive mutations must be closely monitored to rapidly identify viruses with increased zoonotic potential.

Acknowledgments

We acknowledge the authors and submitting laboratories of the sequences from the GISAID EpiFlu Database (Appendix 2, https://wwwnc.cdc.gov/EID/article/27/11/21-1281-App2.xlsx).

This work was funded by the Dutch Ministry of Agriculture, Nature, and Food Quality (project no. WOT-01-003-012).

About the Author

Dr. Rijks is a postdoctoral researcher at the Dutch Wildlife Health Centre in Utrecht, the Netherlands. Her primary research interests are wildlife diseases and epidemiology.

References

1. Van der Poel WH, Van der Heide R, Verstraten ER, Takumi K, Lina PH, Kramps JA. European bat lyssaviruses, the Netherlands. Emerg Infect Dis. 2005;11:1854–9. https://doi.org/10.3201/eid1112.041200
2. Beerens N, Heutink R, Bergervoet SA, Harders F, Bossers A, Koch G. Multiple reassorted viruses as cause of highly pathogenic avian influenza A(H5N8) virus epidemic, the Netherlands, 2016. Emerg Infect Dis. 2017;23:1974–81. https://doi.org/10.3201/eid2312.171062
3. Beerens N, Heutink R, Pritz-Verschuren S, Germeraad EA, Bergervoet SA, Harders F, et al. Genetic relationship between poultry and wild bird viruses during the highly pathogenic avian influenza H5N6 epidemic in the Netherlands, 2017–2018. Transbound Emerg Dis. 2019;66:1370–8. https://doi.org/10.1111/tbed.13169
4. Marschall J, Hartmann K. Avian influenza A H5N1 infections in cats. J Feline Med Surg. 2008;10:359–65. https://doi.org/10.1016/j.jfms.2008.03.005
5. Songserm T, Amonsin A, Jam-on R, Sae-Heng N, Pariyothorn N, Payungporn S, et al. Fatal avian influenza A H5N1 in a dog. Emerg Infect Dis. 2006;12:1744–7. https://doi.org/10.3201/eid1211.060542
6. Lee K, Lee EK, Lee H, Heo GB, Lee YN, Jung JY, et al. Highly pathogenic avian influenza A(H5N6) in domestic cats, South Korea. Emerg Infect Dis. 2018;24:2343–7. https://doi.org/10.3201/eid2412.180290
7. Hu T, Zhao H, Zhang Y, Zhang W, Kong Q, Zhang Z, et al. Fatal influenza A (H5N1) virus infection in zoo-housed tigers in Yunnan Province, China. Sci Rep. 2016;6:25845. https://doi.org/10.1038/srep25845
8. Reperant LA, van Amerongen G, van de Bildt MW, Rimmelzwaan GF, Dobson AP, Osterhaus AD, et al. Highly pathogenic avian influenza virus (H5N1) infection in red foxes fed infected bird carcasses. Emerg Infect Dis. 2008;14:1835–41. https://doi.org/10.3201/eid1412.080470
9. ProMED. Avian influenza (45): Europe (UK, Croatia) seal, fox, wild bird, HPAI H5N8. ProMED 2021 Mar 17. http://www.promedmail.org, archive no. 20210317.8252821.
10. ProMED. Avian influenza, human (02): Russia, H5N8, first case. ProMED 2021 Feb 21. http://www.promedmail.org, archive no. 20210221.8204014.

Address for correspondence: Jolianne Rijks, Dutch Wildlife Health Centre, Utrecht University, Androclus kamer O.177, Yalelaan 1, 3584CL Utrecht, the Netherlands; email: j.m.rijks@uu.nl

Online Registry of COVID-19–Associated Mucormycosis Cases, India, 2021

Shitij Arora, Vagish S. Hemmige, Charuta Mandke, Mayank Chansoria, Sumit Kumar Rawat, Ameet Dravid, Yatin Sethi, Gaurav Medikeri, Sunit P. Jariwala, Yoram A. Puius, the Mycotic Infections in COVID-19 (MUNCO) Network

Author affiliations: Albert Einstein College of Medicine, Bronx, New York, USA (S. Arora, V.S. Hemmige, S.P. Jariwala, Y.A. Puius); Montefiore Medical Center, Bronx (S. Arora, V.S. Hemmige, S.P. Jariwala, Y.A. Puius); HinduHrudaySamrat Balasaheb Thackarey Medical College and Dr. Rustom Narsi Cooper Municipal General Hospital, Mumbai, India (C. Mandke); Netaji Subhash Chandra Bose Medical College, Jabalpur, India (M. Chansoria); Bundelkhand Medical College, Sagar, India (S.K. Rawat); Noble Hospital, Pune, India (A. Dravid); Ventakateshwar Hospital, Delhi (Y. Sethi); HCG Comprehensive Cancer Care Hospital, Bangalore, India (G. Medikeri)

DOI: https://doi.org/10.3201/eid2711.211322

We established an online registry of coronavirus disease–associated mucormycosis cases in India. We analyzed data from 65 cases diagnosed during April–June 2021, when the Delta variant predominated, and found that patients frequently received antibacterial drugs and zinc supplementation. Online registries rapidly provide relevant data for emerging infections.

Coronavirus disease (COVID-19)–associated mucormycosis (CAM) is an emerging systemic fungal infection caused by *Mucorales* species. Reports of CAM are increasing, especially in India, where 187 cases have been described (*1*). Rapid data collection, which can be accomplished through collaborative online registries, is essential to identifying risk factors for CAM (*2*). We analyzed characteristics of the first 65 cases logged in the Mycotic Infections in COVID-19 (MUNCO) registry in India.

We solicited registry participation through social media and contacts at hospitals in India. The study was approved by the Institutional Review Board of the Albert Einstein College of Medicine (approval no. 2021-13086) and ethics boards of the author-affiliated hospitals, where applicable. Cases were entered into a REDCap database (*3*) (https://www.covidmucor.com). CAM diagnosis was based on the judgment of the physician entering the data and not dependent on microbiological, pathologic, or radiographic findings. We had follow-up data for 53 (81.5%) patients; outcomes were defined as full recovery (no residual disease), incomplete recovery (continued treatment at day 42, interrupted treatment, palatal perforation, stroke, or paralysis), vision loss, or death. Because early treatment with orbital exenteration might prevent disease spread to the central nervous system, we did not consider vision loss to be a marker of incomplete recovery. We analyzed data using R (*4*).

Table. Clinical characteristics of patients in an online registry of coronavirus disease–associated mucormycosis, India, 2021*

Characteristic	No. (%)
Total	65 (100)
Sex	
M	48 (74)
F	17 (26)
Underlying conditions	
Diabetes mellitus	52 (80)
Hypertension	13 (20)
Chronic corticosteroid use	2 (3)
Asthma/COPD	1 (1.5)
Hospitalized†	54 (84)
Intensive care unit‡	15 (28)
Required surgical intervention	26 (40)
Site of infection	
Sinus	60 (92)
Eye	34 (52)
Cerebral	5 (7.7)
Gastrointestinal	5 (7.7)
Skin	1 (1.5)
Pulmonary	0
Treatment	
Steroids	53 (82)
Methylprednisolone	32 (49)
Dexamethasone	18 (28)
Prednisone	5 (8)
Budesonide	6 (9)
Steroids ≥10 d§	28 (61)
Antifungal medication	
Posaconazole	43 (66)
Isavuconazole	3 (5)
Amphotericin B	60 (92)
Liposomal	54 (83)
Deoxycholate	14 (22)
Lipid complex	8 (12)
Antiviral medication	
Remdesivir	31 (48)
Favipravir	18 (28)
Zinc supplementation	36 (55)
Other antimicrobial chemotherapy	
Doxycycline	30 (46)
Azithromycin	25 (38)
Ivermectin	25 (38)
No. vaccine doses	
0	56 (86)
1	7 (11)
2	2 (3)

*Totals might exceed 100% when >1 category applies. COPD, chronic obstructive pulmonary disease.
†Data available for 64 patients.
‡Data available for 54 patients.
§Data available for 46 patients.

The reported infections were diagnosed during April–June 2021. During this time, the B.1.617.2 lineage (Delta variant) of severe acute respiratory syndrome coronavirus 2 (SARS-CoV-2) dominated the samples sequenced by the Indian SARS-CoV-2 Genomics Consortium, constituting 58% of isolates in April, 88% in May, and 86% in June (*5*).

Most patients were male (73.8%), and most patients had diabetes (80.0%) (Table). Only 3.1% had been taking long-term corticosteroids. No patients had HIV, cancer, or history of stem cell or solid organ transplant. Among patients with available data, the median age was 56 years, median weight was 64 kg, and median hemoglobin A1c level was 7.80%. The median time between COVID-19 diagnosis and mucormycosis diagnosis was 20 days; patients had a median hospital stay of 11.0 days (Appendix Table, https://wwwnc.cdc.gov/EID/article/27/11/21-1322-App1.pdf). Only 3.1% of patients were fully vaccinated with Covishield (Oxford/AstraZeneca, https://www.astrazeneca.com) or Covaxin (Bhart Biotech, https://www.bharatbiotech.com) at the time of COVID-19 diagnosis.

COVID-19 was treated primarily with corticosteroids, remdesivir, or both. Favipravir, doxycycline, azithromycin, ivermectin, and zinc were also common treatments (Table). No patients were treated with tocilizumab.

We found that most fungal infections occurred in the sinuses or eyes (Table). Amphotericin B, posaconazole, and surgery were the most common antifungal treatments. Among 53 patients with available follow-up data at 42 days, 17 (32.1%) had an incomplete recovery, 20 (37.8%) had a full recovery, 10 (18.9%) had vision loss, and 6 (11.3%) had died (Figure).

In agreement with previous studies, we found that diabetes and steroid use were major risk factors

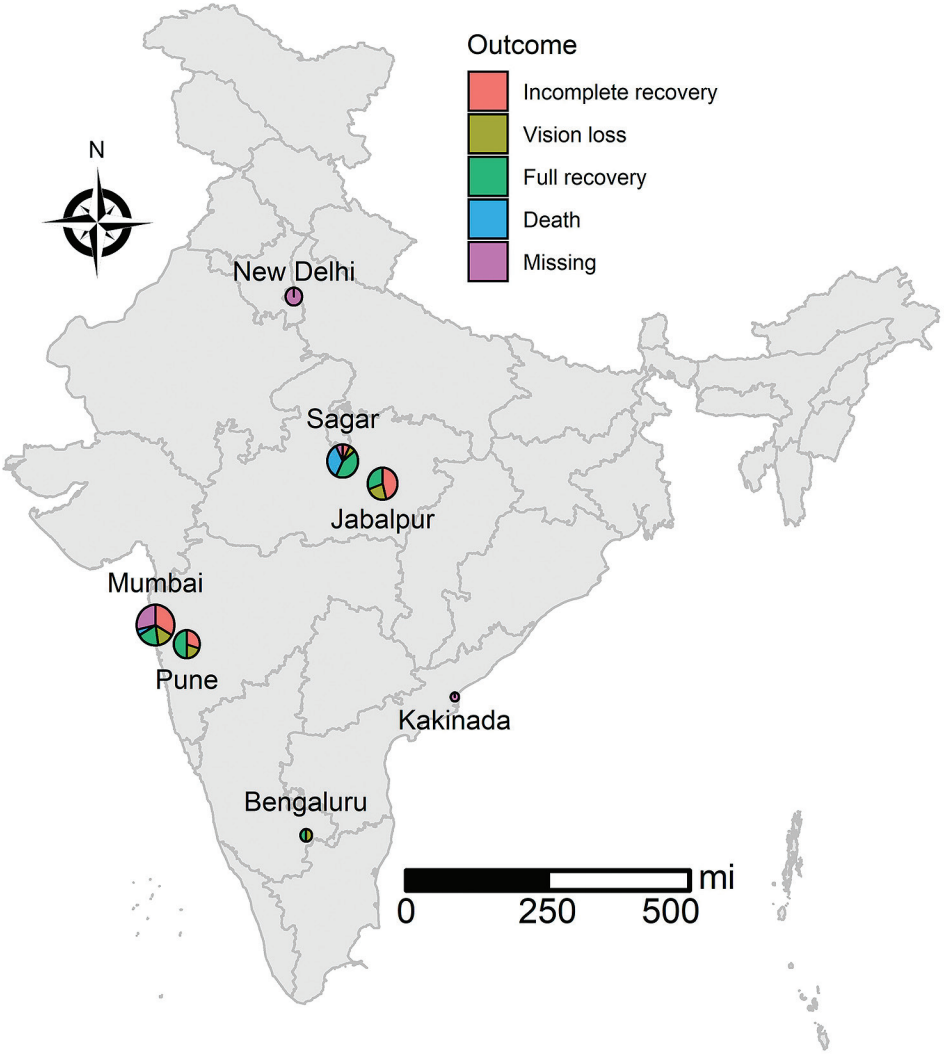

Figure. Geographic distribution of coronavirus disease–associated mucormycosis, India, 2021. Sizes of circles indicates number of cases in that area. Use of the map recognized by the government of India does not endorse the territorial claims of any specific nation.

for CAM (*1*,*6*). We also documented frequent use of antibacterial treatments, a documented risk factor for mucormycosis (*10*), for COVID-19. We found a lower death rate than previously reported (*1*); widespread awareness of CAM might have contributed to increased reporting, earlier diagnosis, and decreased steroid use for treatment of COVID-19. In total, 57% of patients received zinc supplementation, possibly because pathogenic fungi sequester zinc from host tissues. Zinc chelators inhibit the growth of some virulent fungi (*7*,*8*) and enhance the efficacy of antifungal agents against some *Mucorales* strains in vitro (*9*).

This proof-of-concept study shows that rapid, real-time data collection using online registries of CAM cases can provide clinical insights into the disease (*2*). For example, data on these 65 cases were collected in 5 days, enabled by rapid data entry and ease of use. MUNCO is especially useful for physicians in settings where electronic medical records are rarely used and patient follow-up is suboptimal. The major weakness of MUNCO is that pragmatic case definitions are based on the opinions of the clinician entering the data. This study also did not have a control group of non–COVID-19–associated mucormycosis cases, which would enable detection of specific risk factors. By August 2021, we had collected data on 693 cases, which we will soon analyze for additional risk factors associated with poor outcomes. In summary, our results show that online registries are a valuable tool to rapidly provide relevant data for real-time surveillance of emerging infections.

Access to REDCap was paid for by the Einstein-Montefiore Institute for Clinical & Translational Research under grant no. UL1TR002556-06 to S.J.

V.S.H. receives support for unrelated work from Merck Sharp & Dohme Corp., which manufactures antifungal medications.

About the Author

Dr. Arora is an academic hospitalist at Montefiore Medical Center, Bronx, NY, USA. His research interests include coronavirus disease management and outcomes.

References

1. Patel A, Agarwal R, Rudramurthy SM, Shevkani M, Xess I, Sharma R, et al.; MucoCovi Network3. Multicenter epidemiologic study of coronavirus disease–associated mucormycosis, India. Emerg Infect Dis. 2021 Jun 4 [Epub ahead of print].
2. Arora S, Mandke C. Coronavirus disease–associated mucormycosis warrants timely collaborative registers. 2021 Jul 2 [cited 2021 Jul 17]. https://blogs.bmj.com/bmj/2021/07/02/coronavirus-disease-associated-mucormycosis-warrants-timely-collaborative-registers/
3. Harris PA, Taylor R, Thielke R, Payne J, Gonzalez N, Conde JG. Research electronic data capture (REDCap)—a metadata-driven methodology and workflow process for providing translational research informatics support. J Biomed Inform. 2009;42:377–81. https://doi.org/10.1016/j.jbi.2008.08.010
4. R Core Team. A language and environment for statistical computing. R Foundation for Statistical Computing. 2020 [cited 2021 Jun 5]. https://www.R-project.org
5. Council of Scientific and Industrial Research Institute of Genomics and Integrative Biology. Indian COVID-19 genome surveillance. 2021 [cited 2021 Jul 31]. http://clingen.igib.res.in/covid19genomes
6. Sen M, Honavar SG, Bansal R, Sengupta S, Rao R, Kim U, et al.; the Collaborative OPAI-IJO Study on Mucormycosis in COVID-19 (COSMIC) Study Group. Epidemiology, clinical profile, management, and outcome of COVID-19–associated rhino-orbital-cerebral mucormycosis in 2,826 patients in India—Collaborative OPAI-IJO Study on Mucormycosis in COVID-19 (COSMIC), Report 1. Indian J Ophthalmol. 2021;69:1670–92. https://doi.org/10.4103/ijo.IJO_1565_21
7. Laskaris P, Atrouni A, Calera JA, d'Enfert C, Munier-Lehmann H, Cavaillon JM, et al. Administration of zinc chelators improves survival of mice infected with *Aspergillus fumigatus* both in monotherapy and in combination with caspofungin. Antimicrob Agents Chemother. 2016;60:5631–9. https://doi.org/10.1128/AAC.00324-16
8. Staats CC, Kmetzsch L, Schrank A, Vainstein MH. Fungal zinc metabolism and its connections to virulence. Front Cell Infect Microbiol. 2013;3:65. https://doi.org/10.3389/fcimb.2013.00065
9. Leonardelli F, Macedo D, Dudiuk C, Theill L, Cabeza MS, Gamarra S, et al. *In vitro* activity of combinations of zinc chelators with amphotericin B and posaconazole against six *Mucorales* species. Antimicrob Agents Chemother. 2019;63:e00266–19. https://doi.org/10.1128/AAC.00266-19
10. Kaur H, Ghosh A, Rudramurthy SM, Chakrabarti A. Gastrointestinal mucormycosis in apparently immunocompetent hosts—a review. Mycoses. 2018;61:898–908. https://doi.org/10.1111/myc.12798

Address for correspondence: Shitij Arora, Department of Internal Medicine, Montefiore Medical Center, 111 E 210th St, Bronx, NY 10467, USA; email: sharora@montefiore.org; Yoram A. Puius, Division of Infectious Diseases, Montefiore Medical Center, 111 E 210th St, Bronx, NY 10467, USA; email: ypuius@montefiore.org

Spontaneous Bacterial Peritonitis Caused by *Bordetella hinzii*

Grace C. Wang,[1] Miranda J. Wallace,[1] Gayathri Krishnan, Patrick D. Olson, Abigail L. Carlson,[2] Gautam Dantas,[3] James M. Fleckenstein[3]

Author affiliations: Saint Louis University School of Medicine, St. Louis, Missouri, USA (G.C. Wang); Washington University School of Medicine, St. Louis (M.J. Wallace, G. Krishnan, P.D. Olson, A.L. Carlson, G. Dantas, J.M. Fleckenstein); St. Louis Veterans Affairs Health Care System, St. Louis (A.L. Carlson, J.M. Fleckenstein)

DOI: https://doi.org/10.3201/eid2711.211428

Although *Bordetella hinzii* coccobacilli is most commonly identified in respiratory tracts of birds and rodents, this organism has occasionally been isolated in human infections. We describe a case of *B. hinzii* spontaneous bacterial peritonitis in Missouri, USA. Whole-genome sequencing of blood and peritoneal fluid isolates confirmed *B. hinzii* infection.

Bordetella hinzii is a gram-negative aerobic coccobacilli respiratory pathogen in poultry (*1*) and rodents (*2*). Human infections are rare but occur in immunocompromised persons (*3*) or upon exposure to infected animals. Most reported human infections are pulmonary; however, other manifestations include cholangitis (*4*) and periaortic abscess (*5*). We report a case of *B. hinzii* spontaneous bacterial peritonitis (SBP) complicated by bacteremia.

A 71-year-old man with alcoholism, hepatitis C, and decompensated cirrhosis, on day 28 of a 28-day regimen of intravenous vancomycin for *Streptococcus salivarius* bacteremia and SBP, underwent outpatient paracentesis. After paracentesis (7.8 L of fluid removed), the patient experienced hypotension and orthostasis, which resolved after intravenous albumin, and returned home. He later sought care at an emergency department for weakness, abdominal pain, hypotension (68/42 mm Hg), and tachycardia (heart rate 130 beats/min).

Despite intravenous fluid and albumin (1.5 g/kg) resuscitation, daptomycin, and piperacillin/azobactam, the patient experienced septic shock and hepatorenal syndrome, necessitating pressors. We substituted meropenem for piperacillin/tazobactam. On day 3, we discontinued daptomycin; administered albumin (1 g/kg); and initiated octreotide, midodrine, and rifaximin. We discontinued pressors on day 4. The patient improved clinically and his SBP resolved, as indicated by results of serial peritoneal fluid studies. On day 12, we replaced meropenem with ertapenem. After discharge (day 15), the patient completed 2 weeks of ertapenem, followed by daily trimethoprim/sulfamethoxazole prophylaxis.

Further investigation revealed the patient had a dog with cough and a cat with gastroenteritis, and neither pet was receiving veterinary care. His wife maintained several birdfeeders, but she had no symptoms. Five months after seeking care, the patient died after cardiac arrest and transjugular intrahepatic portosystemic shunt occlusion.

Initial ascites fluid studies revealed 1,673 leukocytes with 80% segmented neutrophils. Peritoneal fluid and blood cultures from day 1 of hospitalization had tiny oxidase-positive, indole-negative, gram-negative rods that grew on blood and chocolate agars but not MacConkey or CNA agars. After tentatively identifying the organism as a *Bordetella* species, we performed limited antimicrobial susceptibility testing for levofloxacin (1.5 μg/mL), ertapenem (0.19 μg/mL), meropenem (sensitive), and trimethoprim/sulfamethoxazole (0.004 μg/mL). The Missouri State Public Health Laboratory (Jefferson City, MO, USA) later confirmed identification as *B. hinzii* by using matrix-assisted laser desorption/ionization time-of-flight mass spectrometry.

Blood and peritoneal fluid isolates underwent whole-genome sequencing (WGS) to confirm identification. We suspended isolate plate scrapes in Luria–Bertani broth with 15% glycerol and stored them at –80°C. After thawing 250–500 μL of each suspension, we extracted genomic DNA by using the QIAamp BiOstic Bacteremia DNA Kit (QIAGEN, https://www.qiagen.com). We used 0.5 ng of genomic DNA to prepare sequencing libraries with the Nextera XT DNA Library Preparation Kit (Illumina, https://www.illumina.com). We pooled and sequenced libraries on the NovaSeq 6000 platform (Illumina) to obtain ≈5 million 2 × 150 bp reads. We used Trimmomatic 38.0 (https://github.com/timflutre/trimmomatic) to demultiplex the reads

[1]These first authors contributed equally to this article.

[2]Current affiliation: Centers for Disease Control and Prevention, Atlanta, Georgia, USA.

[3]These authors contributed equally to this article as co–principal investigators.

and remove adaptors. We removed contaminating reads by using Deconseq4.3 (http://deconseq.sourceforge.net) and repaired disordered reads by using BBTools Repair (BBTools 38.26; https://jgi.doe.gov/data-and-tools/bbtools). We assembled de novo genomes by using the Unicycler 0.4.7 Illumina-only assembly process and then annotated by using Prokka 1.14.5 (https://github.com/tseemann/prokka). We determined assembly quality by using QUAST 4.5 (http://quast.sourceforge.net) and checkM 1.0.13 (https://github.com/Ecogenomics/CheckM).

We performed pairwise average nucleotide identity between the isolates and deposited *Bordetella* genomes by using pyani (https://github.com/widdowquinn/pyani). We performed core-genome alignments by using roary 3.12.0 (https://sanger-pathogens.github.io/Roary) and then generated approximate maximum-likelihood trees on the basis of the roary alignment file by using FastTree 2.1.7 (http://www.microbesonline.org/fasttree). We identified single-nucleotide polymorphisms (SNPs) by using Snippy 4.4.3 (https://anaconda.org/bioconda/snippy/files) and antimicrobial-resistance genes by using AMRFinder 3.8.4 (https://github.com/ncbi/amr). We deposited raw sequence data and genomic assemblies to the National

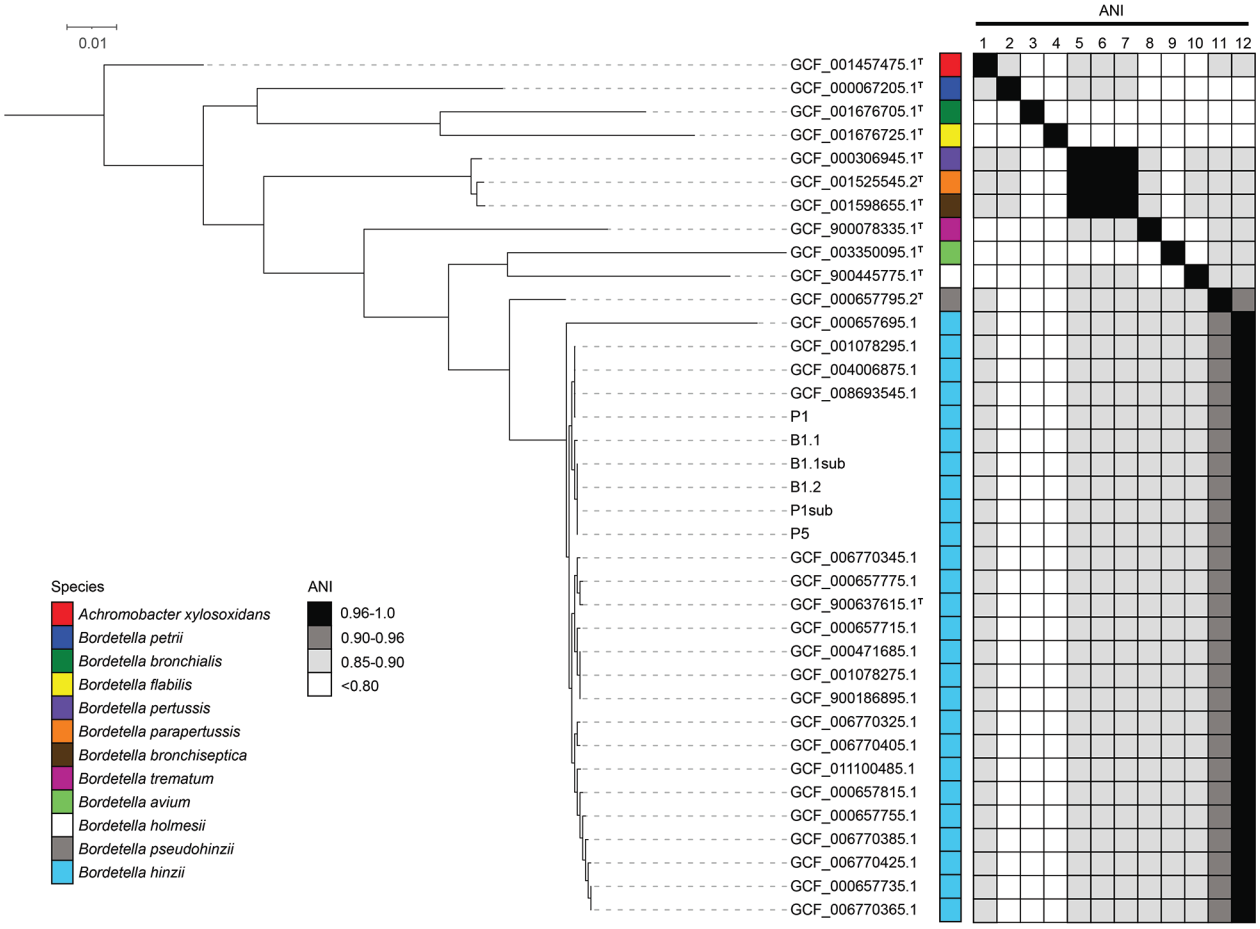

Figure. Comparative genomic analyses of *Bordetella hinzii* isolates from a patient in Missouri, USA, with type and nontype *Bordetella* assemblies. After core-genome alignment (58 total core genes), a neighbor-joining phylogenetic tree rooted with *Achromobacter xylosoxidans* as the outgroup demonstrates the isolates from this study cluster with other previously deposited *B. hinzii* genomes. Pairwise ANI was performed against type assemblies. The isolates in this study meet the ANI threshold (≥0.96%) for species-level identity with *B. hinzii* type assembly GCF_900637615.1 (*7*). Isolates were recovered from peritoneal fluid cultures collected at day 1 and day 5 (P1 and P5, respectively; P2sub is a subculture of P1). Blood isolates were recovered from blood cultures collected on day 1 (B1.1 and B1.2; B1.1sub is a subculture of B1.1). As previously observed (*8*), the type genomes for *B. pertussis*, *B. parapertussis*, and *B. bronchiseptica* represent an instance of previously established, distinct species that exceed the species-level ANI threshold relative to each other. [T] indicates assemblies generated from type material. Type assemblies are numbered 1–12 on vertical axes as follows: 1, GCF_001457475.1; 2, GCF_000067205.1; 3, GCF_001676705.1; 4, GCF_001676725.1; 5, GCF_000306945.1; 6, GCF_001525545.2; 7, GCF_001598655.1; 8, GCF_900078335.1; 9, GCF_003350095.1; 10, GCF_900445775.1; 11, GCF_000657795.2; 12, GCF_900637615.1. ANI, average nucleotide identity.

Center for Biotechnology Information (BioProject no. PRJNA706405).

We performed Illumina short-read WGS on 6 putative *B. hinzii* isolates recovered from peritoneal fluid and blood cultures from day 1 and a peritoneal fluid culture from paracentesis on day 5. Altogether, the isolate assemblies had an average length of 4.8 Mbp (range 4.70–4.84 Mbp) and GC content of ≈67.2%, reflective of published *B. hinzii* genomes (*6*). We built a neighbor-joining phylogenetic tree by using a core-genome alignment of the isolates with publicly available *Bordetella* genomes. The isolates formed a clade with *B. hinzii* genomes, including a type that was distinct from other *Bordetella* species. Pairwise average nucleotide identity analysis showed the isolates meet the species-level threshold (≥96%) (*7*) exclusively with genomes originating from *B. hinzii* (Figure). SNP analyses within the 6 isolates suggested they were clonal because ≤2 SNPs (all nonsynonymous) were found between each strain pair, further confirming the clinical laboratory indications that the isolates are *B. hinzii* and that organisms recovered from peritoneal sites and blood originated from the same source. In addition, we identified a putative novel β-lactamase gene with 51% identity to the class-A LRA-1 β-lactamase (Comprehensive Antibiotic Resistance Database [https://card.mcmaster.ca/home]; accession no. ARO:3002482). This gene is likely endogenous because it appeared in all available *B. hinzii* assemblies.

In summary, WGS of blood and peritoneal fluid isolates confirmed a set of clonal *B. hinzii* isolates from both tissue types from this patient. Our findings provide compelling evidence for serious human infection caused by this organism.

Acknowledgments

We thank Paul Weiland, Mary Ann Smith, and Joan Lorenz; Kimberley V. Sukhum for thoughtful review of this manuscript; and the staff of the Genome Technology Access Center at the McDonnell Genome Institute for their sequencing services.

This work was supported in part by awards to G.D. through the National Institute of Allergy and Infectious Diseases of the National Institutes of Health (grant no. U01AI123394), the Agency for Healthcare Research and Quality (grant no. R01HS027621), and the Congressionally Directed Medical Research Program of the US Department of Defense (grant no. W81XWH1810225). This work also was supported by a T32 fellowship award granted to M.J.W. through the National Cancer Institute of the National Institutes of Health (award no. T32 CA113275-12).

About the Author

Dr. Wang is a resident physician in the Department of Internal Medicine at Saint Louis University School of Medicine. She is interested in both the clinical and translational research aspects of pulmonology and critical care medicine, as well as drug discovery and mechanisms of disease.

References

1. Register KB, Kunkle RA. Strain-specific virulence of *Bordetella hinzii* in poultry. Avian Dis. 2009;53:50–4. https://doi.org/10.1637/8388-070108-Reg.1
2. Jiyipong T, Morand S, Jittapalapong S, Raoult D, Rolain JM. *Bordetella hinzii* in rodents, Southeast Asia. Emerg Infect Dis. 2013;19:502–3. https://doi.org/10.3201/eid1903.120987
3. Cookson BT, Vandamme P, Carlson LC, Larson AM, Sheffield JV, Kersters K, et al. Bacteremia caused by a novel *Bordetella* species, "*B. hinzii*". J Clin Microbiol. 1994;32:2569–71. https://doi.org/10.1128/jcm.32.10.2569-2571.1994
4. Arvand M, Feldhues R, Mieth M, Kraus T, Vandamme P. Chronic cholangitis caused by *Bordetella hinzii* in a liver transplant recipient. J Clin Microbiol. 2004;42:2335–7. https://doi.org/10.1128/JCM.42.5.2335-2337.2004
5. González MM, Romano MPC, de Guzmán García Monge MT, Martín BB, García AS. *Bordetella hinzii* endocarditis, a clinical case not previously described. Eur J Case Rep Intern Med. 2019;6:000994.
6. Weigand MR, Changayil S, Kulasekarapandian Y, Tondella ML. Complete genome sequences of two *Bordetella hinzii* strains isolated from humans. Genome Announc. 2015;3:1–2. https://doi.org/10.1128/genomeA.00965-15
7. Richter M, Rosselló-Móra R. Shifting the genomic gold standard for the prokaryotic species definition. Proc Natl Acad Sci U S A. 2009;106:19126–31. https://doi.org/10.1073/pnas.0906412106
8. Kim M, Oh HS, Park SC, Chun J. Towards a taxonomic coherence between average nucleotide identity and 16S rRNA gene sequence similarity for species demarcation of prokaryotes. Int J Syst Evol Microbiol. 2014;64:346–51. https://doi.org/10.1099/ijs.0.059774-0

Address for correspondence: James M. Fleckenstein, Division of Infectious Diseases, Washington University School of Medicine, 660 S Euclid Ave, Campus Box 8051, St. Louis, MO 63110, USA; email: jfleckenstein@wustl.edu

Resurgence of Respiratory Syncytial Virus Infections during COVID-19 Pandemic, Tokyo, Japan

Mugen Ujiie, Shinya Tsuzuki, Takato Nakamoto, Noriko Iwamoto

Author affiliation: National Center for Global Health and Medicine, Tokyo, Japan

DOI: https://doi.org/10.3201/eid2711.211565

More than a year into the coronavirus-19 pandemic, intensified infection control measures have controlled most viral respiratory infections in Tokyo, Japan. As of July 2021, however, an unusually high number of respiratory syncytial virus infections were reported in Tokyo. This resurgence may have resulted from restarting social activities for children.

The World Health Organization (WHO) declared the novel coronavirus disease (COVID-19) a global pandemic on March 11, 2020 (1). Since then, social activities have been restricted worldwide, and infection control measures including handwashing, mask-wearing, and keeping social distance have been strengthened. These measures reduced the prevalence of respiratory virus infections other than COVID-19, such as influenza, in 2020, and reported case numbers have sharply declined (2). However, the increased burden on healthcare institutions during the COVID-19 pandemic is of concern; it has and will hinder access to healthcare and the promotion of immunization programs, and the reduced number of infected or immunized persons will lead to an overall increase in susceptibility in society, leading in turn to ever-larger epidemics of infectious diseases after the resumption of social activities (3). We report a possible example: an unusual increase in reported cases of respiratory syncytial virus (RSV) infection in Tokyo, Japan.

We compared weekly RSV activity in the 2021 season with activity in 4 previous seasons using data from 2017–2020 from the Tokyo Metropolitan Infectious Disease Surveillance Center (Appendix Table, https://wwwnc.cdc.gov/EID/article/27/11/21-1565-App1.xlsx). The center gathers the number of pediatrician-diagnosed weekly cases of RSV infection on the basis of clinical symptoms and laboratory findings from ≈260 sentinel centers, including hospitals and clinics (4). The most recent information is from epidemiological week 28 of 2021 (July 12–18).

No outbreaks of RSV were reported in 2020, although the previous 3 years had outbreaks in summer and autumn. However, the largest annual increase in cases since monitoring began in 2003 was reported for 2021 (Figure). The cumulative number of cases through week 28 of 2021 was 10,327, rising from a total of 570 in 2020. Whether this upward trend will continue in the latter half of 2021 is unclear as of August, but we expect the peak to be higher than in any year since 2003 and for its timing to be different.

Most children are infected with RSV ≥1 time before age 2. The statistically significant decrease in all cases reported during this epidemic compared with previous epidemics was particularly notable in children ≥2 years of age; by χ^2 testing, they accounted for a significantly lower proportion of cases in 2021 than in the other years ($p<0.001$ for 2017, 2018, 2019, and 2020; p values corrected by the Holm method). This finding suggests that an accumulation of susceptible persons during the pandemic may have contributed to this year's large outbreak. This trend has also been observed nationwide in Japan. In particular, the percentage of children 0–11 months of age with RSV has fallen significantly, from 32%–37% in 2018–2020 to 17% in 2021 (5,6).

The government of Japan has taken active measures to control the spread of COVID-19, including restricting children's group activities. The government requested temporary closure of schools beginning March 2, 2020. According to the Ministry of Education, Culture, Sports, Science and Technology, 86% of schools closed for >10 weeks; 98% reopened at least partially within 14 weeks. School closures

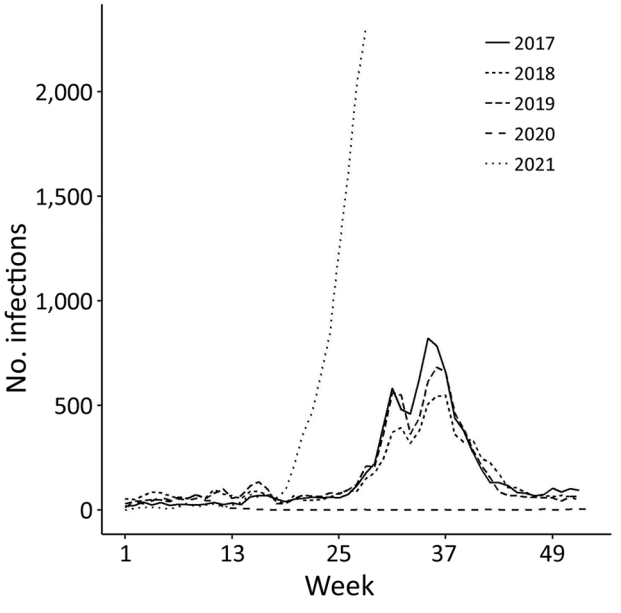

Figure. Respiratory syncytial virus infections in children, by year and epidemiological week, Tokyo, Japan, January 2017–July 2021 (as of epidemiological week 28, 2021).

have been reported to reduce RSV epidemics, and data from Japan, which did not have an epidemic in 2020, supports this hypothesis (7). The importance of school life to society and children was subsequently reevaluated, however, and as a result many children now attend school.

As of July 13, 2021, >25 million (21.9%) eligible persons ≥12 years of age in Japan had completed 2 doses of COVID-19 vaccination (8). As a consequence of vaccination, socioeconomic activity and movement have increased, and children have spent more time in schools and kindergartens than they did previously; therefore, the overall risk for infectious diseases in infants and young children is expected to increase. The increased use of schools and nurseries may also result in more aggressive diagnostic testing for alternative infections, including RSV, to rule out COVID-19, as part of the measures to prevent the spread of COVID-19 infection in patients with fever and respiratory symptoms.

The emergence of RSV epidemics after the COVID-19 pandemic, appearing in different seasons and on a different scale to previous trends, has been observed in other regions, including the Americas and Australia (9,10), and the Tokyo epidemic is therefore not unique. Nevertheless, various local factors such as nonpharmaceutical interventions, travel restrictions, viral competition, and school and nursery closures are likely to have played a role. It remains to be seen whether a similar trend will be observed with other respiratory viral infections such as influenza. New epidemics may increase the already high medical burden and cause further delays in diagnosis amid the continuing pandemic.

In summary, we report a substantial outbreak of RSV infection in Tokyo starting in spring 2021. An adequate response to this increase in patient numbers will include ongoing public infection control, restoring appropriate healthcare measures, and appropriate monitoring of the ongoing RSV epidemic.

About the Author

Dr. Ujiie is the director of the Immunization Support Centre at the National Center for Global Health and Medicine. His research expertise is in immunization, tropical infectious diseases, and travel medicine.

References

1. WHO Director-General's opening remarks at the media briefing on COVID-19—11 March 2020 [cited 2021 Jul 28]. https://www.who.int/director-general/speeches/detail/who-director-general-s-opening-remarks-at-the-media-briefing-on-covid-19—11-march-2020
2. Karlsson EA, Mook PAN, Vandemaele K, Fitzner J, Hammond A, Cozza V, et al. World Health Organization. Review of global influenza circulation, late 2019 to 2020, and the impact of the COVID-19 pandemic on influenza circulation. Wkly Epidemiol Rec. 2021;96:241–64.
3. Mulholland K, Kretsinger K, Wondwossen L, Crowcroft N. Action needed now to prevent further increases in measles and measles deaths in the coming years. Lancet. 2020;396:1782–4. https://doi.org/10.1016/S0140-6736(20)32394-1
4. Tokyo Metropolitan Infectious Disease Surveillance Center. Sentinel disease weekly reports by age [in Japanese]. 2021 [cited 2021 Jul 15]. https://survey.tokyo-eiken.go.jp/epidinfo/weeklyage.do
5. Ministry of Health, Labour, and Welfare of Japan and National Institution of Infectious Disease. Infectious diseases weekly report, July 5 to 11, 2021, as of July 16, 2021 [cited 2021 Jul 28]. https://www.niid.go.jp/niid/ja/diseases/ka/corona-virus/2019-ncov/2487-idsc/idwr-topic/10544-idwrc-2127c.html
6. National Institution of Infectious Disease. RSV infection cases reported per sentinel weekly, as of July 27, 2021 [cited 2021 Jul 28]. https://www.niid.go.jp/niid/ja/10/2096-weeklygraph/1661-21rsv.html
7. van Summeren J, Meijer A, Aspelund G, Casalegno JS, Erna G, Hoang U, et al.; VRS study group in Lyon. Low levels of respiratory syncytial virus activity in Europe during the 2020–21 season: what can we expect in the coming summer and autumn/winter? Euro Surveill. 2021;26:2100639. https://doi.org/10.2807/1560-7917.ES.2021.26.29.2100639
8. Prime Minister's Office of Japan. Information on the COVID-19 vaccination, as of July 13, 2021 [cited 2021 Jul 15]. https://www.kantei.go.jp/jp/headline/kansensho/vaccine.html
9. Pan American Health Organization. Regional update, influenza. Epidemiological week 25—July 6, 2021 [cited 2021 Jul 28]. https://www.paho.org/en/documents/regional-update-influenza-epidemiological-week-25-july-6-2021
10. Government of Western Australia. Paediatric respiratory pathogen report. Week 24, 14th June 2021–20th June 2021 [cited 2021 Jul 28]. https://ww2.health.wa.gov.au/~/media/Corp/Documents/Health-for/Infectious-disease/Paediatric-Respiratory-Pathogen-Weekly-Report/2021/Paediatric-Respiratory-Pathogen-Report-Week-24-2021.pdf

Address for correspondence: Mugen Ujiie, Vaccination Support Center, Disease Control and Prevention Center, National Center for Global Health and Medicine, 1-21-1 Toyama, Shinjuku, Tokyo 162-8655, Japan; email: mgujiie@hosp.ncgm.go.jp

Tracing the Origin, Spread, and Molecular Evolution of Zika Virus in Puerto Rico, 2016–2017

Gilberto A. Santiago,[1] Chaney C. Kalinich,[1] Fabiola Cruz-López, Glenda L. González, Betzabel Flores, Aaron Hentoff, Keyla N. Charriez, Joseph R. Fauver, Laura E. Adams, Tyler M. Sharp, Allison Black, Trevor Bedford, Esther Ellis, Brett Ellis, Steve H. Waterman, Gabriela Paz-Bailey, Nathan D. Grubaugh,[2] Jorge L. Muñoz-Jordán[2]

Author affiliations: Centers for Disease Control and Prevention, San Juan, Puerto Rico, USA (G.A. Santiago, F. Cruz-López, G.L. González, B. Flores, K.N. Charriez, L.E. Adams, T.M. Sharp, G. Paz-Bailey, J.L. Muñoz-Jordán); Yale School of Public Health, New Haven, Connecticut, USA (C.C. Kalinich, A. Hentoff, J.R. Fauver, N.D. Grubaugh); US Public Health Service, Rockville, Maryland, USA (L.E. Adams, T.M. Sharp); Fred Hutchinson Cancer Research Center, Seattle, Washington, USA (A. Black, T. Bedford); US Virgin Islands Department of Health, Charlotte Amalie, St. Thomas, Virgin Islands, USA (E. Ellis, B. Ellis)

DOI: https://doi.org/10.3201/eid2711.211575

We reconstructed the 2016–2017 Zika virus epidemic in Puerto Rico by using complete genomes to uncover the epidemic's origin, spread, and evolutionary dynamics. Our study revealed that the epidemic was propelled by multiple introductions that spread across the island, intricate evolutionary patterns, and ≈10 months of cryptic transmission.

Puerto Rico reported the first confirmed case of Zika virus (ZIKV) disease in November 2015 and subsequently experienced epidemic transmission that peaked by mid-August 2016 (*1*). Despite the large number of confirmed cases detected by traditional surveillance, the origin, spread, and evolutionary dynamics of this epidemic remain undetermined. We sought to reconstruct the epidemic transmission period by using a genomic epidemiology approach and determine evolution of the virus in the island.

To investigate the emergence and subsequent epidemic of ZIKV in Puerto Rico, we generated 83 complete genomes (*2*,*3*) directly from PCR-positive serum samples (*4*) (Appendix, https://wwwnc.cdc.gov/EID/article/27/11/21-1575-App1.pdf) collected from the 8 health regions of Puerto Rico during March 2016–January 2017, congruent to a geotemporal representation of the epidemic in the island. We then performed phylogenetic analysis with an additional 233 published genomes from GenBank that represent the emergence and spread of ZIKV in the Americas during 2015–2017. The resulting reconstructed phylogeny was consistent with published tree topologies, nucleotide substitution rate ranges, and divergence patterns observed elsewhere for the entirety of the Americas (Appendix Figure 1, panel A), providing a pragmatic context to the proposed model of spread and divergence of ZIKV in Puerto Rico (*5*). At least 8 separate foreign-introduction events were captured within the ancestry of the viruses sequenced, including 2 that expanded into autochthonous lineages and 6 separate introduction events represented by individual sequences associated with genomes from the United States, the Caribbean, South America, and Central America, thus suggesting limited spread.

In addition, we analyzed the temporal molecular evolutionary signal in our dataset by reconstructing time-calibrated phylogenies by using genomes annotated with date of sample collection based on year, month, and days for temporal precision. The correlation between date of sample collection and root-to-tip genetic distance supported the heterochronous nature of our dataset. The estimated divergence from the root (i.e., time of most recent common ancestor [tMRCA] of this tree) occurred in February 2013 (because 2013–2014 ZIKV genomes from French Polynesia were used as the root), and the within-epidemic evolutionary rate was 1.09×10^{-3} substitutions/site/year (Appendix Figure 1, panel B).

Bayesian reconstruction of Puerto Rico clade 1 (PR C1) presents the largest autochthonous monophyletic cluster that originated from viruses from South America and the Caribbean, including Brazil, Suriname, French Guyana, the US Virgin Islands, and Dominican Republic (Figure). tMRCA estimates place the divergence of PR C1 in mid-June 2015 (95% highest posterior density [HPD] February 2015–October 2015) and a within-outbreak evolutionary rate of 1.61×10^{-3} (95% HPD $1.13–2.10 \times 10^{-3}$) substitutions/site/year. In addition, PR C1 was observed to diverge further into 2 subclades (SC1 and SC2) spreading across the island. The second clade, Puerto Rico clade 2 (PR C2), presents a smaller autochthonous monophyletic cluster that originated from viruses in Central America, including Nicaragua and Honduras (Figure). Our tMRCA estimates placed the emergence of PR C2 in February 2016 (95% HPD October 2015–April 2016) and its evolutionary rate was similar to PR C1 at 1.87×10^{-3}

[1]These first authors contributed equally to this article.

[2]These senior authors contributed equally to this article.

(95% HPD 1.1–2.64 × 10^{-3}). We compared the ZIKV epidemic history of Puerto Rico to the time-calibrated Bayesian phylogenies and observed that the tMRCA of PR C1 precedes the initial confirmation of ZIKV in the island through traditional surveillance methods by 3–10 months and that expansion of all PR lineages coincides with the peak of the epidemic curve (Figure). We assessed phylogenetic clustering patterns for geographic association with each of the health regions and detected none (Appendix Figure 2).

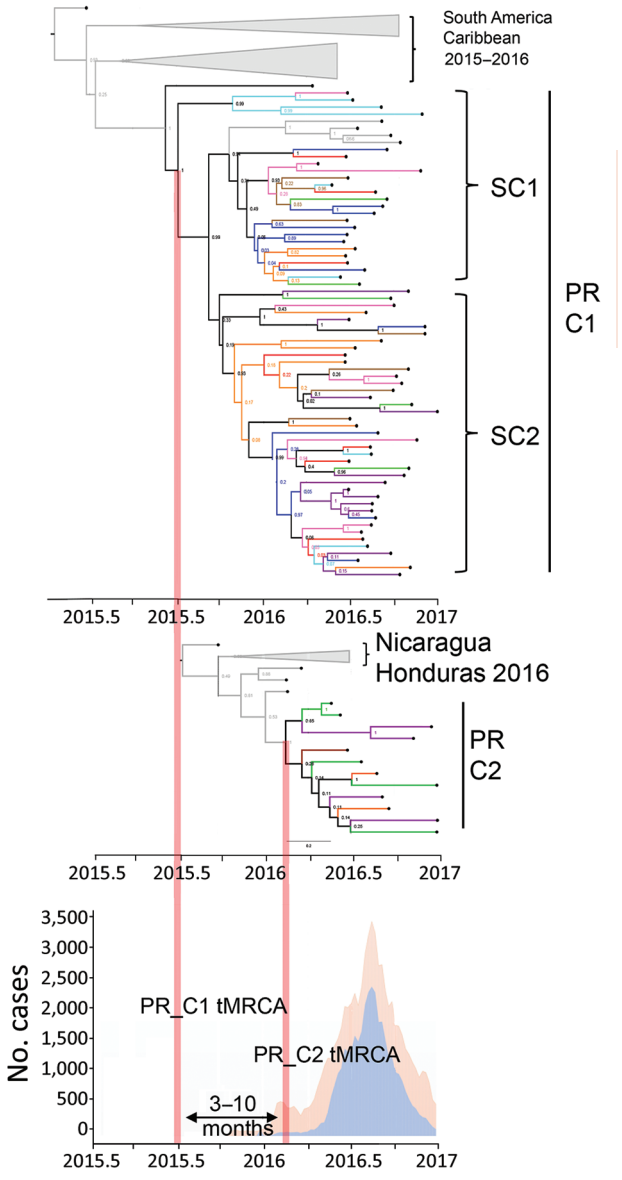

Figure. Intra-island spread and divergence of Zika virus, Puerto Rico, 2016–2017. Bayesian phylogenetic reconstruction using maximum clade credibility trees shows genomes grouping with 2 separate clusters. PR C1 is associated with genomes from South America and the Caribbean (top); this clade diverged into SC1 and SC2. PR C2 is associated with genomes from Central America (center). Epidemic curve of total Zika cases per week (orange shade) and cases confirmed by reverse transcription PCR per week (blue shade) during 2015–2017 (bottom). All external branches representing Puerto Rico genomes are color-coded according to the 8 health regions of Puerto Rico: region 1, red; region 2, blue; region 3, orange; region 4, green; region 5, purple; region 6, cyan; region 7, brown; and region 8, magenta. C, clade; PR, Puerto Rico; SC, subclade; tMRCA, time of most recent common ancestor.

We inferred past viral population dynamics by using Bayesian Skygrid plots, which show an increase in genomic diversity that coincides in time with the emergence of ZIKV in the Americas, followed by a series of fluctuations in the effective population size, characteristic of the virus spreading rapidly through the region (Appendix Figure 3). In Puerto Rico, we observed a similar sharp increase upon emergence and subsequent patterns that mirror the trends observed in the Americas.

Our study revealed the origin and epidemic spread of ZIKV in the island after a period of cryptic transmission undetected by traditional surveillance. Similar cryptic transmission was reported in Brazil and Colombia (*6*–*8*), where case detection was hindered by the difficulty to capture asymptomatic or mild cases with clinical manifestations that overlap endemic arboviruses and other laboratory testing limitations particular to ZIKV (*9*). The dataset we generated in our study presents a relevant contribution to the geotemporal sampling of ZIKV genomes from the region, enabling the study the evolutionary and epidemic dynamics in the Americas.

The integration of genomic epidemiology to arbovirus surveillance has proven to be central to the ascertainment of disease epidemiology, uncovering information otherwise concealed by the nature of the disease and limitations of surveillance systems. Fundamentally, integrated proactive genomic surveillance may help us to predict virus emergence and mitigate more effectively their regional or global expansion.

Acknowledgments

We thank the collaborators from the Ponce Medical School Foundation, Inc. (grant no. U01CK000580), the Puerto Rico Health Department, and members of the Puerto Rico Zika Task Force for the valuable contributions to the enhanced surveillance during the Zika outbreak in 2016.

This project was partially funded by the Centers for Disease Control and Prevention's Advanced Molecular Detection Program and the Yale University's School of Public Health start-up package provided to N.D.G. Additional support for coauthors C.K. and A.H. was provided by the Yale University's Jackson Institute of Global Health Field Experience Award and the Yale Collaborative Action Fellowship.

About the Author

Dr. Santiago is a lead research microbiologist at the Centers for Disease Control and Prevention in San Juan, Puerto Rico. His research is focused on the development of molecular diagnostic tests and genomic epidemiology of dengue virus and severe acute respiratory syndrome coronavirus 2.

References

1. Sharp TM, Quandelacy TM, Adams LE, Aponte JT, Lozier MJ, Ryff K, et al. Epidemiologic and spatiotemporal trends of Zika virus disease during the 2016 epidemic in Puerto Rico. PLoS Negl Trop Dis. 2020;14:e0008532. https://doi.org/10.1371/journal.pntd.0008532
2. Quick J, Grubaugh ND, Pullan ST, Claro IM, Smith AD, Gangavarapu K, et al. Multiplex PCR method for MinION and Illumina sequencing of Zika and other virus genomes directly from clinical samples. Nat Protoc. 2017;12:1261–76. https://doi.org/10.1038/nprot.2017.066
3. Grubaugh ND, Gangavarapu K, Quick J, Matteson NL, De Jesus JG, Main BJ, et al. An amplicon-based sequencing framework for accurately measuring intrahost virus diversity using PrimalSeq and iVar. Genome Biol. 2019;20:8. https://doi.org/10.1186/s13059-018-1618-7
4. Santiago GA, Vázquez J, Courtney S, Matías KY, Andersen LE, Colón C, et al. Performance of the Trioplex real-time RT-PCR assay for detection of Zika, dengue, and chikungunya viruses. Nat Commun. 2018;9:1391. https://doi.org/10.1038/s41467-018-03772-1
5. Metsky HC, Matranga CB, Wohl S, Schaffner SF, Freije CA, Winnicki SM, et al. Zika virus evolution and spread in the Americas. Nature. 2017;546:411–5. https://doi.org/10.1038/nature22402
6. Faria NR, Quick J, Claro IM, Thézé J, de Jesus JG, Giovanetti M, et al. Establishment and cryptic transmission of Zika virus in Brazil and the Americas. Nature. 2017;546:406–10. https://doi.org/10.1038/nature22401
7. Black A, Moncla LH, Laiton-Donato K, Potter B, Pardo L, Rico A, et al. Genomic epidemiology supports multiple introductions and cryptic transmission of Zika virus in Colombia. BMC Infect Dis. 2019;19:963. https://doi.org/10.1186/s12879-019-4566-2
8. Grubaugh ND, Saraf S, Gangavarapu K, Watts A, Tan AL, Oidtman RJ, et al.; GeoSentinel Surveillance Network. Travel surveillance and genomics uncover a hidden Zika outbreak during the waning epidemic. Cell. 2019;178:1057–1071.e11. https://doi.org/10.1016/j.cell.2019.07.018
9. Peters R, Stevenson M. Zika virus diagnosis: challenges and solutions. Clin Microbiol Infect. 2019;25:142–6. https://doi.org/10.1016/j.cmi.2018.12.002

Address for correspondence: Jorge L. Muñoz-Jordan, Centers for Disease Control and Prevention, 1324 Cañada St, San Juan, PR 00920, USA; email jmunoz@cdc.gov.

Fatal Systemic Capillary Leak Syndrome after SARS-CoV-2 Vaccination in Patient with Multiple Myeloma

Gwang-Jun Choi, Seon Ha Baek, Junmo Kim, Jung Ho Kim, Geun-Yong Kwon, Dong Keun Kim, Yeon Haw Jung, Sejoong Kim

Author affiliations: Daegu Metropolitan Government, Daegu, South Korea (G.-J. Choi); Hallym University Dongtan Sacred Heart Hospital, Hwaseong, South Korea (S.H. Baek); National Forensic Service Daegu Institute, Daegu (J. Kim); Yeungnam University College of Medicine, Daegu (J.H. Kim); Korea Disease Control and Prevention Agency, Cheongju, South Korea (G.-Y. Kwon, D.K. Kim, Y.H. Jung); Seoul National University Bundang Hospital, Seongnam, South Korea (S. Kim)

DOI: https://doi.org/10.3201/eid2711.211723

A young man with smoldering multiple myeloma died of hypotensive shock 2.5 days after severe acute respiratory syndrome coronavirus 2 vaccination. Clinical findings suggested systemic capillary leak syndrome (SCLS); the patient had experienced a previous suspected flare episode. History of SCLS may indicate higher risk for SCLS after receiving this vaccine.

Systemic capillary leak syndrome (SCLS) is an extremely rare disease of unknown incidence (*1*). Typical manifestations of SCLS include hypotension, edema, hemoconcentration, and hypoalbuminemia after nonspecific prodromal illnesses (*1*,*2*). Increased capillary vascular permeability is the commonly accepted pathophysiology (*1*,*2*). However, the exact pathogenesis remains unclear.

As part of the efforts to combat the ongoing pandemic of coronavirus disease (COVID-19), caused by severe acute respiratory syndrome coronavirus 2, the US Food and Drug Administration on February 27, 2021, gave emergency use authorization to the Ad26.COV2.S vaccine (Johnson & Johnson/Janssen, https://www.jnj.com). An SCLS case series reported 1 case of SCLS in a patient who received the Ad26.COV2.S vaccine (*3*). The European Medicines Agency reviewed 3 cases of SCLS in Ad26.COV2.S vaccine recipients and issued a report, published July 9, 2021, advising against administering the vaccine in persons with previous SCLS experiences (*4*). We describe a case of SCLS after Ad26.COV2.S vaccination in a patient with smoldering multiple myeloma.

A 38-year-old man reporting vomiting and dizziness sought treatment at an emergency department.

Smoldering multiple myeloma had been diagnosed 1.5 years before, but no laboratory abnormalities had been found in his most recent hospital visit 5 months earlier. He had received the Ad26.COV2.S vaccine 2 days before the emergency department visit and experienced fever, chills, and myalgia 12–24 hours postvaccination, then nausea, recurrent vomiting, and general weakness 24–48 hours postvaccination. At admission, he was afebrile, his heart rate was 130 beats/min, and his blood pressure was 100/90 mm Hg, with no noticeable edema. We administered isotonic saline and initiated diagnostic evaluations: laboratory tests, imaging, and COVID-19 reverse transcription PCR. Test results (Table) showed marked hemoconcentration and hypoalbuminemia. Chest and abdominal computed tomography results were unremarkable. Six hours after admission, the patient was hypotensive (blood pressure 60/40 mm Hg), had a heart rate of 132 beats/min, and reported dyspnea. We obtained blood cultures and treated the patient with broad-spectrum antimicrobials, intravenous fluids, and inotropes. Despite these measures, the patient's hypotensive shock worsened, and he died 10 hours after admission.

Although at admission the patient showed neither peripheral edema nor severe hypoalbuminemia, we suspected SCLS for several reasons. First, we could not entirely rule out infection, but results of blood cultures and COVID-19 testing were negative. Second, autopsy results showed no evidence of acute infection or cardiovascular disease in the internal organs. We identified pulmonary edema, pleural effusion, and pericardial effusion. Although pulmonary edema is atypical in acute SCLS attacks (leak phase), prolonged cardiopulmonary resuscitation and fluid administration might have affected the autopsy findings. Histopathologic findings in both kidneys suggested autolysis or acute tubular necrosis, which helped exclude other possible etiologies of refractory hypotensive shock. Third, through medical chart review, we found that the patient in our study had been admitted 1.5 years earlier for fever, vomiting, myalgia, generalized edema, and hypotension (blood pressure 90/60 mm Hg). Laboratory results showed hemoconcentration (hematocrit 58.4%) and hypoalbuminemia (3.03 g/dL at nadir), but diagnosis was unclear, and the patient recovered spontaneously after fluid administration. We retrospectively assumed a flare episode of SCLS. Fourth, ≈80% of patients with SCLS have monoclonal gammopathy of undetermined significance (MGUS) (*2*,*5*), and there have also been other reports of SCLS in patients with multiple myeloma (*2*). The patient who had the previous reported case of SCLS after Ad26.COV2.S vaccination had MGUS (*3*), and the patient in our study had multiple myeloma. Recently, an additional report described a patient with MGUS who experienced severe SCLS 2 days after receiving the ChAdOx1 nCOV-19 vaccine (Oxford/AstraZeneca, https://www.astrazeneca.com); that patient also had an unrecognized previous episode of presumed SCLS (*6*).

We believe a life-threatening flare developed after COVID-19 vaccination in the patient in our study who had a history suggestive of SCLS. Clinical findings were compatible with a previous report in which life-threatening disease occurred 1–2 days after vaccination (*3*,*6*); we could identify no SCLS triggers other than receiving the COVID-19 vaccine. Data from a review article

Table. Results of laboratory tests in patient with smoldering multiple myeloma who had SCLS develop after vaccination for severe acute respiratory syndrome coronavirus, South Korea*

Clinical measures	Reference range	Test results after SCLS episodes	
		5 mo earlier	Postvaccination
Leukocytes, $\times10^3$/mm^3	4–10	6.88	29.42
Hemoglobin, g/dL	13–17	14.7	22.7
Hematocrit, %	40–52	44.3	63.7
Platelet, $\times10^3$/mm^3	140–440	259	133
Albumin, g/dL	3.5–5.0	4.8	3.3
Blood urea nitrogen, mg/dL	8–23	13.6	33
Creatinine, mg/dL	0.7–1.2	0.94	2.0
Aspartate transaminase, IU/L	10–35	22	30
Alanine transferase, IU/L	0–40	14	4
Total bilirubin, mg/dL	0.1–1.2	0.5	1.46
Calcium, mg/dL	8.6–10.6	10.0	8.9
Erythrocyte sedimentation rate, mm/h	0–20	Not done	13
C-reactive protein, mg/dL	0–0.5	Not done	2.371
Procalcitonin, ng/ml	0–5	Not done	0.641
Troponin I, ng/mL	0–0.04	Not done	0.017
Creatine kinase myocardial band, ng/mL	0.6–6.3	Not done	3.5
N terminal-pro B-type natriuretic peptide, pg/mL	0–125	35.1	4,427
Lactic acid, mmol/L	0.5–1.6	Not done	5.4
Creatine phosphokinase, IU/L	1–171	Not done	276

*Vaccine was Ad26.COV2.S (Johnson & Johnson/Janssen, https://www.jnj.com). SCLS, systemic capillary leak syndrome.

indicated that 44% of 134 patients had identifiable SCLS triggers; 88% of those were infections, usually respiratory, and 11% involved intense physical exertion or extended travel (*7*). There was also a case report of possible SCLS related to the influenza vaccine; although not clearly meeting all the criteria for SCLS, a peritoneal dialysis patient experienced recurrent episodes of hypotension, peripheral edema, and hypoalbuminemia after 2 consecutive seasons of influenza vaccination (*8*). Immunologic response to vaccination has been proposed as a possible mechanism (*8*), but further studies are needed to verify factors predisposing patients to SCLS after COVID-19 immunization.

In South Korea, 1,129,796 people had received the Ad26.COV2.S vaccine as of August 2, 2021 (*9*); we have found no other reports of possible SCLS in vaccine recipients in South Korea. Our report describes the clinical course and characteristics of SCLS after COVID-19 vaccination. SCLS is often difficult to diagnose and may be misdiagnosed as other diseases, such as culture-negative sepsis. Therefore, clinicians should be aware of possible SCLS, especially in at-risk populations, and medical histories should be examined before vaccine is administered.

Acknowledgments

The authors express our deepest condolences to the bereaved family of the patient.

About the Author

Dr. Choi is an epidemic intelligence officer in the Daegu Metropolitan Government in Daegu, South Korea. His current research interest is adverse events following immunization.

References

1. Siddall E, Khatri M, Radhakrishnan J. Capillary leak syndrome: etiologies, pathophysiology, and management. Kidney Int. 2017;92:37–46. https://doi.org/10.1016/j.kint.2016.11.029
2. Druey KM, Greipp PR. Narrative review: the systemic capillary leak syndrome. Ann Intern Med. 2010;153:90–8. https://doi.org/10.7326/0003-4819-153-2-201007200-00005
3. Matheny M, Maleque N, Channell N, Eisch AR, Auld SC, Banerji A, et al. Severe exacerbations of systemic capillary leak syndrome after COVID-19 vaccination: a case series. Ann Intern Med. 2021 June 15 [Epub ahead of print]. https://doi.org/10.7326/L21-0250
4. European Medicines Agency. EMA advises against use of COVID-19 vaccine Janssen in people with history of capillary leak syndrome [cited 2021 July 9]. https://www.ema.europa.eu/en/news/ema-advises-against-use-covid-19-vaccine-janssen-people-history-capillary-leak-syndrome
5. Baek SH, Shin N, Kim HJ, Han MY, Choi DJ, Bang SM, et al. A case of chronic renal failure associated with systemic capillary leak syndrome. Yeungnam Univ J Med. 2012;29:145–9. https://doi.org/10.12701/yujm.2012.29.2.145
6. Julie Robichaud, Catherine Côté, Fanny Côté. Systemic capillary leak syndrome after ChAdOx1 nCOV-19 (Oxford–AstraZeneca) vaccination. CMAJ. 2021 Aug 6 [Epub ahead of print]. https://doi.org/10.1503/cmaj.211212
7. Druey KM, Parikh SM. Idiopathic systemic capillary leak syndrome (Clarkson disease). J Allergy Clin Immunol. 2017;140:663–70. https://doi.org/10.1016/j.jaci.2016.10.042
8. Geerse DA, Meynen FM, Gelens MA, Kooman JP, Cornelis T. Systemic capillary leak syndrome after influenza vaccination in a peritoneal dialysis patient. Perit Dial Int. 2015;35:772–3. https://doi.org/10.3747/pdi.2014.00194
9. Korea Disease Control and Prevention Agency. Cumulative COVID-19 vaccine doses administered in Republic of Korea [cited 2021 August 2]. https://www.kdca.go.kr/board/board.es?mid=a20501010000&bid=0015&list_no=714208&cg_code=&act=view&nPage=7

Address for correspondence: Sejoong Kim, Department of Internal Medicine, Seoul National University Bundang Hospital, 82, Gumi-ro 173beon-gil, Bundang-gu, Seongnam, Gyeonggi-do, South Korea; email: sejoong@snubh.org

The COVID Catastrophe: What's Gone Wrong and How To Stop It Happening Again, 2nd Edition

Richard Horton; Polity, Cambridge, UK, and Boston MA, USA, 2021; ISBN-10: 1509549102; ISBN-13: 978-1509549108; Pages: 180; Price: $59.95 (Hardcover); $6.70 (Paperback)

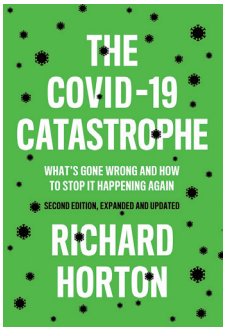

After half of the adult population in the United States has been fully vaccinated against coronavirus disease (COVID-19) to date (*1*), we seem to finally see the light at the end of the tunnel, after a 1.5-year battle with the most unprecedented public health crisis in modern history. We are reckoning with devastating mid-pandemic chaos caused by avoidable mistakes that have added to adverse outcomes.

In this second edition of *The Covid-19 Catastrophe: What's Gone Wrong and How to Stop It Happening Again*, Richard Horton, a medical expert and editor-in-chief of Lancet, leads us to revisit the COVID-19 crisis with his acumen, sharp arguments, and strong conscientiousness. Published in January 2021, this newer edition features updated epidemiologic numbers on COVID-19 and provides better data that account for discoveries and perspectives in the second half of 2020.

Before the main body, the author added a comprehensive introduction to explain the biology of the COVID-19 coronavirus and challenges of vaccine development and distribution. It also summarizes major lessons learned in response to COVID-19. Horton addresses awareness of the "terrible human cost" caused by lockdowns and potential long-term consequences that could afflict COVID-19 survivors.

Chapter 1 describes the origin of the COVID-19 pandemic by reviewing spread of the pandemic and responses from each country and the World Health Organization with a clear timeline. In Chapter 2, Horton engages the reader by asking, "Why were we not prepared?" A critical reason that most countries were unprepared was an underestimation of the danger of the coronavirus by political leaders and the general public, despite lessons learned from outbreaks of Ebola and Zika.

Chapters 3–5 further discuss the "disturbing twists" that might explain why countries were unprepared for COVID-19. Chapter 3 praises the efforts of frontline health workers and scientific groups in providing dependable knowledge regarding COVID-19 and criticizes indecisive policymaking in handling the emergency. In Chapter 4, Horton analyses responses of various countries and identifies elements needed to have a robust and resilient health system capable of responding to such a pandemic. Chapter 5 details the failures of government responses to COVID-19 and discusses how political misinformation played a role in the failure.

Chapter 6 offers a thought-provoking philosophy that emerging risks and problems we encounter today might result from our own developments (*2*). This chapter and the epilogue conclude with Horton's opinions on the impact of COVID-19 on our future, and strategies that help prepare us for the next pandemic. It is indispensable for the World Health Organization to strengthen its global coordinating role by mobilizing resources and establishing an accountability mechanism.

The book is replete with straightforward facts and honest, bold, and sometmes furious arguments that show how COVID-19 is much more than merely a health crisis. "It is a crisis about life itself," Horton writes. Although Horton makes some repetitive points throughout the book, we found it informative and a compelling reflection on the COVID-19 pandemic. It is a fascinating read for health professionals and nonhealth professionals who wish to understand the full scale of the cataclysmic pandemic we are currently experiencing.

Dongzhe Hong, Xin Yin, Lizheng Shi

Author affiliations: Tulane University School of Public Health and Tropical Medicine, New Orleans, Louisiana, USA (D. Hong, L. Shi); Pennsylvania State College of Medicine, Hershey, Pennsylvania, USA (X. Yin)

DOI: https://doi.org/10.3201/eid2711.211257

Bibliography

1. Centers for Disease Control and Prevention. COVID-19 vaccinations in the United States [cited 2021 May 24]. https://covid.cdc.gov/covid-data-tracker/#vaccinations
2. Wimmer J, Quandt T. Living in the risk society: an interview with Ulrich Beck. Journalism Stud. 2006;7:336–47. https://doi.org/10.1080/14616700600645461

Address for correspondence: Lizheng Shi, Health Policy and Management, Tulane University School of Public Health and Tropical Medicine, 1440 Canal St, Ste 1900, New Orleans, LA 70112-2703, USA; email: lshi1@tulane.edu

Berthe Morisot (1841–1895), *Hanging the Laundry Out to Dry* (detail), 1875. Oil on canvas, 13 in x 16 in/33 cm x 40.6 cm. Public domain image, National Gallery of Art, Washington, DC, USA.

Yet Another Potential Age-Old Nonpharmaceutical Intervention

Kathleen Gensheimer and Byron Breedlove

In 1874, members of the *Société Anonyme des Artistes-Peintres, Sculpteurs, Graveurs* staged an exhibition of their work in the highly esteemed Salon de Paris, launching a movement now identified as Impressionism. Art historian Margaret Samu writes, "Their work is recognized today for its modernity, embodied in its rejection of established styles, its incorporation of new technology and ideas, and its depiction of modern life." But this nascent art form was not universally applauded. Art and culture critic Jason Farago notes, "The movement's name was originally a critic's insult. 'Impressionist' came from a venomous review of an 1874 exhibition of paintings by Monet, Renoir, Degas, Pissarro—and one woman." A second exhibition in the spring of 1876 in Paris induced more mixed reactions; one detractor described its participants as "five or six lunatics, one of which is a woman."

That woman, Berthe Morisot, became a leading figure of the Impressionist artistic movement of the 19th century and is perhaps the most underrated Impressionist. The granddaughter of the Rococo painter Jean-Honoré Fragonard, Morisot decided at an early age to become an artist. From 1862 to 1868, she worked under the guidance of landscape artist Camille Corot. Morisot exhibited paintings at the Salon de Paris from 1864 through 1874, when, in support of the burgeoning Impressionist movement, she vowed to never again show her paintings in the officially sanctioned forum. In 1868, Morisot developed a working friendship with French modernist painter Édouard Manet. Manet had a liberating effect on her work, and she in turn aroused his interest in outdoor painting. In 1874, she married Manet's younger brother, Eugène, a writer and painter.

Columnist Tessa Solomon explains that ". . . Morisot's gender also played a role in how she was perceived. Writers in her day used terms like 'flirtatious' and 'charming' to describe her work; neither were labels given to the paintings of Claude Monet, Pierre-Auguste Renoir, and others." Even today, sexist undertones surface in the ways in which Morisot is discussed. In 2018, when the Barnes Foundation in Philadelphia mounted the first US retrospective devoted to her, it was subtitled "Woman Impressionist." "Imagine a parallel case, say, 'Georges Braque: Man Cubist,'" quipped art critic Peter Schjeldahl.

Author affiliations: Food and Drug Administration, College Park, Maryland, USA (K. Gensheimer); Centers for Disease Control and Prevention, Atlanta, Georgia, USA (B. Breedlove)

DOI: https://doi.org/10.3201/eid2711.AC2711

Social conventions of the day kept Morisot from pursuing the same subject matter as her male counterparts, such as Monet and Renoir, who often painted popular sites of leisure around Paris. Because Morisot liked to paint outdoors—and frequenting such sites without a chaperone would have invited scandal—she instead depicted domestic scenes, landscapes, and portraits, stating, "It is important to express oneself, provided the feelings are real and are taken from your own experience." Like Manet, she portrayed contemporary life, taking inspiration from quotidian life. Much of her work focused on the lives of women in French society, and this month's cover image, *Hanging the Laundry Out to Dry,* is an example of her *plein-air* painting; that is, painting outdoors, which better captures the appearance of light and weather conditions.

Morisot depicts several women hanging the washing to dry on a windy day. Clothing hangs off almost everything conceivable object in the garden. In the background, trees dot the countryside, perhaps marking the edges of the property, and steam trains travel across the horizon. Clumps of billowing clouds race across the canvas, revealing glimpses of blue sky. In the foreground, a wood fence that parallels the distant horizon is also draped with laundry. By relying on flickering brushstrokes and a light palette, Morisot succeeds in briskly conveying a scene, not fixating on accuracy or detail.

Art historian Aleid Ford observes, "Figures and features of the scene are roughed-in rapidly. Perspective makes quick sense of the scene but Morisot doesn't dither with sharp or acute detail. Rather, she seems to scrub the view clean with a bleached-out palette of pastels, anchoring the lot with that spindled fence along the front." The large house and extended grounds suggest that a wealthy family lives there and employs a number of workers to handle daily chores such as laundry. According to exhibition notes from the Barnes Foundation, "Working women are a recurring subject in Morisot's painting. The cooks, maids, and servants employed by upper-middle-class households in the late 19th century were as much a part of Morisot's daily life as her family and friends."

A prolific artist, Morisot never enjoyed great commercial success despite having attained significant critical recognition during her lifetime. In 1895, Morisot's daughter Julia was ill with pneumonia, and although Julia recovered, Morisot succumbed to the disease while caring for her daughter and died at the age of 54.

During Morisot's lifetime, today's vaccines and antimicrobials that can prevent or treat pneumonia did not exist. Even with prevention and treatment availability, pneumonia continues to affect hundreds of millions of people, old and young, around the globe. Many cases of pneumonia are caused by transmissible pathogens associated with outbreaks of disease, including influenza A and B virus, parainfluenza, metapneumovirus, measles virus, and respiratory syncytial virus. Of particular importance is the ongoing coronavirus disease pandemic, approaching its second year of circulating globally. Its mitigation requires both vaccines and nonpharmaceutical interventions.

Respiratory infections caused by transmissible pathogens can also be mitigated by wearing masks, maintaining physical distance, practicing hand and face hygiene, cleansing surfaces, avoiding crowds, and increasingly engaging in outdoor activities as feasible. Morisot's portrayal of women working outdoors in the fresh air and sunshine may be a picture of days past, but, nonetheless, it now also conveys a modern message, showing how nonpharmaceutical interventions can help prevent the transmission of respiratory diseases.

Bibliography

1. Barnes Foundation. Berthe Morisot: woman impressionist [cited 2021 Aug 15] https://www.barnesfoundation.org/whats-on/morisot
2. Editors of Encyclopaedia Britannica. Berthe Morisot: French painter [cited 2021 Aug 1. https://www.britannica.com/biography/Berthe-Morisot
3. Centers for Disease Control and Prevention. Pneumonia [cited 2021 Aug 15]. https://www.cdc.gov/pneumonia
4. Farago J. The impressionist art of seeing and being seen [cited 2021 Aug 1]. https://www.nytimes.com/interactive/2021/06/04/arts/design/berthe-morisot-in-england.html
5. Ford A. Sheets to the wind. Head for art [cited 2021 Aug 13]. http://headforart.com/2010/09/18/sheets-to-the-wind
6. Oster Y, Michael-Gayego A, Rivkin M, Levinson L, Wolf DG, Nir-Paz R. Decreased prevalence rate of respiratory pathogens in hospitalized patients during the COVID-19 pandemic: possible role for public health containment measures? Clin Microbiol Infect. 2020;27:5811–2.
7. Sagripanti J-L, Lytle CD. Estimated inactivation of coronaviruses by solar radiation with special reference to COVID-19. Photochem Photobiol. 2020;96:731–7. https://doi.org/10.1111/php.13293
8. Samu M. Impressionism: art and modernity [cited 2021 Aug 5] https://www.metmuseum.org/toah/hd/imml/hd_imml.htm
9. Schjeldahl P. Berthe Morisot, "woman impressionist," emerges from the margins [cited 2021 Aug 31]. https://www.newyorker.com/magazine/2018/10/29/berthe-morisot-woman-impressionist-emerges-from-the-margins
10. Solomon T. Berthe Morisot, Impressionism's most relentless innovator, is finally receiving her due [cited 2021 Aug 5]. https://www.artnews.com/art-news/artists/berthe-morisot-who-is-she-why-is-she-important-1234581283

Address for correspondence: Byron Breedlove, EID Journal, Centers for Disease Control and Prevention, 1600 Clifton Rd NE, Mailstop H16-2, Atlanta, GA 30329-4027, USA; email: wbb1@cdc.gov

EMERGING INFECTIOUS DISEASES®

Upcoming Issue

- Clinical Characteristics of *Corynebacterium Bacteremia* Caused by Different Species, Japan, 2014–2020
- Use of a Novel Serological Assay to Measure the Seroprevalence of Zika Virus in the Philippines
- Surface–Aerosol Stability and Pathogenicity of Diverse Middle East Respiratory Syndrome Coronavirus Strains, 2012–2018
- SARS-CoV-2 Seroprevalence in a Rural and Urban Household Cohort during First and Second Waves of Infections, South Africa, July 2020–March 2021
- Coronavirus Disease Contact Tracing Outcomes and Cost, Salt Lake County, Utah, United States, March–May 2020
- Transmission of Severe Acute Respiratory Syndrome Coronavirus 2 in Households with Children, Southwest Germany, May–August 2020
- Human Melioidosis Caused by Novel Transmission of *Burkholderia pseudomallei* from Freshwater Home Aquarium, United States
- Characterization of Swine Influenza A(H1N2) Variant, Alberta, Canada, 2020
- Four Filoviruses, 1 Hantavirus, and 1 Rhabdovirus in Freshwater Fish, Switzerland, 2017
- Using Serosurveillance to Map Risk for Anthrax Exposure in Feral Swine, Texas, USA
- Novel Use of Capture-Recapture Methods to Estimate Completeness of Contact Tracing during an Ebola Outbreak, Democratic Republic of Congo, 2018–2020
- Mammarenaviruses of Rodents, South Africa and Zimbabwe
- Heartland Virus Transmission, Suffolk County, New York, USA
- Experimental Oronasal Transmission of Chronic Wasting Disease Agent from White-Tailed Deer to Suffolk Sheep
- Detection of SARS-CoV-2 in Wastewater at Residential College, Maine, USA, August–November 2020
- SARS-CoV-2–Specific Antibodies in Domestic Cats during First COVID-19 Wave, Europe
- Incidence Trends for SARS-CoV2 Alpha and Beta Variants, Finland, Spring 2021
- SARS-CoV-2 Variants, South Sudan, January–March 2021
- Large-Scale Screening of Asymptomatic Persons for SARS-CoV-2 Variants of Concern and Gamma Takeover, Brazil

Complete list of articles in the December issue at http://www.cdc.gov/eid/upcoming.htm

Earning CME Credit

To obtain credit, you should first read the journal article. After reading the article, you should be able to answer the following, related, multiple-choice questions. To complete the questions (with a minimum 75% passing score) and earn continuing medical education (CME) credit, please go to http://www.medscape.org/journal/eid. Credit cannot be obtained for tests completed on paper, although you may use the worksheet below to keep a record of your answers.

You must be a registered user on http://www.medscape.org. If you are not registered on http://www.medscape.org, please click on the "Register" link on the right hand side of the website.

Only one answer is correct for each question. Once you successfully answer all post-test questions, you will be able to view and/or print your certificate. For questions regarding this activity, contact the accredited provider, CME@medscape.net. For technical assistance, contact CME@medscape.net. American Medical Association's Physician's Recognition Award (AMA PRA) credits are accepted in the US as evidence of participation in CME activities. For further information on this award, please go to https://www.ama-assn.org. The AMA has determined that physicians not licensed in the US who participate in this CME activity are eligible for AMA PRA Category 1 Credits™. Through agreements that the AMA has made with agencies in some countries, AMA PRA credit may be acceptable as evidence of participation in CME activities. If you are not licensed in the US, please complete the questions online, print the AMA PRA CME credit certificate, and present it to your national medical association for review.

Article Title

Ehrlichiosis and Anaplasmosis among Transfusion and Transplant Recipients in the United States

CME Questions

1. Your patient is a 62-year-old male kidney transplant recipient with fever and respiratory symptoms in whom ehrlichiosis is suspected. On the basis of the case series and literature review by Mowla and colleagues, which one of the following statements about donor-derived ehrlichiosis and anaplasmosis cases in the United States among solid organ transplant recipients is correct?

A. During 1997 to 2020, most cases of ehrlichiosis and anaplasmosis in transplant recipients were donor-derived
B. *Ehrlichia chaffeensis* ehrlichiosis was the most common organ donor-derived infection, occurring in 8 solid organ transplant recipients (7 kidney, 1 liver transplant recipient)
C. Half of cases in transplant recipients had fever
D. None of the donor-derived ehrlichiosis cases died, but two thirds of the confirmed cases were admitted to the intensive care unit (ICU)

2. According to the case series and literature review by Mowla and colleagues, which one of the following statements about donor-derived ehrlichiosis and anaplasmosis cases in the United States among transfusion recipients is correct?

A. Of the 12 cases of transfusion-transmitted ehrlichiosis or anaplasmosis reported from 1997 to 2020, 8 were a result of transfused platelet components
B. Most transfusion-associated cases were ehrlichiosis
C. Among anaplasmosis cases, 2 had ICU treatment for respiratory failure, hypotension, and hypoxia
D. One third of transfusion recipients with donor-derived ehrlichiosis and anaplasmosis died

3. On the basis of the case series and literature review by Mowla and colleagues, which one of the following statements about clinical implications of donor-derived ehrlichiosis and anaplasmosis cases in the United States among solid organ transplant and transfusion recipients is correct?

A. Transfusion- or transplant-transmitted ehrlichiosis and anaplasmosis are rare but cause severe outcomes including recipient death, mandating clinician awareness of these infections
B. Ehrlichiosis and anaplasmosis cases in the US have been stable since 2000
C. Solid organ transplant donors should be screened using approved laboratory screening interventions
D. Studies of asymptomatic infection among blood donors and survivability of infection in blood suggest the risk for transmission is lower than previously recognized